DOE/MC/25031—5097

Original Camera Ready Copy

DOE/MC/25031 -- 5097
(DE96000632)

Secondary Natural Gas Recovery: Targeted Applications for Infield Reserve Growth in Midcontinent Reservoirs -- Boonsville Field, Fort Worth Basin, Texas

Topical Report
May 1993 - June 1995

Bob A. Hardage
David L. Carr
Robert J. Finley
Noel Tyler
David E. Lancaster
Robert Y. Elphick
James R. Ballard

July 1995

Work Performed Under Contract No.: DE-FG21-88MC25031

For
U.S. Department of Energy
Office of Fossil Energy
Morgantown Energy Technology Center
Morgantown, West Virginia

By
University of Texas at Austin
Austin, Texas

DISCLAIMER

DOE/MC/25031 -- 5097
(DE96000632)
Distribution Category UC-132

Secondary Natural Gas Recovery: Targeted Applications for Infield Reserve Growth in Midcontinent Reservoirs -- Boonsville Field, Fort Worth Basin, Texas

Topical Report
May 1993 - June 1995

Bob A. Hardage
David L. Carr
Robert J. Finley
Noel Tyler
David E. Lancaster
Robert Y. Elphick
James R. Ballard

Work Performed Under Contract No.: DE-FG21-88MC25031

For
U.S. Department of Energy
Office of Fossil Energy
Morgantown Energy Technology Center
P.O. Box 880
Morgantown, West Virginia 26507-0880

By
University of Texas at Austin
University Station, Box X
Austin, Texas 78713-8924

July 1995

RESEARCH SUMMARY

Title	Secondary Natural Gas Recovery: Targeted Technology Applications for Infield Reserve Growth in Midcontinent Reservoirs, Boonsville Field, Fort Worth Basin, Texas
Contractor	Bureau of Economic Geology, The University of Texas at Austin GRI Contract No. 5093-212-2630, "Secondary Natural Gas Recovery—Infield Reserve Growth Joint-Venture: Applications in Midcontinent Sandstones."
Principal Investigators	Robert J. Finley and Bob A. Hardage
Report Period	May 1993–June 1995
Objectives	The objectives of this project are to define undrained or incompletely drained reservoir compartments controlled primarily by depositional heterogeneity in a low-accommodation, cratonic Midcontinent depositional setting, and, afterwards, to develop and transfer to producers strategies for infield reserve growth of natural gas. Integrated geologic, geophysical, reservoir engineering, and petrophysical evaluations are described in complex difficult-to-characterize fluvial and deltaic reservoirs in Boonsville (Bend Conglomerate Gas) field, a large, mature gas field located in the Fort Worth Basin of North Texas. The purpose of this project is to demonstrate approaches to overcoming the reservoir complexity, targeting the gas resource, and doing so using state-of-the-art technologies being applied by a large cross section of Midcontinent operators.
Technical Perspective	Reserve growth resources in the Midcontinent region total as much as 41 Tcf. The region contains the second-largest natural gas reserve growth reserve after the Texas Gulf Coast and provided an appropriate resource target for the secondary gas recovery (SGR) research following the Gulf Coast project. Secondary or incremental gas may be contained in reservoirs (even those that have conventional porosity and permeability) that are untapped or bypassed or have incompletely drained areas that are a function of depositional facies, diagenetic, and even structural heterogeneity. The Midcontinent reservoirs selected for this project have more deltaic components than do the dominantly fluvial reservoirs that were the focus of the Gulf Coast SGR project. Further, the Midcontinent reservoirs studied were deposited in a cratonic basin that had relatively low accommodation space and a higher frequency of sea-level fluctuation than did depositional patterns in the Tertiary of the Gulf Coast Basin. Pennsylvanian Midcontinent sandstones are complex, but it is this complexity that creates the opportunity for additional infield gas recovery.
Results	Pressure and production data confirm the existence of compartmented or poorly drained gas reserves throughout much of the Bend Conglomerate, suggesting that additional reserves will be found when well spacing is reduced to 80 acres. Three styles of reservoir compartmentalization were identified in Midcontinent clastic gas reservoirs from the Boonsville analysis: structural, stratigraphic, and a combination of the two.

Structural compartments are caused by low-displacement faulting that acts as a partial barrier to gas flow and is commonly associated with karst collapse in deeper carbonate rocks; these features extend vertically as much as 2,000 ft. This previously unknown karst collapse phenomenon that was identified by means of the 3-D seismic survey may be a widespread influence on the deposition of younger sediments in the Midcontinent.

Stratigraphic compartments may be surface bounded, facies bounded, or cement bounded. Combination-style compartments have both structural and stratigraphic elements and are most commonly surface and fault bounded. The best natural gas reservoirs in Boonsville field occur predominantly as lowstand, valley-fill conglomeratic sandstones overlying erosional surfaces. Isopach mapping indicates a strong relationship between reservoir distribution and structurally low areas on the pre-Atoka seismic time structure surface, suggesting that subtle elevation differences at the pre-Atoka stratigraphic level controlled the geographical location of incised valleys, fluvial and fluvio-deltaic axes in which high-energy reservoir facies were concentrated.

Interpretation of these complex reservoirs was aided by a 26-mi^2 3-D seismic survey. Resolution was maximized using specialized small (10 oz) directional, explosive-source charges; a high data-sampling rate (1 ms); and staggered source and receiver lines that allowed the data to be stacked into high-fold 110- × 100-ft bins for general interpretation or into lower fold 55- × 55-ft bins when detailed interpretations requiring lateral resolution were needed. Precise calibration of thin-bed depths to seismic traveltime was accomplished by recording detailed vertical seismic profile (VSP) data and explosive-source velocity checkshot data at several locations within the 3-D seismic grid.

Whereas the 3-D seismic survey clearly identified the importance of the karst collapse features to reservoir compartmentalization, the ability of the 3-D survey to identify stratigraphic entrapments was more variable. Some sequences, such as the Upper and Lower Caddo, were imaged quite well, once calibrated to well control, and seismic attributes analysis provided excellent agreement with net reservoir distributions generated from sequence stratigraphic interpretations. In other instances, the 3-D data did not always provide conclusive answers. Individual systems tracts and reservoir sandstones that are subsets of genetic sequences are sometimes difficult to trace precisely in the 3-D data, if the acoustic impedance of these units is approximately the same as the acoustic impedance of the bounding beds or if the units are extremely thin.

Judging from the hydrocarbon distribution in the project area, the gas reserves expected in any particular Bend sequence will be approximately 200 MMscf or less on average when well spacing is reduced to 80 acres, whereas gas reserves of at least 400 MMscf will typically be required for new wells to be economically attractive. Although individual Bend completions may still encounter gas reserves in excess of 400 MMscf (some recent wells have), it appears that multiple stacked completion opportunities will be needed in new infield wells. Review of the 3-D data suggests that these stacked trapping geometries often exist throughout the Bend interval. Thus, a reasonable approach to identifying new well

locations may be to focus 3-D seismic evaluation on these apparent stacked trapping geometries in areas having the highest likelihood of encountering multiple completion opportunities. An alternate strategy is to use the 3-D data to identify fault-bounded blocks that have no penetrations in subregional or field-scale areas where the pre-Atoka time structure is low and total Atoka net reservoir isopachs are thick, again increasing the potential for finding multiple vertically stacked completion opportunities.

Technical Approach

This assessment of Midcontinent sandstone natural gas reservoirs in Boonsville field integrated four key disciplines: geology, geophysics, reservoir engineering, and petrophysics. The entire Atoka Group (Lower and Upper) in the project area was divided into 13 third-order genetic stratigraphic sequences. To our knowledge, this is the first public, comprehensive genetic sequence analysis that relates these prolific Pennsylvanian gas reservoirs to their seismic response and to gas productivity. A 26-mi^2 3-D seismic survey was acquired and interpreted to test methods for delineating reservoirs in thin-bed, hard-rock environments. Reservoir facies frameworks, assessed by integrating geological and geophysical approaches, were combined with engineering and petrophysical evaluations of produced gas volumes and reservoir quality.

Project Implications

(To be provided by GRI.)

CONTENTS

Figures

Tables

Appendix A Figures

Appendix A Tables

Appendix B Figures

Appendix C Figures

Appendix C Tables

Appendix D Figures

Appendix D Table

Appendix E Figures

Appendix F Figures

EXECUTIVE SUMMARY

This report documents an assessment of Midcontinent sandstone natural gas reservoirs in Boonsville field, Fort Worth Basin, Texas, conducted as part of the Secondary Gas Recovery (SGR) Infield Reserve Growth Joint Venture between the Gas Research Institute (GRI) and the U.S. Department of Energy (DOE). The objectives of this project are to define undrained or incompletely drained reservoir compartments controlled primarily by depositional heterogeneity in a low-accommodation, cratonic Midcontinent depositional setting, and, afterward, to develop and transfer strategies for infield reserve growth of natural gas to producers. Reserve growth resources in the Midcontinent region total as much as 41 Tcf. The region contains the second-largest natural gas reserve growth resource after the Texas Gulf Coast and is thus an appropriate resource target for SGR research.

Midcontinent gas production is dominantly derived from Pennsylvanian sandstones laid down as fluvial and deltaic deposits (23 plays in Texas, Oklahoma, Arkansas, and Kansas). These are the primary facies in the Atokan Caddo and Bend Conglomerate at Boonsville field, our laboratory for defining heterogeneity in these reservoir types. In this project, interpretation of these complex reservoirs was aided by a 26-mi^2 3-D seismic survey collected to test methods of reservoir delineation in thin-bed, hard-rock environments. The Boonsville test site centers on the 26-mi^2 3-D seismic survey within the field that has been the focal point of this study.

The entire Atoka Group (Lower and Upper) in the project area, between 900 and 1,300 ft thick, has been divided into 13 third-order genetic stratigraphic sequences for purposes of this study. The genetic sequences are defined and bounded by impermeable deep-shelf shales that represent maximum flooding events and are similar in nature to the cycles or cyclothems used in other contexts to describe similarly repetitive, late Paleozoic strata. To our knowledge, this is the first public, comprehensive genetic sequence analysis

that relates these prolific Pennsylvanian reservoirs to their seismic response and to gas productivity.

Pressure and production data confirm the existence of compartmented or poorly drained gas reserves throughout much of the Bend Conglomerate interval in the project area. New wells drilled through the Bend frequently find pressures in one or more of the Bend sequences that are at or near the original pressures encountered more than 40 yr ago when the field was first being developed. Most of these compartmented or poorly drained gas reserves are found in sequences between the Lower Caddo and the Vineyard (the most prolific, basal conglomerate in the Bend section). Median drainage areas in these sequences were found to be 80 acres or less, further confirming the likelihood that compartmented or poorly drained gas reserves will continue to be found as well spacing is reduced to 80 acres (currently the optional well spacing in Boonsville field).

From comprehensive analysis of the Boonsville project area, three styles of reservoir compartmentalization were identified in Midcontinent clastic gas reservoirs: structural, stratigraphic, and a combination of the two. Structural compartments in Boonsville field are caused by low-displacement faulting, most commonly associated with karst collapse in deeper carbonate rocks, that produces structurally isolated fault blocks. The faulting is widespread, but subtle, and neither vertical displacements nor fault-block geometries can be mapped without 3-D seismic data. The importance to reservoir development of structure related to dissolution and karst collapse at depth was previously unknown.

Stratigraphic compartments may be surface bounded, facies bounded, or cement bounded. Surface-bounded compartments result from superposition of reservoir sandstones and other, diachronous impermeable facies at key surfaces. Facies-bounded compartments are caused by high-frequency, autocyclic processes within depositional systems tracts that result in permeability barriers. These facies changes may occur over fairly short, lateral distances. Cement-bounded compartments result from postdepositional

interfacies barriers caused by diagenetic processes (for example, the development of $CaCO_3$ and SiO_2 cements).

Combination-style compartments have both structural and stratigraphic elements. Although they are most commonly surface and fault bounded, some combination compartments result from syntectonic deposition—that is, the preferential buildup of reservoir facies in response to subtle fault-block lows.

The best natural gas reservoirs in Boonsville field occur predominantly as lowstand, valley-fill conglomeratic sandstones; they owe their existence to erosional downcutting (incisement), which occurs during relative sea-level lowstands, followed by subsequent aggradation during the early phase of relative sea-level rises. Highstand deltaic and shoreface sandstones are also important reservoirs that occur as progradational lobes. Lowstand fluvial and deltaic deposits overlie and erosionally truncate highstand deposits; however, their respective sandstone bodies typically occur as separate compartments.

Isopach mapping of net pay within the total Bend Conglomerate section indicates a strong relationship between sandstone reservoir distribution and structurally low areas on the pre-Atoka seismic time structure surface. This fact suggests that subtle differences in the structural elevation at the pre-Atoka, Paleozoic carbonate, stratigraphic level controlled the geographical location of incised valleys, fluvial and fluvio-deltaic axes in which high-energy reservoir facies were concentrated. In addition, many of the thickest valley-fill sandstone reservoirs occur above or immediately adjacent to the vertically faulted, karst collapse zones identified by means of 3-D seismic, although this is not the rule for all Boonsville sequences. Karst collapse appears to have occurred episodically throughout Bend deposition such that slightly different structurally controlled physiographies existed during the deposition of each Bend sequence.

Older ES and IES (resistivity-only) log suites comprised more than half of the available well log data in the project area. In order to include these data in the analysis, as part of this project, we developed an algorithm for estimating porosity and lithologies from

IES logs, and we interpreted the ES logs using commercially available software. In addition, we developed detailed facies identification algorithms for all vintages of well log suites commonly available in the Midcontinent. These log-calculated facies curves were based on careful calibration of geological core observations and multivariate statistical analysis and were useful in backing up the sequence stratigraphic correlations of reservoir zones.

The interpretation of the 3-D seismic data and their application to Bend Conglomerate reservoir types were the cornerstone of this project. In acquiring the 3-D survey, we maximized data resolution using specialized (10 oz), directional explosive source charges, a high data-sampling rate (1 ms), and staggered source and receiver lines that allowed data to be stacked into high-fold 110- × 110-ft bins for geological interpretation or into lower fold 55- × 55-ft bins for detailed interpretations requiring high lateral resolution, when needed. We precisely calibrated thin-bed depths to seismic traveltime by recording detailed vertical seismic profile (VSP) data and explosive-source velocity checkshot data at several locations within the 3-D seismic grid.

At Boonsville, the 3-D data clearly identified a structural component important to reservoir compartmentalization that was unexpected beforehand, in the form of the aforementioned low-displacement faulting, often (but not always) associated with karst collapse in deeper carbonate rocks. These karst collapse features extend vertically as much as 2,000 ft and occur in broadly defined, dominantly north-northwesterly linear groups, suggesting a genetic relationship between karst-dissolution processes and preexisting, subtle basement faulting. Recent Boonsville wells drilled in these small (about 100 acres), structurally high fault blocks have encountered higher than expected pressures in some sequences, suggesting that these low-displacement faults can act as partial barriers to gas flow. Similar karst collapse features occur in Paleozoic outcrops in far West Texas, and hydrocarbon production is known to occur in Ellenburger karst zones of the Val Verde

Basin, suggesting that these features may be a widespread influence on the deposition of younger sediments in the Midcontinent.

In contrast, the ability of the 3-D seismic data to identify stratigraphic entrapments at Boonsville was highly variable. Some sequences, such as the Upper and Lower Caddo, were well imaged in the 3-D data volume, once calibrated to existing well control. Seismic-attribute analysis by means of reflection amplitude and instantaneous frequency in the Upper and Lower Caddo sequences, respectively, provided excellent agreement with net reservoir distributions generated from the sequence stratigraphic interpretations. In some sequences, the 3-D seismic data can thus be highly predictive for identifying interwell properties and siting new wells when an adequate number of wells exist to establish a relationship between seismic attributes and stratigraphic and lithologic facies.

On the other hand, in these complex, surface-dominated stratigraphies that have thin, discontinuous reservoirs, the 3-D seismic data do not always provide conclusive answers. Individual systems tracts and reservoir sandstones that are subsets of genetic sequences are difficult to trace precisely in the 3-D data, especially when units have subtle changes of acoustic impedance or are extremely thin. In addition, some Bend Conglomerate reservoirs appear to be seismically nondescript and difficult to distinguish, even when well control is used to guide the interpretation. In such areas, the 3-D seismic data cannot be used reliably to locate new infield well locations.

An important use of the 3-D seismic survey in this project was in identifying and tracing the geometries of key chronostratigraphic surfaces that manifest themselves as seismic reflectors. This is interpretive seismic stratigraphy at a high resolution, which integrates both well control and the sequence stratigraphic model developed by the geologist. In Midcontinent rocks, it is particularly important to recognize major erosional features that have cut out previously deposited sequences, as well as shingling, clinoform geometries in which several individual sandstone compartments can occur (and that appear to be only a single unit in log-based cross sections). Integration of the 3-D seismic data is

critical to identifying true reservoir architecture, which typically contains significant lateral heterogeneities.

Ultimately the key to successful infield development in an older Midcontinent field such as Boonsville is the volume of gas reserves associated with these compartmented or poorly drained areas of the field. Judging from the hydrocarbon distribution in the project area, the expected gas reserves associated with an individual reservoir compartment or poorly drained area in any particular Bend sequence will be on the order of 200 MMscf or less (on average) as well spacing is reduced to 80 acres, whereas gas reserves of at least 400 MMscf will typically be required for new wells to be economically attractive (depending on operator and completion practices). Although it is still possible that an individual Bend completion may encounter gas reserves in excess of 400 MMscf (some have in recent wells), it is more likely that multiple stacked completion opportunities will be needed to yield gas reserves sufficient for a viable infield well as spacing is reduced.

Analysis of the 3-D data volume in the project area leads us to the conclusion that stacked trapping geometries commonly exist within the 3-D data volume. Further, the influence of the vertical, karst collapse features of Bend Conglomerate stratigraphy also suggests the opportunity and likelihood of finding multiple stacked, and at least partially isolated reservoirs. In the absence of clear geologic or seismic evidence of undeveloped reservoirs, a reasonable approach to identifying new well locations may be to focus 3-D seismic evaluation on these apparent, stacked trapping geometries in areas having the highest likelihood of multiple completion opportunities (that is, multiple pay zones). An alternate strategy for siting new wells is to use the 3-D seismic data to identify fault-bounded blocks having no well penetrations occurring in subregional or field-scale areas where the pre-Atoka time structure is low and total Atoka net reservoir isopachs are thick, again increasing the potential for finding multiple vertically stacked completion opportunities.

This report summarizes the technical results of the Boonsville investigation, but it represents only one facet of the technology transfer from this project. Three short courses based on these results have already been presented and have been well received by industry audiences, not to mention numerous presentations of aspects of the Boonsville project to a variety of professional organizations. Three to six more short courses are anticipated through early 1996, as well as additional technical papers and presentations.

Three technical summaries have been published and two more are in progress, highlighting innovative technological applications in both seismic acquisition and facies determination. Several more technical summaries are planned in the coming months. Executable versions of personal-computer software for applying the IES algorithm will soon be available in both Windows and Macintosh formats. Finally, a digital subset of the 3-D survey data, as well as selected elements of the well data base and digital log curves, will also be made available to industry as part of the technology transfer process.

1. OVERVIEW

The Context for a Natural Gas Reserve Growth Study of Midcontinent Gas Reservoirs

This report documents an assessment of Midcontinent sandstone natural gas reservoirs in Boonsville field, Fort Worth Basin, Texas. The Boonsville test site centers on a 26 mi^2 3-D seismic survey within the field that has been the focal point of this study. The objective of the work, a part of the Secondary Gas Recovery (SGR) Infield Reserve Growth Joint Venture between the Gas Research Institute (GRI) and the U.S. Department of Energy (DOE), is to define advanced approaches to infield natural gas reserve growth. Boonsville field, ranked 28th among U.S. gas fields in cumulative production (as of year-end, 1992), was selected as representative of Pennsylvanian Midcontinent sandstone reservoirs. Pennsylvanian sandstones dominate Midcontinent gas production; 23 out of 41 plays in the region are Pennsylvanian in age and consist dominantly of sandstone reservoirs.

Reserve growth resources in the Midcontinent region total as much as 41 Tcf. The region contains the second-largest gas reserve growth resource after the Texas Gulf Coast and is thus an appropriate resource target after the SGR Gulf Coast project. The Midcontinent reservoirs selected for study have more deltaic depositional components than the dominantly fluvial reservoir targets, such as those at Stratton field, that were the focus of the Gulf Coast SGR project. The Midcontinent reservoirs studied were deposited in a cratonic basin with relatively low accommodation space and a higher frequency of sea-level fluctuation compared with depositional patterns in the Tertiary of the Gulf Coast Basin. Pennsylvanian Midcontinent sandstone reservoirs are therefore complex and difficult to characterize, but it is this complexity that creates the opportunity for additional infield gas recovery. The purpose of the project is to demonstrate approaches to overcoming that complexity, targeting the gas resource, and doing such using

integrated state-of-the-art techniques capable of being applied by a large cross section of Midcontinent operators.

Project team members have worked with three cooperating companies in assessing reserve growth opportunities at Boonsville: OXY USA, Inc., Enserch Operating Limited Partnership, and Threshold Development/Arch Petroleum Co. These companies provided more than 90-percent cofunding of the 3-D seismic survey, made available substantial volumes of existing data, allowed use of proprietary software for reservoir analysis (OXY USA), and cofunded collection of new data as new wells were drilled, completed, and tested. The participation of these companies was an essential and integral part of the SGR Midcontinent project.

This report is organized around a series of case studies that follow a brief overview of the Boonsville test site. The project was very much driven by application of the 3-D seismic data to Boonsville reservoir types within the Bend Conglomerate, an interval generally 1,000 to 1,200 ft in thickness that contains about a dozen depositional cycles. The technical details of the applications made in each of the major disciplines—geology, reservoir engineering, petrophysics, and geophysics—are contained in a series of appendices. This report structure was adopted so that the case studies would not be burdened with excessive methodological detail. Yet it is this detail that operators will want to understand if they are to examine the results of this study and incorporate the insights gained into their own approaches to further development of existing fields for gas reserve growth.

It should be noted that the case studies highlight both insights gained and problems remaining unresolved. Whereas the stratigraphic character of key sequences such as the Upper and Lower Caddo was clearly imaged in the seismic volume, the 3-D seismic data did not provide conclusive answers in all sequences within the Bend Conglomerate. In these complex, surface-dominated stratigraphies with thin, discontinuous reservoirs, not all analogs to prolific reservoirs showed an analogous production response. Structure,

related to carbonate dissolution and karst collapse at depth, was found to play a role in reservoir development that was not previously known. Cases are described where different data, namely engineering analyses of reservoir size compared with geophysical images, gave similar results for reservoir dimensions, whereas in other cases such coherence was not achievable. Initial results from two new wells sited early in the interpretation of the 3-D data are also presented, illustrating the seismic features that suggest reservoir compartmentalization and the procedures used to identify these features in the 3-D seismic image. The authors believe that in documenting these case studies operators gained a realistic sense of the difficulties, as well as potential for successful infield development. One short course participant commented that he liked the case study approach and liked seeing the real problems presented "warts and all."

Technology Transfer: To Date and in the Future

This report documents the technical results of the Boonsville investigation. Three short courses based on these results have already been presented and have been well received by industry audiences. A technology transfer period will now follow, with additional short courses and the generation of additional technology transfer products. The second generation of short course notes will provide additional detail for the case studies and, in particular, better integrate geophysical and sequence stratigraphic interpretations with other aspects of the investigation. The latter particularly includes reconciliation of reservoir extent with engineering tests of reservoir volumes in communication with a given completion interval. No new data will be incorporated into this additional integration. The focus will be on greater depth of analysis of existing data to develop key relationships that have extrapolation potential to wider areas within Midcontinent cyclic reservoir sequences.

Overview of the Boonsville Project Area

Introduction

The primary focus of this study was Boonsville (Bend Conglomerate Gas) field located in the Fort Worth Basin of north-central Texas. Figure 1.1 shows the location of the field, which covers most of Wise and Jack Counties, Texas. Actually there are several Boonsville field designations in the area, depending on the particular completion interval(s), but the area of primary interest in the study is officially designated as Boonsville (Bend Conglomerate Gas) field by the Railroad Commission of Texas. This field covers several hundred thousand acres and is one of the largest natural gas fields in the United States. To date, the field has produced in excess of 2.6 Tscf (trillion standard cubic feet) of natural gas; there are just over 2,000 active wells in the field.

In Figure 1.1, the region designated by the solid rectangle on the Wise–Jack County line is the primary area of interest in this project. This is where 26-mi^2 of 3-D seismic data were gathered and where the vast majority of research work reported here was performed. This location will be referred to as the Boonsville project area throughout this report.

Figure 1.2 shows a history of drilling activity in the Boonsville project area. This figure plots the number of wells drilled in, and immediately adjacent to, the project area against the year drilled. Whereas this figure does not include all wells in the field, the trends shown in the figure are representative of the field as a whole.

Boonsville field was discovered in 1945, but in the late 1940's and early 1950's, there was not much market for the gas. In fact, operators commonly abandoned, or shut in and temporarily abandoned, a number of gas-producing wells in this time period. Drilling boomed in the mid- to late 1950's, following the construction of a large gas pipeline that went from Wise County to Chicago. Figure 1.2 illustrates the large increase in drilling

activity in the project area in the mid- to late 1950's owing to the existence of the new pipeline market.

In November 1957, the Railroad Commission of Texas officially established field rules for Boonsville (Bend Conglomerate Gas) field. These initial field rules permitted one well to be drilled on a 320-acre unit. This field designation consolidated more than 29 separate fields in existence at the time, and other fields have been merged with Boonsville (Bend Conglomerate Gas) field since then.

Drilling activity tapered off in the 1960's and 1970's; then in 1980, the Railroad Commission of Texas modified the field rules to permit wells to be drilled on optional 160-acre units. As Figure 1.2 shows, this ruling sparked new drilling activity in the field in the early- to mid-1980's. Recently, in 1991, the Railroad Commission reduced the spacing requirements again, permitting wells to be drilled on optional 80-acre units. Again, there has been a small upturn in the drilling activity as a result of this reduced spacing.

Geologic Setting

Natural gas production in Boonsville field comes from conglomeratic sandstones deposited in the Fort Worth Basin during the Atoka stage of the Middle Pennsylvanian period (Figs. 1.3 and 1.4; Blanchard and others, 1968; Thompson, 1982). The primary trapping mechanisms are facies and permeability pinch-outs (Glover, 1982; Lahti and Huber, 1982; Thompson, 1982), and effective exploitation of these fields is difficult because the typically thin and discontinuous sandstone reservoirs represent a variety of complexly intermingled depositional environments and facies and commonly contain pore-occluding diagenetic cements. The complexities found in many Upper Paleozoic sandstones of the U.S. Midcontinent are the result of unique fundamental geological controls that combined to produce complex, compartmentalized reservoirs. Specifically the primary geological controls were

- relatively low accommodation setting (i.e., shallow basin),
- high-amplitude, high-frequency sea level fluctuations,
- tectonic jostling during sedimentation,
- temporal variations in sediment source material,
- high rates of sediment supply, and
- tropical paleoclimate.

The Fort Worth Basin is a late Paleozoic foreland basin that contains a maximum thickness of approximately 13,000 ft (~4,000 m) of sedimentary strata, the majority of which are Pennsylvanian in age (Turner, 1957; Thompson, 1988). In addition to the dominantly Pennsylvanian basin fill, major sequences of Cambrian, Ordovician, Mississippian, and Permian rocks are also present. The Paleozoic units are unconformably overlain and onlapped by Cretaceous strata in the eastern and southeastern parts of the basin (Flawn and others, 1961; Lahti and Huber, 1982; Thompson, 1982).

In map view, the Fort Worth Basin is an asymmetric, inverted triangle that is approximately 80 mi across and 250 mi long, from apex to base (Figure 1.3). Fault-bounded structural uplifts define the eastern (Ouachita Thrust Belt) and northern limits (Muenster Uplift, Red River-Electra Uplift) of the basin, but the less distinct western limit is bounded by the Bend Arch, which is a low, north-plunging fold. The Muenster and Red River–Electra Uplifts are both thought to be part of the northwest-trending Amarillo–Wichita Mountain Uplift, which resulted from reactivation of Precambrian boundary faults when Ouachitan compressive stresses were transmitted to the craton (Walper, 1977).

Ouachita foreland basin gas accumulations, including Bend Conglomerate gas in the Fort Worth Basin, occur as large, pervasive, deep basin accumulations (Masters, 1979; Meckel and others, 1992). Pennsylvanian gas reservoirs in these basins, typically underpressured, are rarely water productive, are relatively tight (typically less than

10 md), and are hydraulically separated from updip–overlying, more permeable, normally pressured water-bearing units (Meckel and others, 1992). The source of the natural gas is probably the abundant humic materials (land-derived, macerated plant material) in shales that encase the sandstone reservoirs (Meckel and others, 1992). Other Ouachita foreland basins having similar habitats include the Arkoma, Val Verde, and Black Warrior Basins, and possibly the Kerr and Marfa Basins.

Stratigraphy and Nomenclature

Figure 1.5 presents a typical log from the Bend Conglomerate interval in the project area. The Bend Conglomerate is defined as those intervals between the base of the Caddo Limestone and the top of the Marble Falls Formation (Railroad Commission of Texas, 1991). The Bend interval is treated as a common source of supply, and wells completed in more than one of the Bend productive sequences may be commingled and produced from a single wellbore. Recently the Railroad Commission has also allowed operators to commingle both Caddo and Bend Conglomerate production in a single wellbore, especially when necessary for economic reasons.

For practical purposes, the terms "Bend Conglomerate" and "Atoka Group" are essentially synonymous and can be used interchangeably. We have retained Thompson's (1982) "Lower Atoka" and "Upper Atoka" division, which splits the Bend Conglomerate interval into two geologically distinctive halves. A time-stratigraphic correlation chart for comparing units across the many basins of the U.S. Midcontinent appears in Figure 1.4.

A variety of nomenclatures have been developed to divide the major intervals of the Bend Conglomerate, but the complex stratigraphy, lack of outcrop exposures, and paucity of good index fossils have led to a proliferation of schemes that are not rigorously correlative to one another. As a result of the confusion in the published literature, individual operating companies have developed their own local nomenclatures. Even

within the Boonsville project area, there were considerable differences in interval definitions, correlations, and names used by our operator partners.

To facilitate communication between the project participants, and to permit unrestricted geological interpretation of the Bend Conglomerate interval, it was necessary to construct a new, more broadly applicable nomenclature, in which major reservoir intervals were divided by using the concepts of sequence stratigraphy (see discussion that follows and Appendix A). The log section shown in Figure 1.5 illustrates the stratigraphic framework we used to define the major reservoir zones in the Boonsville project area. These intervals represent major, time-equivalent sequences that were subsequently named for local cultural and geographic features in the project area; the widely used terms Caddo and Davis were preserved because they fit within our sequence stratigraphic framework.

Reservoir Characteristics

The Bend Conglomerate ranges from 100 to 1,700 ft thick across Boonsville field, and in the project area, the interval ranges from about 900 to more than 1,300 ft in thickness. As Figure 1.5 illustrates, there are numerous potentially productive sequences throughout the Bend. Of these intervals, the Caddo and the Vineyard have been by far the most prolific producing reservoirs in the project area, but there have been completions in all the major sequences. Typically these intervals are gas productive, but several of these sequences are also oil productive in the northeast and southeast portions of the project area. The Caddo sequences are primarily oil productive in the project area.

Table 1.1 lists some of the key characteristics of the Bend Conglomerate in the project area. As shown, the Bend Conglomerate is found at depths ranging between 4,500 and 6,000 ft and is somewhat underpressured. Depending on the interval and the depth, the best estimate for initial pressure ranges from 1,400 psi to 2,200 psi, which is a pressure gradient of about 0.35 to 0.4 psi/ft. The reservoir temperature is about 150° F, and the typical gas gravity is 0.65 to 0.75 (1,100 to 1,200 BTU/MMscf).

Table 1.1. Bend Conglomerate characteristics in Boonsville project area.

Property/item	Typical values
Depth	4,500 to 6,000 ft
Initial pressures	1400 to 2200 psi - somewhat underpressured
Temperature	150°F
Gas gravity	0.65 to 0.75
Gross thickness	900 to 1,300 ft
Net thickness	Multiple pays from a few ft to 20–30 ft each
Permeability	Varies from <0.1 md to >10 md; 0.1 to 5 md typical
Porosity	5 to 20 percent
Production	Varies from 10 MMscf to 8 Bscf; 1.5 Bscf Median

Net pay thickness ranges from several feet to 20 to 30 ft in each sequence; thus, a typical well may have anywhere from just a few feet of net pay to more than 100 ft of net pay. Permeabilities vary widely from less than 0.1 md to greater than 10 md, but values in the range of 0.1 to 5 md are typical. Gas production also varies widely. In the project area alone, gas recoveries range from as little as 10 MMscf to as much as 8 Bscf, with a median per-well recovery of about 1.5 Bscf.

Major reservoir intervals in the Bend Conglomerate strata correspond to "genetic sequences" (similar to cycles or cyclotherms in other terminology) averaging approximately 100 ft in thickness. Genetic sequences consist of upward-coarsening facies successions that are defined and bounded by impermeable marine shales marking key maximum flooding surfaces (Figure 1.6). Natural gas reservoirs at Boonsville occur predominantly in lowstand valley-fill conglomeratic sandstones; they owe their existence to erosional downcutting, which occurs during relative sea-level lowstands, followed by subsequent aggradation during the early phase of relative sea-level rises. Highstand deltaic and shoreface sandstones are also important reservoirs that occur as progradational lobes. Lowstand deposits overlie and erosionally truncate highstand deposits; however, their respective reservoir sandstone bodies typically occur as separate compartments.

Completion Practices

Figure 1.7 illustrates the typical completion practices in the Boonsville project area over the years. New wells drilled in the 1950's were most likely completed as (1) single or multiple, commingled completions in the Bend only or (2) dual completions in the Bend and the Caddo, with the latter typically being oil productive. Operators generally pumped small, hydraulic fracture treatments to stimulate production from the Bend reservoirs. Typical fracture treatments in the 1950's consisted of a treated lease oil with 10,000 lb of sand per zone.

As the productivity of the lower Bend intervals declined over time (into the 1970's), additional intervals were commonly added up-hole. Sometimes operators abandoned the original completion intervals. At other times production from these zones was simply commingled with that from the newly completed zones up-hole.

Today, production from multiple zones is commingled in most of the older, original completions. As mentioned previously, the Bend Conglomerate may now also be commingled with production from the Caddo in certain instances. Many of these older wells are on some sort of artificial lift, such as beam pumps or plunger lifts. The newer completions may be either single or dual completions. Often multiple Bend Conglomerate intervals may be completed together. Today these intervals are usually fractured by means of a 70- to 75-quality nitrogen foam carrying 30,000 to 70,000 lb of sand per interval treated.

Detailed Project Area

Figure 1.8 is a detailed map of the project area showing all wells having a total depth of more than 4,000 ft, which includes all wells that have penetrated the Caddo or below. The project area is just to the west of Lake Bridgeport, and the outline shown on the map illustrates the boundaries of the 26-mi^2 area where 3-D seismic data were recorded.

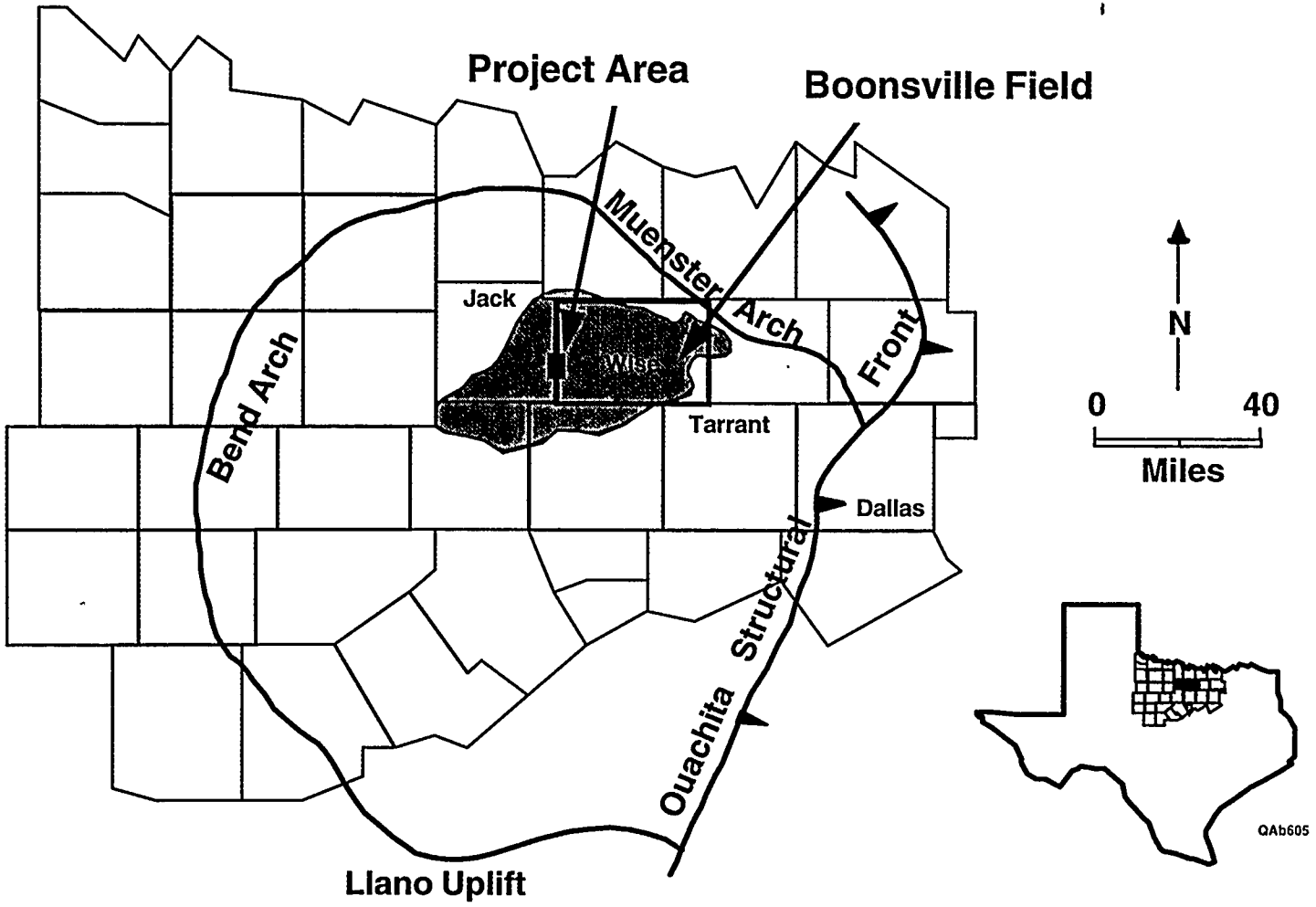

Figure 1.1. Location of Boonsville field in Wise and Jack Counties, Texas. The solid rectangle on the Wise-Jack County line designates the area where the 3-D seismic data were gathered and where the vast majority of the research work was performed.

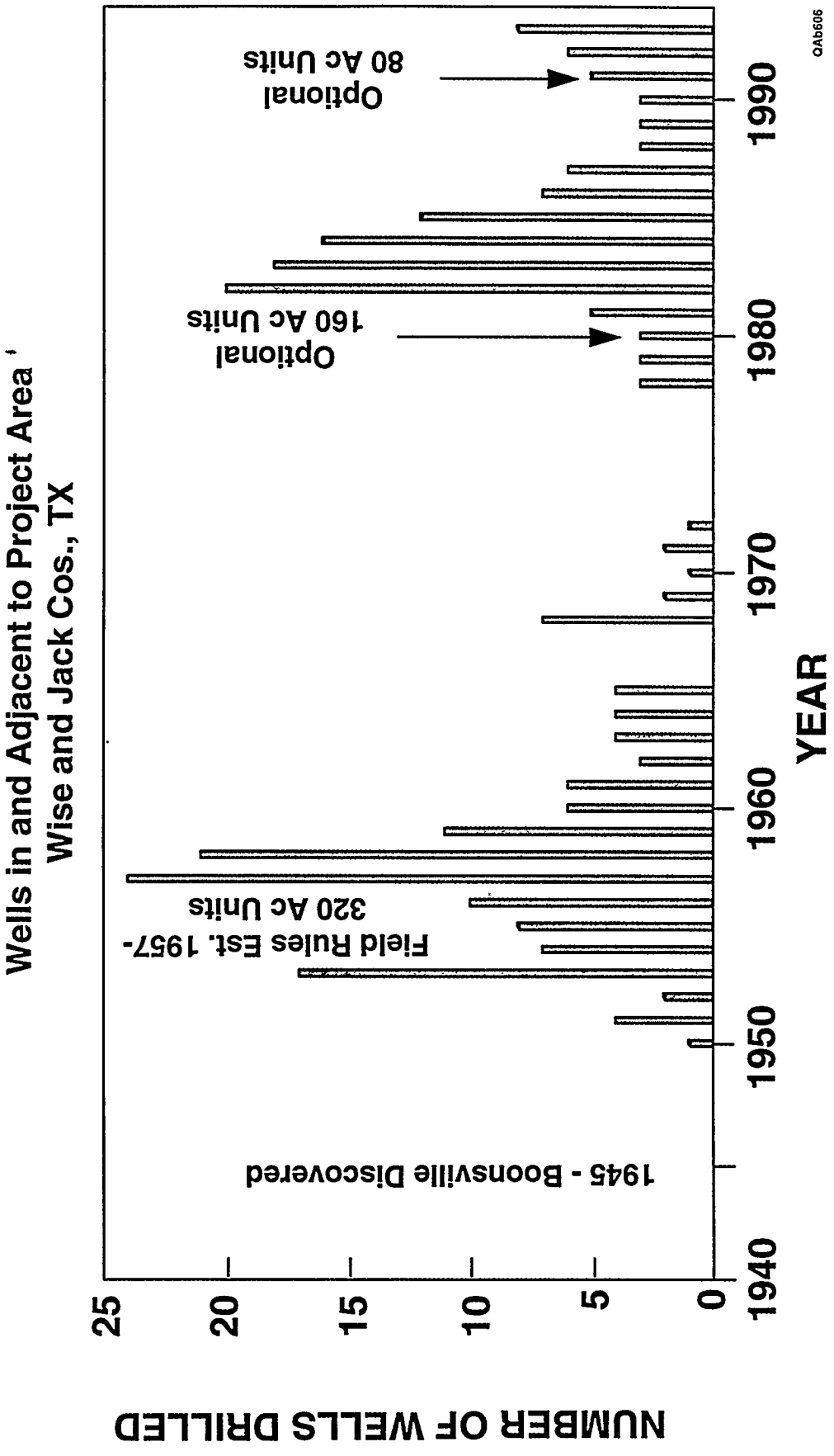

Figure 1.2. History of drilling activity for wells drilled in, and immediately adjacent to, the Boonsville project area.

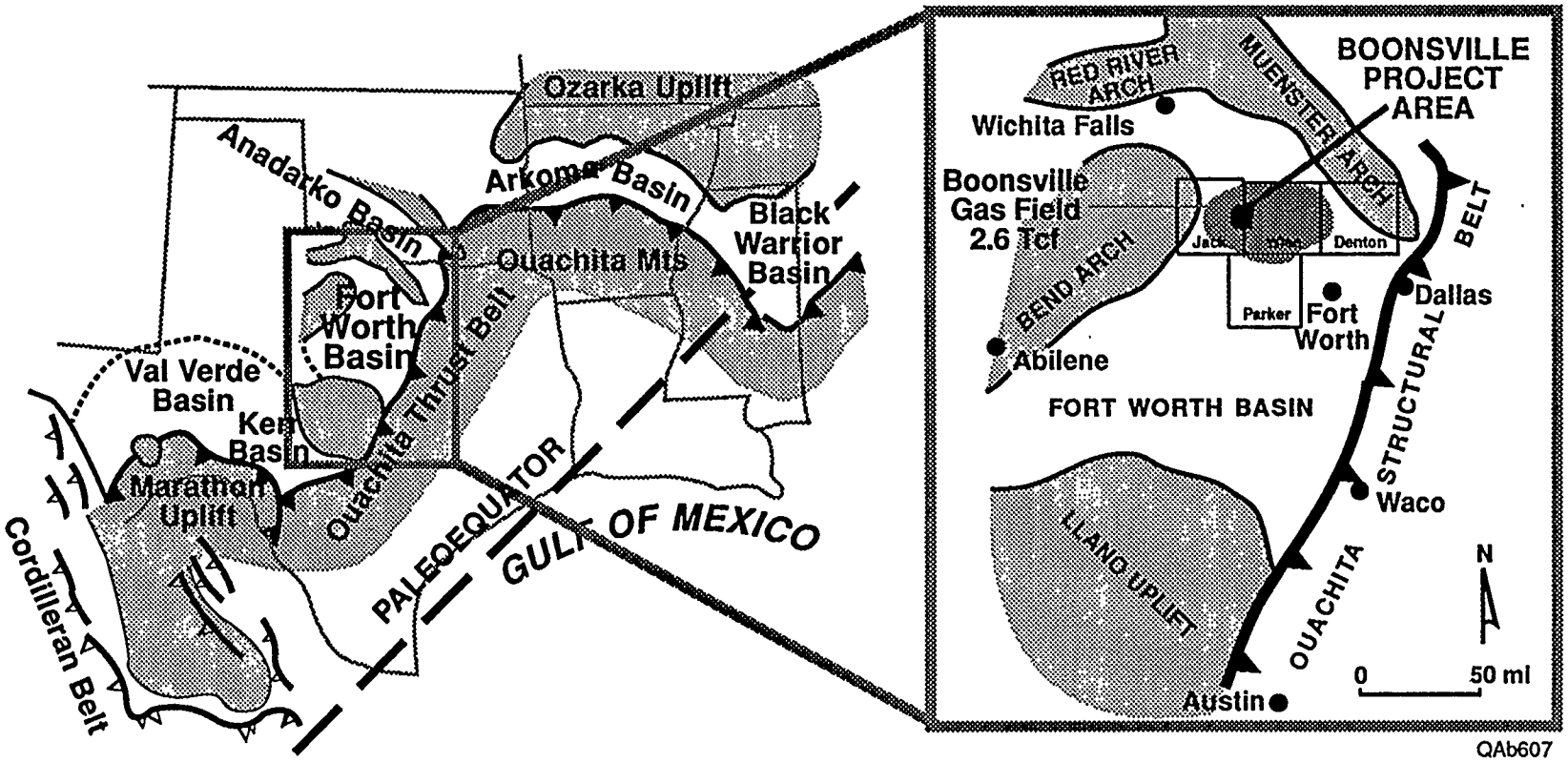

Figure 1.3. Middle Pennsylvanian paleogeographic map showing the Fort Worth Basin and Boonsville project area. Modified from Thompson (1982) and Lahti and Huber (1982).

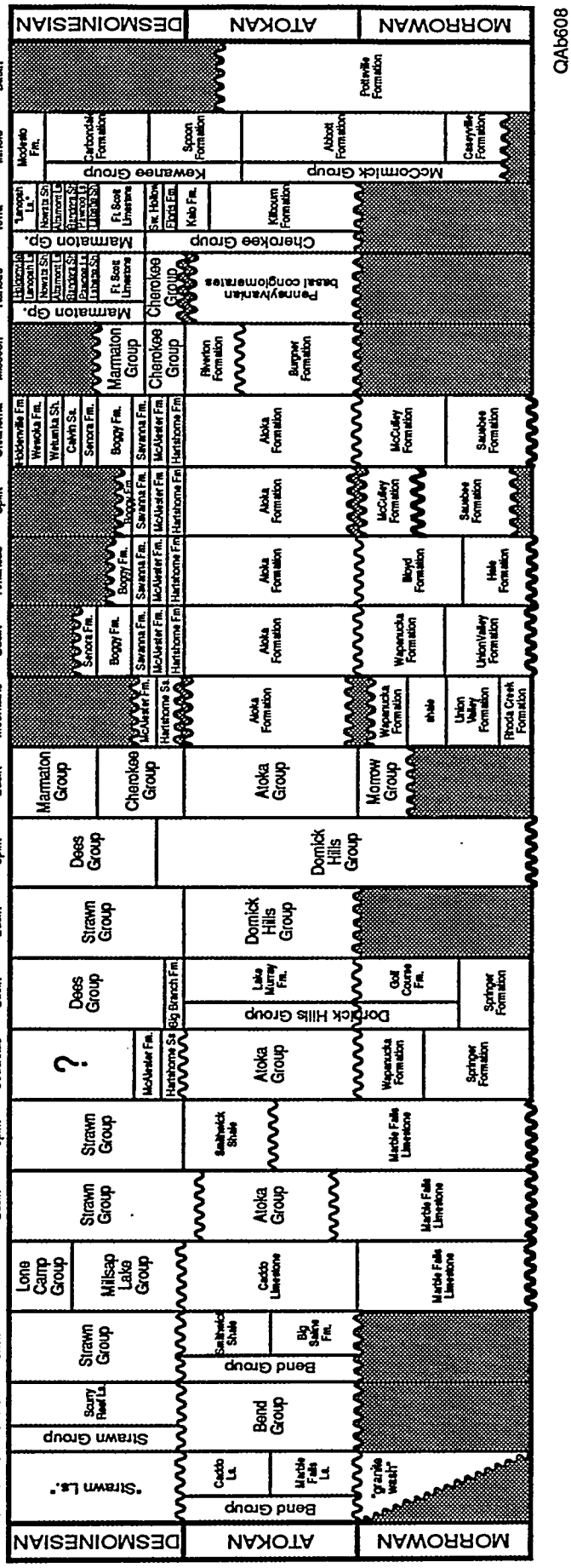

Figure 1.4. Time-stratigraphic correlation for Middle Pennsylvanian rocks of the U.S. Midcontinent region. Based on Sutherland and others (1982), Thompson (1982), Chapin and others (1983), Ravn and others (1984), Shaver and others (1984), Zachry and Sutherland (1984), Adler and others (1986), Carlson and others (1986), Grayson (1990), Manger and others (1992), and Sutherland and Grayson (1992).

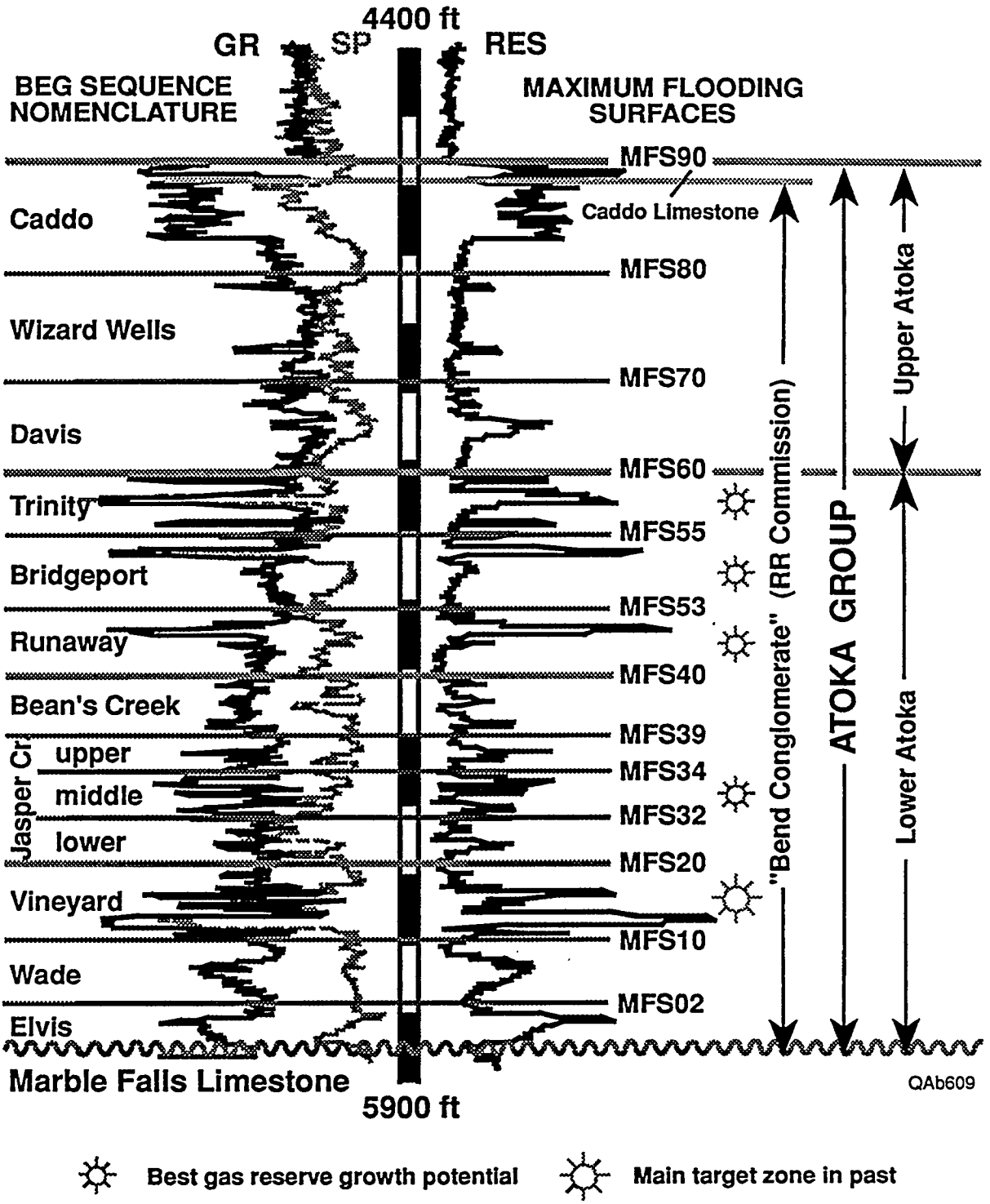

Figure 1.5. Type log from Boonsville project area, Threshold Development, Fayette Yates No. 11. Major reservoir zones were defined by genetic sequences, which are upward-coarsening units bounded by impermeable, maximum-flooding shales.

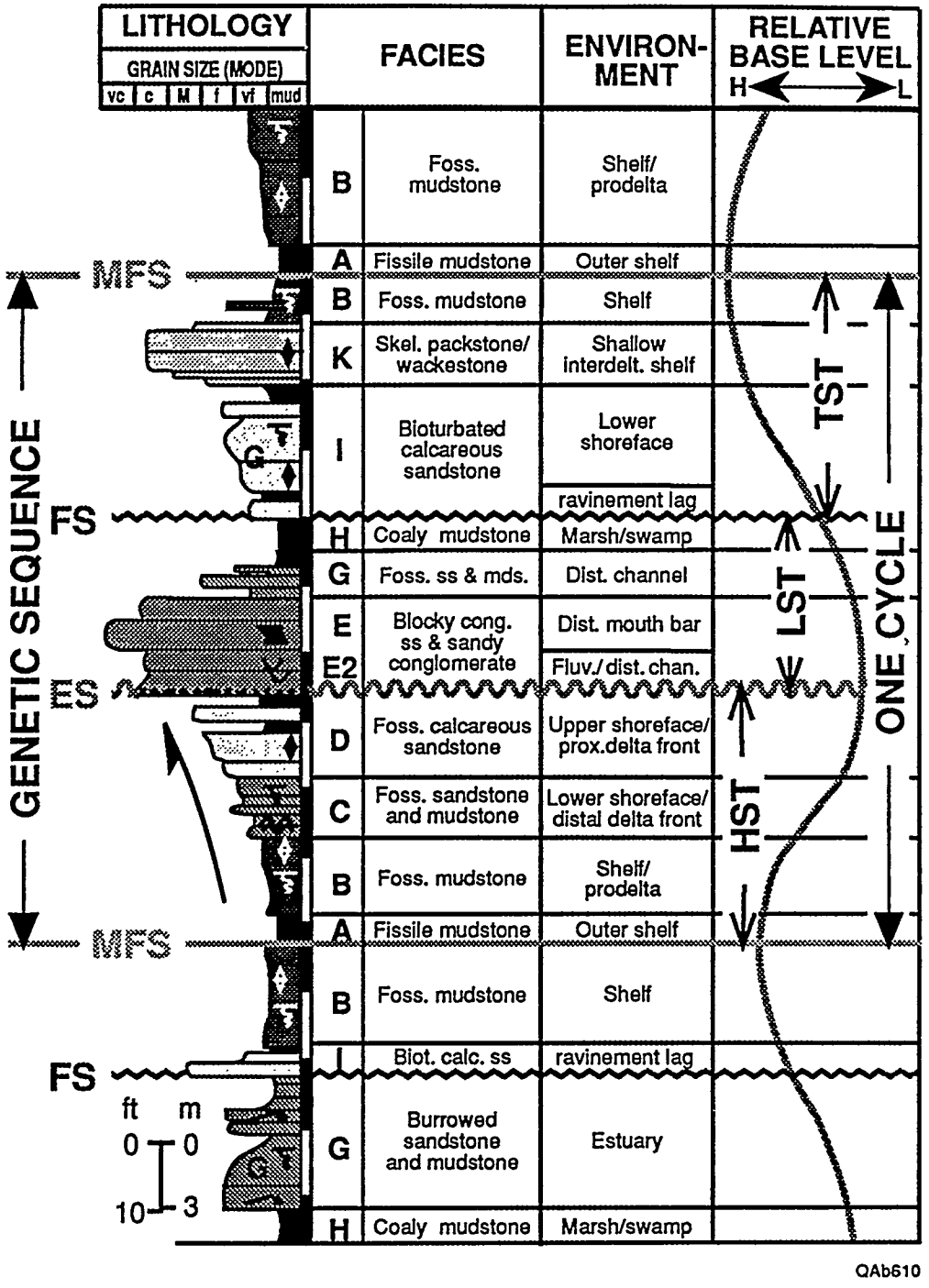

Figure 1.6. Composite genetic sequence illustrating key chronostratigraphic surfaces and typical facies successions. Constructed from actual core data spanning four Boonsville sequences. One relative base level cycle is commonly represented by highstand (HST), lowstand (LST), and transgressive (TST) systems tracts. Cycles beginning and ending with maximum flooding surfaces (MFS) typically contain one or more erosion surfaces (ES) and flooding surfaces (FS), which are commonly ravinement surfaces. Reservoir sandstone facies, if present, usually occur in the LST.

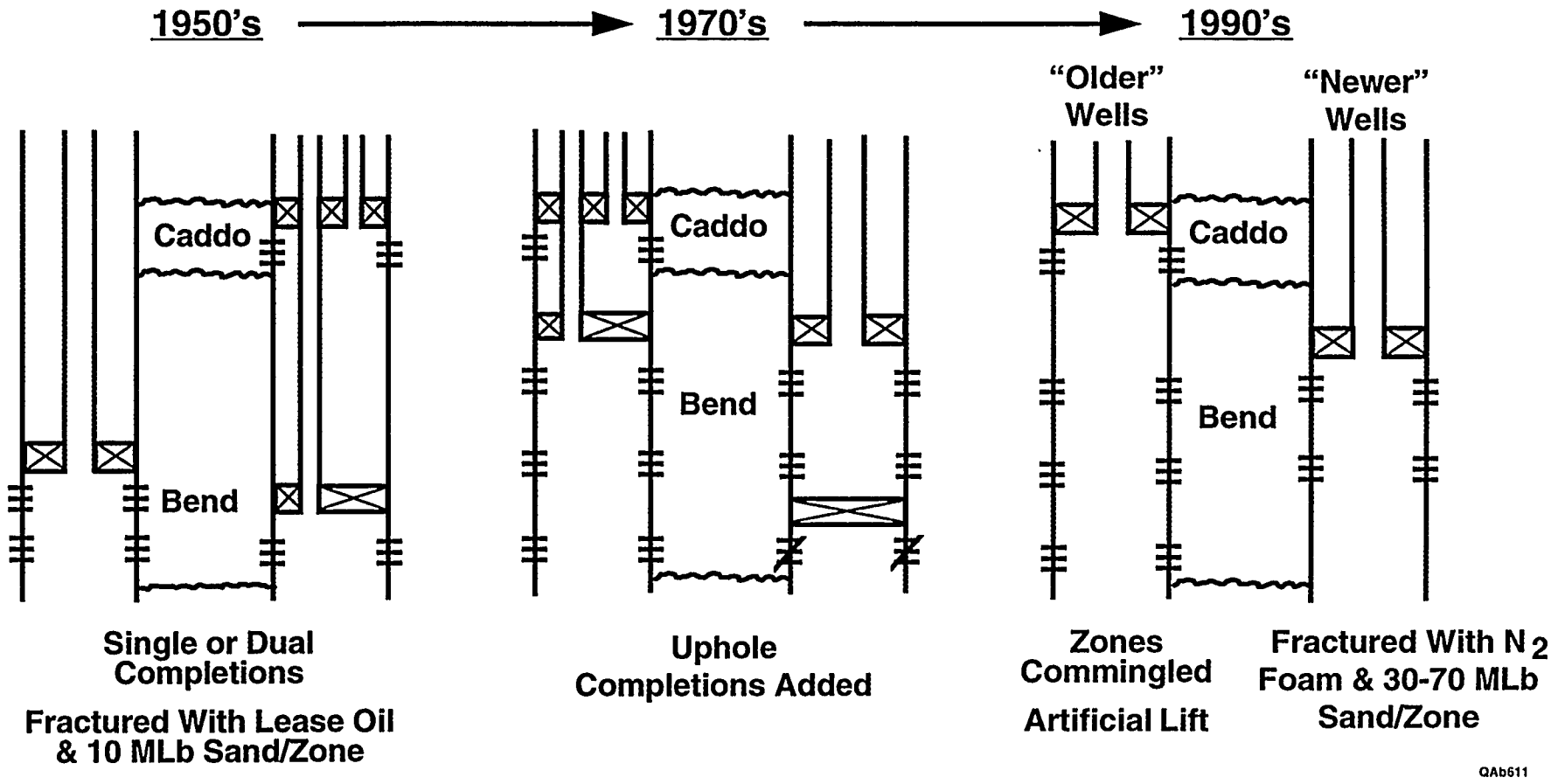

Figure 1.7. History of typical completion practices in the Boonsville project area.

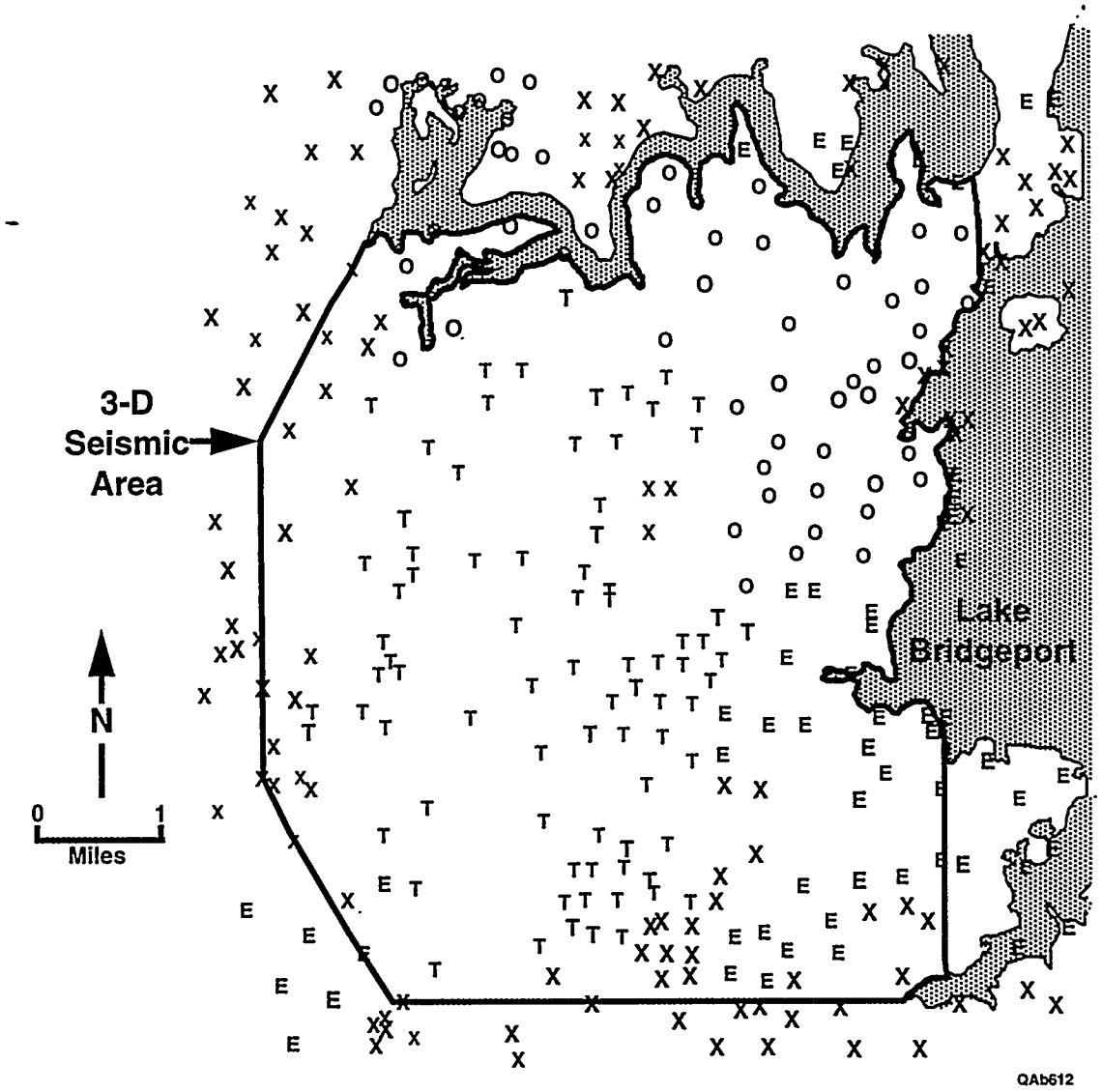

Figure 1.8. Detailed map of the Boonsville project area, located just to the west of Lake Bridgeport. Threshold Development/Arch Petroleum Co., OXY USA, Inc., and Enserch Operating Limited Partnership were the key operating partners in the project area.

2. INFLUENCE OF PALEOZOIC CARBONATE KARST COLLAPSE ON BEND CONGLOMERATE STRATIGRAPHY AND RESERVOIR COMPARTMENTALIZATION

One unique aspect of Bend Conglomerate stratigraphy which is best revealed by 3-D seismic imaging is the manner in which Atokan-age sedimentation has been influenced by karsting in deep, Ordovician age and perhaps younger Paleozoic carbonate rocks. Although there are hints that small grabenlike structural features are present in well control, neither the vertical displacements nor the fault-block geometries can be mapped without 3-D seismic data. This karsting phenomenon can be illustrated by inspecting seismic-derived structure maps traversing the base and top of the Bend Conglomerate interval. The maps produced during the course of the Boonsville 3-D seismic interpretation are presented as Figures 2.1 and 2.2 and show, respectively, the topography at the base of the Bend Conglomerate (or the Vineyard surface) and the topography at the top of the Bend Conglomerate (or the Caddo surface).

Inspection of the Vineyard structure map (Fig. 2.1) shows that several depressions occur in a seemingly random pattern across the Vineyard chronostratigraphic surface. These depressions tend to have circular to oval shapes, with diameters ranging from about 600 to about 3,000 ft. The caption for Figure 2.1 identifies the locations of several of these interesting structural depressions. Groups of karst collapse features sometimes occur along poorly defined linear trends, suggesting that subtle north-northwest-trending basement faults provided favorable sites for $CaCO_3$ dissolution that often resulted in "rows" of sinkholes.

Inside the 3-D seismic grid, well log control defines the Caddo surface (top of the Bend Conglomerate) to be 1,000 to 1,200 ft above the Vineyard surface (basal unit of the Bend Conglomerate). The seismic-interpreted Caddo surface developed in this study is displayed in Figure 2.2. This map shows that depressions similar to those at the Vineyard level also occur across the Caddo surface. An important observation is that these Caddo

depressions, particularly the three prominent ones labeled 1, 2, and 3, are positioned directly above equivalent depressions in the Vineyard surface, approximately 1,000 ft deeper, implying that there is a genetic relationship between the Caddo depressions and the older Vineyard depressions.

The seismic reflection response inside each of these structural depressions differs significantly from the reflection response in nondepressed areas. This variation in seismic reflection behavior can be well documented whenever the reflection response is displayed across an interpreted chronostratigraphic surface. One example of the seismic sensitivity to these surface depressions is shown in Figure 2.3, which is a display of the reflection amplitude magnitude on the Vineyard time structure surface (Fig. 2.1). Because this chronostratigraphic surface is interpreted so that it follows the apex of a reflection peak, the reflection amplitudes on the surface have the same algebraic sign but variable magnitudes. When the seismic wiggle trace data are displayed so that all positive reflection amplitudes are one color and all negative reflection amplitudes are a different color, as is done in this instance, the reflection amplitude map should have the same color, but with varying intensity, across the entire surface (refer to the shading bar in Fig. 2.3). Inspection of this map shows that quasi-circular disruptions (appearing as white areas) occur across this seismic amplitude response map, and correlating this disruption pattern with the Vineyard structure map (Fig. 2.1) confirms that each of the dramatic alterations in the seismic reflection response corresponds to a depression in the Vineyard surface topography.

The location of the arbitrary profile ABC shown in Figure 2.3 is chosen so that it traverses three of these seismic reflection anomalies on the Vineyard surface. A section view of the seismic behavior along this profile is provided as Figure 2.4, and, in this view, the consistently near-vertical attitude and the extreme height of these stratigraphic disruptions are striking. Each structural depression begins at seismic basement (not far below 1.2 s), which is the Ellenburger (Ordovician age), and extends vertically into, or

completely through, the Bend Conglomerate (Pennsylvanian Atokan age), causing the vertical extent of these disrupted zones to vary from 2,000 to 2,500 ft throughout the Boonsville 3-D seismic grid. In a few instances, a disruption continues into the Strawn above the Bend Conglomerate.

These structural collapse zones occur at a rather high spatial density, with adjacent collapses often separated by only 1 mi or less (see Fig. 2.3), and as noted, each zone extends completely through the Bend Conglomerate, or at least through a significant part of the Bend interval. Because of the severe stratigraphic disruption that these collapses cause within the Bend Conglomerate, some of these basement-related collapses were a significant influence on Bend sedimentation and, thus, these basement-related phenomena need to be considered when evaluating Bend Conglomerate prospects.

Geological Mechanism for Collapse Structures

These extensive vertical collapse zones are interpreted to be the result of Ellenburger and post-Ellenburger karsting. This karst model is adopted because karst-generated vertical collapse zones can be observed in Ellenburger outcrops in the Franklin Mountains at El Paso, Texas, and because Ellenburger karst plays are pursued by some West Texas operators. In the Franklin Mountains outcrops, the measured lateral dimensions of the collapsed features correspond to the diameters of the disrupted zones observed in the 3-D seismic image at Boonsville. The outcrop features also have extensive vertical dimensions, as do the seismically imaged collapses at Boonsville, with some of these outcrop collapses extending vertically for at least 1,200 ft in the larger outcrop exposures.

It is important to note that the Ellenburger karst collapse zones observed in outcrops in the Franklin Mountains and the Ellenburger-related collapse zones observed in the Boonsville 3-D data document that this Paleozoic karsting phenomenon spans a distance of at least 400 mi. The influence of this deep karsting on younger sedimentation needs to

be studied at several sites between these two widely separated control points to better document how this karsting phenomenon affects hydrocarbon production and exploration strategy throughout the Permian and Delaware Basins.

Although no Ellenburger cores are available within the Boonsville project area, these regional outcrop observations and the Boonsville seismic images allow the following karst-related hypothesis to be put forward regarding the genesis of the Boonsville collapse structures.

1. Post-Ellenburger/pre-Bend basement faulting (apparently strike-slip(?) faults trending north-northwest) occurred across the Boonsville area.

2. Karst solution weathering then occurred, particularly along subtle faults where water seepage was enhanced, and produced large caverns in some carbonate units.

3. As Atokan clastic sediment accumulated, sediment loading by the Bend Conglomerate sequences caused sporadic and intermittent collapsing of these karst-induced caverns.

4. The presence of the resultant collapse structures influenced the distribution of sandstone reservoir facies within the various Atokan sequences. Periods of active collapse would have produced a hilly, hummocky physiography; downcutting fluvial systems would occupy these subtle, collapsed areas and allow site-preferential aggradation of high-energy, active-fluvial and deltaic facies to be deposited during late phases of base-level lowstands.

5. The locations of active collapsing apparently varied with time and caused each Bend Conglomerate sequence to be affected differently. For example, the Davis and Wizard Wells genetic sequences appear to have been relatively unaffected by underlying karst collapse; however, the Caddo and some members of the Jasper Creek were strongly influenced by some of these features.

Fault-Bounded Reservoir Compartmentalization Resulting from Karst Collapse Processes

The previous section presented an important factor that needs to be considered when evaluating the compartmentalization of Bend Conglomerate reservoirs—deep Paleozoic karsting significantly influences shallower sedimentation processes. One example of deep-seated karsts creating at least partial reservoir compartmentalization at the Caddo level, some 2,500 ft above the onset of the karsting, is the situation associated with the Sealy C-2 well.

Figure 2.5 shows the location of the OXY Sealy C-2 well in the northeast portion of the project area. This well is currently producing gas from the Upper Caddo. There are 32 Upper Caddo completions in the project area, the majority of which are oil productive. Oil recoveries from the Upper Caddo are quite variable, ranging from as little as 5,000 STB to as much as 200,000 STB. The gas completions in the Upper Caddo have estimated ultimate recoveries ranging from only about 50 MMscf to as much as 700 MMscf. Drainage areas tend to range anywhere from about 10 to 170 acres; typical values are about 40 to 60 acres.

Figure 2.6 presents an expanded view of the area around the Sealy C-2 well. The Sealy B-3 well to the north is also a fairly recent Upper Caddo gas completion, having produced 346 MMscf of gas since June 1991. There are also a number of Upper Caddo completions immediately to the southwest of the Sealy C-2. Most of these wells produce oil, and some, like the OXY Ashe B-2 and the OXY Ashe B-4, have been quite prolific, producing 129,000 STB and 83,000 STB, respectively, from the Caddo.

Most of these wells were completed in the Upper Caddo in the mid- to late 1950's, but some, such as the Threshold Development Cap Yates 3, 10, and 11 wells are more recent Upper Caddo recompletions during the late 1980's and early 1990's. Many of these recompletions found significant depletion in the Upper Caddo and produced only

5,000 to 10,000 STB of oil. The Sealy B-2 to the northeast tested the Upper Caddo when drilled in the mid-1960's, but despite testing gas, the well was completed in several lower intervals in the Bend Conglomerate. In addition to the Upper Caddo, there are also a number of other Bend intervals completed in wells in the immediate vicinity of the Sealy C-2, including the Lower Caddo, Trinity, Bridgeport, Runaway, Beans Creek, Lower Jasper Creek, and Vineyard.

The Sealy C-2 was spudded in September 1992 and drilled through the Vineyard to a total depth of 5,830 ft. Table 2.1 presents the log-derived reservoir properties, as well as the bottomhole pressures measured in the various Bend intervals. The pressures measured in the Vineyard and the Upper Caddo were higher than expected and suggest only partial pressure depletion in these intervals. The Trinity and Bridgeport intervals appear to be more pressure depleted based on the RFT results, but both zones still offer behind-pipe completion opportunities.

Initially the Sealy C-2 was completed and tested in the Vineyard. The measured bottomhole pressure of 1,129 psi in the Vineyard was higher than generally found in the project area today; Vineyard pressures of 500 psi or less are far more common. The Vineyard interval produced only a small show of gas following a 2,000-gal acid treatment. This was not surprising, however, because the Sealy C-2 is located in a northwest-southeast-trending portion of the Vineyard reservoir that appears to have considerably lower permeability and much less productivity than usually observed in the Vineyard throughout the project area. A bridge plug was set above the Vineyard, and the operator moved uphole to complete the Upper Caddo.

The Upper Caddo was perforated from 4,886 to 4,902 ft and treated with 2,000 gal of 15 percent HCl. Following cleanup of the acid treatment, a pressure buildup test was conducted, and an average reservoir pressure of 1,300 psi was estimated for the Upper Caddo (Table 2.1). Following the shut-in period, the Sealy C-2 produced at 1.04 MMscf/d during a 24-h flow test.

Figure 2.7 is a plot of initial pressures in the Upper Caddo measured from wells in the project area over time. The values of initial pressure for the Sealy C-2 and Sealy B-3 wells are similar to those reported in wells drilled and completed in the 1950's. Note that, in each case, the pressures reported are the best estimates that could be obtained for particular wells using available data sources (both operator and public domain records). The estimated initial reservoir pressure for the Sealy C-2 of 1,300 psi represents a pressure gradient of about 0.3 psi/ft. This pressure suggests that although the Sealy C-2 location has been partially drained by surrounding production, the pressure is higher than might have been expected given the extent of the offsetting production from the Upper Caddo.

Figure 2.8 shows the logs recorded in the Sealy C-2 across the Upper Caddo sequence. The Upper Caddo shows good sand development on both the SP and gamma-ray logs. Note, too, the well-developed gas effect on the neutron–density crossover. Below this sand is a classic marine, shale-dominated sequence. Figure 2.9 presents an interpreted log for the Upper Caddo sequence. A net pay of 16.5 ft, with a porosity of 11.7 percent and a water saturation of 44.5 percent, was calculated for the Upper Caddo sand (see Table 2.1). Facies analysis described the majority of the Upper Caddo sand as facies "E," the cleanest, most productive sand facies in the project area (see Appendix C for additional details on the facies analysis).

The northeast quadrant of the Caddo time structure map (Fig. 2.2) is enlarged in Figure 2.10, and the locations of the Sealy C-2 and several neighboring wells are identified. This map shows that the Sealy C-2 well was drilled on the flank of what appears to be a structural high. However, when the structural and stratigraphic details associated with the Sealy C-2 well are viewed in section views along profiles such as A, B, C, or D (Fig. 2.10), it is apparent that the well is not positioned on a structural high created by tectonic uplift, but rather is on a portion of the Caddo surface where the terrain completely surrounding the well collapsed because of underlying karsting.

Profiles B and C are presented as Figures 2.11 and 2.12, respectively, to support this karst compartmentalization model. Both profiles show that vertical, seismically disrupted, collapse zones extend from the Caddo surface down to the Ellenburger (approximately 1.2 s), and that these collapse zones surround and isolate the Sealy C-2 well. These vertical seismic sections indicate that numerous low-displacement, vertical faults (often with throws of only 20 to 30 ft) separate the Sealy C-2 fault block from the surrounding terrain. The estimated Upper Caddo reservoir pressure of 1,300 psi encountered in the C-2 well and the subsequent production history (Fig. 2.13) suggest these low-displacement faults acted as at least partial barriers to fluid flow. The area inside the circumference defined by this ring of collapse is approximately 130 acres. If it is assumed that the karst collapse zones are partial flow barriers at the Caddo level, then the Sealy C-2 well is producing from a Caddo reservoir compartment that appears to span about 130 acres.

Figure 2.13 shows the actual production from the Sealy C-2 well. This is a log-log plot of gas flow rate versus time. The well came on line in November 1992 and produced 800 to 900 Mscf/d for the first couple of months. Since then, the gas flow rate has gradually declined to about 200 Mscf/d, after just over 2 yr of production. The Sealy C-2 has produced about 350 MMscf of gas to date. The production data, when plotted this way, show the influence of reservoir boundaries, as evidenced by the concave downward shape of the later-time data.

The production data were history-matched with an analytical reservoir model to estimate reservoir properties and gas in place. As Figure 2.13 shows, the analytical model provides a good match of the actual production data. From this analysis, a permeability of 2.2 md, a skin factor of –2 (indicating slight stimulation following the acid treatment), and a drainage area of 128 acres were determined. The estimated reservoir area of 128 acres agrees well with the 130-acre reservoir size identified from the seismic interpretation, as described previously.

Using this reservoir description, future performance of the Sealy C-2 was projected. The Sealy C-2 is expected to recover another 200 MMscf over the next several years, resulting in an ultimate gas recovery of about 550 MMscf. This projected ultimate recovery is at the high end of what might be expected statistically from an Upper Caddo gas completion in the project area (see Appendix B). In addition, this projected future recovery is for the Upper Caddo reservoir only; there still appear to be behind-pipe opportunities in both the Trinity and Bridgeport sequences, which may lead to additional gas recovery from this well.

As mentioned earlier, the reservoir size estimated from the production data analysis was essentially the same as that predicted from the 3-D seismic interpretation. The reservoir performance supports the seismic interpretation of an Upper Caddo reservoir compartment created by the karst-collapse zones surrounding the Sealy C-2 well. None of the reservoir pressures measured in the Bend intervals from the Caddo through the Vineyard, however, could be considered initial reservoir pressures; all indicated varying degrees of pressure depletion at this location. Therefore, the low-displacement faults associated with these karst collapse features may act as partial, but not total, barriers to gas flow, at least in this case. The degree of isolation caused by this low-scale faulting may also vary from sequence to sequence.

In May 1995, OXY USA drilled the Sealy C-3 well approximately 1,500 ft northwest of the Sealy C-2, as shown in Figure 2.6. This well penetrated the northern part of the structure shown in Figure 2.10 near its structural apex. The primary objective of this well was to test the Ellenburger Formation below the Bend. RFT's were run throughout the Bend section, however, to evaluate potential completion zones in these sequences as well. Table 2.2 presents these RFT results.

Similar to the Sealy C-2 (see Table 2.1), potential completion opportunities were identified in the Upper Caddo, Trinity, Bridgeport, and Vineyard sequences. As in the Sealy C-2, the Vineyard interval was found to be a low-permeability, low-productivity

reservoir at this location. Pressures in the Trinity and Bridgeport sequences suggest partial drainage of the gas in these intervals, but both still offer behind-pipe completion opportunities. The pressure of 1,005 psi in the Upper Caddo reflects communication with the gas production from the Sealy C-2 well. This pressure supports the seismic interpretation of the structural feature shown in Figure 2.10 and is in line with the value expected at this location given the size of the structure, the well locations, and the total production (degree of depletion) from the Sealy C-2 well.

Table 2.1. Estimated reservoir properties for the Sealy C-2 well.

Sequence	Net pay (ft)	Porosity (%)	Water saturation (%)	Bottomhole pressure (psi)	Source of pressure data
Upper Caddo	16.5	11.7	44.5	1,300*	PBU**
Lower Caddo	0	—	—	—	
Wizard Wells	3	10.6	51.7	—	
Davis	0	—	—	—	
Trinity	11.5	11.5	35.1	750	RFT
Bridgeport	7.5	11.8	37.1	540/660	RFT's
Runaway	0	—	—	—	
Beans Cr	0	—	—	—	
U Jasper Cr	0	—	—	—	
M Jasper Cr	0	—	—	—	
L Jasper Cr	0	—	—	—	
Vineyard	24.5	9.3	45.6	1129	PBU

* Estimated average reservoir pressure.
** Pressure buildup test.

Unlike the Sealy C-2, however, an excellent 10- to 12-ft sand in the upper part of the Jasper Creek sequence was also encountered in the Sealy C-3. As shown in Table 2.2, pressures of 2,196 and 2,200 psi were measured during two RFT tests in this interval. Pressure built up rapidly during both RFT's, indicating good permeability in this zone as well. These pressures are considered to be initial pressure at this depth, and, thus, the Sealy C-3 has encountered a previously undrained portion of the Jasper Creek or an isolated, reservoir compartment. Figure 2.14 shows the open-hole logs recorded across

this interval. Notice the excellent SP development and the gas effect observed from the density–neutron crossover.

Following an Ellenburger test, OXY elected to complete the Sealy C-3 well in the Vineyard from 5,742 to 5,752 ft. Only a small gas show was reported after an acid treatment, and this interval was subsequently abandoned. Next, in mid-June, OXY completed the Jasper Creek sand from 5,540 to 5,550 ft. This zone tested 3 MMscf/d at 1,500 psi flowing tubing pressure. As of the end of June, this well was still making in excess of 1 MMscf/d at about 1,600 psi flowing tubing pressure.

We will continue to monitor the performance of the Sealy C-3 well to determine the effective size of this Jasper Creek reservoir. If this sand should cover most of the structure illustrated in Figure 10, as did the Upper Caddo in the Sealy C-2, the gas reserves associated with this Jasper Creek reservoir could be in excess of 500 MMscf. The discovery of this reservoir in the Sealy C-3 well further illustrates the influence of these karst collapse features on stratigraphy and potential reservoir compartmentalization in the Bend Conglomerate.

Table 2.2. RFT pressures measured in the Sealy C-3 well.

Sequence	RFT pressure (psi)
Upper Caddo	1005
Lower Caddo	—
Wizard Wells	—
Davis	—
Trinity	708
Bridgeport	902
Runaway	—
Beans Cr	—
Upper Jasper Creek	2,196/2,200
Middle Jasper Creek	—
Lower Jasper Creek	—
Vineyard	840

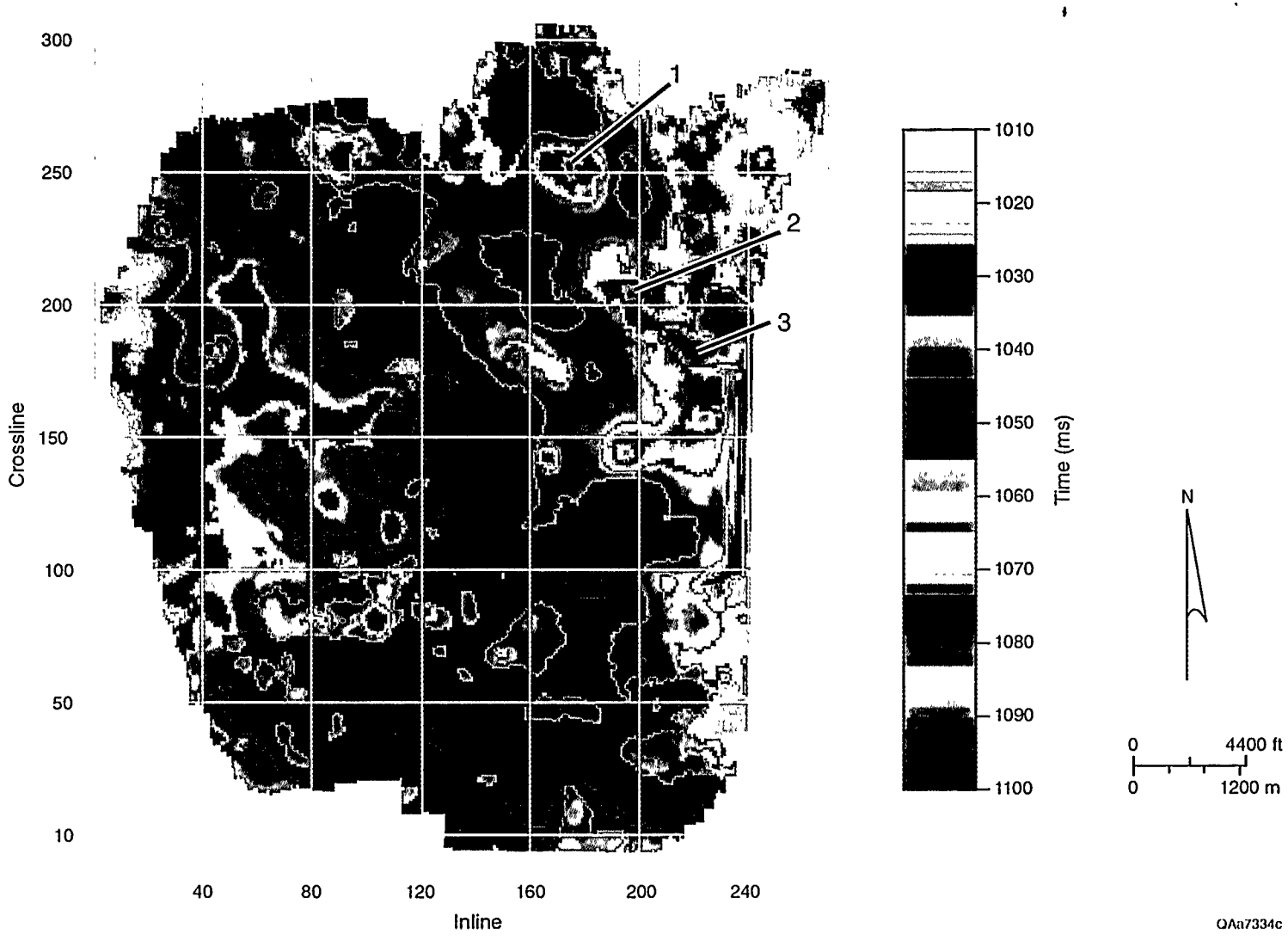

Figure 2.1. Seismic time structure map showing the topography of the Vineyard chronostratigraphic surface (base of the Bend Conglomerate). The numbered features identify karst collapse areas.

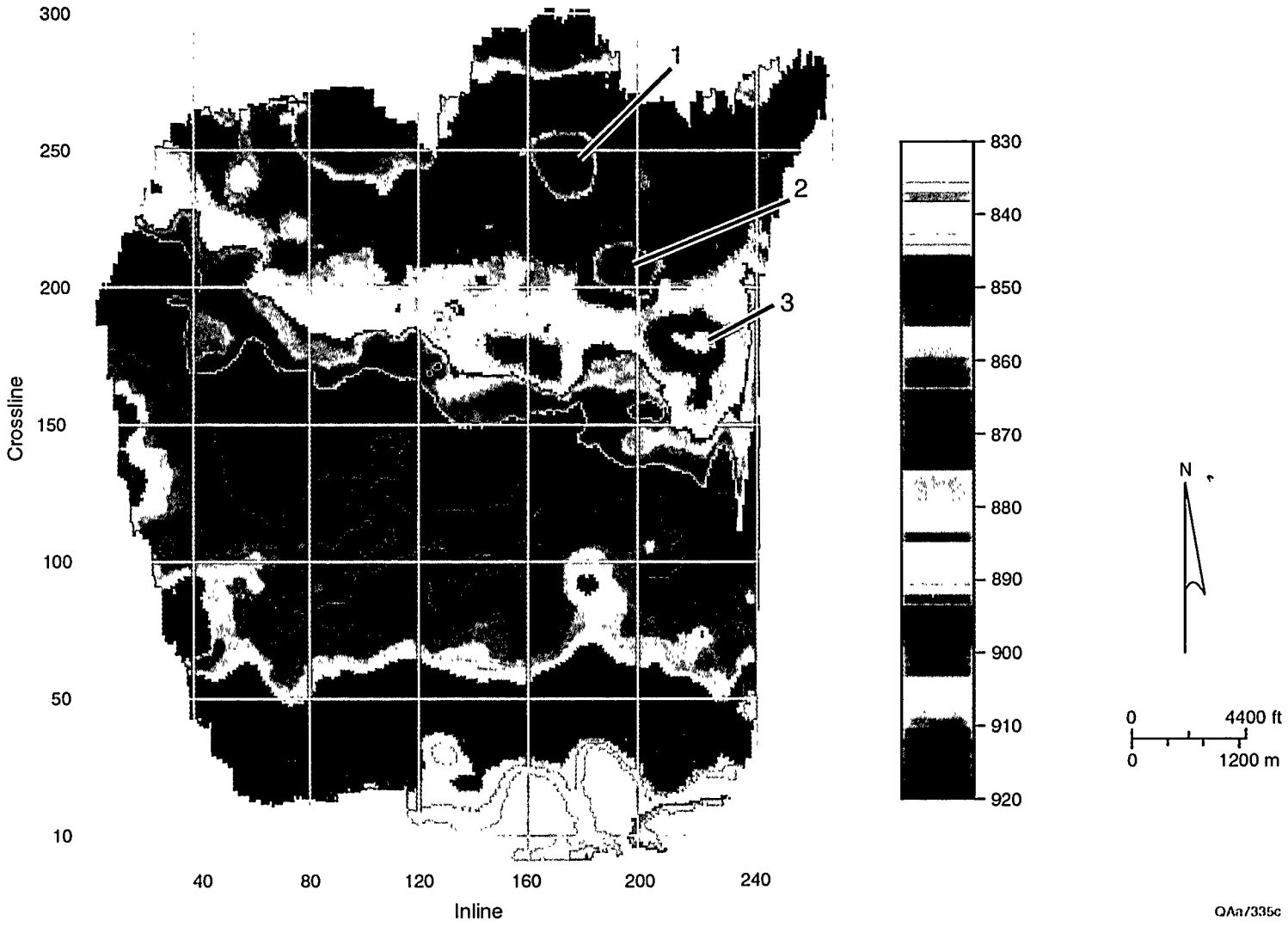

Figure 2.2. Seismic time structure map showing the topography of the Caddo chronostratigraphic surface (top of the Bend Conglomerate). The numbered features identify karst collapse areas. Note that these karst depressions are positioned directly above the depressions in the Vineyard surface (previous figure).

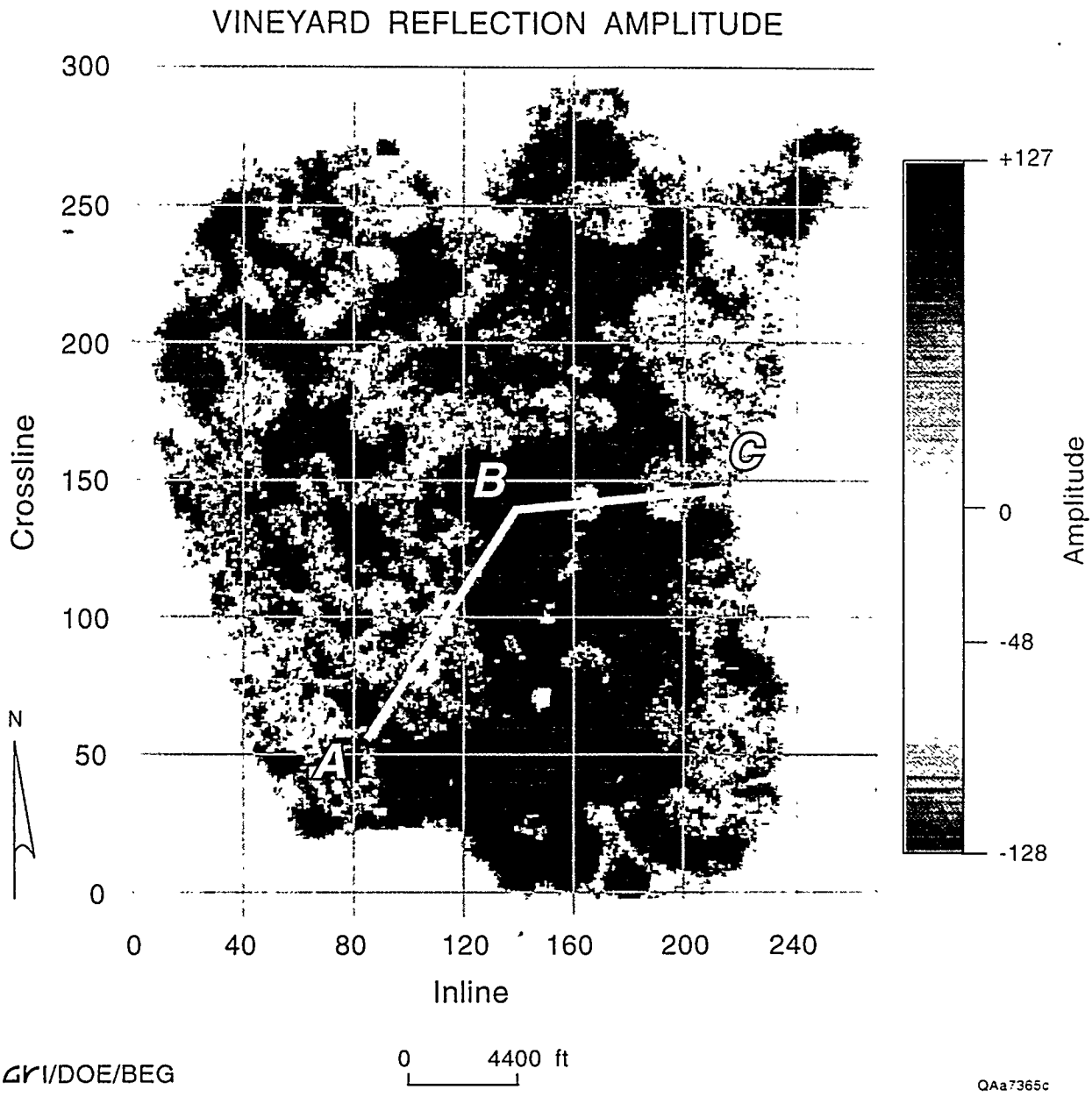

Figure 2.3. Behavior of the seismic reflection amplitude across the Vineyard chronostratigraphic surface. The reflection response on this surface should have a constant polarity, shown by the dark color. The white areas define regions where the polarity of the Vineyard reflection changes algebraic sign. Each white area corresponds to a karst depression in the Vineyard surface.

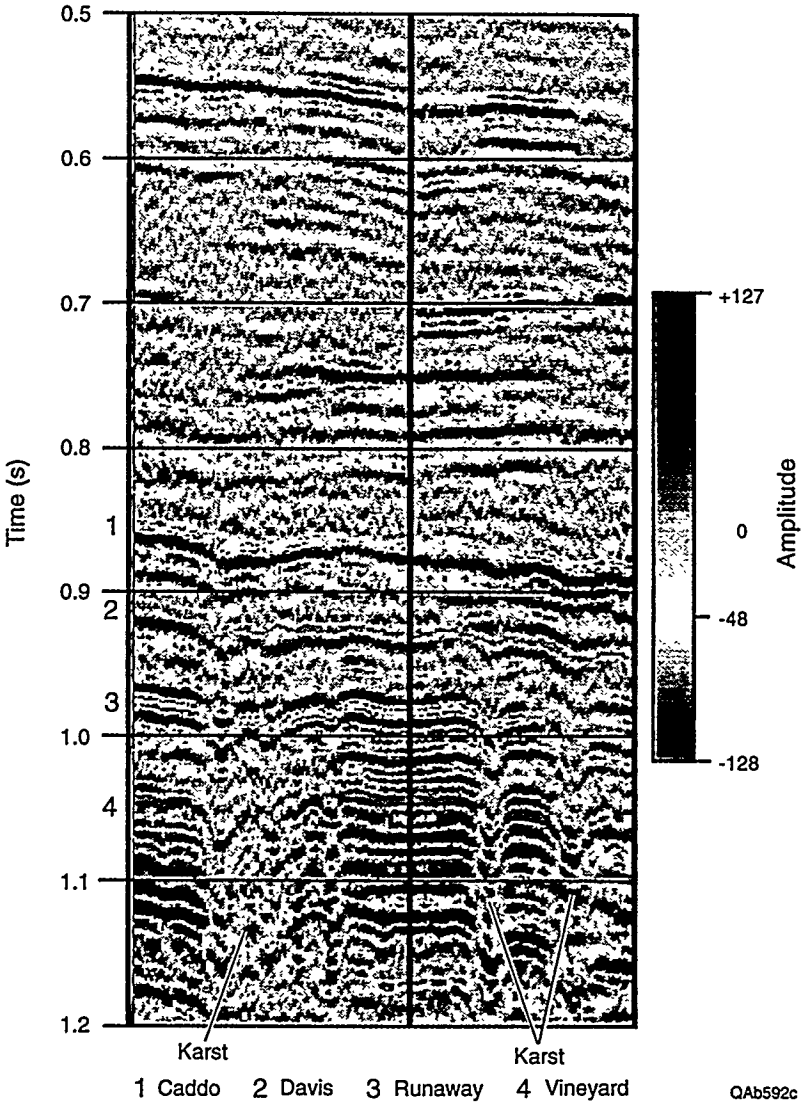

Figure 2.4. Vertical seismic section along profile ABC shown in Figure 2.3, which traverses three of the white reflection anomalies on the Vineyard surface. This section view shows that these reflection disturbances are vertical collapse zones that start at seismic basement (just below 1.2 s) and extend all the way to the Caddo level. These collapses are thought to be karst-driven phenomena that initiated at the Ellenburger level (seismic basement) and continued for an unknown length of time.

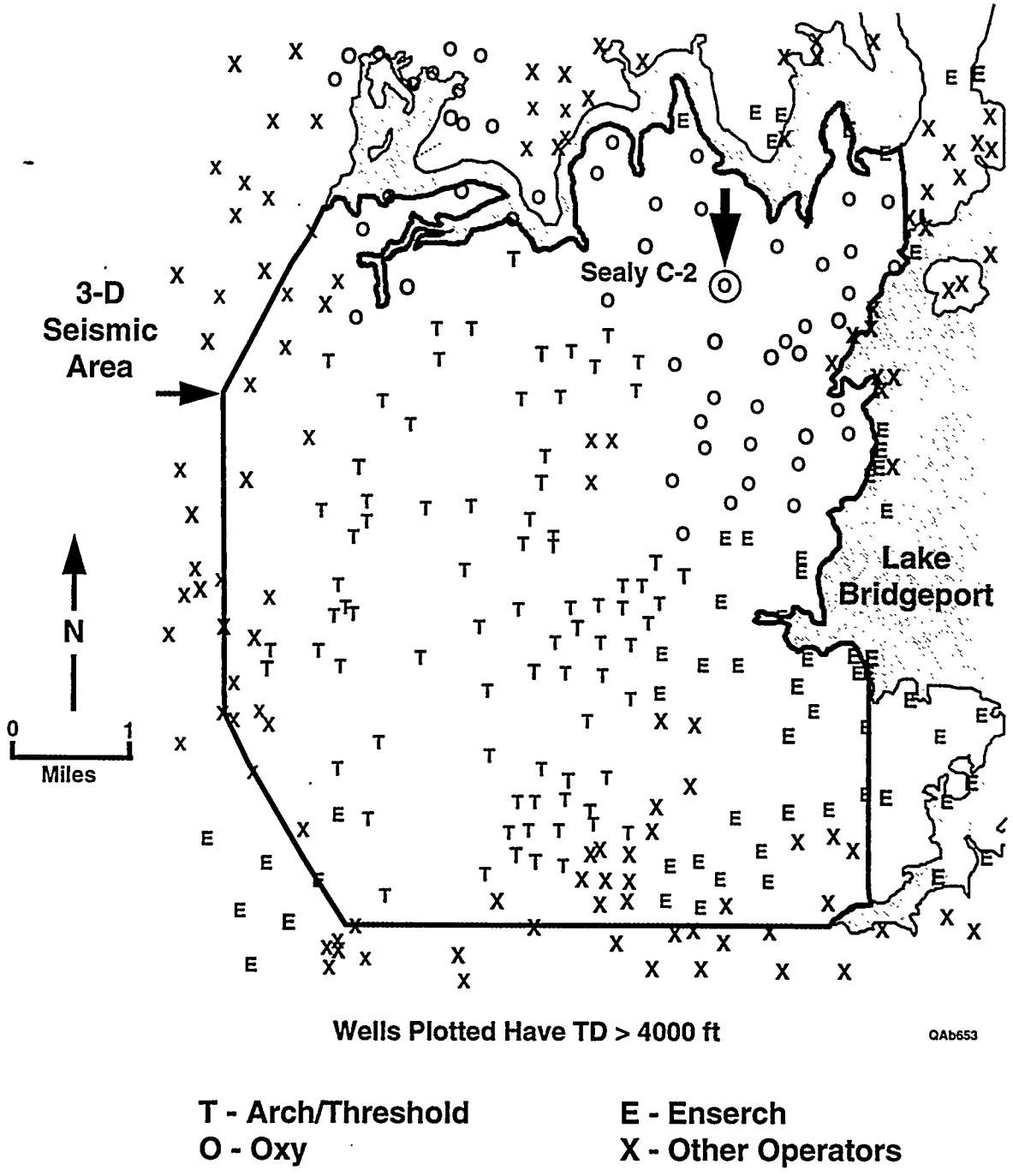

Figure 2.5. Location of the Sealy C-2 well in the northeast part of the project area.

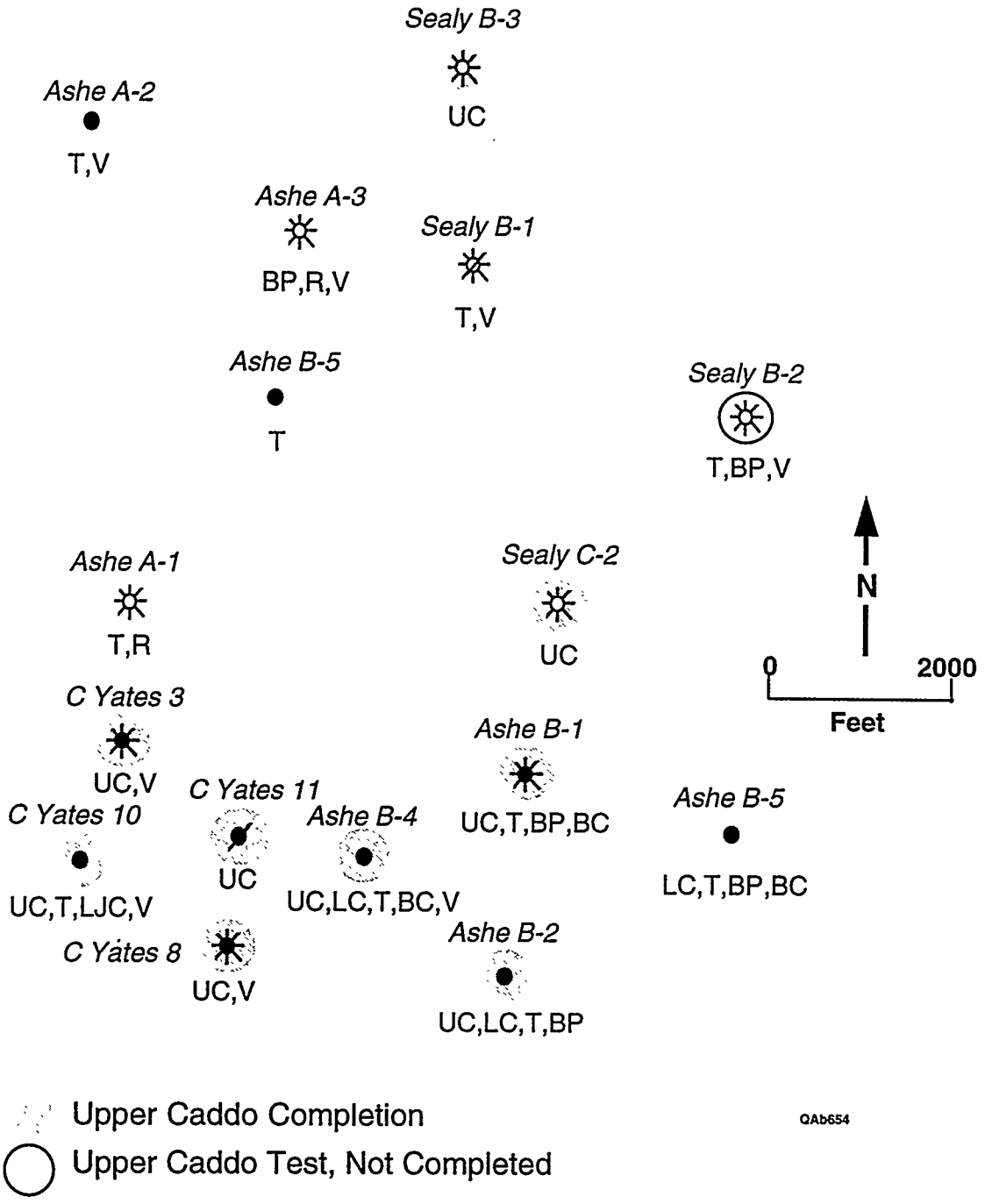

Figure 2.6. Expanded view showing Upper Caddo completions near the Sealy C-2 well. Most are southwest of the Sealy C-2 location and tend to be oil wells. Many other Bend zones are also completed in nearby wells.

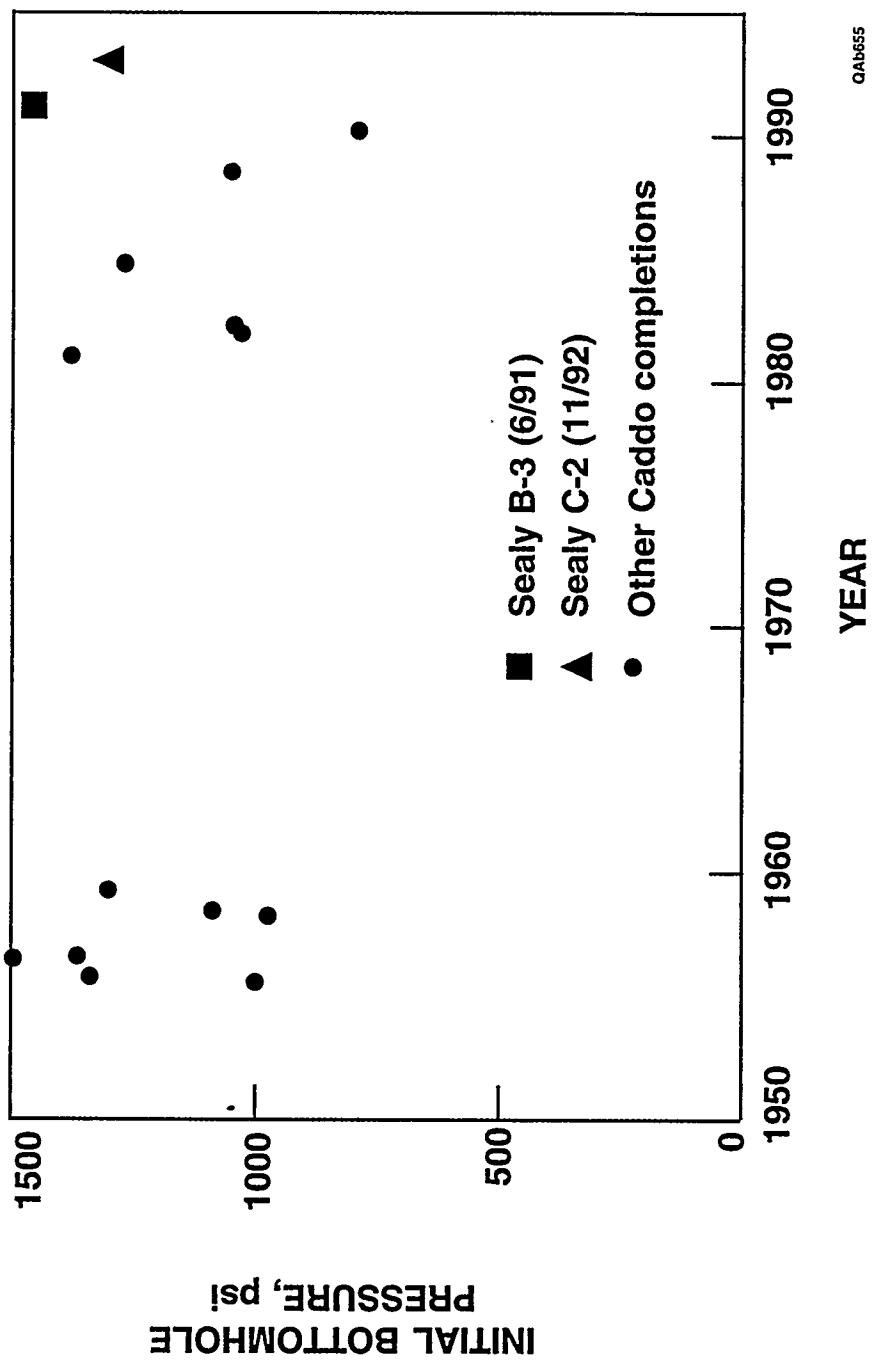

Figure 2.7. Initial pressures measured in the Sealy C-2 and Sealy B-3 Upper Caddo completions. These pressures are comparable to initial pressures reported in other wells drilled in the Upper Caddo sequence over the past 40 yr.

2.19

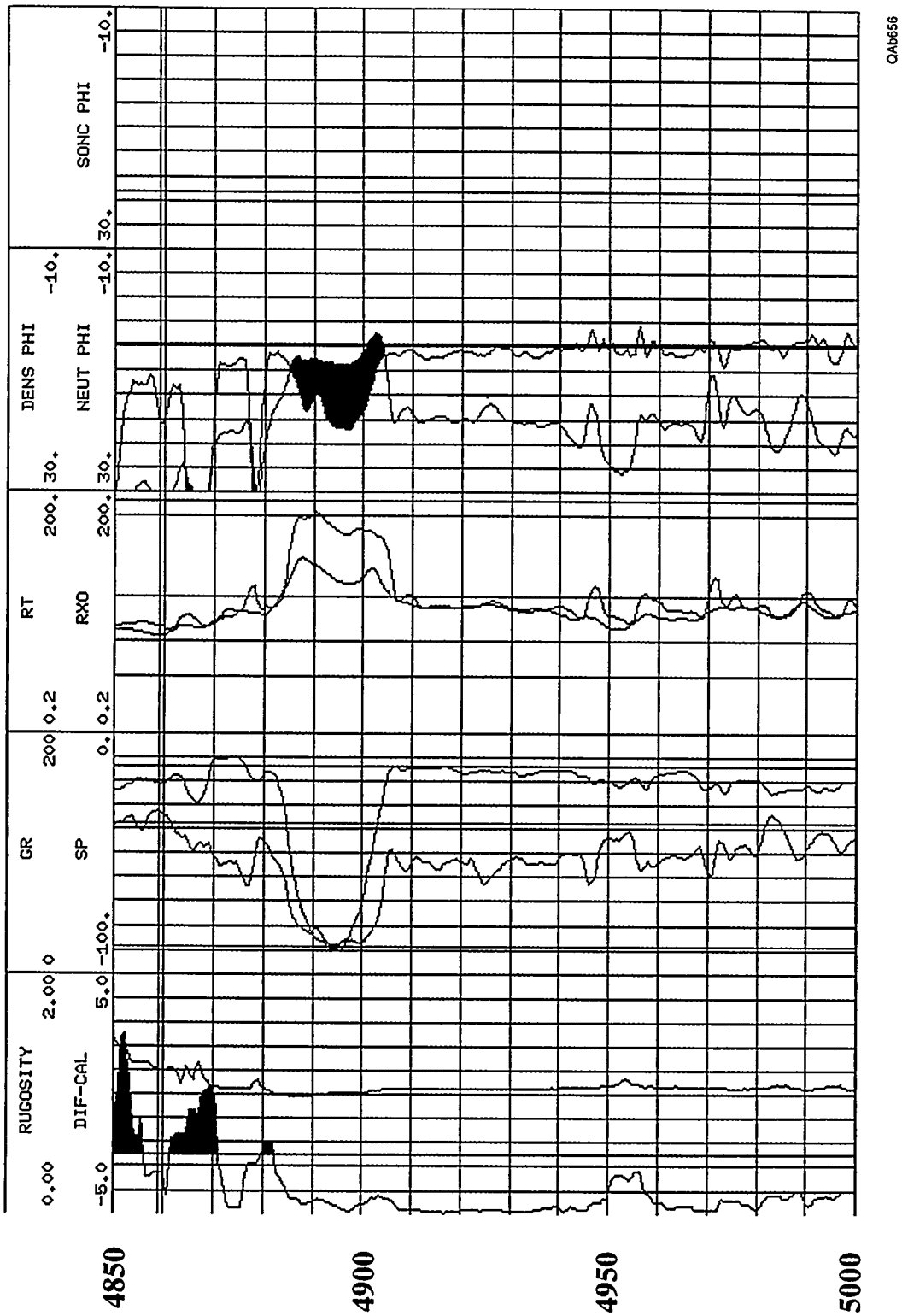

Figure 2.8. Open-hole logs recorded over the Upper Caddo sequence in the Sealy C-2 well.

2.20

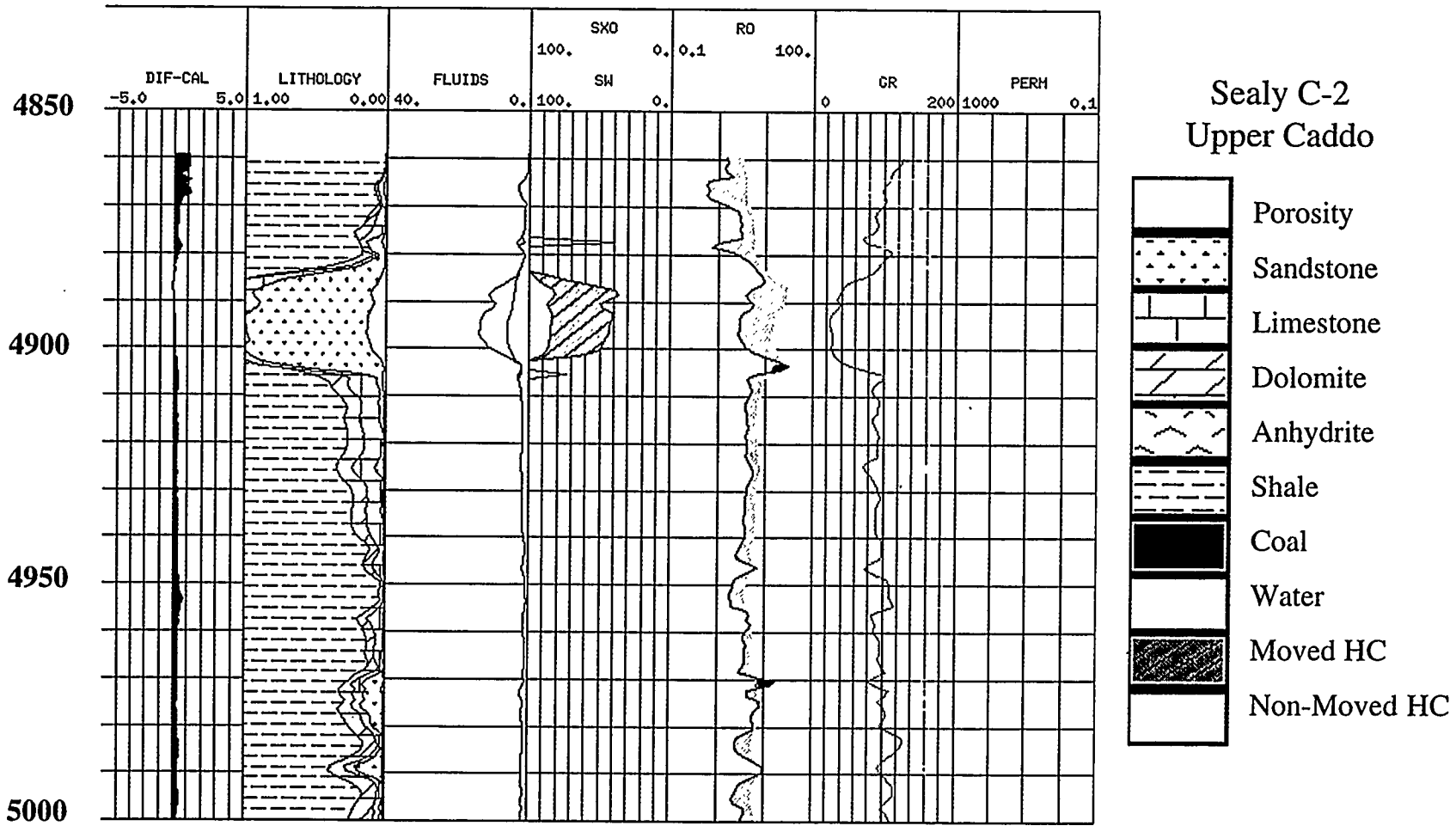

Figure 2.9. Interpreted log for the Upper Caddo sequence in the Sealy C-2 well.

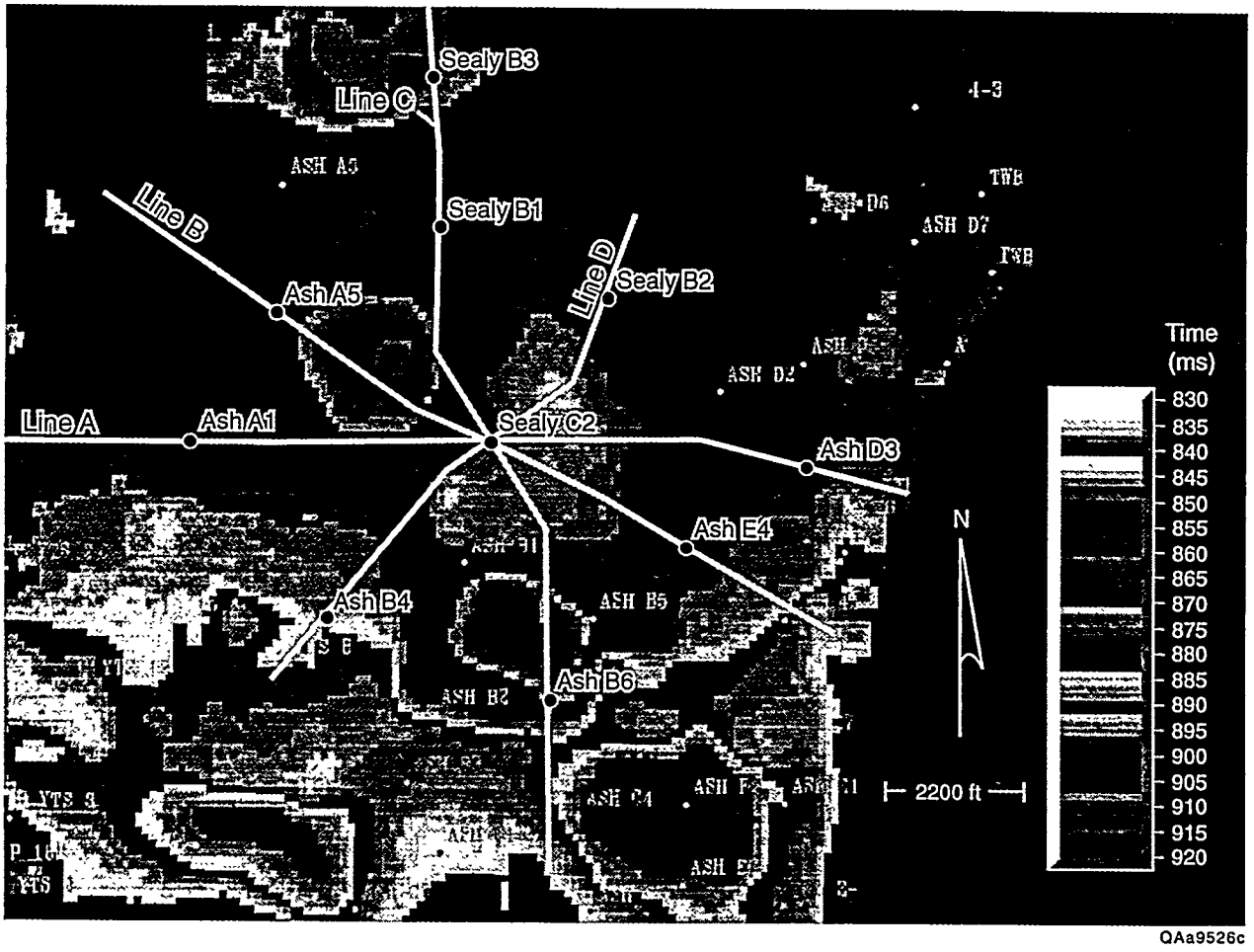

Figure 2.10. Northeast quadrant of the Caddo time structure map showing a ring of karst collapse surrounding the Sealy C-2 well.

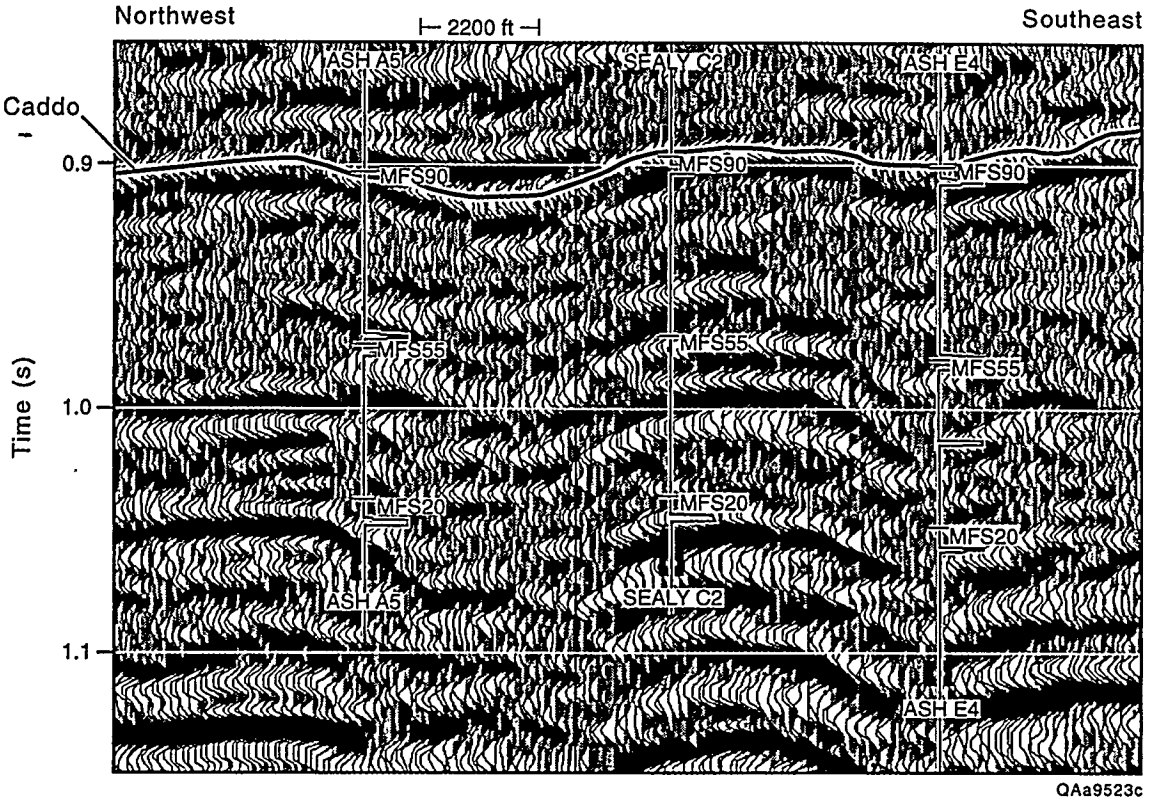

Figure 2.11. Vertical section along profile B defined in Figure 2.10. This section view emphasizes how the Sealy C-2 well is positioned on an apparent structural high, which actually is not a structural uplift, but rather is an area that remained in place after the surrounding terrain fell into a series of karst collapses. The curve plotted at each well location identifies where reservoir quality facies occur within the Bend Conglomerate section.

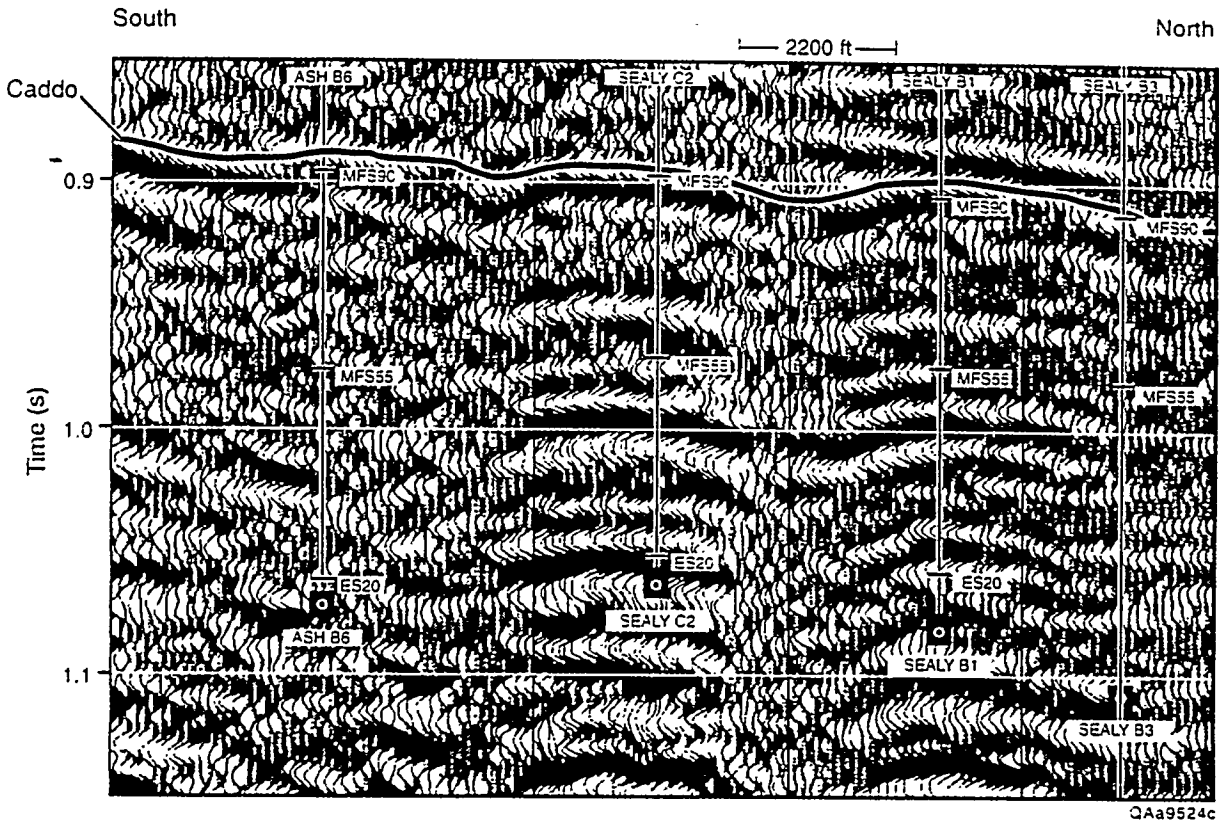

Figure 2.12. Vertical section along profile C defined in Figure 2.10. See caption for Figure 2.11 for explanation of key features.

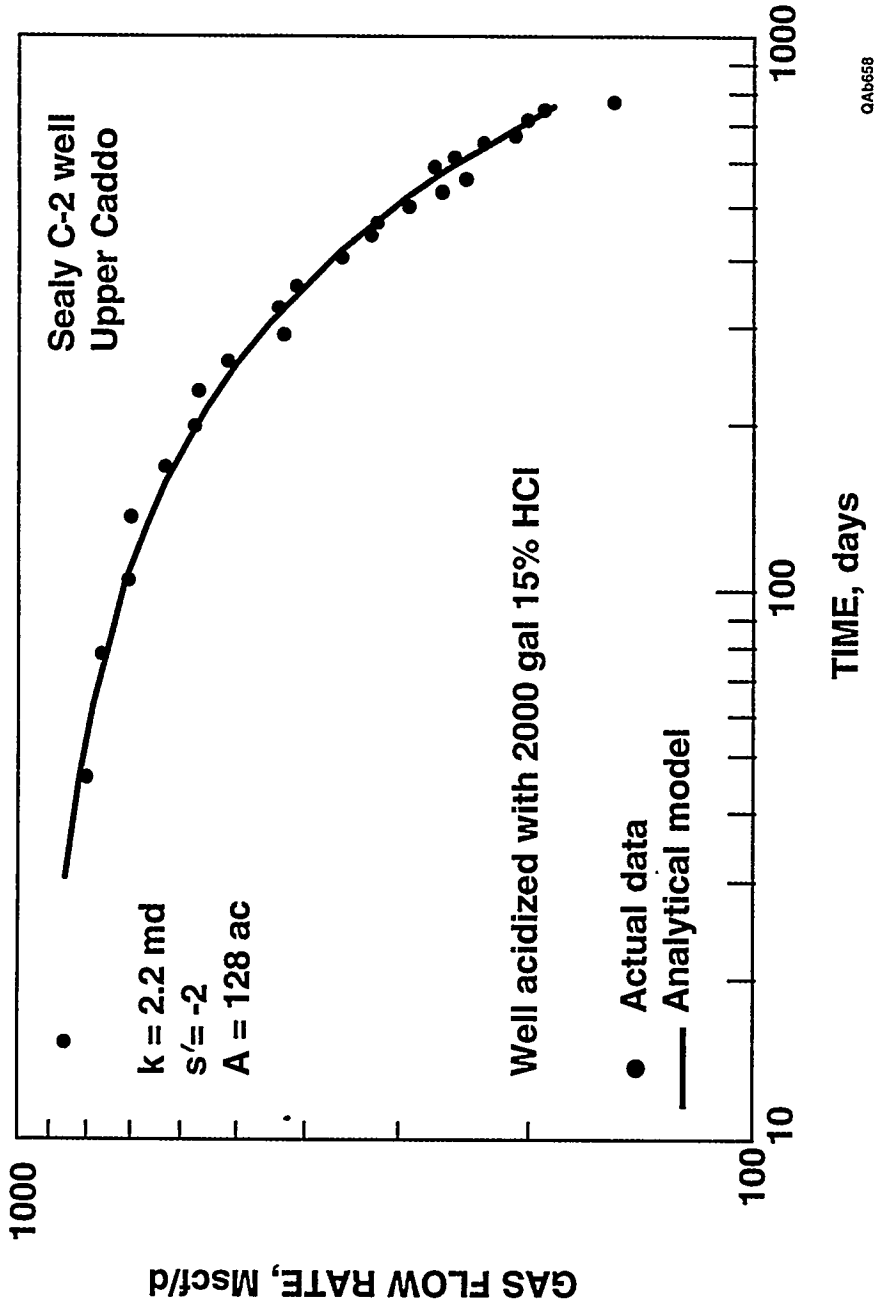

Figure 2.13. History-match of production data from the Sealy C-2 well.

2.25

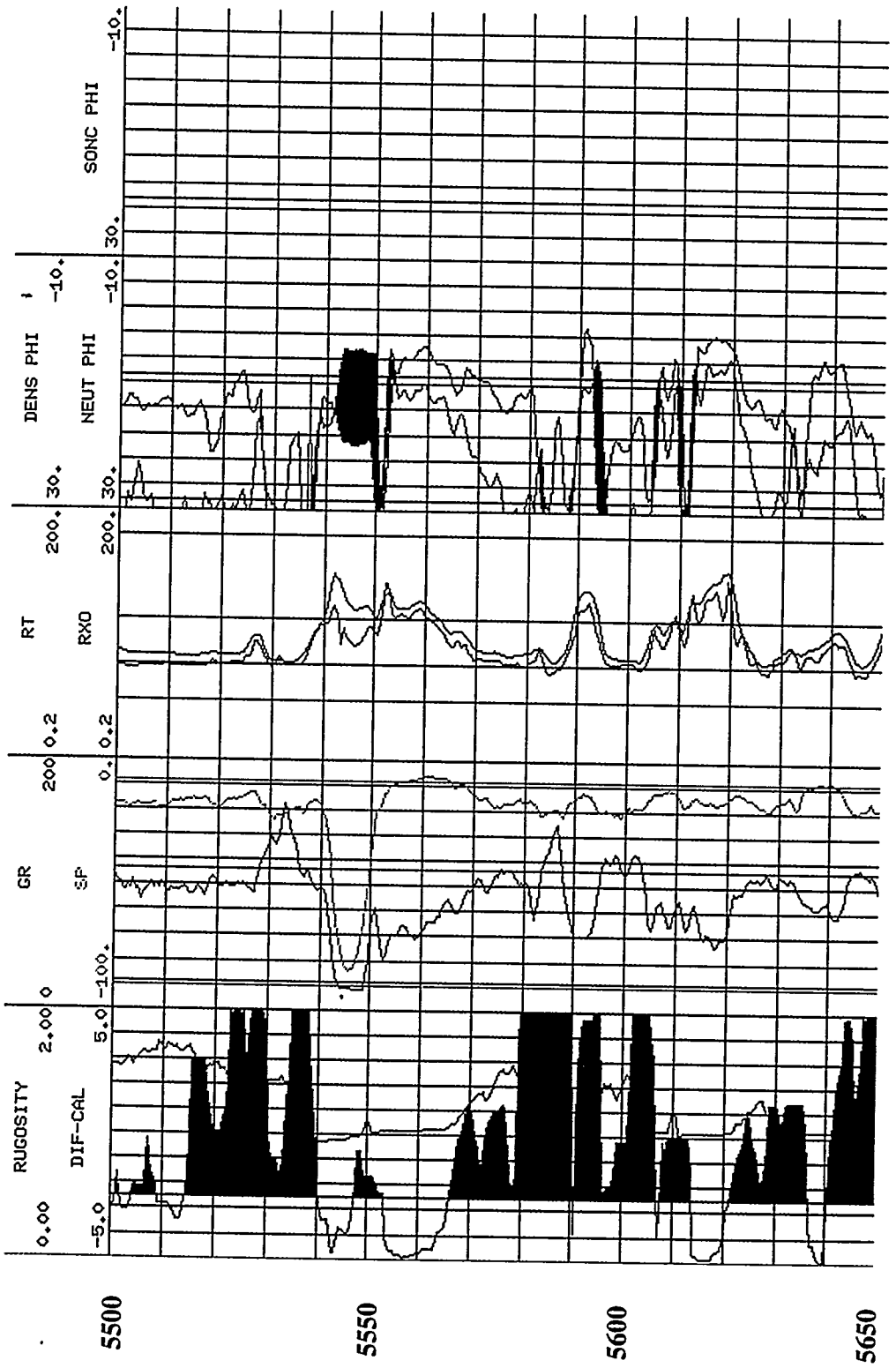

Figure 2.14. Open-hole logs recorded across the Jasper Creek sequences in the Sealy C-3 well.

3. CORRELATION BETWEEN SEISMIC ATTRIBUTES AND CADDO RESERVOIR PROPERTIES

One research activity that was pursued in the Boonsville seismic interpretation was to investigate whether a seismic parameter could be found that was a reliable indicator of a critical reservoir property. This effort focused on the Caddo interval because Caddo reservoirs are among the most productive in the area and because the Caddo sequence creates a relatively good seismic response across the study area. Numerically the investigation concentrated on analyzing the Hilbert transform seismic attributes described in detail in Appendix E. These attributes are commonly referred to as instantaneous amplitude, instantaneous phase, and instantaneous frequency.

Lower Caddo

One of the better correlations discovered in this investigation was the relationship between instantaneous seismic frequency and the amount of net reservoir within the Lower Caddo. This correspondence between net reservoir and seismic frequency is illustrated by maps in Figures 3.1 and 3.2, which cover the southern third (approximately) of the 26-mi^2 3-D seismic grid. The Lower Caddo seismic attribute analysis is limited to this portion of the project area because the Lower Caddo is a pervasive, major producing reservoir within these bounds, whereas Lower Caddo reservoirs are sparsely distributed in the northern two-thirds of the seismic area.

The value, net reservoir feet, plotted in Figure 3.1 is a log-based parameter determined by calculating the cumulative number of vertical feet within the Lower Caddo, where the deep resistivity exceeds 10 ohm-m and the SP value is less than –30 API units. The seismic frequency value in Figure 3.2 is the average instantaneous frequency in a 10-ms window starting 10 ms below, and remaining conformable with, the

interpreted Caddo seismic horizon, which is the time window where several Lower Caddo reservoirs are located. Comparing the two maps shows that this average instantaneous frequency parameter produces a rather accurate map of the Lower Caddo net reservoir, which leads to the conclusion that there are some stratigraphically trapped reservoirs in the Boonsville study area that can be seismically imaged with considerably accuracy. To produce reliable seismic maps of these stratigraphic reservoir facies, we found that several seismic attributes, but principally just reflection amplitude and instantaneous frequency, had to be calculated within the narrow, precisely defined seismic time window that spanned the targeted sequence, and that each calculated attribute then had to be displayed with a variety of color bars until a color bar was found that caused a certain numerical range of the attribute to be distributed in an areal pattern that reasonably matched the areal facies pattern implied by well control.

In this Lower Caddo example, the best seismic attribute for using to map net reservoir seemed to be instantaneous frequency, and the best choice for a color bar seemed to be the one shown in Figure 3.2. This interpretational approach requires that two forms of supporting data be available to the interpreter:

1. An accurate depth-to-time conversion function must exist so that the log-derived depths of the thin Lower Caddo sequence can be converted into the correct narrow time window in the Boonsville 3-D seismic data volume.
2. A reasonable number of wells must exist so that the amount of Lower Caddo net reservoir can be determined at several locations and so that a color bar can then be found that will cause the areal distribution of a certain numerical range of instantaneous frequencies to reasonably match the areal net reservoir pattern suggested by these control wells.

Upper Caddo

Upper Caddo reservoirs are found primarily in the northern half of the Boonsville study area, and a particularly important trend of Upper Caddo producers occurs in the northwest third of the 3-D seismic grid. A well-log-based map defining the distribution of the Upper Caddo sandstone thickness in this northwest area is shown in Figure 3.3. From log analyses, these Upper Caddo sandstones are interpreted to be a valley-fill facies, and log control indicates that this valley-fill system trends northeast-southwest between the CYTS5 and DCN3 wells (Fig. 3.3). This log-derived map implies that the Upper Caddo valley-fill system bifurcates into two channels in the vicinity of the BYTS6, 12, and 17D wells, resulting in no reservoir facies being present in these three wells.

Examination of the Boonsville 3-D seismic data shows that in the northwest portion of the seismic grid, the seismic reflection associated with the Caddo sequence boundary undergoes a significant amplitude reduction along the trend where the well-log-based map shows that the Upper Caddo reservoir sandstone exists. A display of this Caddo reflection behavior is shown as Figure 3.4, and the northeast-southwest trend of low-amplitude responses in this seismic attribute map is remarkably similar to the trend in the log-derived sandstone thickness map in Figure 3.3.

The particular seismic attribute displayed in Figure 3.4 is the average of the negative reflection amplitudes occurring in a 30-ms window immediately below the Caddo sequence boundary. The seismic analysis window slightly exceeds the thickness of the Caddo sequence, but the average negative amplitude in this data window differs little from the average negative amplitudes calculated in shorter data windows. Other estimates of the Caddo seismic reflection amplitude might be equally as diagnostic of Upper Caddo sandstone thickness as in the parameter displayed in Figure 3.4.

The principal difference between the maps in Figures 3.3 and 3.4 is that the sandstone distribution shown in Figure 3.3 is a computer generated contouring of only 40

(approximately) widely separated data points calculated in the existing control wells, whereas the seismic display in a composite of approximately 30,000 reflection amplitude values occurring at closely spaced points separated by only 110 ft across the map area. Because of this dense spatial sampling, the seismic display (Fig. 3.4) is assumed to be a more accurate depiction of the distribution of the Upper Caddo reservoir facies in the interwell spaces than is the spatially aliased computer-contoured map in Figure 3.3.

Two profiles, labeled as Line 1 and Line 2, are shown connecting key control wells on the seismic attribute map, and the seismic images along the two profiles are depicted in Figures 3.5 and 3.6. In each profile, that portion of the Caddo sequence boundary where the reflection amplitude undergoes a significant reduction is enclosed by a dashed circle. This amplitude dimming is the key seismic attribute that maps the Upper Caddo channel fill. The relationship between the reflection amplitude magnitude where the channel-fill reservoir facies occurs and the reflection amplitude magnitude at other locations on the Caddo sequence boundary is probably best illustrated by the color bar in Figure 3.4 that defines the parameter range used to display the Caddo seismic reflection attribute. The valley-fill facies consistently produces a reflection magnitude that is approximately one-fourth the maximum reflection amplitude found on the Caddo surface in this imaged area.

Like the previously discussed Lower Caddo example, this Upper Caddo analysis shows that by carefully calibrating a series of seismic attributes with well control, a key attribute can often be found that is sensitive to facies changes within the targeted sequence.

Figure 3.1. Lower Caddo net reservoir in the southern third of the project area as determined from well log control, using the criteria that Lower Caddo reservoir facies exist whenever the resistivity exceeds 10 ohm-m, and simultaneously, the SP curve reads less than –30 API units. This map was created using data from approximately 75 wells; only 7 of the wells are labeled.

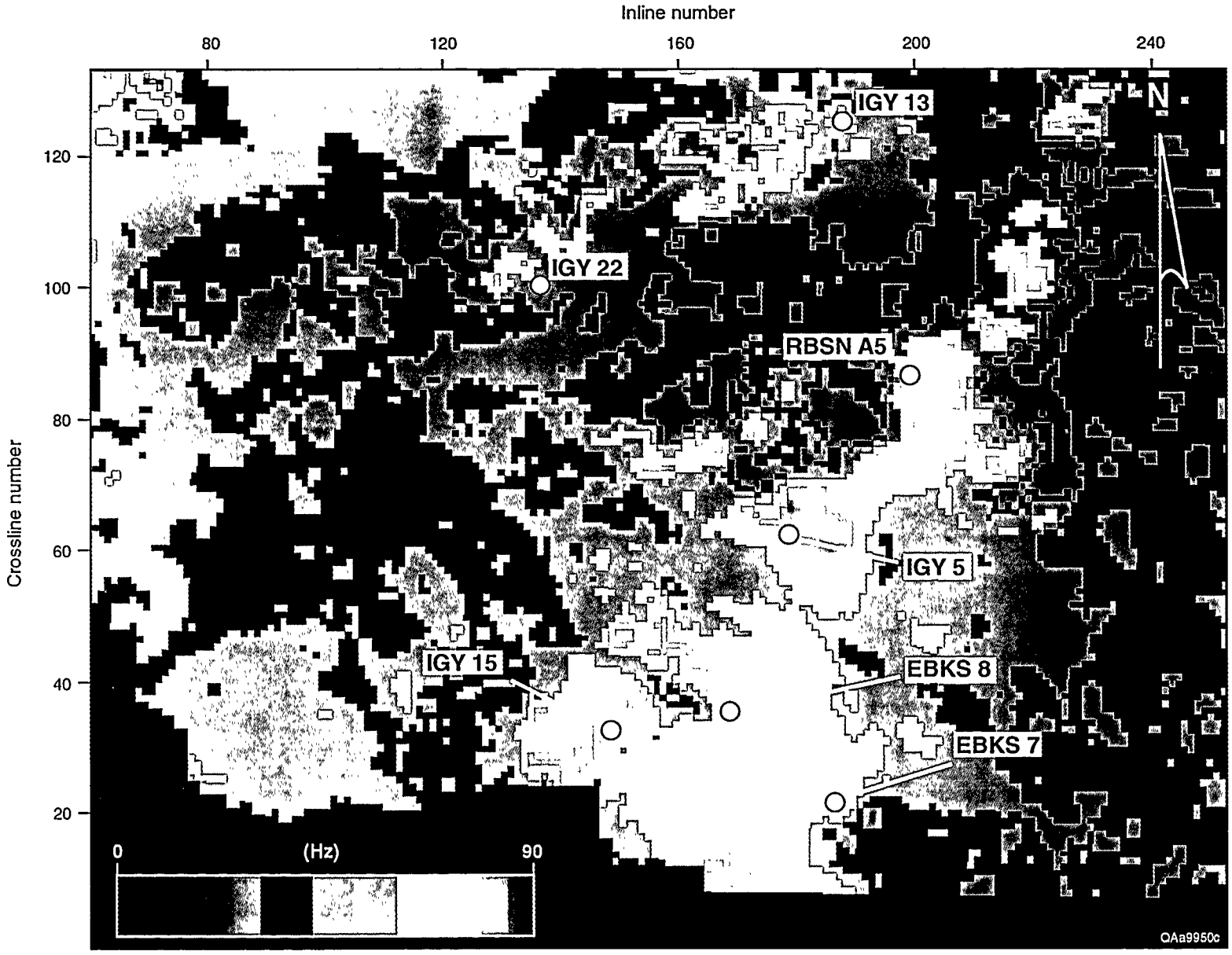

Figure 3.2. Average instantaneous seismic frequency calculated within the Lower Caddo sequence. This map should be compared with the preceding Lower Caddo net reservoir map. The parameter that is mapped is the average instantaneous frequency in a 10-ms window that is conformable to the seismically derived Caddo chronostratigraphic boundary and starting 10 ms below that boundary. The correspondence between this seismic attribute map and the log-based net reservoir map is striking, and shows that, in some circumstances, 3-D seismic data provide a valuable predictive tool for locating stratigraphically trapped reservoirs. The theory of instantaneous frequency is discussed in Appendix E.

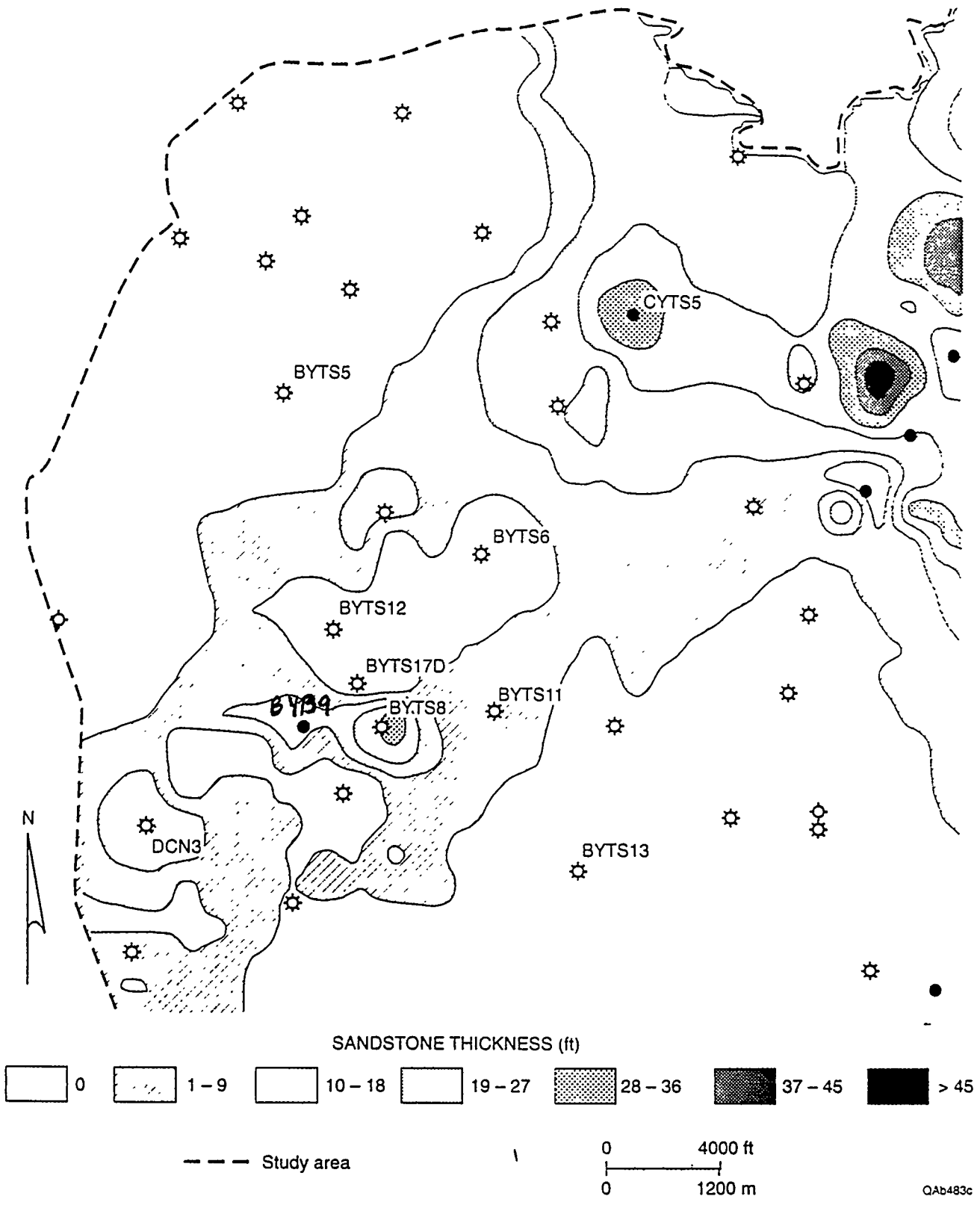

Figure 3.3. Upper Caddo sandstone thickness in the northwest third of the Boonsville project area as defined by well log control. This map is a computer-contoured product generated from only 40 (approximately) control points.

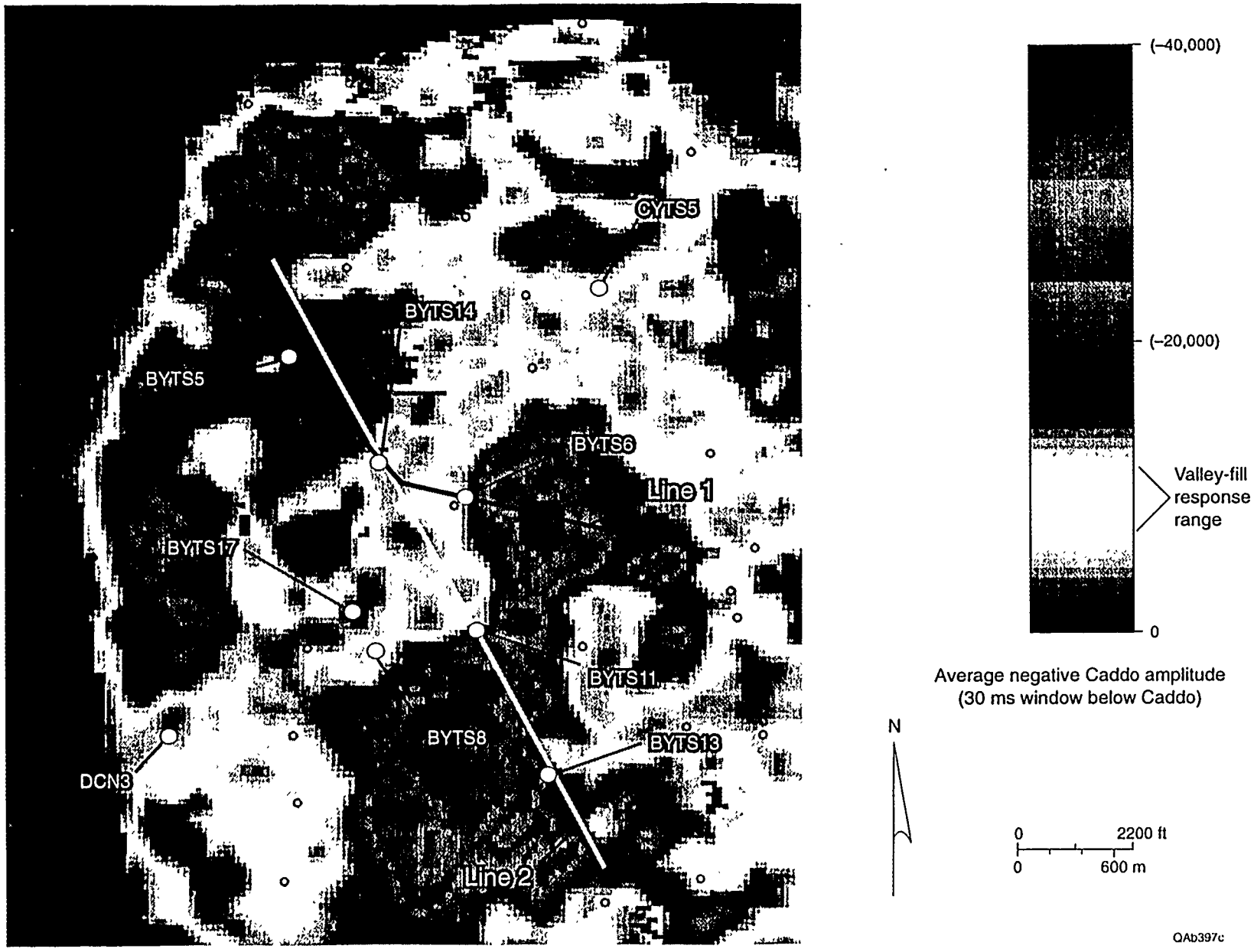

Figure 3.4. Map of a seismic amplitude attribute calculated within the Caddo sequence in the northwest third of the project area. The parameter that is displayed is the average of the negative reflection amplitudes occurring in a 30-ms window immediately below the Caddo sequence boundary. The amplitude values falling inside the interval labeled "valley-fill response range" define a trend that is remarkably similar to the valley-fill trend shown in Fig. 3.3, implying that seismic reflection amplitude is a reliable indicator of Upper Caddo valley-fill facies in this portion of the study area.

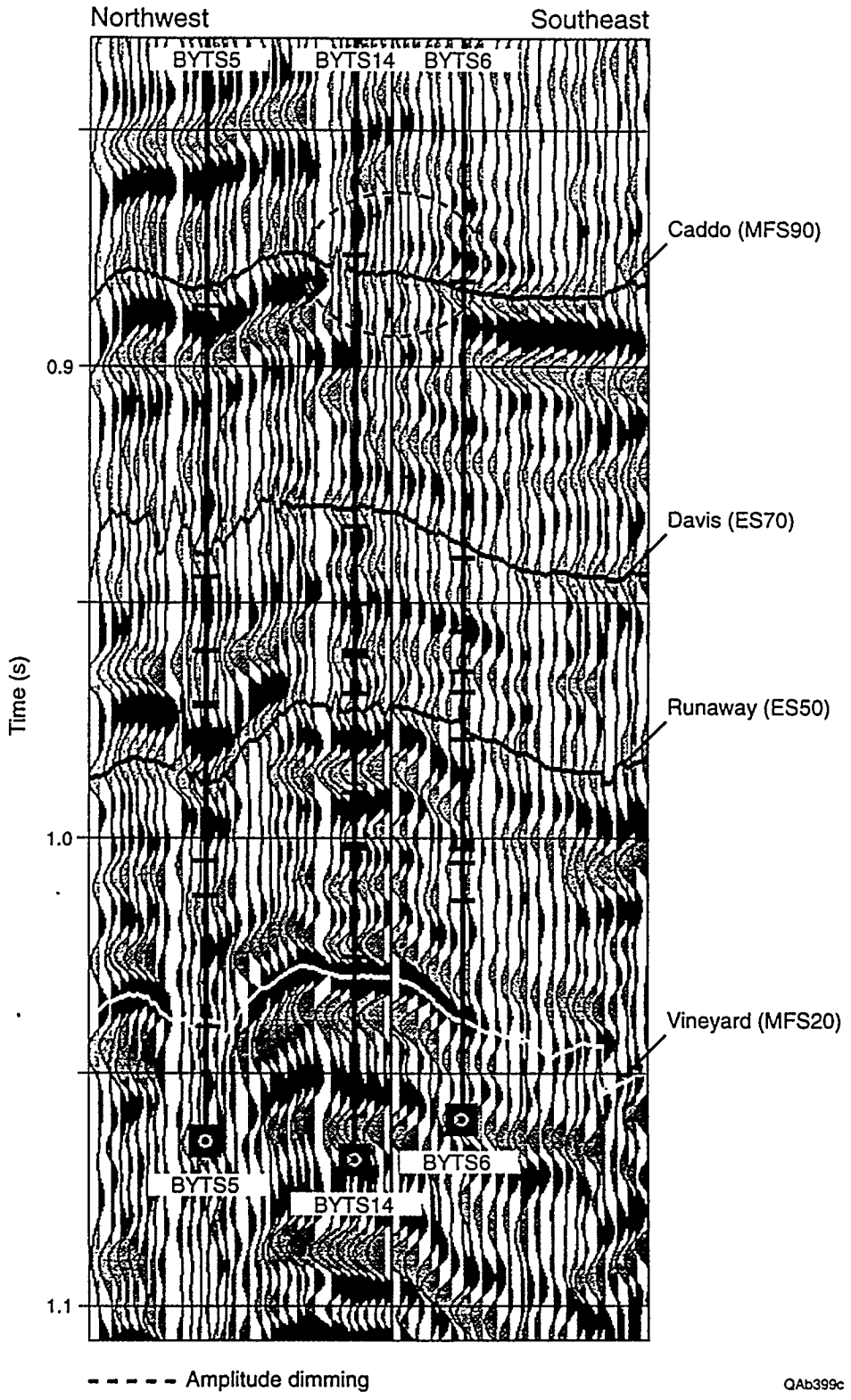

Figure 3.5. Seismic profile along the surface track labeled "Line 1" in Figure 3.4. The amplitude dimming of the Upper Caddo reflection response inside the dashed circle is a key seismic parameter that maps the position of the Upper Caddo valley-fill facies.

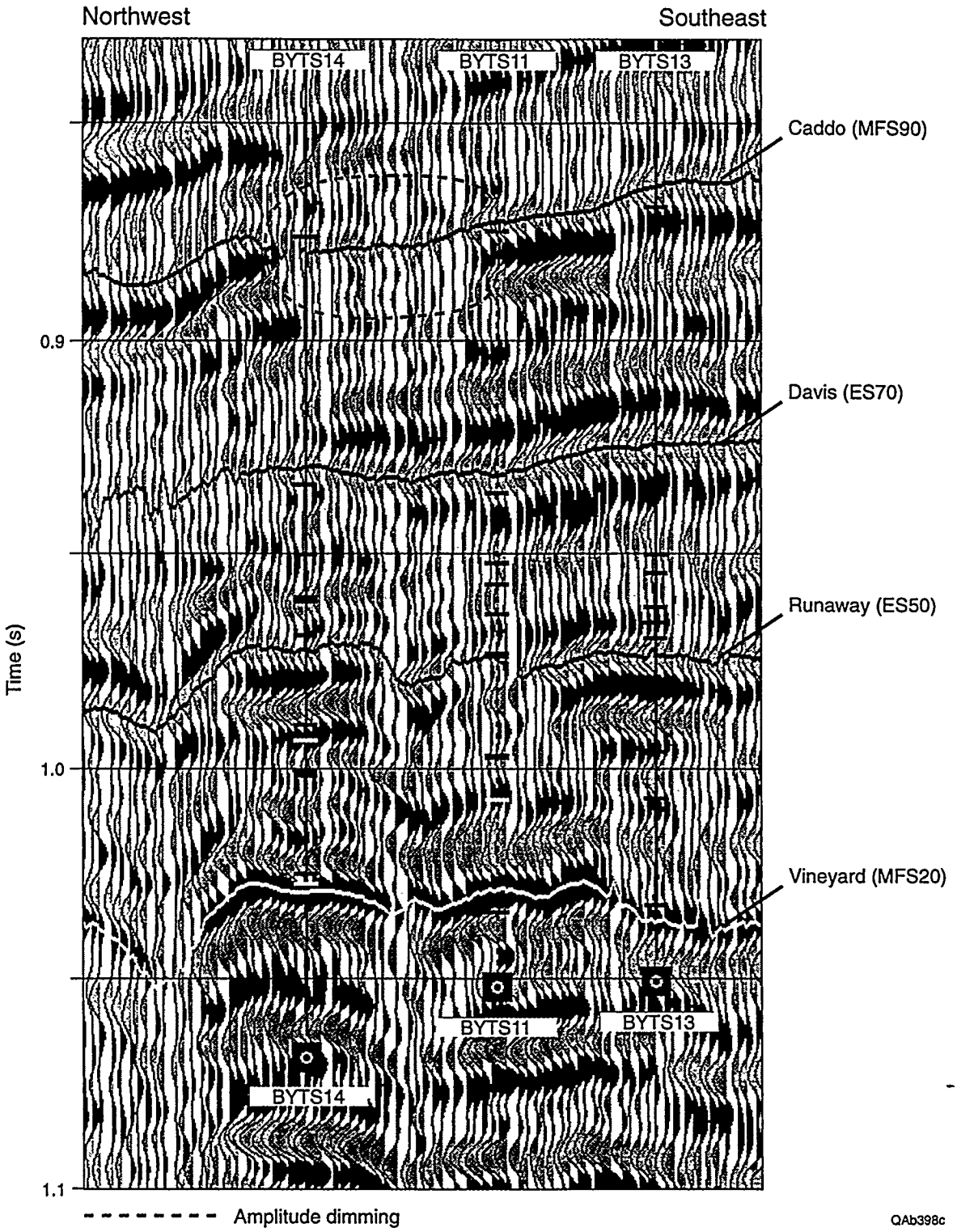

Figure 3.6. Seismic profile along the surface track labeled "Line 2" in Figure 3.4. The amplitude dimming of the Upper Caddo reflection response inside the dashed circle is a key seismic attribute that maps the position of the Upper Caddo valley-fill facies.

4. COMPLEX BEND CONGLOMERATE STRATIGRAPHY CAN LEAD TO SMALL-SCALE RESERVOIR COMPARTMENTALIZATION

One of the best examples illustrating how the complex stratigraphy in the Bend Conglomerate can lead to small-scale reservoir compartmentalization involves several closely spaced wells drilled and completed in the Jasper Creek sequence in the south-central part of the project area. Figure 4.1 shows the location of the four primary wells of interest, the Threshold I. G. Yates 33 (IGY 33) and I. G. Yates A9 (IGY A9) wells to the west and the Enserch W. Dewbre 2 (WD 2) and W. Dewbre 3 (WD 3) wells to the east. What is particularly interesting about this area is that it occurs at the lease boundaries of several operators. As indicated on the map, Threshold's acreage is to the west, Enserch's acreage is to the east, and Mitchell Energy is the operator of the wells immediately to the south.

In the project area, 72 wells have been completed in one or more of the Jasper Creek sequences. About 75 percent of the Jasper Creek completions are gas productive, but the Jasper Creek does make some oil in the northeast and southeast portions of the project area. Gas recoveries from the Jasper Creek in this vicinity have ranged from as little as 10 MMscf to as much as 3.5 Bscf. Drainage areas calculated for the Jasper Creek range from less than 10 acres to more than 500 acres (see Appendix B), so there is quite a range in effective Jasper Creek reservoir size across the project area.

Figure 4.2 is an expanded view of the IGY 33 area. In addition to the four wells of primary interest in this discussion, three other offset wells have been completed in the Jasper Creek—the Threshold I. G. Yates 4 (IGY 4), the Enserch Craft Water Board 12-1 (CWB 12-1), and the Mitchell J. M. Robinson A-5 (JMR A5) wells. In the figure, each well completed in the Jasper Creek is designated by a gas symbol. Next to the symbol for each completion is listed the best estimate for initial bottomhole pressure and the date

that the Jasper Creek was completed, the cumulative gas produced from the interval, and the current status of the Jasper Creek completion. In some wells, the cumulative production came from multiple zones (in addition to the Jasper Creek); if so, the designation MZ appears after the cumulative production figure. Those wells in the figure shown by open circles penetrated, but were not completed in the Jasper Creek.

The IGY 4 well produced only about 10 MMscf when recompleted to the Jasper Creek in 1979; this zone was subsequently abandoned in 1981. The Jasper Creek interval in the CWB 12-1 had an initial pressure greater than 740 psi (based on a shut-in surface pressure measurement) when completed in 1970, but this zone would not produce against line pressure on test. Although the zone is still open and part of a commingled Bend completion, it is unlikely that the Jasper Creek has made much gas at this location. The JMR A5 was completed in five different Bend intervals in late 1993 and is producing commingled from all zones; the initial pressure reported is for the well as a whole, not just for the isolated Middle Jasper Creek interval.

Figure 4.3 presents some additional information about the four primary wells of interest. These wells were completed in either one or two intervals in the Jasper Creek; the intervals shown in Figure 4.3 are the Middle and Lower Jasper Creek sequences. As mentioned previously, these wells are fairly closely spaced; the distance between the IGY 33 and the WD 3 is about 1,200 ft; the distance between the WD 2 and the WD 3 is about 1,500 ft.

The WD 2 was drilled and completed in the Middle Jasper Creek in March 1982. On completion, the bottomhole pressure in the interval was estimated to be just over 1,600 psi. This zoned tested about 2 MMscf/d initially. The well was completed in two other intervals uphole (both in the Trinity sequence); the Trinity intervals did not test much gas after an acid treatment, and they were not tested separately after a subsequent fracture treatment. All three intervals in the Trinity and Middle Jasper Creek were then commingled and produced together. The WD 2 produced 552 MMscf from the combined

Trinity and Middle Jasper Creek intervals, although it is not possible to determine how much gas came from each interval. In December 1993, the Caddo zone was also commingled with the Trinity and Middle Jasper Creek production.

Almost 10 yr after the WD 2 was drilled, Enserch drilled the WD 3 well in December 1992. This well was perforated in both the Middle and Lower Jasper Creek intervals. RFT's measured pressures of just over 1,900 psi in the Middle Jasper Creek, which reflects initial pressure in the Jasper Creek sequence, and it appears that the WD 3 encountered an isolated gas compartment in the Jasper Creek. This zone tested about 2.2 MMscf/d during a short flow test and came on line making about 1 MMscf/d. Unfortunately the flow rate declined very quickly, and within a few months, the well was making less than 50 Mscf/d. The combined Middle and Lower Jasper Creek intervals produced a total of only 76 MMscf through October 1993, before being abandoned. The well is currently completed uphole in the Trinity and Lower Caddo intervals.

The IGY A9 was recompleted from the Lower Caddo to both the Middle and Lower Jasper Creek in February 1993. The completion interval tested 400 to 500 Mscf/d during a short flow test, but the production from these zones also declined quickly. Within about 6 mo, the IGY A9 was making only 10 to 15 Mscf/d, and through November 1993, the Jasper Creek zones produced only about 15 MMscf. These intervals are now commingled with the original Lower Caddo perforations uphole.

As a result of the encouraging early results from the WD 3, Threshold drilled the IGY 33 well in April 1993 as a direct offset to the WD 3. RFT's run on the IGY 33 also recorded pressures of about 1,900 psi in the Middle Jasper Creek, again suggesting no pressure depletion at this location. The IGY 33 flowed at rates above 2 MMscf/d, without stimulation, during initial flow tests. Unfortunately, as with the WD 3 and IGY A9 wells, the production from this zone declined very quickly. The IGY 33 came on line making 2 MMscf/d but declined to less than 50 Mscf/d in 2 to 3 mo. This zone also made a few barrels of oil per day as well, and a pumping unit was installed to help lift the liquids. The

Middle Jasper Creek made only about 60 MMscf of gas before being abandoned in September 1994; the IGY 33 is currently producing from the Caddo uphole.

Figure 4.4 is a plot of initial pressures in the Jasper Creek measured from wells in the project area over time. The values of initial pressure measured for the IGY 33 and the WD 3 wells are similar to those reported in wells drilled and completed since the 1950's. Note, in each case, that the pressures reported are the best estimates that could be obtained for particular wells using available data sources (both operator and public domain records). This figure suggests that the IGY 33 and WD 3 encountered original pressure in the Jasper Creek.

Figure 4.5 presents a comparison of production from these four offsetting Jasper Creek completions. As mentioned previously, the WD 2, WD 3, and the IGY 33 wells all tested the Jasper Creek at rates of about 2 MMscf/d initially, but production from the WD 3 and IGY 33, as well as the IGY A9, declined very rapidly. The WD 2 well showed a more typical decline with time, but the data presented in Figure 4.5 reflect commingled production from both the Trinity and the Jasper Creek. Because production from the WD 2 has always been commingled, it is not possible to separate the contributions of the Trinity and Jasper Creek intervals. Given the performance of the offsetting Jasper Creek completions, it appears likely that much of the gas produced by the well may have come from the Trinity interval, with the Jasper Creek being a high-productivity, but low volume contributor to the overall production of the well. If most of this gas was produced from the Jasper Creek, however, the Middle Jasper Creek in the WD 2 does not appear to have been in communication with the Jasper Creek intervals at the IGY 33 and WD 3 locations.

Several pressure buildup tests were run on the IGY 33, WD 3, and IGY A9 wells. Table 4.1 summarizes key results from the test analyses. These buildup tests show considerable variability in reservoir quality over a small area in the Jasper Creek, with permeabilities varying from 28 md in the IGY 33 to 0.2 md in the IGY A9. Notice, too,

how rapidly reservoir pressure declined in the IGY 33 and WD 3 wells over a short time period. Tests conducted in the IGY 33 well showed a drop in average reservoir pressure of about 1,300 psi in just 4 mo, after only about 40 MMscf of gas had been produced. Likewise, reservoir pressure in the WD 3 declined from approximately 1,900 psi to about 700 psi in just 8 mo, after only about 70 MMscf had been produced. Both wells were apparently draining high-productivity, but low-volume Jasper Creek reservoirs. Drainage areas of 8 and 20 acres were estimated for the IGY 33 and WD 3 wells, respectively.

Table 4.1. Summary of well test results in I.G. Yates 33 area.

Well	Test date	k, md	s′	$\bar{p}$ psi	Remarks
I. G. Yates 33	4/93	–	–	1,890	RFT pressure
	4/93	28	+2	1,560	After 7 MMscf produced
	8/93	28	-2	~600	After 42 MMscf produced
Dewbre 3	12/92	–	–	1909	RFT pressure
	8/93	2	+3	~700	After 71 MMscf produced
I. G. Yates A9	2/93	0.2	–3	1,066(?)	Highest pressure measured

In addition to providing estimates for average pressure and reservoir quality, the wells tests also provided insight into the size and shape of the Jasper Creek reservoirs. An example illustrating this type of detailed analysis is shown in Figures 4.6 through 4.8. These figures present the analysis of the first pressure buildup test conducted on the IGY 33 well in April 1993. The well flowed for about 4 d before being shut in for this 3-d buildup test.

Figures 4.6 and 4.7 show the log-log and semilog plots prepared to interpret the test data. In the log-log plot shown in Figure 4.6, both the change in pressure and its derivative are plotted versus the time since shut-in on a log-log scale. In this figure, adjusted pressure change versus equivalent adjusted time is plotted. These plotting functions are similar to actual pressure and time but include the corrections necessary to account for changes in gas fluid properties with time (Al-Huissany, 1966; Agarwal, 1979;

Lee, 1986). The equivalent time correction allows the use of drawdown type curves to analyze buildup test data (Agarwal, 1980).

The earliest data are approximately unit-slope, suggesting a very brief period of wellbore storage. The flattening of the derivative curve at an equivalent adjusted time of about 0.1 h indicates the beginning of pseudo-radial flow, when a straight line would be expected on the semilog plot whose slope is inversely proportional to permeability. The fact that the derivative flattens like this so early in the test suggests a high-permeability sand. The sharp upturn in the pressure derivative data at a time of about 0.3 h indicates that a near-well boundary has been encountered, although not all boundaries have yet been felt. The flattening and subsequent decline in the pressure derivative data during the later stages suggest that all reservoir boundaries may have been encountered during the test.

Figure 4.7 is the semilog plot of the test data. Using the slope of the straight line shown in the figure, a permeability of 28 md was calculated for the Middle Jasper Creek reservoir. This permeability was higher than generally observed for the Bend intervals in this area (permeabilities of 0.1 to 5 md are more typical), but this value is consistent with the abnormally high values measured from core analysis in this well. In addition, as Table 4.1 shows, the same permeability was also calculated from the second pressure buildup test run in August 1993.

Figure 4.8 presents a history-match of the pressure buildup test generated by a reservoir simulator. Although several different reservoir descriptions were tried, the best match of the actual test data was obtained using a long, narrow (16 × 1) rectangular-shaped reservoir, with the well located near one end of the drainage area. The permeability used in generating the simulated test data was 28 md, the same value calculated from the conventional analyses shown in Figures 4.6 and 4.7. The total reservoir size was about 8 acres. This high-permeability, rectangular-shaped sand body,

as deduced from the well test analysis, was consistent with the geologic interpretation of the Jasper Creek reservoirs in this immediate vicinity.

In summary, it appears that both the IGY 33 and the WD 3 wells encountered original pressure and untapped gas reserves in the Jasper Creek interval. In fact, there is no clear evidence of communication among any of these four closely spaced wells in the Jasper Creek sequence. Unfortunately the drainage areas and, hence, the volumes of these compartments found in the Jasper Creek are small, on the order of 100 MMscf or less, which when considered on their own, are insufficient to be economical infill development targets. This example clearly indicates the stratigraphic complexity found in the Bend intervals and confirms the need for multiple completion opportunities in any new wells drilled.

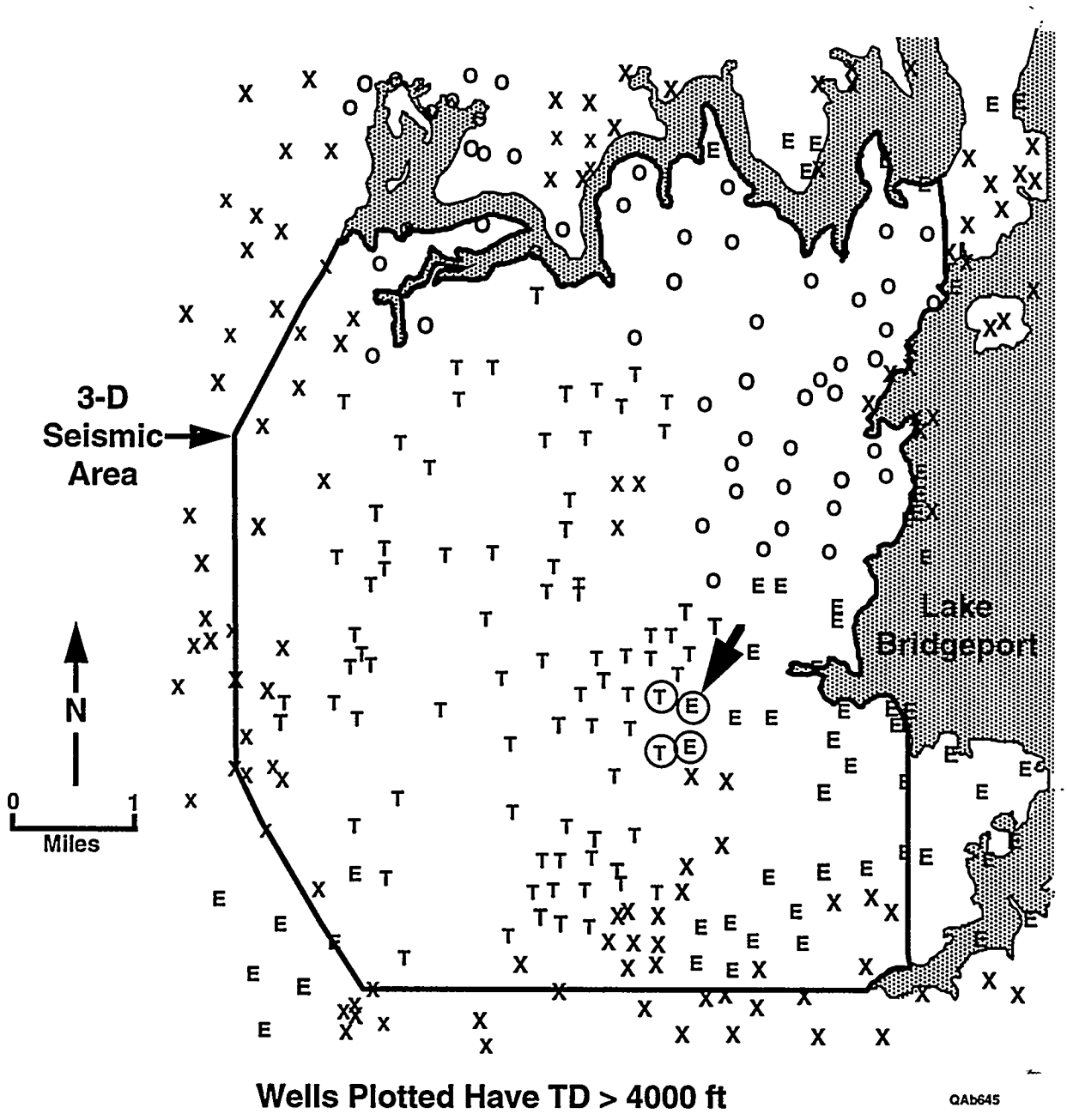

Figure 4.1. Location of several closely spaced Jasper Creek completions in the southeast portion of the project area. Moving clockwise from the southwest corner, the four wells highlighted on the map are the Threshold I. G. Yates 33 and A9 wells and the Enserch W. Dewbre 2 and 3 wells.

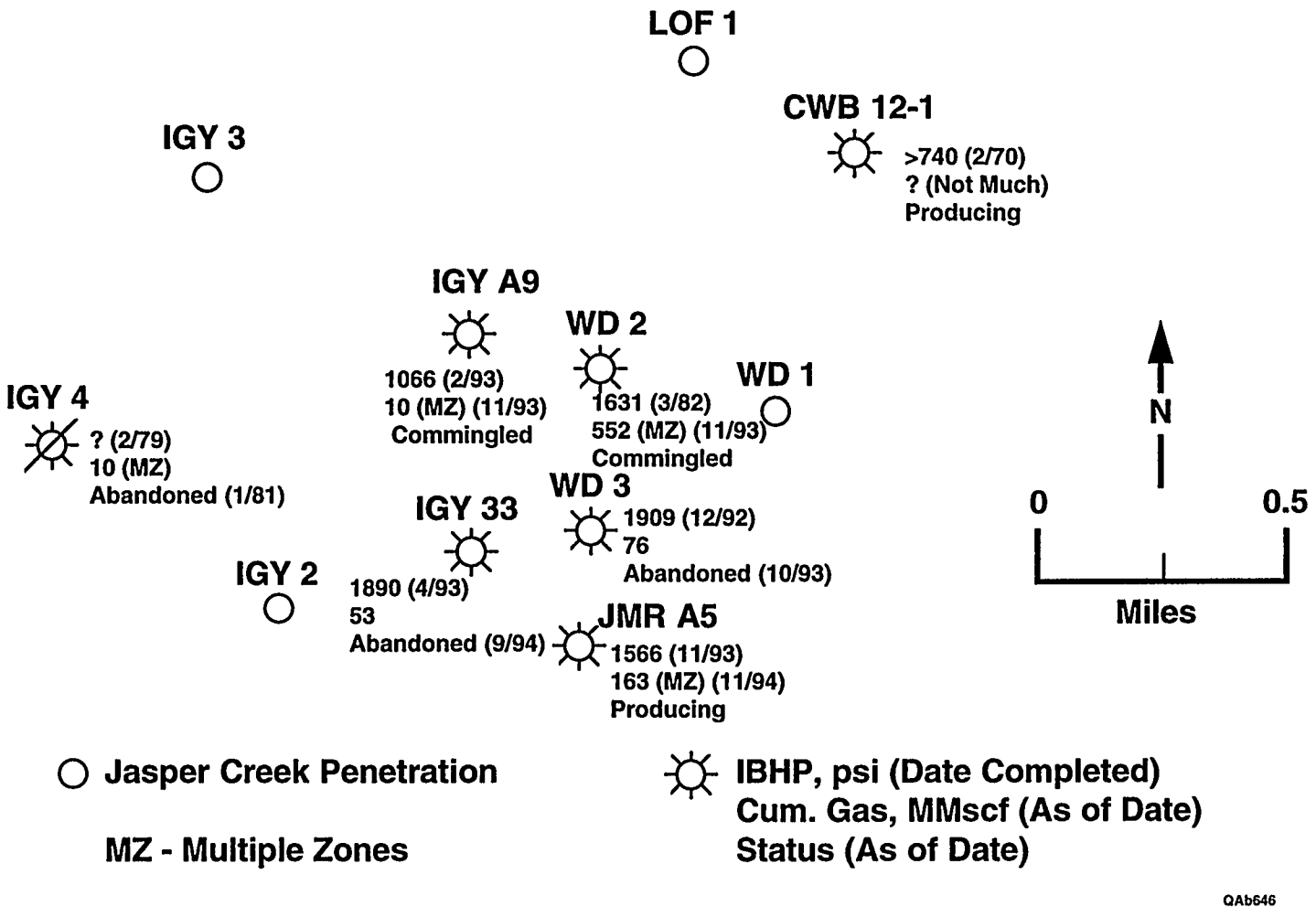

Figure 4.2. Expanded view of the wells presented in Figure 4.1, showing the status of the Jasper Creek completions.

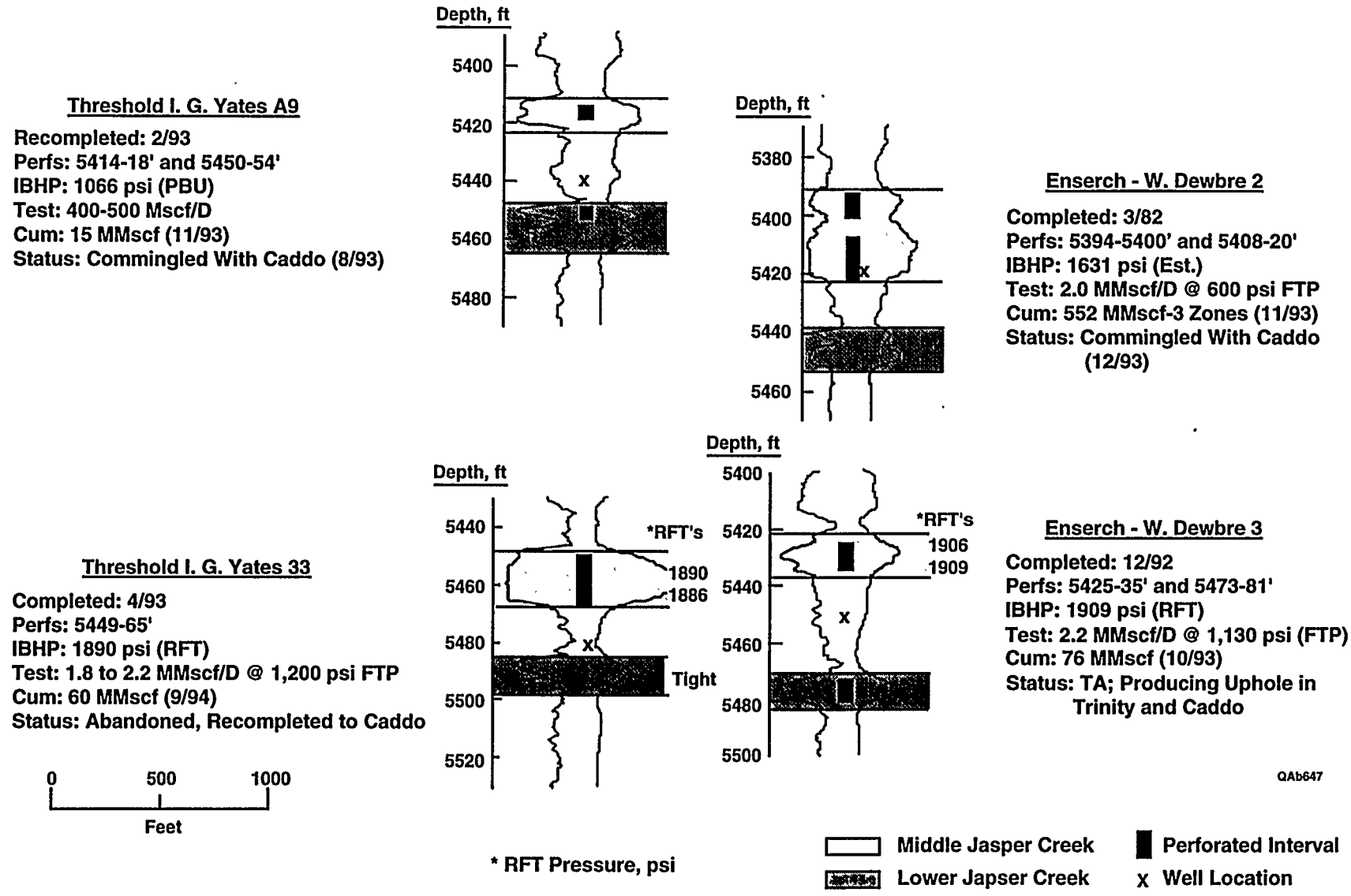

Figure 4.3. Additional completion and production information on the IGY A9 and 33 wells and the WD 2 and 3 wells.

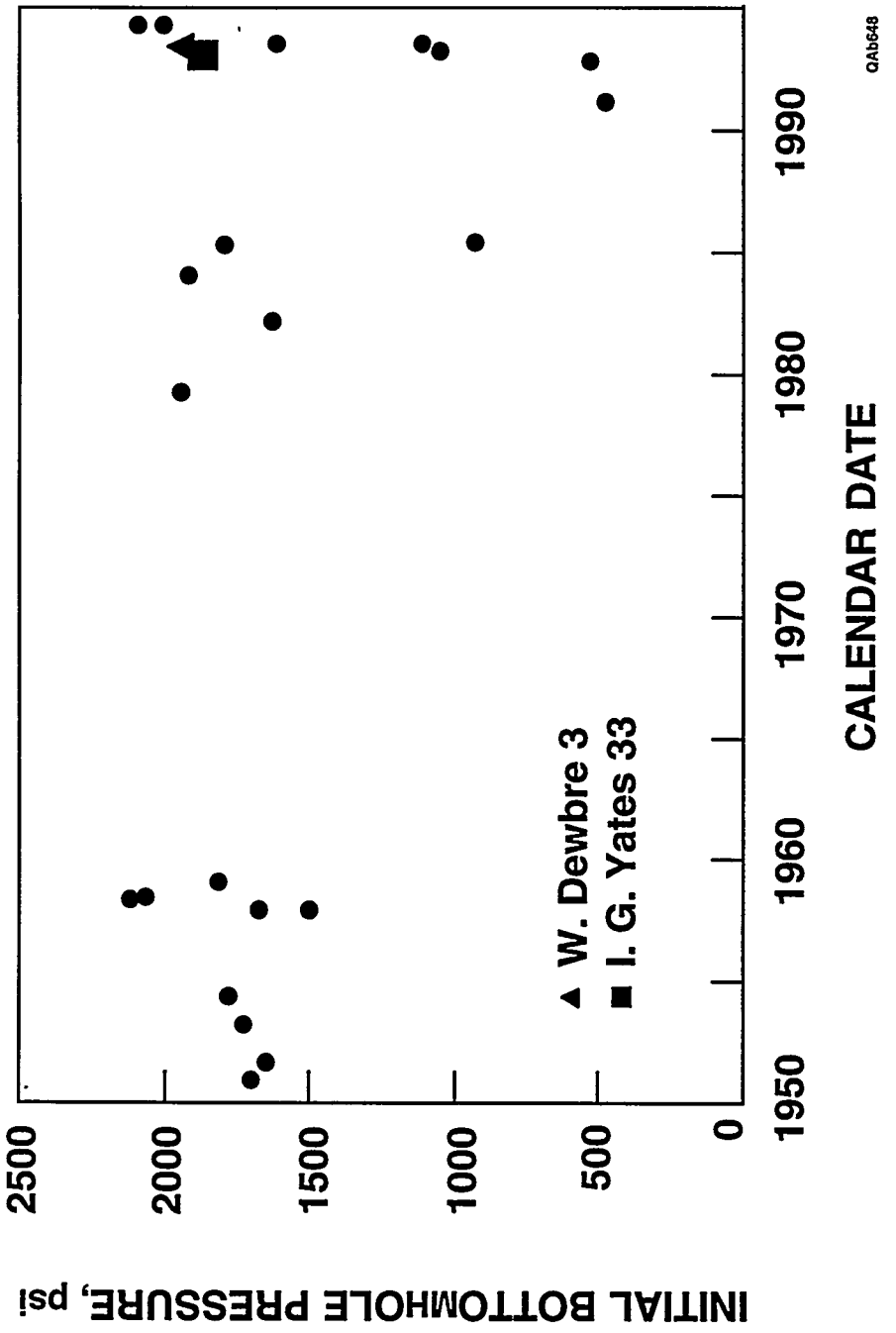

Figure 4.4. Comparison of initial pressures measured in the IGY 33 and WD 3 wells to initial pressures reported in other Jasper Creek completions.

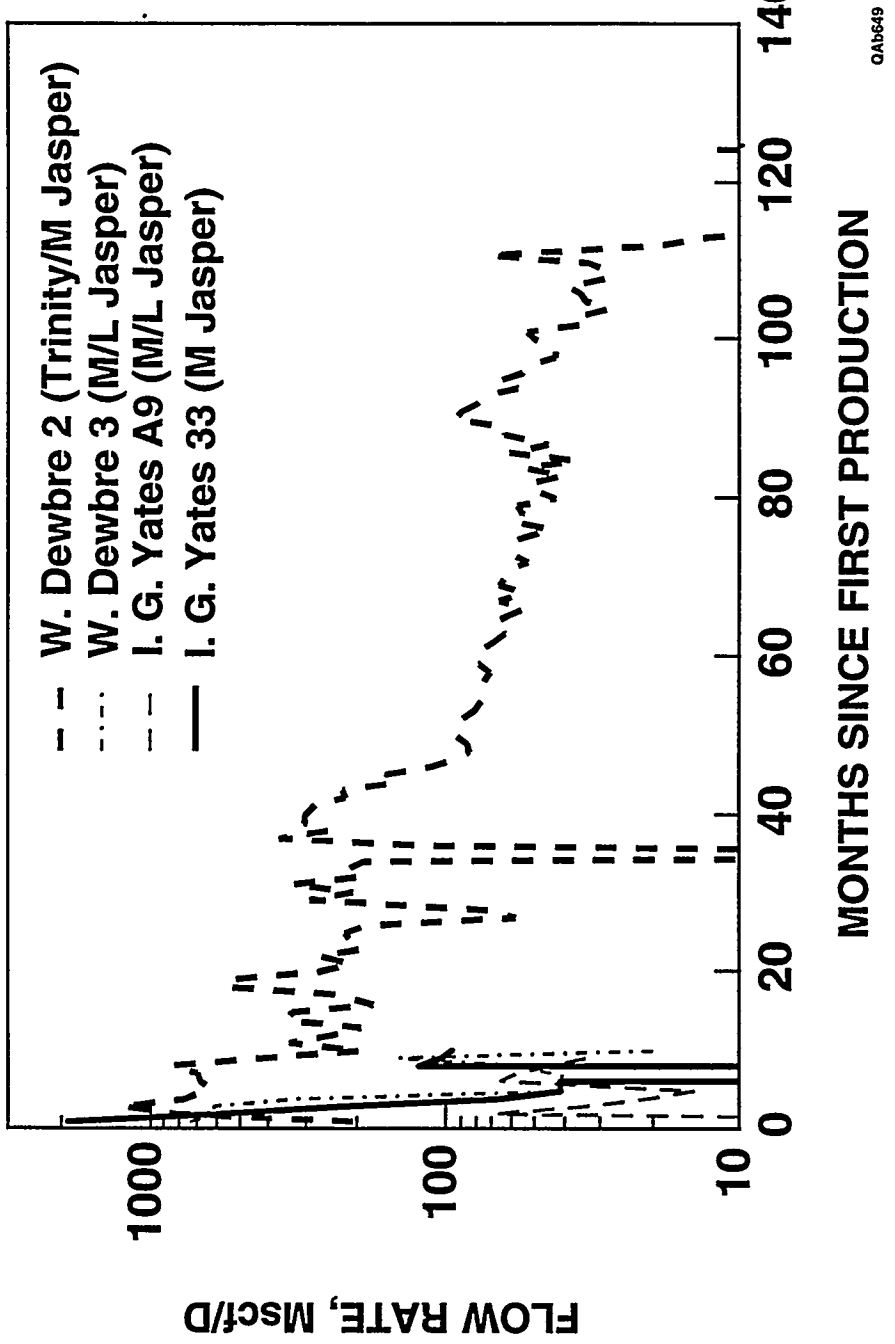

Figure 4.5. Production histories from the IGY A9 and 33 wells and the WD 2 and 3 wells.

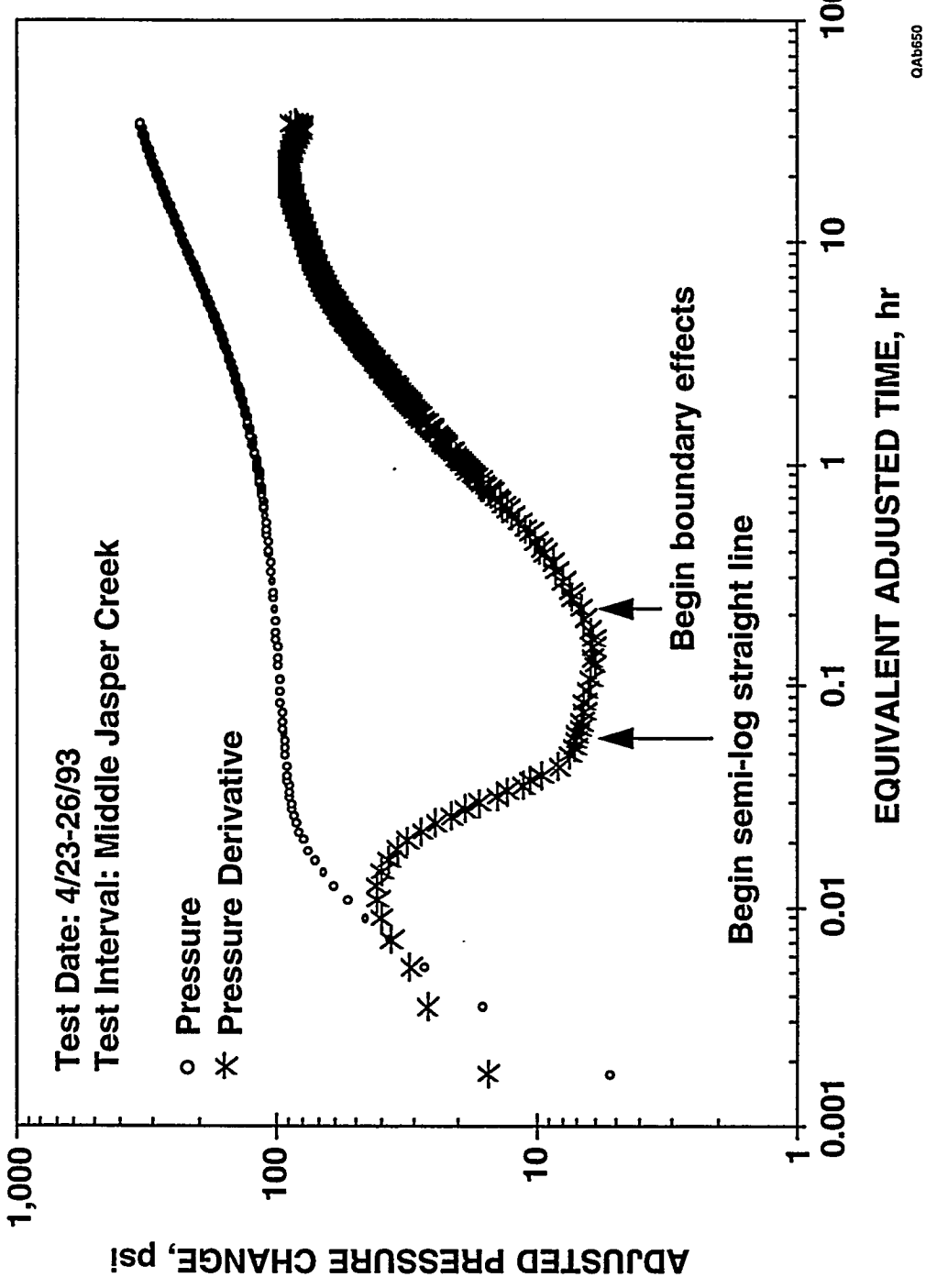

Figure 4.6. Log-log plot of test data from the April 1993 pressure buildup test conducted in the IGY 33 well.

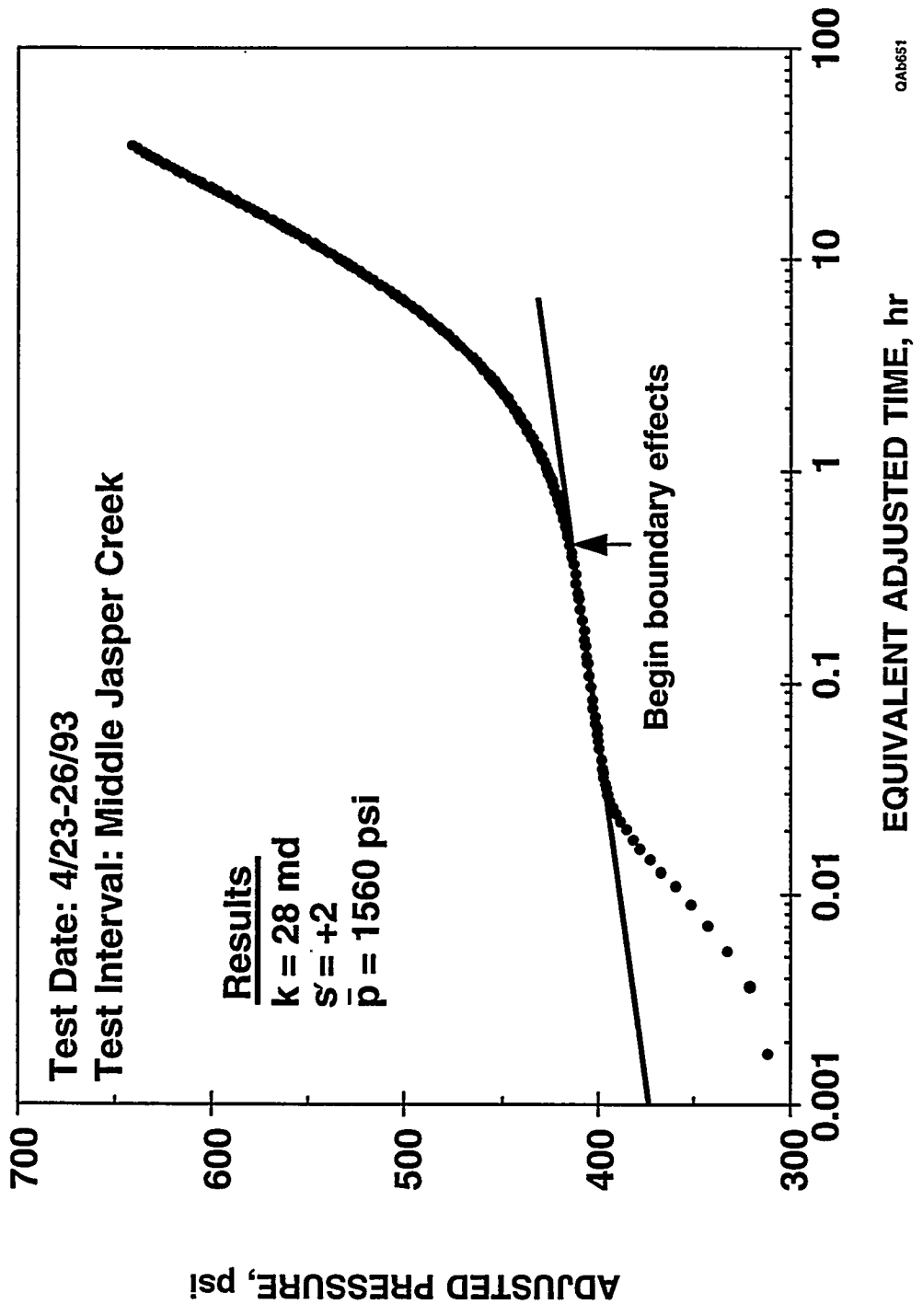

Figure 4.7. Semilog analysis of the April 1993 pressure buildup test conducted in the IGY 33 well.

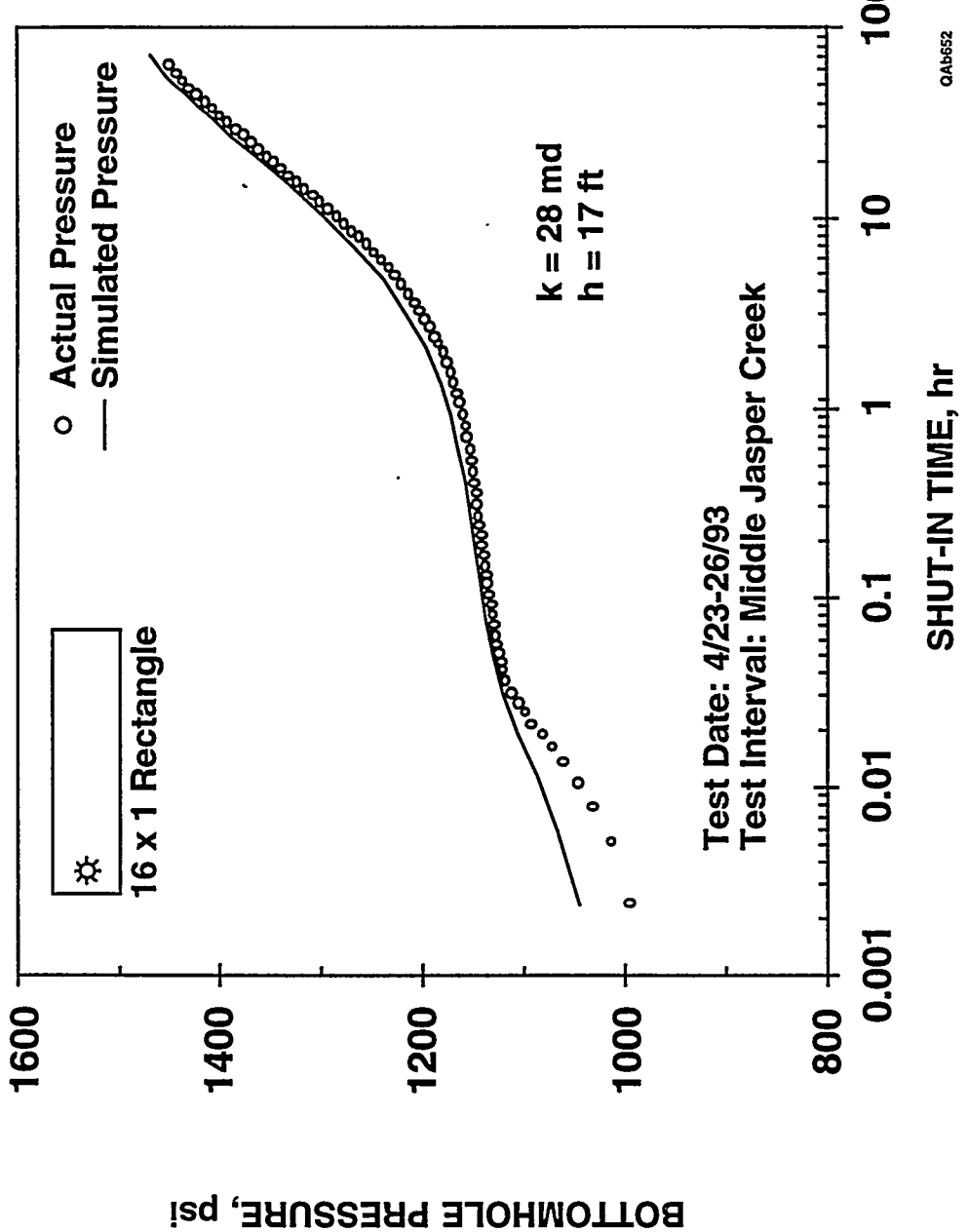

Figure 4.8. History-match of the April 1993 pressure buildup test conducted in the IGY 33 well.

5. SIGNIFICANT BUT ELUSIVE RESERVOIRS

One objective of the Boonsville research was to determine what combinations of modern technology, if any, can reliably predict where to find uncontacted Bend Conglomerate reservoirs. Considerable emphasis was placed on determining whether 3-D seismic images, or some combination of numerically derived seismic attributes, could locate isolated Bend Conglomerate compartments. The ability to see Bend reservoirs using 3-D seismic data is quite variable, with clear, almost unarguable images produced in some instances (for example, the Upper and Lower Caddo reservoirs illustrated in Figures 3.1 through 3.4), whereas in other locations only faint, elusive seismic evidence of certain Bend Conglomerate reservoirs can be seen. This section analyzes one of these elusive reservoir situations.

The Trinity reservoir penetrated by the C Yates 9 well was selected as one example that illustrates how 3-D seismic data may not satisfactorily image the lateral heterogeneity associated with a Bend Conglomerate stratigraphic trap compartment boundary. The Trinity interval at the C Yates 9 well is particularly significant because it contains a reservoir that is one of the most prolific Trinity producers within the 26-mi^2 seismic grid.

The Threshold Development C Yates 9 well was drilled and completed in early 1971. Figure 5.1 shows the location of the well in the north-central part of the project area. The C Yates 9 was initially perforated in the Vineyard interval from 5,688 to 5,701. Following a small fracture treatment (12,000 gal gelled water and 12,000 lb 20/40 sand), the Vineyard tested 668 Mscf/d and 2 STB/d condensate at 100 psi flowing tubing pressure on a 3/4-inch choke.

Immediately thereafter, a bridge plug was set above the Vineyard, and the Trinity interval was perforated from 5,206 to 5,210 ft. After a small fracture treatment (10,000 gal gelled water and 9,000 lb 20/40 sand), the Trinity reservoir tested

2.45 MMscf/d and 14 STB/d condensate at 580 psi on a 1/2-inch choke. The C Yates 9 was turned to sales and produced only from the Trinity interval from June 1971 to September 1989, making 1.91 Bscf of gas. At that time, the bridge plug was removed, and the lower Vineyard perforations were put on production. Currently both the Vineyard and Trinity zones are commingled, and the well has produced a total of 2.11 Bscf.

Although the C Yates 9 was not drilled until 1971, the nearest Trinity completion at the time was more than 1 mi away, and it had not produced much gas from the Trinity (only about 60 MMscf). The reported initial bottomhole pressure of 1,411 psi would not be considered initial pressure in the Trinity, but this pressure was estimated from a surface shut-in pressure that was not fully built up and is considered to be lower than the actual Trinity reservoir pressure at the time. That any significant drainage from the Trinity reservoir had been at this location at the time the C Yates 9 was completed is unlikely.

Figure 5.2 presents an expanded view of the area around the C Yates 9 well. The OXY Ashe 1 well was completed in the Trinity interval in January 1961, which was the only nearby well completed in the Trinity before the C Yates 9 being drilled, and it had produced only about 60 MMscf of gas to that time (cumulative Trinity production to date is only 185 MMscf). Trinity perforations were added in the C Yates 6 well in May 1983, but because the Trinity is one of six Bend intervals commingled in this wellbore, it was impossible to estimate its gas production individually.

The C Yates 10 and 12 wells were drilled in 1984 and 1985, respectively. Both wells were multiple completions in the Trinity, Lower Jasper Creek, and Vineyard sequences. Upper Caddo perforations were added in the C Yates 10 in 1990. Both these wells are structurally lower than the C Yates 9 by about 40 to 50 ft, and each tested and produced both oil and gas from the Trinity; both were actually classified as oil wells. The C Yates 10 has produced about 25,000 STB of oil and 184 MMscf of gas from the three

commingled intervals, whereas the Cap Yates 12 has produced only about 3,400 STB of oil and 165 MMscf of gas.

In December 1992, the B Yates 3 well was recompleted in the Trinity. There was significant pressure depletion in the Trinity on recompletion; this zone had an estimated reservoir pressure in the Trinity of about 200 psi on the basis of surface pressure measurements. The C Yates 9 had apparently drained the Trinity reservoir at the B Yates 3 location. The same is true at the Lewis 1 location, where the initial pressure on completion of the Trinity interval was 508 psi in March 1982.

Figure 5.3 presents an interpreted log across the Trinity sequence penetrated by the C Yates 9. The upper part of the sequence from 5,197 to 5,218 ft had excellent sand development and good porosity and gas saturation; this was the interval that was completed. The lower sands are highly carbonate cemented with a resulting loss of porosity and productivity.

Figure 5.4 shows the Trinity-only gas production from the C Yates 9 well and is a semilog plot of gas flow rate versus time. The well came on line making in excess of 2 MMscf/d and declined to a rate of about 20 Mscf/d over an 18-yr period.

Figure 5.5 is a log-log plot of gas flow rate versus time. This plot indicates boundary-dominated flow during most of the well's producing life, as evidenced by the concave downward shape of the production data after about 300 to 500 d of production. Using an analytical model to history-match the production data, the Trinity reservoir was estimated to have a permeability of about 3.3 md and a drainage area of approximately 300 acres. This estimated drainage area is based on a constant, average net pay thickness of 14 ft calculated for the C Yates 9. If the average net thickness of the Trinity reservoir in communication with the C Yates 9 wellbore is less that 14 ft, then the apparent reservoir size of 300 acres is a minimum value. The estimated total gas in place of 2.1 Bscf in the Trinity reservoir should be correct for any combination of net pay thickness and drainage area.

Two seismic profiles that traverse the C Yates 9 well and connect with adjacent wells are used to illustrate the seismic subtlety of this particular Trinity reservoir. These vertical seismic sections are shown as uninterpreted and interpreted wiggle trace data in Figures 5.6 through 5.9, and as uninterpreted and interpreted instantaneous phase data in Figures 5.10 through 5.13 (see Appendix E for a discussion of how instantaneous phase is calculated and used).

In this situation, it is easier to use instantaneous phase to interpret the position of the Trinity surface than it is to use the traditional approach of using wiggle trace data. The advantage of instantaneous phase is that the phase behavior of seismic data is independent of the magnitude of the reflection signal amplitude; consequently, instantaneous phase displays show stratigraphic relationships in low-amplitude portions of a 3-D seismic data volume with the same degree of fidelity and robustness as they do in high-amplitude portions. Because the reflection response associated with the Trinity surface is low amplitude, the Trinity sequence boundary can be tracked more easily in instantaneous phase displays. In all instances where any Bend Conglomerate sequence boundary had to be interpreted in low-amplitude wiggle trace data, the interpretations were usually done using instantaneous phase volumes.

The seismic two-way traveltime positions of several log-interpreted sequence boundaries are marked by heavy horizontal dashes on each well profile in these seismic displays, and these sequence boundary control points are expanded into continuous sequence boundaries on each interpreted section. The MFS60 (Trinity) surface is the target reservoir that needs to be imaged. The wiggle trace displays in Figures 5.6 and 5.7 show that, along this particular profile, the Trinity surface is marked by a low-amplitude event that has an erratic time onset and a variable waveshape. In this instance, the Trinity surface follows a reasonably consistent phase trend (Figs. 5.10 and 5.11). In contrast, no definitive reflection event is associated with the Trinity surface along the profile shown in Figures 5.8 and 5.9, and in the associated phase displays (Figs. 5.12 and 5.13), the phase

exhibits rapid lateral changes along the time surface where well control defines the Trinity sequence boundary to be located. Thus, even though the Trinity sequence penetrated by the C Yates 9 well is a significant reservoir, the reservoir is quite elusive in a seismic sense, and some interpreters might refer to the reservoir as being seismically invisible in this particular 3-D seismic data volume.

The principal point to make concerning the seismic image of this stratigraphy is that this Trinity reservoir is not seismically invisible; it is simply nondescript in a seismic sense because the reflection waveshapes defining the sequence are low amplitude, variable in character, irregular in their time onset, and not conformable to any nearby reflection event. No distinctive seismic property therefore causes an interpreter to focus on that portion of the 3-D data volume where this Trinity reservoir is located, and well control must be used to identify the precise location of the Trinity sequence boundary.

Once sequence boundary picks from the C Yates 9 and neighboring wells are incorporated into the interpretation, the two-way seismic traveltime of the Trinity reservoir can be defined, and the sequence boundary associated with the reservoir can be extended away from the control wells. Maps of seismic attributes calculated on the resulting Trinity horizon show that there is a distinctive reflection amplitude behavior (Fig. 5.14), with the Trinity sequence being expressed by low reflection amplitudes having both positive and negative algebraic signs immediately around the C Yates 9 well, and by larger, positive-only reflection amplitudes at greater distances around the well. We assumed that the low amplitude seismic facies indicated Trinity reservoir facies, and that the larger valued, positive seismic amplitude facies mapped nonreservoir Trinity facies. The exact way to position the boundary that segregates these two seismic amplitude facies is a matter of subjective judgment, but the configuration shown in Figure 5.14 is thought to be reasonably consistent. This boundary encloses an area of almost 300 acres, which is a reservoir size similar to what the production data imply. The B Yates 3 well is positioned inside the south edge of this interpreted Trinity compartment.

A distinctive boundary of anomalous frequency values (Fig. 5.15) also encircles the C Yates 9 well. If we assume that the boundary defined by the anomalous frequencies also marks the lateral extent of the C Yates 9 reservoir compartment, as is suggested by the data examples presented in Appendix E, the seismic data imply that the areal size of this Trinity reservoir is a little over 100 acres, which is not as large a reservoir as the production data imply. Reflection profiles along Lines 1 and 2, shown on the seismic amplitude and frequency maps, are provided as Figures 5.16 and 5.17 to support the claim that this particular Trinity reservoir is a highly elusive target in the 3-D seismic image.

A significant conclusion provided by this C Yates 9 reservoir analysis is that other Bend Conglomerate reservoirs, not just Trinity reservoirs, may also not be easily seen in 3-D seismic images, even when seismic attributes such as instantaneous frequency are used in the analysis. Stated another way, it will be difficult for 3-D seismic data to be used as a predictive tool to site exploration wells for some, but not all, Bend Conglomerate reservoirs in undrilled areas, if the reservoir trapping mechanism is caused strictly by lateral facies change rather than by some type of structural disruption. Even when an elusive reservoir of this type is the primary interpretation target, however, 3-D seismic imaging is still valuable for estimating the areal size of the stratigraphic trap, because once the reservoir has been penetrated by a well, the reservoir sequence can then be accurately positioned in the 3-D data volume and seismic attribute maps can be made to imply compartment size and shape.

Thus, the role of 3-D seismic technology in low accommodation Midcontinent fields similar to Boonsville seems to be the following.

1. 3-D seismic imaging can be used as a predictive tool for siting exploration wells when the reservoir trapping mechanism is associated with a structural disruption, such as a fault or a collapse zone, and also for many stratigraphic traps, such as has been documented for the Upper and Lower Caddo (Figs. 3.1 through 3.4).

2. 3-D seismic imaging may not serve as a reliable predictive tool for some subtle stratigraphic traps, but in such cases, the imaging can be used as a property management tool to estimate the areal size and shape of these subtle stratigraphic traps once the reservoir has been penetrated by a well. This increased value of 3-D seismic data at the production phase of an elusive reservoir play occurs because the well data allow the sequence boundary of the reservoir to be accurately positioned in the 3-D seismic data volume, even if the seismic response at that boundary has no obvious, distinctive waveform character.

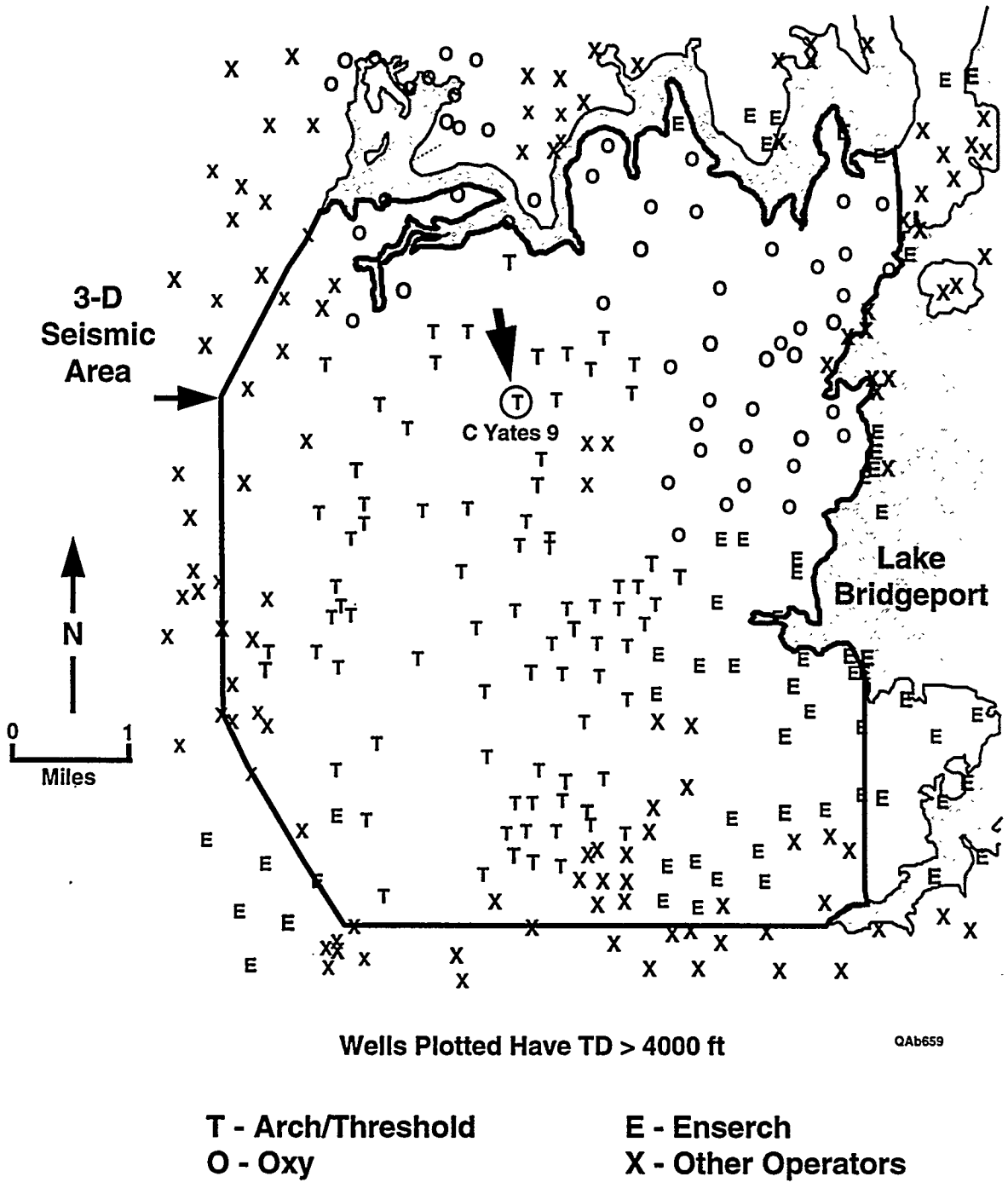

Figure 5.1. Location of the C Yates 9 well in the north-central portion of the project area.

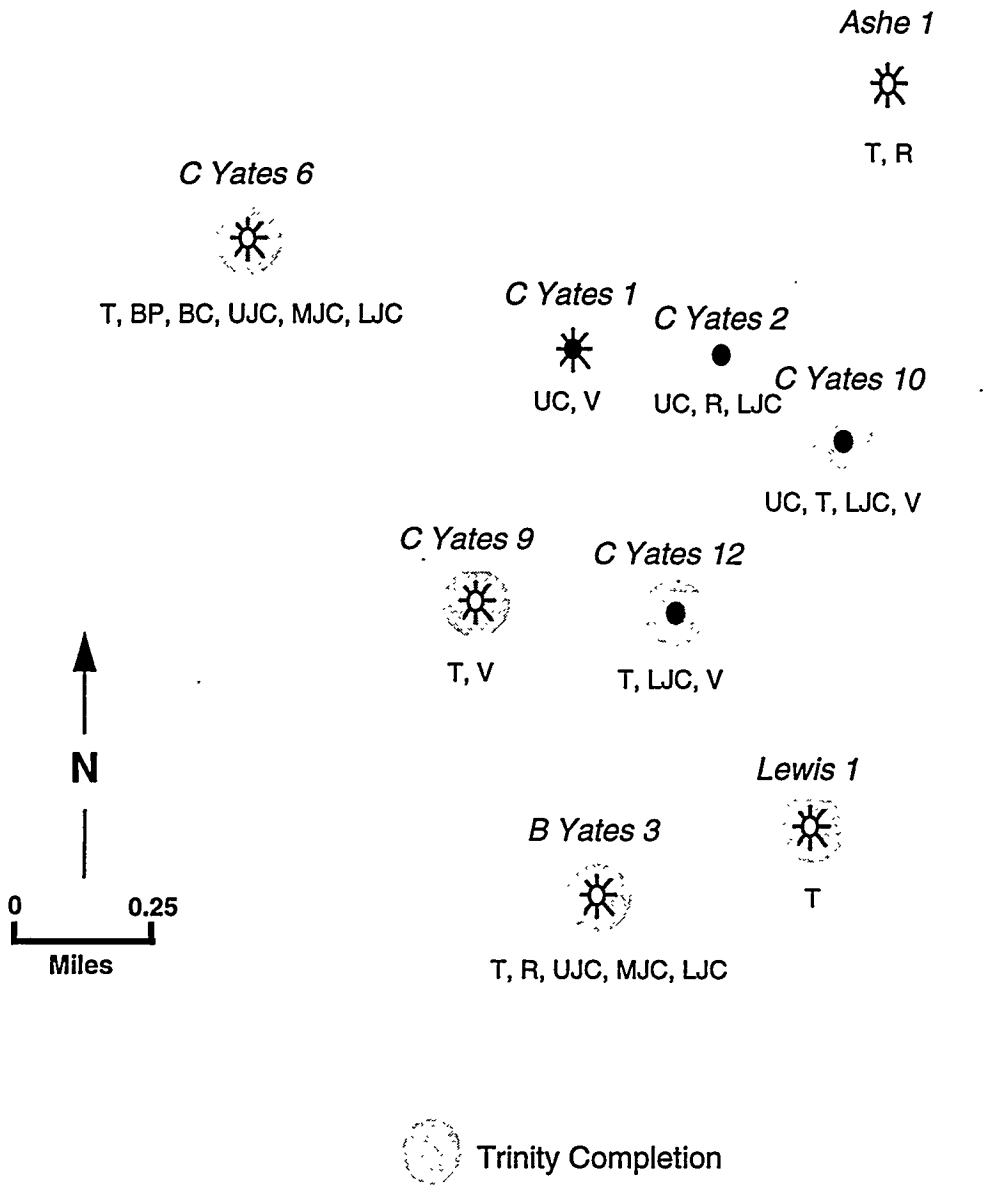

UC - Upper Caddo
T - Trinity
BP - Bridgeport
R - Runaway
BC - Beans Creek
UJC - Upper Jasper Creek
MJC - Middle Jasper Creek
LJC - Lower Jasper Creek
V - Vineyard

Figure 5.2. Expanded view of wells offsetting the C Yates 9 location.

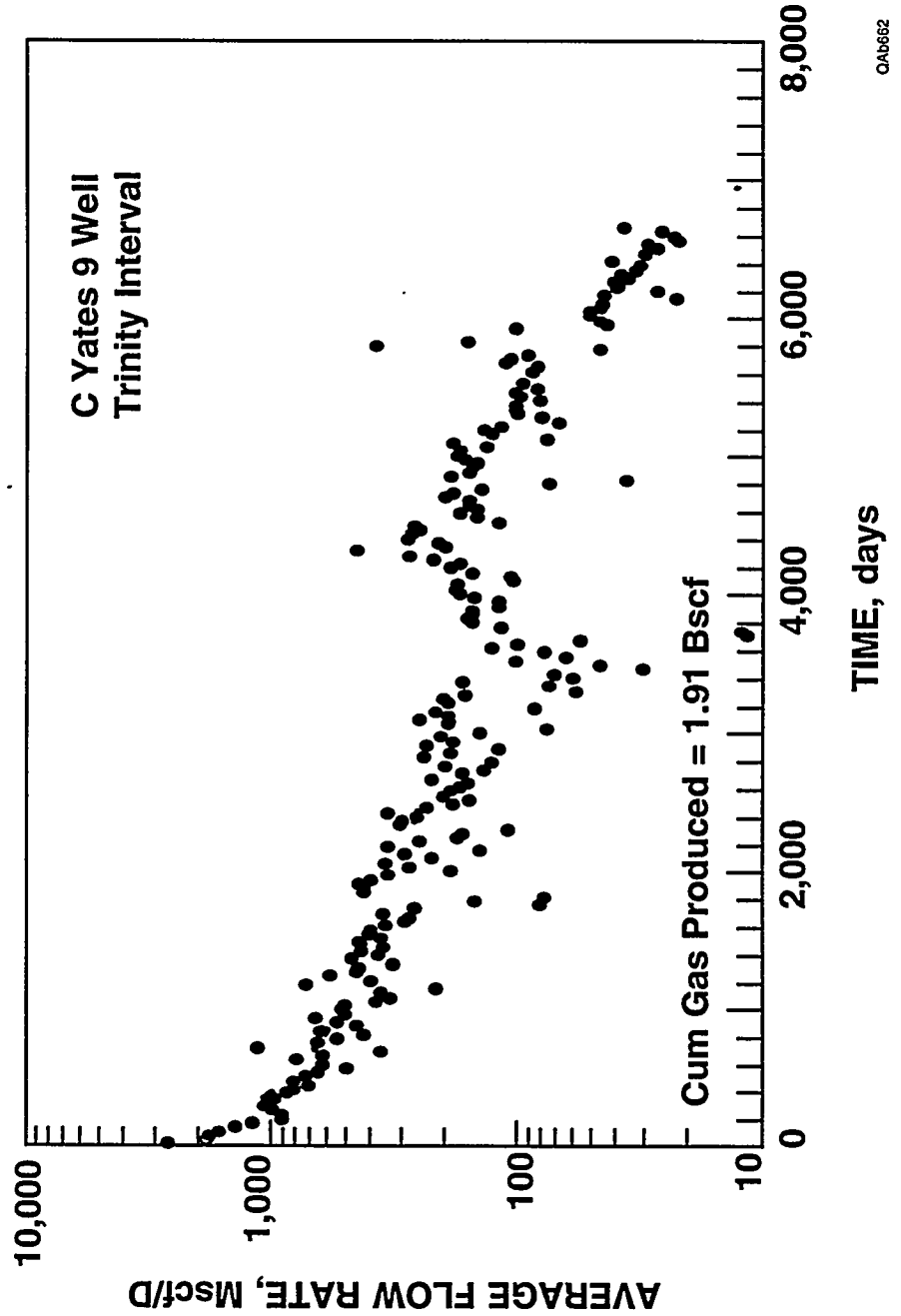

Figure 5.4. Trinity-only production history from the C Yates 9 well.

5.12

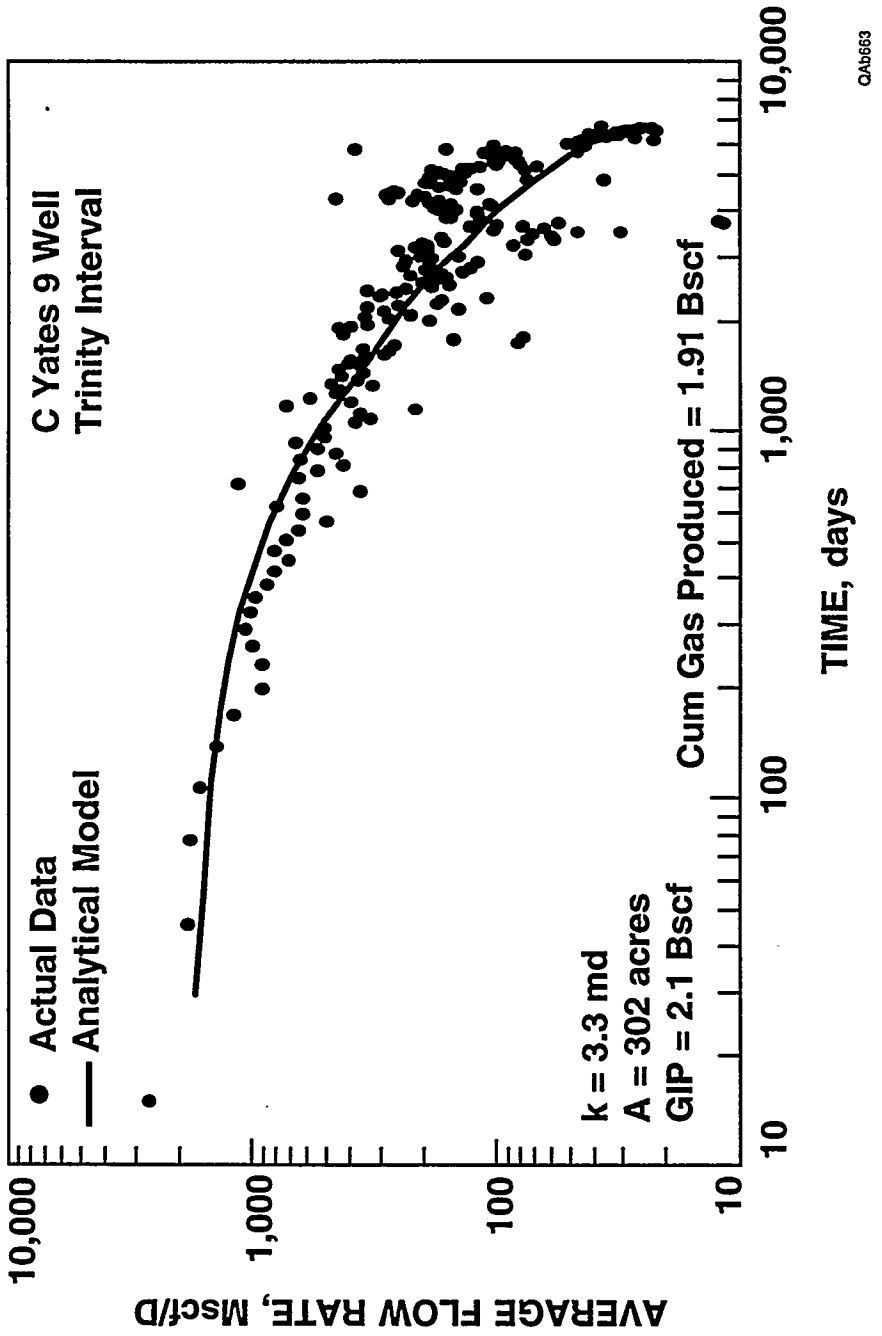

Figure 5.5. History-match of production data from C Yates 9 well.

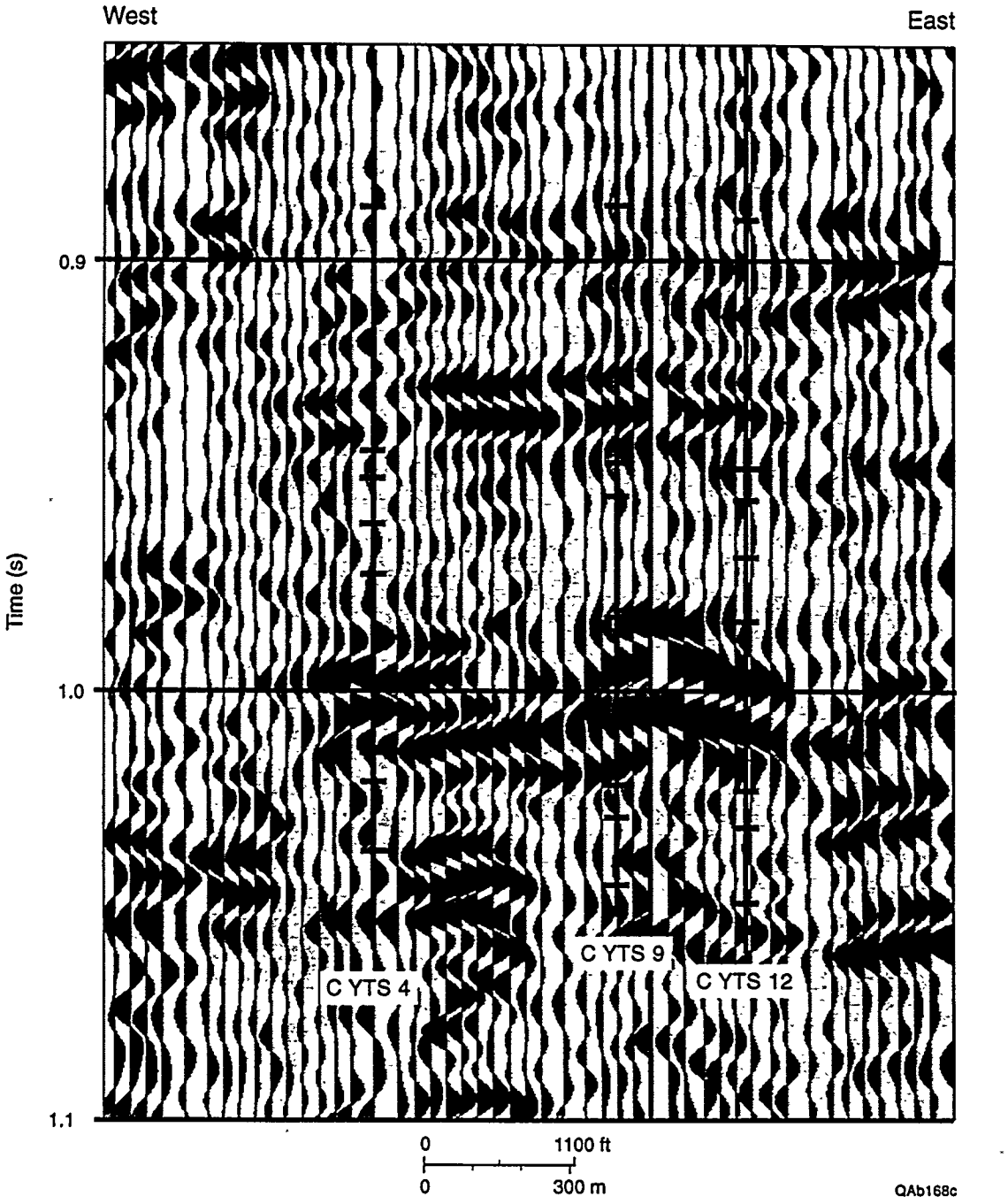

Figure 5.6. An uninterpreted east-west seismic section connecting the C Yates 9 well with neighboring wells. The horizontal dashes on each well profile show where key sequence boundaries are positioned by the depth-to-time conversion function developed for the study area.

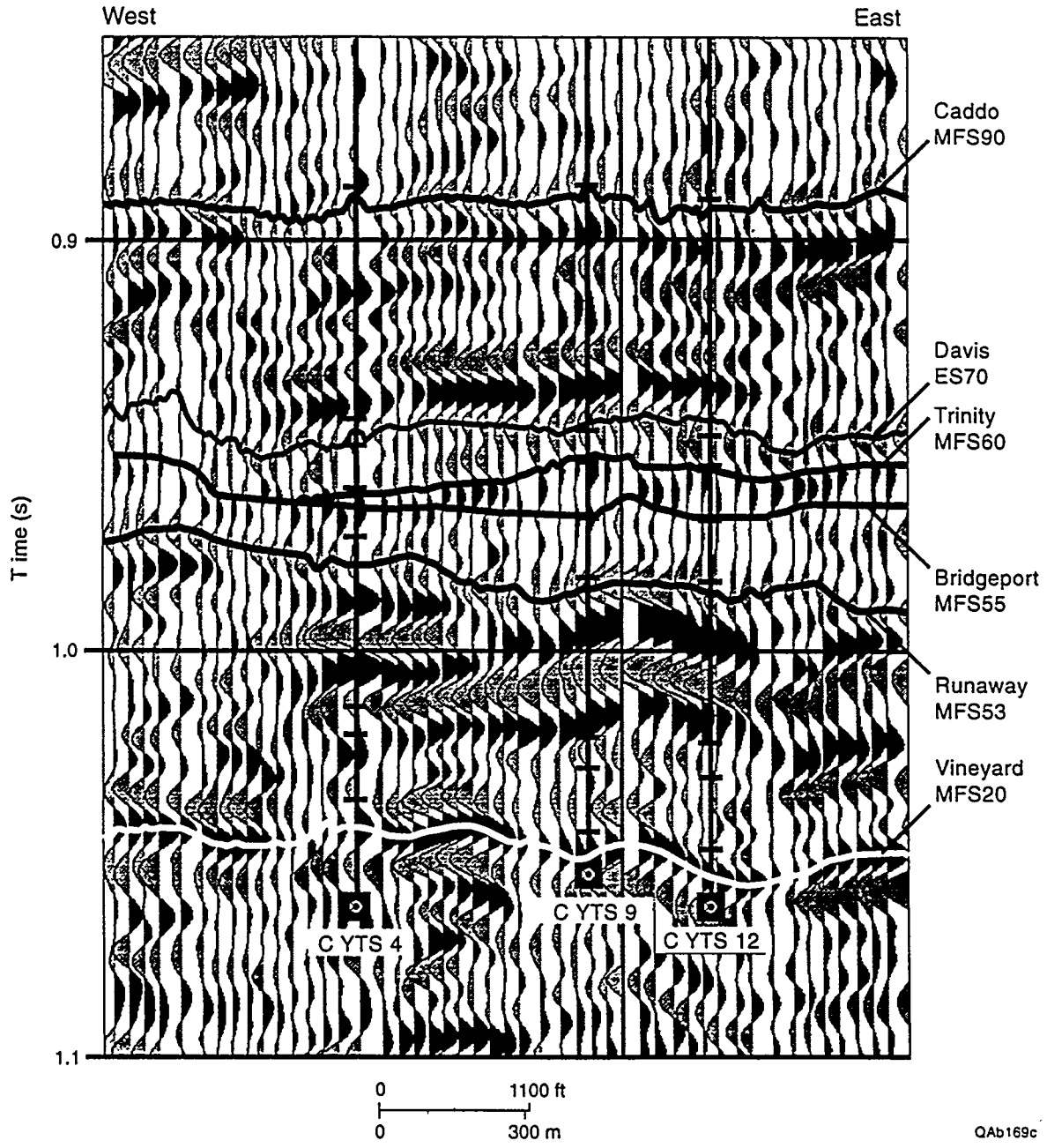

Figure 5.7. An interpreted version of the seismic line shown in Figure 5.6. The imaging objective is a major reservoir immediately below the Trinity (MFS60) sequence boundary.

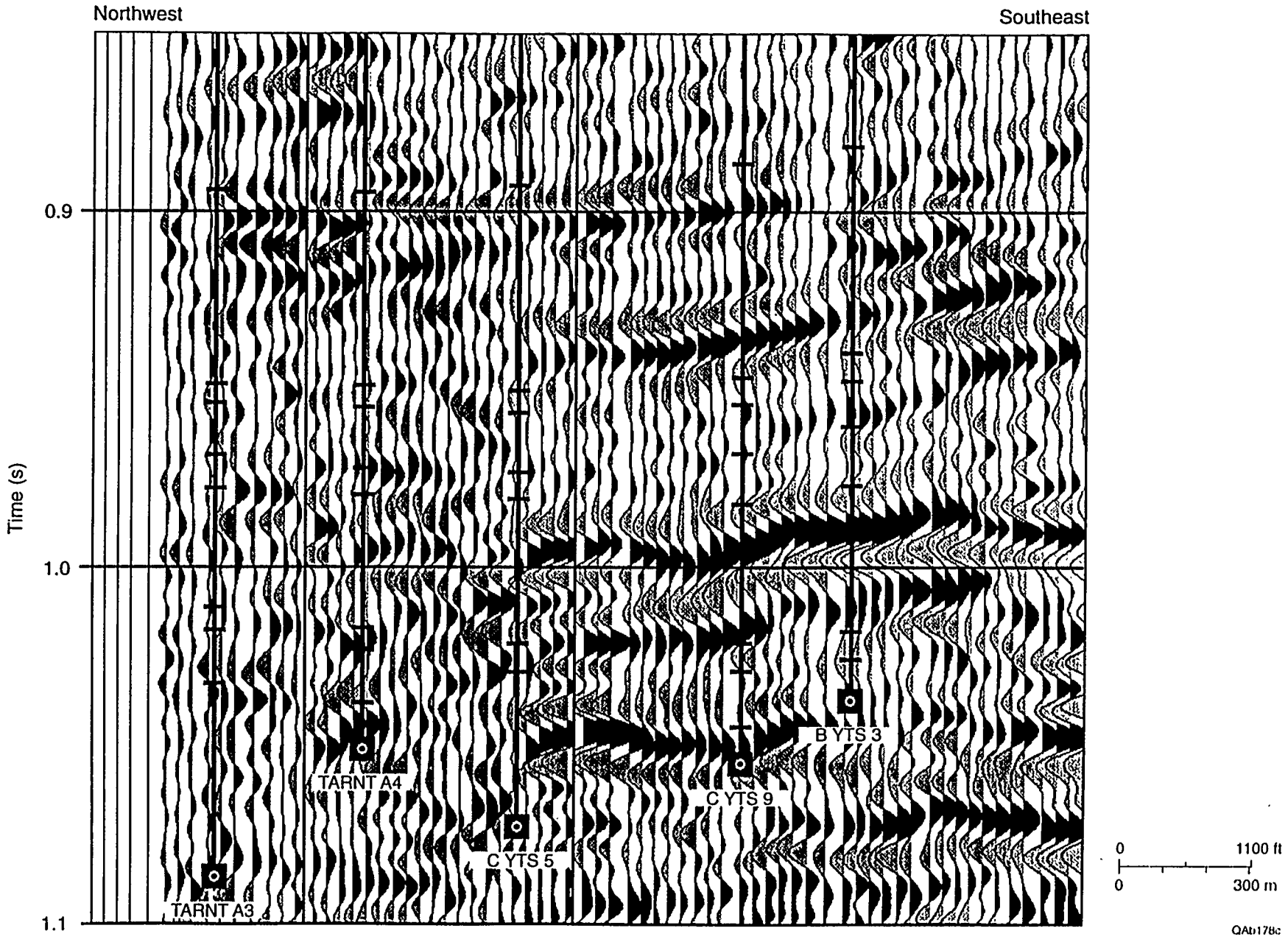

Figure 5.8. An uninterpreted northwest-southeast seismic section connecting the C Yates 9 well with neighboring wells. The horizontal dashes on each well profile show where key sequence boundaries are positioned by the depth-to-time conversion function developed for the study area.

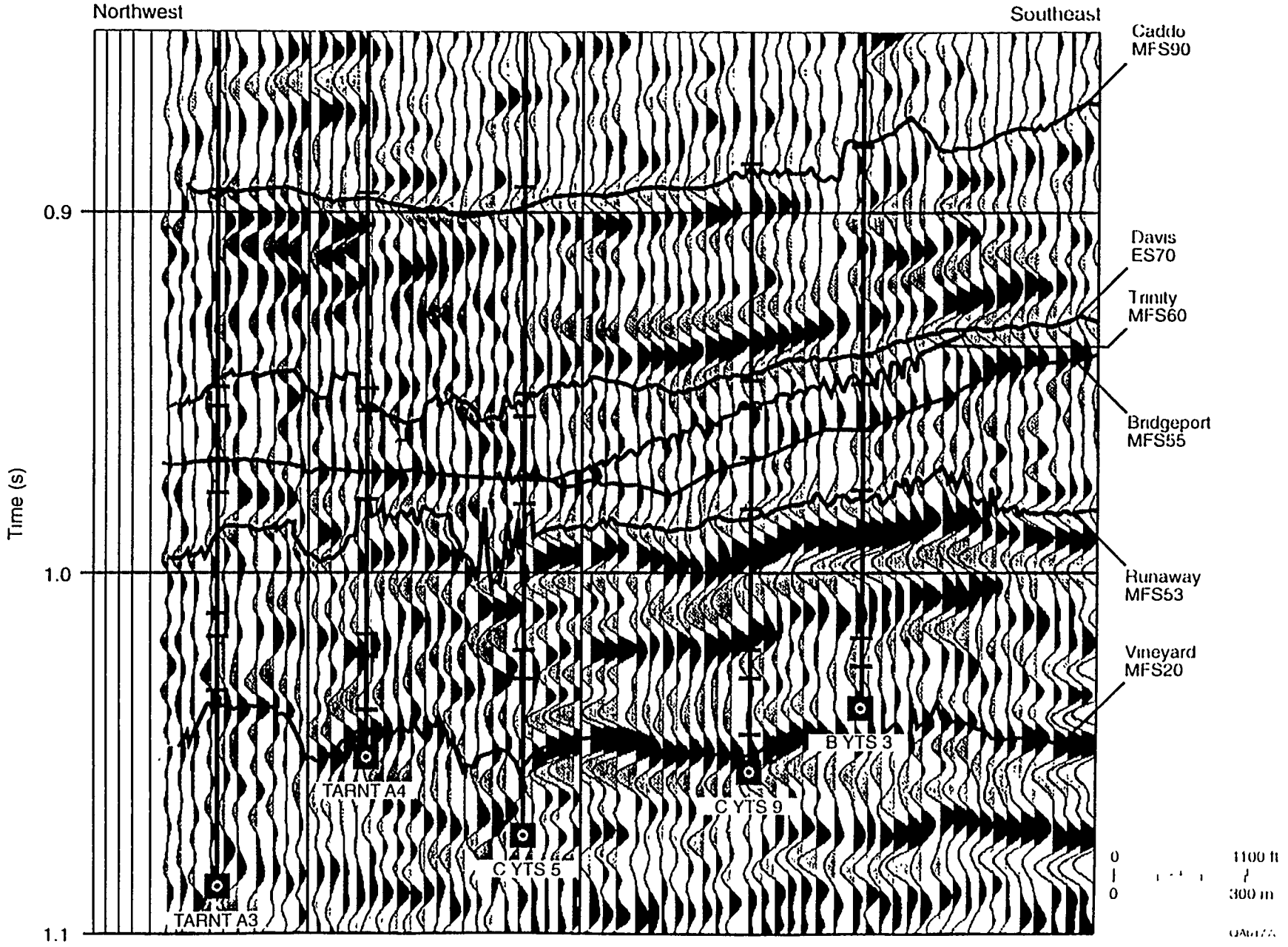

Figure 5.9. An interpreted version of the seismic line shown in Figure 5.8. The imaging objective is a major reservoir immediately below the Trinity (MFS60) sequence boundary.

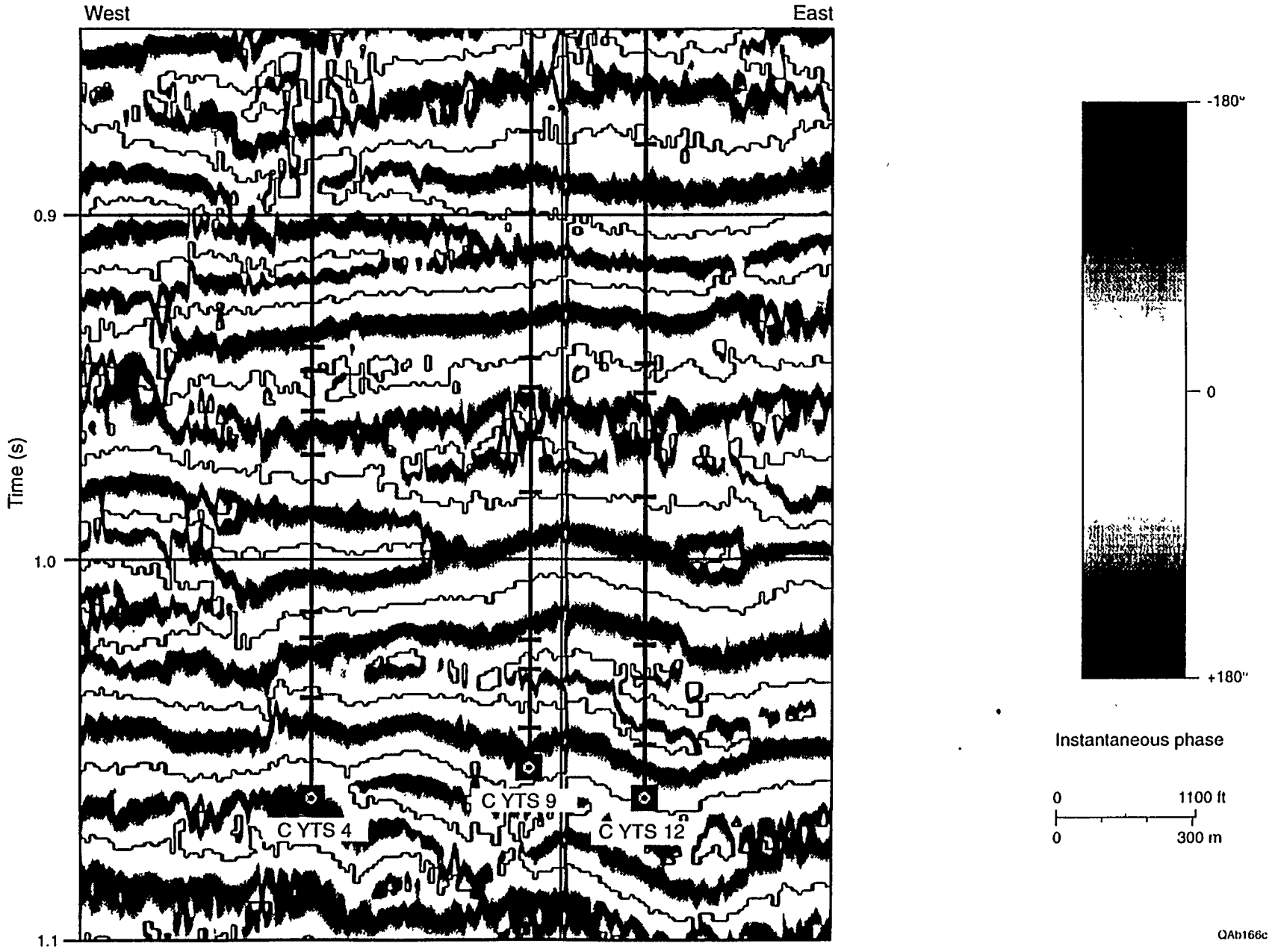

Figure 5.10. The data in Figure 5.6 converted to instantaneous phase. The thin black line passing through the center of each white phase zone shows where the phase function undergoes a 360° wrap-around when the phase function cycles through the 0° value. This helpful phase surface is automatically provided by the Landmark software used to interpret the Boonsville 3-D seismic data.

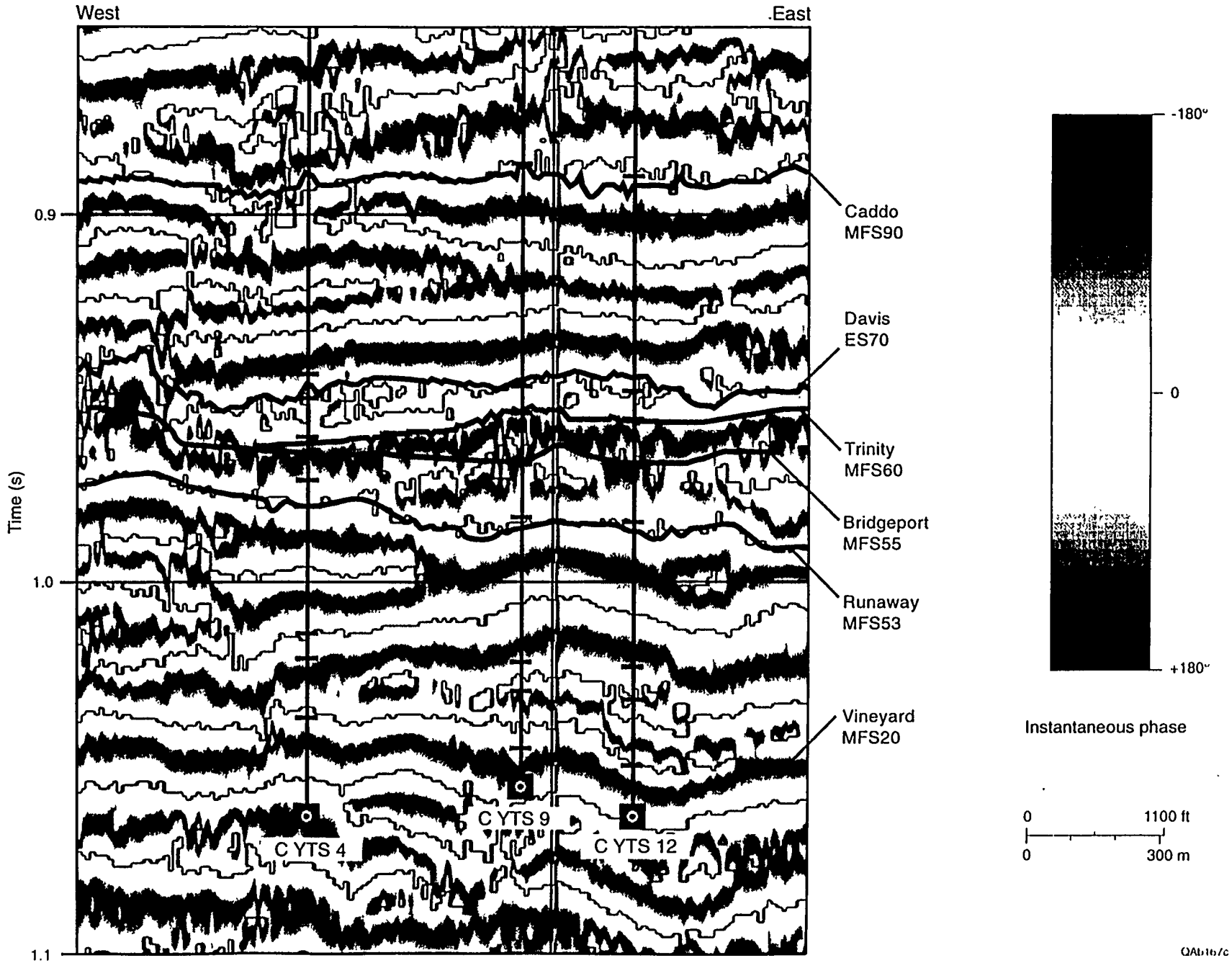

Figure 5.11. The data in Figure 5.7 converted to instantaneous phase. Note that each sequence boundary, including the Trinity surface, follows a constant phase surface.

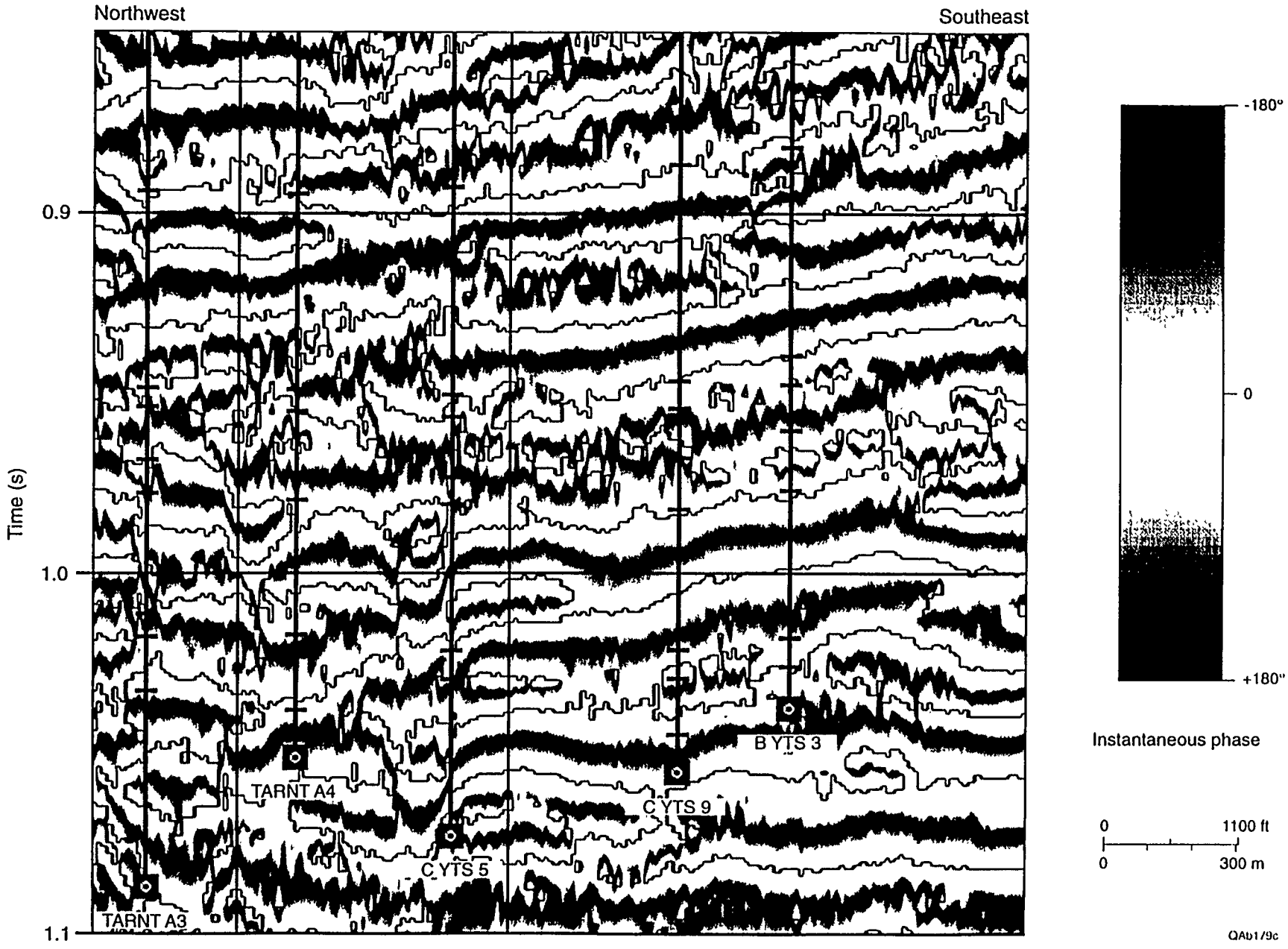

Figure 5.12. The data in Figure 5.8 converted to instantaneous phase. The thin black line passing through the center of each white phase zone shows where the phase function undergoes a 360° wrap-around when the phase function cycles through the 0° value. This helpful phase surface is automatically provided by the Landmark software used to interpret the Boonsville 3-D seismic data.

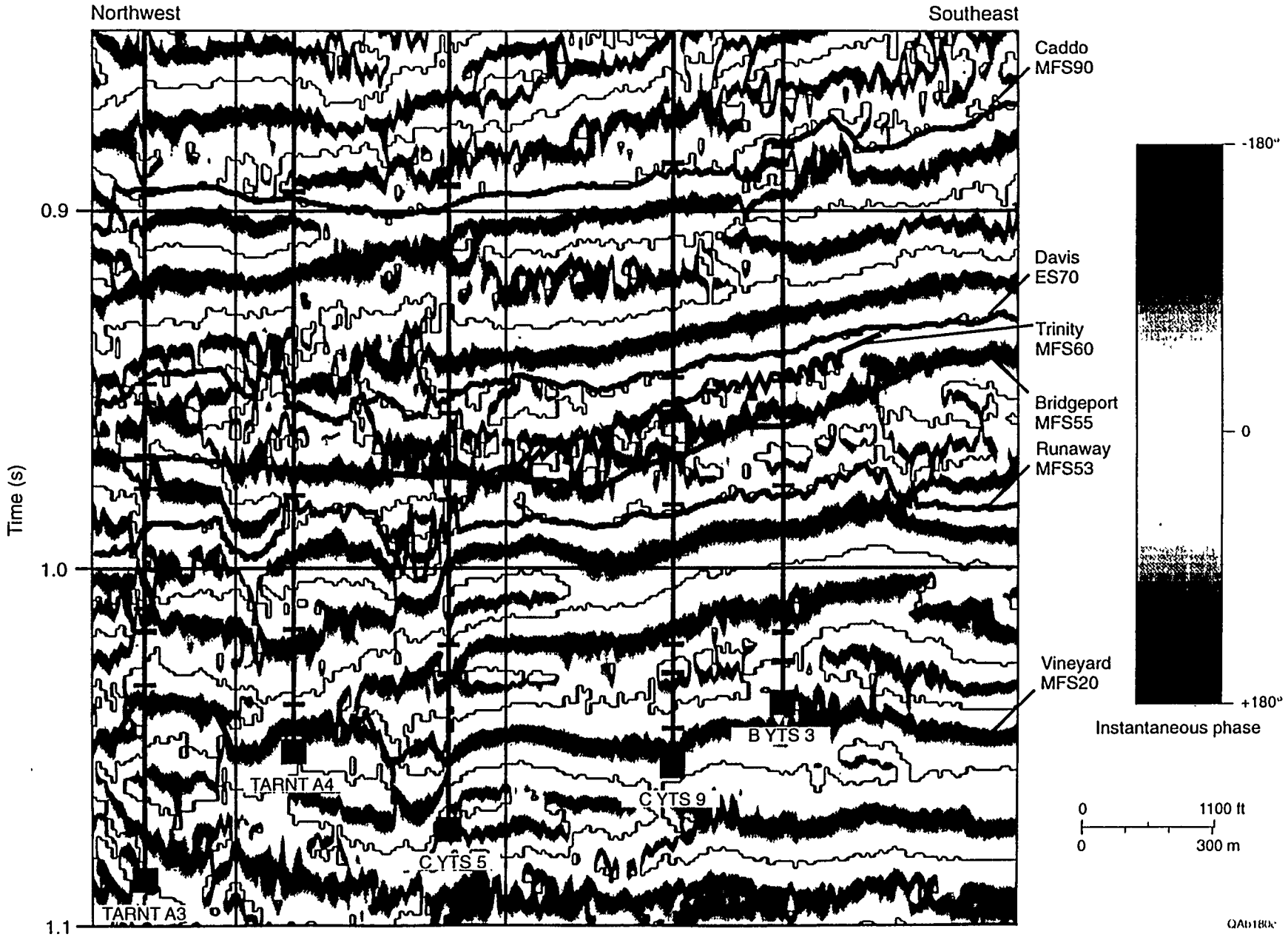

Figure 5.13. The data in Figure 5.9 converted to instantaneous phase. Note that the Davis and Runaway surfaces that bracket the Trinity sequence follow a constant phase surface, but the Trinity boundary is located in a time window where the phase attribute has a highly erratic behavior.

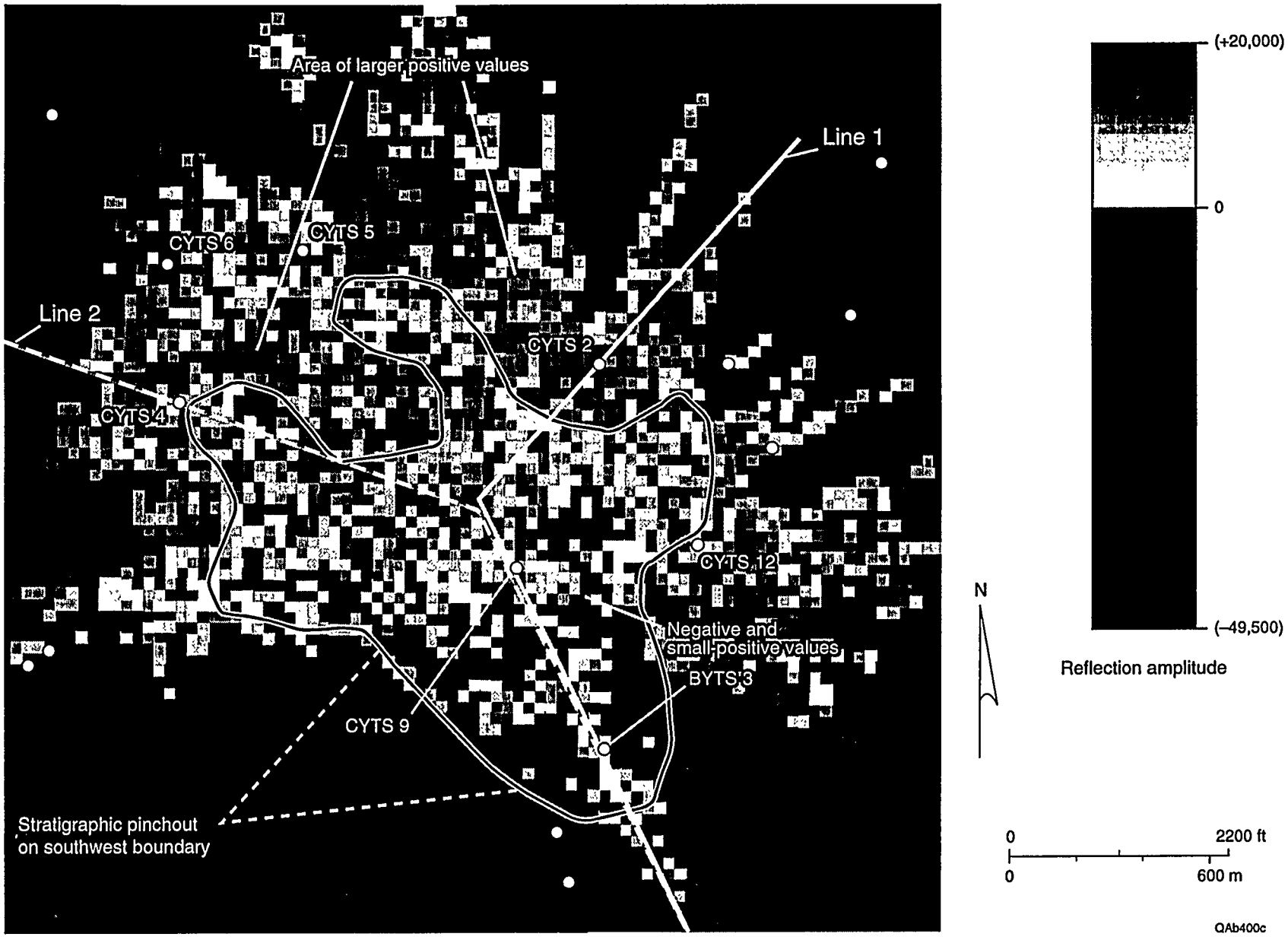

Figure 5.14. Reflection amplitude behavior on the interpreted Trinity surface near the C Yates 9 well. This is a black-and-white copy of a color display. The heavy outline encloses an area of approximately 300 acres, where the reflection amplitude is either positive or negative, but always of quite low amplitude. Outside of this boundary, the reflection amplitudes are positive and have relatively high amplitudes. Seismic reflection profiles along Line 1 and Line 2 are displayed as Figures 5.16 and 5.17.

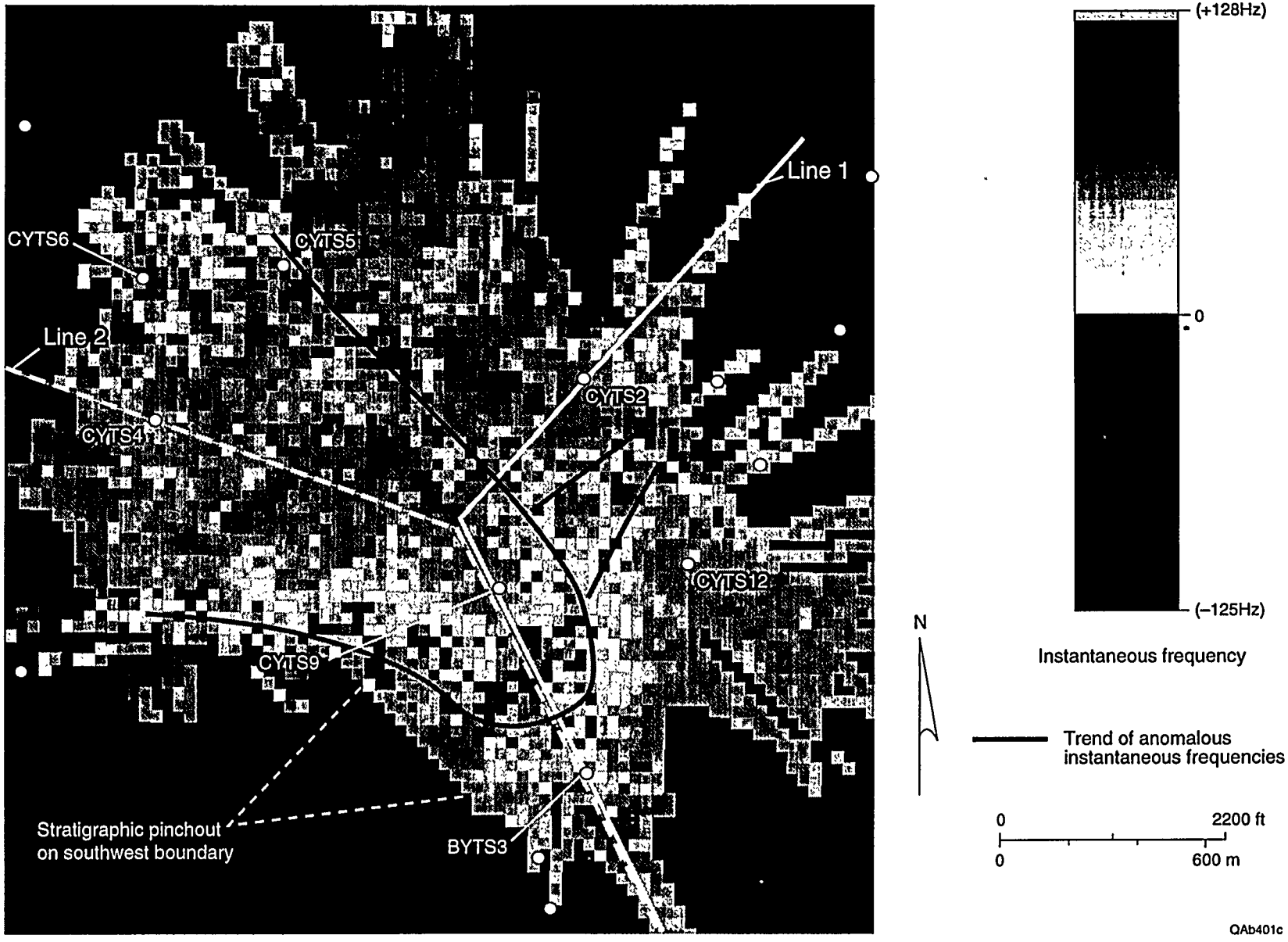

Figure 5.15. Instantaneous frequency behavior on the interpreted Trinity surface near the C Yates 9 well. The thick, dark lines trace trends where there are negative frequency values, which indicate trends where the reflection waveform is distorted. Such distorted waveforms often imply compartment boundaries, but if that interpretation rule is invoked here, the Trinity reservoir covers an area only slightly greater than 100 acres, which does not agree with the production data. Thus, the reservoir size implied by the amplitude image (Fig. 5.14) agrees more closely with the size implied by the production performance. Seismic reflection profiles along Line 1 and Line 2 immediately follow.

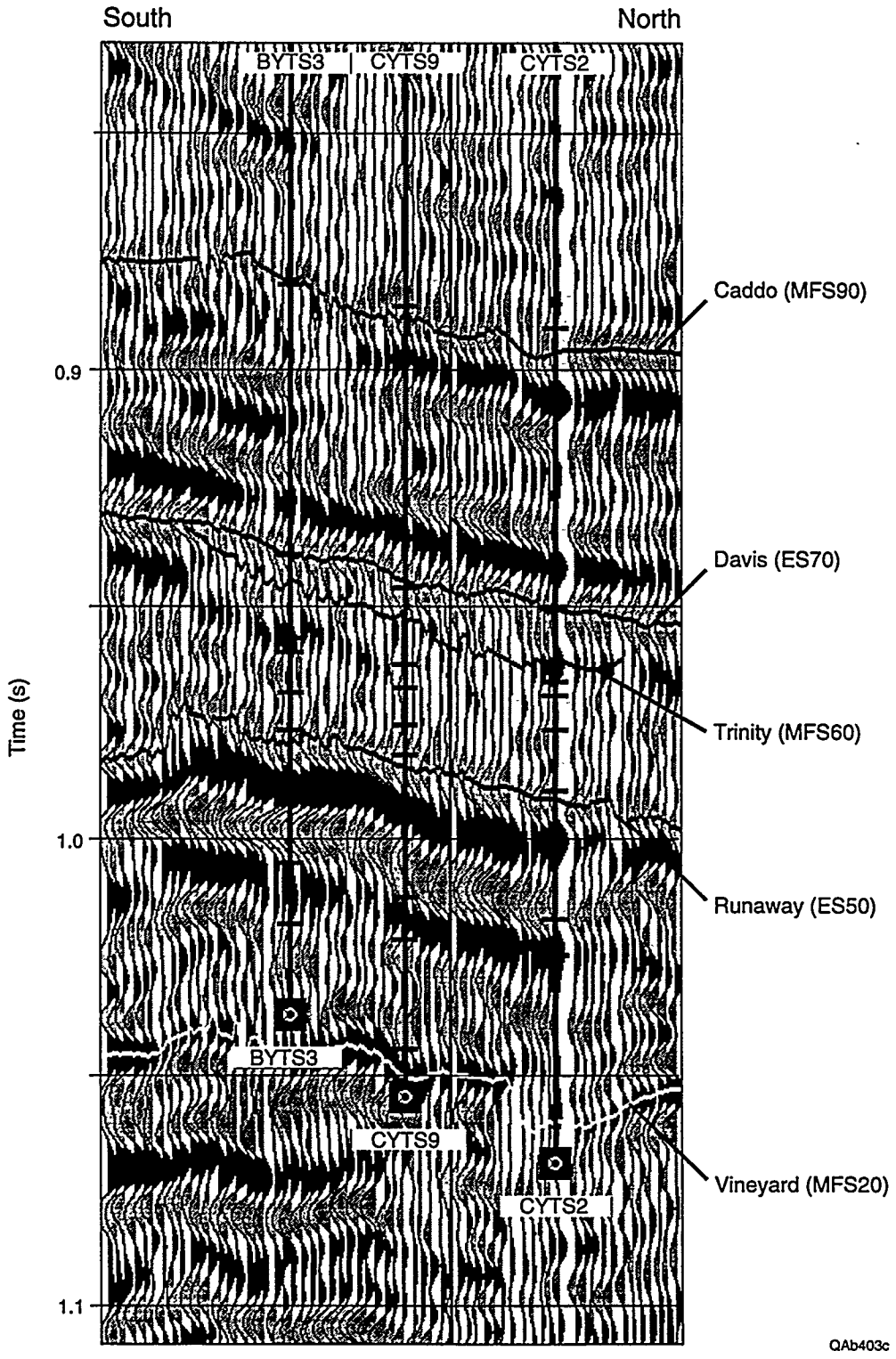

Figure 5.16. Reflection profile along Line 1. Note that the Trinity surface is essentially invisible in a seismic sense in the interval from near the BYTS3 well to near the CYTS2 well. To the right of the CYTS2 well (toward the northeast), the Trinity surface follows a positive peak of reasonable amplitude.

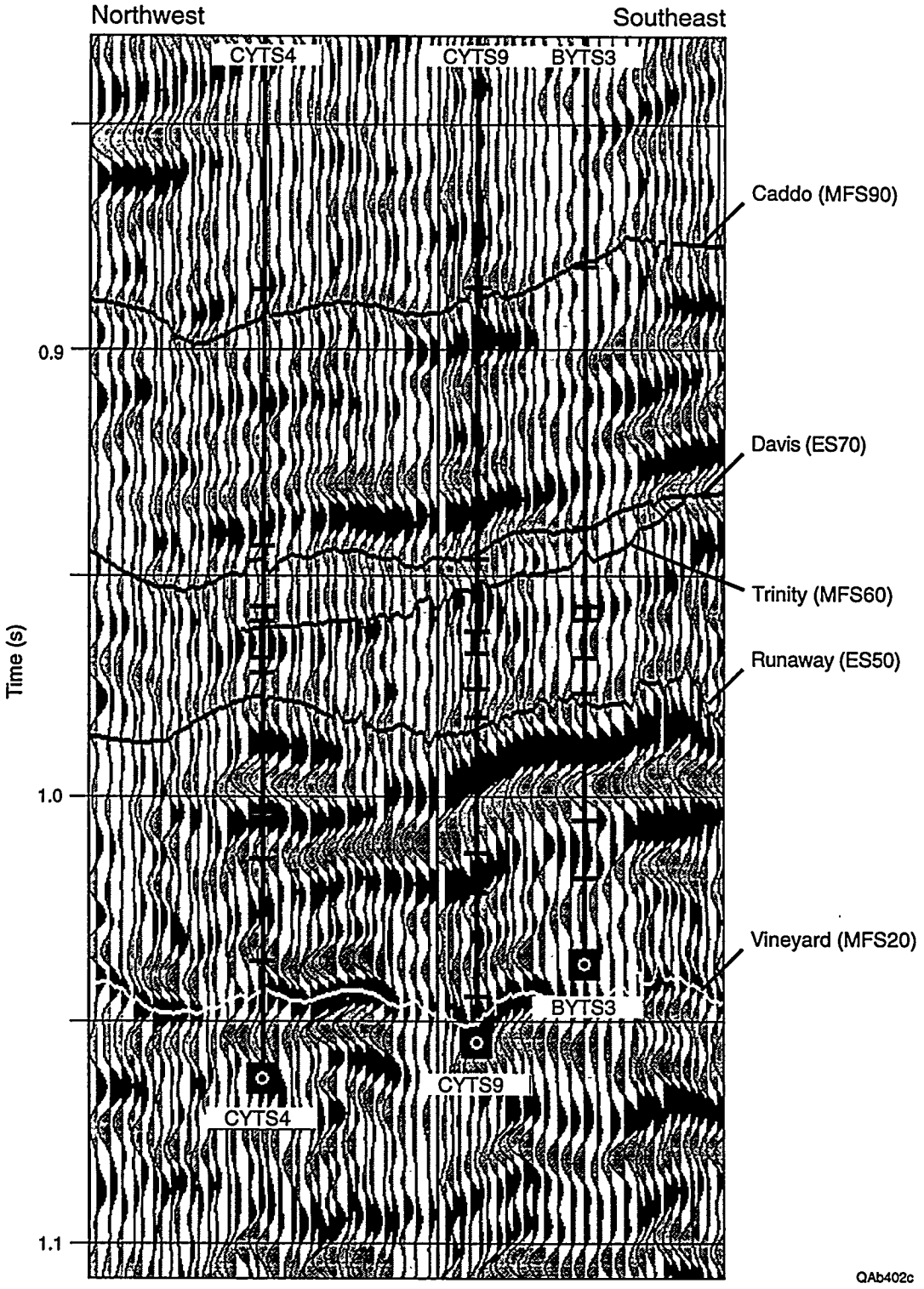

Figure 5.17. Reflection profile along Line 2. Again, the Trinity surface along much of this profile is a trend of low-amplitude responses of variable waveshapes that have either positive or negative amplitudes, which indicates a low reflection signal that is contaminated by noise and by interference from nearby reflecting surfaces.

6. SITING BOONSVILLE DEVELOPMENT WELLS—CASE HISTORIES

Two wells, the B Yates 17D and 18D, were drilled inside the 26-mi^2 Boonsville 3-D seismic survey area shortly after interpretation of the seismic data was initiated, but before 3-D interpretation was completed and properly integrated with the geologic and engineering control. There are numerous reasons why a drilling program must be started before a prospect is fully interpreted, so the urgency to select drill sites for the B Yates 17D and 18D wells before a detailed Bend Conglomerate stratigraphic model was constructed is typical of situations that confront many operators.

B Yates 18D

Figure 6.1 shows the location of the B Yates 18D well in the central part of the project area. This well was drilled by Threshold Development in November and December 1994 and is the first of several infill development wells that Threshold has planned in the immediate project area. The B Yates 18D was the first well drilled in the project area following collection of the 3-D seismic data.

Figure 6.2 presents an expanded view of the B Yates 18D location and the surrounding wells. Of the two closest wells, the B Yates 4 did not penetrate the Bend interval, and the B Yates 1 was drilled in the late 1940's, found gas, but was abandoned owing to a lack of market and pipeline facilities at the time. The other nearby wells produce from a variety of intervals from the Caddo through the Vineyard.

Briefly reviewing the completion history of the wells offsetting the B Yates 18D location, the B Yates 2 was initially completed in the Lower Jasper Creek in 1950 but did not produce much gas. This well was tested unsuccessfully in the Vineyard in 1956 but then recompleted successfully in the Runaway shortly thereafter. The B Yates 2 has produced over 1.1 Bscf from the Runaway interval and is still actively producing.

The B Yates 3 produced in excess of 3.4 Bscf from the Middle and Lower Jasper Creek from 1951 through 1992. In 1992, the well was recompleted in the Trinity, Runaway, and Upper Jasper Creek sequences, but these intervals have not contributed much, if anything, to the overall production from the well.

The B Yates 7 is one of the best Vineyard wells in the project area, producing over 5.7 Bscf. That interval is now abandoned, and the well has recently been recompleted in the Middle and Lower Jasper Creek. These zones were partially drained when recompleted, apparently from the B Yates 3 but are still producing about 200 Mscf/d.

The B Yates 13 was drilled and completed in the Vineyard in 1984. Despite being substantially drained at this location and finding only 457 psi bottomhole pressure in the Vineyard, the well has still produced about 350 MMscf to date. The B Yates 15 was drilled and completed in the Trinity, Middle and Lower Jasper Creek, and the Vineyard in 1985. The well has produced 544 MMscf from the combined intervals.

The I. G. Yates 3 was completed in the Trinity, Bridgeport, and Vineyard intervals in 1958. It is one of the best wells in the project area, producing in excess of 5.4 Bscf from these commingled zones. The I. G. Yates 32 was drilled to the Lower Caddo in 1992. This well found a bottomhole pressure of 618 psi, indicating significant depletion in the Lower Caddo. The I. G. Yates 32 was oil productive and was converted to a water injection well as part of a Lower Caddo waterflood project being conducted just to the southeast of the area shown in this figure.

From a review of the offsetting production history and the distribution of net pay and net hydrocarbon in the vicinity, Table 6.1 provides the projected reservoir conditions expected at the B Yates 18D location prior to drilling. Less than 5 ft of pay was expected in the Caddo, and the interval was expected to have poor reservoir quality and limited productive potential. Only 2 to 3 ft of net pay was anticipated in the Wizard Wells; this interval was expected to exhibit poor reservoir quality. There was no sand development projected in the Davis sequence.

Table 6.1. Reservoir conditions projected at B Yates 18D location based on offset well data.

Interval	Net pay (ft)	Projected reservoir conditions
Caddo	<5	Poor reservoir quality, limited productive potential
Wizard Wells	2–3	Very poor reservoir quality, no potential
Davis	0	No sand development
Trinity	5–6	Low permeability, limited potential, depletion from B Yates 15
Bridgeport	0–1	Almost no sand development
Runaway	2–3	Limited sand development, drained by B Yates 2
Beans Creek	0	No sand development
U Jasper Creek	0	No sand development
M Jasper Creek	5–6	Partial depletion from B Yates 3, 15?
L Jasper Creek	7–8	Partial depletion from B Yates 3, 15?
Vineyard	30–35	Substantial depletion from B Yates 7, 13, 15

The Trinity sequence looked as though it might encounter 5 to 6 ft of net pay, but this interval appeared to be low permeability. In addition, there was also the likelihood of some depletion from the B Yates 15 well to the east. There was almost no sand development expected in the Bridgeport, and only 2 to 3 ft of net pay projected in the Runaway. In addition, any pay in the Runaway was expected to be substantially drained by the B Yates 2 well to the northeast. There did not appear to be any sand development in the Beans Creek or the Upper Jasper Creek at the B Yates 18D location.

About 6 to 8 ft of net pay was expected in both the Middle and Lower Jasper Creek intervals. It appeared likely, however, that the Jasper Creek reservoirs at this location could be at least partially drained by Jasper Creek gas production from the B Yates 3 and 15 wells. Finally, some 30 to 35 ft of net pay was projected in the Vineyard. There was no doubt that a thick Vineyard interval would be found, but it was expected to be substantially depleted by gas production from the B Yates 7, 13, and 15 wells.

All in all, from an engineering and geological perspective, the B Yates 18D location appeared to offer multiple completion possibilities, but the degree of pressure depletion or reservoir quality to be expected in any particular sequence was somewhat uncertain. The location was, in fact, in a favorable part of the project area where at least four net pay

intervals with a total of at least 1.5 net hydrocarbon feet were expected between the Lower Caddo and the Vineyard (see Figures B19 and B20 in Appendix B). Ultimately, however, the B Yates 18D location was chosen primarily from the 3-D seismic information.

One objective that Threshold Development hoped to achieve with the B Yates 18D was to locate an uncontacted Caddo reservoir. Thus, a dual-objective, seismic interpretation approach was employed in the short time allowed to locate possible drill sites: the primary objective being to find a Caddo seismic image that was a look-alike to the seismic image at a known productive Caddo reservoir, and the secondary objective being to ensure that attractive trapping geometries existed within several Bend Conglomerate sequences below any productive Caddo look-alike that could be found.

The distinctive seismic response associated with the productive Caddo reservoir penetrated by the Mitchell J. M. Robinson A5 well was selected as the look-alike target that was kept in mind while reviewing the Caddo reflection response over the entire 26-mi^2 survey area. The reflection character at the Robinson A5 well is illustrated in Figure 6.3a. A Caddo seismic response much like the one occurring at the Robinson A5 well was found at crossline-inline coordinates 151, 111 and is presented in Figure 6.3b. This 3-D seismic coordinate point, which is where the B Yates 18D well was drilled, thus satisfied the primary objective for a drilling site—that an attractive Caddo drilling target existed at the location. The secondary drilling objective—that the site also had additional attractive Bend Conglomerate targets—was also satisfied as is documented in Figure 6.4. This seismic section passing through the well coordinates shows that a vertical sequence of potential reservoir entrapments, consisting either of pinch-outs or small-throw faults, was stacked throughout the Bend interval at the B Yates 18D location.

Caddo Facies

Even though the Caddo seismic response at the B Yates 18D well site resembled the seismic response at the productive Robinson A5 well, the Caddo facies found by the B Yates 18D well was not productive. Logs from the Robinson A5 and from the B Yates 18D wells are compared in Figure 6.5 and show that the Caddo response at the B Yates 18D location is caused by two thin limestone units, not by a productive sand as at the Robinson A5. (The B Yates 18D well log data are presented in more detail in Figures 6.6, 6.7, and 6.8.) The discrepancy between the depositional facies at these two Caddo seismic look-alikes illustrates a principle known by all experienced seismic interpreters—seismic responses are not unique, and often two or more stratigraphic relationships can produce the same seismic response. Thus, even though the search for look-alikes to the seismic response at a known productive reservoir is a sound and rather widely practiced procedure for identifying potential drill sites, the technique does involve an element of risk, as it did in this Caddo situation.

Well Operations

The B Yates 18D was drilled to a total depth of 5,750 ft through the Vineyard. As discussed earlier, the Lower Caddo sand was not developed as suggested by the initial seismic interpretation, but the Trinity, Jasper Creek, and Vineyard sequences were present much as expected. In addition, there was some sand development in the uppermost part of the Jasper Creek that had not been anticipated. The most encouraging feature encountered in the B Yates 18D was the development of a 20-ft sand in the upper part of the Runaway sequence. This sand was not (and really could not have been) predicted from the available engineering or geologic data available prior to drilling this well.

Figure 6.6 presents the upper section of the open-hole well logs recorded in the B Yates 18D. The logs shown in the figure include the SP, gamma-ray, deep-resistivity, neutron, density, microlog, and RFT tools. The section shown in Figure 6.6 includes the Caddo and the upper part of the Wizard Wells. As the logs indicate, there was no sand development in the Caddo and almost no porosity. The Caddo was not a productive interval, and, as expected, neither was the Wizard Wells sequence.

Figure 6.7 shows the open-hole logs recorded across the Trinity, Bridgeport, Runaway, and part of the Beans Creek sequences. As expected, the Trinity interval had 4 to 5 ft of net pay; notice the crossover in both the porosity logs and the microlog. Two attempts were made to measure pressures with an RFT in this interval. The behavior of the tests suggested that the zone is tight. One test did record a pressure of 310 psi, although pressure was still building when the test was concluded after about 15 minutes. This low measured pressure may suggest depletion from the Trinity reservoir in the B Yates 15, but it more likely indicates a lower permeability interval in the Trinity and insufficient time for the pressure to build up completely.

In the Runaway sequence, the 2 to 3 ft of lower sand was what had been expected. RFT's run in this interval suggest that this sand is tight. As mentioned previously, however, what was not anticipated was the 20 ft of sand encountered in the upper part of the Runaway. Qualitatively, according to the logs, this Upper Runaway sand has good gas effect on the porosity logs, and the microlog indicates that the reservoir is permeable. The RFT measured a pressure of 1,685 psi in this interval after about 20 minutes. This is as high a pressure as any ever recorded in the project area in the Runaway sequence. This sand appeared to be an isolated Runaway reservoir at original reservoir pressure.

Figure 6.8 shows the open-hole logs recorded across the Jasper Creek and Vineyard sequences. All three Jasper Creek intervals should be productive, but the Upper and Middle Jasper Creek appear to have the best reservoir quality. The pressures measured with the RFT of 2,113 and 2,075 psi in the Middle and Lower Jasper Creek, respectively,

are essentially original pressure, suggesting no drainage of gas at this location. Because the pressure of 1,354 psi recorded in the Upper Jasper Creek was still building at the rate of several psi/min when the RFT was concluded, it should be considered only a lower-bound estimate of the current reservoir pressure. Even so, this pressure would indicate only partial drainage from the Upper Jasper Creek at this location at best. As mentioned previously, however, sand development in the Upper Jasper Creek was not anticipated in the B Yates 18D, because this sequence is not encountered in nearby offsetting wells. Thus, if the Upper Jasper Creek has been partially drained, it is not clear where the communication exists; geologically, this sequence appears to be isolated at this location.

Finally, Figure 6.8 shows that the Vineyard has 25 to 30 ft of net pay as expected and that the reservoir is substantially depleted at this location, as indicated by the 456 psi pressure in the interval measured with the RFT. Although the pressure in the Vineyard is far below its original value, it should be remembered that this is the thickest, best connected, most productive gas producing interval in the project area. Thus, depending on the reservoir pressure level in the Vineyard reservoir surrounding this well location and the effective drainage area, this zone may still contribute as much as 150 to 200 MMscf (or more) to the total gas recovery from this well. Note that the B Yates 13 well (Figure 6.2) recorded an initial pressure of 457 psi in the Vineyard in 1985 and has produced in excess of 350 MMscf from the Vineyard reservoir alone since then. The Vineyard is neither compartmented nor poorly drained at this location, but it still may be an important completion interval in this well from the standpoint of ultimate gas recovery.

In summary, the B Yates 18D did not encounter an isolated Caddo compartment as anticipated, but it did find at least four intervals that encountered original or near original pressure in the Runaway and Jasper Creek sequences. All in all, including the Vineyard interval, there may be as many as 5 to 6 viable completion zones in this well. The key to

the successful long-term performance of this well, however, will be the size of the gas reserves associated with these compartments or poorly drained areas.

Reservoir Analysis

Initially, Threshold elected to complete only the Upper Runaway sand from 5,317 to 5,331 ft. The zone was treated with 1,250 gal of acid and fractured with about 22,000 gal of nitrogen foam and 34,000 lb of sand. The well was produced for about 1 mo, and then shut in for a 2-week pressure buildup test.

The initial Runaway production from the B Yates 18D is shown in Figure 6.9. The well came on line producing about 1.4 MMscf/d, but both the flow rate and the flowing tubing pressure declined rapidly during the first month. The flow rate prior to shut-in for the well test was 420 Mscf/d. Cumulative gas production prior to the well test was about 20 MMscf.

Figures 6.10 and 6.11 present the well test results, which indicate that the Upper Runaway interval is a very small reservoir. As shown in the figures, the bottomhole pressure built up to only about 650 psia after 2 weeks of buildup and was beginning to level off. A quantitative analysis of the test data yields an average reservoir pressure of 720 psia. The initial reservoir pressure, as measured with the RFT, was at least 1,685 psia. Thus, the reservoir pressure had apparently declined more than 1,000 psi after only about 20 MMscf of gas was produced. This suggest a reservoir size of about 8 acres.

Figure 6.11 shows a log-log plot of the pressure change and pressure derivative for this well test. In this figure, adjusted pressure change versus adjusted equivalent time (Al-Huissnay, 1966; Agarwal, 1979, 1980; Lee, 1986) is plotted. The upper curve is the pressure data, and the lower curve is the derivative data. What these plots show are very early wellbore storage effects, followed by a period of bilinear flow, indicative of a finite conductivity hydraulic fracture. At an adjusted equivalent time of about 0.2 h, boundary effects are first observed in the test data. In this case, the boundaries appear to be the

side(s) of a channel. Ultimately, near the end of the test, both the pressure and the pressure derivative begin to decrease, and the derivative data roll over and start to decline. This behavior suggests that we have likely encountered all reservoir boundaries during the test.

Figure 6.11 also shows the results of a history-match of the actual test data generated using a finite-difference reservoir simulator and the reservoir description shown in Figure 6.12. The reservoir description used to match the test data consists of a long, narrow channel that widens somewhat away from the well. The channel is only about 90 ft wide near the wellbore. The total areal extent of the reservoir is just more than 8 acres. Whereas this is a reasonable model for the test data, it is not unique, and other, similar reservoir descriptions may fit the data equally well. Even so, a small reservoir size and a near-well boundary are features that must be included in any reasonable interpretation of the test data. The model presented here fits well with the geologic interpretation of the Upper Runaway reservoir in this vicinity.

Following the well test, the B Yates 18D was returned to production. As a result of the pressure buildup in the reservoir, the well came back on line making 1.05 MMscf/d. The flow rate declined quite rapidly, however, as shown in Figure 6.9, and within a matter of days, the well was producing at rates below those prior to the well test. Threshold produced the Upper Runaway reservoir for about another month following the well test, and in that time, the well recovered another 10 MMscf of gas. Finally, in mid-April, after producing only about 30 MMscf, Threshold abandoned the Upper Runaway, and recompleted the well in the three Jasper Creek intervals, commingling the production from all three zones.

Figure 6.13 shows the first few weeks of production from the Jasper Creek reservoirs; these results look somewhat more encouraging. The combined production from the Jasper Creek intervals was in excess of 1 MMscf/d initially, and these zones are currently flowing about 600 Mscf/d, with little decline in flowing tubing pressure.

Cumulative production from these Jasper Creek reservoirs is approximately 40 MMscf after only 7 weeks on line.

B Yates 17D

Figure 6.14 shows the location of the B Yates 17D well in the west-central part of the project area. The B Yates 17D well was drilled about 1 mo after the B Yates 18D, and like the B Yates 18D, the B Yates 17D was sited at a location (crossline, inline coordinates = 171, 53) where there appeared to be a vertical sequence of several stratigraphic and structural entrapments throughout the Bend Conglomerate interval (Fig. 6.15). From a seismic standpoint, the primary targets were the Trinity and the Jasper Creek, where the 3-D seismic data suggested possible isolation from offsetting gas production.

Figure 6.16 presents an expanded view of the B Yates 17D location and the surrounding wells. Briefly reviewing the completion history of the wells offsetting the B Yates location, the B Yates 8 and 9 wells were drilled in 1957 and completed as oil wells in the Upper Caddo. Neither well penetrated the Bend intervals below the Caddo. The B Yates 8 well produced 70,000 STB of oil from the Upper Caddo through July 1979; the well is currently completed as a gas well in the Strawn sands up-hole. The B Yates 9 made 110,000 STB of oil from the Upper Caddo through December 1989; currently, this well is also producing from the Strawn sands up-hole.

The B Yates 10 was initially completed in the Vineyard, producing 3.43 Bscf from April 1958 through June 1980. From June 1980 through June 1993, this well was completed and commingled in the Davis, Trinity, and Beans Creek reservoirs, producing a total of 210 MMscf of gas and about 6,000 STB of oil–condensate from the three zones combined. In July 1993, this well was recompleted to the Strawn sands.

The B Yates 12 was drilled in September 1983 and initially completed in the Vineyard, Middle Jasper Creek, and Runaway zones. The Vineyard interval did not

produce much gas after fracturing and was subsequently isolated below a bridge plug in May 1984. The Middle Jasper Creek and Runaway intervals were produced together, making a total of only about 90 MMscf. In February 1990, perforations were added in the Trinity, Beans Creek, and Lower Jasper Creek sequences. All five zones were commingled, and the well recovered another 45 MMscf through August 1992. The well has been shut in since then.

The B Yates 6 well was drilled in July 1957 and produced 1.44 Bscf from the Vineyard through December 1979. The Vineyard perforations were abandoned, and the well was recompleted in the Bridgeport and Runaway intervals. These zones are still producing commingled at 30 Mscf/d and have made about 440 MMscf to date.

The B Yates 11 well was drilled in July 1971 and completed in the Vineyard with an initial bottomhole pressure of 938 psi, indicating prior depletion in the Vineyard at this location. This well is still producing from the Vineyard at about 30 Mscf/d; it has recovered about 900 MMscf of gas to date. The Dallas Royalty Swetnam 1 was completed in the Trinity in April 1973. It was originally classified as an oil well and has been a marginal producer. The well is currently making about 10 Mscf/d.

From a review of the offsetting production history and the distribution of net pay and net hydrocarbons in the area, the B Yates 17D location appeared to offer multiple completion opportunities. As with the B Yates 18D well, the B Yates 17D location was also in a favorable part of the project area where at least four net pay intervals were expected between the Lower Caddo and the Vineyard. Reservoir-quality sand development was anticipated in the Trinity, Bridgeport, Runaway, and Jasper Creek sequences prior to drilling, but the degree of pressure depletion or reservoir quality in any particular sequence was not certain. Reservoir-quality sands were also anticipated in the Upper Caddo and Vineyard sequences, but both these intervals were expected to be substantially depleted by offsetting production.

The B Yates 17D was drilled to a total depth of 5,650 ft through the Vineyard. From an analysis of the openhole logs run in the Bend interval, potential completion opportunities were identified in the Trinity, Runaway, and Lower Jasper Creek sequences. There was some sand development observed in the Lower Jasper Creek and Bridgeport sequences as well, although not enough for these zones to be viable completion targets. Most of these sands were thin (less than 10 ft), with fairly low porosity (5 to 7 percent). The prolific Upper Caddo reservoir present in the B Yates 8 and 9 wells was not found in the B Yates 17D; rather, the Upper Caddo is mostly limestone at this location. The Vineyard reservoir was present and substantially depleted (reservoir pressure of 500 psi) as expected.

RFT pressures were measured on only two intervals in this well, the Vineyard and the Lower Jasper Creek, because of problems with the tool itself. Lost circulation materials were added to the mud system in this well to combat a lost circulation problem encountered while drilling through the Vineyard. Due to this lost circulation material in the wellbore, the RFT tool plugged frequently and would not seat on occasion. The tool was removed twice from the wellbore to clean it and resume testing, but each time, it plugged again quickly after being run back in the hole.

The only RFT value considered reliable from this well was the first test conducted in the Vineyard interval, which yielded a pressure of 500 psi. RFT pressures of 2,384 and 2,596 psi were measured in the Lower Jasper Creek interval, but these values do not appear to reflect actual reservoir pressure. First, these pressures are much higher than the values of 1,900 to 2,100 psi generally associated with initial pressure in the Jasper Creek sequence in the project area (depending on depth). Further, considering that (1) the lower pressure of 2,384 psi was still increasing about 20 psi/min when the test was concluded and (2) the hydrostatic pressure of the mud column was about 2,630 psi at this depth

(5,500 ft), it appears the tool was leaking and that these pressures reflect hydrostatic head and not the reservoir pressure in the Lower Jasper Creek. Unfortunately, because of the problems with the RFT tool, it was not possible to conclude whether most of the potential Bend reservoirs are isolated compartments or are in communication with production from offset wells.

Initially Threshold elected to complete only the Lower Jasper Creek sand from 5,496 to 5,502 ft in mid-January 1995. Figure 6.17 is an interpreted log across the Jasper Creek intervals in the well. The Lower Jasper Creek has 6 ft of net pay, with a porosity of 7.2 percent and a water saturation of 43.4 percent. This zone was hydraulically fractured with about 19,000 gal of fluid and 31,000 lb of 20/40 Ottawa sand. Following the treatment, the well was swabbed and cleaned up for several days; then it began flowing about 200 Mscf/d at 80 psi tubing pressure on a 20/64-inch choke. The well was put on production several days later making 250 Mscf/d against 60 psi flowing tubing pressure, producing into a compressor.

Figure 6.18 shows the early production from the Lower Jasper Creek interval. In the first few months of production, the B Yates 17D well has averaged between 150 and 250 Mscf/d. The periodic declines in flow rate are due to liquid loading in the wellbore; the well makes 1 to 2 bbl of condensate periodically. When the liquids are swabbed from the wellbore, the flow rate jumps back up to about 250 Mscf/d. Threshold has recently installed a plunger lift in this well to keep the wellbore fluids lifted on a regular basis.

The B Yates 17D was shut in for a 2-week pressure buildup test in mid-May 1995. The final flow rate prior to shut-in was 140 Mscf/d at a flowing bottomhole pressure of 414.3 psi. The Lower Jasper Creek reservoir had produced about 20 MMscf of gas prior to the well test.

Figure 6.19 is a log-log plot of the pressure buildup test data, with adjusted pressure change plotted vs. equivalent adjusted time (Al-Huissany, 1966; Agarwal, 1979, 1980; Lee, 1986). The upper curve is the actual pressure change data, whereas the lower curve

is the pressure derivative. The buildup test data were matched to a type curve developed by Cinco and others (Cinco and Samaniego, 1981) for analyzing wells with finite conductivity hydraulic fractures. This type curve is usually best when analyzing test data from hydraulically fractured wells with moderate permeability, as was the case for this Lower Jasper Creek reservoir.

The "hump" observed early in the test data (at an equivalent adjusted time of about 0.1 h) is most likely due to phase segregation (Fair, 1981); at this point, the pressure in the wellbore had built up sufficiently to force any liquid accumulated at the bottom of the hole back into the formation. Beyond this point, the test data match the type curve well, and the later-time data exhibit pseudoradial flow, suggesting that a straight line should develop on the semilog plot, whose slope can be used to calculate permeability. In addition, the type curve analysis shows no indications of reservoir boundaries being encountered during the test.

Figure 6.20 shows the semilog (Horner) plot of the test data (Horner, 1951). Using the slope of the straight line identified in the figure, a permeability of 3.6 md was calculated, using the net pay of 6 ft computed for the Lower Jasper Creek reservoir. This analysis also yielded an apparent skin factor (s') of –5.4, indicating successful stimulation of the formation by the fracture treatment. Extrapolating this semilog straight line to infinite shut-in time yields a pressure (p*) of 678 psi. This pressure should be a reasonable approximation of the current average reservoir pressure; the actual value for current average reservoir pressure depends on the actual reservoir size and geometry, but no attempt was made to assume any particular size or geometry and make that calculation.

The radius of investigation calculated at the end of this 2-week shut-in period was 1,232 ft. Because no reservoir boundaries were observed during the test, this reservoir should have a minimum areal extent of about 109 acres, assuming a circular drainage

area. The actual drainage area is larger that this, but the exact value cannot be determined from the available data.

Returning to the log-log analysis in Figure 6.19, a fracture half-length of 174 ft was calculated using the permeability of 3.6 md. In addition, a fracture conductivity of about 2,000 md-ft was computed. Both values were considered reasonable, given the size of the fracture treatment and the fact that sand was used as the proppant.

Overall the interpretation of the pressure buildup test data appears to be quite consistent with the well performance and the way the well was stimulated. Further, given the well's initial performance (150 to 250 Mscf/d at 60 psi tubing pressure), the calculated permeability of 3.6 md, an estimated current reservoir pressure of about 700 psi, and the fact that this reservoir has a drainage area in excess of 100 acres, the pressure at the time of completion in the Lower Jasper Creek must have been on the order of 750 to 800 psi. This adds further support to the conclusion that the RFT pressures of 2,400 and 2,600 psi did not reflect reservoir pressure in the Lower Jasper Creek.

A pressure of 750 to 800 psi in the Lower Jasper Creek at the time of completion, however, suggests that this interval was not isolated at this location, but, instead, is in communication with offsetting production. The closest well completed in the Lower Jasper Creek is the B Yates 12, about 1,000 ft to the northwest (see Figure 6.16). As mentioned previously, however, the B Yates 12 has been completed in the Trinity, Runaway, Vineyard, and Middle and Lower Jasper Creek intervals, with a total gas production of only 135 MMscf for all zones combined. The Trinity and Lower Jasper Creek perforations were added in 1990, and the well produced only about 45 MMscf after these zones were completed.

Because the contributions from the Lower Jasper Creek reservoir cannot be isolated, it is unclear whether there was sufficient production from this reservoir in the B Yates 12 to result in the degree of pressure depletion observed at the B Yates 17D location; however, due to the small volumes of gas produced from the Lower Jasper Creek, it

appears unlikely that the drainage observed at the B Yates 17D location could all be associated with gas production from the B Yates 12. This suggests that the Lower Jasper Creek reservoir at this location may be in communication with the B Yates 7 well or the prolific B Yates 3 well (3.4 Bscf from the Middle and Lower Jasper Creek) to the east, even though these wells are approximately 4,000 and 7,000 ft away, respectively.

On the basis of the interpretation of the test data, the ultimate gas recovery from this Lower Jasper Creek completion is projected to be about 75 to 100 MMscf, assuming the plunger lift equipment can successfully keep the liquids lifted from the borehole. Future completion attempts are expected in the Trinity, Runaway, and Vineyard sequences.

Lower Jasper Creek Reservoir

North-south and east-west seismic profiles through the B Yates 17D well, with the interpreted position of the Lower Jasper Creek sequence boundary identified, are shown in Figures 6.21 and 6.22, respectively. These profiles show that small-throw faults occur in several directions about the well site. When the Lower Jasper Creek sequence interpretation is extended laterally away from the well location, a continuous sequence boundary is created, which allows areal distributions of seismic attributes to be calculated within an accurately defined Lower Jasper Creek seismic time window. Two of the more diagnostic seismic attributes found at this site are instantaneous frequency and average reflection amplitude.

The instantaneous frequency behavior is plotted in Figure 6.23. This map shows that an almost continuous boundary of anomalous instantaneous frequencies encloses the B Yates 17D location. These anomalous frequency values start at a fault located between the B Yates 17D and B Yates 12 wells, extend north to the edge of the map, turn southeast and pass by the B Yates 6 well, then turn west along a fault system at the B Yates 11 well and pass just north of the B Yates 10 well. The B Yates 17D well appears to be sited just inside the southwest edge of the area encompassed by these

anomalous frequencies. Referring to the examples in Appendix E that illustrate how anomalous instantaneous frequency values pinpoint stratigraphic pinch-outs and/or faults, it is not unreasonable to assume that the closed, continuous boundary of anomalous frequencies described above possibly defines the areal size and shape of the Lower Jasper Creek reservoir found by the B Yates 17D well.

The reflection amplitude behavior associated with the Lower Jasper Creek sequence is displayed as Figure 6.24. This reflection strength attribute was derived by calculating the average positive reflection amplitude in a 16-ms window centered on the Lower Jasper Creek sequence boundary. The same fault systems occurring in the instantaneous frequency map (Fig. 6.23) are repeated in this average amplitude map. This display shows that the B Yates 17D well is located in the southwest corner of a dark (high amplitude) area that extends almost to the B Yates 12 and B Yates 11 wells. The areal extent of this amplitude anomaly is somewhat smaller than the area encompassed by the ring of anomalous instantaneous frequency values in Figure 6.23, and for the present, this amplitude map will be assumed to be the better estimate of size and shape of the Lower Jasper Creek reservoir compartment at the B Yates 17D well. This high-amplitude reflection area covers approximately 100 acres.

Analysis of the early well performance and the pressure buildup data described previously indicates that the Lower Jasper Creek reservoir at the B Yates 17D location is in communication with offsetting production. As mentioned previously, a possible source of some of this communication is the Lower Jasper Creek production from the B Yates 12 well. The seismic interpretation shown in Figures 6.23 and 6.24, however, indicates a fault between the B Yates 12 and the B Yates 17D wells in the Lower Jasper Creek, although it is unclear the degree to which this fault may isolate the Lower Jasper Creek in the two wells. Further, as Figure 6.24 shows, the area of high amplitude associated with the B Yates 17D location may also connect with an area of equally high amplitude to the east and north of the B Yates 11 well, toward the B Yates 3 well, which is a prolific

Jasper Creek completion. Although the B Yates 3 well is over 1 mi away, gas production from this well may be the primary source of the pressure depletion observed in the Lower Jasper Creek reservoir at the B Yates 17D location. The dimming in the amplitude response just north of the B Yates 11 well may simply indicate a thinning of the Jasper Creek reservoir that cannot be detected well with the 3-D data.

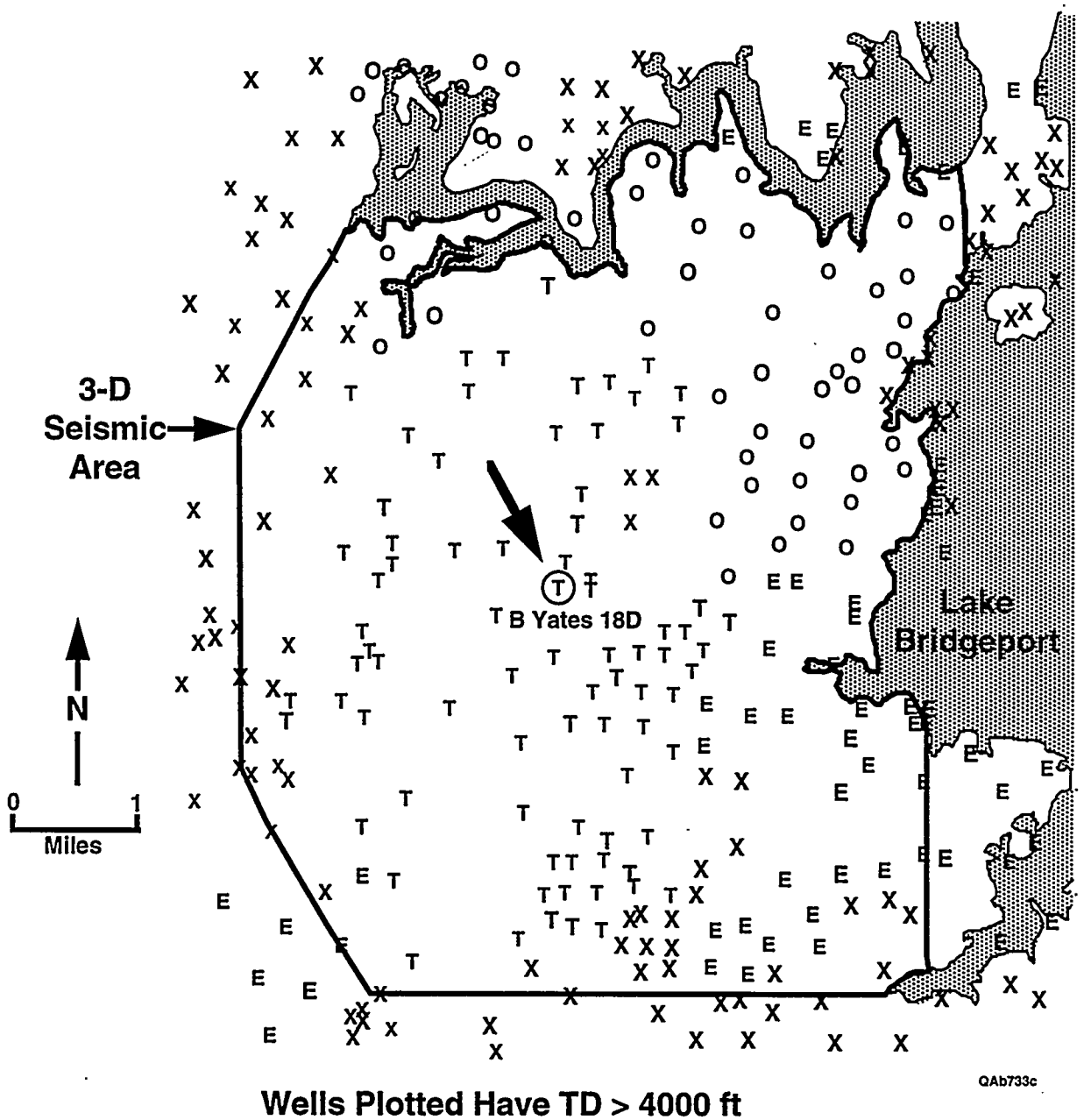

Figure 6.1. Location of the B Yates 18D well in the central part of the project area.

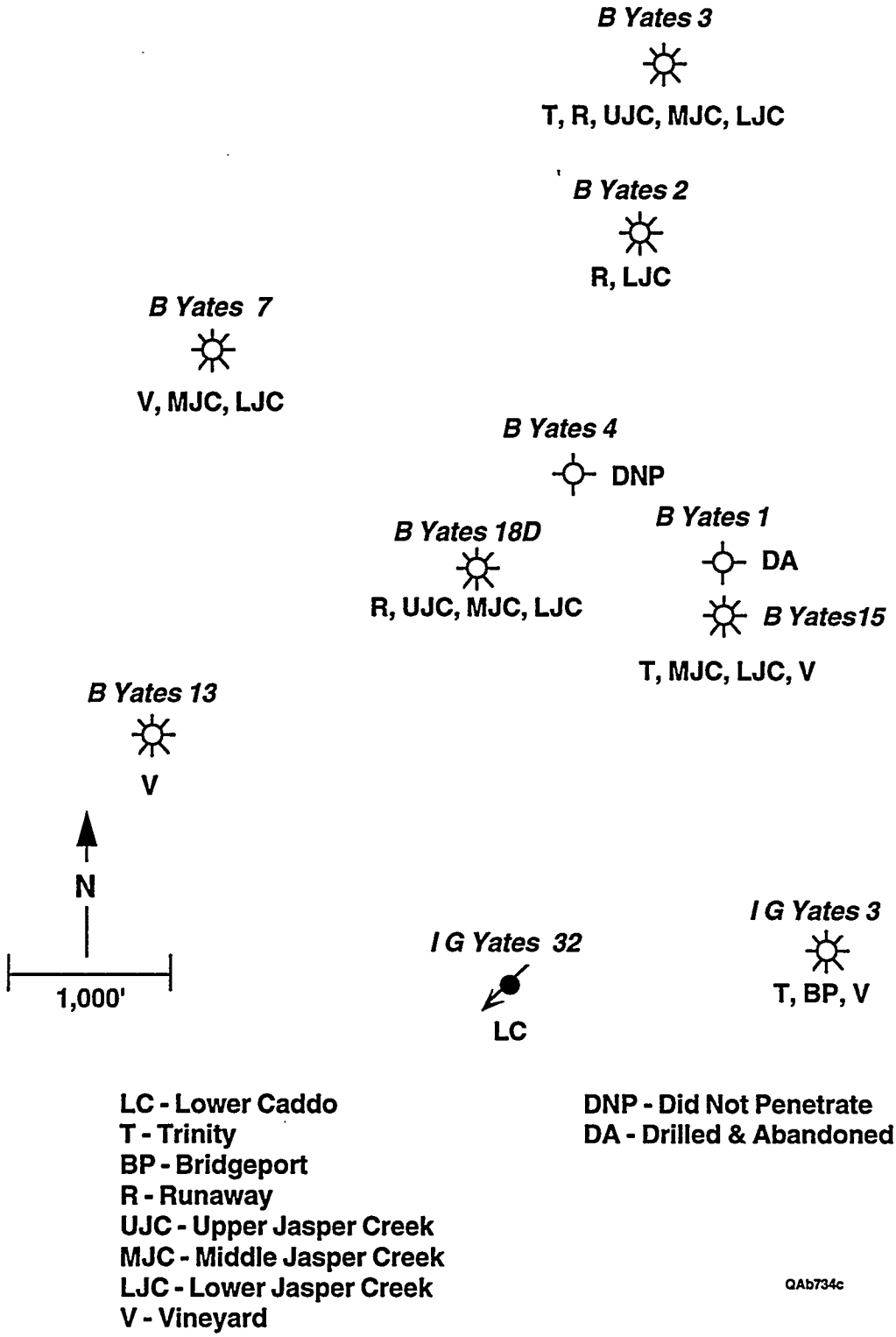

Figure 6.2. Expanded view of wells offsetting the B Yates 18D location.

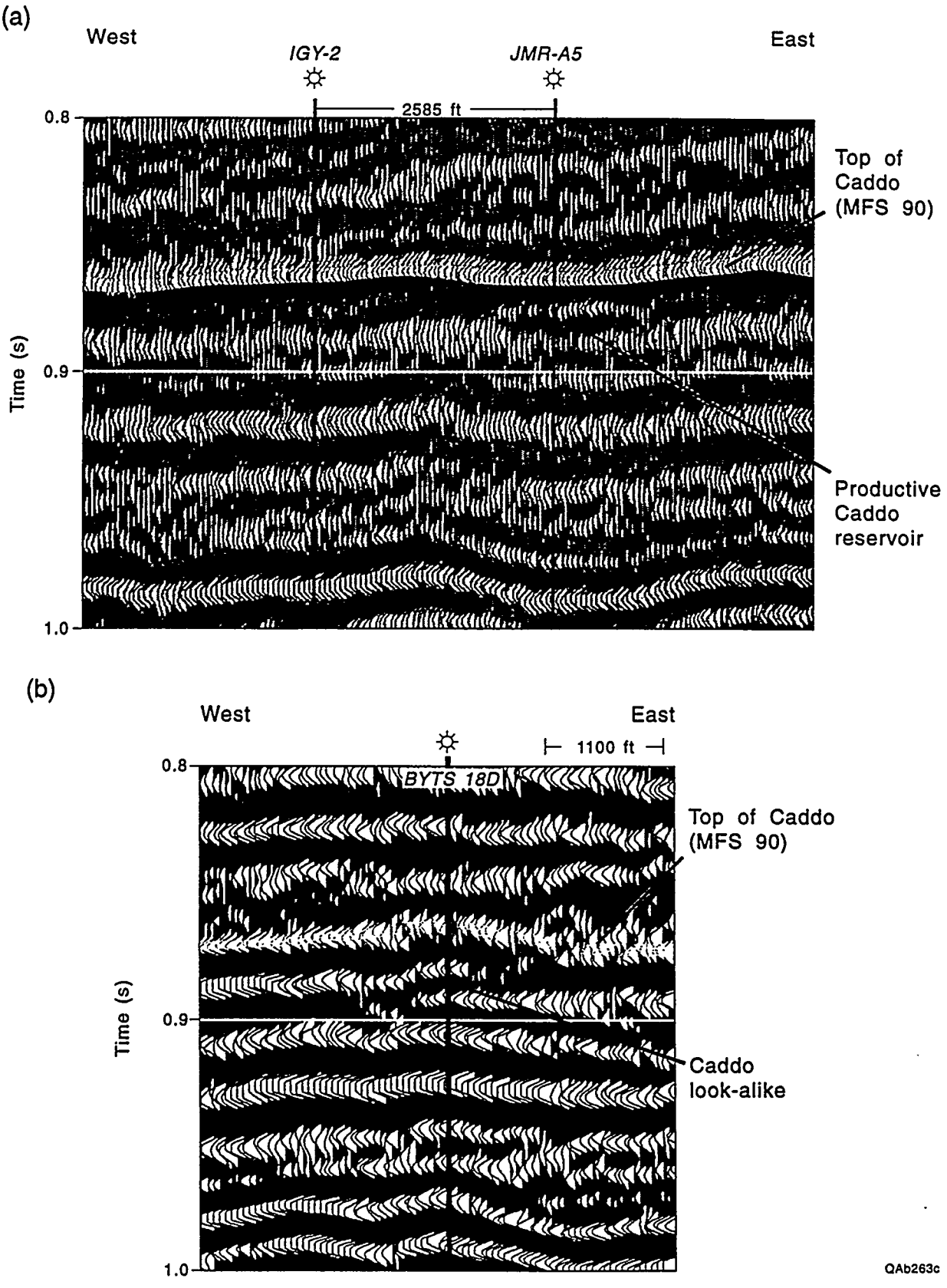

Figure 6.3. (a) East-west seismic profile showing the seismic response of a productive Caddo reservoir penetrated by the Robinson A5 well (JMR-A5). (b) East-west seismic profile showing the seismic response of a Caddo look-alike to the JMR-A5 response. The B Yates 18D well was drilled to test this look-alike feature.

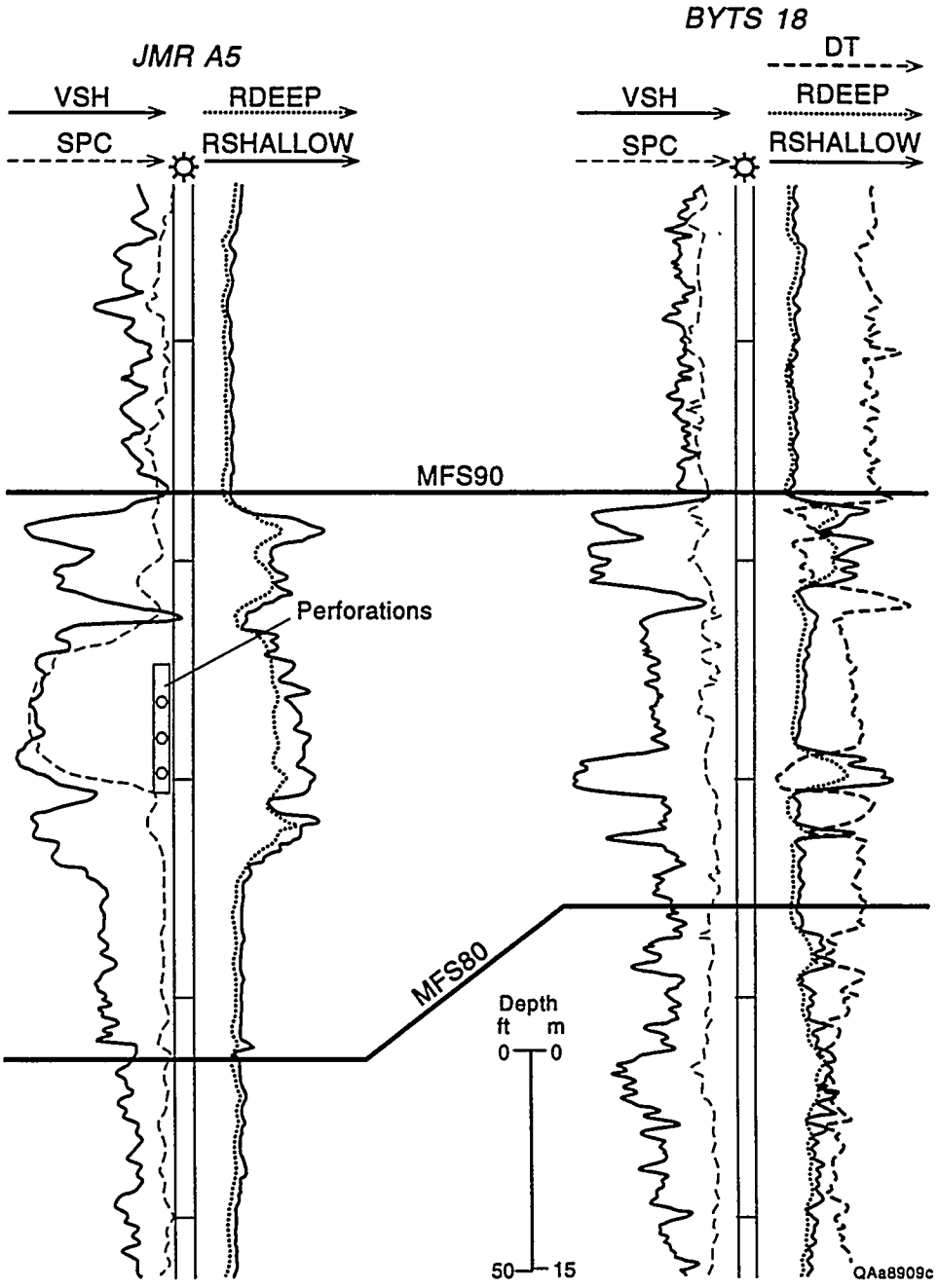

Figure 6.5. Comparison of log data from the productive Caddo interval at the Robinson A5 well with the log data from the Caddo interval at the B Yates 18D. The Caddo seismic response at the B Yates 18D is caused by two thin limestone units within the sequence, and no productive facies are present.

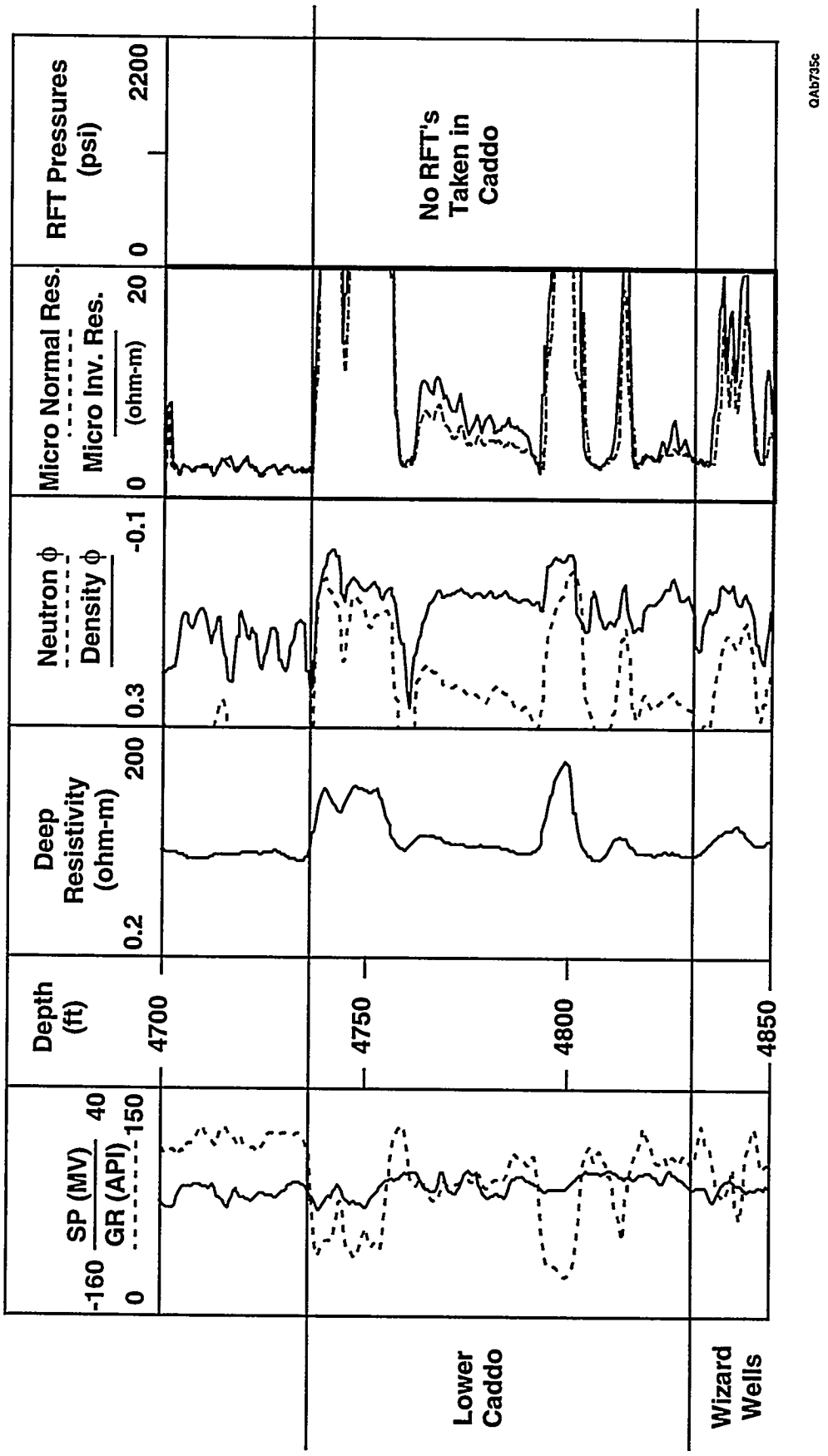

Figure 6.6. Open-hole logs run across the upper portion of the Bend intervals in the B Yates 18D well showing no Lower Caddo sand development.

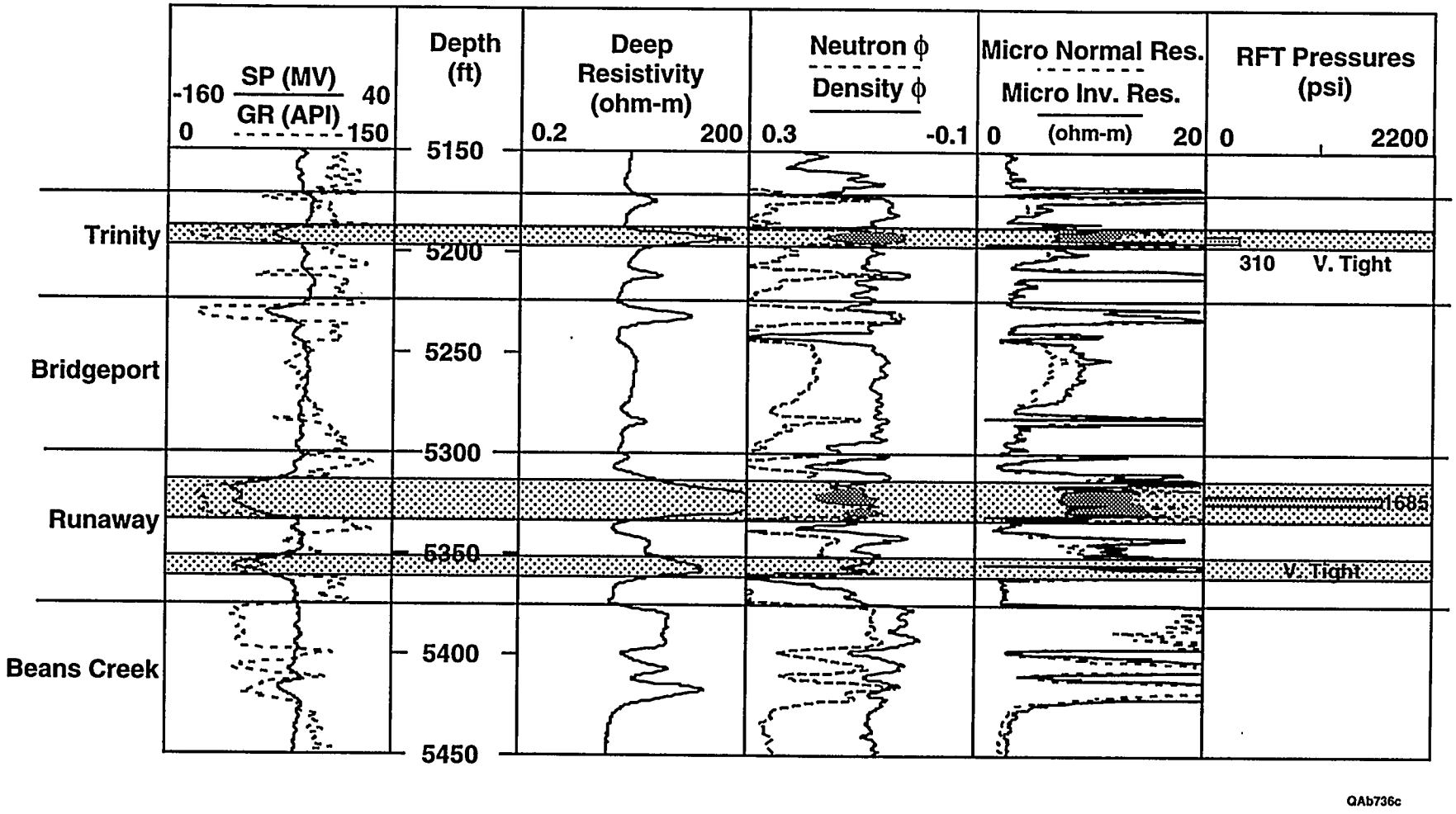

Figure 6.7. Open-hole logs run across the Trinity, Bridgeport, Runaway, and part of the Beans Creek sequences in the B Yates 18D well. The 20-ft sand encountered in the Upper Runaway appears to be an isolated reservoir at original pressure.

6.25

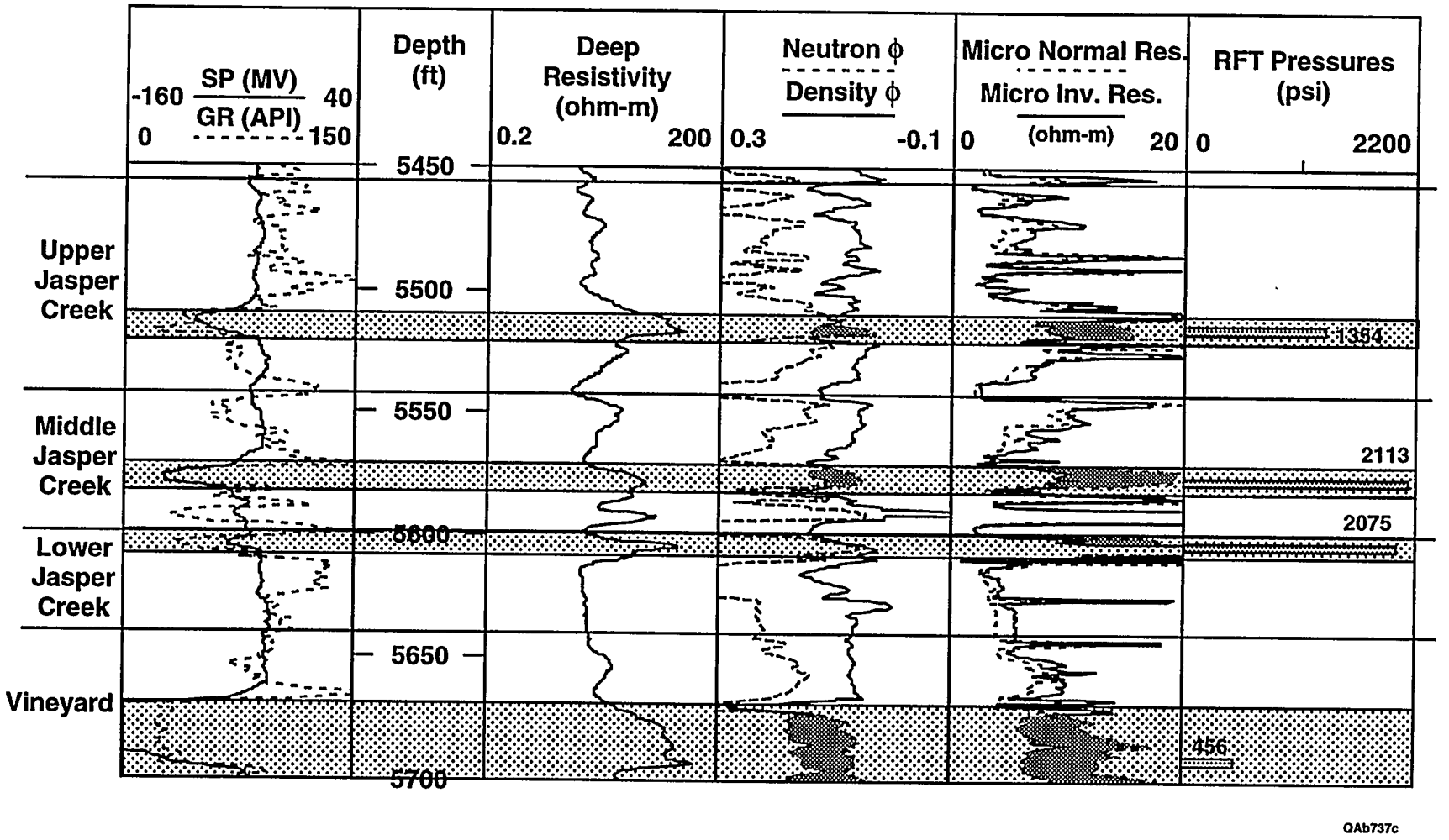

Figure 6.8. Open-hole logs run across the Jasper Creek and Vineyard sequences in the B Yates 18D well. Several of the Jasper Creek intervals appear to be isolated reservoirs. Good Vineyard zone encountered, as expected, with substantial pressure depletion.

6.26

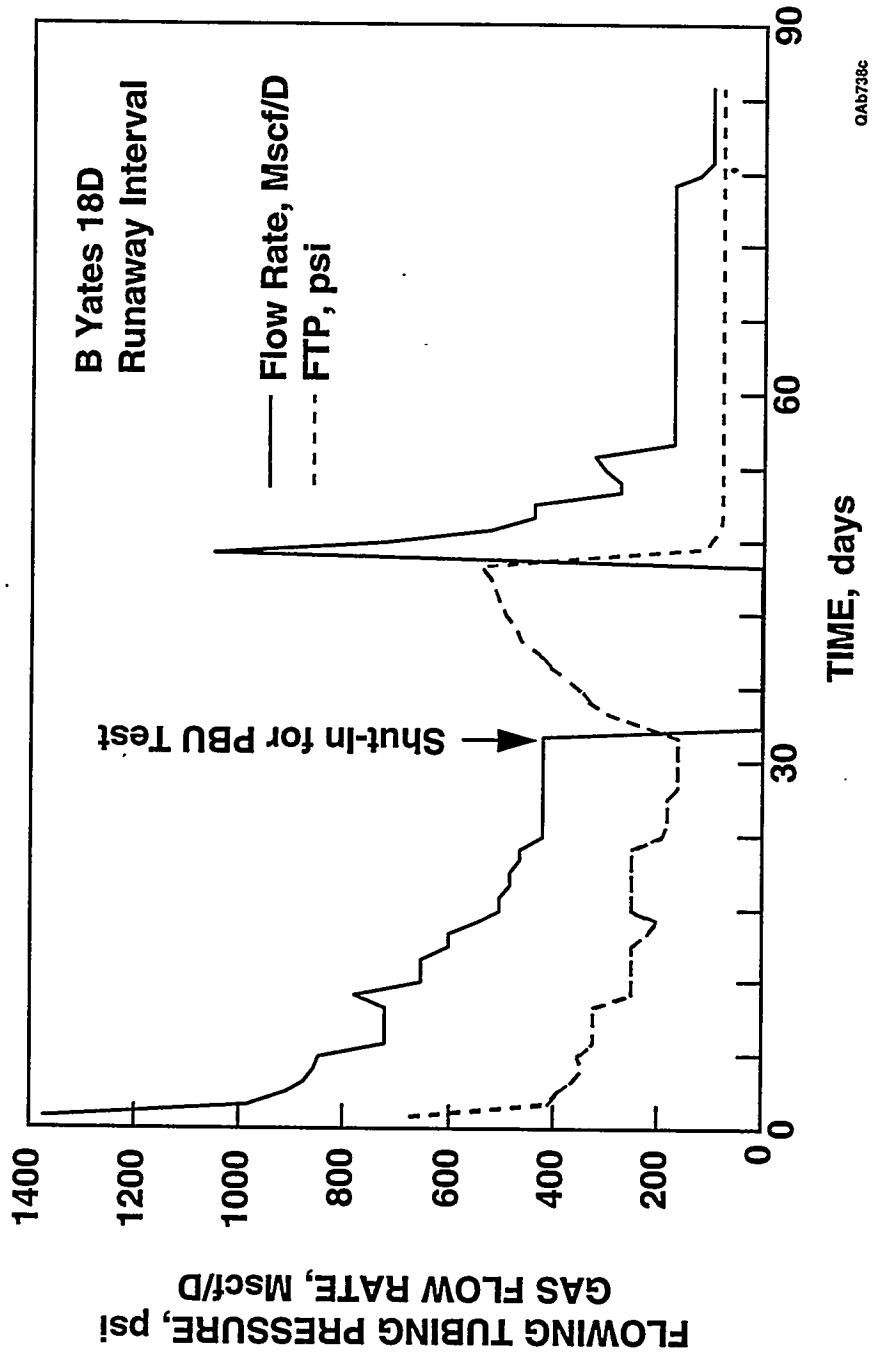

Figure 6.9. Flow rates and pressures for the Upper Runaway interval in the B Yates 18D well.

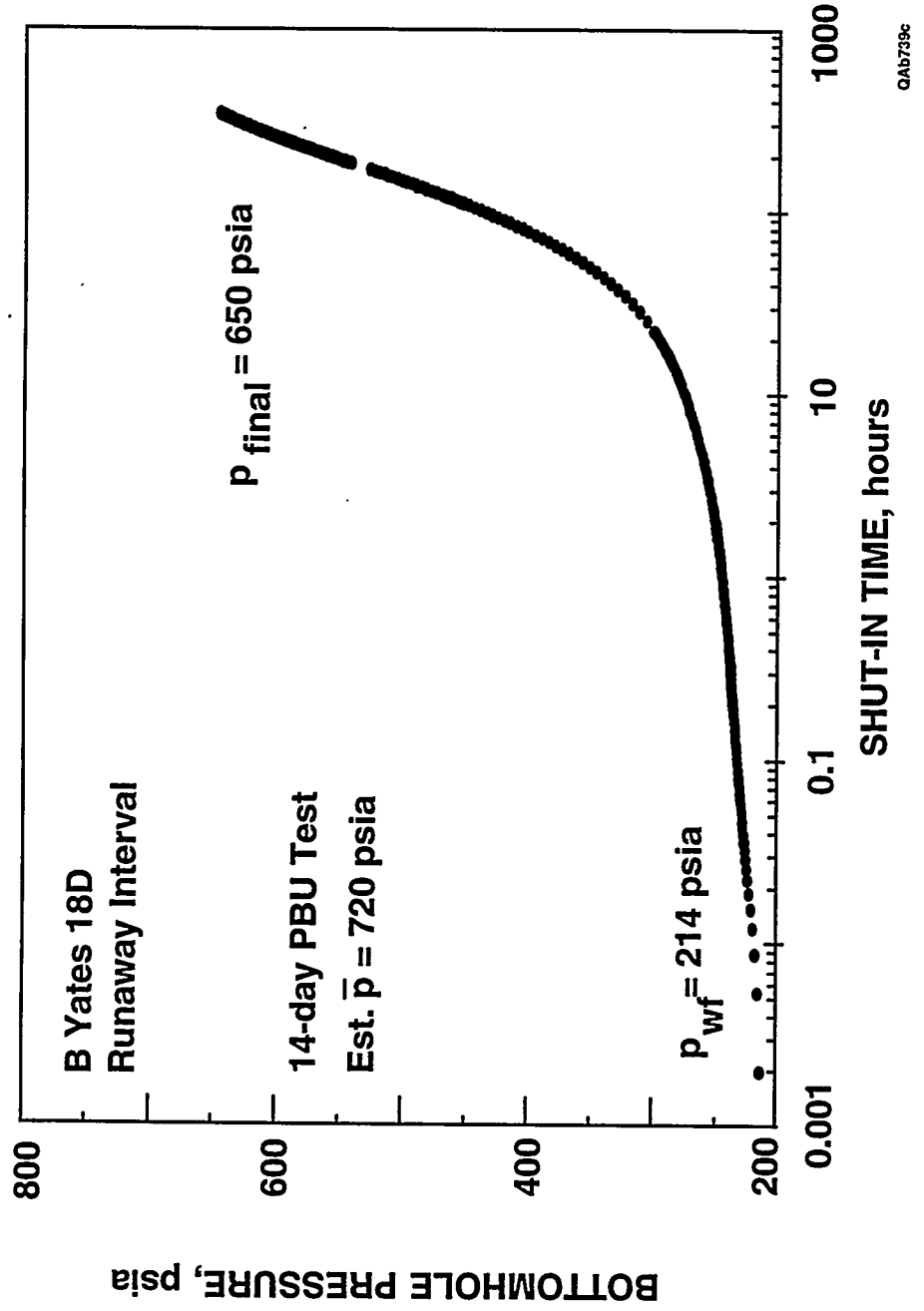

Figure 6.10. Pressure data recorded during the 2-week buildup test conducted in the Upper Runaway reservoir in the B Yates 18D well.

6.28

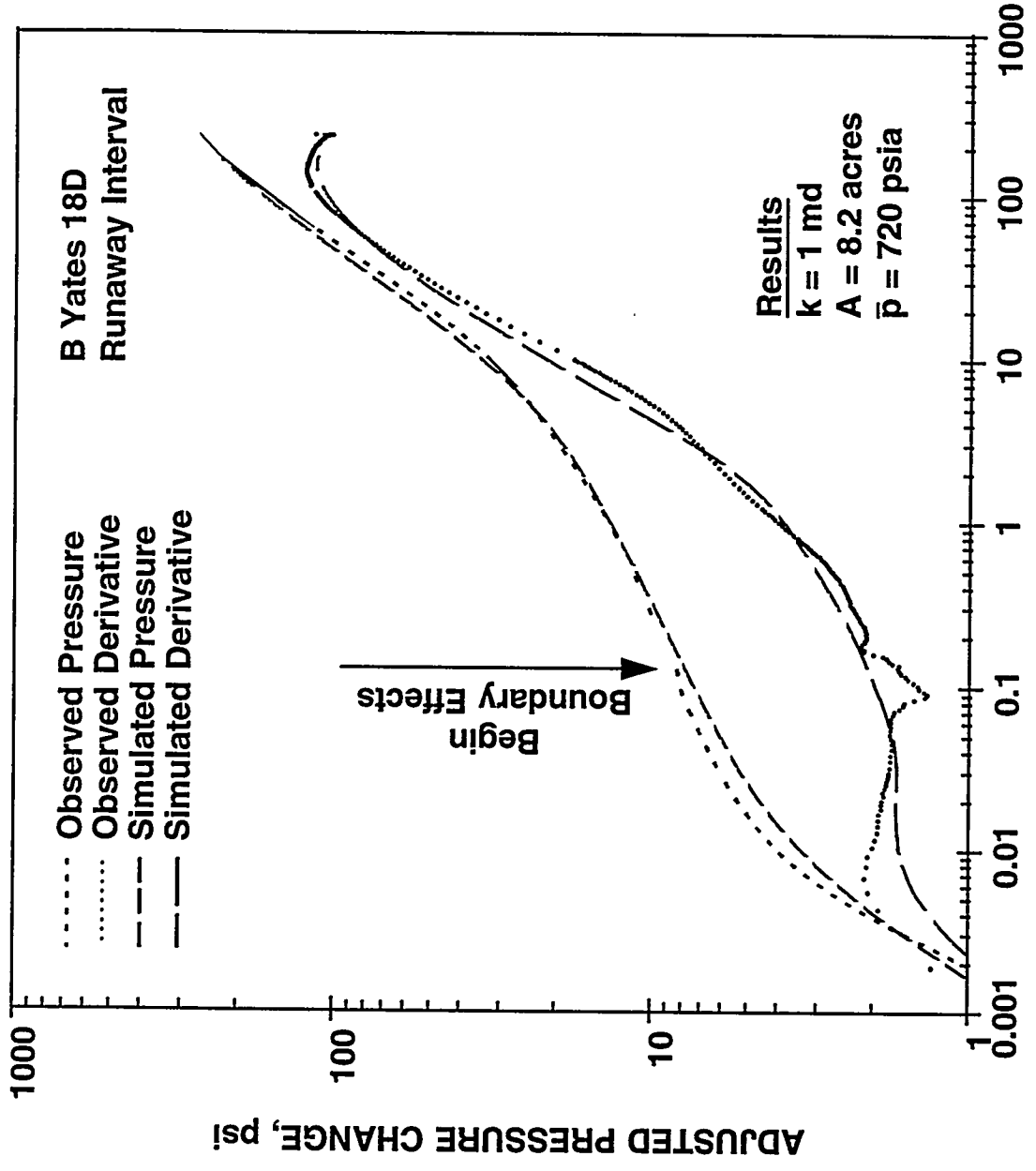

Figure 6.11. History-match of B Yates 18D Upper Runaway well test. These data suggest a reservoir size of about 8 acres.

6.29

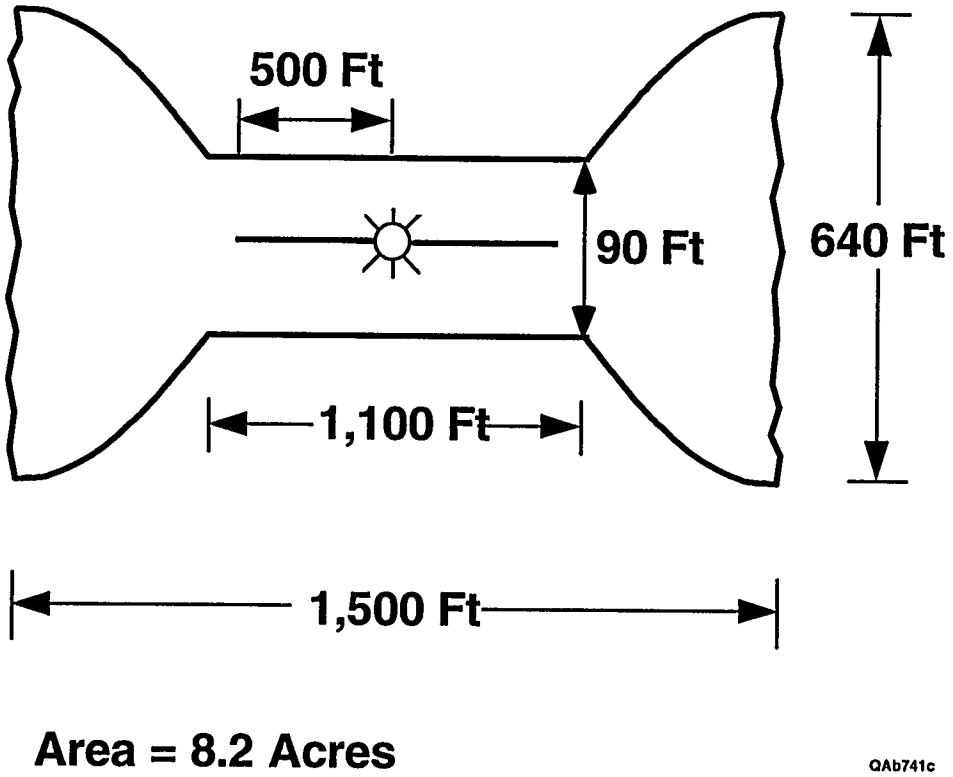

Figure 6.12. Schematic diagram of reservoir model used to history-match B Yates 18D Upper Runaway well test data.

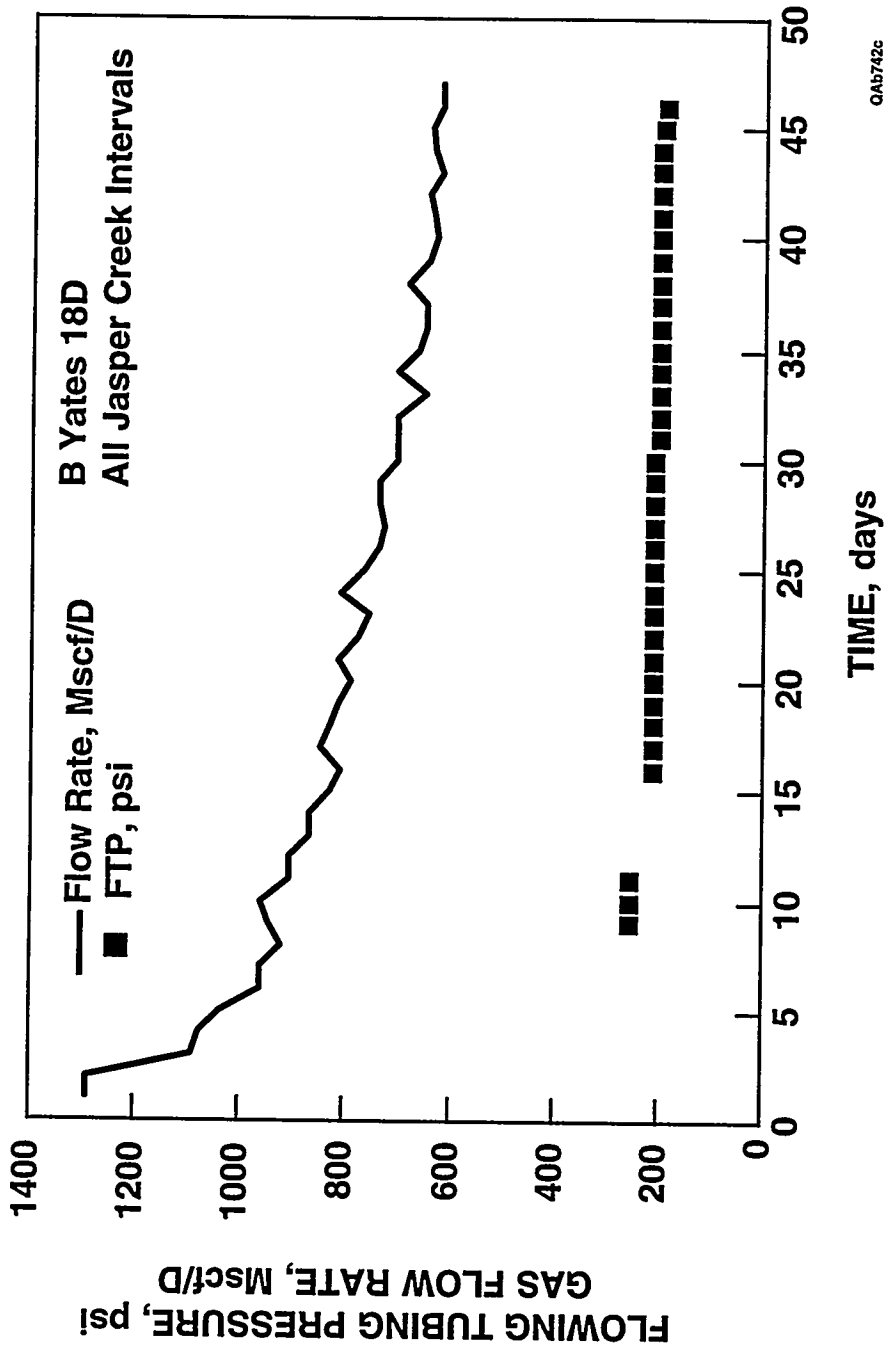

Figure 6.13. Initial production from the Jasper Creek reservoirs in the B Yates 18D well.

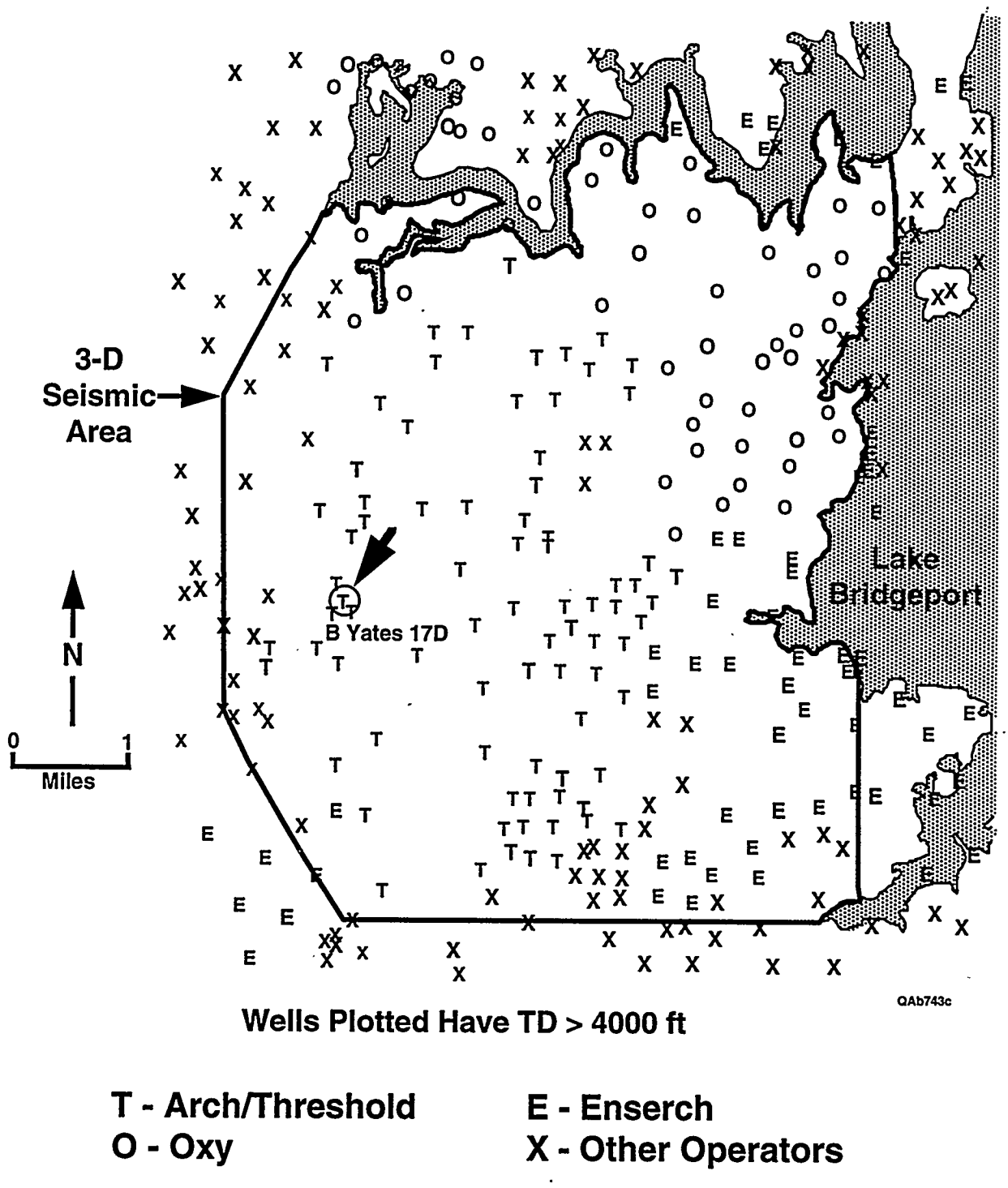

Figure 6.14. Location of the B Yates 17D well in the west-central part of the project area.

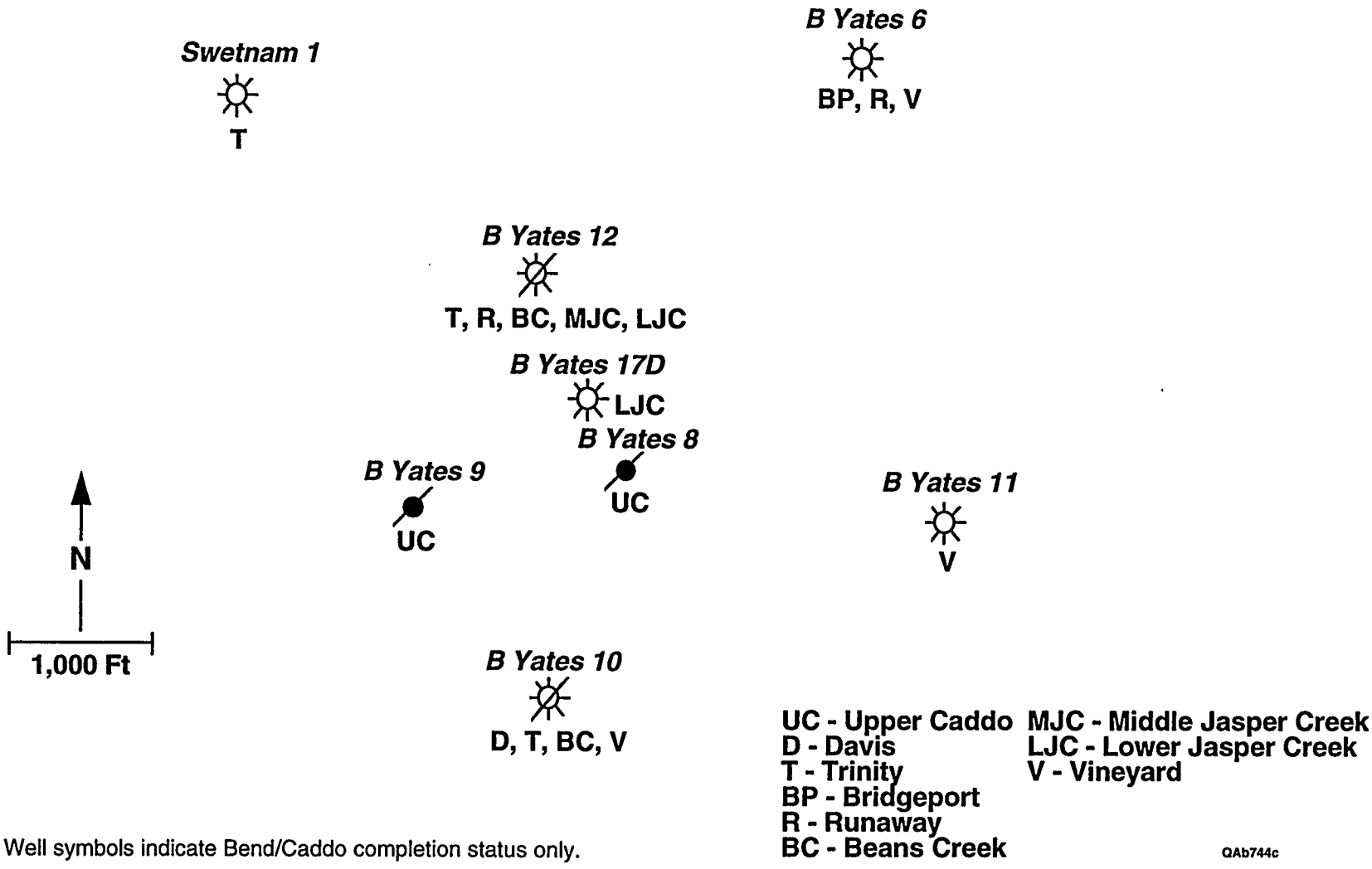

Note: Well symbols indicate Bend/Caddo completion status only.

Figure 6.16. Expanded view of wells offsetting the B Yates 17D location.

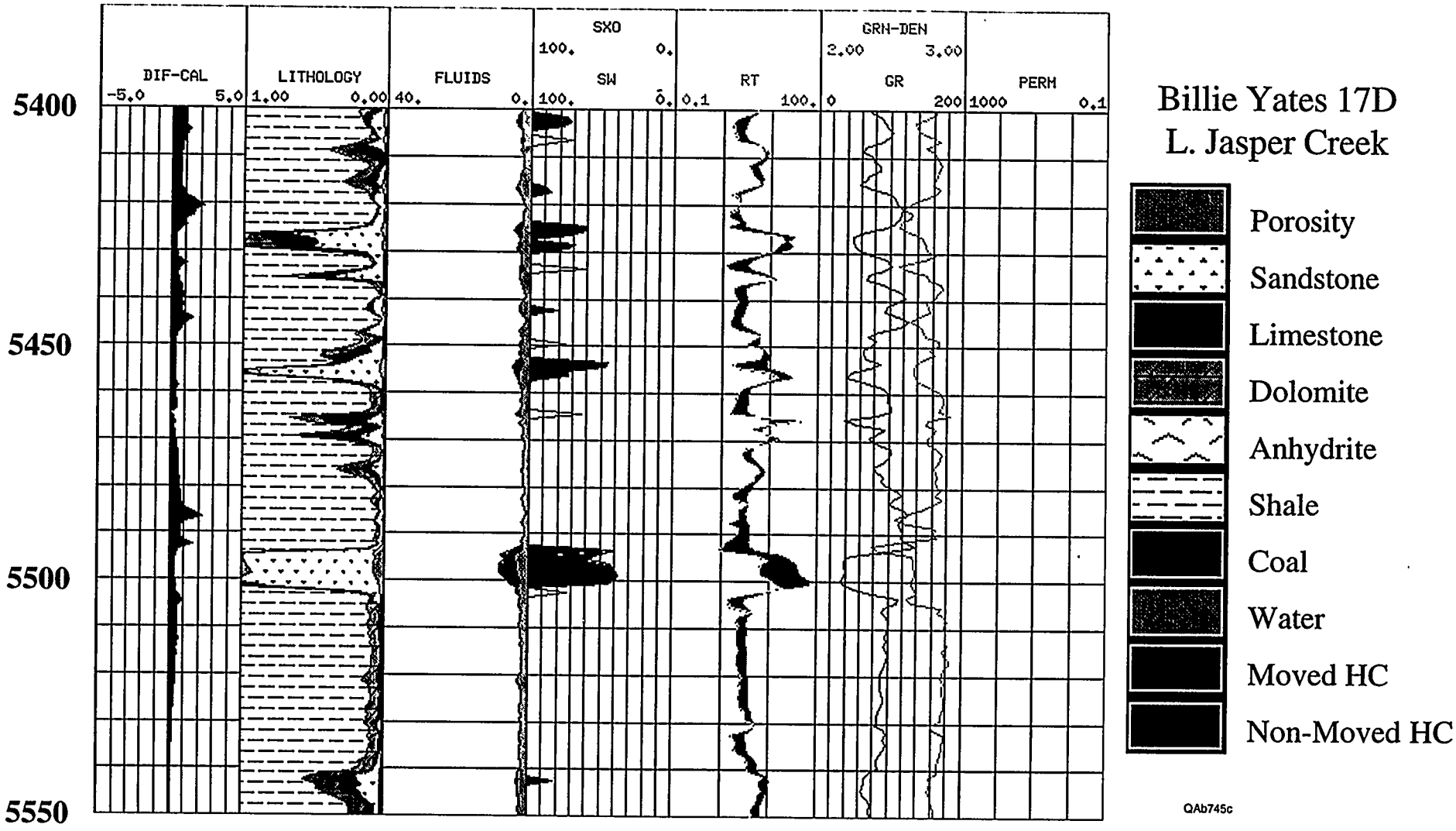

Figure 6.17. Interpreted log for the Jasper Creek sequences penetrated by the B Yates 17D well. The well is completed in the Lower Jasper Creek from 5,496 to 5,502 ft.

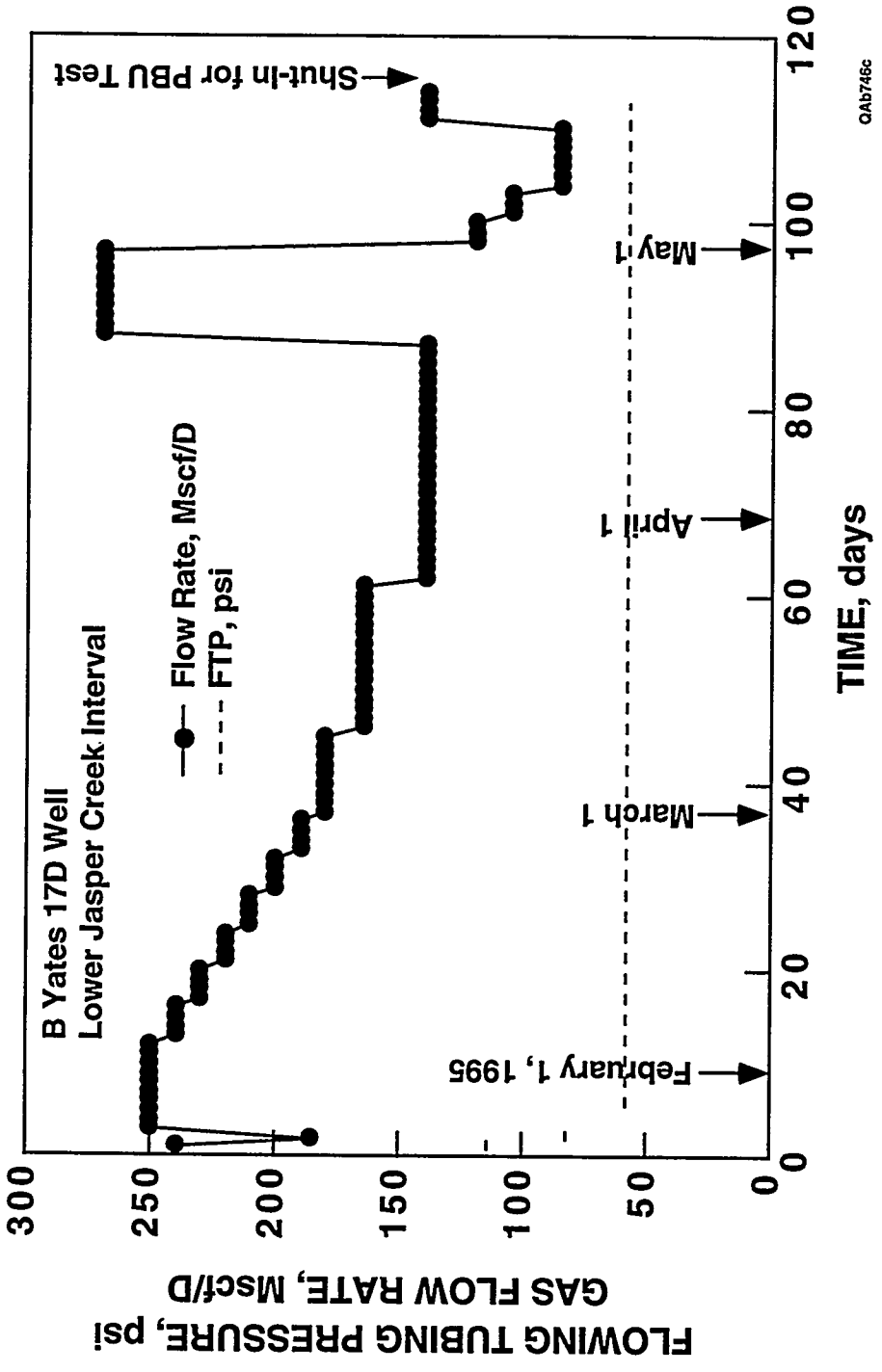

Figure 6.18. Initial production from the Lower Jasper Creek in the B Yates 17D well.

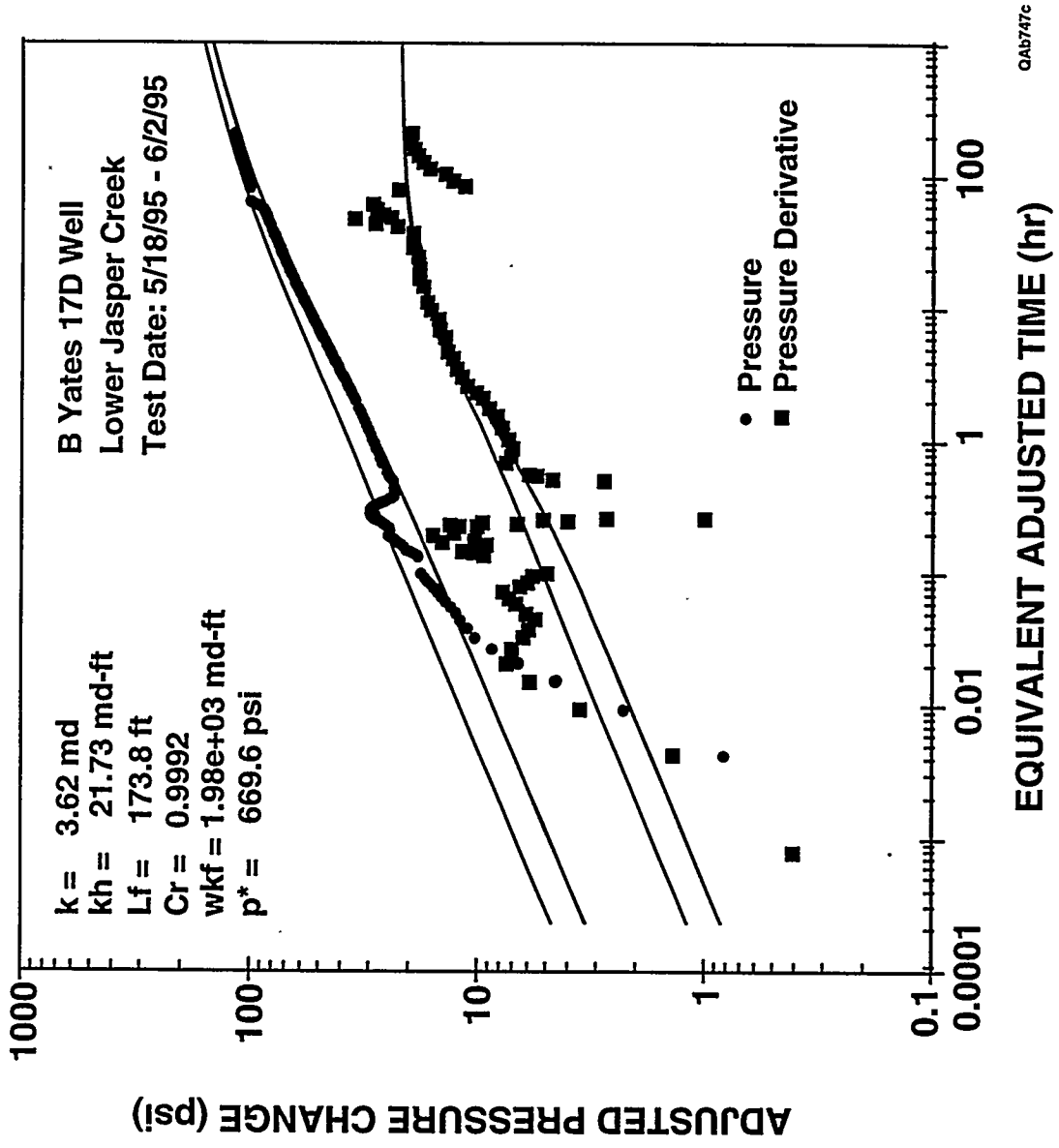

Figure 6.19. Log-log analysis of the pressure buildup test conducted in the Lower Jasper Creek reservoir in the B Yates 17D well.

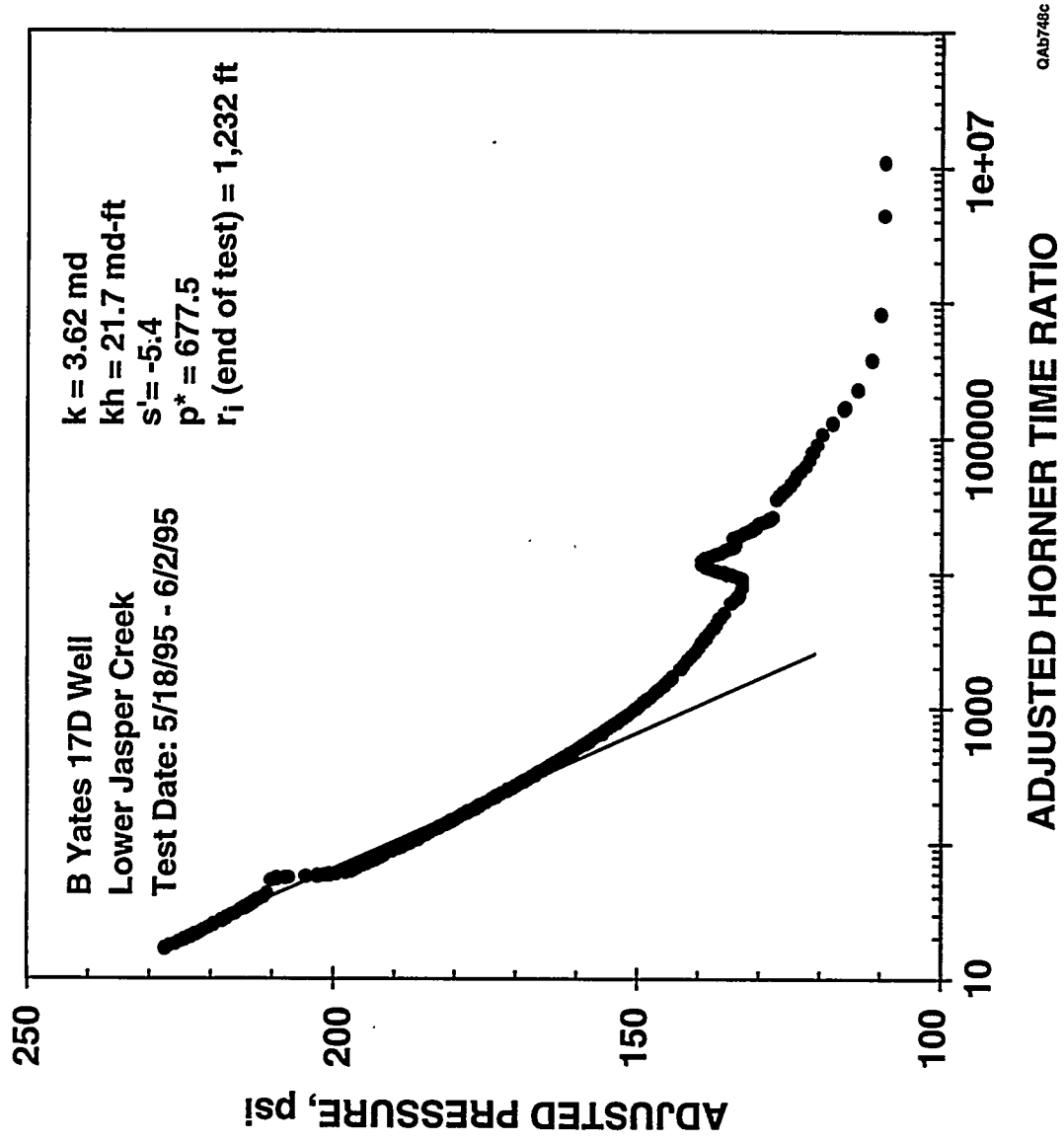

Figure 6.20. Semilog analysis of the pressure buildup test conducted in the Lower Jasper Creek reservoir in the B Yates 17D well.

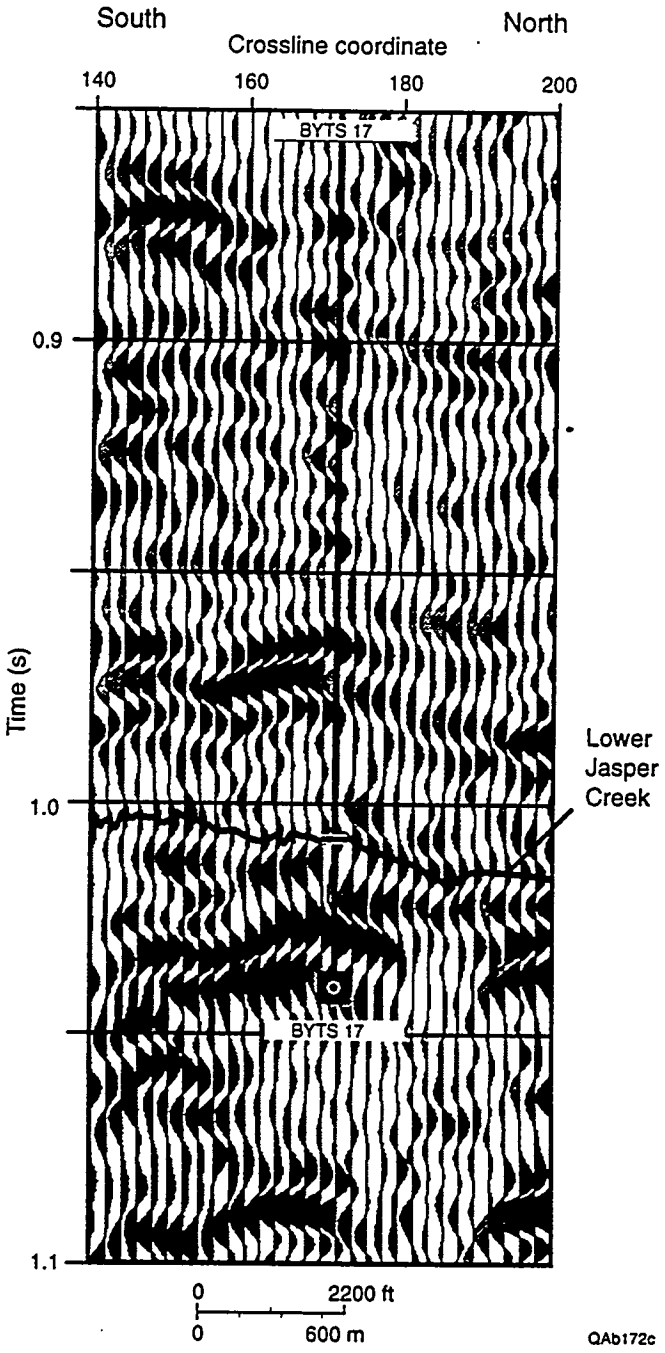

Figure 6.21. North-south profile through the B Yates 17D well location showing the position of the Lower Jasper Creek (heavy dash on the well profile) as determined by the depth-to-time calibration function used in the project area and the resulting interpretation of the Lower Jasper Creek sequence boundary.

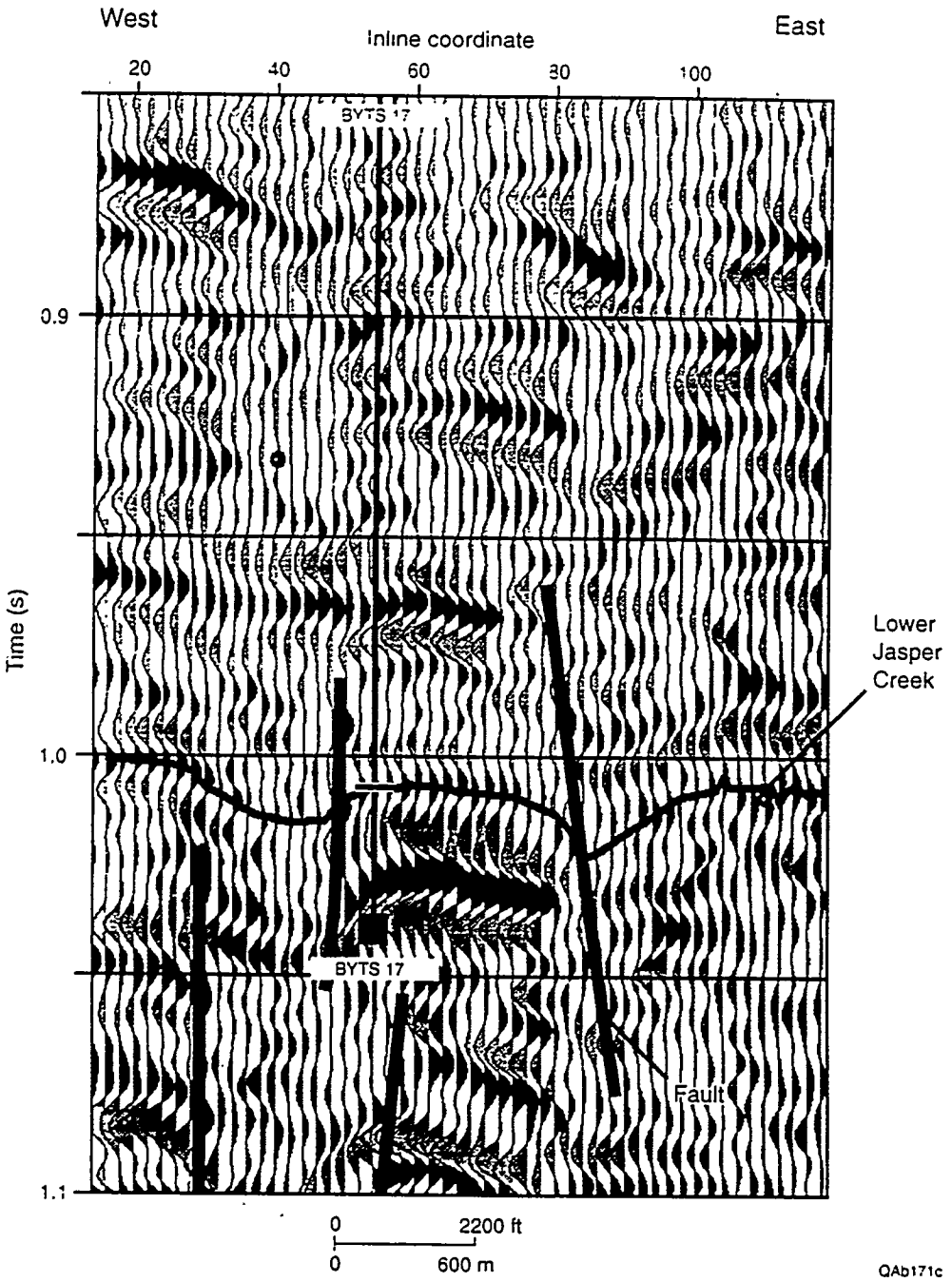

Figure 6.22. East-west profile through the B Yates 17D well location showing the position of the Lower Jasper Creek (heavy dash on the well profile) as determined by the depth-to-time calibration function used in the project area and the resulting interpretation of the Lower Jasper Creek sequence boundary. Several interpreted faults are also indicated.

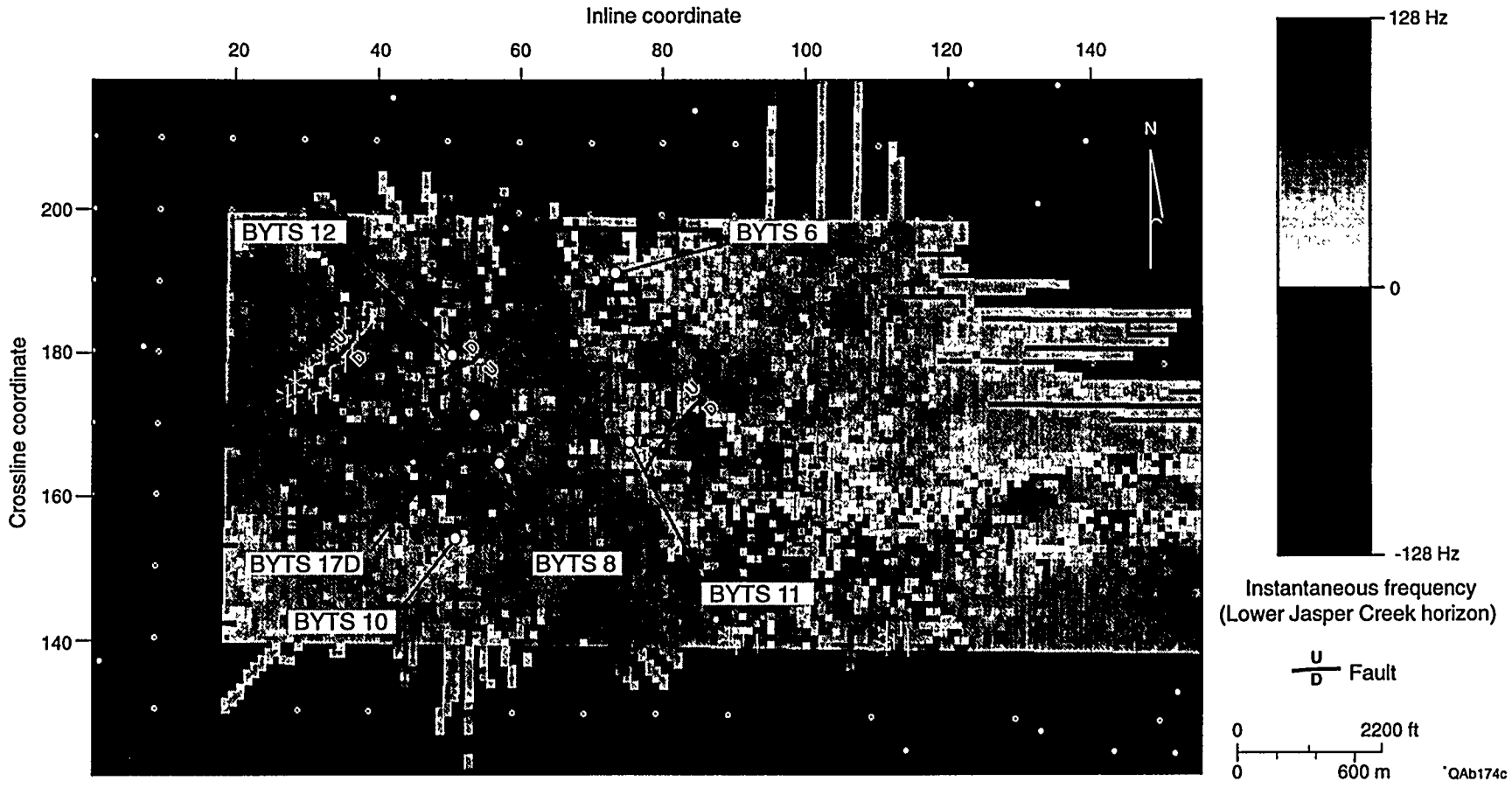

Figure 6.23. Instantaneous frequency behavior across the interpreted Lower Jasper Creek surface. The darkest bins show where the reflection waveform is distorted, which implies that a possible compartment boundary may occur at these coordinates.

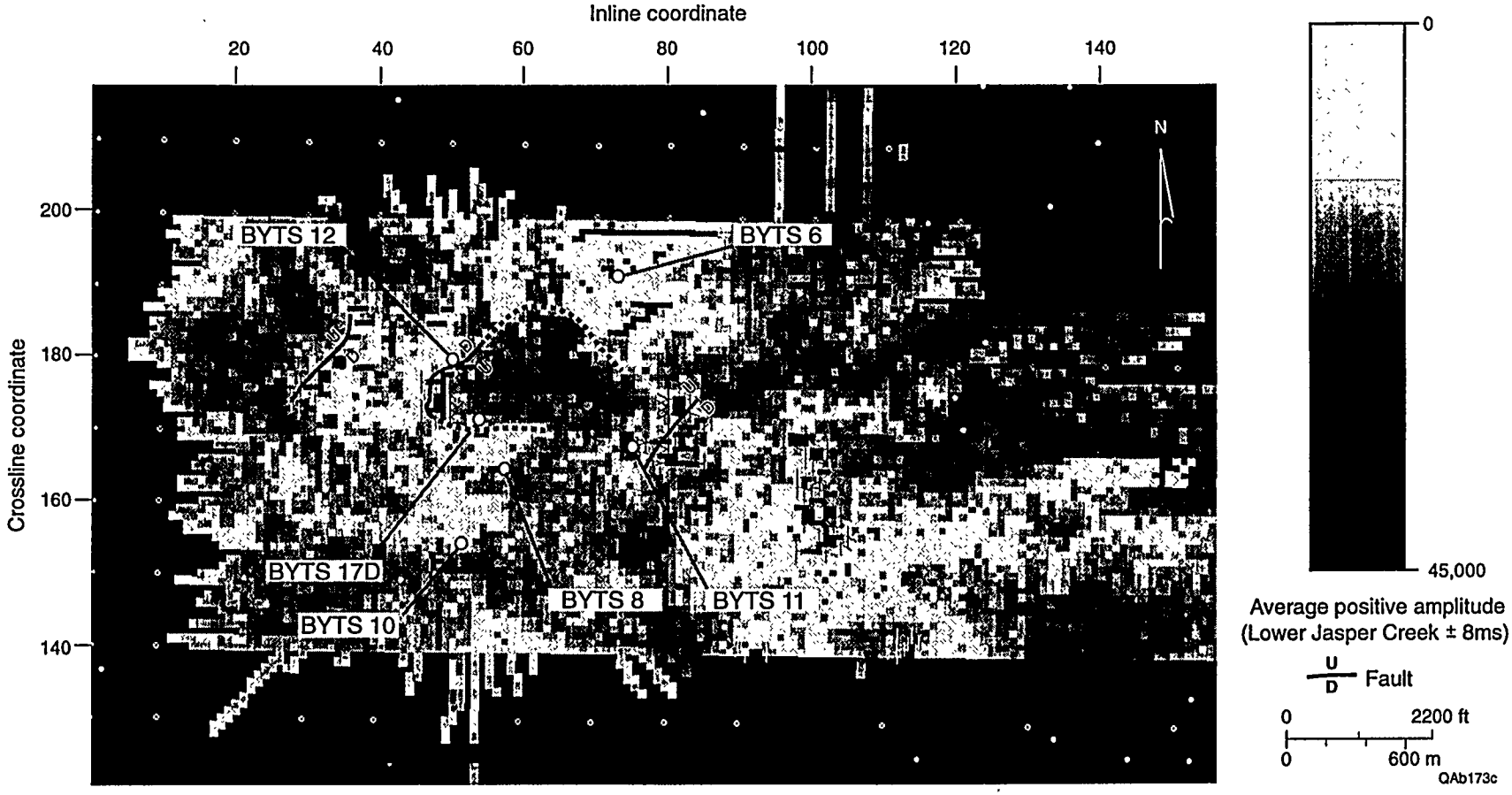

Figure 6.24. Reflection amplitude behavior across the interpreted Lower Jasper Creek surface. The parameter that is plotted is the average of the positive amplitudes occurring in a 16-ms window centered on the Lower Jasper Creek surface. The B Yates 17D well is positioned near the edge of an area where the reflection amplitudes have a moderate positive range, as indicated on the color bar. Assuming that these seismic amplitude facies map a consistent stratigraphic facies, they indicate that the compartment size (area inside the dashed boundary) is perhaps as large as 100 acres and may connect with a larger, equivalent seismic amplitude facies extending southward between the B Yates 8 and B Yates 11 wells.

7. REFERENCES

Adler, F. J., Amsden, T. W., Anderson, E. G., Barnes, V. E., Bennett, J., Bennison, A. P., Brown, L. F., Jr., Caplan, W. M., Caylor, J. W., Clendening, J. A., Copeland, C. W., Craig, W. W., Culp, E. F., Deford, R. K., Denison, R. E., Downs, H. R., Ethington, R. L., Furnish, W. M., Jr., Gatewood, L. E., Gilbert, M. C., Glick, E. E., Groat, C. G., Hannum, C. E., Hansen, T. A., Harrison, W. E., Hart, G. F., Hills, J. M., McCord, D. L., McFarland, J. D., III, Milling, M. E., Morgan, W. A., Osborne, W. E., Pope, D. E., Rascoe, B., Jr., Repetski, J., Sprinkle, J., Stanton, R. J., Sutherland, P. K., Takken, S., Thomas, W. A., Wermund, E. G., Jr., Wilson, L. R., Wise, O. A., Jr., Yancey, T. E., and Young, K. P., 1986, Texas–Oklahoma tectonic region correlation chart, *in* Mankin, C. J., ed., Correlation of stratigraphic units in North America: American Association of Petroleum Geologists.

Agarwal, R. G., 1979, Real gas pseudo-time—a new function for pressure buildup analysis of MHF gas wells: Society of Petroleum Engineers, Paper SPE 8279.

_____ 1980, A new method to account for producing time effects when drawdown type curves are used to analyze pressure buildup and other test data: Society of Petroleum Engineers, Paper SPE 9289.

Al-Hussainy, R., Ramey, H. J., and Crawford, P. B., 1966, The flow of real gas through porous media: Journal of Petroleum Technology, May, p. 623–636.

Blanchard, K. S., Denman, O., and Knight, A. S., 1968, Natural gas in Atokan (Bend) section of northern Fort Worth Basin: Beebe, B. W., and Curtis, B. F., eds., Natural

gases of North America: American Association of Petroleum Geologists Memoir 9, v. 2, p. 1446–1454.

Carlson, M. P., Nodine-Zeller, D. E., Thompson, T. L., and White, B. J., 1986, Mid-Continent region correlation chart, *in* Adler, F. J., ed., Correlation of stratigraphic units in North America: American Association of Petroleum Geologists.

Chapin, C., Clemons, R. E., DeWitt, E., Harding, J. M., Hills, J. M., Hook, S. C., Knepp, R. A., Kottlowski, F. E., LeMone, D. V., Maxwell, C., McBride, E. F., Mear, C. E., Moore, G., Nicholson, J., Peirce, H. W., Pray, L. C., Scarborough, R. B., Seager, W., Stewart, W. J., Thompson, S., III, Wilde, G. L., Wolberg, D., and Wright, W., 1983, Southwest/southwest Midcontinent correlation chart, *in* Hills, J. M., and Kottlowski, F. E., eds., Correlation of stratigraphic units in North America: American Association of Petroleum Geologists.

Cinco Ley, H., and Samaniego-V. F., 1981, Transient pressure analysis for fractured wells: Journal of Petroleum Technology, September, p. 1759–1766.

Fair, W. B., Jr., 1981, Pressure buildup analysis with wellbore phase redistribution: Society of Petroleum Engineers Journal, April, p. 259–270.

Flawn, P. T., Goldstein, A. G., Jr., King, P. B., and Weaver, C. E., 1961, The Ouachita System: University of Texas, Austin, Bureau of Economic Geology Publication No. 6120, 401 p.

Glover, G., 1982, A study of the Bend Conglomerate in S. E. Maryetta Area, Boonesville [sic] Field, Jack County, Texas: Dallas Geological Society.

Grayson, R. C., 1990, Canyon Creek: a significant exposure of a predominantly mudrock succession recording essentially continuous deposition from the Late Devonian

through the Middle Pennsylvanian, *in* Ritter, S. M., ed., Early to Middle Paleozoic conodont biostratigraphy of the Arbuckle Mountains, southern Oklahoma: Oklahoma Geological Survey, Guidebook for the South-Central Section of the Geological Society of America Field Trip No. 27, p. 85–105.

Horner, D. R., 1951, Pressure buildup in wells, *in* Proceedings, Third World Petroleum Congress: The Hague, Section II, p. 503–523.

Lahti, V. R., and Huber, W. F., 1982, The Atoka Group (Pennsylvanian) of the Boonsville Field area, north-central Texas, *in* Martin, C. A., ed., Petroleum geology of the Fort Worth Basin and Bend Arch area: Dallas Geological Society, p. 377–399.

Lee, W. J. 1986, Characterizing formations with pressure tests textbook for videotape short course: Dallas, Society of Petroleum Engineers.

Manger, W. L., Miller, M. S., Mapes, R. H., 1992, Age and correlation of the Gene Autry Shale, Ardmore Basin, southern Oklahoma, *in* Sutherland, P. K., and Manger, W. L., eds., Recent advances in Middle Carboniferous biostratigraphy—a symposium: Oklahoma Geological Survey Circular 94, p. 101–109.

Masters, J. A., 1979, Deep basin gas trap, Western Canada: American Association of Petroleum Geologists Bulletin, v. 63, p. 152–181.

Meckel, L. D., Jr., Smith, D. G., Jr., Wells, L. A., 1992, Ouachita foredeep basins: Regional paleogeography and habitat of hydrocarbons, chapter 15, p. 427–444.

Railroad Commission of Texas, 1991, Field rules, section VI, Boonsville Field (Bend Conglomerate Gas), Order No. 9-36, 420.

Ravn, R. L., and Swade, J. W., Howes, M. R., Gregory, J. L., Anderson, R. R., and Van Dorpe, P. E., 1984, Stratigraphy of the Cherokee group and revision of

Pennsylvanian stratigraphic nomenclature in Iowa: Iowa Geological Survey Technical Information Series, No. 12, 76 p.

Shaver, R. H., Clayton, L., Mudrey, M. G., Jr., Peters, R. M., Mikulic, D. G., Ells, G. D., Eschman, D. F., Fisher, J. H., Lilienthal, R., Collinson, C., Atherton, E., Baxter, J. W., Kolata, D. R., Jacobson, R. J., Lineback, J. A., Norby, R. D., Palmer, J. E., Sargent, M. L., Trask, C. B., Willman, H. B., Droste, J. B., Patton, J. B., Gray, H. H., Goldthwait, R. P., Rexroad, C. B., Noger, M. K., Dever, G. R., Jr., Smith, H. J., Williamson, A. D., Schwalb, H. K., Luther, E. T., and Copeland, C. W., 1984, Midwestern basin and arches region correlation chart, *in* Correlation of stratigraphic units in North America: American Association of Petroleum Geologists.

Sutherland, P. K., Archinal, B. E., and Grubbs, R. K., 1982, Morrowan and Atokan (Pennsylvanian) stratigraphy in the Arbuckle Mountains area, Oklahoma, *in* Sutherland, P. K., ed., Lower and Middle Pennsylvanian stratigraphy in south-central Oklahoma: Oklahoma Geological Survey, prepared for Geological Society of America Field Trip No. 2, p. 1–17.

Sutherland, P. K., and Grayson, R. C., Jr., 1992, Morrowan and Atokan (Pennsylvanian) biostratigraphy in the Ardmore Basin, Oklahoma, *in* Sutherland, P. K., and Manger, W. L., eds., Recent advances in Middle Carboniferous biostratigraphy—a symposium: Oklahoma Geological Survey Circular 94, p. 81–99.

Thompson, D. M., 1982, Atoka Group (Lower to Middle Pennsylvanian), northern Fort Worth Basin, Texas: terrigenous depositional systems, diagenesis, and reservoir distribution and quality: The University of Texas at Austin, Bureau of Economic Geology Report of Investigations No. 125, 62 p.

_____ 1988, Fort Worth Basin, *in* Sloss, L. L., ed., The geology of North America: Boulder, Geological Society of America, v. D-2, p. 346–352.

Turner, G. L., 1957, Paleozoic stratigraphy of the Fort Worth Basin, *in* Bell, W. C., ed., Abilene and Fort Worth Geological Societies 1957 Joint Field Trip Guidebook, p. 57–77.

Walper, J. L., 1977, Paleozoic tectonics of the southern margin of North America: Gulf Coast Association of Geological Societies Transactions, v. 27, p. 230–239.

Zachry, D. L., and Sutherland, P. K., 1984, Stratigraphy and depositional framework of the Atoka Formation (Pennsylvanian) Arkoma Basin of Arkansas and Oklahoma, *in* Sutherland, P. K., and Manger, W. L., eds., The Atokan Series (Pennsylvanian) and its boundaries—a symposium: Oklahoma Geological Survey Bulletin 136, p. 9–17.

APPENDIX A

GEOLOGIC EVALUATION OF THE BOONSVILLE PROJECT AREA

Introduction

More than 90 percent of the 2.6 Tcf of natural gas produced at Boonsville has come from conglomeratic sandstones deposited in the Fort Worth Basin during the Atoka Stage of the Middle Pennsylvanian Period (Fig. A1; Blanchard and others, 1968; Thompson, 1982). The distribution, porosities, and permeabilities of Boonsville sandstones and many other Upper Paleozoic sandstone reservoirs in Midcontinent basins are typically erratic and unpredictable. Previous investigations have concluded that trapping mechanisms are due predominantly to sandstone facies pinch-outs and permeability pinch-outs due to diagenetic cements (Glover, 1982; Lahti and Huber, 1982; Thompson, 1982). Effective characterization and exploitation of these fields is difficult because the sandstone reservoirs, typically thin and discontinuous, represent a variety of complexly intermingled depositional environments and facies and commonly contain pore-occluding diagenetic cements. As compared with other times in geologic history, the fundamental geological controls on reservoir architecture and stacking patterns in marine basins were unique during the Pennsylvanian Era. Specifically the mechanisms that combined to produce complex, compartmentalized reservoirs at the Fort Worth, and many other Midcontinent Basins were:

- Relatively low accommodation setting (i.e., shallow basin)
- High-amplitude, high-frequency sea-level fluctuations
- Tectonic jostling during sedimentation
- Temporal variations in sediment source material
- High rates of sediment supply

- Tropical paleoclimate

The purpose of the geological investigation was to determine how these unique geological circumstances shaped reservoir architecture in this important natural gas province and to outline predictive development strategies that pinpoint optimal infill drilling sites. This appendix describes the geological conditions and concepts, data base, methods of evaluation, and general geological interpretations of the Boonsville Project Area that represent the foundation upon which development strategies were built.

Hydrocarbon Habitat

Ouachita foreland basins gas accumulations, including Bend Conglomerate gas in the Fort Worth Basin, occur as large, pervasive, *deep basin accumulations* (Masters, 1979; Meckel and others, 1992). Pennsylvanian gas reservoirs in these basins, typically underpressured, produce little to no water and are relatively tight (typically less than 10 md). They are hydraulically separated from updip/overlying, more permeable, normally pressured water-bearing units (Meckel and others, 1992). The source of the natural gas is probably the abundant humic materials (land-derived, macerated plant material) in shales that encase the sandstone reservoirs (Meckel and others, 1992). Other Ouachita foreland basins having similar habitats, include the Arkoma, Val Verde, and Black Warrior Basins, and possibly the Kerr and Marfa Basins (Fig. 1.3).

Global Stratigraphic Context

Present-day continental margins are comprised of thick, well-preserved Mesozoic and Cenozoic deposits that contain seismically resolvable depositional sequences (Vail and others, 1977; Ross and Ross, 1988). Thick continental margin wedges also formed during the Late Paleozoic; however, individual depositional sequences are much more difficult to identify in the Late Paleozoic wedges because, generally too extensively deformed, they

contain long-ranging, deep-water fossils that are difficult to correlate with shallow-water fossils and many of the wedges have been consumed by subduction zones and no longer exist (Ross and Ross, 1988). Thus, most Late Paleozoic strata preserved today, including those containing hydrocarbon reservoirs, represent the thin, updip stratigraphic remnants of sea-level highstands deposited in stable cratonic areas, such as the U.S. Midcontinent region (Ross and Ross, 1988).

Eustatic Sea Level

The southern supercontinent, Gondwana, drifted through the south-polar region during the Paleozoic, resulting in continental glaciation that controlled ocean water volume and, thus, eustatic (worldwide) sea level (Crowell and Frakes, 1970; Crowell and Frakes, 1975; Crowell, 1982; Caputo and Crowell, 1985). Similar to the more recent Pleistocene ice age, astronomical factors caused glacial ice volume and its reciprocal, ocean-water volume, to vary cyclically with periodicities ranging from about 20,000 to 400,000 yr (Donovan and Jones, 1979; Berger, 1988; Heckel, 1989a, b; Goldhammer and others, 1991; Connolly and Stanton, 1992). The magnitudes of Late Paleozoic sea-level variations are estimated to be on the order of 60 to 200 m (200 to 650 ft) (Heckel, 1977, 1989; Crowley and Baum, 1991), which is a magnitude large enough alternately to expose and drown continental shelves and continental interior seaways.

The high-amplitude, high-frequency signal has been recognized in Late Paleozoic strata worldwide (for example, Heckel, 1977, 1980; Brown and others, 1990; Goldhammer and others, 1991; Youle and others, 1994). Global and regional sea-level histories have been reconstructed from seismic data (Vail and others, 1977) and, in considerably finer detail, from Late Paleozoic rocks (Heckel, 1977, 1986; Ramsbottom, 1979; Saunders and others, 1979; Ross and Ross, 1985; Boardman and Heckel, 1989). Using data from three continents, Ross and Ross (1988) constructed a comprehensive, Atokan eustatic sea-level estimate, which details six major eustatic cycles (Fig. A2).

Late Paleozoic Paleoclimate

During the Pennsylvanian, the U.S. Midcontinent was located in the tropics (Fig. A3), a conclusion supported by both paleomagnetic data (McElhinny, 1973; Morel and Irving, 1978) and paleontological information (Nassichuk and Bamber, 1978; Phillips and Peppers, 1984). The Appalachians lay just south of, and parallel to, the equator, which ran in a line from approximately southern Texas to Maine (Scotese and others, 1979; Heckel, 1980). The Fort Worth Basin and Ouachita Mountains were located in the doldrums, whereas the rest of what is now the central United States straddled the northern trade wind belt (Heckel, 1980). Euramerica remained approximately in this position during the entire Pennsylvanian (Scotese and others, 1979). Phillips and Peppers (1984) analyzed the florae preserved in coals and coal balls from North America and Europe, and, on the basis of palynological changes, were able to document synchronous, global changes in climate. The Early Atokan climate was seasonally dry and wet but became very wet from the Middle Atokan to the Desmoinesian Epoch; the increase in humidity and rainfall parallels, and resulted from, the Atokan global transgression (Fig. A2). The tropical paleoclimate provided optimal conditions for biogenic production of skeletal calcite, which later became an important diagenetic component in sandstone units or formed limestone beds during brief cessations of terrigenous clastic influx.

Fort Worth Foreland Basin: A Mixed Accommodation Basin

The Fort Worth Basin is a Late Paleozoic foreland basin that contains a maximum thickness of approximately 13,000 ft of sedimentary strata, the majority of which are Pennsylvanian in age (Turner, 1957a; Thompson, 1988). In addition to the dominantly Pennsylvanian basin fill, major sequences of Cambrian, Ordovician, Mississippian, and Permian rocks are also present. The Paleozoic units are unconformably overlain and

onlapped by Cretaceous strata that occur in the east and southeast parts of the basin (Flawn and others, 1961; Lahti and Huber, 1982; Thompson, 1982, 1988).

In map view, the Fort Worth Basin is an asymmetric, inverted triangle that is approximately 80 mi across and 250 mi long, from apex to base (Fig. A4). Fault-bounded structural uplifts define the eastern (Ouachita Thrust Belt) and northern limits (Muenster Uplift, Red River [=Electra] Uplift) of the basin, but the less distinct western limit is bounded by the Bend Arch, which is a low, north-plunging fold. The Muenster and Red River–Electra Uplifts are both thought to be part of the northwest-trending Amarillo–Wichita Mountain Uplift, which resulted from reactivation of Precambrian boundary faults when Ouachitan compressive stresses were transmitted to the craton (Walper, 1977). A concise synopsis of Fort Worth Basin structural elements can be found in Lahti and Huber (1982).

The Fort Worth Basin is one of several foreland basins formed by, and lying immediately adjacent to, the leading edge of the Ouachita–Appalachian Fold Thrust Belt (Fig. 1.3) (Lahti and Huber, 1982; Thompson, 1982, 1988; Meckel and others, 1992). The Ouachita–Appalachian Fold Thrust Belt is the result of continental collision between the carbonate-dominated, Euramerican (previously fused plates containing parts of North America and Europe) passive margin and the Gondwana supercontinent, which was comprised of parts of present-day Africa, South America, Antarctica, and Australia (Wickham and others, 1976; Meckel and others, 1992). The initial compressional effects began in Early Pennsylvanian time and moved southwestward along the belt in sporadic waves, from the Middle Atlantic region to the southwest Texas–Mexican border area, where it culminated in Early Permian time (Wickham and others, 1976).

Foreland basins are created by subsidence in areas immediately adjacent to complexly folded and faulted overthrust belts (Fig. A4). Subsidence in the overthrust foreland occurs by incremental loading of the lithosphere as successive thrust sheets are emplaced. The load-induced subsidence creates a deep, asymmetric *flexural moat* next to the belt; the

flexural moat becomes shallower away from the belt, and, in fact, grades into a slightly positive, upwarped *peripheral bulge* (Quinlan and Beaumont, 1984). The axis of the Fort Worth Basin represents the flexural moat, and the Bend Arch may represent the peripheral bulge that formed in response to Ouachita thrust loading.

Foreland basins are cratonic (or continental) basins that have widely varying amounts of *accommodation*, which is defined as the space below base level (commonly sea level) available for sediment to accumulate (Jervey, 1988). Depending on relative geographic position with respect to the adjacent thrust belt, the flexural moat or the peripheral bulge, a spectrum of accommodation settings are present, ranging from high in the moat or basin axis, to low near the peripheral bulge. If one considers oceanic, continental margin basins to be *high-accommodation basins*, and at the other extreme, shallow intracratonic basins (for example, Lower Paleozoic U.S.A.) to be *low-accommodation basins*, then foreland basins could be characterized as *mixed-accommodation basins* that, intermediate in total accommodation, nonetheless have wide, intrabasinal variations in local accommodation. The Fort Worth Basin is a mixed-accommodation basin by this definition (Table A1).

Table A1. Accommodation settings of marine sedimentary basins.

Accommodation setting	Structural classification(s)	Generalized stratal architecture	Examples
HIGH	Oceanic continental margins	Vast, thick (tens of thousands of feet and greater); architecture dominated by progradational elements; high preservation potential for diverse facies assemblages: lithology-dominated strata	Gulf of Mexico; other post-Jurassic oceanic basins worldwide
MIXED	Foreland basins, rift basins	Deposits restricted to local–regional areas; varying thicknesses that typically do not exceed thousands of feet; variety of architectural elements that vary through time (vertically in stratigraphic section) and space.	Fort Worth Basin, Val Verde Basin, Arkoma Basin, Appalachian Basin, Cretaceous Western Interior Basin
LOW	Shallow cratonic basins	Thin, sand-rich, surface-dominated strata	Lower Paleozoic interior U.S.A.

Reservoir architecture within mixed-accommodation basins is complex. In a mixed setting, small base-level changes result in accommodation changes over short distances that can have a profound impact on depositional environments, facies, and reservoir architecture. These same small changes might not greatly affect sedimentation in a high-accommodation setting. For example, a 100-ft drop in sea level would not change sedimentary environments significantly on a 300-ft deep continental shelf, whereas the same sea-level fall in a 100-ft-deep cratonic shallow seaway would cause a major facies dislocation from shelf mudstones to upper shoreface sandstones or deltaic sediments.

Accommodation Settings and Stratal Architecture

There is a process–response relationship between accommodation, sediment volumes distribution, and the resulting stratal stacking patterns (Gardner and Cross, in preparation). Accommodation is the key variable that determines whether sediment is preserved and is thus intimately related to the relative proportions of time represented by either erosion surfaces or strata.

Sedimentary rocks preserved in thin, intracratonic wedges deposited in mixed-/low-accommodation settings are typically *surface-dominated strata* (Gardner and Cross, in preparation). For a given unit of geologic time, these strata contain many surfaces of erosion or nondeposition. The net time required for the deposition of strata may have been relatively small compared with the erosional–nondepositional breaks in sedimentation (hiatuses or disconformities) represented by the surfaces that separate stratal units. By contrast, in a typical *stratal-dominated* package, such as Mesozoic or Cenozoic continental margin strata, the thick strata themselves represent much greater net time than do the intervening surfaces, which are generally less numerous and less severe in erosional character.

Surface-dominated, terrigenous clastic strata are typically thin and commonly contain sand-prone, lowstand systems tracts that are rarely fully preserved. Once deposited, parts

of the originally complete systems tracts were commonly stripped away by repeated erosional events. Many cycles of erosion and subsequent thin-bed aggradation produce a complex mosaic comprised of the erosional remnants of several or many diachronous (deposited at different times) systems tracts. The overall effect is such that tracing fossil depositional environments is difficult because the rock record in low-accommodation sequences commonly contains only incomplete pieces of individual, time-equivalent strata. It is analogous to reconstructing a jigsaw puzzle after your Irish Setter has chewed up or eaten half the pieces.

The relative amounts of time represented by surfaces or rocks in depositional sequences are controlled by the accommodation history. Fort Worth Basin strata tend to be surface dominated, especially compared with Mesozoic and younger continental margin deposits, such as those in the Gulf of Mexico Basin. Because of their cratonic, mixed- and low-accommodation settings, Midcontinent strata are surface dominated and are typically made up of complex mosaics of thin, incompletely preserved slivers of systems tracts in which sandstone reservoirs occur.

Reservoir Heterogeneity Varies with Accommodation Setting

Facies characteristics within reservoir sandstone bodies vary with accommodation setting (Gardner and Cross, in preparation). In general, preserved assemblages of bedforms are diverse, and greater numbers and volumes of shale interbeds occur in high-accommodation sequences. Because of the ample available space, sediment reworking is minimal and preservation potential for a given depositional event is high. The opposite is true in low-accommodation reservoirs: constant reworking of sediments winnows clays and concentrates framework sand grains in low-accommodation sequences. Crossbed sets in low-accommodation reservoirs are commonly truncated and incomplete and represent *micro*surface-dominated sandstone facies that are, in effect, the small-scale, fractal equivalents of the surface-dominated strata in which they occur. Although systems tracts

tend to be fragmented and sandstone-body geometries hard to predict in low-accommodation, Midcontinent sequences, once found, internal sandstone heterogeneity is generally low in the absence of diagenetic cements, and these units tend to be productive reservoirs.

Well Log Correlation of Surface-Dominated Strata

Log correlations and mapping of depositional environments and facies tracts in surface-dominated strata are especially difficult and prone to error because it is not uncommon for systems tracts and sometimes even entire sequences to be truncated or absent in some of a field's wells. The process of well-log correlation is inherently biased toward lithostratigraphic correlation: the interpreter typically attempts to recognize and relate specific rock units that display a distinctive pattern on the logs. It is easy for the interpreter to string together rock units having a similar log character or units that appear at similar depths, when in reality, time lines, true reservoir compartment geometries, and flow-unit architectures can be vastly different from layer cake lithostratigraphic interpretations. Today's successful geologist must understand and apply chronostratigraphic concepts, which, in subsurface work, means that one must identify and trace the key time lines or chronostratigraphic surfaces that separate rock units in subsurface reservoirs. The process of tracing chronostratigraphic surfaces between wells can be abstract and difficult, requiring the synthesis of cores, logs, and seismic data containing regional information on tectonics, sea-level history, paleoclimates, and sediment supply. However, it is critical to perform the task properly because without an accurate chronostratigraphic framework, subsequent interpretations and mapping of depositional systems and sandstone reservoir geometries are likely to be incorrect.

rigorously correlative to one another (Fig. A5). As a result of the confusion in the published literature, individual operating companies have been forced to develop their own local nomenclatures. Even within the Boonsville Project Area, there were considerable differences in zone definitions, correlations, and names used by our operator-partners. To facilitate communication between the many project participants, and to allow unrestricted geological interpretation of the Bend Conglomerate interval, it was necessary to create a new, more broadly applicable nomenclature system in which the major reservoir zones were divided by using the concepts of *sequence stratigraphy* (see later discussion). The type log shown in Figure 1.5 illustrates the stratigraphic framework we used to define the major reservoir zones in the Boonsville Project Area. The zones represent major time-equivalent sequences that were subsequently named for local cultural and geographic features in the project area; the widely utilized terms, Caddo and Davis, were preserved because they fit within our sequence stratigraphic framework.

Sediment Sources

All the Boonsville sequences (Fig. 1.5) that we mapped in the project area, except perhaps for the Davis, were sourced from the north, namely from the Muenster and Red River–Electra elements of the Wichita mountain system. Crossbed dip directions within reservoir sandstones throughout the Atoka section analyzed by means of FMI/FMS borehole imaging tools clearly indicate a north-to-south sediment transport direction (Fig. A6). Petrographic and infrared spectroscopic analyses show increasing percentages of feldspars and igneous–metamorphic rock fragments in sandstones upward through the Atoka section, reflecting the erosional unroofing of the granitic core of the Wichita mountain system (Fig. A7).

There is considerable variation in previous interpretations of Lower Atoka sandstone sediment sources. Brown (1973), Ng (1979) and Thompson (1982, 1988) suggested an eastward Ouachitan source, whereas Lahti and Huber (1982), Lovick and others (1982),

Meckel and others (1992), and Ammentorp and Cleaves (1990) agreed with our interpretation for a northern Wichitan source. Review of published literature and communications with Boonsville operators suggests that Thompson's (1982) Ouachitan interpretation may be the most widely applied regional framework in use today, although our data and that of the several others cited above support a northern source.

The Davis sequence (Thompson, 1982; Collins and others, 1992) and the overlying "Grant Deltaic System," which is not present in the SGR Project Area (Lahti and Huber, 1982; also called "Upper Atoka" by Ng, 1979; "Grant Sands" by Lovick and others, 1982; "Post Davis" by Thompson, 1982), both appear to have been derived predominantly from the Ouachitas. The post-Davis, Upper Atoka in our terminology (Wizard Wells and Caddo sequences; Fig. 1.5), were both sourced from the north; well log and seismic clinoform dip directions, FMI-derived paleocurrents, and petrographic analyses point to a feldspar-rich Wichitan source.

Boonsville Geological Data Set

The data available for evaluating Boonsville Bend Conglomerates in the project area primarily consisted of well log data and cores from 222 wells (Table A2) in and around the 3-D seismic survey. Figure A8 shows the aerial distribution of well log suites and the location of cored wells used in the evaluation.

Table A2. Logging suites from 222 wells available for geological evaluation of Boonsville Project Area.

Suite	Logs typically available	Number of wells	% of total wells
MODERN	Gamma ray; density-neutron, SP; resistivity: dual induction, array induction, phaser induction; microlog; +or- PEF (23 wells); +or– Sonic (15 wells)	105	47.3
IES	SP; resistivity: deep induction, 16" (short) normal; microlog	74	33.3
ES	SP; resistivity: lateral; 64" (long) normal; 16" (short) normal; microlog	43	19.4

Methods of Geologic Analysis

OXY U.S.A.'s *Stacked Curves* (*SCPC*) software system was utilized to conduct the geologic evaluation. *Stacked Curves* is a proprietary package developed on a mainframe computer by OXY in the 1980's and recompiled for the IBM-PC platform in the 1990's. It is used extensively throughout the company to determine detailed knowledge of reservoir geometry and associated parameters crucial in infill drilling, field extension, and enhanced recovery projects (Srivistava, 1994). In this project, *SCPC* was used to display, normalize, and perform petrophysical transforms on digital log curves; conduct sequence stratigraphy and correlate reservoir zones; run summations of reservoir parameters; construct reservoir isopach maps; and integrate well data with 3-D seismic data.

OXY also provided a comprehensive digital well data base for the project area and digital well log curves for their acreage. All available log hardcopies from wells within and proximal to Arch-Threshold's and Enserch's properties were digitized and loaded into *SCPC*. Production data for most wells in the project area was also provided by the operator-partners. The SGR reservoir engineering team reviewed production files and constructed an electronic spreadsheet detailing completion zones, dates and other pertinent data, which were input to the *SCPC* database.

Cores from four wells, totaling 358 ft, were slabbed and described, focusing on lithology, facies and depositional environments, key surfaces, and the impact of each of these parameters on reservoir rock quality. Graphical core descriptions and key symbols are shown in Figures C13 through C17. Three of the four cores were collected cooperatively with each one of the three operator-partners. Fifty thin sections were cut from the cores and analyzed to complement core description observations and to determine porosity types, clast provenance, and diagenetic cements.

A log-calculated facies transform was developed by integrating efforts of the geological and petrophysical teams (detailed in Appendix C). Core-calibrated, log-calculated facies curves can help identify the complex lithologies in the Bend Conglomerate interval, which include pyrite, ferroan calcite, and dolomite-cemented sandstone facies and marine limestones that are difficult to distinguish from one another in most of the older log data and many of the modern suites lacking a PEF curve. It is critical to identify the major facies and lithologies accurately, even nonreservoir facies, to make the key surface correlations that define the reservoir architecture.

Application of Sequence Stratigraphy to Boonsville Bend Conglomerates

The concept of *sequence stratigraphy* was instrumental in defining the major time-equivalent or *chronostratigraphic* rock units containing the main reservoir zones in the Boonsville Bend Conglomerates. Sequence stratigraphy is a recent advance representing the synthesis and integration of process sedimentology–depositional systems analysis with seismic stratigraphy research that was created primarily by Exxon Production Research (EPR; for example, Vail and others, 1977). EPR's main premise was that seismic reflections represent *key chronostratigraphic surfaces* that closely approximate time lines, and these surfaces bound genetically related, time-equivalent rock units. Key surface recognition was combined with facies analysis to interpret outcrops, cores, and well logs in the 1980's; refinement and application of sequence stratigraphy continues today (for example, Van Wagoner and others, 1990; Mulholland, 1994). Recognition of key chronostratigraphic surfaces is important in reservoir characterization because these surfaces commonly define sandstone body and internal flow-unit geometries.

Key chronostratigraphic surfaces separate the major types of *depositional systems tracts* that are deposited during distinct phases of a given *base-level cycle*. Base-level cycles (or relative sea-level cycles) result from eustatic sea-level changes, sediment supply, tectonic subsidence, and physiography of the depositional substrate (Cross, 1988; Van

Wagoner and others, 1990; Gardner and Cross, in preparation). *Depositional systems* are three-dimensional assemblages of lithofacies, linked by active (modern) or inferred (ancient) processes and environments (Fisher and McGowen, 1967). A *depositional systems tract* (Brown and Fisher, 1977) is a linked assemblage of contemporaneous depositional systems. The sedimentary deposits of depositional systems tracts are commonly bounded by key surfaces that can manifest themselves as seismic reflections if the combination of bed thickness, acoustic-impedance contrast across surface boundaries, and seismic data-frequency content are favorable.

Boonsville–Atoka Sequences

In the Boonsville Project Area, complexly arranged key chronostratigraphic surfaces are a major control on compartmentalization and architecture of Atokan reservoirs (Fig. 1.6). Key surfaces are widespread physical surfaces that separate younger strata from underlying older strata. Facies offsets, or facies dislocations as they are sometimes called, that interrupt normal Walther's Law facies successions commonly occur at these surfaces. The familiar methods of depositional systems analysis and facies modeling are valid only within time-rock units bounded by key surfaces. After core-calibration, facies, key surfaces, and systems tracts could be inferred from well log responses (Fig. A9), but the degree of reliability varied with data vintage and quality.

Three types of key surfaces were identified, correlated, and used as defining boundaries for Boonsville Bend Conglomerate reservoir zones: flooding surfaces (FS), maximum flooding surfaces (MFS), and erosion surfaces (ES). *Flooding surfaces* are widespread surfaces where evidence of a upward-deepening facies dislocation occurs, such as the contact between rooted, unfossiliferous floodplain mudstones and overlying fossiliferous marine shale. A *ravinement surface* is a type of flooding surface where evidence suggests that transgressive passage of a surf zone has slightly eroded the

underlying shallower water facies. Several ravinement-type flooding surfaces occur in Bend Conglomerate cores (for example, the lowermost FS illustrated in Figure 1.6), suggesting that these surfaces are a common and typical component of Atokan cyclothems.

Maximum flooding surfaces are widespread, upward-deepening surfaces associated with the inferred, deepest water facies encountered in a succession of strata. The MFS is commonly represented by a thin *condensed section*, typically a black, organic-rich shale having a low-diversity fossil assemblage representing deep-water, sediment-starved conditions. Boonsville Bend Conglomerate maximum flooding shales are slightly bioturbated, sparsely fossiliferous, fissile black shales that typically occur near the base of upward-coarsening facies successions (Fig. 1.6).

The maximum flooding surfaces bound and define the upward-coarsening facies successions and are termed *genetic sequences* (Galloway, 1989; Gardner and Cross, in preparation), which are similar to cycles or cyclothems in other terminology (for example, Wanless and Weller, 1932; Moore and others 1944). At least a dozen genetic sequences averaging approximately 100 ft in thickness have been observed in the Boonsville–Atokan strata of the project area.

One or more *erosion surfaces* occur within the Boonsville–Atokan genetic sequences, where evidence of a facies offset indicating an abrupt decrease in water depth occurs. Many of the erosion surfaces are widespread, and truncation of older strata can be documented on well log cross sections, suggesting that these particular surfaces may be unconformities representing downcutting during periods of subaerial exposure caused by *allocyclic* (extrabasinal) mechanisms, such as eustatic sea-level changes. Other erosion surfaces appear to be local diastems, such as fluvio-deltaic channel avulsion within depositional systems tracts caused by *autocyclic* (intrabasinal) mechanisms. When working at the field or reservoir scale, to precisely determine the significance and dimension of a particular erosion surface such that an allocyclic or autocyclic distinction could be made is difficult to impossible. A large-scale, Fort Worth Basin analysis would be required to begin an

understanding of the regional context of erosion surfaces encountered in a particular field or reservoir. However, speculative inferences regarding the relative significance of erosion surfaces were made by comparing the relative ease of ES identification and breadth of occurrence in the project area, sandstone net reservoir isopach map patterns, and depths of truncation. Understanding the regional context of erosion surfaces can help transfer correlation and play concepts to other fields and even other basins where time-equivalent, hydrocarbon-productive strata occur.

Some of the Boonsville–Atokan reservoir units can be more precisely defined by erosion surfaces or a combination of flooding and erosion surfaces. Delineation of depositional sequences that have unconformities or erosion surfaces is a common practice advocated by Exxon Production Research, and in this report, reservoir units defined by erosion surfaces are referred to as Exxon sequences (Fig. A10).

Base-Level Cycles and Systems Tracts

The repetitive pattern of stacked genetic sequences or cyclothems comprising the Bend Conglomerate interval was produced as a result of cyclically fluctuating base level superimposed upon long-term subsidence. Stratigraphic base level is an equilibrium surface, below which sediments can accumulate and above which the processes of erosion are dominant. There are more complex definitions of base level (for example, Shanley and McCabe, 1994; Gardner, 1995a), but for the practical purposes of this field-scale project, base level can be considered to be similar to relative sea level. The term is used herein without specific reference to particular forcing mechanisms, such as eustatic sea level, tectonic movement, sediment supply and sediment loading, and physiography, although global stratigraphic evidence suggests that cyclic stacking of many of the Boonsville–Atokan genetic sequences resulted from glacioeustatically induced base-level changes superimposed upon long-term subsidence of the Fort Worth Foreland Basin.

Boonsville–Atokan genetic sequences are made up of three depositional systems tracts associated with highstand, lowstand, and transgressive phases of inferred base level (Fig. 1.6). The deposits of a typical *highstand depositional systems tract* consist of an upward-coarsening facies succession beginning with dark gray, maximum flooding mudstones, and grading upward into highstand calcareous shoreface–delta front sandstones that represent progradational facies that filled accommodation available during base-level maxima and subsequent fall. Highstand tracts are truncated by an erosion surface and overlain by the *lowstand depositional systems tracts* comprising complex, fluvial, and deltaic conglomeratic sandstones, which are capped by estuarine and carbonaceous floodplain mudstones and thin, fine-grained sandstones. *Transgressive depositional systems tracts* consist of bioturbated, calcareous sandstones or shallow-marine limestones that commonly overlie a ravinement surface.

New Interpretation for Bend Conglomerate Reservoirs

We introduce a new interpretation of the Boonsville–Atoka section on the basis of application of sequence stratigraphic concepts: most of the productive, Bend Conglomerate sandstone bodies represent complex mosaics of fluvial and deltaic deposits that formed during base-level lowstands. The sandstone bodies most commonly occur immediately above mappable erosion surfaces, some of which are probably unconformities related to periods of maximum continental (Gondwana) glaciation at the Atokan south pole. The Boonsville Project Area is close to the Fort Worth Basin's peripheral bulge, namely the Bend Arch, which was a shallow area where accommodation was relatively low, such that repeated exposure and incision was followed by inundation and backfilling as base level fell and rose, respectively. These rather severe swings in sedimentary conditions, coupled with high rates of sediment supply and a subtle, complex, structurally controlled physiography resulted in a highly compartmentalized, complex reservoir architecture.

General Geologic Parameters of the Project Area

Gross Stratigraphic Architecture

The Bend Conglomerate interval thins markedly but relatively smoothly from southeast to northwest in the project area (Figures 1.5, 1.6, 1.7), reflecting the onlap of strata onto the Bend Arch, which was the active peripheral bulge of the Fort Worth Foreland Basin during sedimentation. Within the boundaries of the 3-D seismic survey, Atokan strata range from 869 to 1,334 ft, and average 1,078 ft in gross isopach thickness (Fig. A11). In this report, the Atokan interval is defined by the MFS90, which is the top of the Caddo zone, to MFS10, the base of the Vineyard (Fig. 1.5). Most of the Bend Conglomerate wells in the project area targeted the basal Vineyard zone but stopped short of the Marble Falls to avoid lost circulation of drilling fluids in porous karst zones within the limestone. Because only 13 project area wells penetrated the Marble Falls Limestone, which is the true base of the Atoka interval, the estimate of MFS90 to MFS10 interval made from 117 wells is slightly thinner (91 to 145 ft) but representative of total Atokan–Bend Conglomerate thickness trends.

Total Atoka net reservoir sandstone (Fig. A14) averages 77 ft, but varies considerably within the project area, ranging from 0 to 189 ft, and has strikingly different isopach trends compared with the gross isopach. Net reservoir sandstone values for particular zones were determined for each well by summing the total well log curve footage meeting petrophysical cutoff criteria, namely an SP curve value of less than –30 millivolts and a resistivity of greater than 10 ohm-m. The 75-ft contour in Figure A14 defining two major regions of thin (0 to 75 ft) and thick (75 to 125 ft) net reservoir sandstone roughly corresponds to the west-southwest and east-northeast halves of the project area, respectively. The distribution of net reservoir sandstone indicates that high-energy, fluvio-deltaic systems preferentially occupied the east-northeast half of the area. Structure mapping from both well control and

3-D seismic suggests a link between basement Paleozoic carbonate structure and thick, multistoried sandstone reservoirs.

Structure

Maps representing structural elevations of well-defined, maximum flooding surfaces that occur near the base, middle, and top of the Bend Conglomerates are presented in Figures A15, A16, and A17, respectively. Structure in the project area is more complex at the base of the Atoka (Fig. A15) and becomes simpler upward through the section, and overall structural dip rotates from east-northeastward to northward upsection. Structure at the MFS20 (or Vineyard) level exhibits a high west side and a southeast-plunging structural nose (referred to as Noles Nose), with lower areas falling off both limbs. Only a small vestige of Noles Nose is apparent at the MFS60 (or Trinity; Fig. A16) level, and the feature is essentially absent at the MFS90 (or Caddo; Fig. A17) level.

Many small-scale, near-vertical fault zones having ovoid time-structure map patterns are present throughout the Bend Conglomerate section and are particularly prevalent in the Lower Atoka and underlying Paleozoic carbonate horizons (Chapter 2). Most of these high-angle, normal and reverse faults have less than 100 ft of displacement and are typically on the order of 20 to 30 ft. The faults rarely penetrate the overlying Strawn Group, indicating that structural movements occurred predominantly during Atoka time. Figures A18 and A19 illustrate the subtle, near-vertical faults, which were added to the well log cross sections after examination of arbitrary 3-D vertical sections coincident with the well control. Although hints of faulting can be detected from well control, confident estimates of vertical displacements and fault-block geometries cannot be determined without 3-D seismic data.

We interpret these features to have resulted from dissolution and subsequent, episodic collapse of karst cavities in the Paleozoic platform carbonate units, namely, the Marble Falls (Pennsylvanian Morrow), Comyn (Mississippian), and Ellenburger (Cambro-Ordovician) Formations underlying the Atoka interval. In map view, the karst collapse

features occur in broadly defined, dominantly north-northwesterly linear groups (Figs. 2.1 and 2.2), suggesting a genetic relationship between karst-dissolution processes and preexisting, subtle basement faulting. The faults are consistently vertical, but horizontally discontinuous, and the extent of vertical displacement at a particular stratigraphic level varies significantly across the project area, suggesting that sites of collapse were anchored in space, but that the collapse events were episodic and localized. The karst collapse features probably represent buried caverns and sinkholes, perhaps similar to those found in Florida, Kentucky, and Central Texas, that were covered by Bend Conglomerate sequences, whose sediment-loading effects most likely triggered collapse.

Structure and Sedimentation

Figure A20 is a near Marble Falls seismic time-structure map that has the total Atokan net reservoir isopach contours of Figure A14 superimposed upon it. A strong relationship exists between structurally low areas on the pre-Atoka surface and areas where thick net reservoir sandstone occurs. The majority of the differences in the two map patterns can be explained by data differences in data resolution. The net reservoir isopach map was derived from 117 wells, whereas the time-structure map was constructed from 81,204 data traces: the 3-D seismic map has a nearly 700-fold horizontal resolution advantage over the well-control isopach map.

This positive relationship implies that subtle differences in structural elevation at the pre-Atoka, Paleozoic carbonate stratigraphic level controlled the geographical locations of incised valleys, fluvial and fluvio-deltaic axes in which high-energy reservoir facies were concentrated. Many of the thickest valley-fill sandstone reservoirs occur above or immediately adjacent to vertically faulted karst collapse zones (for example, see Chapter 3). Modern stream and river courses (some now drowned in Lake Bridgeport's waters) also appear to be controlled to a certain extent by the basement structure at the Paleozoic

carbonate level, suggesting that structure has continued to influence the position of depositional systems up to the present time (Fig. A21).

Geologic Controls on Gas Production

The lion's share of natural gas produced within the Boonsville Project Area has come from the Vineyard zone (Fig. 1.5), which is commonly referred to as the basal conglomerate of the Bend interval (Appendix B). The Vineyard is the most predictable, widespread, and least compartmentalized of the Atoka reservoir sandstones. Although early production data was not available for most wells, productivity estimated from cumulative production data suggests that the best production has occurred where thick Vineyard sandstone sweetspots are draped over subtle structural highs (Fig. A22).

After more than 30 yr of steady production, the Vineyard zone is widely depleted (Appendix B). It is likely that most future reserve growth will be derived from smaller, more stratigraphically compartmentalized zones overlying the Vineyard.

Reservoir Compartmentalization Styles in Atokan-Bend Conglomerates

The predominant compartmentalization mechanisms observed in the Boonsville Project Area are *stratigraphic*, comprising surface-bounded, facies-bounded and cement-bounded compartments; *structural*, mainly fault-bounded compartments; and perhaps the most common type encountered at Boonsville is a *combination* of stratigraphic and structural mechanisms.

Stratigraphic Compartmentalization

Surface-bounded compartments result from the juxtaposition of reservoir sandstones and impermeable facies at key chronostratigraphic surfaces. This type of stratigraphic compartmentalization is typically a broad-scale phenomenon because of the widespread

nature of key surfaces. Lowstand valley-fill sandstones common in many Bend Conglomerate sequences are examples of surface-bounded compartments. Most of the stratigraphic compartmentalization in the surface-dominated strata of low–mixed accommodation Midcontinent basins is likely to be of the surface-bounded type.

Facies-bounded compartments result from high-frequency autocyclic processes within the depositional systems tract. For example, mud-drape barriers deposited on point-bar sands during waning flood stages, or, on a larger scale, an abandoned delta lobe can founder and be encased in inner shelf or prodelta mudstones.

Diagenetic cements can occlude porosity in Midcontinent reservoir sandstone units and may be significant intrafacies flow barriers in some instances. Quartz overgrowths, calcite, ferroan calcite, and dolomite are common in project area cores, and secondary porosity is also common, indicating a complex fluid migration history and a high degree of postdepositional redistribution of mineral matter.

Structural Compartmentalization

Several Boonsville wells drilled in small (~ 100 acres), structurally high fault blocks encountered gas at higher than expected pressures in otherwise hydraulically well connected reservoir zones (Caddo, Vineyard), suggesting that the vertical faults can act as partial barriers to fluid flow (see Chapter 2 for details). Because potential fault-bounded compartmentalization can be quickly and easily identified from 3-D seismic, a quick-look infill drilling strategy is to identify fault-bounded blocks having no well penetrations that occur in subregional or field-scale areas where (1) the pre-Atoka time structure is low, (2) total Atoka net reservoir isopachs are thick, and (3) net pay interval maps indicate good potential for finding multiple reservoir zones.

The apparently episodic fault movements, inconsistent vertical displacements, and the general lack of lateral continuity suggest that the sealing properties may be variable as well. Even so, knowledge of fault-block geometries can nonetheless help in identifying areas

having a higher potential for isolating fluid communication between otherwise continuous reservoir zones, and can therefore be used to upgrade locations and reduce risks in development drilling programs.

Combination of Stratigraphic and Structural Compartmentalization

It is likely that a spectrum of compartment types exist between those of purely structural and those of purely stratigraphic origin. In addition, because of the structural influence on sandstone distribution, and because of the limited degree to which stratigraphic compartments can be resolved, it is sometimes difficult to precisely determine the relative impact of structural versus stratigraphic mechanisms.

Detection Resolution of Compartment Types

As mentioned earlier, most types of stratigraphic compartments in Atokan-Bend Conglomerates are difficult to predict using existing technologies. Large-scale, surface-bounded reservoir zones can be differentiated using well control, and the numerous lowstand valley-fill sandstone reservoirs throughout the Atoka section provide many good examples. Surface-bounded compartmentalization can also be detected using seismic attributes analysis, where stratigraphically calibrated isochrons (i.e., seismic reflectors) can be readily traced in zones where net reservoir values in sandstone bodies significantly exceed 25 to 30 ft in thickness over large areas (for example, Upper and Lower Caddo, Chapter 3). It is difficult to detect surface-bounded compartments by means of seismic attributes analysis in most of the Lower Atoka, thin-bed zones having the most reserve growth potential.

We were unable to document facies- or cement-bounded compartmentalization definitively using well control or 3-D seismic because they occur within surface-bounded systems tracts and thus operate at a very small scale (tens to hundreds of feet). A large core

data base coupled with detailed petrographic analyses would be required to properly assess compartmentalization at scales relevant to lateral changes in facies and cements. However, this type of compartmentalization is probably common in the Bend Conglomerates; several case history examples document closely spaced wells that are hydraulically isolated from one another because of fine-scale barriers likely to be the result of facies changes, cements, or both (for example, I. G. Yates No. 33).

Although nearly impossible to delineate using well control, structural, fault-bounded compartments can be quickly and easily identified in the 3-D seismic data. Very fine scale fault displacements of less than 20 ft, and fault-block geometries can be mapped with confidence from the 3-D seismic data. The seismic does not, however, provide information regarding the sealing qualities of the faults nor estimates of reservoir pressures: these must be inferred from well log geology and engineering assessments of pressure regimes in the targeted reservoir zones.

Relationship between Compartment Size and Relative Accommodation

Although the Fort Worth Basin accommodation setting was low–intermediate during the Atoka, accommodation varied through Atoka time such that each of the Bend Conglomerate sequences (Fig. 1.5) was deposited under unique conditions that affected their respective reservoir properties. Accommodation is the amount of space that was available below base level, in which the sediment of a particular sequence could accumulate, and, thus, it cannot be determined precisely. However, geological parameters such as gross thickness, average net reservoir sandstone thickness, average net:gross ratio, and number of individual sandstone beds per zone can help provide a comparative estimate of the relative amount space available during deposition of each reservoir-bearing sequence at Boonsville (Table A3).

Table A3. Semiquantitative relationship between relative accommodation and typical compartment size.

Relative accommodation setting	Estimate of typical compartment sizes	Geologic description
HIGH	?<100 MMcf ?<50 acres	High gross (G); low net/gross; small, relatively tight facies-bounded compartments: for example, downlapping deltaic lobes separated by shale barriers
INTERMEDIATE	100–250 MMcf 10–75 acres	Intermediate gross; variable net/gross; commonly surface bounded compartments; variable permeability: for example, multistoried channel-fill or valley-fill deposits
LOW	200 MMcf to >1 Bcf 50 to > 160 acres	Low-intermediate gross; high net/gross; hydraulically well connected; variable permeability: for example, relatively sheetlike, continuous sandstone with multiple, internal erosion surfaces; best potential for structural compartmentalization

Figure A23 illustrates the semiquantitative relationship between estimated relative accommodation and typical reservoir compartment-size estimates (in MMcf reserves), which were calculated in the engineering analysis (Appendix B). Most of the lower accommodation settings (for example, Vineyard, Trinity) occurred during deposition of the bottom half of the Atoka section, whereas the highest accommodation settings (for example, Davis, Wizard Wells) are younger, upper Atoka sequences. Three specific examples of Boonsville sequences are presented below to illustrate the characteristics of reservoirs deposited in high, intermediate, and low relative accommodation settings.

High-Accommodation Example: Wizard Wells Sequence

The Wizard Wells genetic sequence is defined by the interval between maximum flooding surfaces MFS80-MFS70, which averages approximately 200 ft in gross thickness

(Fig. 1.5). Despite its great thickness relative to all the other sequences, only a small volume of productive sandstone reservoir occurs in this largely shale prone unit (Fig. A24). The majority of the net reservoir sandstone occurs near the top of the sequences in several discreet lobes in the north-northeastern portion of the project area.

Careful tracing of resistivity patterns indicates that the Wizard Wells is comprised of southward-dipping clinoforms representing a highstand delta prograding south-southeastward into a relatively deep body of water (Fig. A25). Local erosion surfaces that probably represent channel-cut diastems can be identified in the sandstone-rich lobes in the northwest quadrant of the project area, but there is not a single, through-going erosion surface as is typical of many other Boonsville sequences. Low net-reservoir volume, preservation of several small facies-bounded sandstone bodies, very high gross thickness, and overwhelming predominance of mudstones suggest that a relatively high amount of accommodation was available during Wizard Wells deposition.

Intermediate-Accommodation Example: Jasper Creek Sequences

The Jasper Creek sequences represent an intermediate relative accommodation example in the comparative examination of reservoir types found within Bend Conglomerate sequences. Intermediate relative accommodation type reservoirs are the most attractive targets for future gas reserve growth because they are highly compartmentalized and thus likely to contain untapped reserves. In addition, the upside potential for finding relatively large compartments is high: several more recent wells—for example, the Billie Yates No. 2 (Runaway) and the Billie Yates No. 3 (Lower Jasper Creek)—have produced more than 1 Bcfg in these types of compartments.

The Jasper Creek sequence is a thick, erosion-surface-bounded sequence that consists of four subsequences, each one of which contains sinuous belts of reservoir sandstone (Figs. A26, A27). Severe erosional truncation of the uppermost Jasper Creek sequences by the ES40 (Beans Creek) occurs in the northern part of the project area (Fig. A28). Oldest to

youngest, these ES-based subsequences are Lower (ES30-ES34), Middle (ES34-ES36), Upper (ES38-ES36), and 4th Jasper Creek (FS39-ES38). The bases of the ES30 and ES34 exhibit significant erosional truncation across the project area, suggesting they represent unconformities. The thick uppermost Jasper Creek strata (above FS34) contain numerous upward-shoaling lobes (parasequences), and it is more difficult to trace erosion surfaces (ES36, ES38) in areas where sharp-based, channel-fill sandstones are absent, suggesting that the ES36 and ES38 may be local diastems. Review of individual Jasper Creek net reservoir sandstone isopachs (Figs. A29 through A32) indicates a progressive upward decrease in net reservoir sandstone volume, suggesting that a large-scale transgressive event occurred during Jasper Creek deposition.

Reservoir compartments in the Jasper Creek sequences are mostly surface-bounded valley-fill deposits, with varying degrees of internal facies- and cement-bounded barriers. The Jasper Creek net reservoir sandstone isopach shown in Figure A27 contains a greater area where net reservoir is present (exceeds zero) as compared with the Wizard Wells isopach (Fig. A24), which has a vast area containing no reservoir rock; decrease in accommodation favors greater lateral distribution of sand in the depositional system. Both sequences are similar in that they contain several discrete sandstone bodies; however, the Jasper Creek sequences are dominated by fluvio-deltaic valley-fill and distributary-channel deposits, several of which may represent entirely different base-level cycles, whereas the Wizard Wells sandstone bodies appear to be the result of shifting of lower energy deltaic environments within a large-scale progradational event during the highstand of a single base-level cycle.

Low-Accommodation Example: Caddo

In contrast to the Wizard Wells and Jasper Creek isopachs (Figs. A24 and A27), the total Caddo net reservoir sandstone isopach in Figure A33 illustrates a more widespread sandstone distribution typically found in a relatively low accommodation setting. The

Caddo contains only two discrete sandstone bodies that occur within a Lower Caddo highstand systems tract (MFS80-ES95) and Upper Caddo lowstand systems tract (MFS90-ES95). Judging from clinoform geometries, rock types and high feldspar contents, and FMI paleocurrent indicators, Caddo sediment transport is inferred to have been southward from Red River (Electra) and Muenster granitic terrains.

The Lower Caddo is a southward-prograding deltaic system, exhibiting low-angle, shingled clinoforms (Fig. A34). "The Caddo Limestone" in the project area actually comprises two separate carbonate units representing the abandonment and transgression of two distinct delta-lobe platforms. Figure A35 shows a northeast-trending net reservoir thick in the south half of the project area that is interpreted to be a strike-oriented, delta-front deposit. Sinuous, south-trending ribbons of thin sandstone north of the delta front sandstone may represent minor fluvial or distributary channels. The Lower Caddo is an oil-productive zone and it occurs in the area of highest structural elevation at the Caddo level (Fig. A17).

The Upper Caddo sandstone is a broad southeast-trending belt of sandstone with several smaller sinuous fingers extending from it to the south and southwest (Fig. A36). Overall, the Upper Caddo represents a large incised valley-fill system that was filled by high-energy fluvial and deltaic-channel deposits.

The Upper Caddo overlies a conspicuous erosional surface, ES95, which is inferred to be an unconformity. Caddo limestones do not occur above the sharp-based, blocky to upward-fining Upper Caddo sandstone (Fig. A39), and sharp-based upward-fining sandstones are generally not present below Caddo limestones. In the northeastern part of the project area, Upper Caddo sandstone sharply overlies shelf mudstones, a marked facies dislocation suggesting that erosional stripping of units has occurred.

Although most of the Caddo production in the project area is oil, significant gas reserves have been found in Upper Caddo wells (for example, Sealy "C" No. 2 and "C" No. 3) located structurally downdip relative to the Lower Caddo oil accumulation in the

south, indicating that the two units are physically separate reservoir compartments. The Upper and Lower Caddo Sandstones occur in distinctly different systems tracts and provide an excellent example of surface-bounded reservoir compartmentalization on a fieldwide scale.

Summary and Conclusions of Geologic Evaluation

A computer-based geologic evaluation of well log curves and cores from an approximately 30-m^2 portion of Boonsville Bend Conglomerate Gas field was conducted by part of an interdisciplinary team assigned the task of developing infill drilling strategies to increase natural gas reserves in the mature Midcontinent region. The following has been uncovered as a result of this endeavor:

- Late Paleozoic strata of the U.S. Midcontinent region, including those containing hydrocarbon reservoirs, represent the thin, updip stratigraphic remnants of sea-level highstands deposited in stable cratonic areas. These rocks can be described as surface-dominated strata; there is relatively more geologic time represented by surfaces than by preserved strata.
- Surface-dominated, terrigenous clastic strata are typically thin and commonly contain sand-prone, lowstand systems tracts that are rarely fully preserved. The Fort Worth Foreland Basin provided a mixed-accommodation setting into which Atokan surface-dominated strata were deposited.
- When performing geological correlations in surface-dominated, Midcontinent reservoirs, researchers must recognize major erosional features that have cut out previously deposited sequences and shingling, clinoform geometries in which several individual sandstone compartments can occur that appear to be one unit in well log cross sections.
- The Bend Conglomerate stratigraphic interval averages 1,100 ft in thickness in the Boonsville Project Area and consists of sandstone, limestone, and mudstone

deposits representing the 2- to 7-million-yr-long Atoka Epoch, which is part of the Early Middle Pennsylvanian Period (Carboniferous Upper Westphalian Series).

- The Boonsville Bend Conglomerate stratigraphic interval is composed of 10 genetic stratigraphic sequences (or genetic sequences) that average about 100 ft in gross thickness. The genetic sequences are defined and bounded by impermeable, deep-shelf shales that represent relative maximum flooding events. Genetic sequences are similar to cycles or cyclothems used by many workers to describe repetitive stratigraphic successions in upper Paleozoic strata.
- Individual genetic sequences contain a well-defined succession of *depositional systems tracts*, including *highstand*, *lowstand* and *transgressive* tracts. The inferred systems tracts are defined and bounded by key chronostratigraphic surfaces, namely *maximum flooding surfaces* (MFS), *erosion surfaces* (ES), and transgressive *flooding surfaces* (FS). Highstand, lowstand, and transgressive systems tracts are inferred to coincide broadly with high and falling base level, base-level minima and early-phase base-level rise, and rising base level, respectively.
- Thickness and lithologic trends in Bend Conglomerate genetic sequences suggest that eustasy may have been the dominant variable controlling base-level cycles that created the complex stratal architecture. Atokan relative sea-level interpretations of Ross and Ross (1988) indicate an overall increase in eustatic sea level punctuated by high amplitude (100 to 300 m) and high-frequency (100,000 to 400,000 yr) sea-level cycles. The Boonsville Project Area was probably alternately subaerially exposed then inundated by marine waters at least 6, and perhaps as many as 10, times during Atoka time.
- Natural gas reservoirs at Boonsville occur predominantly as lowstand, valley-fill conglomeratic sandstones; they owe their existence to erosional downcutting (incisement), which occurs during relative base-level lowstands, followed by

subsequent aggradation during the early phase of relative base-level rises. Highstand deltaic and shoreface sandstones are also important reservoirs that occur as progradational lobes. Lowstand fluvial and deltaic deposits overlie and erosionally truncate highstand deposits; however, their respective reservoir sandstone bodies typically occur as separate compartments.

- Many small-scale, near-vertical fault zones, which cannot be mapped without 3-D seismic data, have oval or circular patterns present on time-structure maps. Most of these high-angle normal and reverse faults have less than 100 ft of displacement; they rarely penetrate the overlying Strawn Group; and they are closely associated with karst collapse features in the underlying Paleozoic platform carbonate units.
- In map view, the karst collapse features occur in broadly defined, dominantly north-northwesterly linear groups, suggesting a genetic relationship between karst-dissolution processes and preexisting, subtle basement faulting.
- Isopach mapping of the sum of all net reservoir (i.e., total Atoka net reservoir) contained in the Bend Conglomerate within the project area indicates a strong relationship between sandstone-reservoir distribution and structurally low areas on the pre-Atoka, seismic time-structure surface. This fact implies that subtle differences in structural elevation at the pre-Atoka, Paleozoic carbonate stratigraphic level controlled the geographical locations of incised valleys, fluvial and fluvio-deltaic axes in which high-energy reservoir facies were concentrated. Many of the thickest valley-fill sandstone reservoirs occur above or immediately adjacent to vertically faulted, karst collapse zones.
- The predominant compartmentalization mechanisms observed in the Boonsville project area are (1) stratigraphic, comprising surface-bounded, facies-bounded and cement-bounded compartments; (2) structural, mainly fault-bounded

compartments; and perhaps the most common type encountered at Boonsville, (3) a combination of stratigraphic and structural mechanisms.

- Three types of stratigraphic compartmentalization mechanisms occur in the Boonsville project area. Surface-bounded compartments result from the juxtaposition of reservoir sandstones and impermeable facies at key chronostratigraphic surfaces. Facies-bounded compartments result from high-frequency autocyclic processes within the depositional systems tract. Diagenetic cements can occlude porosity in Midcontinent reservoir sandstone units to the extent that cement-bounded compartments arise.
- Accommodation varied through Atoka time such that each of the Bend Conglomerate sequences was deposited under unique conditions that controlled compartment size. Geological parameters such as gross thickness, average net reservoir sandstone thickness, average net:gross ratio, and number of individual sandstone beds per zone can help provide a comparative estimate of the relative amount of space available during deposition of each reservoir-bearing sequence, and an estimate of expected compartment sizes can be made and used as a screening tool.
- Seismic attribute analysis of confidently interpreted reservoir zones (i.e., genetic sequences) holds great promise for identifying stratigraphic prospects in some of the thicker, low-accommodation reservoir zones, such as the Caddo. Although attribute analysis can in some instances provide startling, magic-bullet identification of interwell reservoir properties, in Midcontinent thin-bed reservoirs, it is an advanced task requiring very accurate horizon interpretations and expert workstation data-manipulation techniques that go well beyond a quick-look interpretation of the 3-D data.

References

Ammentorp, A. D., and Cleaves, A. W., 1990, Depositional systems, petrography, and hydrocarbon entrapment in the upper Atokan "Caddo" clastics interval on the northwestern margin of the Fort Worth Basin: Transactions of the American Association of Petroleum Geologists, Southwest Section, 1990 Annual Convention &, & eds., p. 121–130.

Berger, A., 1988, Milankovitch theory and climate: Reviews of Geophysics, v. 26, no. 4, p. 624–657.

Blanchard, K. S., Denman, O., and Knight, A. S., 1968, Natural gas in Atokan (Bend) section of northern Fort Worth Basin, *in* Beebe, B. W., and Curtis, B. F., eds., Natural gases of North America: American Association of Petroleum Geologists Memoir 9, v. 2, p. 1446–1454.

Boardman, D. R., II, and Heckel, P. H., 1989, Glacial-eustatic sea-level curve for early Late Pennsylvanian sequence in north-central Texas and biostratigraphic correlation with curve for midcontinent North America: Geology, v. 17, no. 9, p. 802–805.

Brown, L. F., Jr., 1973, Pennsylvanian rocks of north-central Texas: an introduction, *in* Brown, L. F., Jr., Cleaves, A. W., II, and Erxleben, A. W., Pennsylvanian depositional systems in north-central Texas: a guide for interpreting terrigenous clastic facies in a cratonic basin: The University of Texas at Austin, Bureau of Economic Geology, Guidebook No. 14 prepared for Geological Society of America field trip, p. 1–9.

Brown, L. F., Jr., and W. L. Fisher, 1977, Seismic-stratigraphic interpretation of depositional systems: examples from Brazilian rift and pull-apart basins, *in* Payton,

C. E., ed., Seismic stratigraphy—applications to hydrocarbon exploration: American Association of Petroleum Geologists Memoir 26, p. 213–248.

Brown, L. F., Jr., Solis-Iriate, R. F., and Johns, D. A., 1990, Regional depositional systems tracts, paleogeography, and sequence stratigraphy, Upper Pennsylvanian and Lower Permian strata, north- and west-central Texas: The University of Texas at Austin, Bureau of Economic Geology Report of Investigations No. 197, 116 p.

Caputo, M. V., and Crowell, J. C., 1985, Migration of glacial centers across Gondwana during the Paleozoic Era: Geological Society of America Bulletin, v. 96, no. 8, p. 1020–1036.

Cheney, M. G., and Goss, L. F., 1952, Tectonics of central Texas: American Association of Petroleum Geologists Bulletin, v. 36, no. 12, p. 2237–2265.

Collins, E. W., Laubach, S. E., Dutton, S. P., and Hill, R. E., 1992, Depositional environments, petrology and fractures of the Atoka Davis Sandstone: a low-permeability gas-bearing sandstone of the Fort Worth Basin, north-central Texas, *in* Cromwell, D. W., Moussa, M. T., Mazzullo, L. J., eds., Transactions of the American Association of Petroleum Geologists, Southwest Section, Publication 92-90, p. 221–230.

Connolly, W. M., and Stanton, R. J., Jr., 1992, Interbasinal cyclostratigraphic correlation of Milankovitch band transgressive-regressive cycles: correlation of Desmoinesian–Missourian strata between southeastern Arizona and the midcontinent of North America: Geology, v. 20, no. 11, p. 999–1002.

Cross, T. A., 1988, Controls on coal distribution in transgressive-regressive cycles, Upper Cretaceous, Western Interior, U.S.A., *in* Wilgus, C. K., Hastings, B. S., Ross, C. A., Posamentier, H., Van Wagoner, J., and Kendal, C. G. St. C., eds., Sea-level

changes: an integrated approach: Society of Economic Paleontologists and Mineralogists Special Publication No. 42, p. 371–380.

Crowell, J. C., 1982, Continental glaciation through geologic times, *in* Climate in Earth history: Washington, National Academy Press, p. 77–82.

Crowell, J. C., and Frakes, L. A., 1970, Phanerozoic glaciation and the causes of ice ages: American Journal of Science, v. 268, no. 3, p. 193–224.

_____ 1975, The Late Paleozoic glaciation, *in* Campbell, K. S. W., ed., Gondwana geology: papers presented at the third Gondwana symposium, Canberra, Australia, 1973, p. 313–331.

Crowley, T. J., and Baum, S. K., 1991, Estimating Carboniferous sea-level fluctuations from the Gondwanan ice extent: Geology, v. 19, no. 10, p. 975–977.

Donovan, D. T., and Jones, E., 1979, Causes of world-wide changes in sea level: Journal of the Geological Society of London, v. 136, p. 187–192.

Fisher, W. L., and McGowen, J. H., 1967, Depositional systems in the Wilcox Group of Texas and their relationship to occurrence of oil and gas, *in* Gulf Coast Association of Geological Societies Transactions, v. 17, p. 105–125.

Flawn, P. T., Goldstein, A. G., Jr., King, P. B., and Weaver, C. E., 1961, The Ouachita System: University of Texas, Austin, Bureau of Economic Geology Publication No. 6120, 401 p.

Galloway, W. E., 1989, Genetic stratigraphic sequences in basin analysis I: architecture and genesis of flooding-surface bounded depositional units: American Association of Petroleum Geologists Bulletin, v. 73, no. 2, p. 125–142.

Gardner, M. H., 1995a, Tectonic and eustatic controls on the stratal architecture of Mid-Cretaceous stratigraphic sequences, Central Western Interior Foreland Basin of North America, *in* SEPM (Society for Sedimentary Geology) Special Publication No. 52, p. 243–281.

Gardner, M. H., 1995b, The stratigraphic hierarchy and tectonic history of the Mid-Cretaceous Foreland Basin of central Utah, *in* SEPM (Society for Sedimentary Geology) Special Publication No. 52, p. 283–303.

Gardner, M. H., and Cross, T. A., in preparation, Time-space partitioning of sediment volumes in facies tracts: a primary control on stratal geometry and facies architecture of depositional sequences.

Glover, G., 1982, A study of the Bend Conglomerate in S. E. Maryetta Area, Boones-ville [sic] Field, Jack County, Texas: Dallas Geological Society &

Goldhammer, R. K., Oswald, E. J., and Dunn, P. A., 1991, Hierarchy of stratigraphic forcing: example from Middle Pennsylvanian shelf carbonates of the Paradox Basin, *in* Franseen, E. K., and others, eds., Sedimentary modeling: computer simulations and methods for improved parameter definition: Kansas Geological Survey Bulletin No. 233, p. 361–413.

Heckel, P. H., 1977, Origin of phosphatic black shale facies in Pennsylvanian cyclothems of mid-continent North America: American Association of Petroleum Geologists Bulletin, v. 61, no. 7, p. 1045–1068.

_____ 1980, Paleogeography of eustatic model for deposition of midcontinent Upper Pennsylvanian cyclothems, *in* Fouch, T. D., and Magathan, E. R., eds., Paleozoic paleogeography of the west-central United States: Rocky Mountain Section of the

Society of Economic Paleontologists and Mineralogists, Rocky Mountain Paleogeography Symposium 1, p. 197-215.

_____ 1986, Sea-level curve for Pennsylvanian eustatic marine transgressive-regressive depositional cycles along midcontinent outcrop belt, North America: Geology, v. 14, no. 4, p. 330–334.

_____ 1989a, Implications for Texas of glacial eustatic control over Middle and Upper Pennsylvanian cyclothems in midcontinent North America (abs.): Geological Society of America Abstracts with Programs, South-Central Section, v. 21, no. 1, p. 14.

_____ 1989b, Updated Middle-Upper Pennsylvanian eustatic sea level [sic] curve for midcontinent North America and preliminary biostratigraphic characterization: XI^{e} Congrés International de Stratigraphie et de Géologie du Carbonifère Beijing 1987, Comptes Rendu, v. 4, p. 160–185.

Jervey, M. T., 1988, Quantitative geological modeling of siliciclastic rock sequences and their seismic expression, *in* Wilgus, C. K., Hastings, B. S., Ross, C. A., Posamentier, H., Van Wagoner, J., and Kendal, C.G.St.C., eds, Sea-level changes: an integrated approach: Society of Economic Paleontologists and Mineralogists Special Publication No. 42, p. 47–69.

Lahti, V. R., and Huber, W. F., 1982, The Atoka Group (Pennsylvanian) of the Boonsville Field area, north-central Texas, *in* Martin, C. A., ed., Petroleum geology of the Fort Worth Basin and Bend Arch area: Dallas Geological Society, p. 377–399.

Lovick, G. P., Mazzini, C. G., and Kotila, D. A., 1982, Atokan clastics—depositional environments in a foreland basin: Oil and Gas Journal, v. 80, no. 5, p. 181–199.

Masters, J. A., 1979, Deep basin gas trap, Western Canada, American Association of Petroleum Geologists Bulletin, v. 63, p. 152–181.

McElhinny, M. W., 1973, Palaeomagnetism and plate tectonics: Cambridge, Cambridge University Press, 358 p.

Meckel, L. D., Jr., Smith, D. G., Jr., Wells, L. A., 1992, Ouachita foredeep basins: regional paleogeography and habitat of hydrocarbons, Chapter 15, p. 427–444.

Moore, R. C., Wanless, H. R., Weller, J. M., Williams, J. S., Read, C. B., Bell, W. A., Ashley, G. H., Cheney, M. G., Cline, L. M., Condra, G. E., Dott, R. H., Dunbar, C. O., Elias, M. K., Glenn, L. C., Grene, F. C., Hendricks, T. A., Jewett, J. M., Johnson, J. H., King, P. B., Knight, J. B., Levorsen, A. I., Miser, H. D., Newell, N. D., Plummer, F. B., Thompson, M. L., Tomlinson, C. W., and Westheimer, J., 1944, Correlation of Pennsylvanian formations in North America: Geological Society of America Bulletin, v. 55, no. 6, p. 657–706.

Morel, P., and Irving, E., 1978, Tentative paleocontinental maps for the Early Phanerozoic and Proterozoic: Journal of Geology, v. 86, no. 5, p. 535–561.

Mulholland, J. W., 1994, Sequence stratigraphic correlation of well-log cross sections: Mountain Geologist, v. 31, no. 3, p. 65–75.

Nassichuk, W. W., and Bamber, E. W., 1978, Middle Pennsylvanian biostratigraphy, eastern Cordillera and Arctic islands, Canada—a summary, *in* Stelck, C. R., and Chatterton, B. D. E., Western and Arctic Canadian biostratigraphy: Geological Society of Canada Special Paper 18, p. 395–413.

_____ 1979, Subsurface study of Atoka (Lower Pennsylvanian) clastic rocks in parts of Jack, Palo Pinto, Parker, and Wise Counties, north-central Texas: American Association of Petroleum Geologists Bulletin, v. 63, v. 1, p. 50–66.

Phillips, T. L., and Peppers, R. A., 1984, Changing patterns of Pennsylvanian coal-swamp vegetation and implications of climatic control on coal occurrence: International Journal of Coal Geology, v. 3, no. 3, p. 205–255.

Quinlan, G. M., and Beaumont, Christopher, 1984, Appalachian thrusting, lithospheric flexure, and the Paleozoic stratigraphy of the Eastern Interior of North America: Canadian Journal of Earth Sciences, v. 21, no. 9, p. 973–996.

Railroad Commission of Texas, 1991, Field rules, Section VI, Boonsville Field (Bend Conglomerate Gas), Order No. 9-36, 420.

Ramsbottom, W. H. C., 1979, Rates of transgression and regression in the Carboniferous of NW Europe: Journal of the Geological Society of London, v. 136, no. 2, p. 147–153.

Ross, C. A., and Ross, J. R. P., 1985, Late Paleozoic depositional sequences are synchronous and worldwide: Geology, v. 13, no. 3, p. 194–197.

_____ 1988, Late Paleozoic transgressive-regressive deposition, *in* Wilgus, C. K., Hastings, B. S., Ross, C.A., Posamentier, H., Van Wagoner, J., and Kendal, C. G. St. C., eds, Sea-level changes: an integrated approach: Society of Economic Paleontologists and Mineralogists Special Publication No. 42, p. 227–247.

Saunders, W. B., Ramsbottom, W. H. C., and Manger, W. L., 1979, Mesothermic cyclicity in the mid-Carboniferous of the Ozark shelf region?: Geology, v. 7, no. 6, p. 293-296.

Scotese, C. R., Bambach, R. K., Barton, C., Van der Voo, R., and Zeigler, A. M., 1979, Paleozoic base maps: Journal of Geology, v. 87, no. 3, p. 217–277.

Shanley, K. W., and McCabe, P. J., 1994, Perspectives on the sequence stratigraphy of continental strata: American Association of Petroleum Geologists Bulletin, v. 78, p. 544–568.

Srivastava, G. S., 1994, Interactive software integrates geological and engineering data: Oil and Gas Journal, September, p. 85–91.

Thompson, D. M., 1982, Atoka Group (Lower to Middle Pennsylvanian), Northern Fort Worth Basin, Texas: terrigenous depositional systems, diagenesis, and reservoir distribution and quality: The University of Texas at Austin, Bureau of Economic Geology Report of Investigations No. 125, 62 p.

_____ 1988, Fort Worth Basin, *in* Sloss, L. L., ed., The geology of North America: Boulder, Geological Society of America, v. D-2, p. 346–352.

Turner, G. L., 1957, Paleozoic stratigraphy of the Fort Worth Basin, *in* Bell, W. C., ed., Abilene and Fort Worth Geological Societies 1957 Joint Field Trip Guide- book, p. 57–77.

Vail, P. R., Mitchum, R. M., Thompson, S., III, 1977, Seismic stratigraphy and global changes of sea level, part 4: global cycles of relative changes of sea level, *in* Payton, C. E., ed., Seismic stratigraphy—applications to hydrocarbon exploration: American Association of Petroleum Geologists Memoir 26, p. 83–97.

Van Wagoner, J. C., Mitchum, R. M., Campion, K. M., and Rahmanion, V. D., 1990, Siliciclastic sequence stratigraphy in well logs, cores, and outcrops: concepts for high-

resolution correlation of time and facies: American Association of Petroleum Geologists Methods in Exploration Series, No. 7, 55 p.

Walper, J. L., 1977, Paleozoic tectonics of the southern margin of North America, *in* Gulf Coast Association of Geological Societies Transactions, v. 27, p. 230–239.

Wanless, H. R., and Weller, J. M., 1932, Correlation and extent of Pennsylvanian cyclothems: Geological Society of America Bulletin, v. 43, p. 1003–1016.

Wickham, J., Roeder, D., and Briggs, G., 1976, Plate tectonic models for the Ouachita foldbelt: Geology, v. 4, no. 2, p. 173–176.

Youle, J. C., Watney, W. L., and Lambert, L. L., 1994, Stratal hierarchy and sequence stratigraphy—Middle Pennsylvanian, southwestern Kansas, U.S.A., *in* Klein, G. D., ed., Pangea: paleoclimate, tectonics, and sedimentation during accretion, zenith, and breakup of a supercontinent: Boulder, Colorado, Geological Society of America Bulletin Special Paper 288.

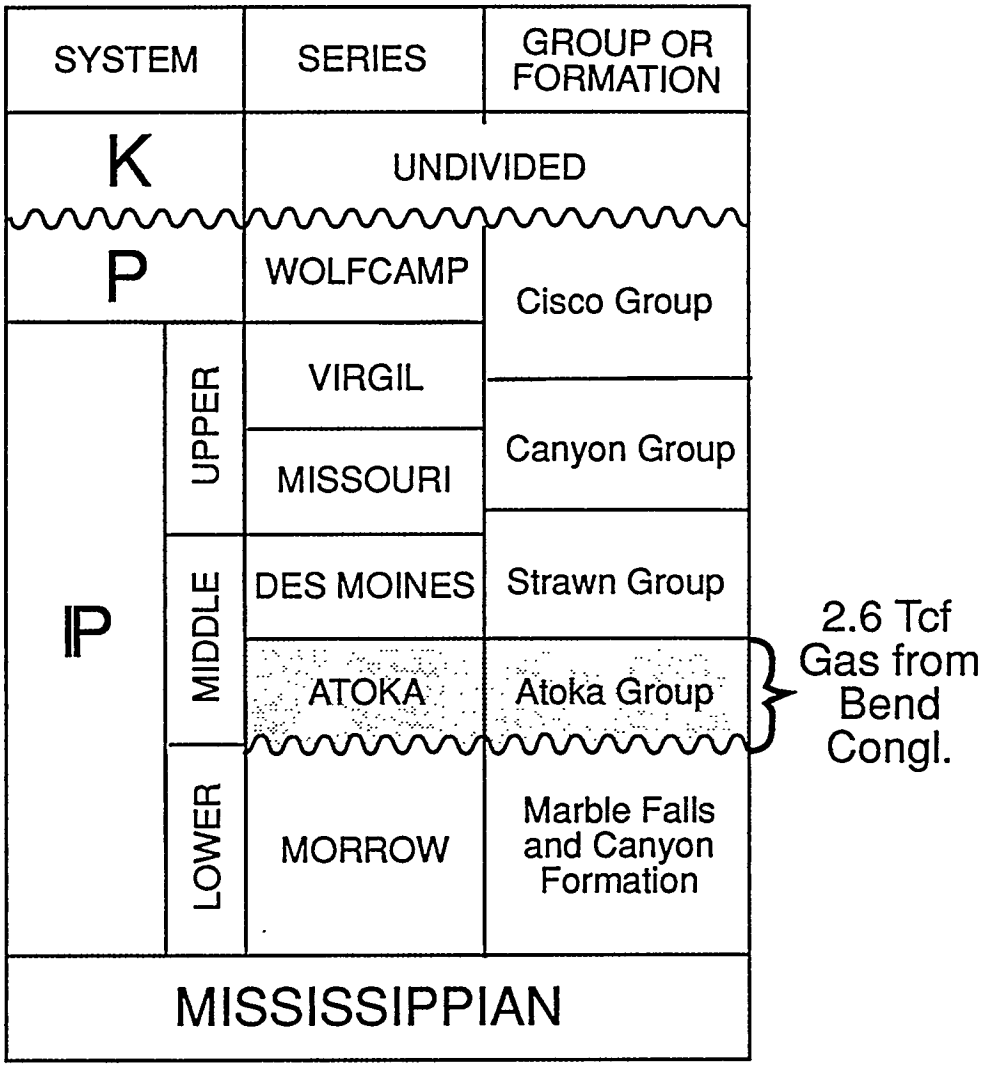

Figure A1. Time-rock stratigraphic column for post-Mississippian strata in the Boonsville project area. Modified from Thompson (1982).

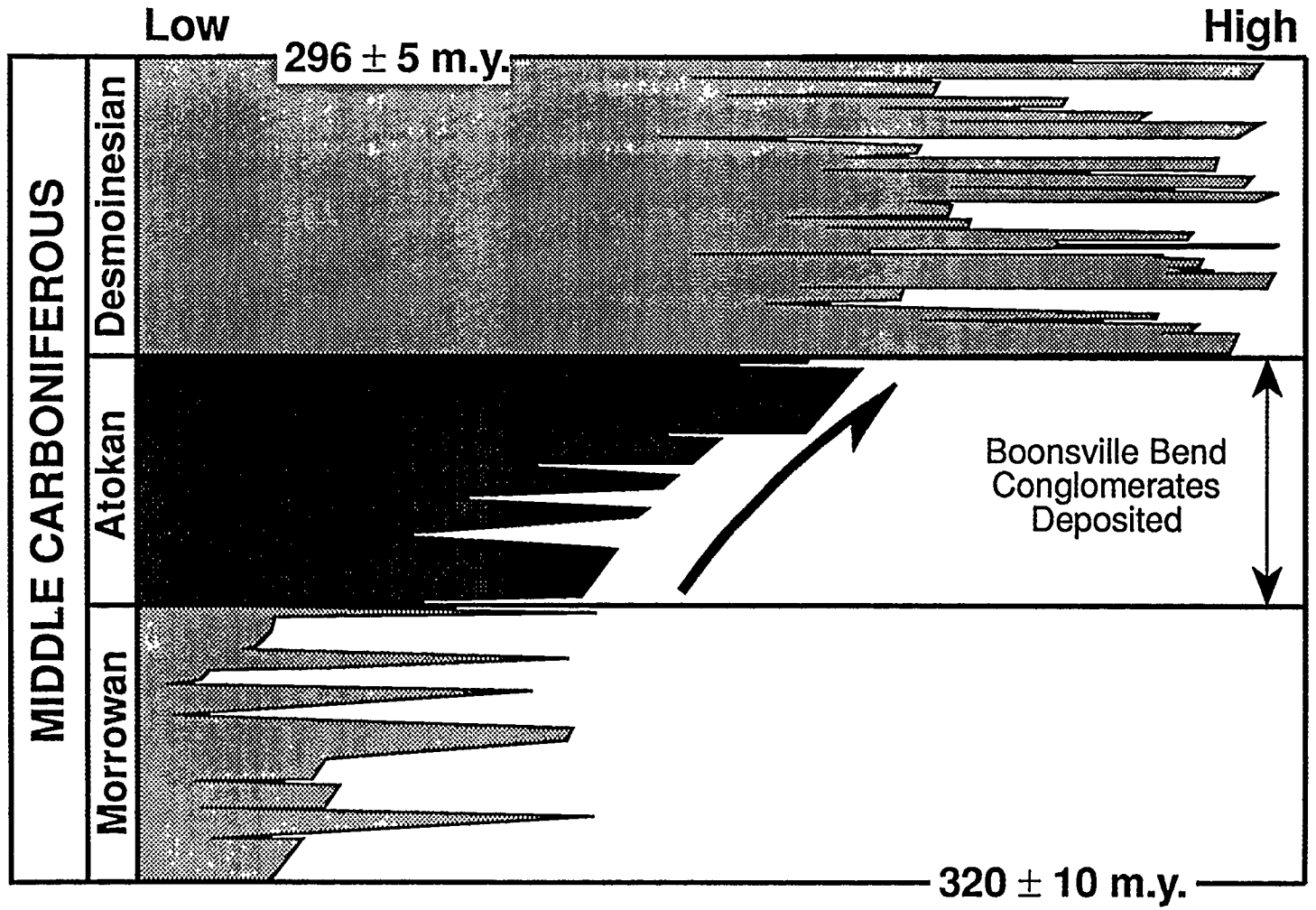

Figure A2. Middle Carboniferous eustatic sea level changes derived from coastal onlap data. After Ross and Ross (1988).

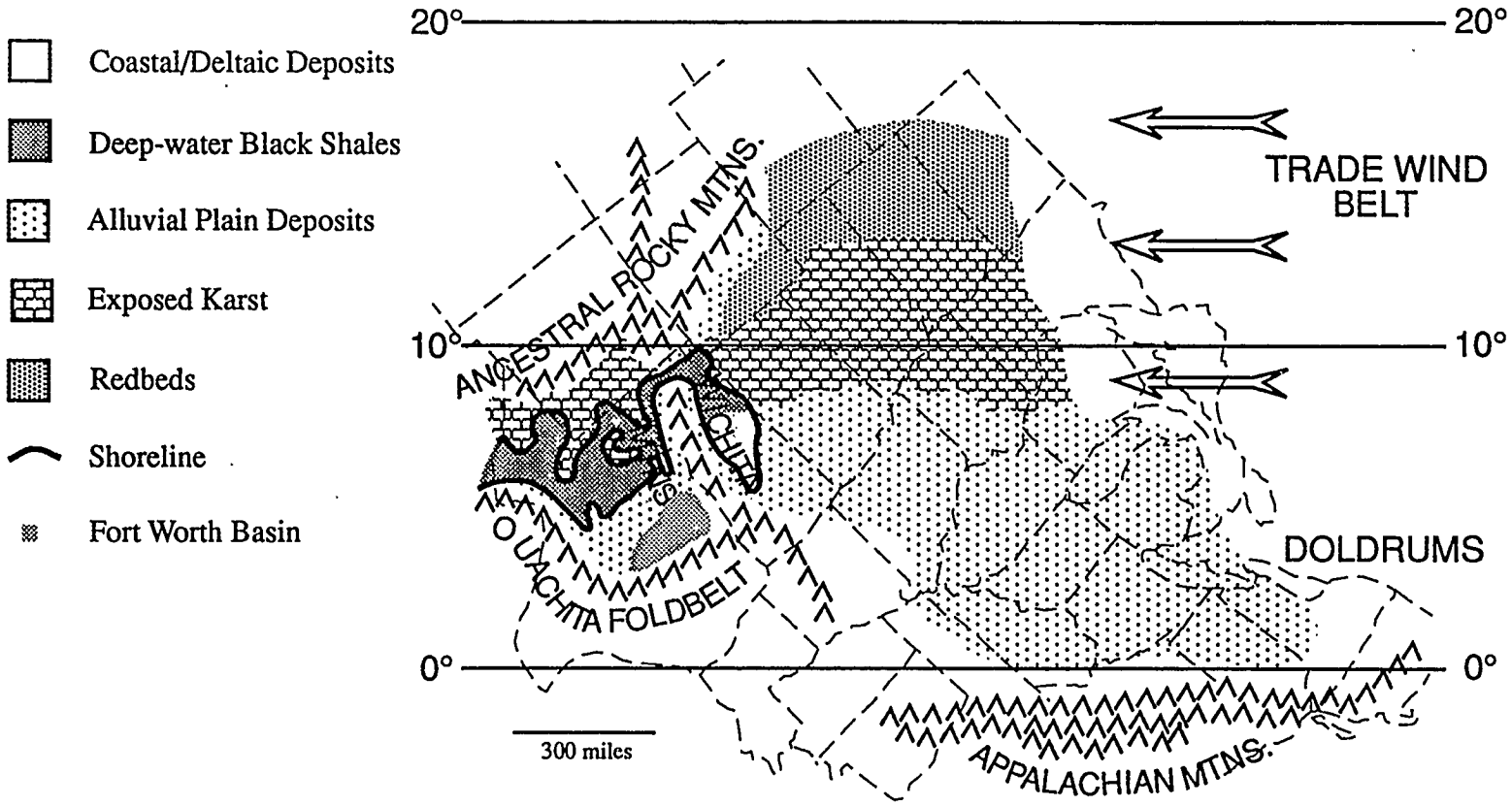

Figure A3. Pennsylvanian paleogeography and lithofacies distribution of the Midcontinent United States during maximum regression (lowstand). After Heckel (1980).

A.45

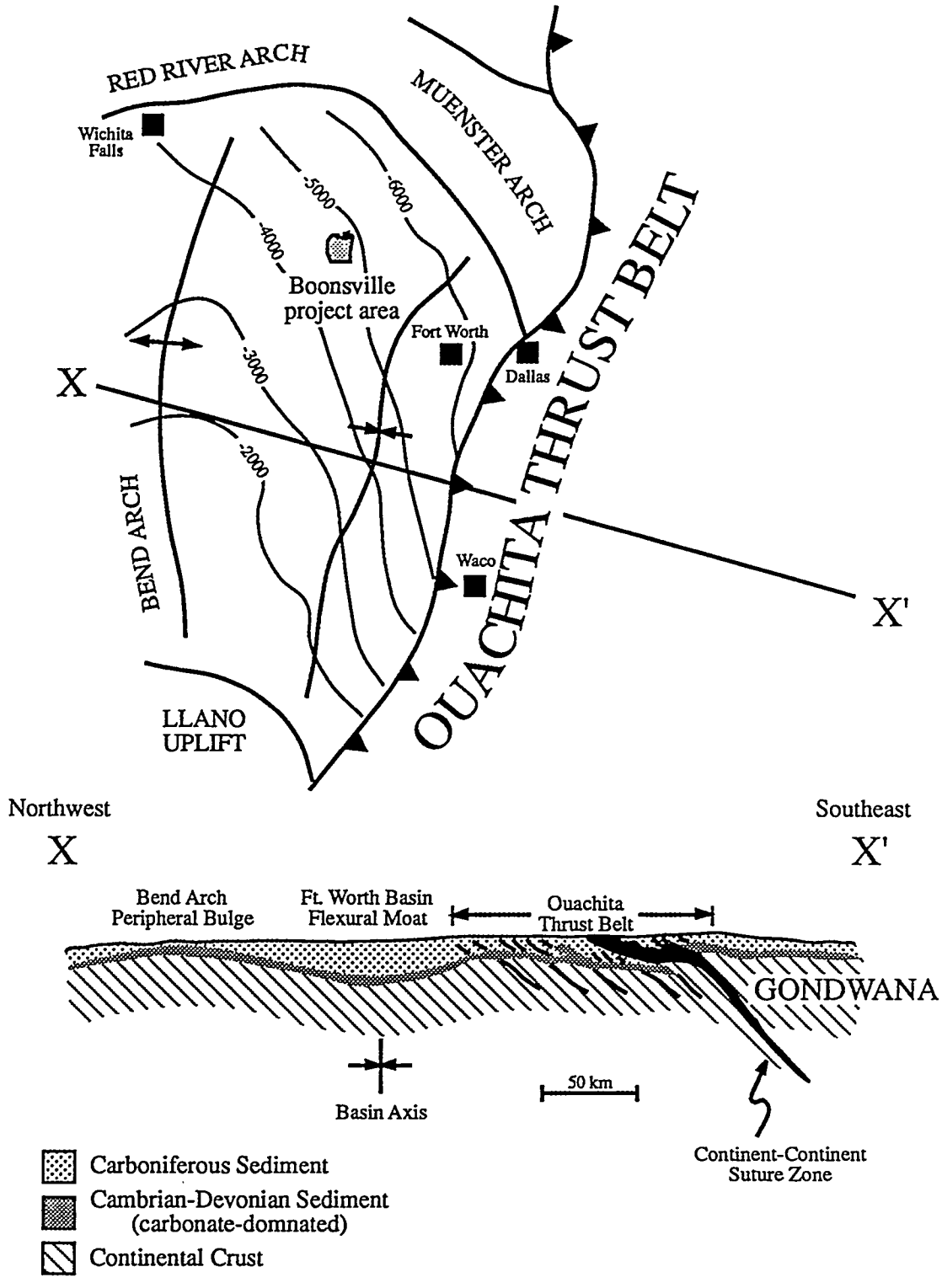

Figure A4. Tectonic and structural framework of the Fort Worth Foreland Basin. Contours represent depth below sea level of the top of the Marble Falls Formation. Structure map after Meckel and others (1992), tectonic cross-section after Wickham and others (1976).

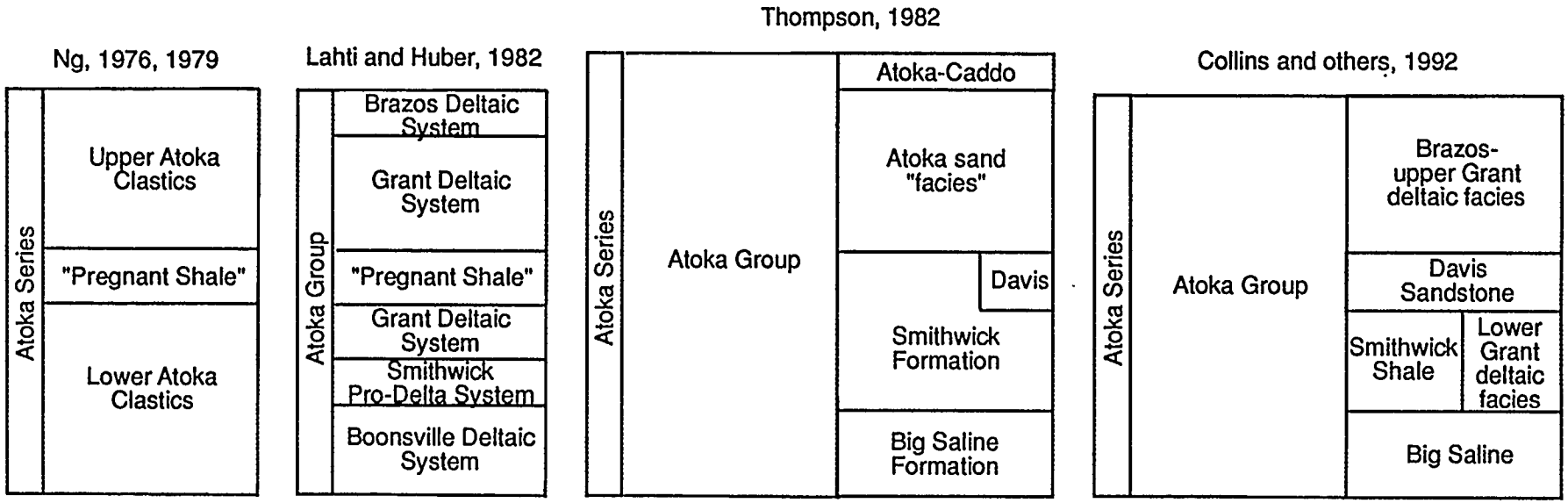

Figure A5. Comparison of stratigraphic nomenclatures for Atokan rocks in the Fort Worth Basin presented by previous workers. The complex geologic relationships have contributed to a proliferation of nomenclatural systems.

A.47

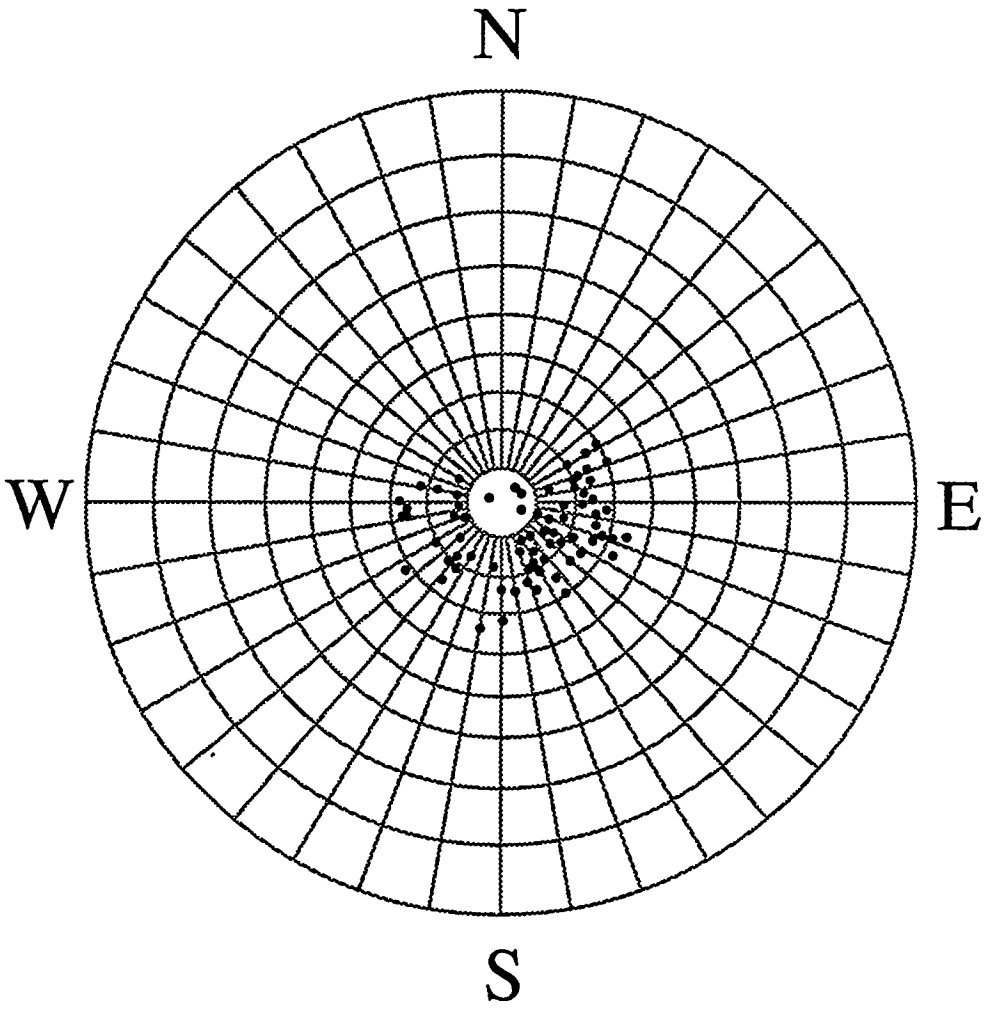

Figure A6. Crossbed dip orientations based on FMI log data from the Lower Atoka, Billie Yates No. 18D.

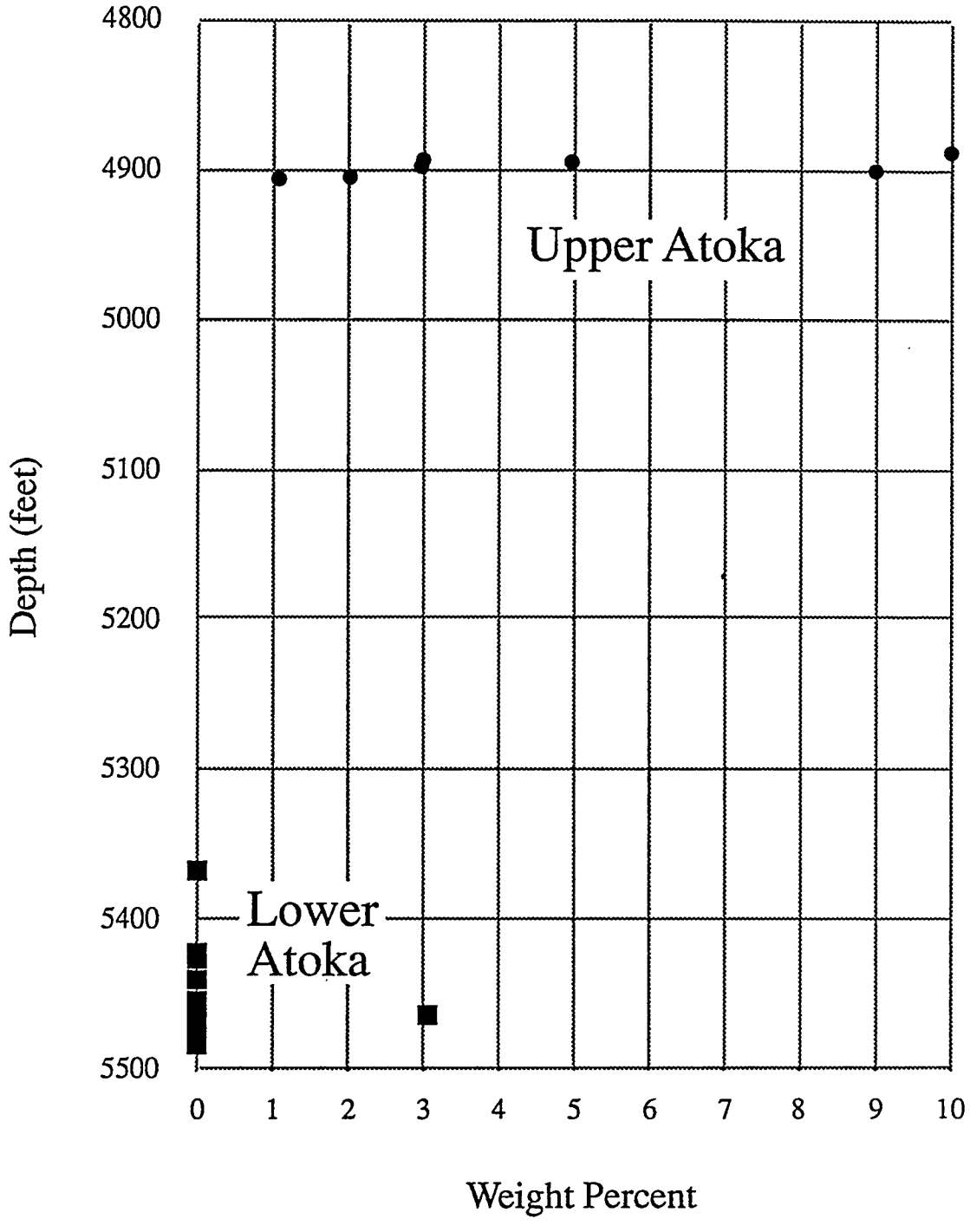

Figure A7. Depth distribution of potassium feldspars determined from infrared spectroscopic analysis of core samples.

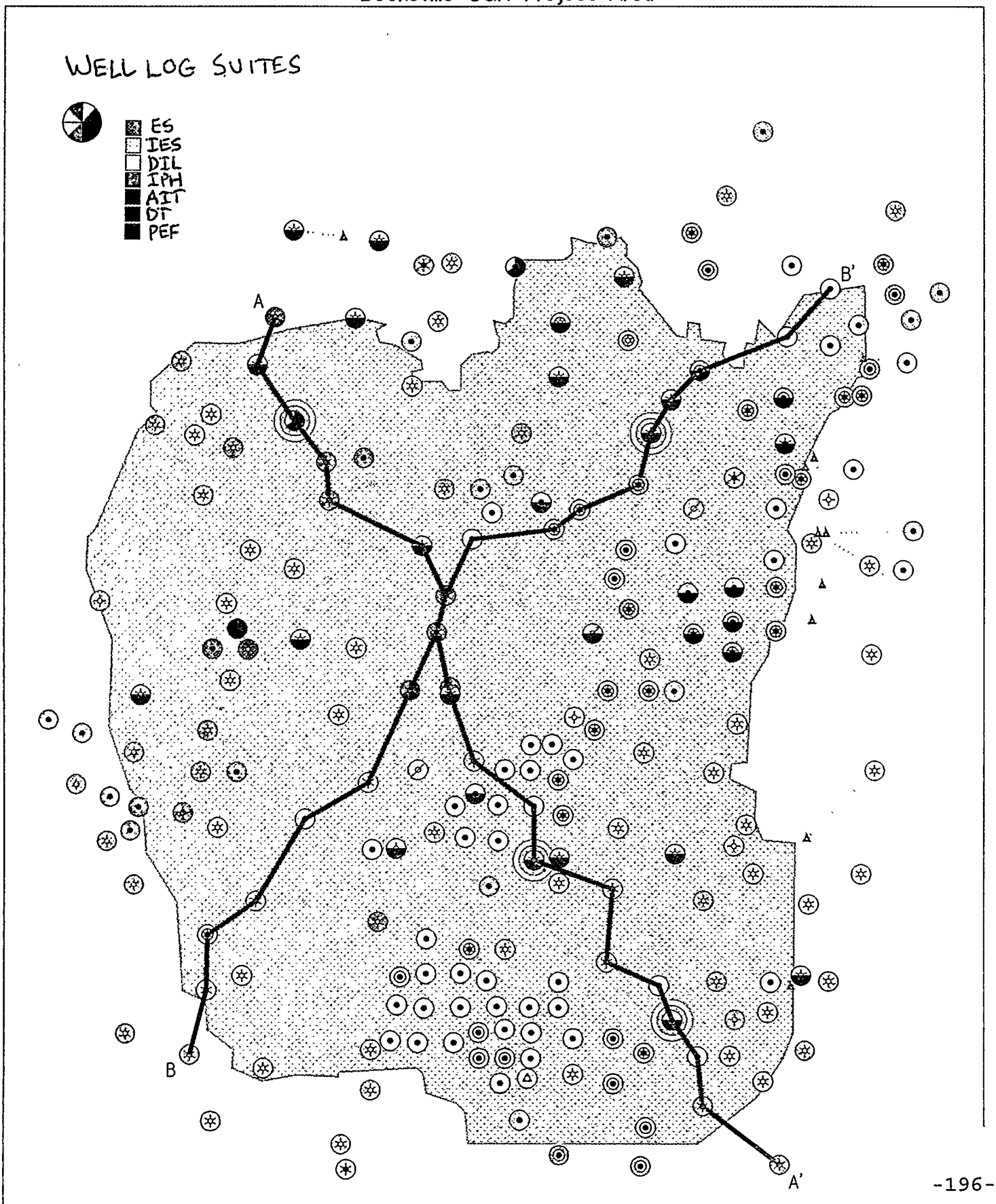

Figure A8. Distribution of well-log suites and cores (yellow open circles) used in the geologic evaluation of the Boonsville Project Area. Dark cyan colored-filled area represents outline of the 3-D seismic survey

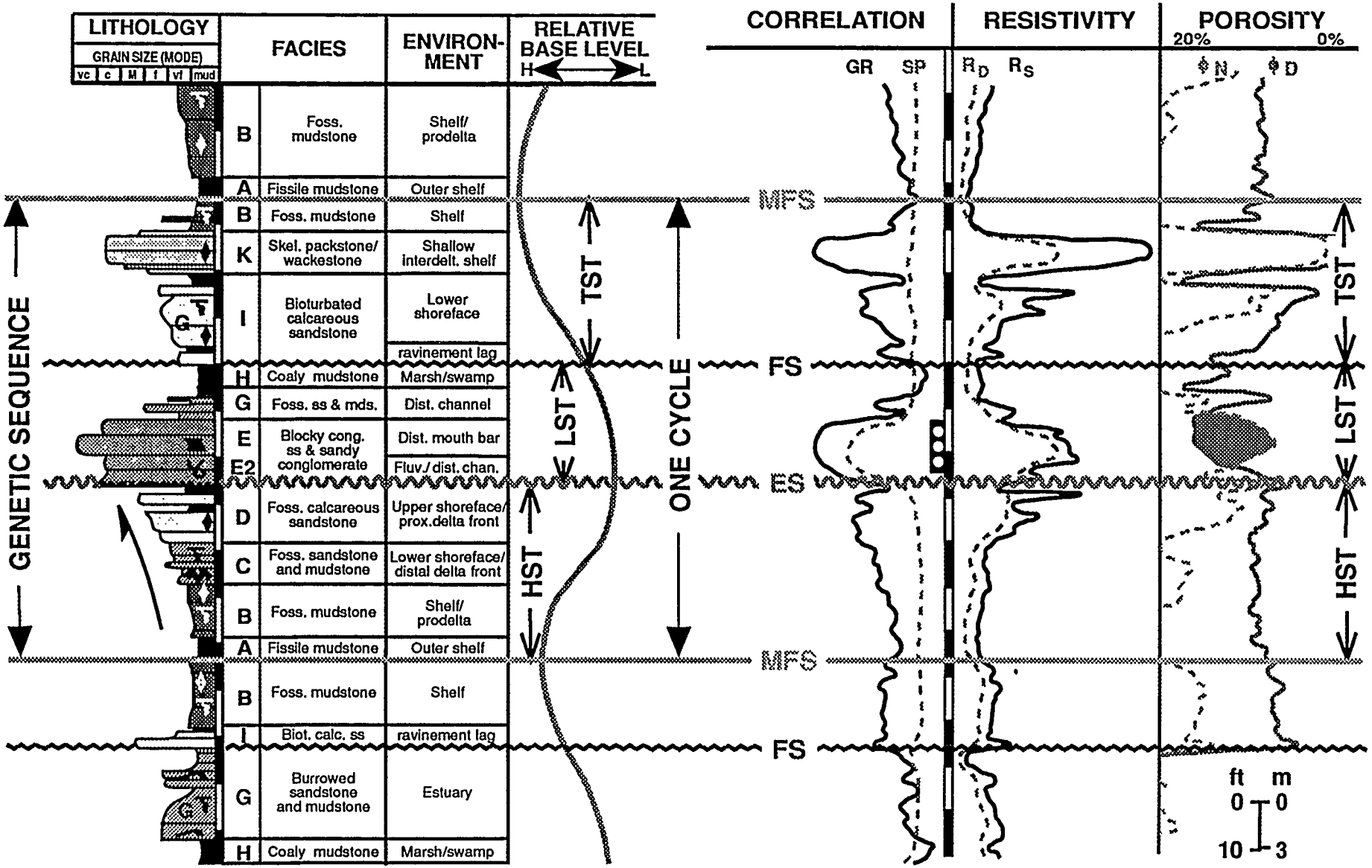

Figure A9. Typical log responses for composite Boonsville Bend Conglomerate genetic sequence.

A.51

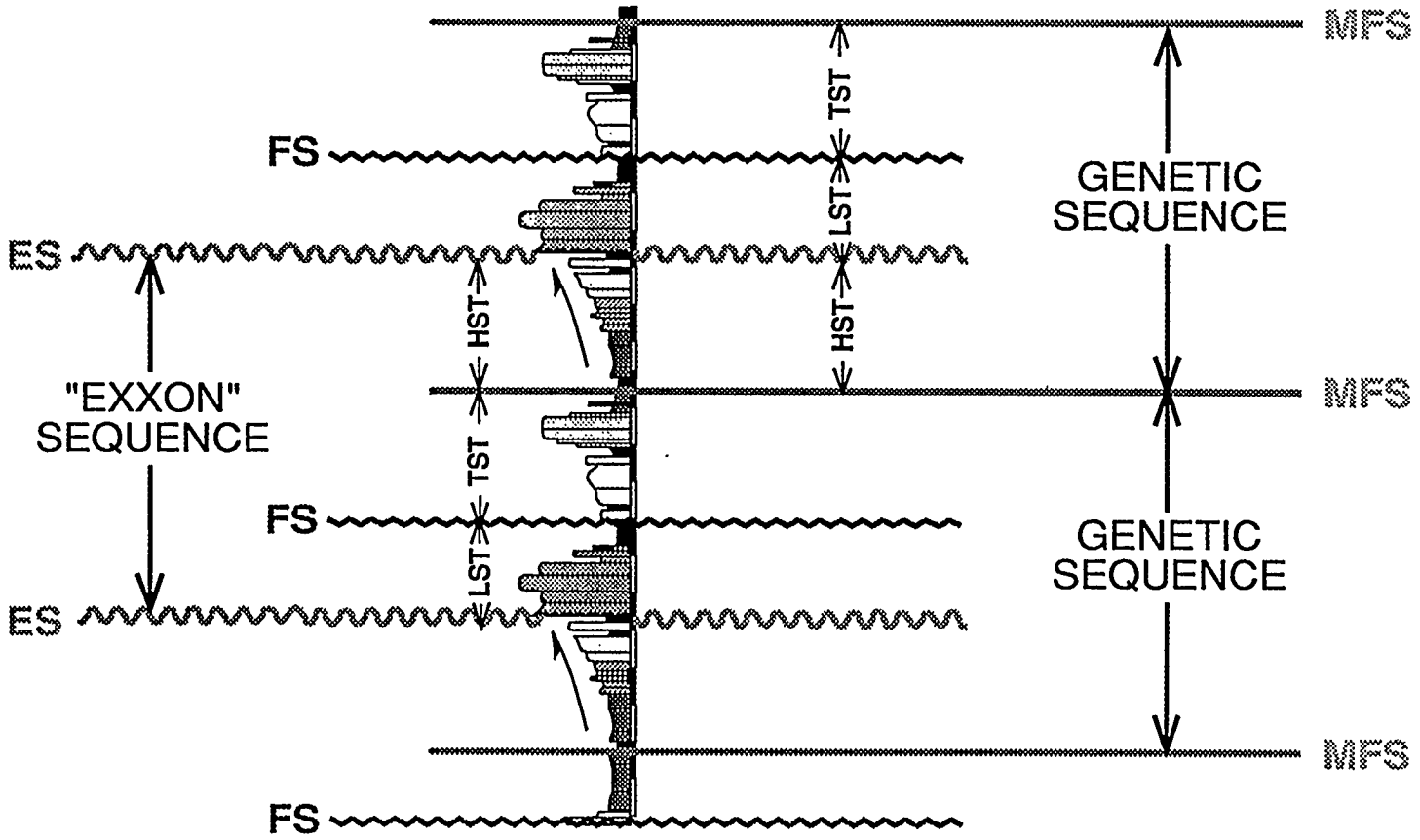

Figure A10. Core graphic illustrating key surface-based sequence terminologies in common use. "Exxon" sequences are defined by erosion surfaces, whereas genetic sequences are defined by flooding or maximum flooding surfaces.

A.52

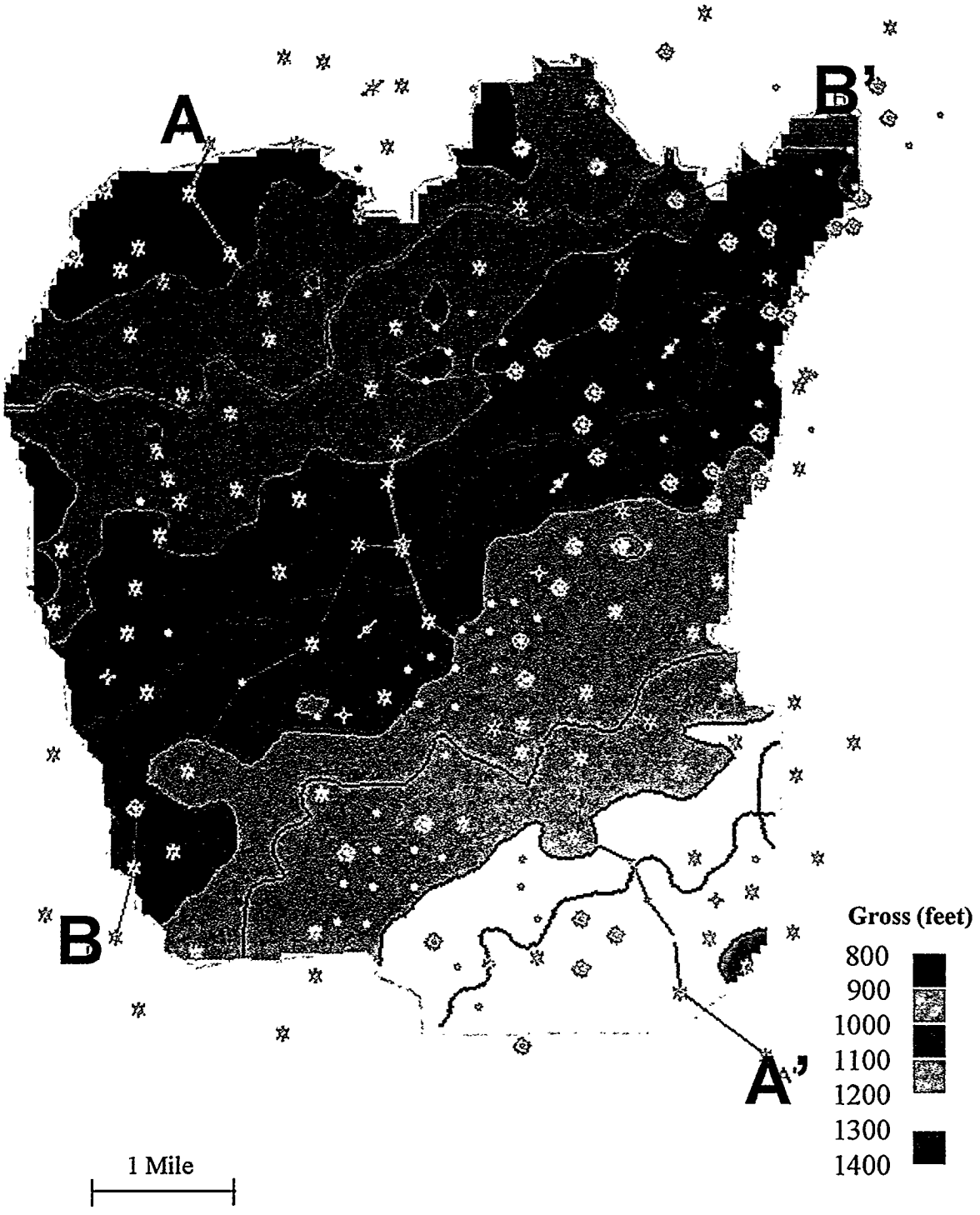

Figure A11. Total Bend Conglomerate (= total Atoka) gross isopach (MFS90-MFS10). Contour interval = 50 feet.

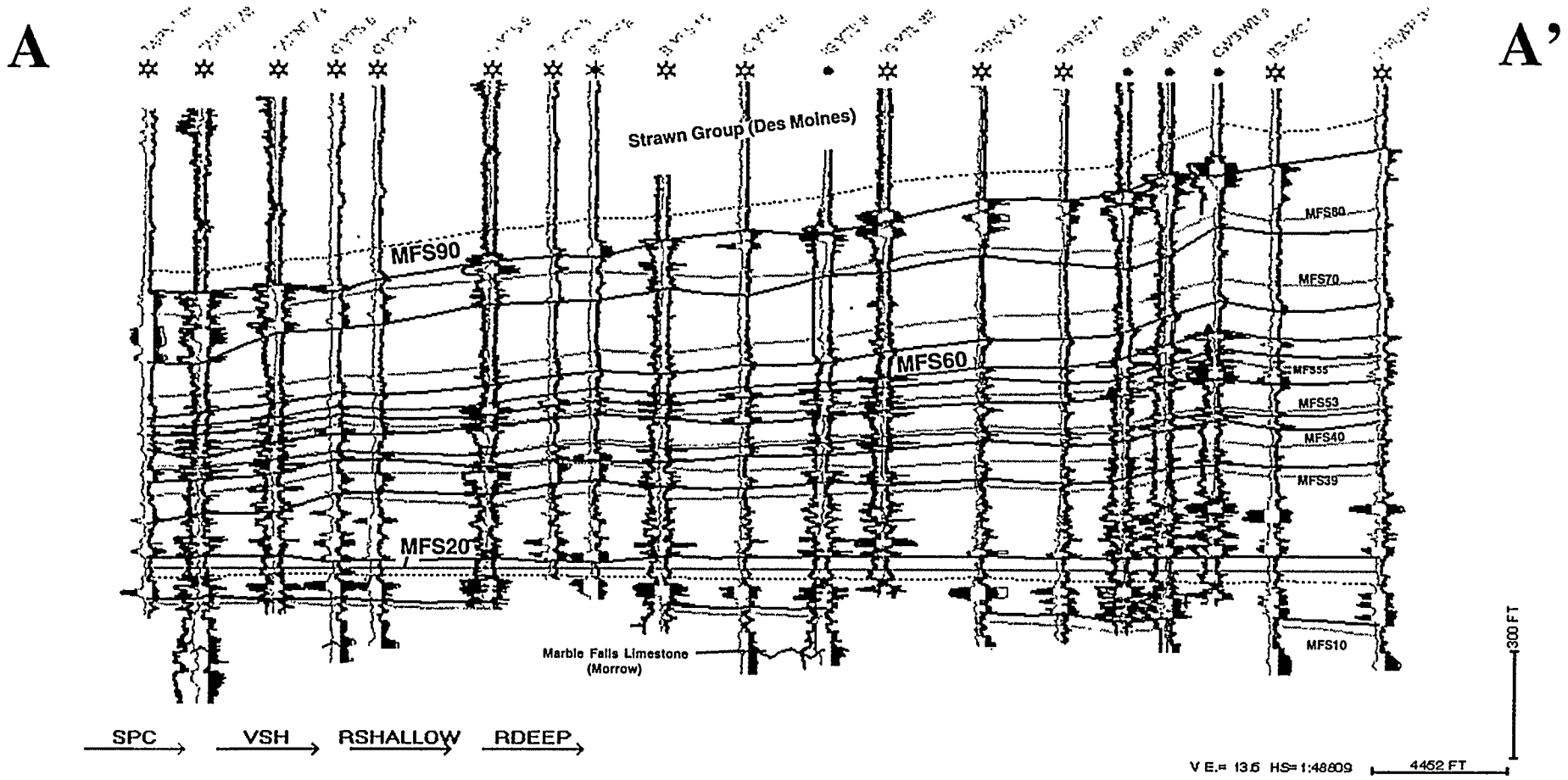

Figure A12. Boonsville stratigraphic cross-section A-A' through Bend Conglomerate using MFS20 (the top of the Vineyard genetic sequence) as a datum.

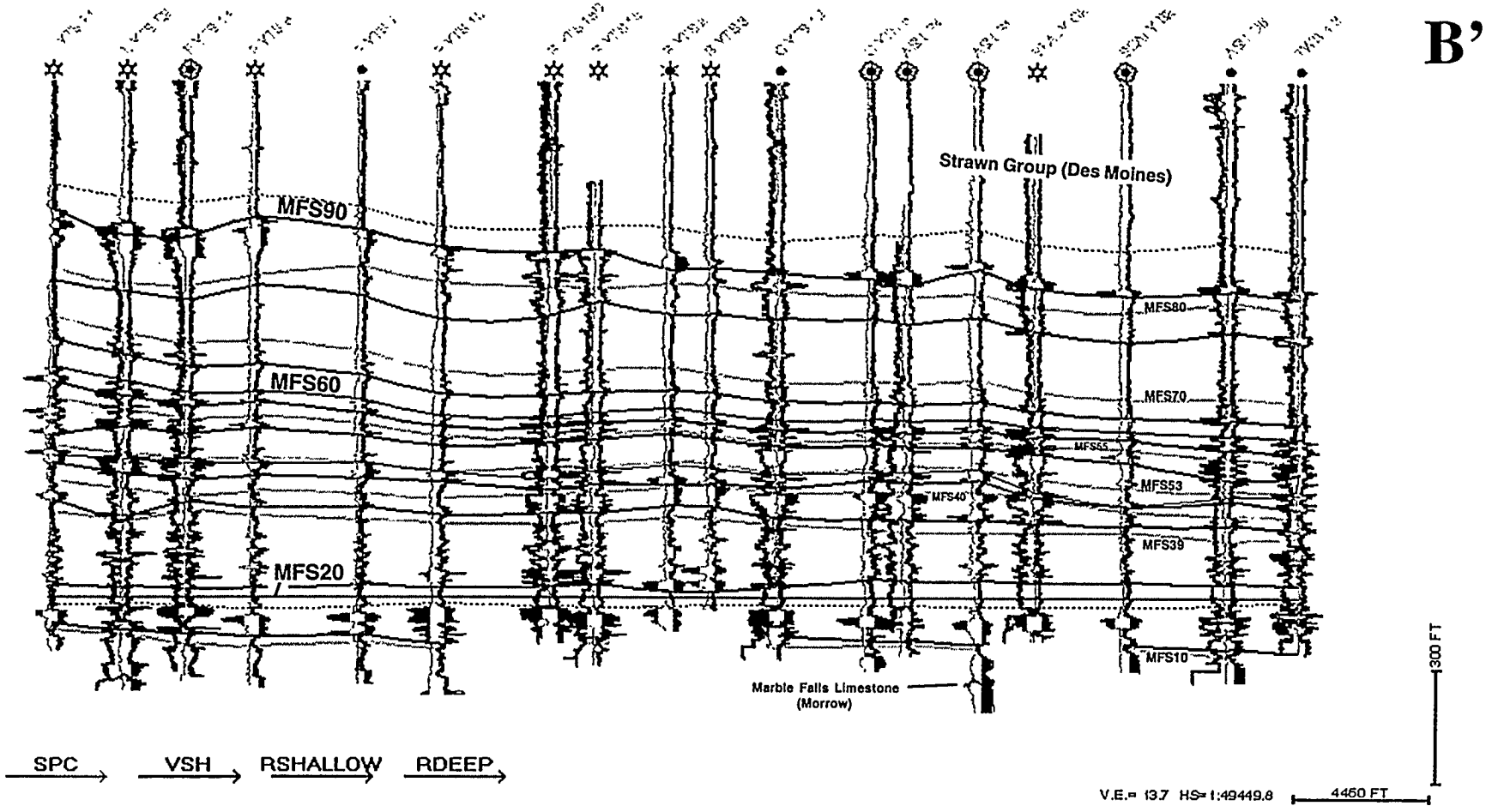

Figure A13. Boonsville stratigraphic cross-section B-B' through Bend Conglomerate using MFS20 (the top of the Vineyard genetic sequence) as a datum.

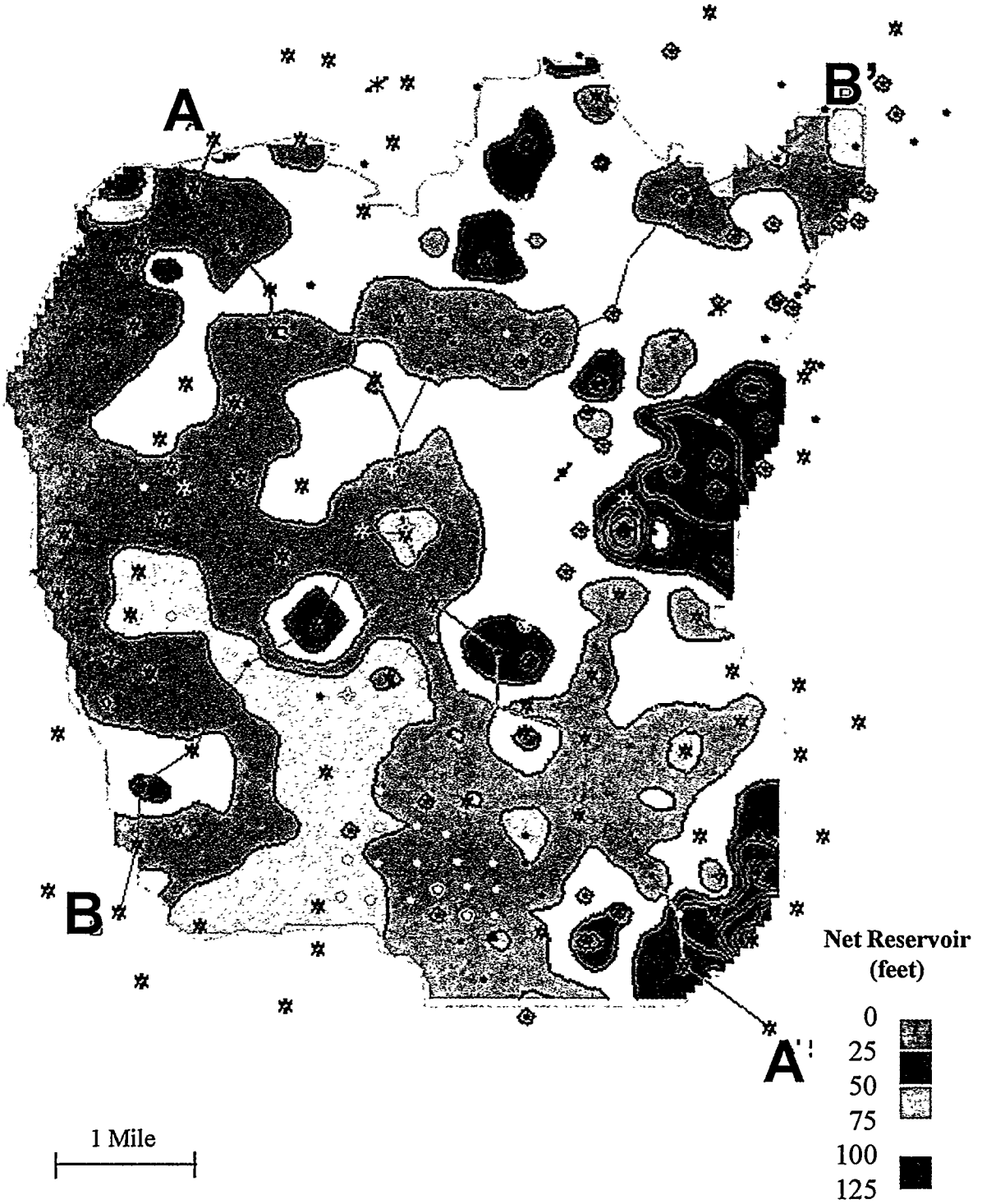

Figure A14. Total Bend Conglomerate net reservoir isopach (MFS90-MFS10). Net reservoir cutoffs: SP < -30 mv, Res > 10 ohmm.

A.56

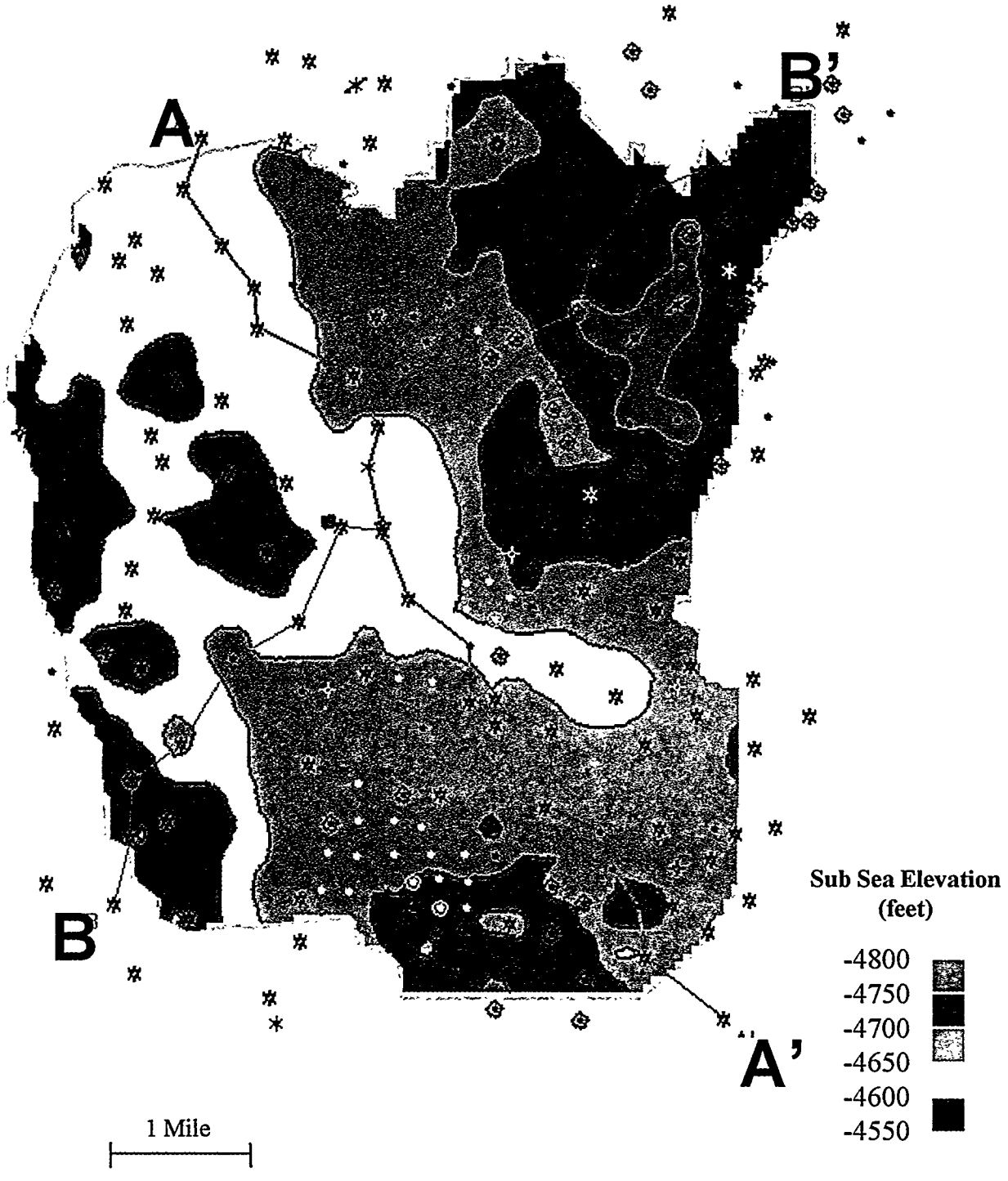

Figure A15. Top of Vineyard genetic sequence (MFS20) measured in depth below sea level. Contour interval = 50 feet.

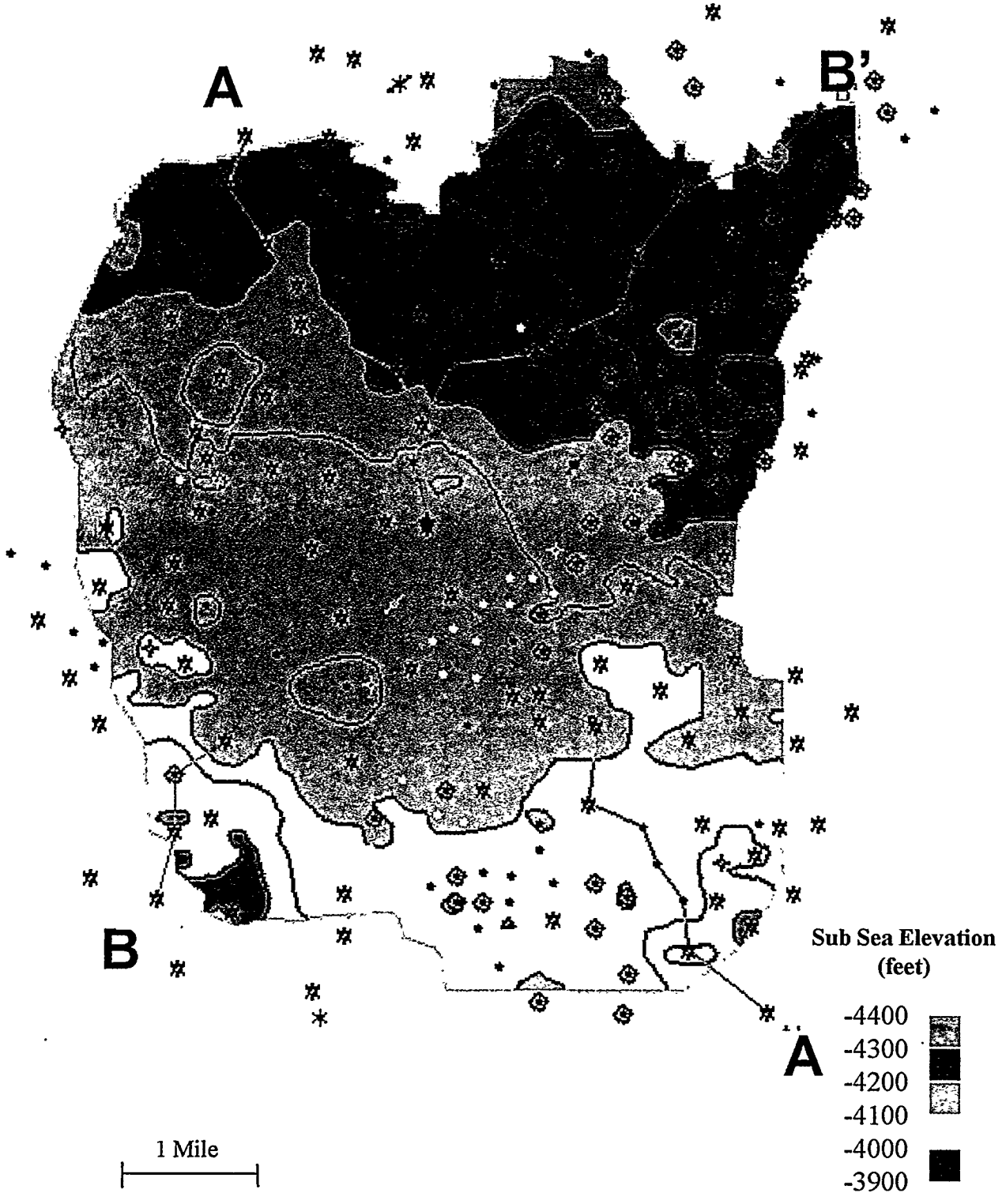

Figure A16. Top of Trinity genetic sequence (MFS60) measured in depth below sea level. Contour interval = 50 feet.

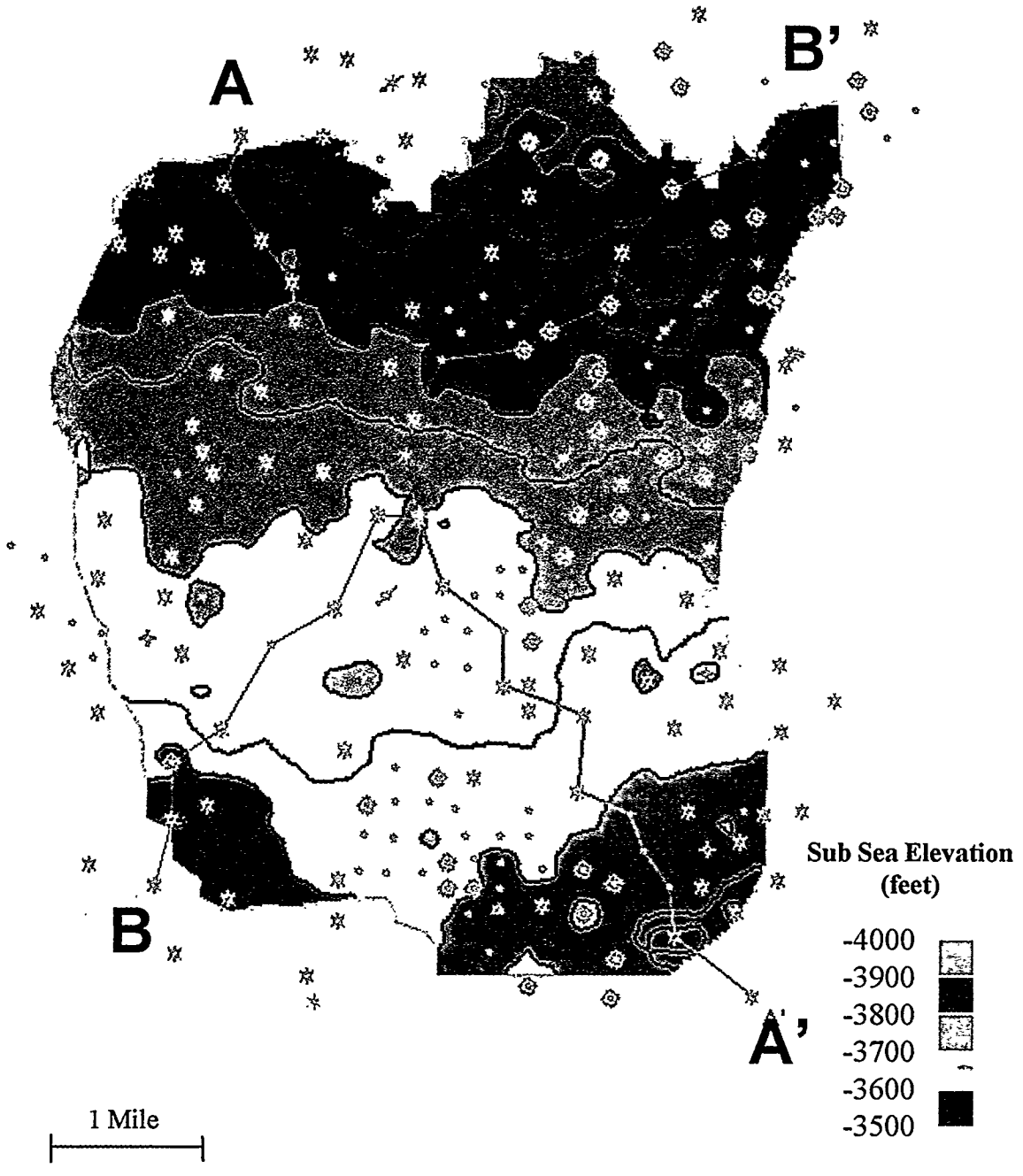

Figure A17. Top of Caddo genetic sequence (MFS90) measured in depth below sea level. Contour interval = 50 feet.

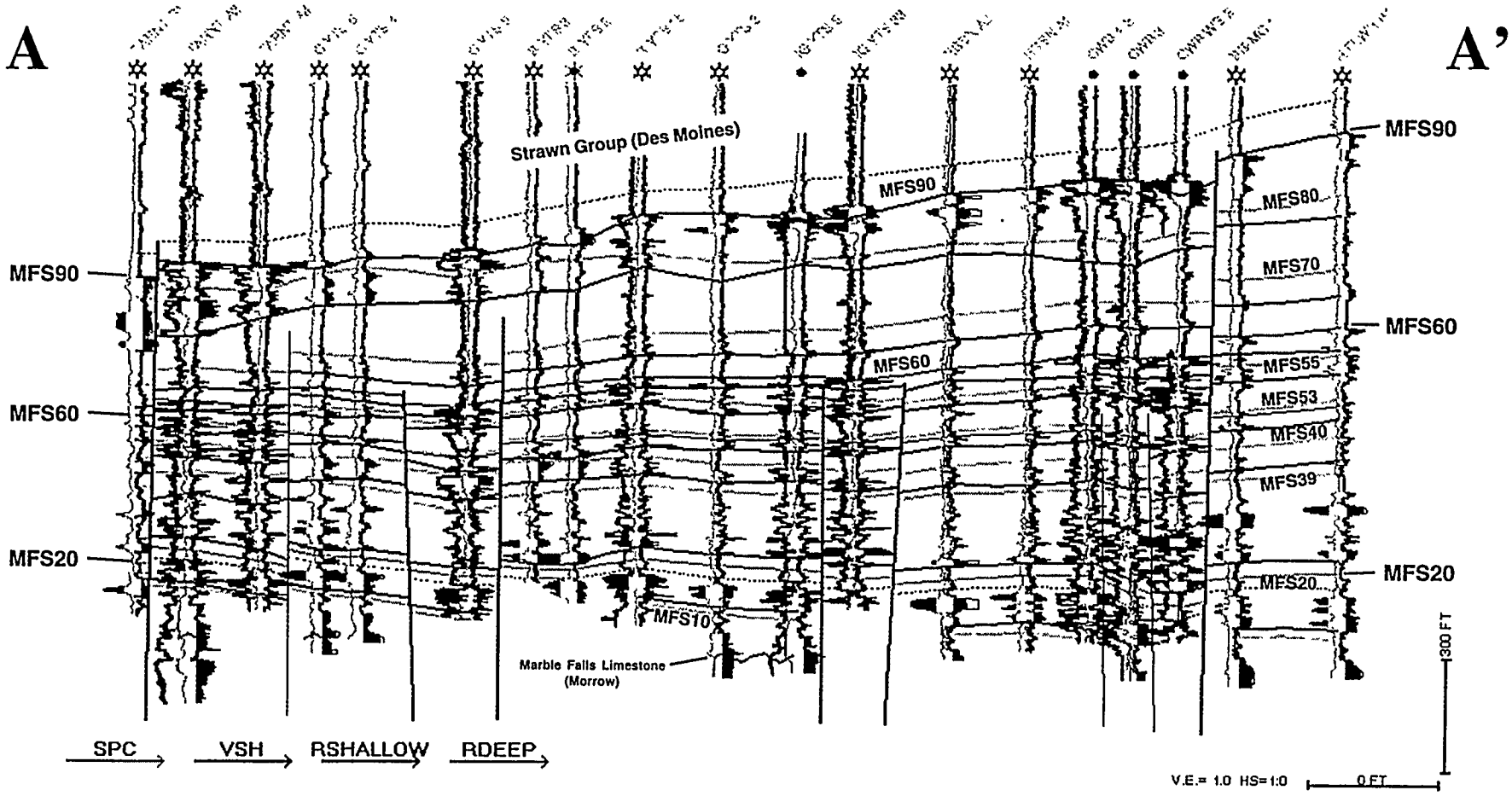

Figure A18. Boonsville structural cross-section A-A' through Bend Conglomerate illustrating faults interpreted from 3D seismic information.

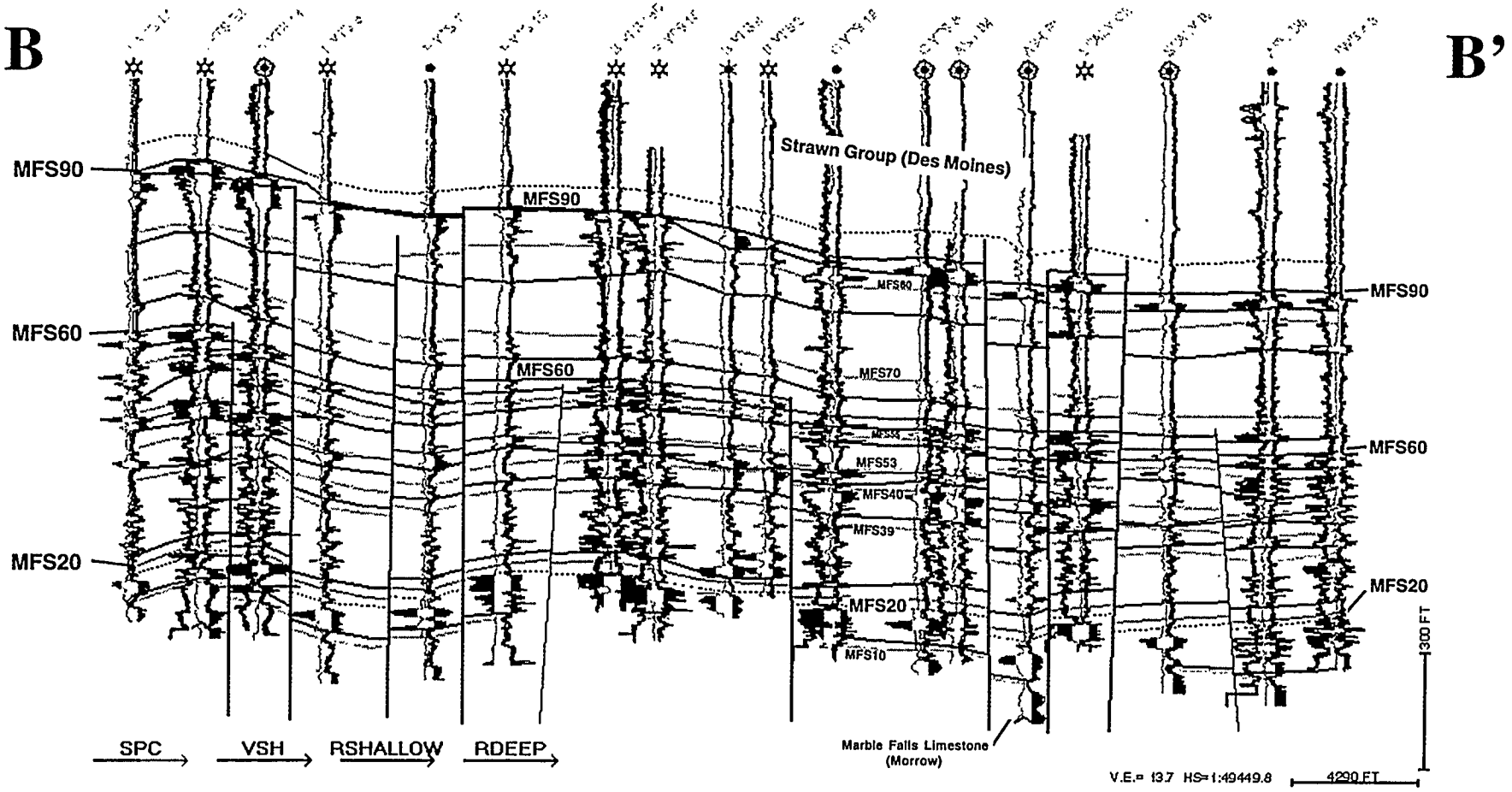

Figure A19. Boonsville structural cross-section B-B' through Bend Conglomerate illustrating faults interpreted from 3D seismic information.

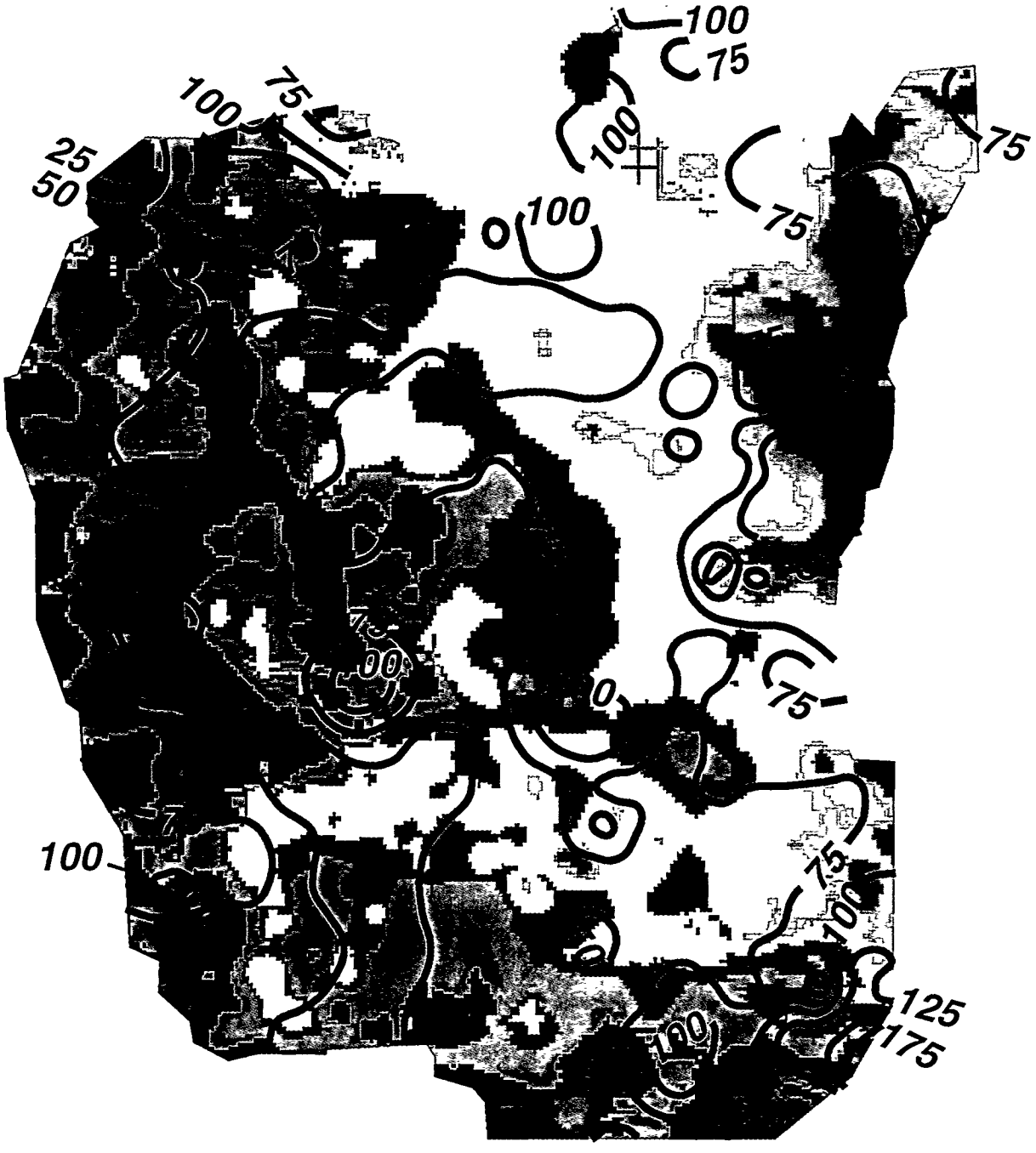

Figure A20. Map of Boonsville project area showing the relationship between total Atoka (MFS90-MFS10) net reservoir thickness and deep subsurface structure, as indicated by the top of the Marble Falls Limestone interpreted from 3D seismic data. Dark colors represent higher elevations and grade to lower elevations colored in lighter shades.

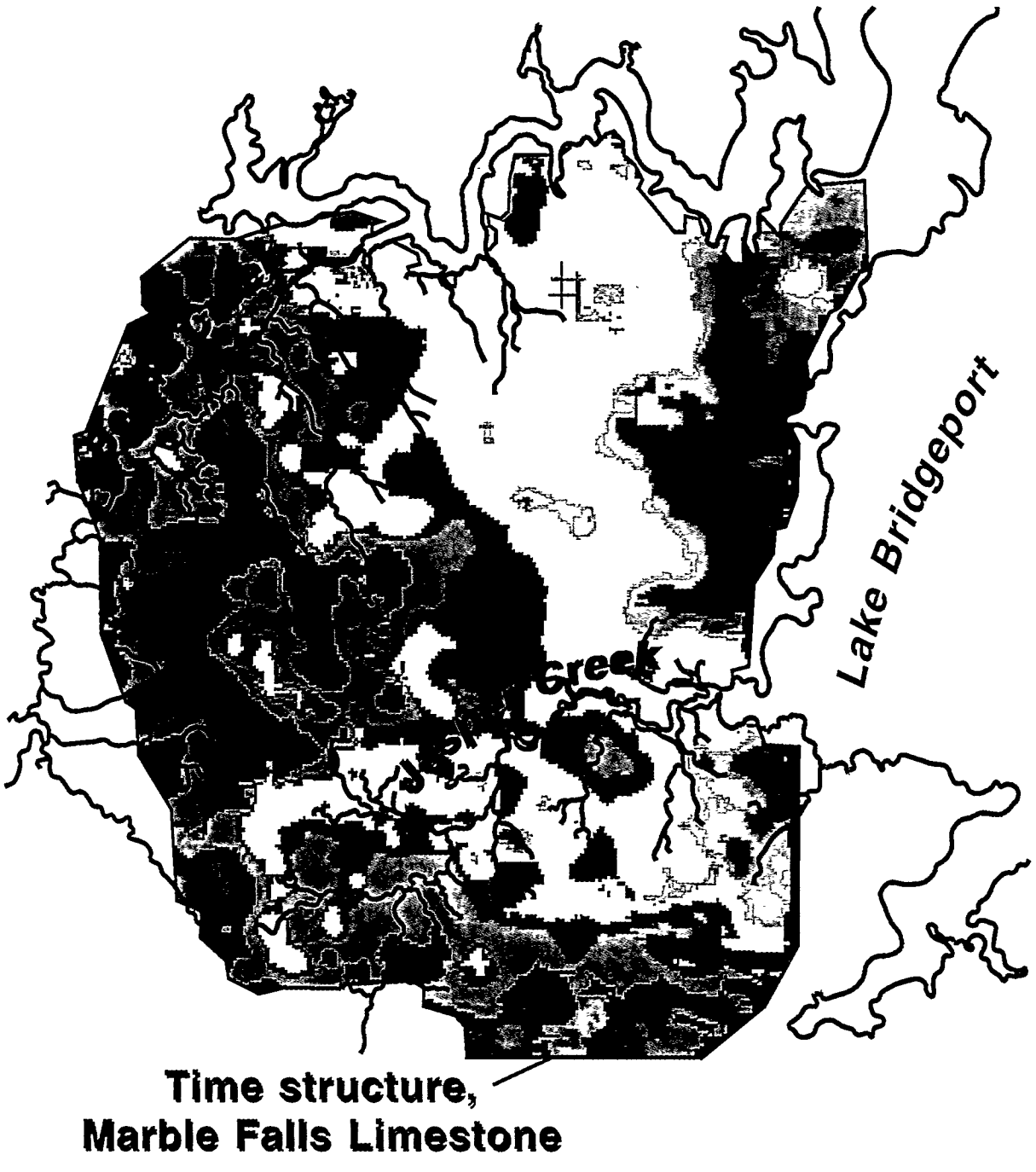

Figure A21. Map of Boonsville project area showing the relationship between modern stream drainage and deep subsurface structure, as indicated by the top of the Marble Falls Limestone interpreted from 3D seismic data. Dark colors represent higher elevations and grade to lower elevations colored in lighter shades.

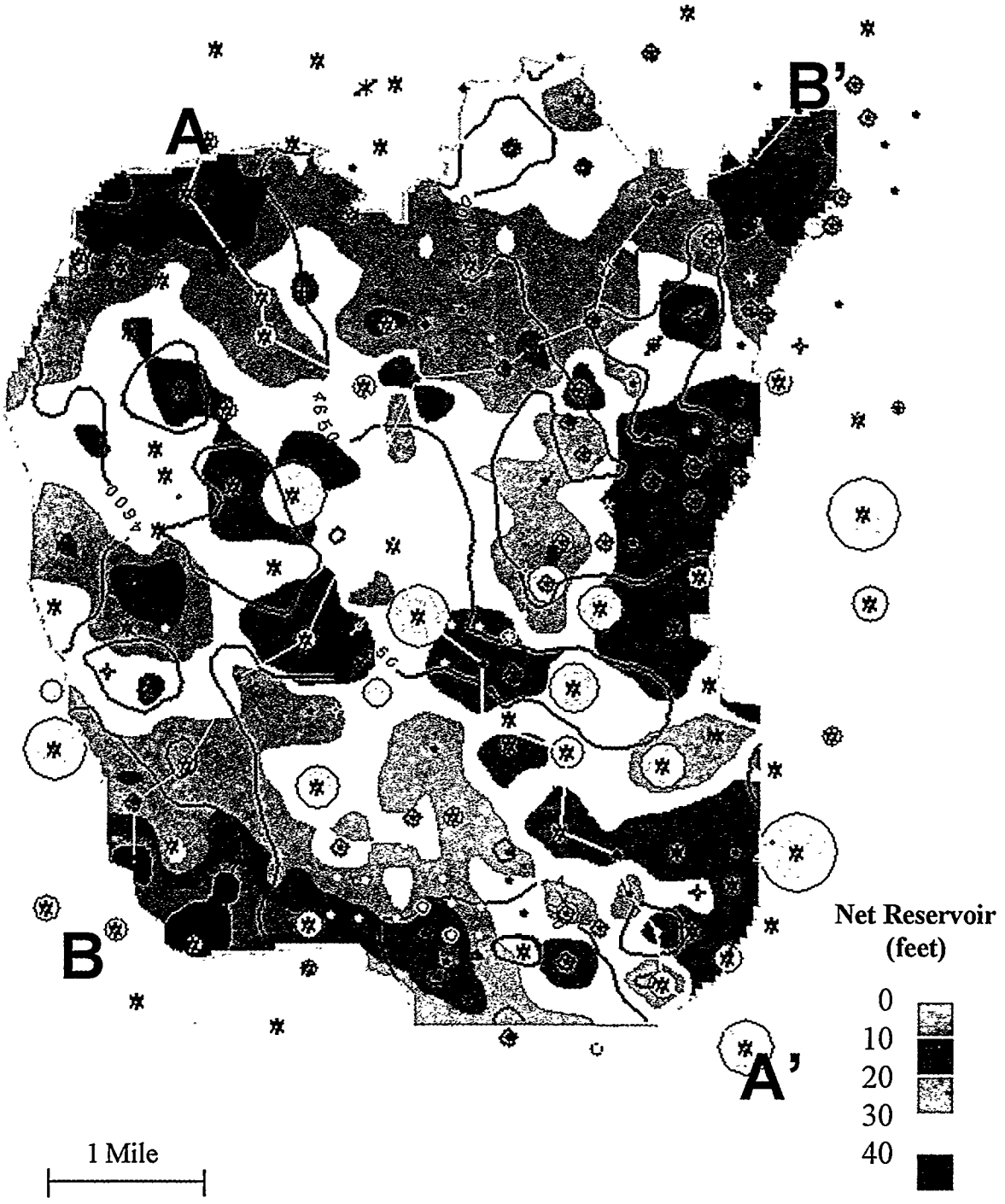

Figure A22. Thick sandstone and subtle structural controls on gas production in the Vineyard sequence. Note the southeast-northwest trending line of large cumulative gas production coincides with the thick net reservoir "sweetspot" draped over "Noles' Nose". Color fill = Vineyard net reservoir isopach; bubbles = cumulative gas production. Net reservoir cutoffs: SP < -30 mv, res > 10 ohmm.

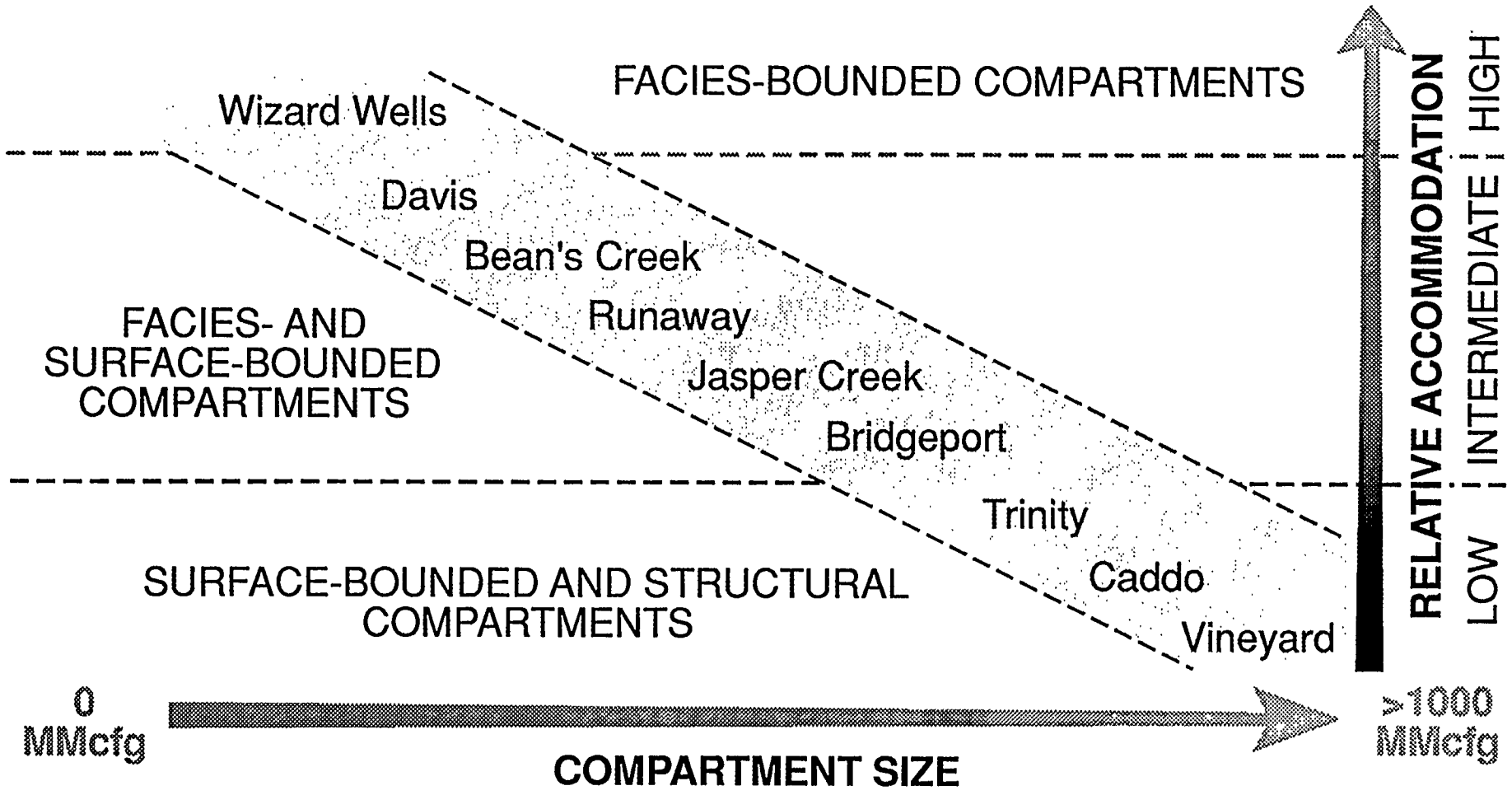

Figure A23. Semi-qualitative relationship established between relative accommodation available during deposition of the Boonsville sequences and compartment size in terms of typical, expected gas reserves.

A-65

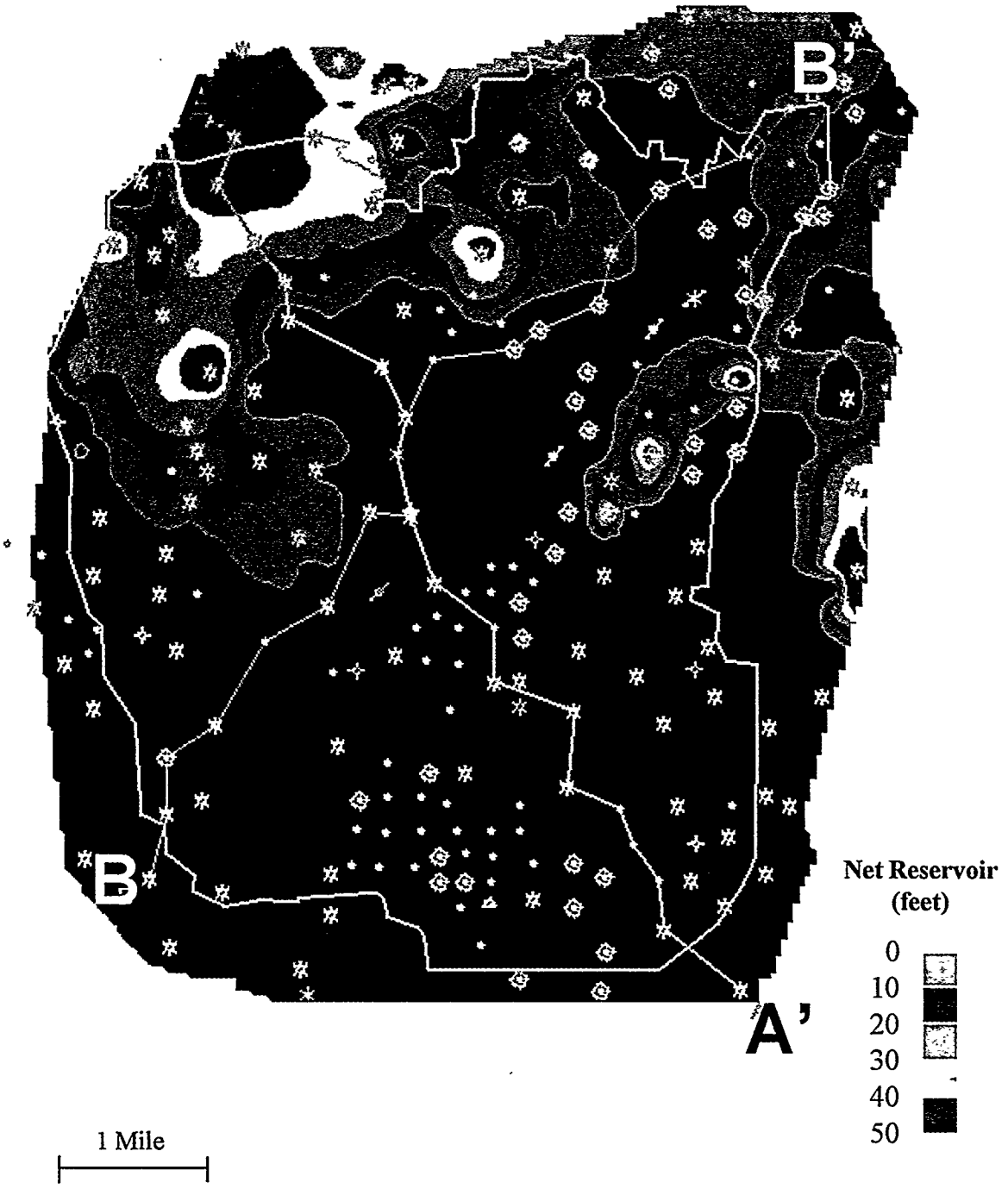

Figure A24. Wizard Wells genetic sequence net reservoir isopach (MFS80-MFS70). Net reservoir cutoffs: SP < -30 mv, Res > 10 ohmm.

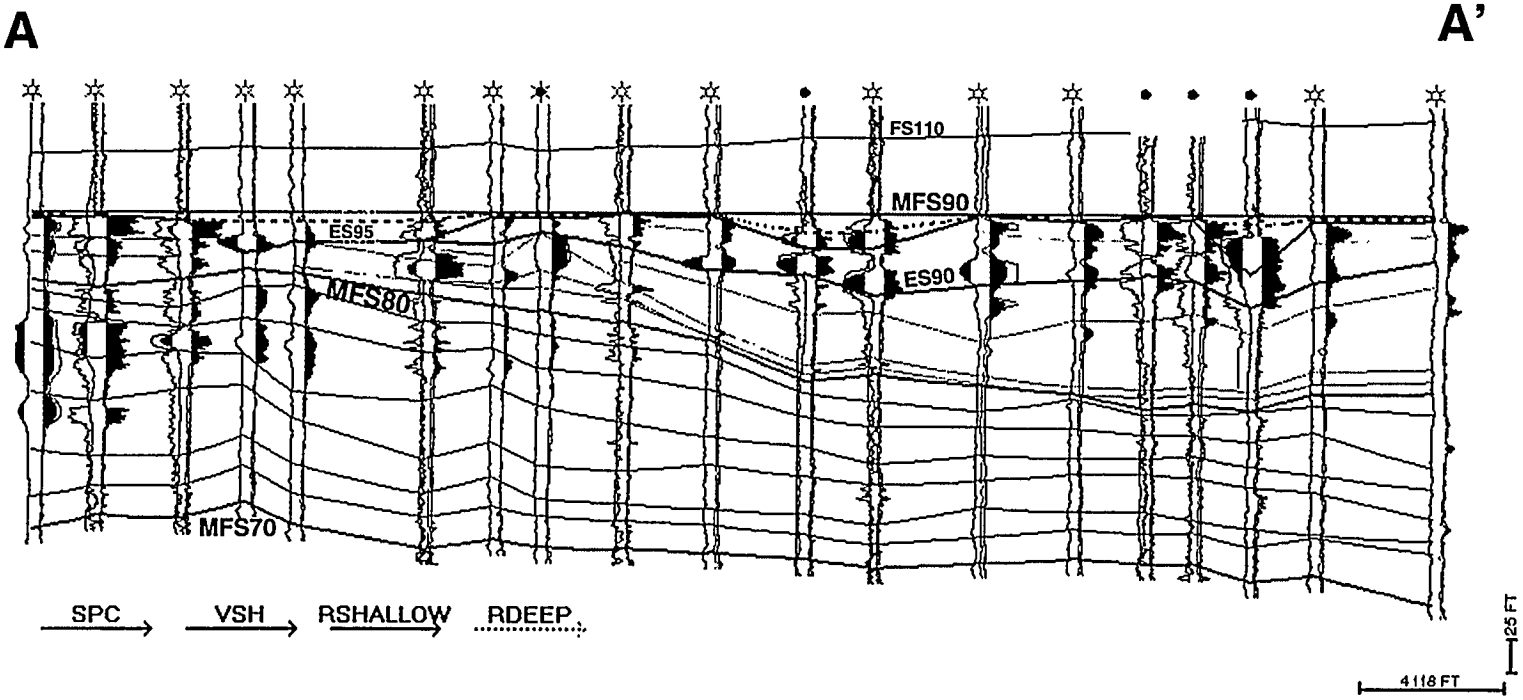

Figure A25. Stratigraphic cross-section A-A' of Wizard Wells genetic sequence (MFS80-MFS70) illustrating clinoforms (thin black lines between MFS80-MFS70) comprising this highstand delta system. Stratigraphic datum = MFS90.

A.67

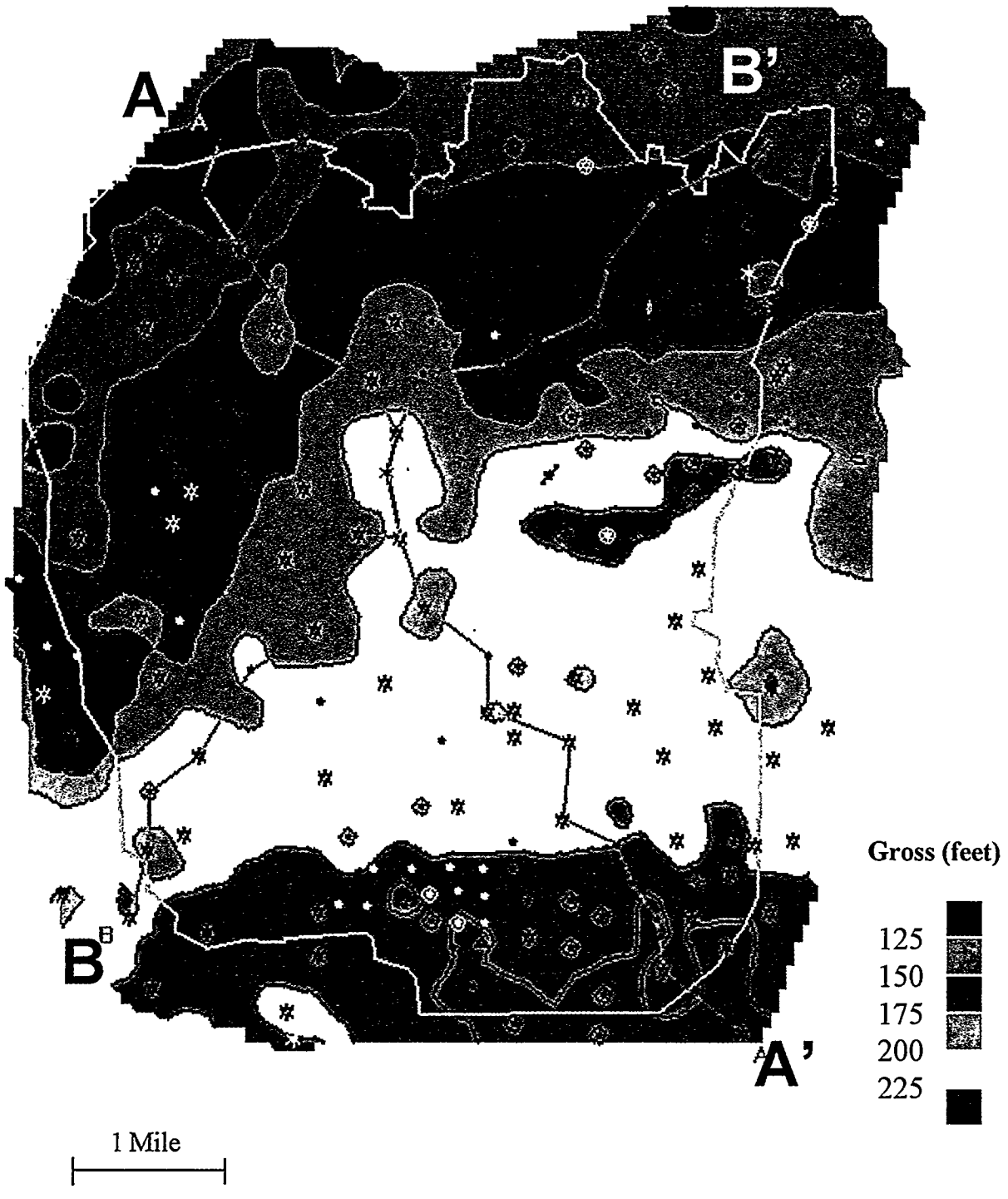

Figure A26. Jasper Creek "Exxon" sequence total gross interval isopach (ES40-ES30).

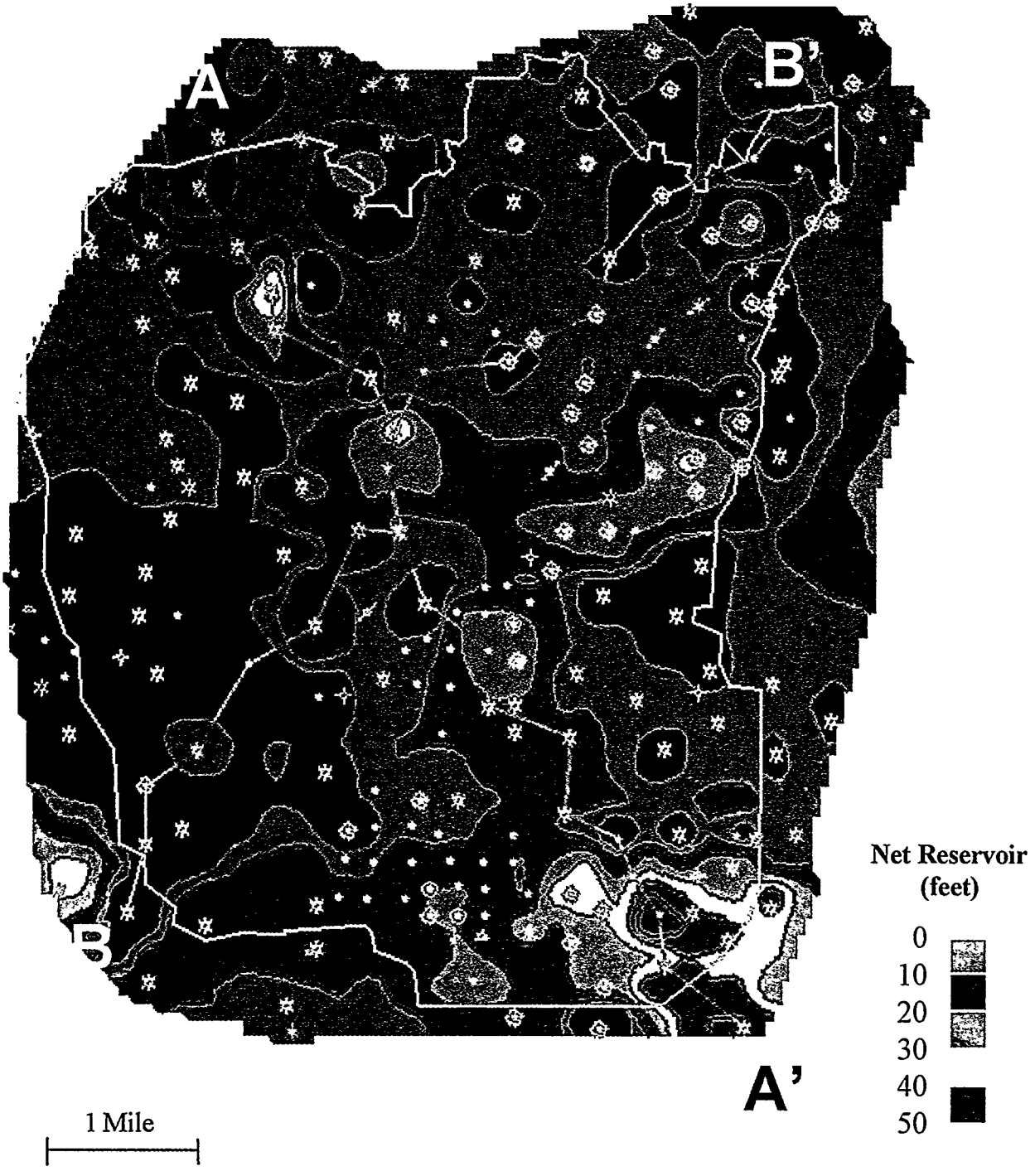

Figure A27. Jasper Creek "Exxon" sequence total net reservoir isopach (ES40-ES30). Net reservoir cutoffs: SP < -30 mv, Res > 10 ohmm.

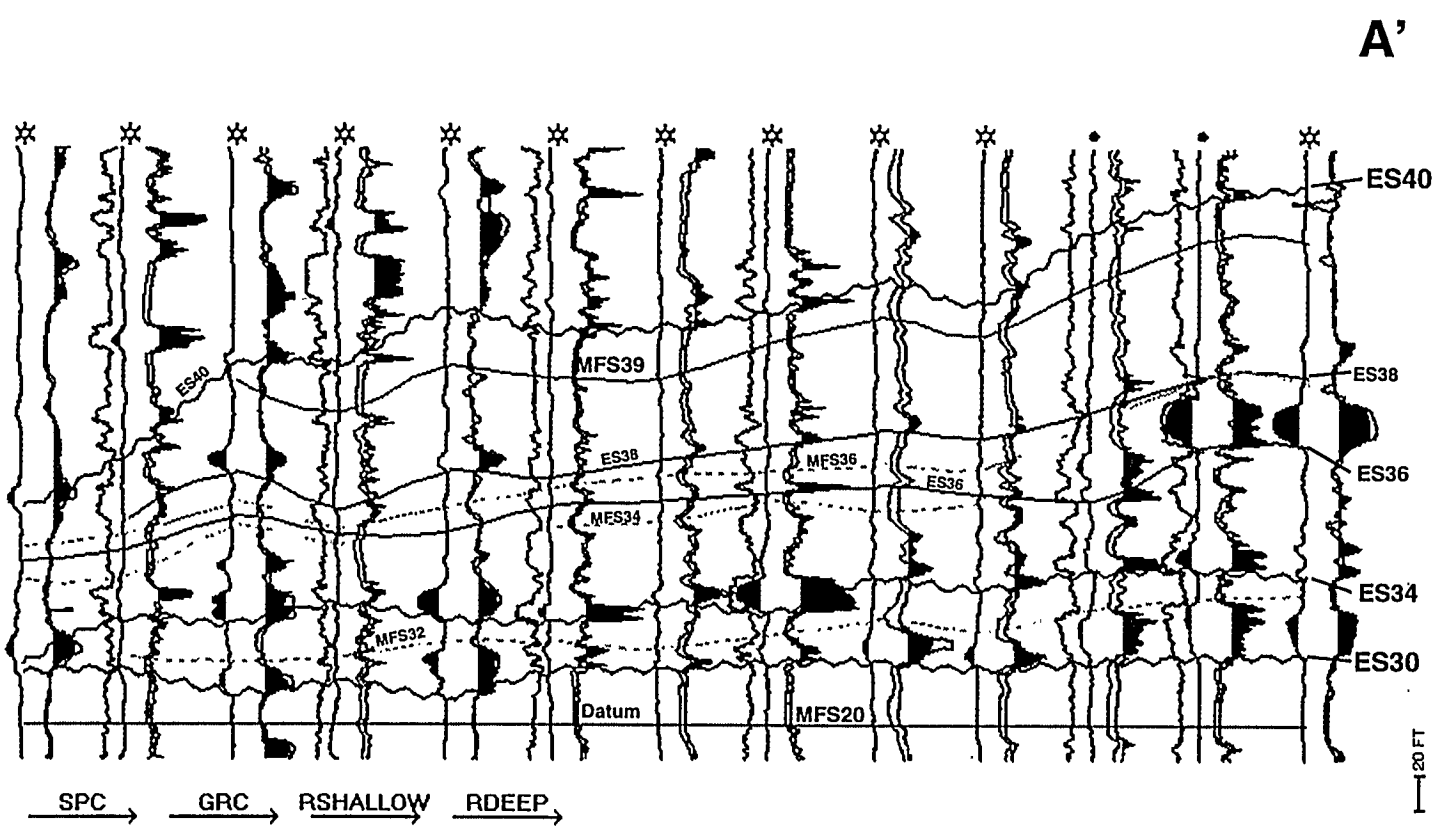

Figure A28. Stratigraphic cross-section A-A' illustrating the Jasper Creek "Exxon" sequence (ES30-ES40). The Jasper Creek sequence contains 4 subsequences in which sinuous belts of reservoir sandstone occur. Note the severe erosional truncation of Jasper Creek sequences by the ES40 (Bean's Creek) in the northern part of the Project Area. Stratigraphic datum = MFS20.

A.70

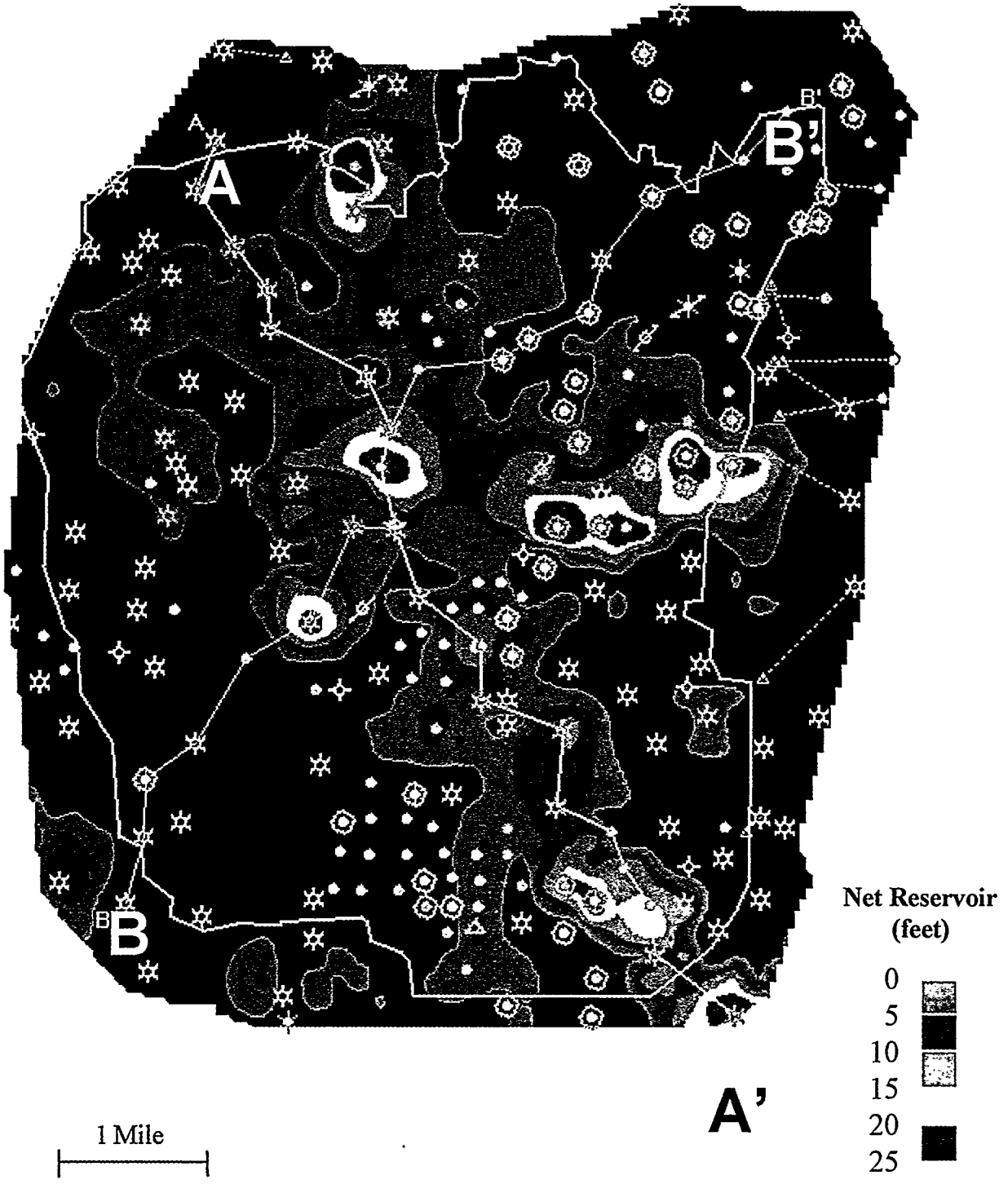

Figure A29. Lower Jasper Creek "Exxon" sequence total net reservoir isopach (ES34-ES30). Net reservoir cutoffs: SP < -30 mv, Res > 10 ohmm.

A.71

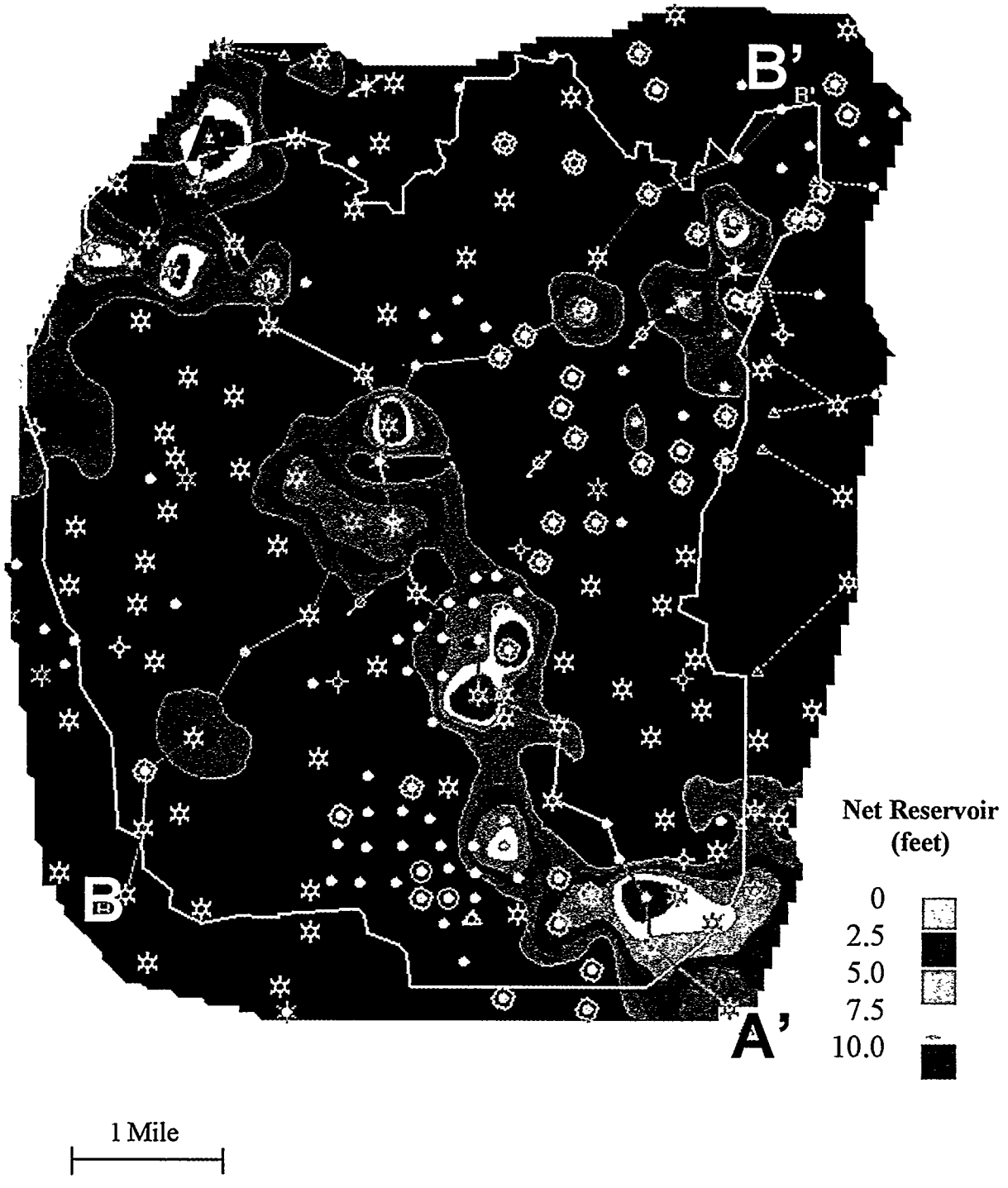

Figure A30. Middle Jasper Creek lowstand valley fill net reservoir isopach (FS34-ES34). Net reservoir cutoffs: SP < -30 mv, Res > 10 ohmm.

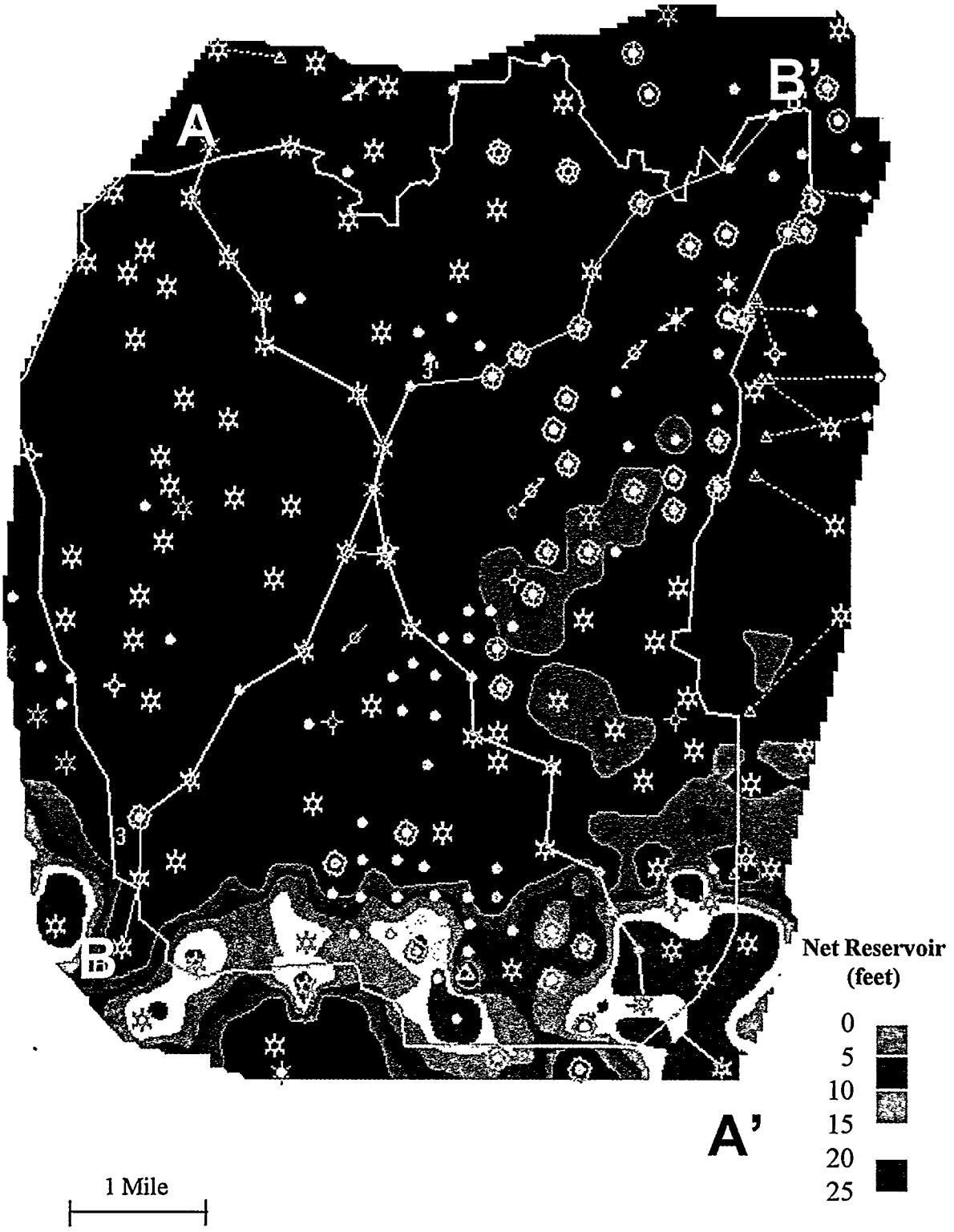

Figure A31. Upper Jasper Creek "Exxon" sequence net reservoir isopach (ES38-ES36). Net reservoir cutoffs: SP < -30 mv, Res > 10 ohmm.

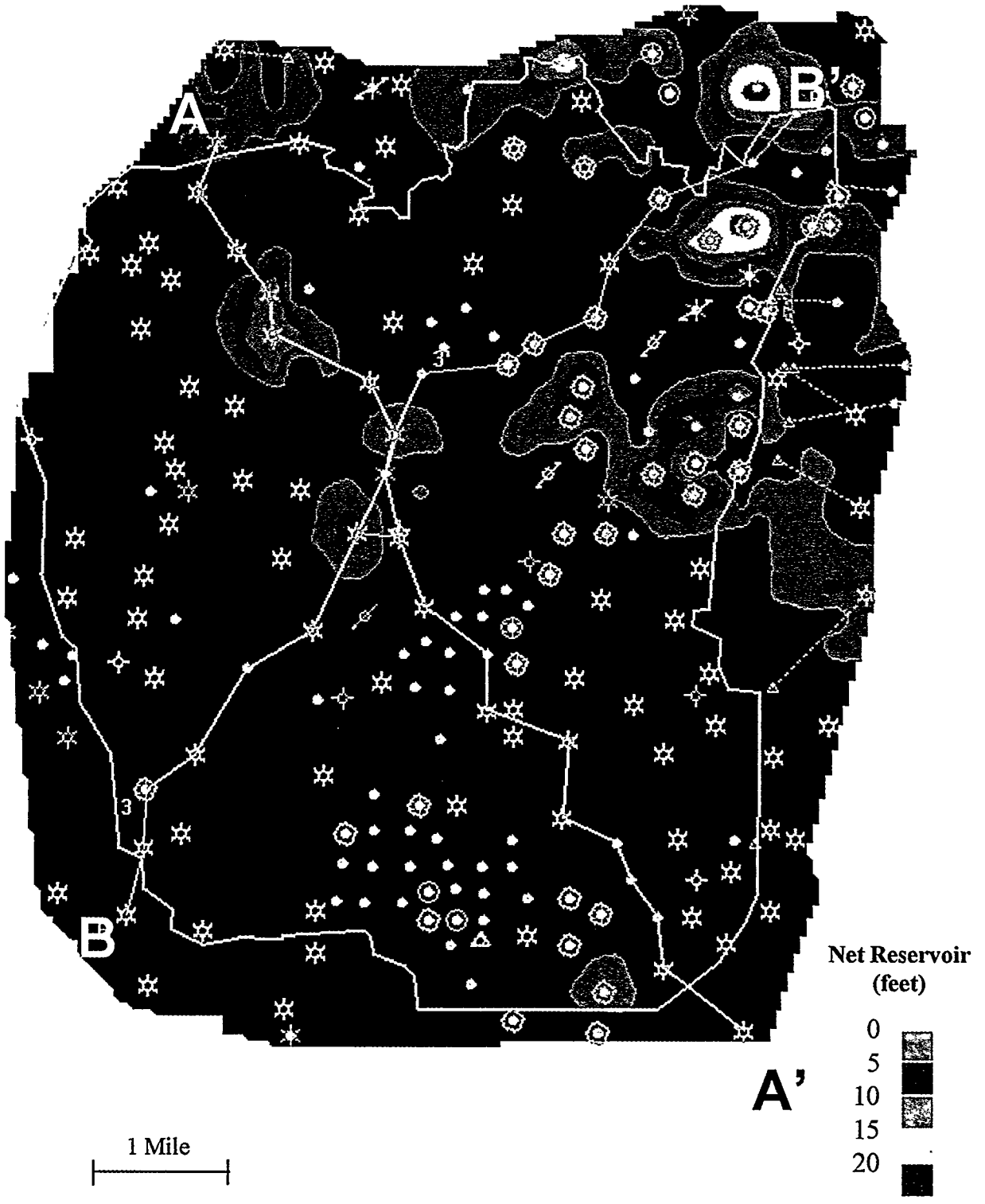

Figure A32. Fourth Jasper Creek "Exxon" sequence net reservoir isopach (ES40-ES38). Net reservoir cutoffs: SP < -30 mv, Res > 10 ohmm.

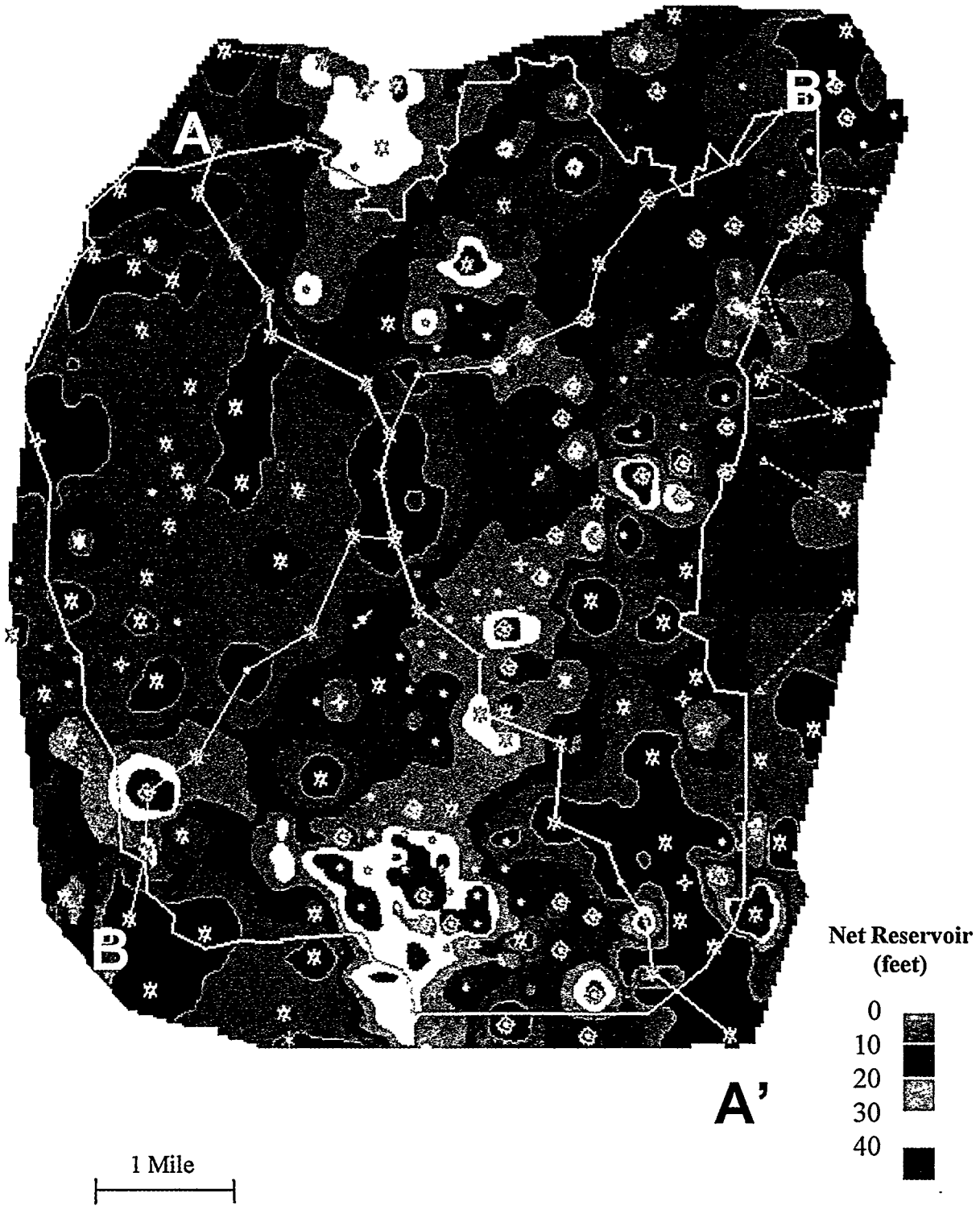

Figure A33. Caddo genetic sequence total net reservoir isopach (MFS90-MFS80). Net reservoir cutoffs: SP < -30 mv, Res > 10 ohmm.

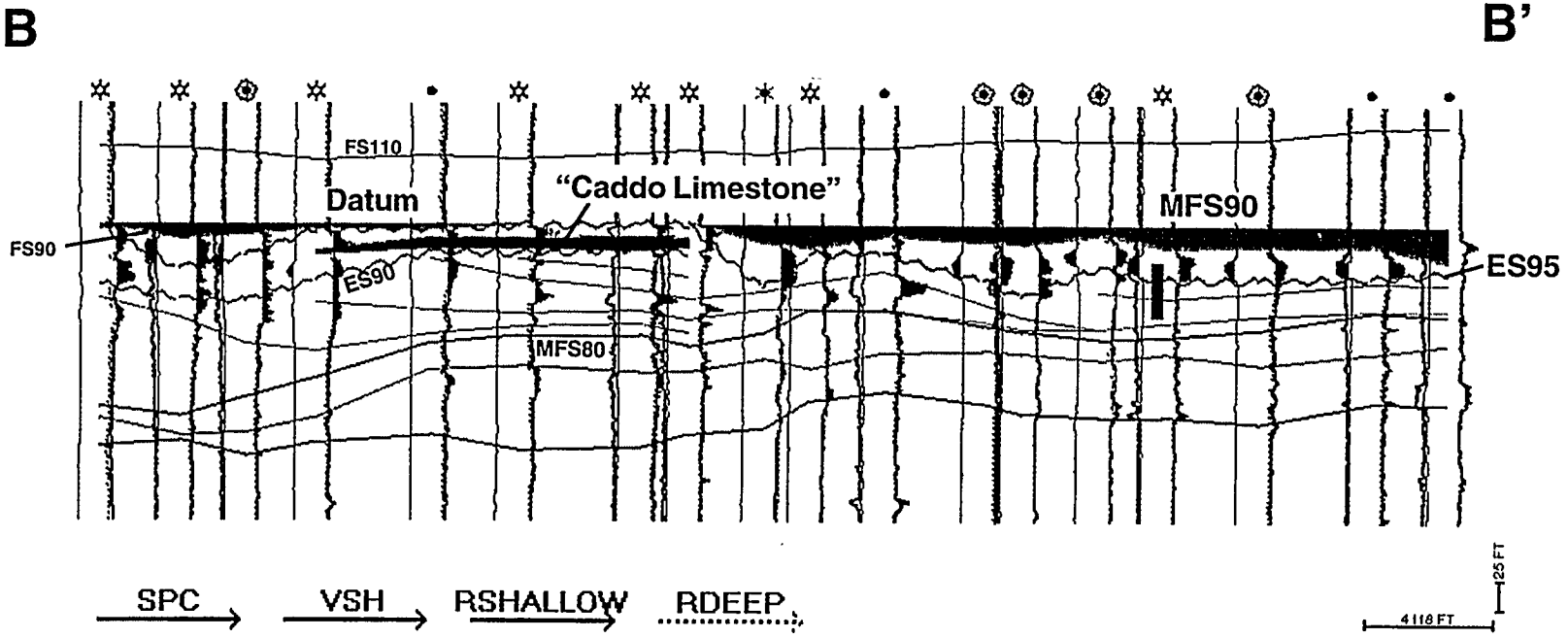

Figure A34. Stratigraphic cross-section B-B' illustrating Lower Caddo shingling clinoforms and limestone erosionally truncated by ES95. Upper Caddo valley-fill reservoirs are shaded in light gray. Stratigraphic datum = MFS90.

A.76

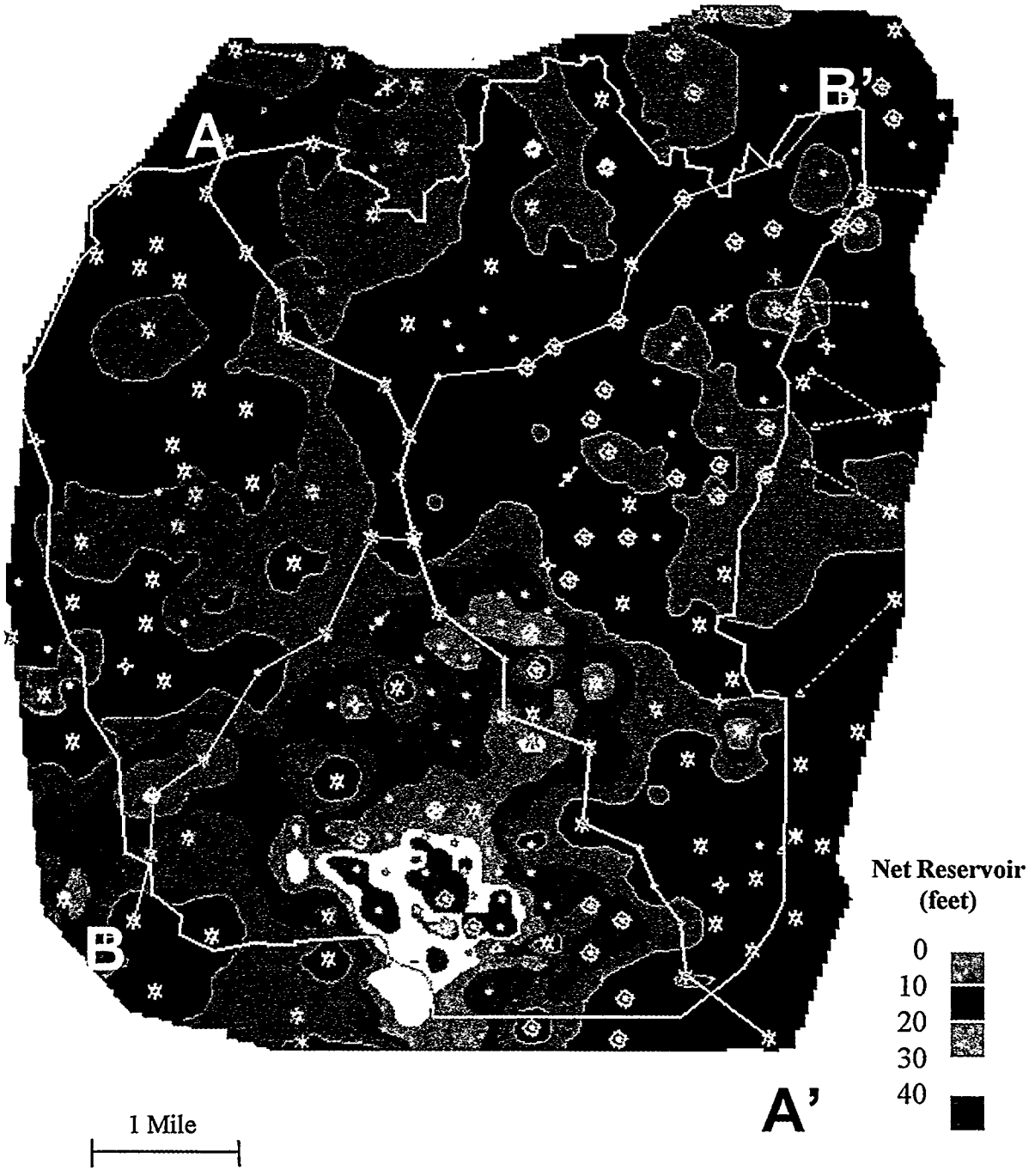

Figure A35. Lower Caddo lowstand wedge net reservoir isopach (ES95-MFS80). Net reservoir cutoffs: SP < -30 mv, Res > 10 ohmm.

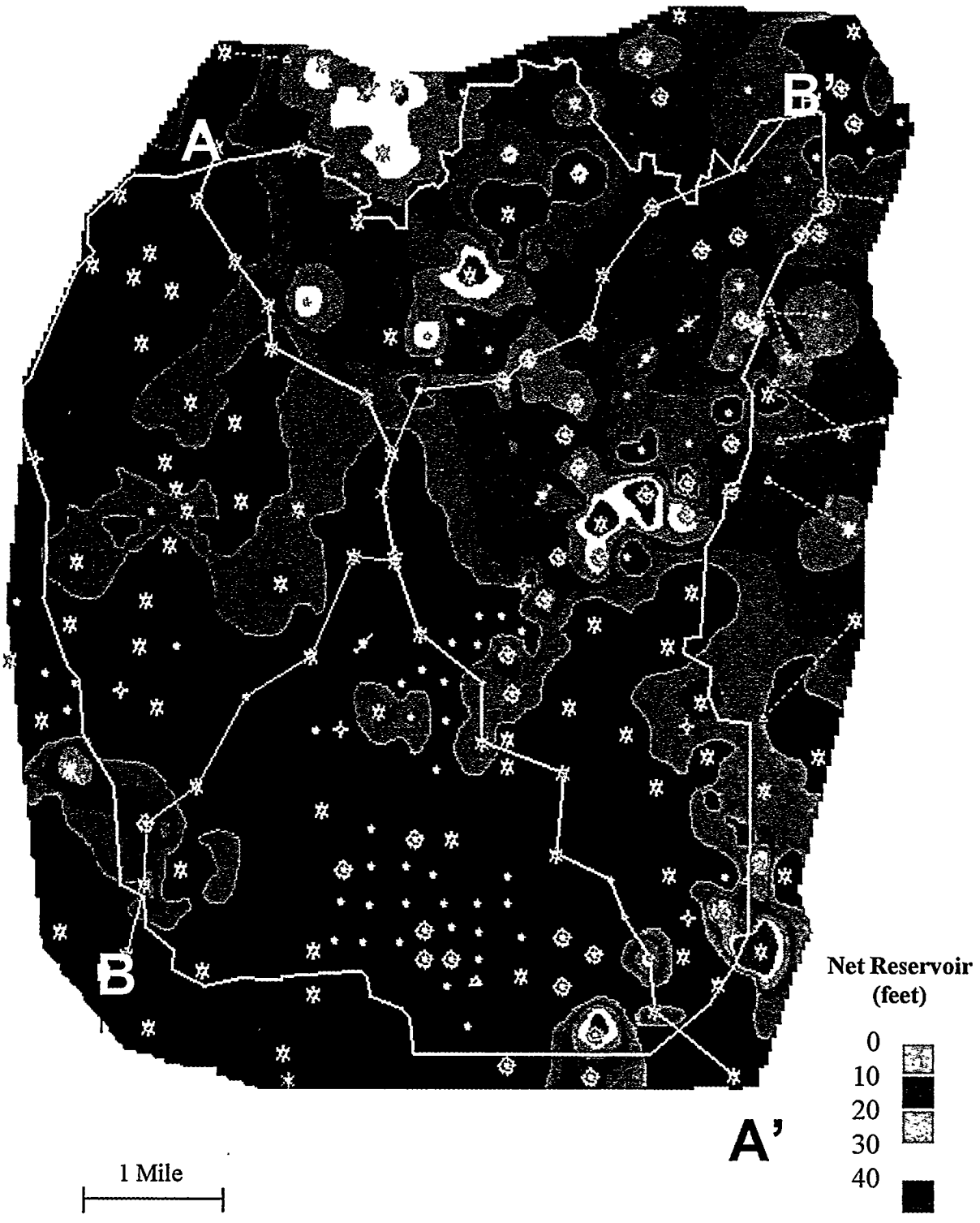

Figure A36. Upper Caddo genetic lowstand wedge net reservoir isopach (MFS90-ES95). Net reservoir cutoffs: SP < -30 mv, Res > 10 ohmm.

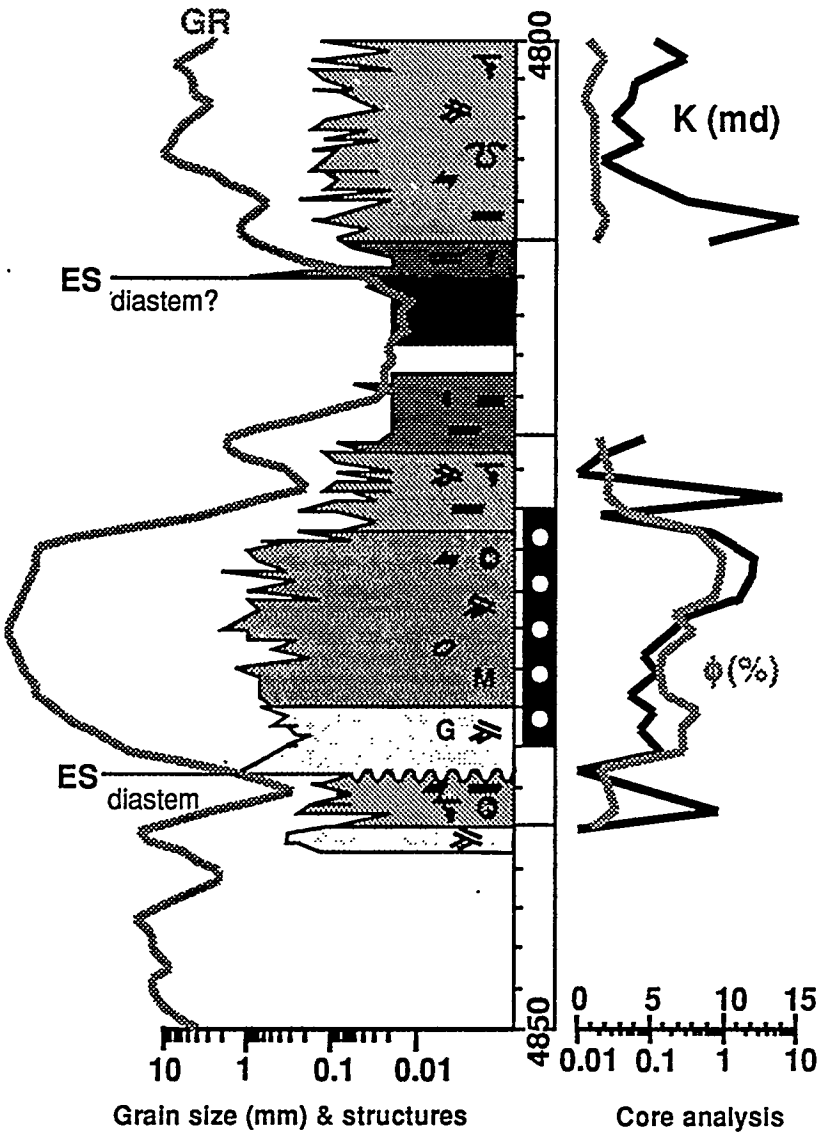

Figure A37. Wizard Wells genetic sequence from OXY, U.S.A., Tarrant "A" No. 4 core.

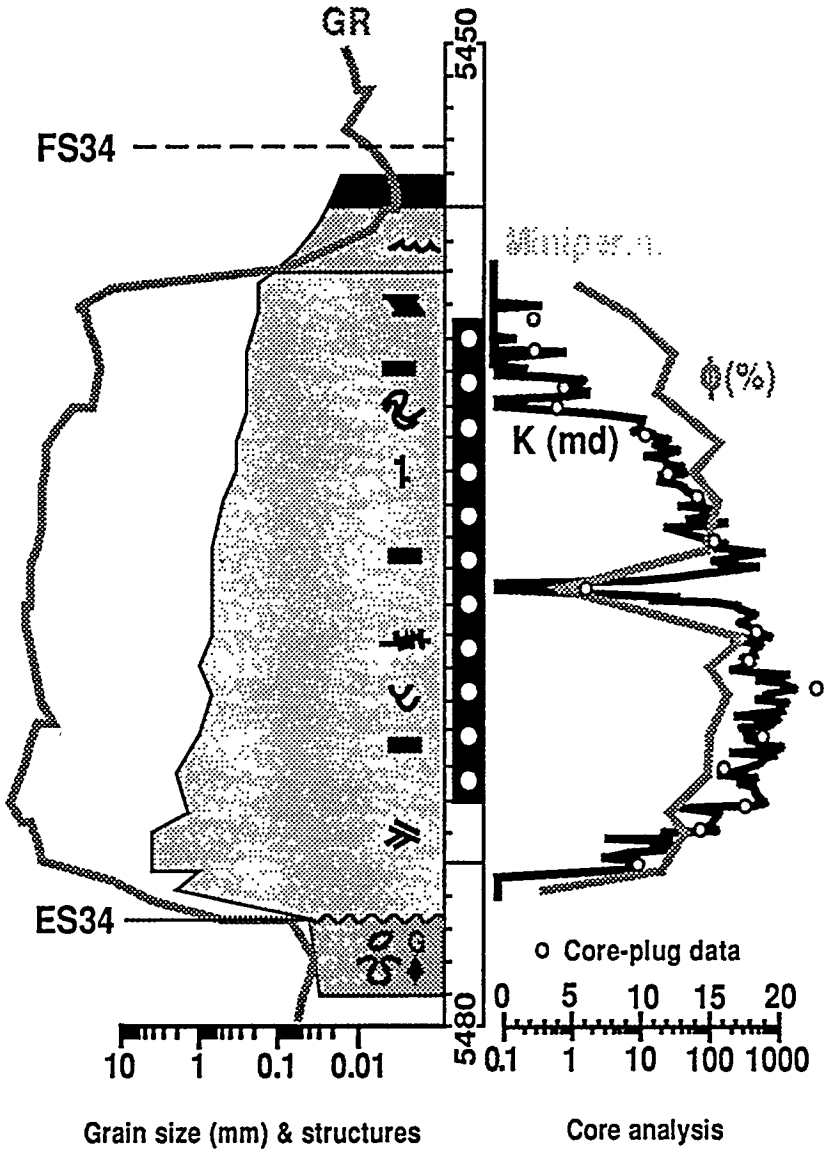

Figure A38. Middle Jasper Creek genetic sequence from Threshold Development I. G. Yates No. 33 core.

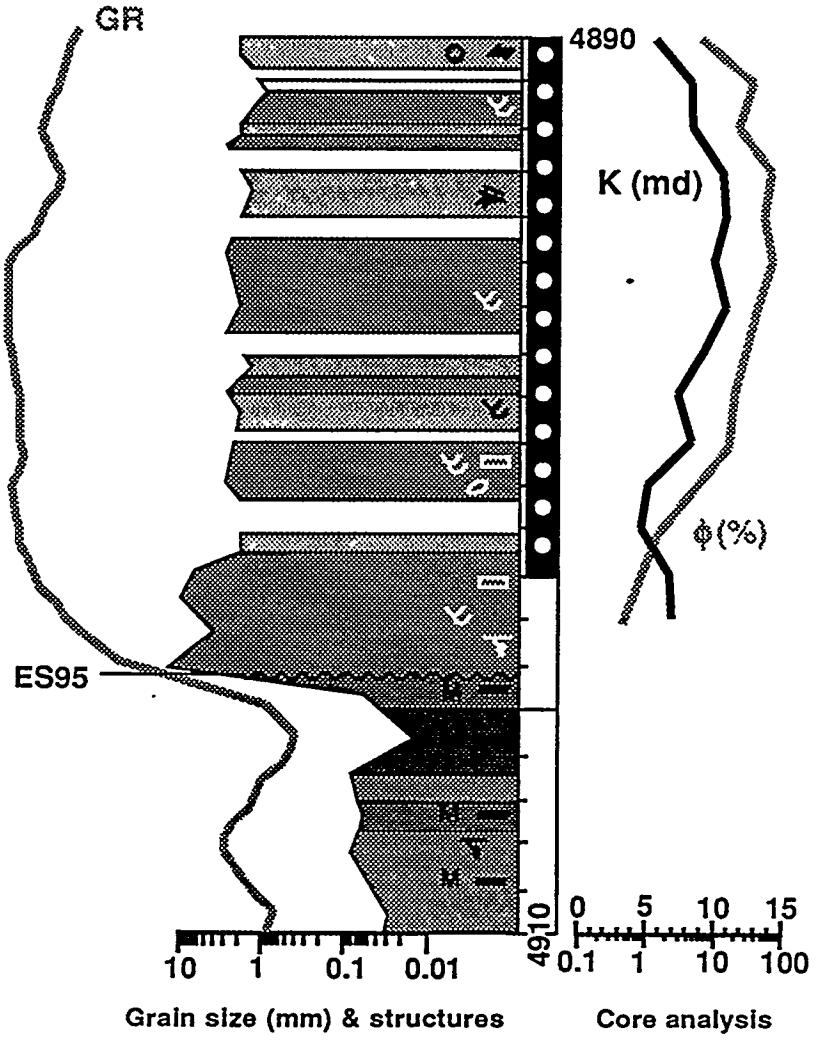

Figure A39. Upper Caddo sequence from OXY, U.S.A., Sealy "C" No. 2 core.

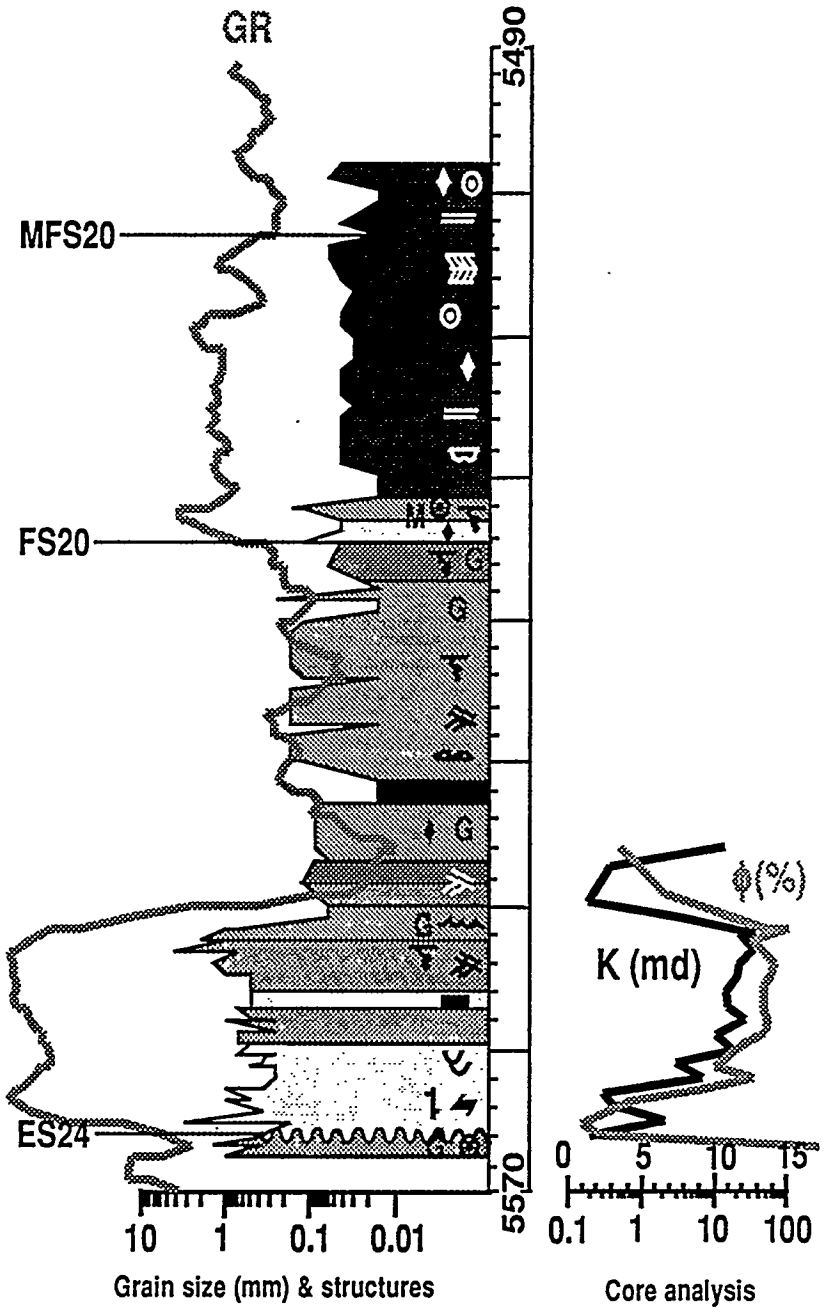

Figure A40. Vineyard genetic sequence from OXY, U.S.A., Tarrant "A" No. 4 core.

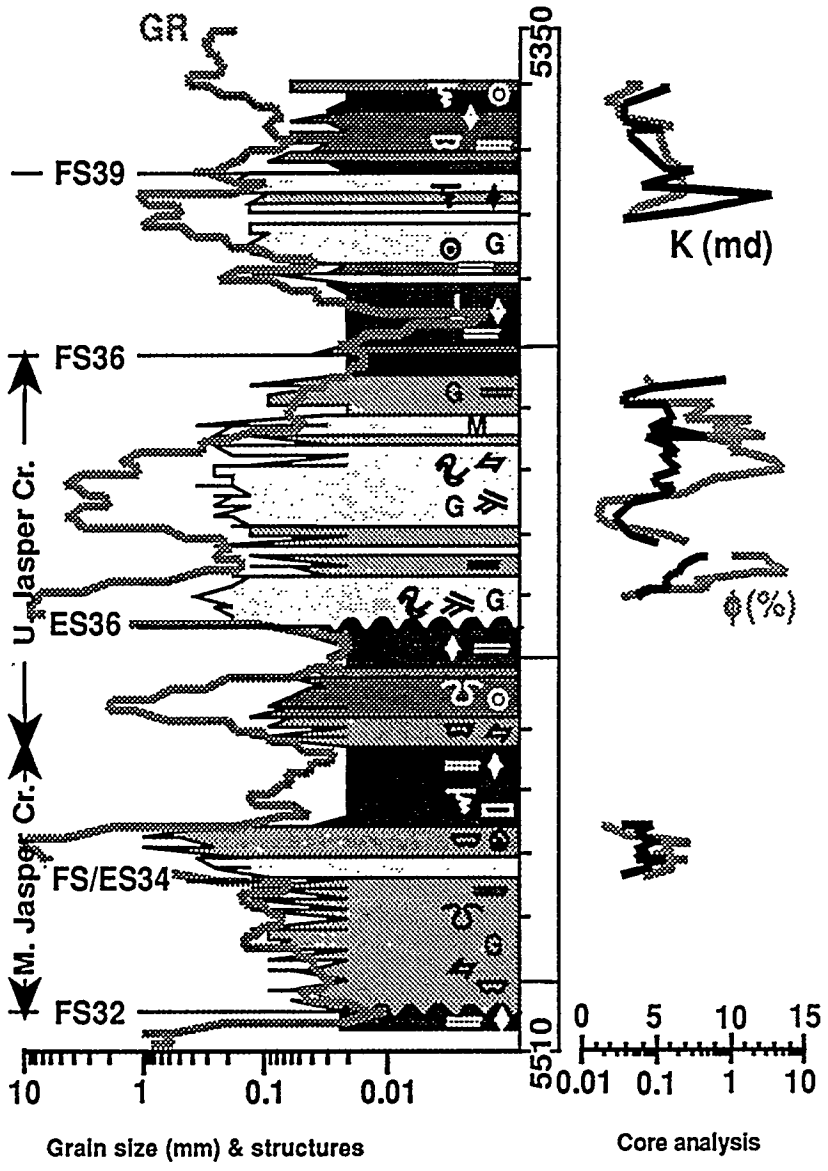

Figure A41. Middle and Upper Jasper Creek genetic sequence from E.P. Operating, Craft Tarrant Water Board No. 3 core.

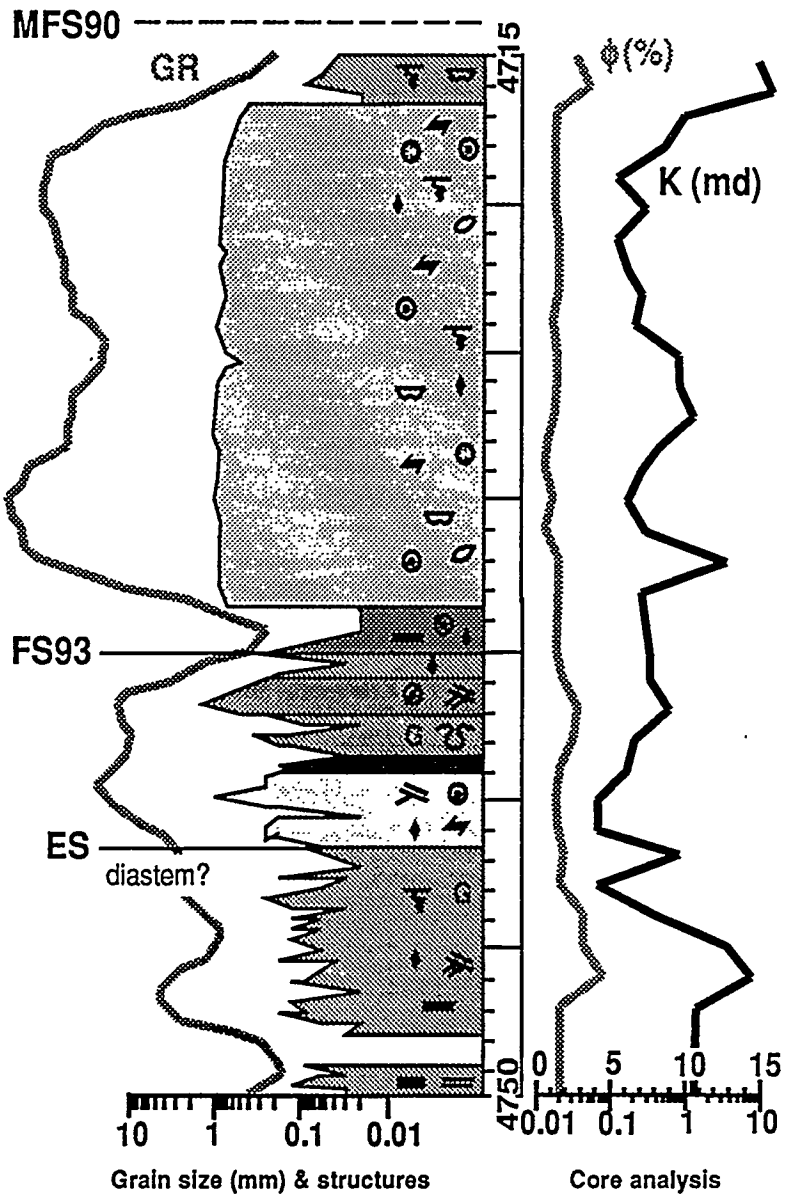

Figure A42. Upper Caddo genetic sequence from OXY, U.S.A., Tarrant "A" No. 4 core.

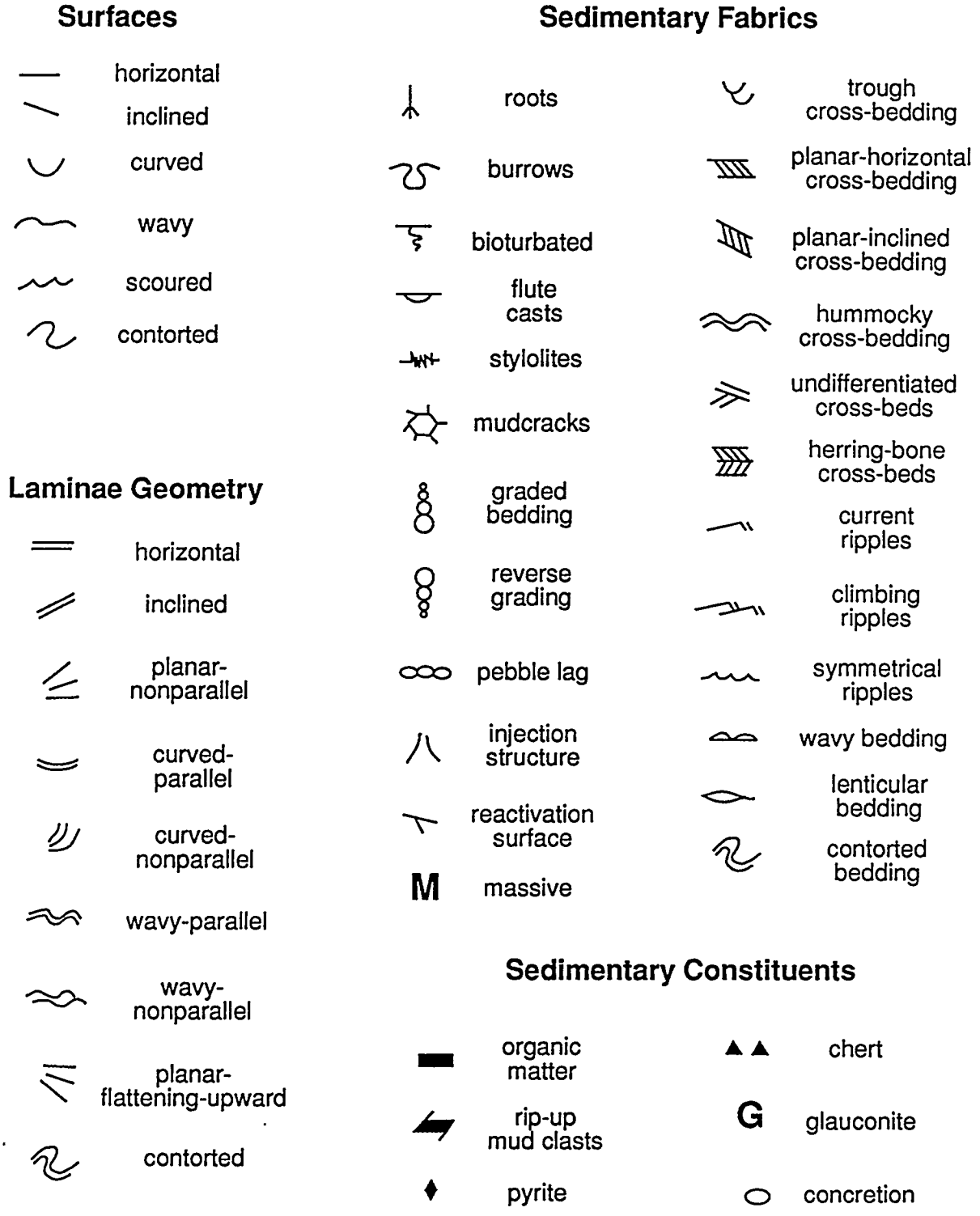

Figure A43. Key to symbols used in core description figures.

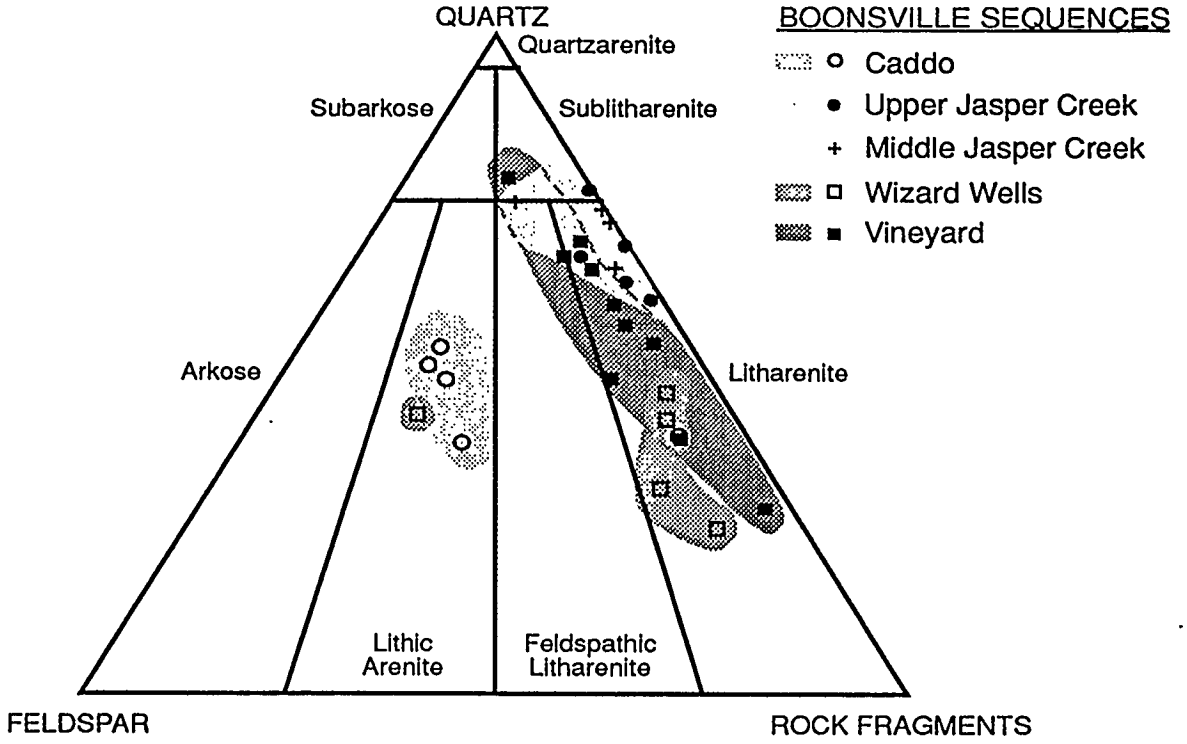

Figure A44. Variations in Boonsville reservoir sandstone lithologies by sequence.

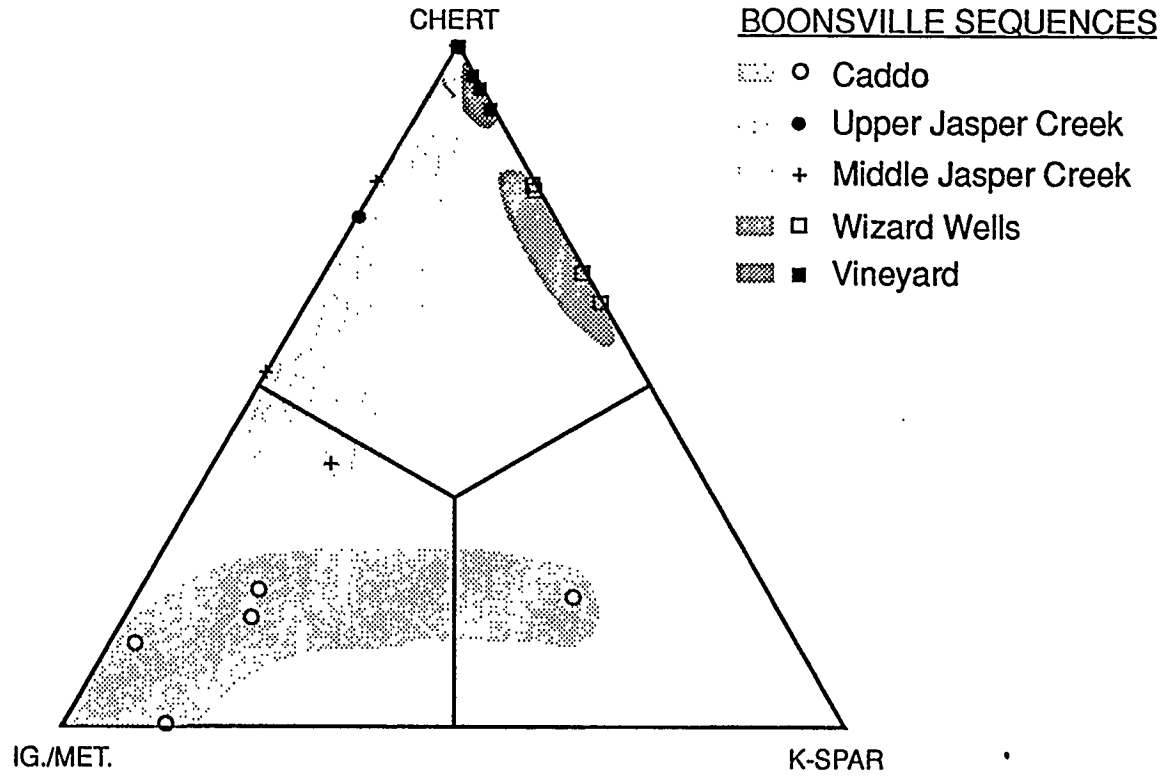

Figure A45. Relative proportions of non-quartz clasts (chert, K-spar, and igneous/metamorphic rock fragments) in Boonsville reservoir sandstones.

A.87

APPENDIX B

RESERVOIR ENGINEERING ANALYSIS OF THE BOONSVILLE PROJECT AREA

Introduction

This appendix highlights key results and conclusions derived from the reservoir engineering analysis conducted in the 26-mi^2 project area in Boonsville (Bend Conglomerate Gas) field in Wise and Jack Counties, Texas. Reservoir engineering plays an important role in an integrated study such as the one conducted in this project. The reservoir engineer must review available well-completion and well-performance data to establish the existence (or lack thereof) of compartmented or incompletely drained reserves and then to estimate the incremental gas reserves that may be expected from additional development. Well-test and production-data analysis and reservoir simulation can then be used to estimate reservoir properties and reservoir size, and, in some instances, to determine reservoir geometry. Reservoir properties may be mapped for regional trends that correlate with larger scale geologic and geophysical analyses; likewise, detailed reservoir engineering analyses of individual wells can provide valuable insight into reservoir architecture. Ultimately, the role of the reservoir engineer is to help focus and refine geological/geophysical interpretations being developed. Any geological/geophysical interpretations of reservoir geometry and reservoir compartmentalization must honor the known well-performance data.

As a result of the engineering analysis conducted in this project area, the following observations were made:

1. Engineering data, particularly pressure and production data, provide evidence of compartmented or incompletely drained gas in the Boonsville project area.

2. The expected gas volumes associated with these isolated compartments or poorly drained areas in most individual stratigraphic intervals will be small (200 MMscf or less on average), and multiple completion opportunities will typically be needed to achieve economic success in new infill wells.
3. Production and well test data can be used in many instances to estimate reservoir properties and to focus and refine the geological and geophysical interpretations of reservoir size and geometry.
4. Careful, strategic targeting of new wells will be the key to maximizing economic success.

Evidence of Compartmented or Incompletely Drained Gas

As part of the general overview of the Boonsville project, Figure 1.5 (see Overview section) presents a typical log through the Bend Conglomerate interval. As that figure shows, there are numerous, potentially productive sequences throughout the Bend Conglomerate. Of these intervals, the Upper Caddo and the Vineyard have been by far the most prolific producing reservoirs in the project area, although there have been completions in all the major sequences. In addition, the Upper and Lower Caddo are primarily oil-productive, although there is some gas production in both sequences.

Of particular importance to the engineering evaluation is that the Bend Conglomerate is treated as a common source of supply, and wells completed in more than one of the Bend productive sequences may be commingled and produced from a single wellbore. This poses particular problems in trying to determine total production volumes that can be attributed to specific stratigraphic sequences and in estimating interval-by-interval reservoir properties. Recently the Railroad Commission of Texas has also granted operators permission to commingle production from the Caddo and the Bend intervals in some instances.

The engineering analysis conducted in this project area included all wells drilled to the Caddo or deeper (total depth greater than 4,000 ft) within the 26^2-mi area where the 3-D data were shot and wells adjacent to, but just outside, the 3-D area. There are just over 200 wells in the 3-D area and approximately 350 wells in the engineering data base. Well logs were available for almost all of the wells in the 3-D area. Completion information and production history were also obtained for the additional wells in the engineering data base.

As additional background to the completion history in the Boonsville project area, Figure B1 illustrates the relative completion frequency of wells in the various Bend sequences. This summary includes all completions from the early 1950's to the mid-1990's for wells with log data. This figure shows all completions in the particular sequences, taking into account that one well is often completed in more than one interval. In fact, in the project area, an average of about three sequences are completed per well. The figure shows both producing and attempted completions in each interval; not all sands completed and tested in each interval were subsequently produced.

The basal Vineyard conglomerate has been the most widely completed sequence in the project area because the Vineyard is encountered throughout the project area, and it typically has 20 to 25 ft or more of net pay. Almost 70 percent of the wells in the project area have been completed in the Vineyard at some point. Quite a few wells have also tested, but not produced, the Vineyard interval. Most of these nonproductive Vineyard zones are located in the northeast portion of the project area, where the Vineyard, although thick, is deeper and has less porosity, higher water saturation, and apparently, much lower permeability.

Both the Caddo sequences and the Trinity have also been widely completed across the project area. The Bridgeport, Runaway, and Jasper Creek intervals have been completed in 15 to 30 percent of the project area wells. The other sands, including the

Wizard Wells, the Davis, and the Beans Creek are encountered only sparsely throughout the project area, as reflected in the small number of completions recorded.

As infill wells have been added at closer spacings, operators have completed in the sequences above the Vineyard with relatively greater frequency. This is illustrated in Figures B2 and B3 for wells drilled since 1980 and 1990, respectively. The Vineyard is now widely depleted across the project area, and reservoir pressures of 500 psi or less are often encountered in this sequence. As described later, the higher pressures associated with poorly drained or isolated reservoirs are found in the sequences above the Vineyard in the newer wells, accounting for the greater frequency of completion in these intervals.

With this understanding of well-completion history, one of our first steps undertaken in the engineering analysis was to look for evidence of compartmented or incompletely drained gas in the Boonsville project area. Figure B4 is a plot of initial pressures reported for wells in the project area as a function of time. These pressures are taken from multiple sources, including operator well files, state completion records, and commercial services such as Dwight's and Petroleum Information. These pressures may represent single or multiple commingled completions in different intervals throughout the Bend. In some cases, it is almost certain that these pressures are not fully built up and represent lower bound estimates of initial pressure. In all cases, however, these are the best estimates of initial pressure available for wells in the project area, and these data do provide at least a qualitative idea of the pressure history in the Bend Conglomerate over time.

In the 1950's, when most initial drilling occurred, most initial pressures reported ranged from about 1,500 to about 2,200 psi. The cluster of pressures reported in the 2,000- to 2,200-psi range reported in the mid- to late 1950's reflects the fact that most of the deeper Vineyard wells were drilled and completed during this time. As the figure shows, however, a number of the more recent wells drilled in the 1980's and 1990's still encounter initial pressures that are at or near the pressures measured in the 1950's. Clearly, there is additional scatter in the more recent data, indicating that many new wells

also encounter partially or significantly depleted areas in these reservoirs. Still, these higher pressures indicate that isolated, untapped reservoir compartments and poorly drained areas of the Bend Conglomerate reservoirs can still be found today.

This behavior is encountered widely throughout the Bend section. Figures B5 and B6 show similar plots generated for the Upper Caddo and the Jasper Creek sequences. In both cases, the initial pressures measured in several of the more recent completions in these intervals are comparable to original pressures reported in wells drilled 40 yr ago. Again, these data indicate that within individual stratigraphic sequences, there still appear to be isolated reservoir compartments or, at a minimum, very poorly drained areas of these reservoirs.

Figure B7 presents a summary of pressures measured by interval in wells drilled since 1990. These pressures also come from a variety of sources, including RFT's run during logging, actual wells tests, and completion records. Because the RFT (see Appendix C for discussion of RFT tool) has been used routinely by operators in the project area to measure pressure in potential completion intervals, a number of pressure measurements are available throughout the section, even in intervals that were not subsequently completed. In almost every sequence, pressures have been measured at or very near the expected original reservoir pressure for that interval, indicating poorly drained or compartmented gas reserves in these intervals. Generally, a wide range of pressures are recorded in many of these sequences, and even those where higher pressures have been measured also show evidence of significant depletion in other instances—e.g., Upper Caddo, Trinity, Bridgeport, and Jasper Creek intervals.

In two intervals, the Lower Caddo and the Vineyard, no pressures have been measured in recent wells in the project area that could be considered initial reservoir pressure. The initial pressure in the Vineyard is on the order of 2,200 psi, but the highest pressure measured in any well drilled since 1990 in the project area is about 1,500 psi. Most are significantly lower, in the range of 500 psi or less. The same is true in the

Lower Caddo, where most pressures measured in recent wells have been far less than the estimated original pressure of about 1,600 to 1,700 psi. This behavior in the Vineyard and the Lower Caddo is not surprising. As mentioned earlier, these intervals have been the best producing intervals in the area historically, and, as described in the geologic analysis (see Appendix A), these sequences were deposited in a very low accommodation space environment suggesting less likelihood of compartmentalization, especially at spacings of less than 160 acres.

Although the pressure data indicate that isolated or poorly drained gas reserves are still encountered in the Bend Conglomerate, a look at the production statistics in the project area indicates that these pressures are associated with decreasing gas volumes. Figure B8 plots the estimated ultimate gas recovery from project area wells drilled between the 1950's and 1970's as a function of the probability of occurrence; this was the first phase of drilling when wells could only be drilled on 320-acre units. There has been a wide range of gas recoveries from these wells, from as little as less than 10 to 20 MMscf to as much as 8 Bscf. The median ultimate gas recovery from wells drilled in this time period (the value occurring at a 50-percent probability) is 1.55 Bscf.

When the spacing requirements were reduced in 1980, permitting wells on optional 160-acre spacing, a number of new wells were drilled. Figure B9 presents the estimated gas recovery from these wells. These values again range from less than 50 MMscf to between 2 and 3 Bscf. The median gas recovery from wells drilled in this time period is expected to be about 600 MMscf. This decrease in expected ultimate recovery is largely influenced by the fact that more wells were completed in the Vineyard early in the development of this area. As mentioned previously, by the 1980's drilling phase, the Vineyard was already widely produced and substantially depleted in many areas. Because of this, it was completed less frequently, and when it was, it was less of a contributor to overall well performance. Thus, the gas recoveries shown in this figure are more

reflective of the contributions of uphole sequences, including especially the Trinity, Bridgeport, Runaway, and Jasper Creek.

Figure B10 shows estimated gas recoveries from wells drilled since 1990 in the immediate project area. Current field rules permit wells to be drilled on optional 80-acre units, but some wells shown in this figure have somewhat larger well spacings. Not many wells have been drilled in the project area since 1990, but those that have been drilled have estimated ultimate gas recoveries ranging from less than 100 MMscf to about 700 MMscf. Unlike the previous two figures, these estimated gas recoveries include only the zones currently producing; several still have behind pipe completion opportunities that may contribute additional gas to the overall well recovery. In Figures B8 and B9, there are almost no remaining behind-pipe opportunities in those wells; essentially all potential reservoirs have been completed and tested.

Based on currently producing zones, the median recovery from these recently drilled wells is only about 250 MMscf from the Bend Conglomerate. Again, however, this value is low, and the dashed line in Figure B10 is intended to suggest that behind-pipe opportunities will raise this distribution somewhat, although it is unlikely to go much above about 400 MMscf. Gas reserves of 300 to 400 MMscf are at the lower end of what operators in this field need for wells to be attractive investments. The goal of this project is to improve the overall distribution of ultimate gas recoveries through strategic targeting of new infill wells. Through strategic targeting, it is anticipated that poorer wells can be eliminated and that better wells will be drilled more routinely; this, in turn, will shift the distribution of gas recoveries to the right and up, into a range of gas recovery that is economical and that pays for the technology necessary to achieve it.

All of the wells represented in Figure B10 were completed initially in one or more reservoirs with a measured pressure at or near the expected original pressure. In several instances, these wells were tested at 1 to 2 MMscf/d, but both reservoir pressure and gas flow rates decline rapidly with time (see case histories on the I. G. Yates 33 area and the

B Yates 18D in the main body of the report). Ultimately the gas reserves associated with these higher pressures in a particular stratigraphic sequence were quite small—less than 100 MMscf in several cases. On the other hand, two recent wells drilled and completed in the Upper Caddo and also included in Figure B10, the Sealy C-2 and Sealy B-3 wells (see case history in the main body of the report), are projected to have ultimate gas recoveries of 500 to 600 MMscf from the Upper Caddo alone.

This is the reality faced by operators in this area as wells are drilled on closer spacings. Sometimes these higher (original or near original) pressures are associated with significant gas volumes, resulting in economically successful wells. At other times, however, these higher pressures occur in reservoirs of very limited size. These results point to the need for a better understanding of reservoir architecture and a more strategic approach to targeting new wells.

Hydrocarbon Distribution and Volumetric Estimates

Pressure data establish the existence of compartmented or poorly drained gas reserves throughout much of the Bend Conglomerate interval. The next step in the engineering analysis is to look at how the hydrocarbons are distributed within the Bend interval and to establish the expected size of the infill well reserves. To do this, a detailed petrophysical evaluation of the well log data was conducted as explained in Appendix C. Using the quantitative results of this log analysis, useful information was developed about the distribution of hydrocarbons and reservoir size within the Bend sequences.

Figure B11 illustrates the distribution of net pay and net hydrocarbon feet among the Bend intervals. As used in this analysis, net pay is defined as the hydrocarbon-bearing portion of the reservoir having a shale volume of less than 50 percent, a porosity of greater than 4 percent, and a water saturation of less than 60 percent. Net hydrocarbon feet is defined as the product of net pay, porosity, and hydrocarbon saturation (one minus the water saturation).

As the figure shows (and as has been alluded to previously), the Vineyard sequence alone contains about 40 percent of the total net hydrocarbons found between the top of the Caddo and the base of the Vineyard in the project area. The combined Upper and Lower Caddo zones contribute another 20 percent to the total. All other intervals combined, from the Wizard Wells through the Lower Jasper Creek, make up the remaining 40 percent of the net pay and net hydrocarbon feet. The median net pay for wells in the project area is 73 ft; the median value of net hydrocarbon is 5.2 ft.

The pressure data in Figure B7 demonstrated that most high pressures measured that are indicative of original reservoir pressure have been found in the intervals between the Lower Caddo and the Vineyard. Thus, although there is recent evidence of compartmented gas reserves in the Upper Caddo, it appears likely that most isolated or poorly drained gas in the project area will be found in the sequences between the Lower Caddo and the Vineyard. Because of this, most of the subsequent analyses considered only those zones between the Lower Caddo and the Vineyard.

That said, however, the Vineyard may still be a viable completion target in certain infill wells drilled within the project area, even if it is substantially depleted. Because of the Vineyard's overall reservoir quality—large net pays (20 to 30 ft), low water saturations (20 to 25 percent), and good permeabilities (0.5 to 5 md), this zone may still produce as much as 100 to 300 MMscf, depending on its effective drainage area, even if the average reservoir pressure is as low as 500 psi. Often, because many earlier Vineyard completions have been abandoned, newer wells drilled to the Vineyard may drain substantial areas. Clearly these reserves are neither isolated nor compartmented, but they should not be overlooked in planning the completion strategy for future infill wells. In some cases, these potential reserves may represent as much as half of the gas recovery needed to make an infill well in this area successful economically. One word of caution is appropriate, however; these low pressure intervals in the Bend Conglomerate are easily

damaged by fluid contact, so operators must be careful to minimize exposure to fluids when attempting completions in these zones (Darden, 1994).

Figures B12 and B13 show the distribution of total net pay and total net hydrocarbon feet in the intervals between the Lower Caddo and the Vineyard. Total net pay in these intervals, when present, ranges from as little as 1 ft to more than 110 ft, but the median value is 30 ft. This means that, historically, half the wells drilled in the project area have found less than a total of 30 ft of net pay and half the wells have found greater than 30 ft of net pay between the Lower Caddo and Vineyard sequences. The median value for net hydrocarbon is 1.9 ft.

As Figures B12 and B13 illustrate, significantly less net pay and net hydrocarbon are found between the Lower Caddo and the Vineyard on the west side of the project area as compared with the east side. As demonstrated in the geologic evaluation of the project area (see Appendix A), the west portion of the project area is structurally higher than the east side. Because of this, overall less sand was deposited on the west side of the project area (see Figure A15 in Appendix A).

As a result, the west side of this area has a median total net pay and net hydrocarbon between the Lower Caddo and the Vineyard of only 21 and 1.3 ft, respectively, compared with values of 40 and 2.2 ft to the east. This superior distribution of net pay and net hydrocarbon to the east may suggest better infill opportunities in that part of the project area. Conversely, the lack of net pay to the west may suggest conditions more favorable to additional reservoir isolation.

Operators in and near the project area have indicated that gas reserves of 300 to 500 MMscf are needed for new Bend wells to be economically viable; the exact value depends on the operator's drilling and completion practices. Wells drilled through the Bend cost about $200,000 to $250,000 to drill and complete on average, but this can vary considerably among operators. For purposes of this evaluation, an ultimate recovery per well of 400 MMscf has been used as an economic infill well target.

Figures B14 and B15 are nomographs prepared for the project area showing total hydrocarbon feet required as a function of reservoir pressure and drainage area to yield recoverable gas reserves of 400 MMscf. For drainage areas of 60 to 80 acres and an average reservoir pressure of 1,500 psi, between 1.5 and 2 ft of net hydrocarbon or between 20 and 25 ft of net pay are required to have recoverable gas reserves of about 400 MMscf. As both pressure and drainage area increase, these net pay and net hydrocarbon requirements are less; likewise, if average reservoir pressure and compartment size decrease, even more total net pay and net hydrocarbon feet are needed to have recoverable reserves of 400 MMscf. These values of 1,500 psi for pressure and 60- to 80-acre drainage areas appear reasonable, however, for evaluating potential infill wells to be drilled in the project area.

Figure B16 is a summary of estimated drainage areas computed by completion interval using production data from wells in the project area. As mentioned previously, many wells in this project area are commingled in multiple zones, and it is difficult to allocate production back to specific intervals. This figure, however, is based solely on those completions where the actual production could be attributed to a particular zone with a high degree of certainty. Thus, it should be a reliable indicator of the range of drainage areas to be expected in the project area.

Most of the sequences have quite a wide range of estimated drainage areas. That should not be surprising because some really good wells (greater than 1 Bscf) can be found in almost every major sequence. What the figure shows is that for an interval such as the Trinity, drainage areas range from as small as 10 to 20 acres to in excess of 500 acres, but the median value is about 80 acres. In fact, most median values are in the 50- to 80-acre range for all zones except the Vineyard. The Vineyard has a median drainage area of about 160 acres.

It should be noted that these estimated drainage areas may be somewhat conservative. These values are based on the value of net hydrocarbon feet calculated at

the wellbore and assume constant reservoir properties away from the well. To the extent that reservoir quality may decrease away from the wellbore, the calculated drainage areas may be somewhat smaller than they actually are. Nevertheless, these median values and the range of results presented in Figure B16 appear quite consistent with earlier observations that we are more likely to find poorly drained or compartmented reserves in those intervals above the Vineyard as the well spacing is reduced to 80 acres. Likewise, it is not surprising that most Vineyard completions show signs of substantial depletion at spacings of 160 acres and less.

If 20 to 25 ft of net pay and 1.5 to 2 ft of net hydrocarbon are needed in the Bend intervals between the Caddo and the Vineyard for a successful infill well, where will these hydrocarbons be found? Figure B17 provides some insight. This figure plots the range of net pay and net hydrocarbon found in each major sequence throughout the project area. For an interval such as the Trinity, when present, the net pay may range from as little as 1 to about 20 ft; the net hydrocarbon ranges from 0.1 to about 2 ft. The median values are about 10 and 0.6 ft, respectively. Thus, while it is possible to find sufficient net pay and net hydrocarbon in a single completion in most of these sequences, it is far more likely that multiple, stacked completion opportunities will be needed to yield sufficient gas reserves for an economical infill well.

Figure B18 shows this even more clearly. In this figure, the values in Figure B17 were used along with an average drainage area of 80 acres to calculate typical gas reserves by interval. As the figure illustrates, an 80-acre Trinity reservoir may contain gas reserves of up to about 600 MMscf, but gas reserves of about 200 MMscf are more likely. The same is true for the other sequences as well. Thus, on average, it will take multiple, compartmented or poorly drained completion opportunities in those sequences above the Vineyard to result in a successful infill well. This observation should not discourage the use of geological or geophysical information in an effort to identify superior sand development in particular sequences. It does suggest, however, that a reasonable

approach to identifying infill locations may be to focus geological/geophysical evaluation in those areas having the highest likelihood of stacked completion opportunities.

Using that premise, Figures B19 and B20 were prepared. These figures show the distribution of net hydrocarbon and net pay across the project area. Figure B19 highlights those areas, with net hydrocarbon less than 1.5 ft, between 1.5 and 2 ft, and greater than 2 ft between the Caddo and the Vineyard. Figure B20 shows those areas with 3, less than 3, and 4 or more net pay intervals, also between the Caddo and the Vineyard. Comparing these two figures, one can see a band across the center of the project area from east to west that has the highest number of potential pay intervals and the best values of net hydrocarbon feet. This information was provided to both the geologist and the geophysicist in an effort to focus their analyses into areas that appear to have the greatest opportunity for finding multiple, higher volume completion opportunities.

Is there reason to expect that multiple, stacked reservoir compartments (or poorly drained areas) may exist at any one location in the project area? Generally speaking, there probably would not be, but in the Boonsville project area (and perhaps in other Mid-continent reservoirs as well), review of the 3-D seismic data leads to the observation that apparent, stacked, trapping geometries often exist within the 3-D data volume. This is actually one important approach that has been used to identify potential infill well locations (see 6. Siting Boonsville Development Wells—Case Histories—discussion in the main body of the report). Furthermore, the influence of karst-collapse features on Bend Conglomerate stratigraphy as described in the main body of the report also suggests the opportunity and the likelihood for finding multiple, stacked, and at least partially isolated compartments with the Bend.

In fact, these multiple, stacked reservoir compartments have been observed in at least one recent infill well drilled in the project area—the Billie Yates 18D (see discussion in the main body of the report). This well location was actually sited using the 3-D seismic data in an area of both greater than 1.5 net hydrocarbon feet and greater than

4 net pay intervals according to Figures B19 and B20. When drilled, the well found more than 2 net hydrocarbon feet and 5 net pay intervals between the Lower Caddo and the Vineyard. Four of these intervals encountered original or near-original pressure. Unfortunately, at least one of these intervals, the Upper Runaway, was limited in size (about 8 acres) and produced only about 30 MMscf. Additional high pressure intervals recently completed in the Jasper Creek look more promising, however, having produced about 40 MMscf in just 7 weeks and flowing at 600 Mscf/d, with little decline in flowing tubing pressure.

Estimating Reservoir Characteristics with Pressure, Production, and Well Test Data

Another reservoir engineering goal in an integrated reservoir study of this type is the ability to estimate reservoir properties and reservoir size, and, where possible, to provide some insight about reservoir geometries in order to help focus and refine the geological/geophysical interpretations being developed. To do this, reservoir engineers use these primary sources of data: pressure, production, and well test data.

p/z Analysis

As demonstrated earlier in this appendix, pressure data were used extensively in this analysis to establish the existence (or lack thereof) of isolated or poorly drained reserves in the various stratigraphic sequences that make up the Bend Conglomerate. Another way that long-term pressure data may be used to infer the presence of a partially drained reservoir compartment in communication with an already producing reservoir is by using gas well material balance or "p/z" analysis. This approach has been described elsewhere (Lord and Collins, 1991, 1992), and it was used extensively in the Gulf Coast phase of the Bureau's Secondary Gas Recovery research.

Figure B21 describes how p/z analysis may be used to infer communication with an incompletely drained reservoir compartment. In a volumetric gas reservoir, a plot of average reservoir pressure divided by the z-factor (compressibility factor for real gases) vs. the cumulative gas production will be a straight line whose x-axis intercept is equal to the original gas in place in the reservoir. This behavior is illustrated by the straight line in Figure B21. It should be noted that in order for this straight-line relationship to hold true, the value of pressure used to calculate p/z must be average reservoir pressure.

Often, the only source of long-term reservoir pressure data available in many wells comes from periodic deliverability tests required by State regulatory agencies. These tests may be conducted annually or biannually, and the shut-in periods required during these tests generally range from 24 to 72 h. As Figure B21 shows, as long as these short-term shut-in pressures reflect average reservoir pressure at various times, they can be used to construct a reliable p/z plot. In gas reservoirs, a reservoir permeability of greater than 5 to 10 md is typically required for 24-h shut-in pressures to build up sufficiently to represent average reservoir pressure. This was true of many of the high productivity Gulf Coast sands investigated in the Bureau's earlier research (Levey and others, 1992, 1993).

Sometimes, as shown by the dashed line in Figure B-21, the p/z vs. cumulative gas plot may begin to deviate from the straight line and flatten with time. Such behavior may suggest communication between the producing reservoir and an adjacent, supporting reservoir volume or compartment. Flow between these two sands may be restricted by a permeability contrast between the two; thus, it takes some period of depletion in the primary reservoir compartment before the response of the secondary reservoir compartment is observed. As the figure shows, as gas from the secondary compartment migrates into the primary compartment, it acts to maintain the average reservoir pressure at a level higher than would be anticipated, causing the flattening in the p/z curve. In some instances, using these data and the G-WIZ software developed as part of the Gulf Coast research (Lord and Collins, 1991, 1992), quantitative estimates of both primary and

secondary reservoir volumes and the degree of communication between the two can be determined.

Although this approach has been used with some success to identify incompletely drained compartments in the Gulf Coast, an engineer must still be cautious when using it. First, as stated previously, it works well only in higher gas permeability reservoirs (5 to 10 md or greater), where the short-term pressures typically used in the p/z plots accurately reflect average reservoir pressure. In addition, the flattening of the p/z curve may be caused by factors other than communication with a secondary reservoir compartment, including water drive, compaction drive, or multiple layers of different permeabilities being produced simultaneously. Even operational changes may result in this type of behavior. Therefore, the inference of a secondary reservoir volume based on a flattening in the p/z curve should also be based on supporting geological and geophysical interpretations.

The p/z curves from wells in the Boonsville project area were not found to be useful for inferring incompletely drained reservoir compartments. As discussed in the Overview section of this report, permeabilities in the Bend Conglomerate reservoirs tended to range between 0.1 and 5 md; thus, the 24-h shut-in pressures typically available for constructing the p/z plots did not represent average reservoir pressure. This is illustrated in Figure B22, for a reservoir with a permeability of 0.5 md. As the figure shows, although the 24-h shut-in pressures do not reflect average reservoir pressure, they do approach the average pressure with time in tighter reservoirs. This behavior, in itself, causes the p/z plot to appear to flatten with time, but it reflects nothing other than the fact that the short-term pressures used to construct the plot do not represent average reservoir pressure.

In addition to the behavior illustrated in Figure B22, many of the wells in the project area have been completed and produced from multiple zones simultaneously. Typically these zones have different pressures, permeabilities, and drainage areas. These variations in interval productivity can also result in a flattening of the p/z curve as the more

permeable intervals dominate the early production and later, the lower productivity intervals begin to contribute more to the overall production. Again, this flattening in the p/z curve is due to reservoir behavior other than communication with a secondary reservoir volume.

Because of the typical permeabilities of the Bend sequences and the way in which many of the wells were completed and produced, the use of p/z analysis to infer secondary reservoir compartments was not a useful technique in this study. This should not rule out the approach in other Midcontinent gas reservoirs, however. In other Mid-continent sands where the permeabilities are a little higher and the reservoirs are completed and produced separately, this p/z analysis may be just as effective in inferring incompletely drained reservoir compartments as in the previous Gulf Coast research.

Production Data Analysis

Production data analysis, or advanced decline curve analysis, was used extensively in the Boonsville engineering analysis to estimate reservoir properties, such as permeability and drainage area, and to evaluate the relative degree of depletion in specific reservoirs. Typically, in any study of this type, production data are usually the most readily available and easily obtained data. Using production data to determine reservoir characteristics is not new, having been introduced by Fetkovich in the early 1970's (Fetkovich, 1973). Still, however, production data, though often used to predict future performance, are not widely used to estimate reservoir properties. The advanced decline-curve analysis methods originally introduced by Fetkovich and extended by others (Fraim and Wattenbarger, 1987; Blasingame and others, 1991; Spivey and others, 1992; Spivey and Lee, 1993; Spivey and Frantz, 1994) enable production data to be analyzed in a manner similar to that used for well test data to estimate reservoir properties such as permeability, the degree of damage or stimulation (skin factor), and drainage area.

Figure B23 presents the Fetkovich type curves, which are composites of both analytical and empirical curves. These type curves combine analytical solutions with the radial flow equation describing transient flow, with empirical decline curve equations describing pseudo-steady-state or boundary-dominated flow. The curves are log-log plots of dimensionless rate, q_{Dd}, vs. dimensionless time, t_{Dd}, and assume constant bottomhole pressure production. The early stems are functions of dimensionless wellbore radius, r_D (ratio of drainage radius to effective wellbore radius), which is an indicator of damage or stimulation; the smaller the value of r_D, the greater the degree of stimulation. The later stems are functions of the decline exponent "b," also known as the Arps exponent (Arps, 1945), where a b value of zero indicates exponential decline and a b value of 1 represents harmonic decline. The evenly spaced b stems in between represent different types of hyperbolic decline. A b value between 0 and 0.7 is most common. For gas wells, Fraim and Wattenbarger (Fraim and Wattenbarger, 1987) showed that when gas reservoir properties are evaluated properly with time, all gas production data will follow the b stem of 0 on the type curve. This is particularly useful when analyzing gas well data quantitatively.

As Figure B23 shows, when the production data are plotted as log rate vs. log time, two important flow periods can be identified: transient flow and depletion or boundary-dominated flow. The transient flow period occurs first and is characterized by no influence from the reservoir boundaries. During this time, reservoir performance does not depend on reservoir size, but rather on permeability and the degree of damage or stimulation of the reservoir. This portion of the data can be used to estimate permeability and skin factor. Once reservoir boundaries begin to influence well performance, the log-log plot of flow rate vs. time begin to take on a concave downward shape. This portion of the data can be used to estimate ultimate recovery and drainage area.

Analyzing gas well data using the type curves is quite simple. First, a log-log plot of actual gas flow rate vs. time is generated as shown in Figure B24 at the same scale as the

type curve plot. Then the actual data are moved up and down and left to right until the best match of the production history is achieved with one of the type curves. From this match, values of permeability, skin factor, ultimate gas recovery, and drainage area can be estimated. This analysis can be accomplished by hand (Fetkovich, 1973), but automated Fetkovich-type analyses are also included in many popular decline-curve analysis software packages available in the petroleum industry today.

For analyzing production data from several hundred wells in a project such as this, however, an automated form of production data analysis is preferred. In this study, the production data analysis was actually accomplished using a GRI-developed software package known as PROMAT (Watson and Lee, 1986; Murtha and others, 1987; PROMAT, 1992). PROMAT is a single-phase production data analysis and forecasting tool developed as part of previous GRI research. The software includes a wide variety of analytical solutions modeling a number of different reservoir types and inner and outer boundary conditions. PROMAT is particularly useful because it includes an automatic history matching option that allows the engineer to enter and match actual production data easily and quickly to obtain estimates for reservoir permeability, skin factor, drainage area, and other reservoir properties, such as the degree of fracture storage and matrix-to-fracture transmissibility in naturally fractured reservoirs. PROMAT also permits variable flowing bottomhole pressures to be modeled over the life of a well (Spivey and Frantz, 1994), which can be important when trying to capture a known flowing bottomhole pressure history and operational events such as curtailment and compression.

Production data from all wells in the Boonsville project area were analyzed using PROMAT to estimate reservoir properties. Wherever possible, production from individual sequences was analyzed separately to develop estimates for reservoir characteristics by stratigraphic interval. Often, however, production from multiple zones had always been commingled, and it was not possible to allocate production back to

individual sequences. In these instances, total production from all zones was analyzed as a single zone, but with the knowledge that only estimates of overall gas recovery were generally reliable and not the reservoir properties themselves.

Age of the wells was also a problem in analyzing some Boonsville production data. Many wells in the project area were drilled in the 1950's, before the public data sources such as Dwight's and Petroleum Information began keeping records. In addition, the operators of these wells changed over the years in many cases, and much of the early production records are no longer available. Thus, in a number of the older wells, the first 5 to 10 yr of production data were missing. Again, this impacts the reliability of the estimates for reservoir permeability and especially skin factor in some cases, but the estimates for ultimate recovery and reservoir size should be largely unaffected.

As an example of how the production data were analyzed, Figure B25 shows the Trinity-only production history from the Threshold C Yates 9 well (see case history in the main body of the report). This decline behavior is typical of many project area wells. This well was completed in the Trinity sequence in June 1971 and produced about 1.9 Bscf from this interval through September 1989. The well came on line making about 2.5 MMscf/d and declined to about 20 Mscf/d over the 18 yr of production. This zone is still producing but is now commingled with the Vineyard reservoir below.

Figure B26 shows the more diagnostic log-log plot of the flow rate vs. time data. This plot suggests a period of transient flow for the first year or so; then the concave downward shape of the production data thereafter indicates boundary-dominated flow during most of the well's producing life. Using the analytical model (PROMAT) to history-match the production data, we estimated the Trinity reservoir to have a permeability of 3.3 md and a drainage area of about 300 acres. The estimated gas in place was 2.1 Bscf. Thus, the Trinity reservoir at this location has been essentially depleted by this well.

This same type of behavior can be seen throughout the project area. Figure B27 is another example of long-term production data analysis from the Upper Jasper Creek reservoir in the Threshold F Yates 9 well; this well produced for over 30 yr from this interval. Using the analytical reservoir model to history-match the production data, we found the Upper Jasper Creek reservoir to have a permeability of 0.33 md, a gas in place of 2.4 Bscf, and a drainage area of 232 acres. Again, the data suggest that this reservoir is substantially depleted.

Although the vast majority of production histories evaluated suggest substantial reservoir depletion, as shown in Figures B26 and B27, not all do. Figure B28 is a semilog plot of average flow rate vs. time from the Threshold B Yates 2 well. This well was completed in the Runaway sequence in 1956 and has produced for almost 40 yr from this reservoir alone. Although much of the first 10 yr of production history is unavailable, completion records suggest that the well came on production making 700 to 800 Mscf/d. Over time, however, the well has declined slowly and has maintained an average flow rate of about 50 to 100 Mscf/d over the last 30 yr. Overall, the decline is much flatter than observed in most project area wells.

In the late 1960's, the B Yates 2 was shut in and apparently curtailed for a couple of years. Once the well came back on line, however, the production jumped up to 400 to 500 Mscf/d and then declined back to a 50 to 100 Mscf/d average rate. The same was true following another apparent period of curtailment in the late 1970's.

When plotted on a log-log plot, as shown in Figure B29, the production data show only limited influence of boundary-dominated flow. This suggests that the B Yates 2 well is in communication with a larger gas volume than it can drain efficiently. Using the analytical model, we estimated the Runaway reservoir to have a permeability of 0.34 md, a gas in place of about 2.6 Bscf, and a drainage area of almost 600 acres. Because the B Yates 2 well has produced about 1.13 Bscf to date and is currently making about

50 Mscf/d, this evaluation suggests that another well may be needed to produce the gas from this reservoir effectively (or perhaps that this well should be restimulated).

Observations of this type signal areas where additional geological and geophysical interpretation should be focused. If, as the production data suggest, a reasonably large Runaway reservoir is communication with the B Yates 2 and a second well is needed, this area needs to be mapped and evaluated using the 3-D seismic data to both identify the reservoir extent and the optimal location for an additional well. Clearly this analysis does not infer the existence of an isolated reservoir compartment in the Runaway, but it does suggest an incompletely drained reservoir that may benefit from an additional well to accelerate the production of gas reserves in a more timely and economical manner.

Other uses of production data analysis results have been to map certain key properties across the project area and to compare the results with those from other disciplines. Figure B30 shows one such plot of drainage areas estimated for Middle Jasper Creek completions from production data analysis. The Middle Jasper Creek is a valley-fill sandstone that run diagonally from northwest to southeast across much of the project area. Interestingly, in the central and southeast parts of the project area, the Middle Jasper Creek is characterized by smaller drainage areas on the order of 60 acres or less, whereas much larger drainage areas (up to about 300 acres) are found in the northwest part of the project area. Similar maps were prepared for other sequences and were provided to aid and refine the geological and geophysical interpretations of these sequences.

Figure B31 presents another example of how the results of production data analyses were integrated with analyses from the other disciplines. This figure presents cumulative gas production as a function of time from the OXY Sealy B-3 and Sealy B-2 wells, both drilled since 1991 and completed in the Upper Caddo (see case history in the main body of the report). Both wells encountered near-original pressures upon completion in the Upper Caddo. As shown in the figure, both wells recovered about 350 MMscf through

the end of December 1994; the Sealy C-2 well has produced at somewhat higher flow rates than the Sealy B-3.

Also shown in Figure B31 are the values of permeability estimated for the Upper Caddo reservoir in each well from production data analysis. Permeabilities of 2.2 and 0.5 md were determined for the Sealy C-2 and Sealy B-3 wells, respectively. These permeabilities were then compared with those of the facies calculated for the Upper Caddo in both wells as determined from the petrophysical analysis (see Appendix C). The Upper Caddo facies determined for the Sealy C-2 well was "E," indicative of the cleanest sand in the Boonsville project area; the facies in the Sealy B-3 was found to be "E2," the shalier, lower quality productive sand type in the area. The permeability contrast between the two wells correlated nicely with this change in facies. In fact, additional comparisons between calculated facies and permeabilities suggest that a permeability of about 1 md may distinguish E from E2 facies in the project area. That is, E facies sands appear to have permeabilities greater than 1 md, whereas E2 facies reservoirs appear to have permeabilities of less than 1 md.

Well Test Analysis

Another useful source of reservoir information in a study of this type is well test data, particularly from pressure buildup tests. Well tests, when available, should provide superior estimates of permeability and skin factor (the degree of near-well damage or stimulation) as compared with production data because the test data are more concentrated at early times when transient flow generally dominates well performance. In some instances, depending on reservoir properties, pressure buildup tests may also provide insight into reservoir size and shape. This information about reservoir geometry can then be integrated with corresponding geological and geophysical interpretations to develop a better understanding of reservoir architecture.

Unfortunately, in an old field such as Boonsville (and, no doubt, many other older Mid-continent fields), not many well tests are available. Pressure buildup tests were rarely run in wells in the project area, and even when they were, many of the older test data were not always preserved. During the course of the research, however, several pressure buildup tests were run. Figure B32 presents the results from one of the well tests conducted in the Threshold I. G. Yates 33 well.

The I. G. Yates 33 well was drilled in April 1993 and completed in a high-permeability, 17-ft sand in the Middle Jasper Creek. RFT's run during openhole logging recorded pressures of about 1,900 psi in the Middle Jasper Creek, leading to the conclusion that this was a previously untapped reservoir compartment. The well flowed at rates above 2 MMscf/d initially without stimulation, but both flow rate and flowing tubing pressure declined very quickly, indicating a small reservoir volume. The Middle Jasper Creek interval made only about 60 MMscf of gas and some oil prior to being abandoned in September 1994.

The well test presented in Figure B32 was run only several days after the I. G. Yates 33 well was placed on production, but it provided early evidence of the limited reservoir size. Figure B32 is a semilog plot of the test data. From a quantitative analysis of the data, a permeability of 28 md was calculated for the Middle Jasper Creek reservoir. This permeability was higher than generally observed in the Bend intervals in this area, but this value was consistent with the abnormally high pressures measured from core analysis in this well. At a shut-in time of only about 0.5 h, a sharp upturn in the pressure data was observed, indicating that a near-well boundary had been encountered. The estimated average reservoir pressure of 1,560 psi was about 350 psi below the initial measured pressure of approximately 1,900 psi in this reservoir, after only less than 10 MMscf of gas had been produced. Again, these results suggested a very small reservoir volume.

Figure B32 also presents a history-match of the pressure buildup test data generated by a reservoir simulator. Although several different reservoir descriptions were tried, the

best match of the actual test data was obtained using a long, narrow (16 × 1) rectangular reservoir, with the well located near one end of the drainage area. The permeability used in generating the simulated test data was also 28 md, and the total reservoir size was about 8 acres. This high permeability and rectangular shape, as deduced from the well test analysis, were consistent with subsequent well performance, and, ultimately, with the geologic description of the complex Middle Jasper Creek stratigraphy in this area.

Well tests run in other project area wells were analyzed in a similar fashion to provide estimates of reservoir permeability, skin factor, reservoir size, and reservoir geometry for integration with the corresponding geological and geophysical interpretations. The results of several of these interpretations are included in the discussions found in the main body of this report.

Summary

In summary, engineering data, particularly pressure and production data, confirm the existence of compartmented or poorly drained gas reserves throughout much of the Bend Conglomerate interval in the project area. New wells drilled through the Bend Conglomerate still frequently encounter pressures in one or more of the Bend sequences that are at or near the original pressures encountered more than 40 yr ago. Most of these compartmented or poorly drained gas reserves are found between the Lower Caddo and the Vineyard intervals, particularly in the Trinity, Bridgeport, Runaway, and Jasper Creek sequences. Median drainage areas in these sequences were found to be 80 acres or less, further confirming the likelihood that compartmented or poorly drained gas reserves will continue to be found as well spacing is reduced to 80 acres.

Although higher pressures are still being found, the gas volumes associated with these pressures are the key to successful infill development. On the basis of the hydrocarbon distribution in the project area, we expect gas volumes associated with these isolated compartments or poorly drained areas (i.e., higher pressures) in most

stratigraphic intervals will be small, on the order of 200 MMscf or less on average (using an estimated drainage of 80 acres and typical volumetric properties). Recent wells having pressures at or near original in various sequences have found gas reserves in these zones ranging from less than 50 MMscf to about 700 MMscf. Thus, whereas it is possible that any single Bend sequence may include gas reserves sufficient to be economically attractive as well spacing is reduced, it is more likely that multiple, stacked completion opportunities will be needed to yield gas reserves sufficient for an economical infill well. More careful strategic targeting of new wells, incorporating insight gained from 3-D seismic and supporting geologic analysis, will therefore be needed to maximize economic success in Boonsville field.

Petrophysical, production, and well test data were analyzed wherever available throughout the Boonsville project area to estimate reservoir properties, drainage areas, and reservoir geometries. These results, in turn, were used to focus and refine the geological and geophysical interpretations developed. In particular, engineering estimates of reservoir size and geometry proved particularly important in understanding the stratigraphic complexities of the Bend Conglomerate and in calibrating 3-D seismic interpretations.

Review of 3-D seismic data in the project area leads us to the conclusion that apparent, stacked, trapping geometries often exist within the 3-D data volume. Further, influence of karst-collapse features on Bend Conglomerate stratigraphy also suggests the opportunity and likelihood for finding multiple, stacked, and at least partially isolated compartments. In the absence of clear geologic or seismic evidence of undeveloped reservoirs, a reasonable approach to identifying infill well locations may therefore be to focus 3-D seismic evaluation on these apparent, stacked, trapping geometries in those areas having the highest likelihood of multiple completion opportunities (i.e., multiple net pay zones).

References

Arps, J. J., 1945, Analysis of decline curves: Transactions of the American Institute of Mining, Metallurgical, and Petroleum Engineers, v. 160, p. 228.

Blasingame, T. A., McCray, T. C., and Lee, W. J., 1991, Decline curve analysis for variable pressure drop/variable flowrate systems: Society of Petroleum Engineers, Paper SPE 21513.

Darden, D. P., 1994, Plunger lift applications in wells with set packers or permanent tubing (abs.): Journal of Petroleum Technology, January, p. 6.

Fetkovich, M. J., 1973, Decline curve analysis using type curves: Society of Petroleum Engineers, Paper SPE 4629.

Fraim, M. L., and Wattenbarger, R. A., 1987, Gas reservoir decline-curve analysis using type curves with real gas pseudopressure and normalized time, *in* Society of Petroleum Engineers Formation Evaluation, p. 671–682.

Levey, R. A., and others, 1992, Infield gas reserve growth potential: Gulf Coast sandstone reservoirs (Frio, Vicksburg, Wilcox): The University of Texas at Austin, Bureau of Economic Geology, short course notes prepared for the Gas Research Institute, U.S. Department of Energy, and State of Texas, 392 p.

Levey, R. A., and others, 1993, Secondary natural gas recovery: targeted technology applications for infield reserve growth in fluvial reservoirs, Stratton field, South Texas: The University of Texas at Austin, Bureau of Economic Geology topical report prepared for the Gas Research Institute and the U.S. Department of Energy, GRI-93/0187, GRI Contract No. 5088-212-1718 and DOE Contract No. DE-FG21-88MC25031.

Lord, M. E., and Collins, R. E., 1991, Detecting compartmented gas reservoirs through production performance: Society of Petroleum Engineers, Paper SPE 22941, p. 575–581.

_____ 1992, Simulation system for compartmented gas reservoirs: targeted technology applications for infield reserve growth: Research & Engineering Consultants, Inc., topical report prepared for the Gas Research Institute and the U.S. Department of Energy, GRI-92/0104, GRI Contract No. 5088-212-1718 and DOE Contract No. DE-FG21-88MC25031.

Murtha, J. A., Gatens, J. M., Lancaster, D. E., Lane, H. S., Lee, W. J., Olarewaju, J. S., and Watson, A. T., 1987, Practical analysis methods for well test and production data: S. A. Holditch & Associates, Inc., topical report prepared for the Gas Research Institute, GRI-88/0017, GRI Contract No. 5084-213-0980.

PROMAT, 1992, A production data history matching and performance forecasting program for oil and gas wells: S. A. Holditch & Associates, Inc., User's Manual, Version 3.1.

Spivey, J. P., and Frantz, J. H., 1994, History matching production data using analytical solutions for linearly varying bottomhole pressure: Society of Petroleum Engineers, Paper SPE 29167.

Spivey, J. P., Gatens, J. M., Semmelbeck, M. E., and Lee, W. J., 1992, Integral type curves for advanced decline curve analysis: Society of Petroleum Engineers, Paper SPE 24301.

Spivey, J. P., and Lee, W. J., 1993, Production data analysis for wells that have been subject to periodic curtailment: Society of Petroleum Engineers, Paper SPE 26182.

Watson, A. T., and Lee, W. J., 1986, A new algorithm for automatic history matching production data: Society of Petroleum Engineers, Paper SPE 15228.

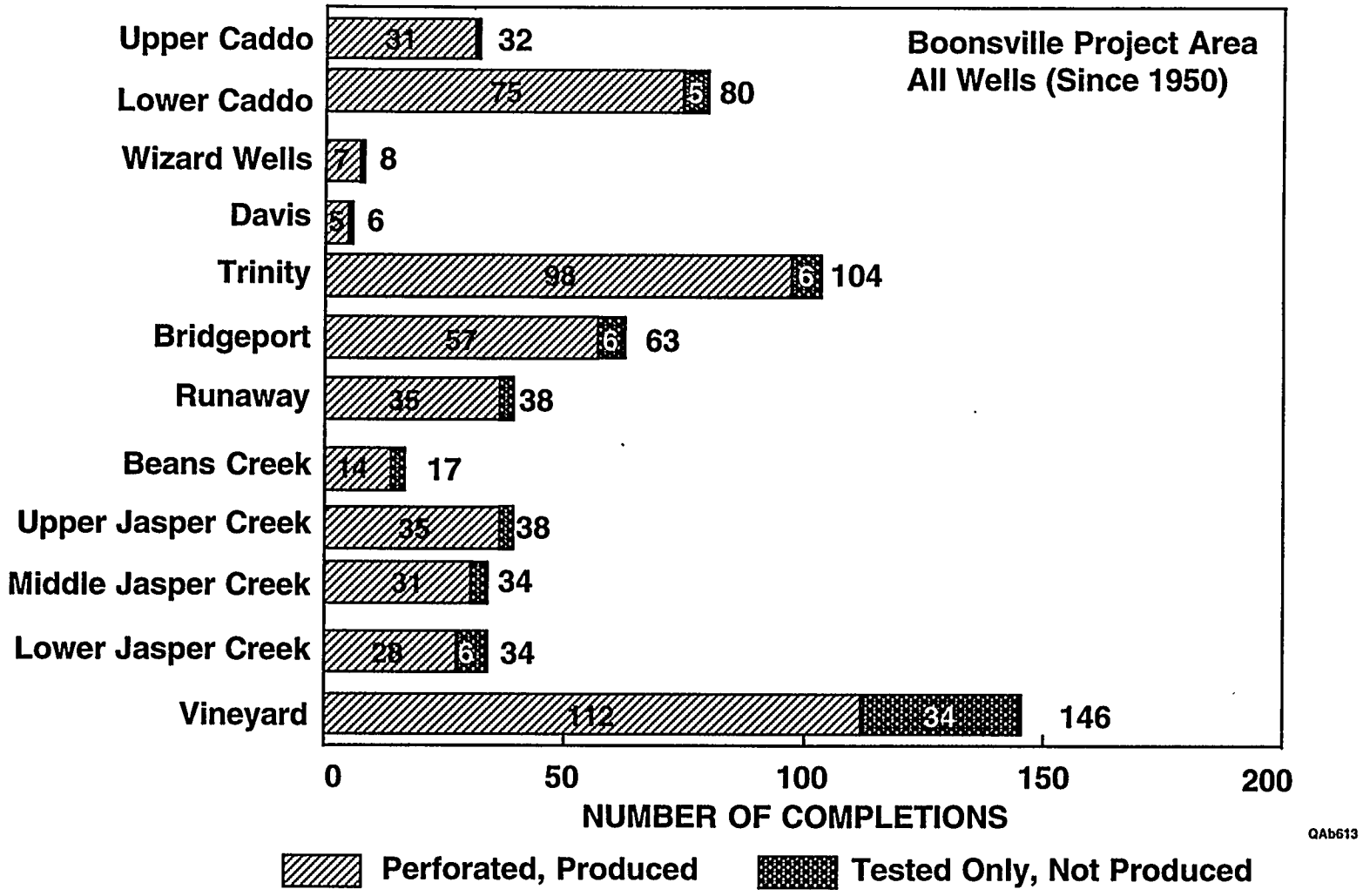

Figure B1. Completion frequency in various stratigraphic sequences for all wells in the Boonsville project area.

B.31

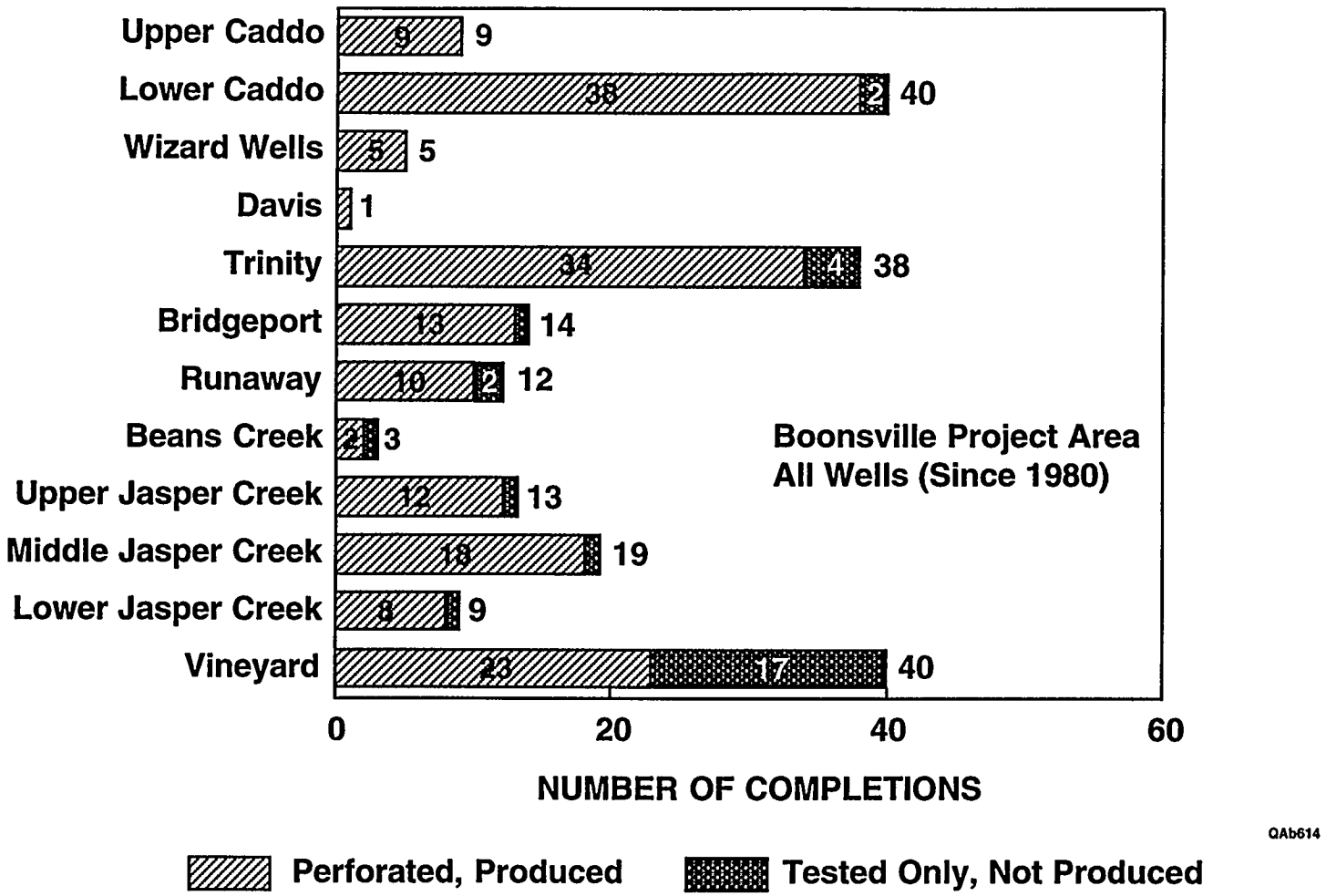

Figure B2. Completion frequency in various stratigraphic sequences for wells drilled since 1980 in the Boonsville project area.

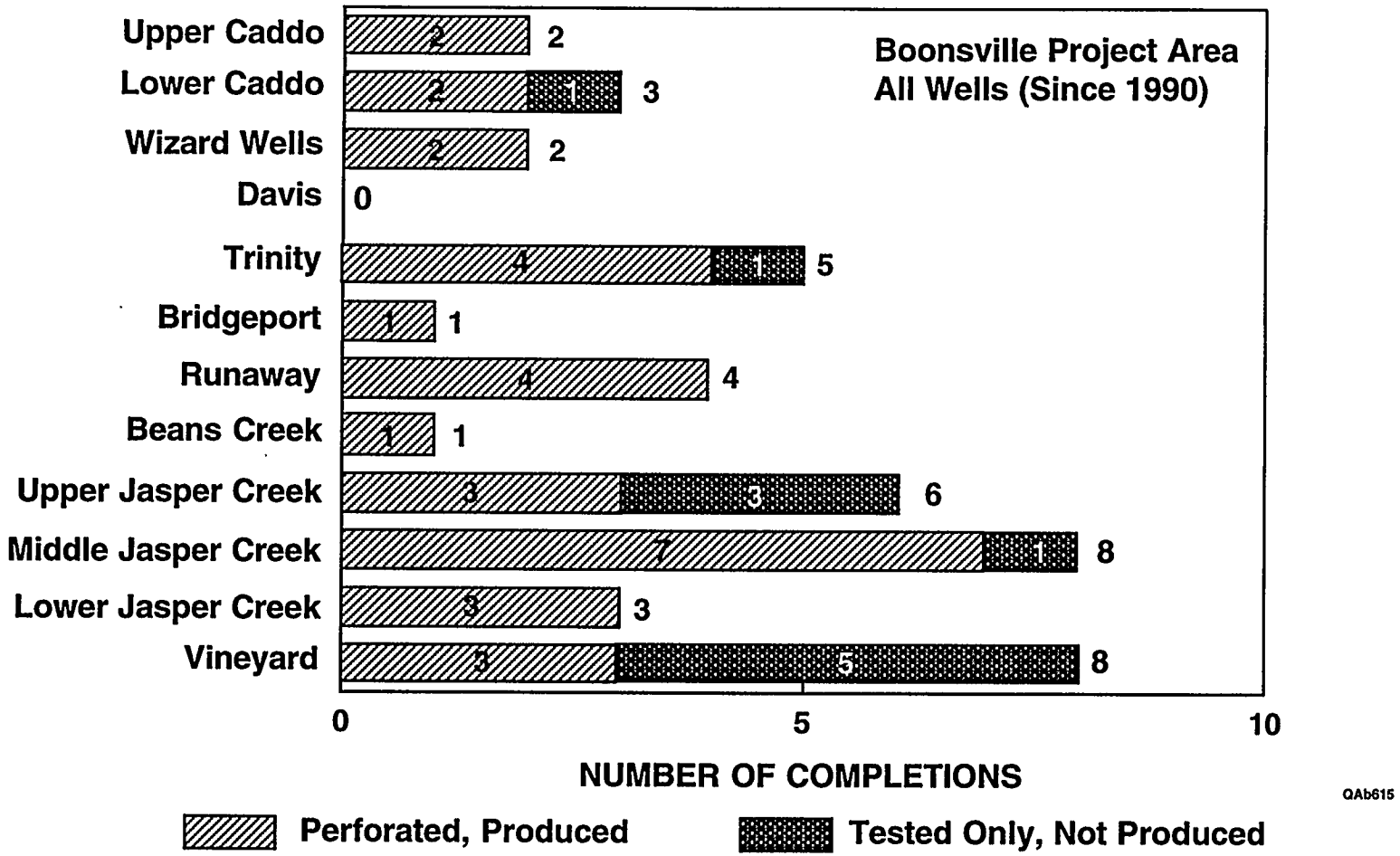

Figure B3. Completion frequency in various stratigraphic sequences for wells drilled since 1990 in the Boonsville project area.

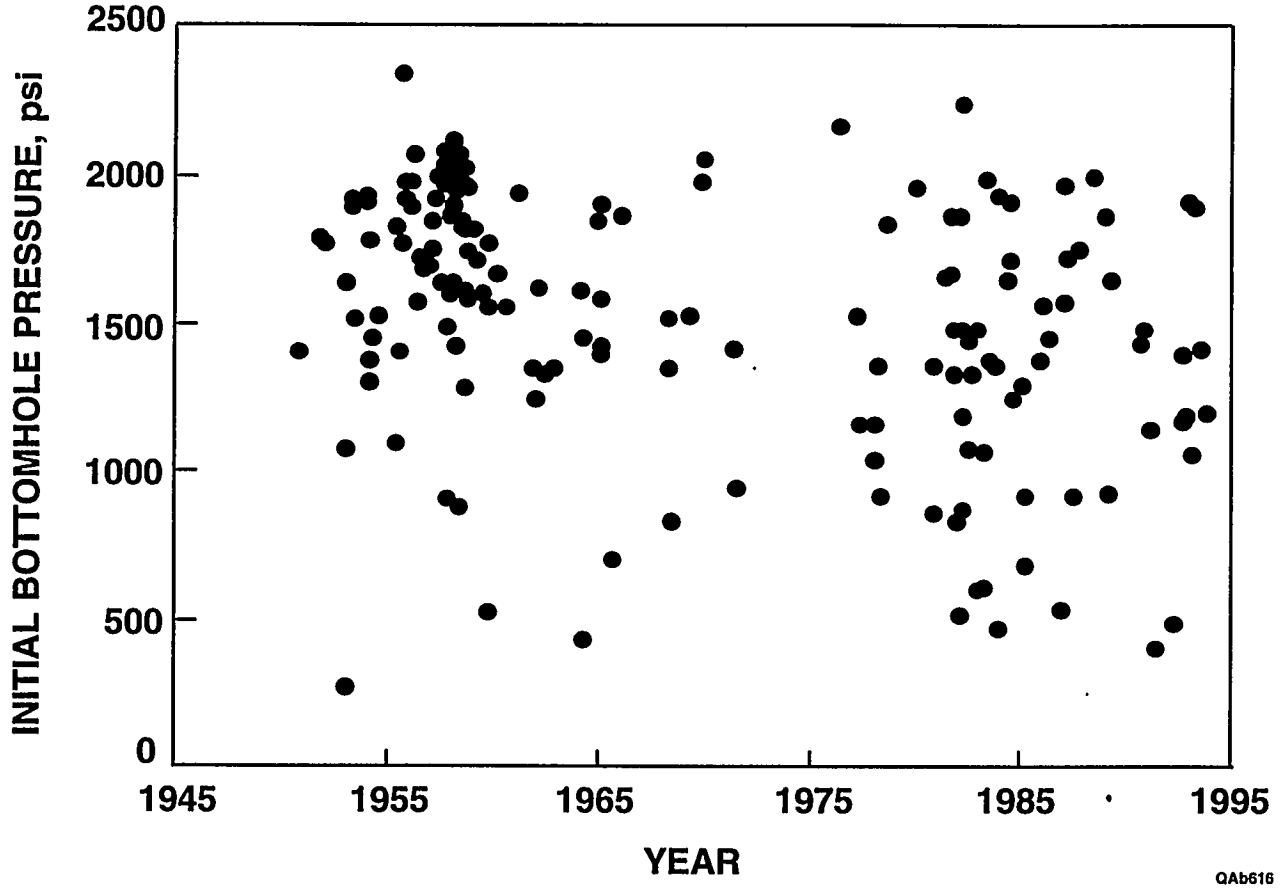

Figure B4. Best estimates of original pressure available from wells in the Boonsville project area. A number of new wells still encounter pressures near the original pressures measured 40 yr ago.

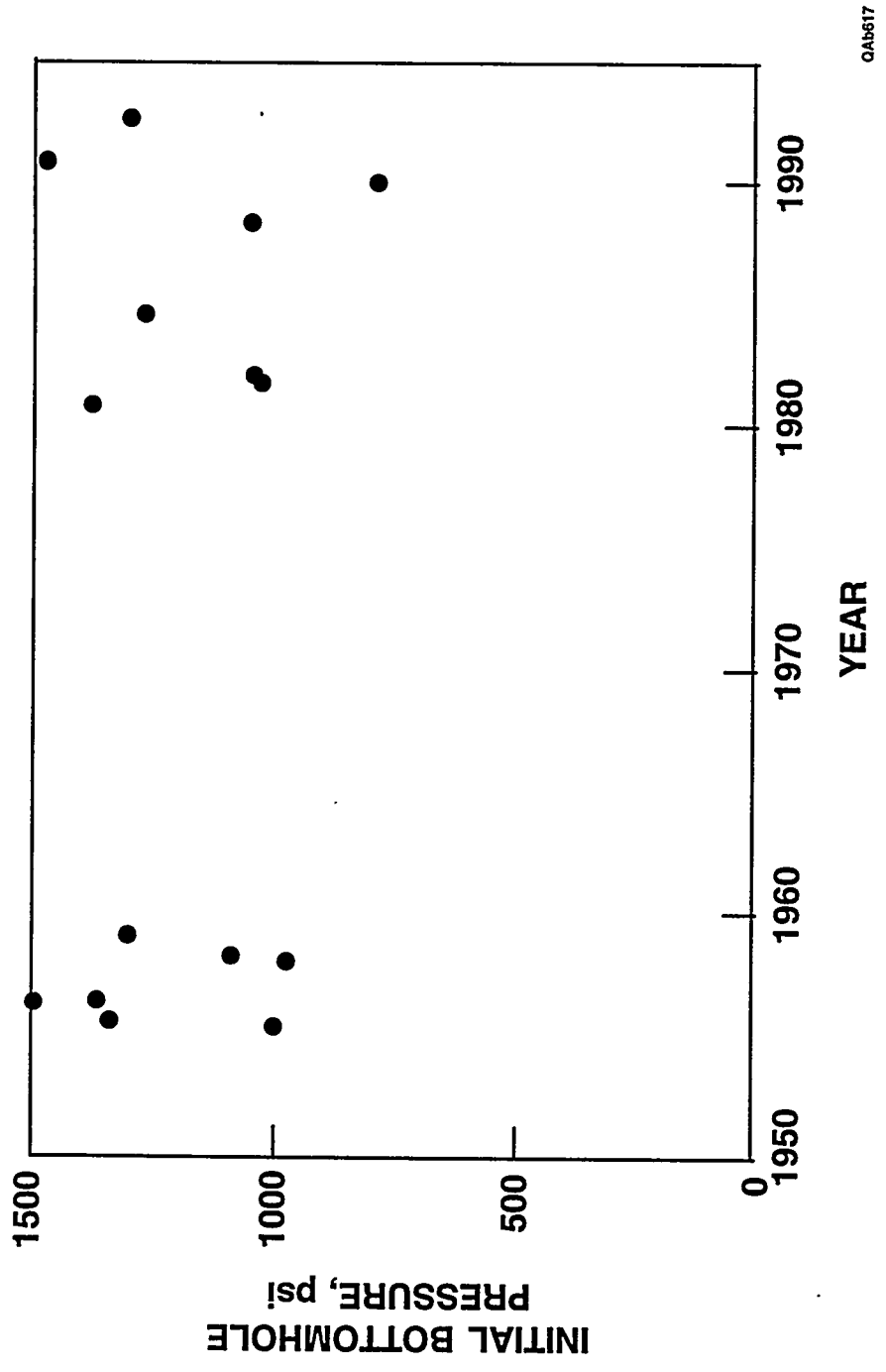

Figure B5. Comparison of initial pressures measured in more recent Upper Caddo completions to original pressures reported in the Upper Caddo sequence in the 1950's.

B.35

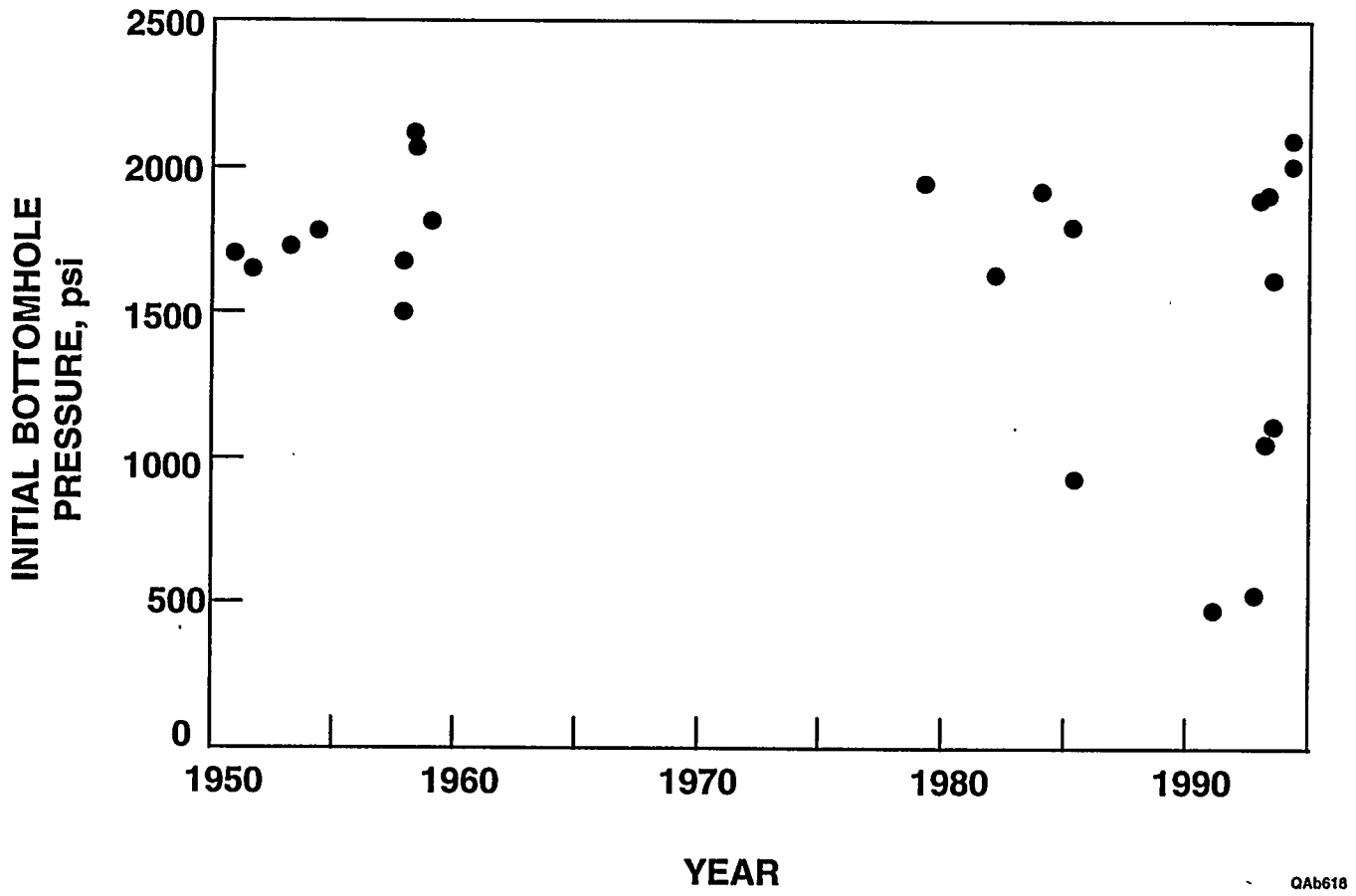

Figure B6. Comparison of initial pressures measured in more recent Jasper Creek completions to original pressures reported in the Jasper Creek sequence in the 1950's.

B.36

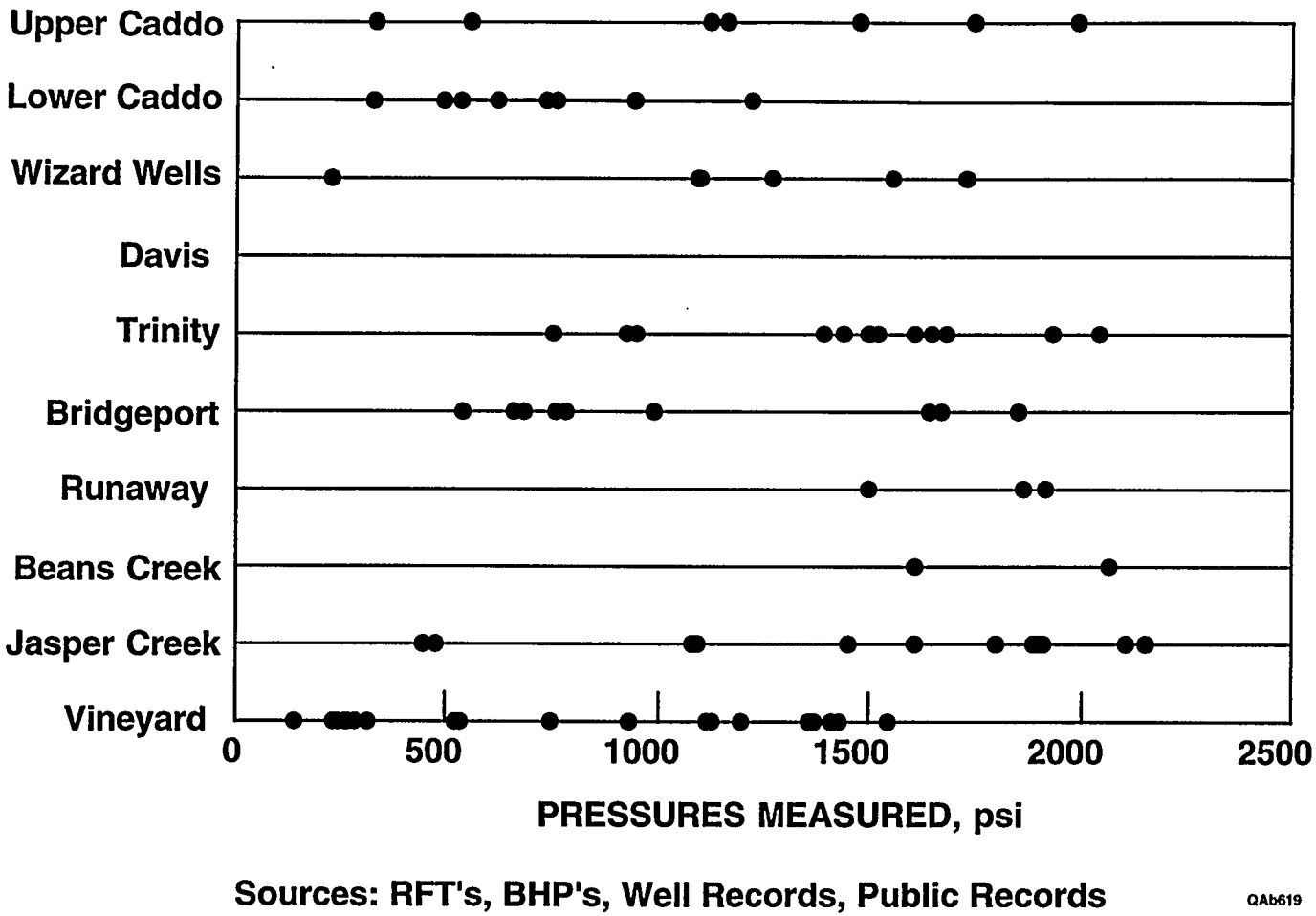

Figure B7. Pressures measured in various stratigraphic sequences in wells drilled since 1990 in the Boonsville project area. With the exception of the Lower Caddo and Vineyard sequences, original or near-original pressures have been found in almost all sequences.

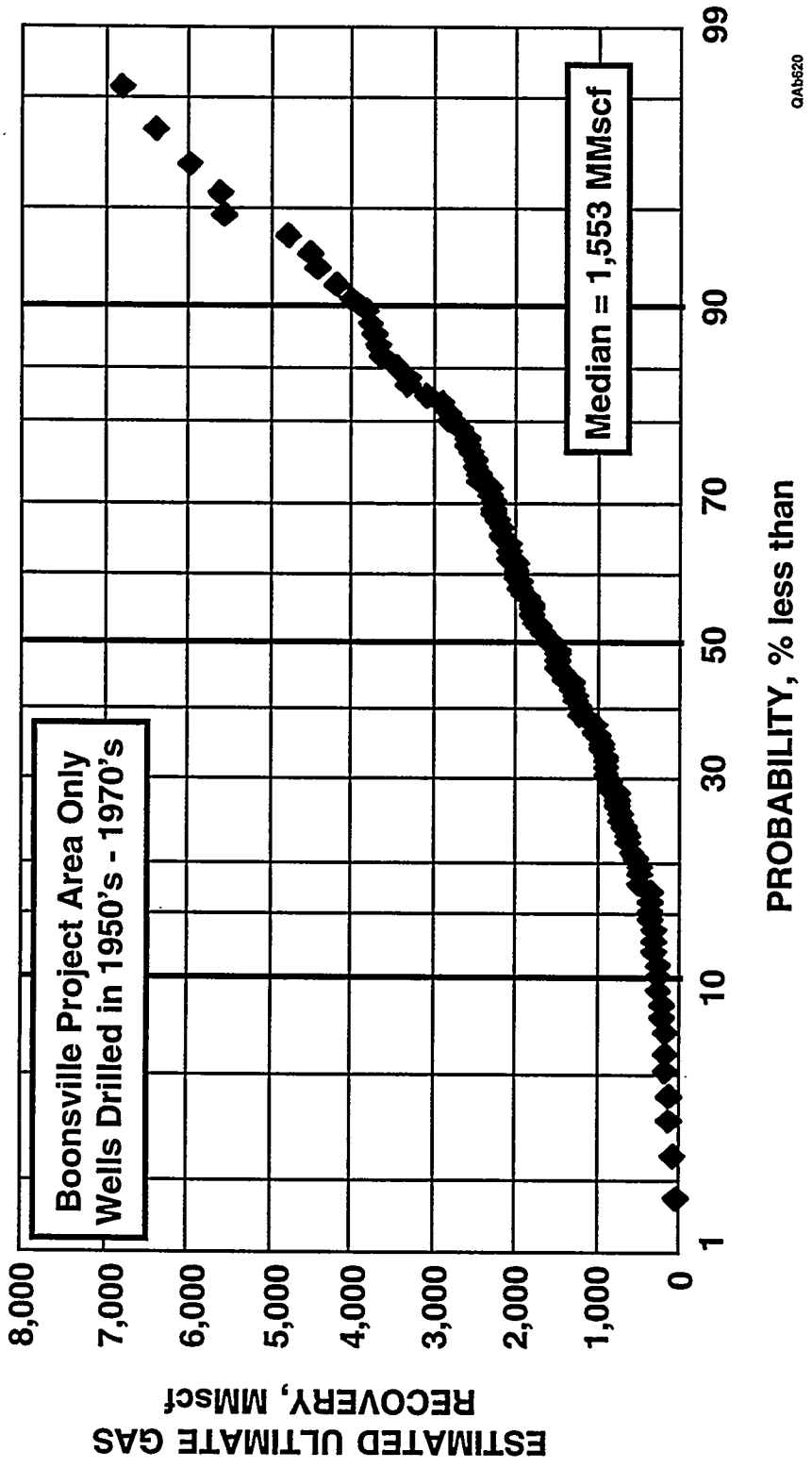

Figure B8. Distribution of estimated ultimate gas recoveries from wells in the project area drilled in the late 1950's through 1970's. The median gas recovery is about 1.5 Bscf.

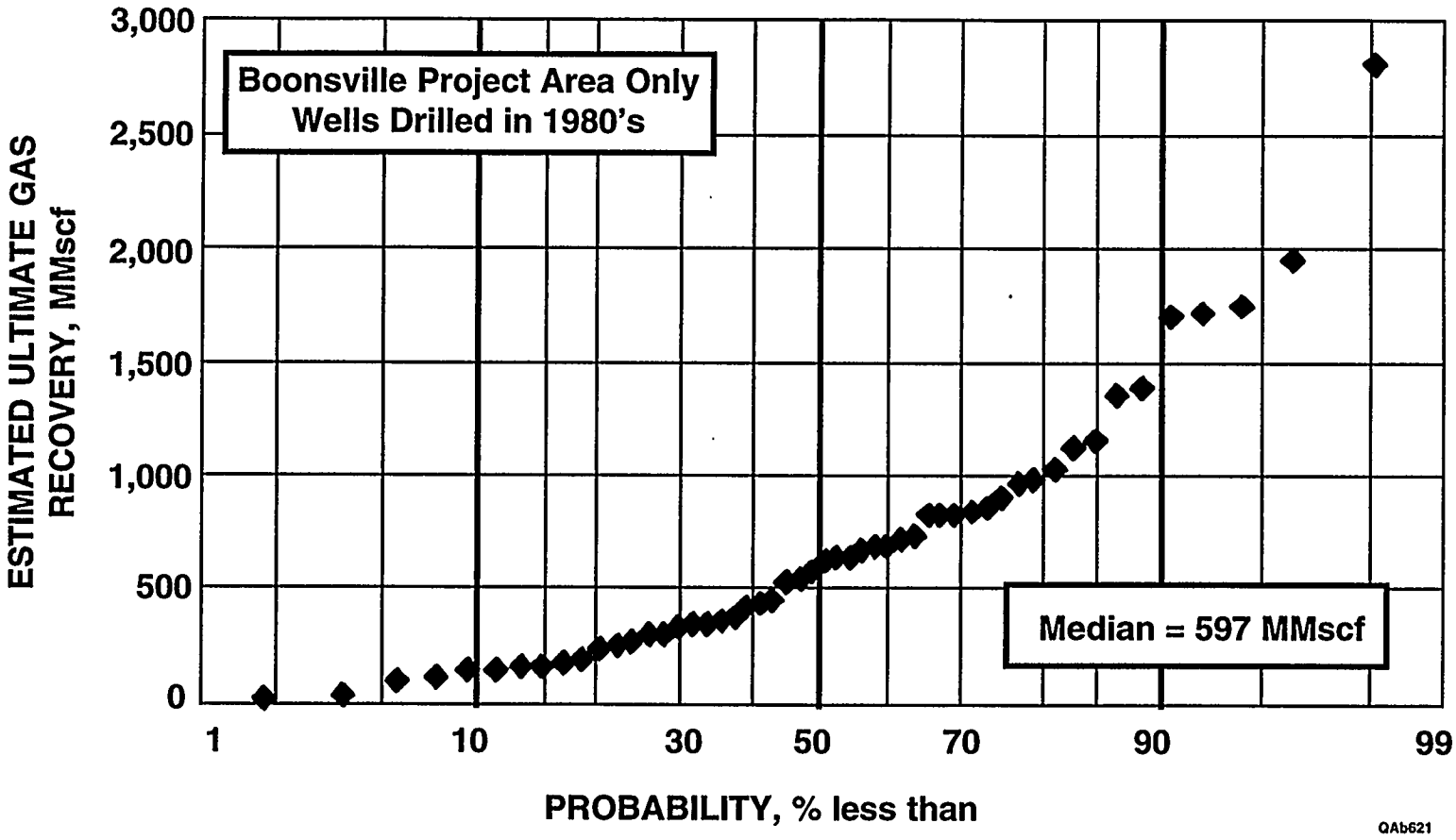

Figure B9. Distribution of estimated ultimate gas recoveries for wells in the project area drilled in the 1980's. The median gas recovery is about 600 MMscf.

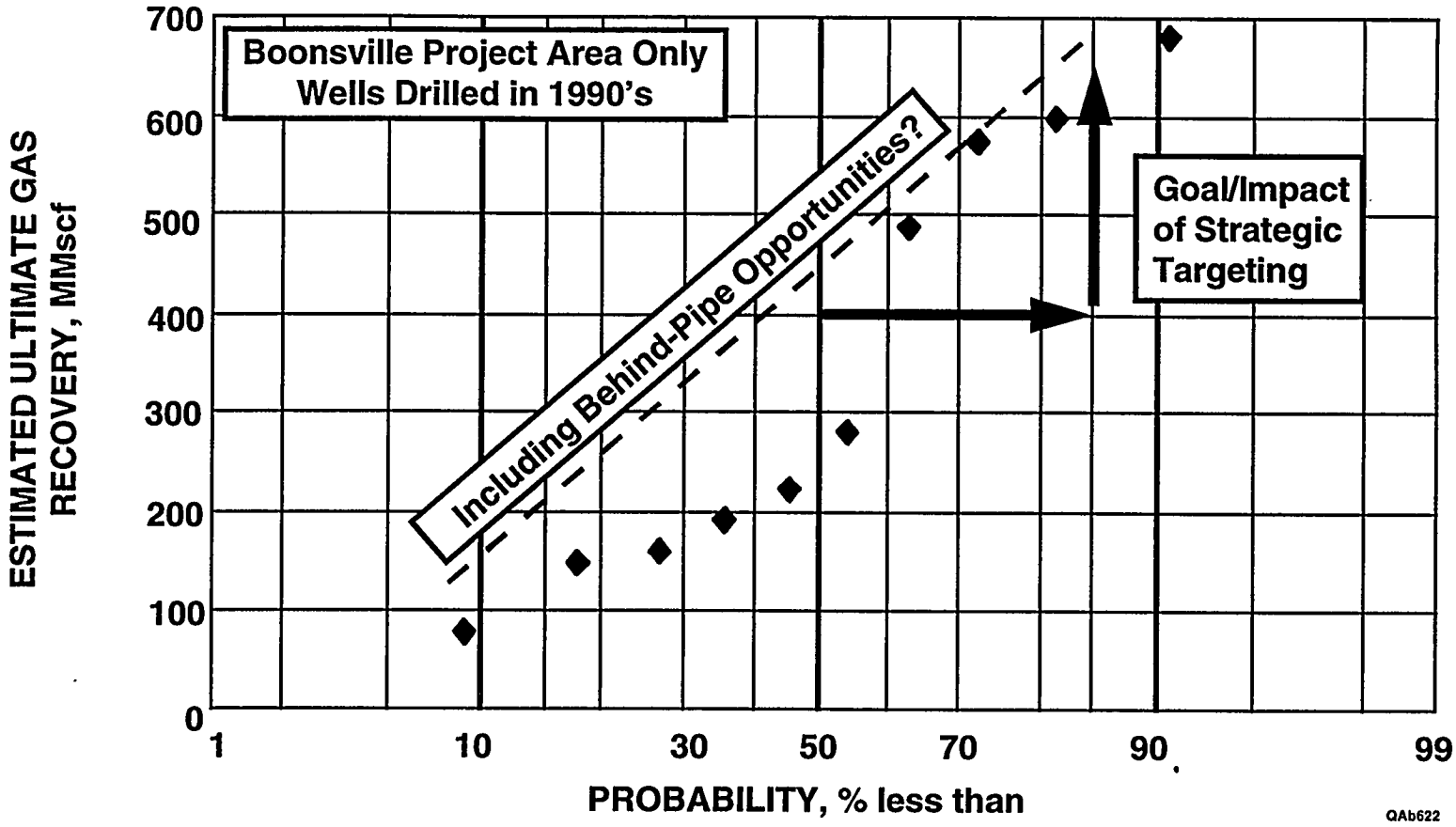

*** Only Zones Currently Producing; Does Not Include Behind Pipe Opportunities.**

Figure B10. Distribution of estimated ultimate gas recoveries, not including behind-pipe opportunities, for wells in the project area drilled in the 1990's. The goal of the secondary gas recovery research is to increase gas recovery through strategic targeting of new wells.

B.40

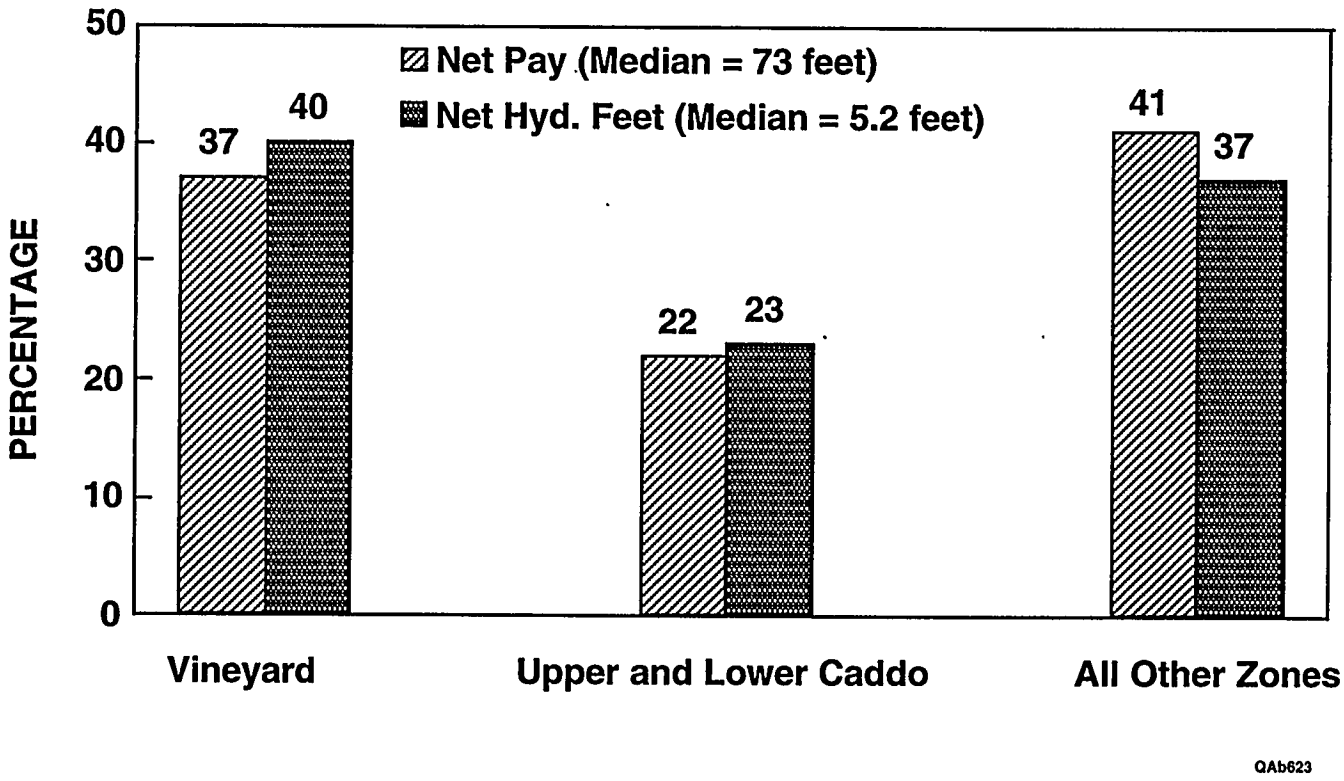

Figure B11. Distribution of net pay and net hydrocarbons among the Bend intervals in the project area.

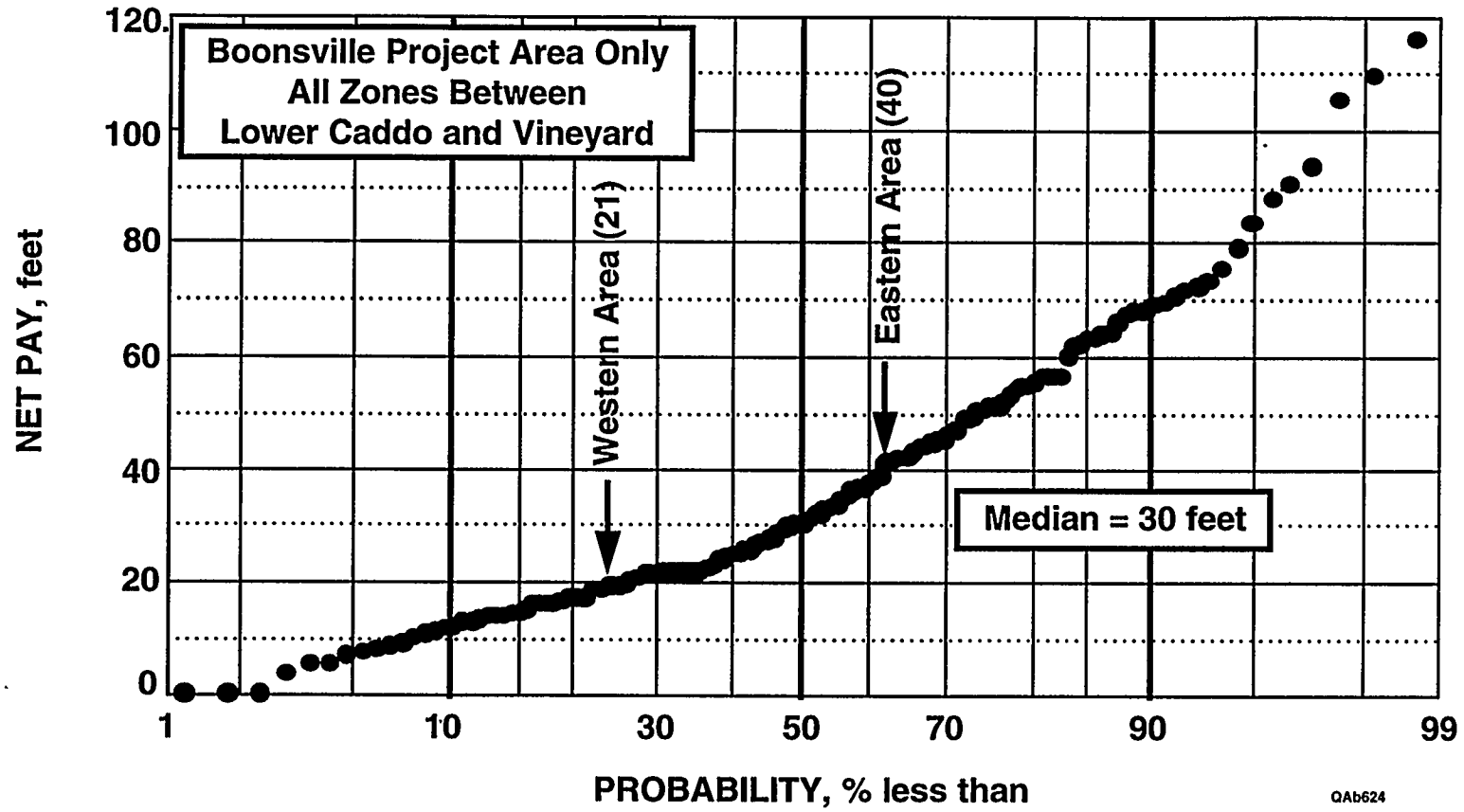

Figure B12. Distribution of net pay thickness in all zones between the Lower Caddo and the Vineyard; the median net pay is 30 ft.

B.43

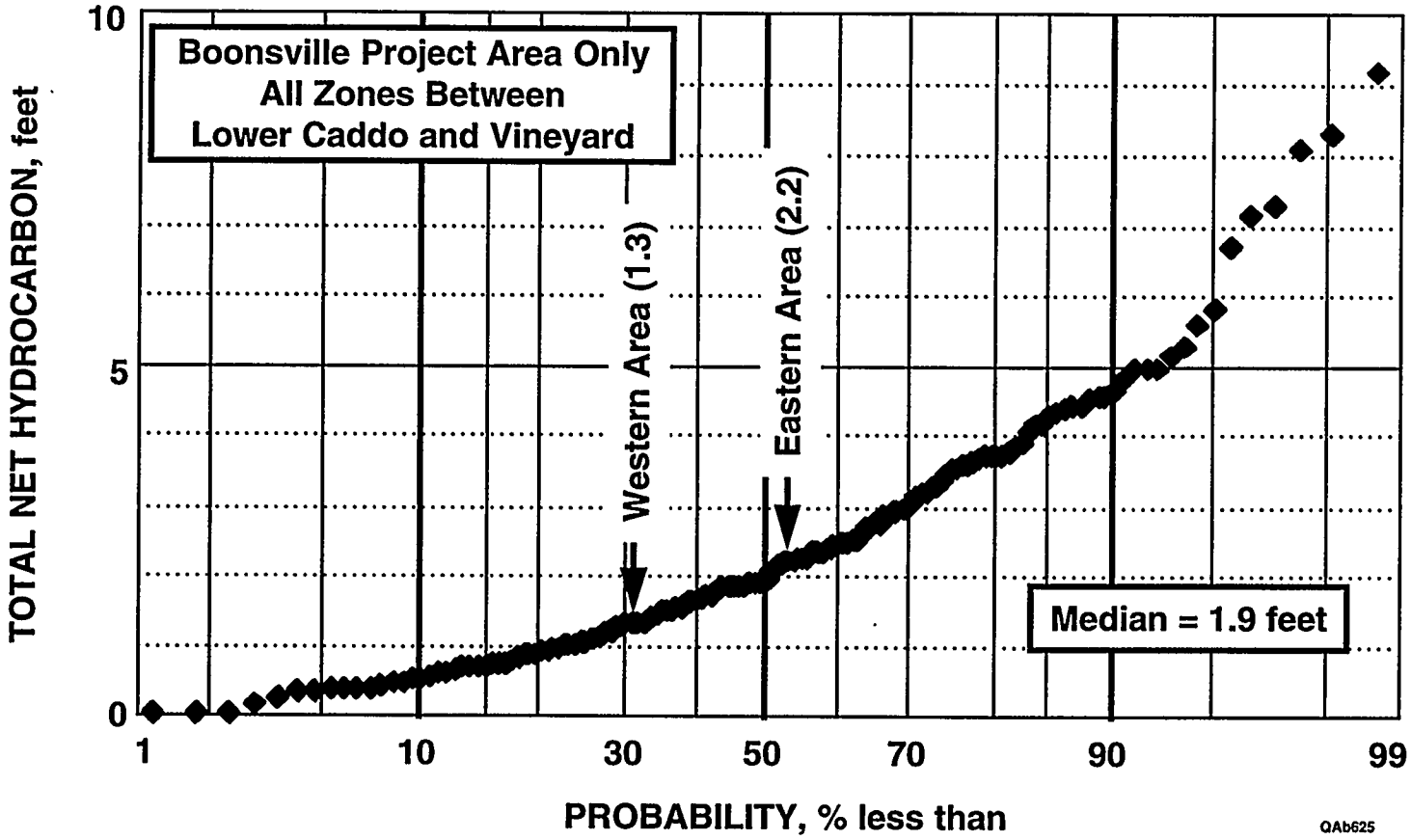

Figure B13. Distribution of net hydrocarbon thickness in all zones between the Lower Caddo and the Vineyard; the median net hydrocarbon thickness is 1.9 ft.

B.43

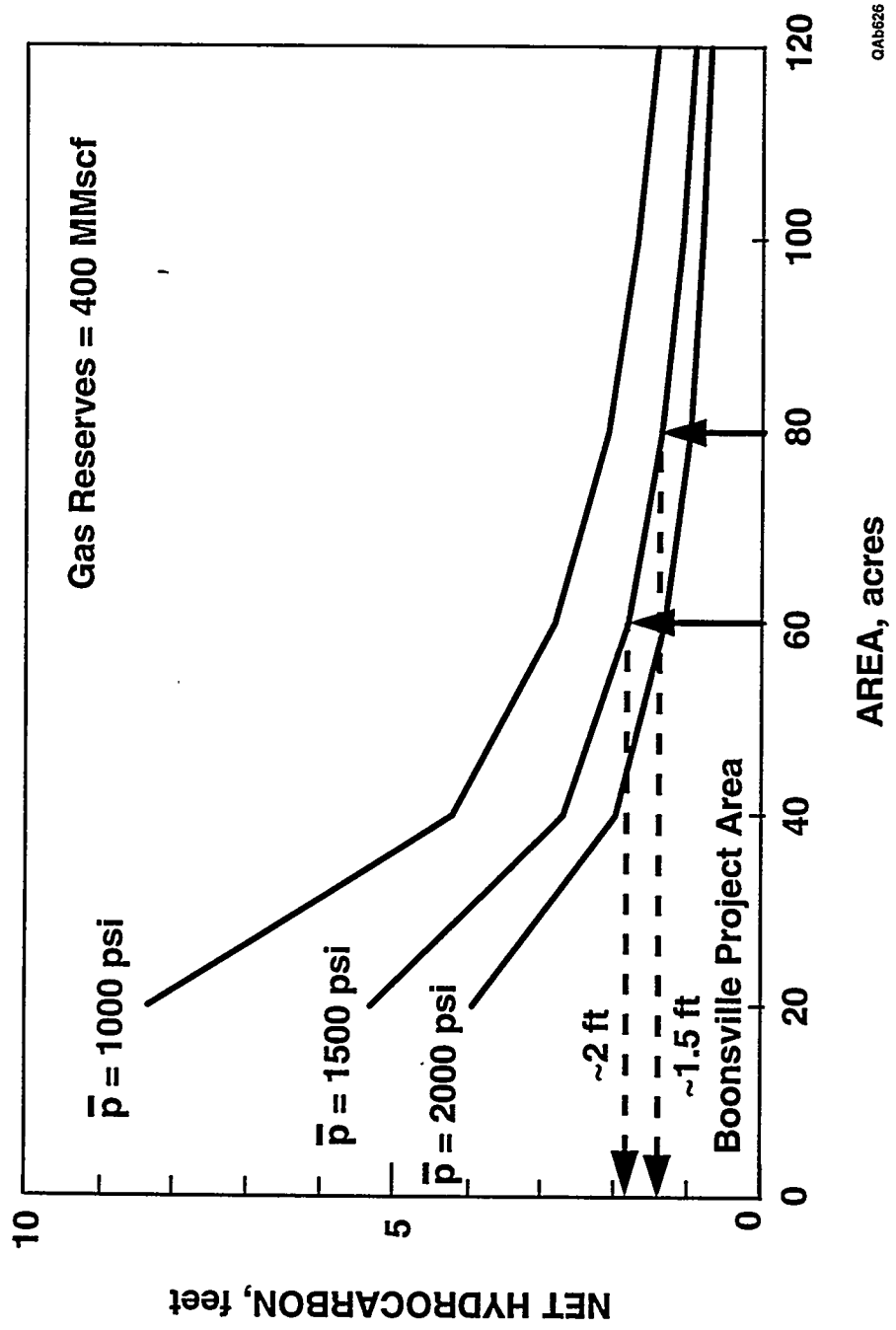

Figure B14. Nomograph prepared for the Boonsville project area, showing the net hydrocarbon feet required as a function of pressure and drainage area to obtain recoverable gas reserves of about 400 MMscf.

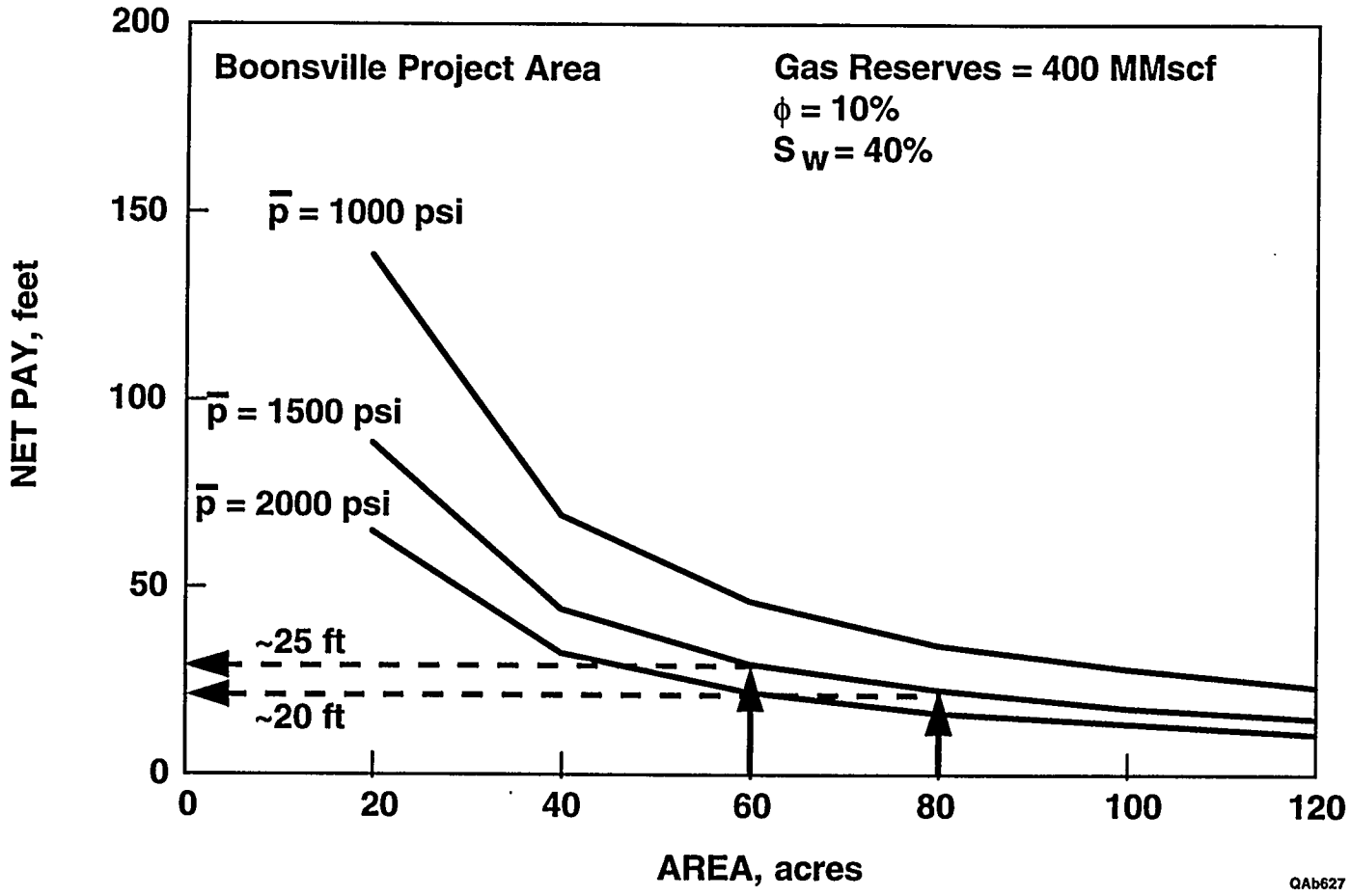

Figure B15. Nomograph for the Boonsville project area showing the net pay required as a function of pressure and drainage area to obtain recoverable gas reserves of about 400 MMscf.

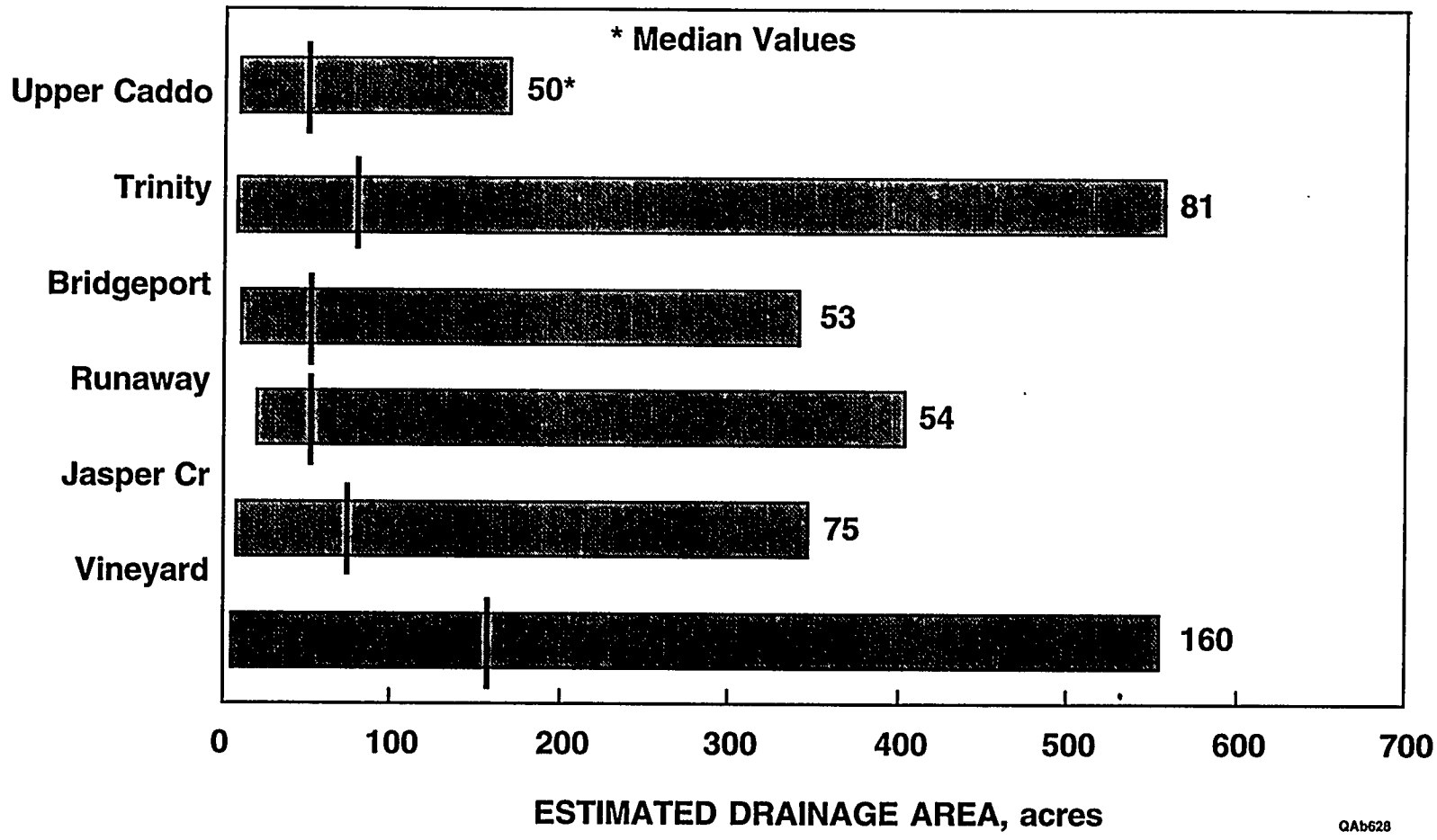

Figure B16. Estimated drainage areas computed for the major stratigraphic sequences using production data from wells in the project area.

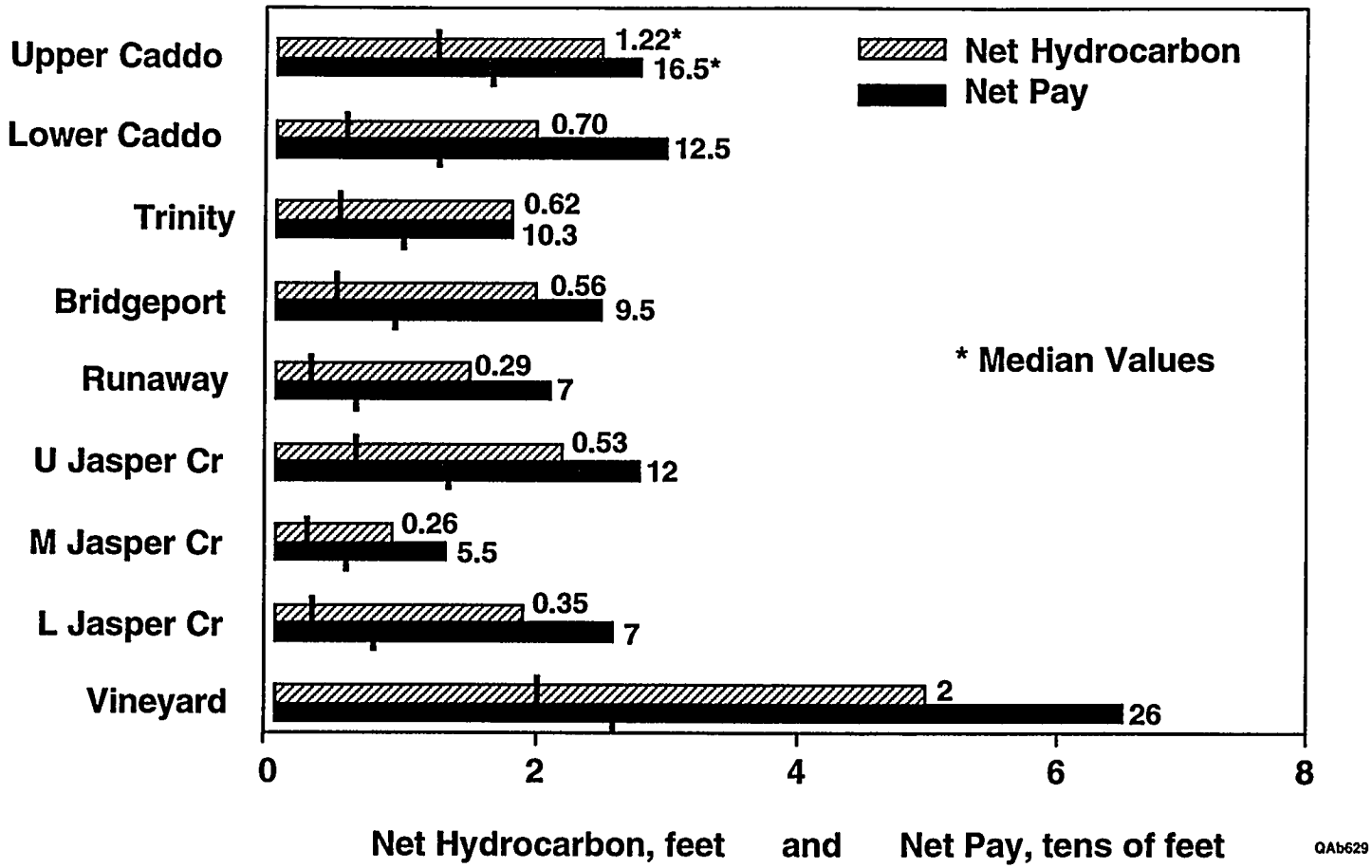

Figure B17. Range of net pay and net hydrocarbons found in each major sequence throughout the project area.

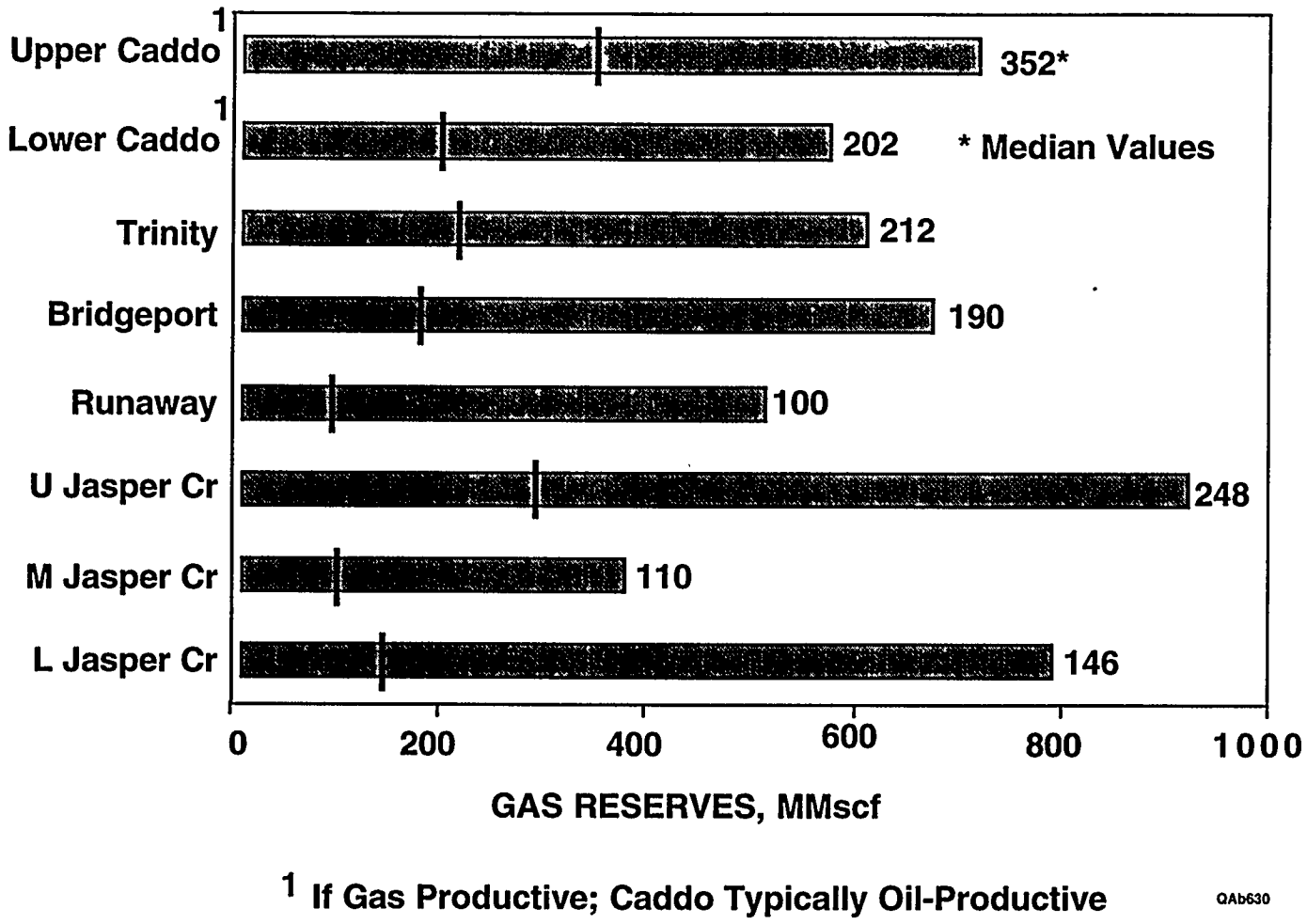

Figure B18. Range of potential gas reserves associated with an 80-acre drainage area in each major sequence throughout the project area.

Figure B19. Distribution of net hydrocarbons between the Lower Caddo and the Vineyard mapped across the project area.

Figure B20. Distribution of the number of net pay intervals between the Lower Caddo and the Vineyard mapped across the project area.

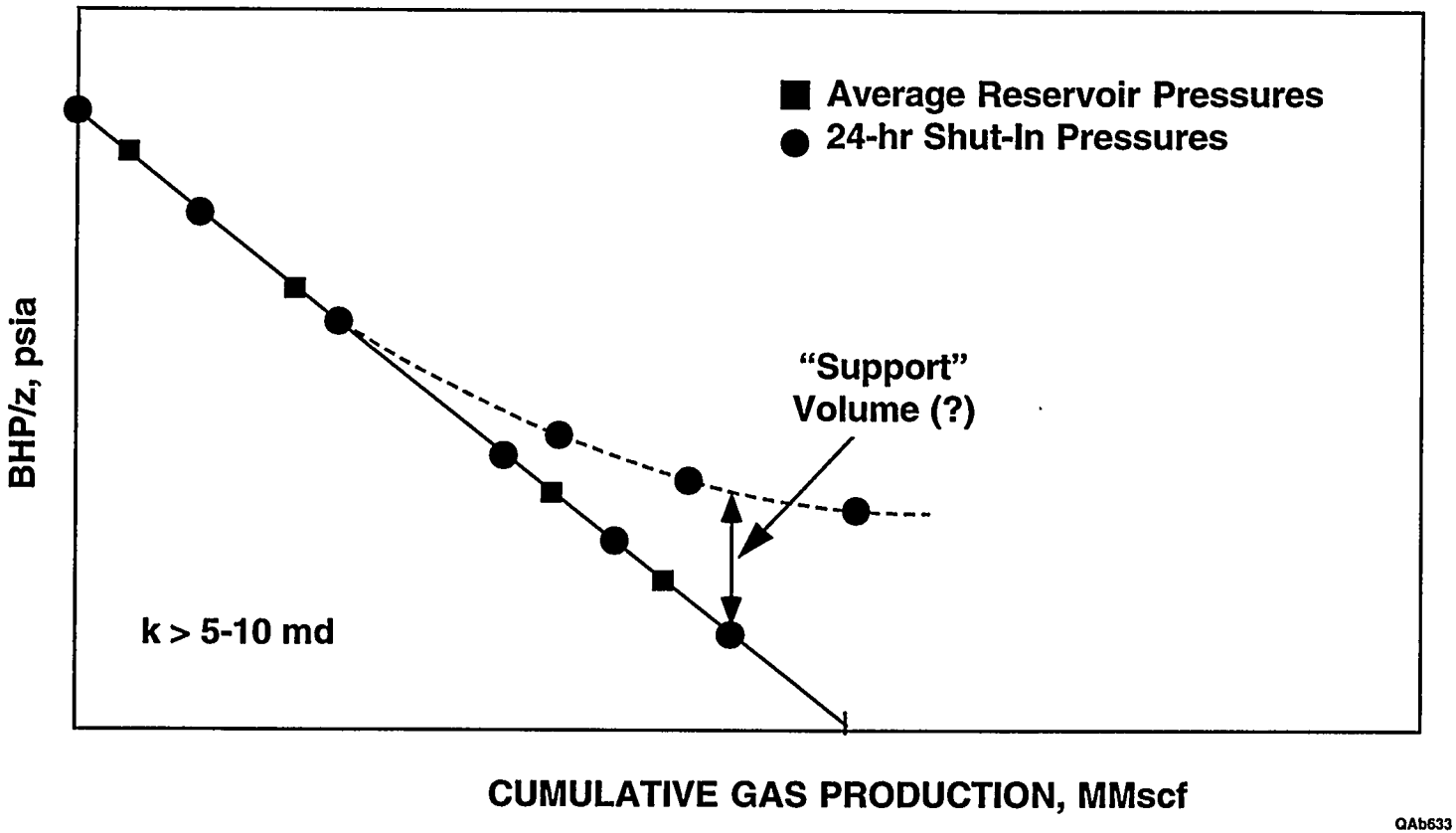

Figure B21. Flattening of the p/z curve with time may suggest communication with an incompletely drained reservoir compartment in high-permeability gas reservoirs (permeability greater than 5 to 10 md). Water drive, production from multiple layers, compaction drive, and even operational changes may also cause this behavior.

B.51

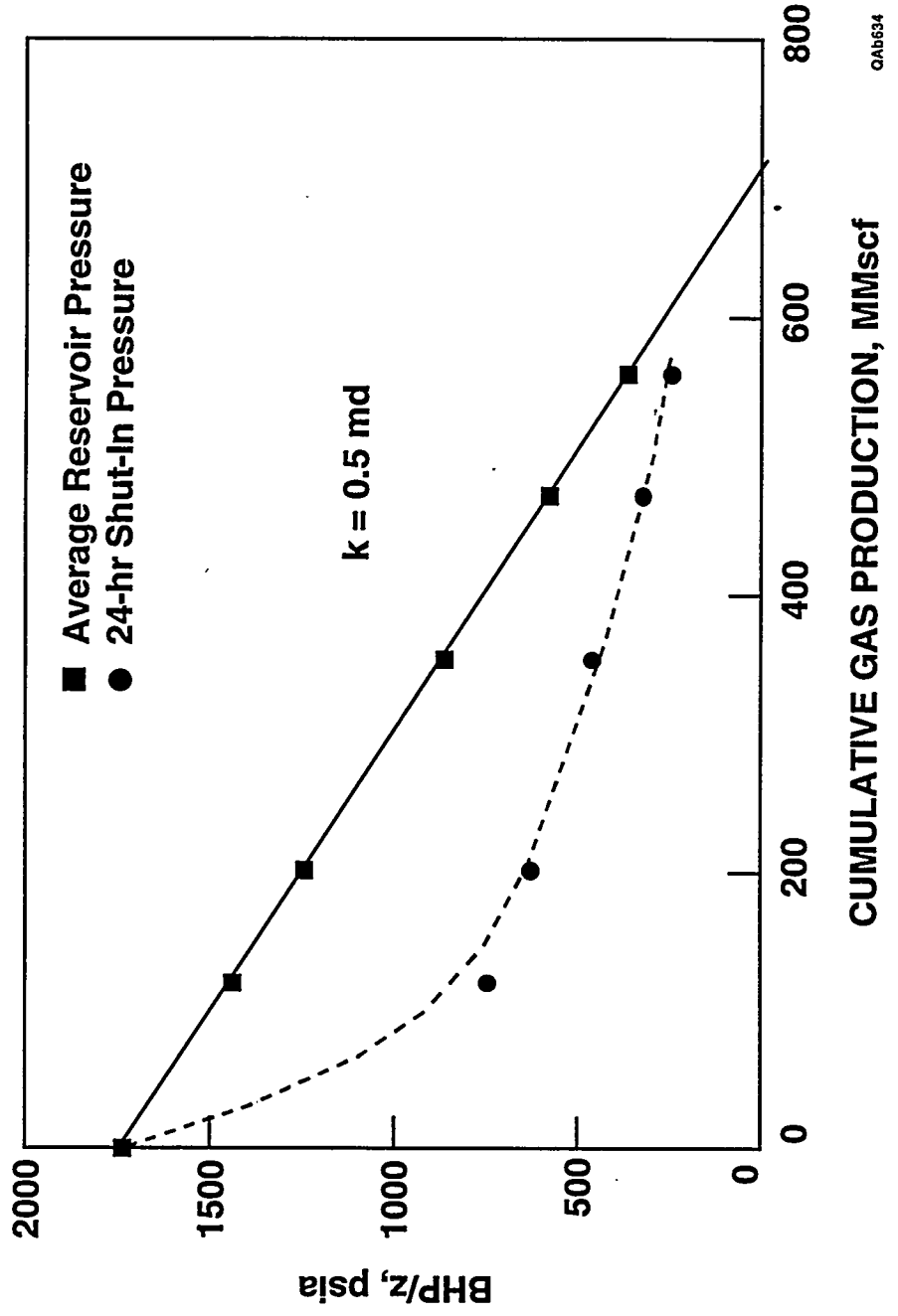

Figure B22. p/z curves may flatten in lower permeability reservoirs but primarily because 24-hr shut-in pressures do not reflect average reservoir pressure. This is true of the Bend Conglomerate reservoirs, where typical permeabilities are 0.1 to 5 md. This flattening behavior may also be due to differential depletion of multiple, commingled producing intervals, which is also common for Bend Conglomerate wells.

B.52

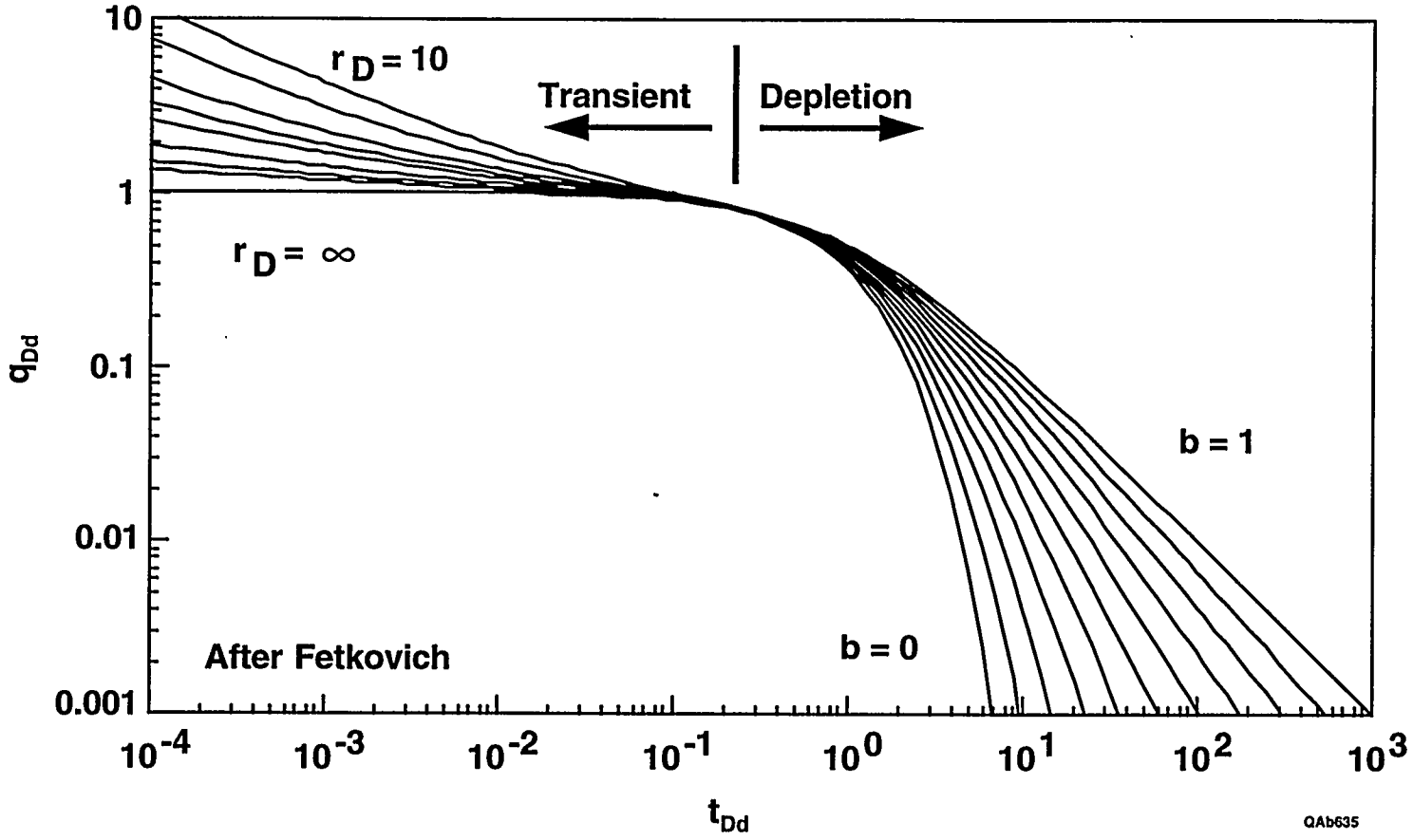

Figure B23. Example of a Fetkovich type curve that can be used for quantitative production data analysis to estimate reservoir properties, predict drainage area and gas in place, and forecast future performance.

B.53

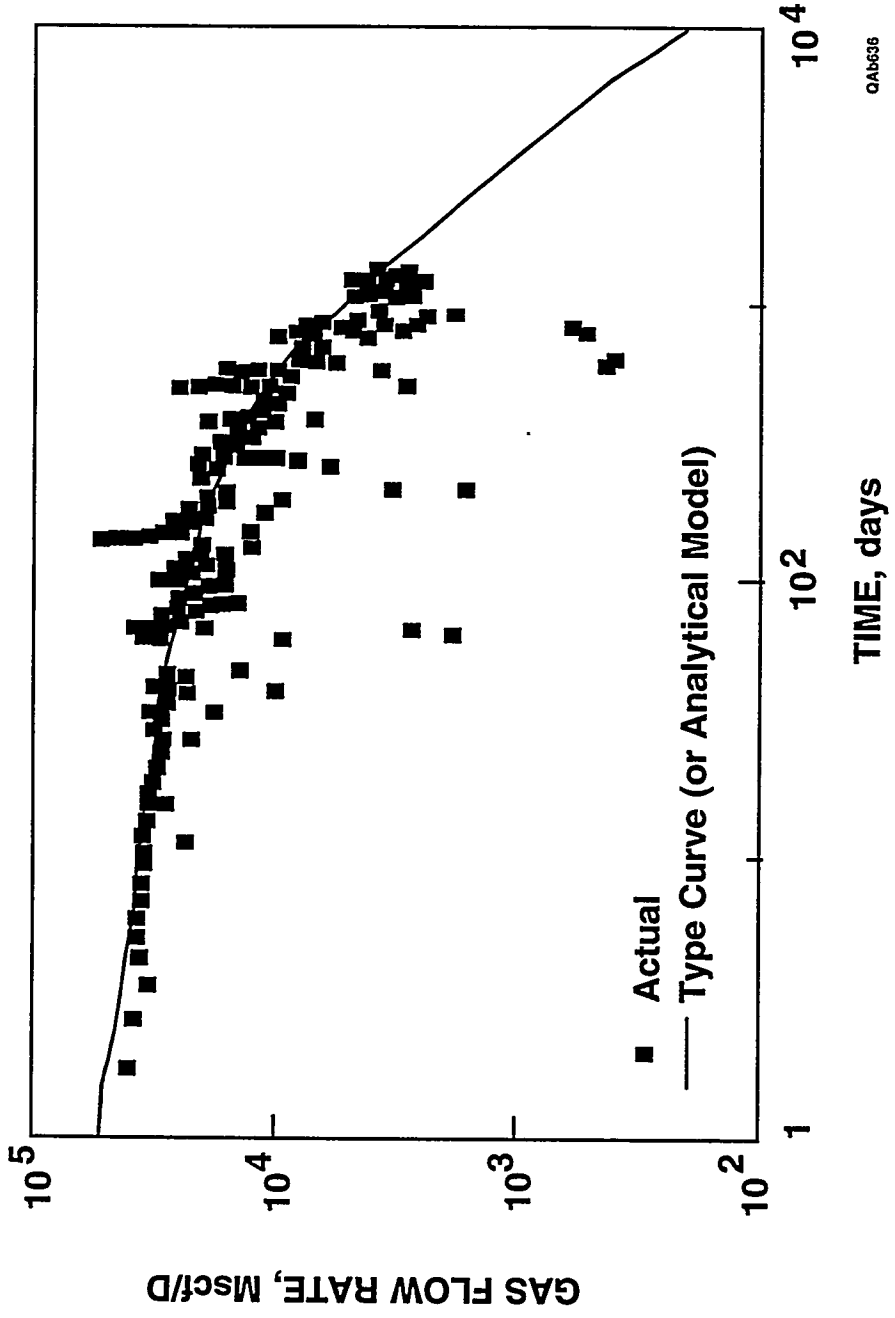

Figure B24. Example production data analysis using the Fetkovich type curves (or an equivalent analytical model).

B.54

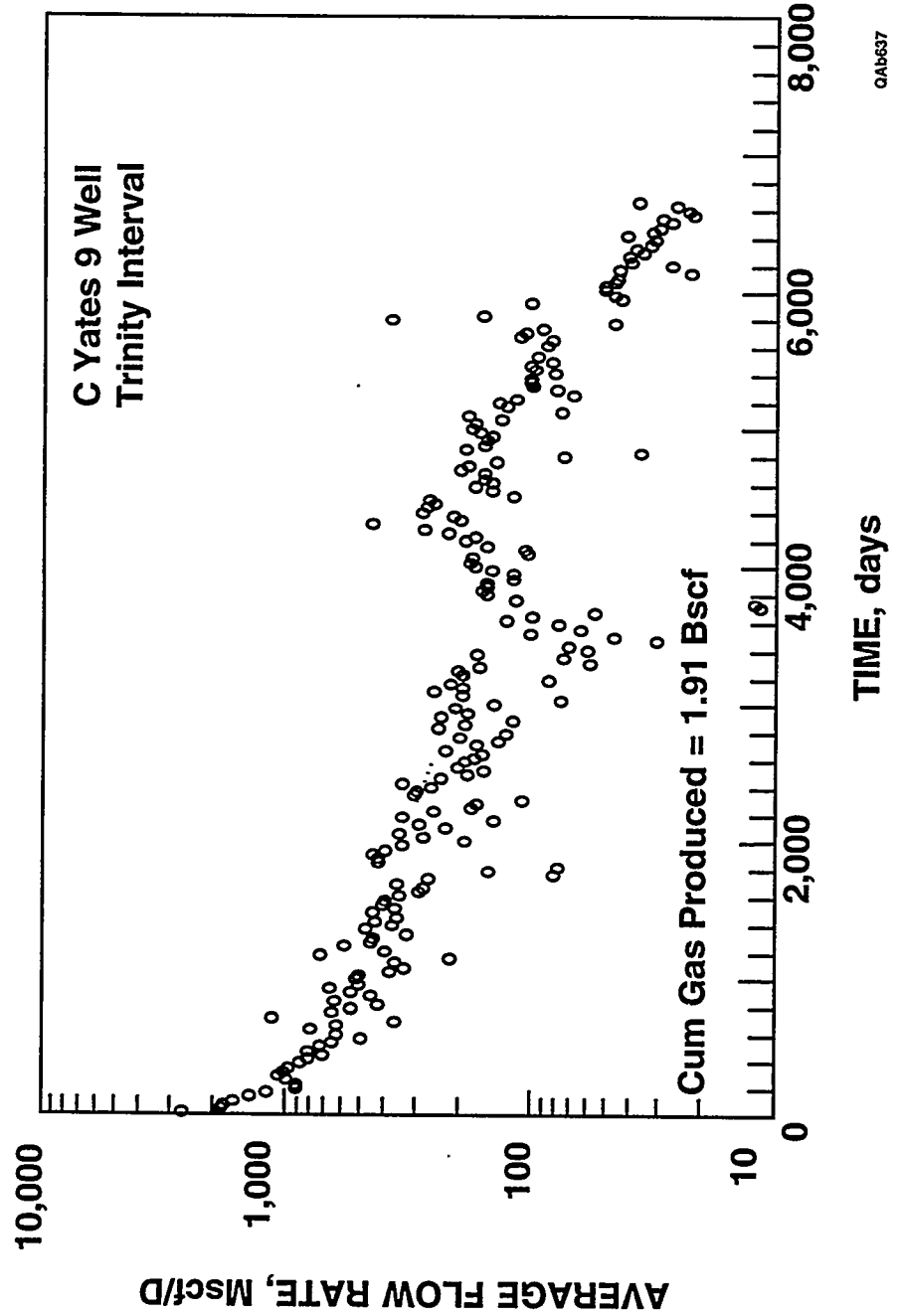

Figure B25. Semilog plot of flow rate vs. time for the Trinity interval in the C Yates 9 well; this production decline behavior is typical of many wells in the project area.

B.55

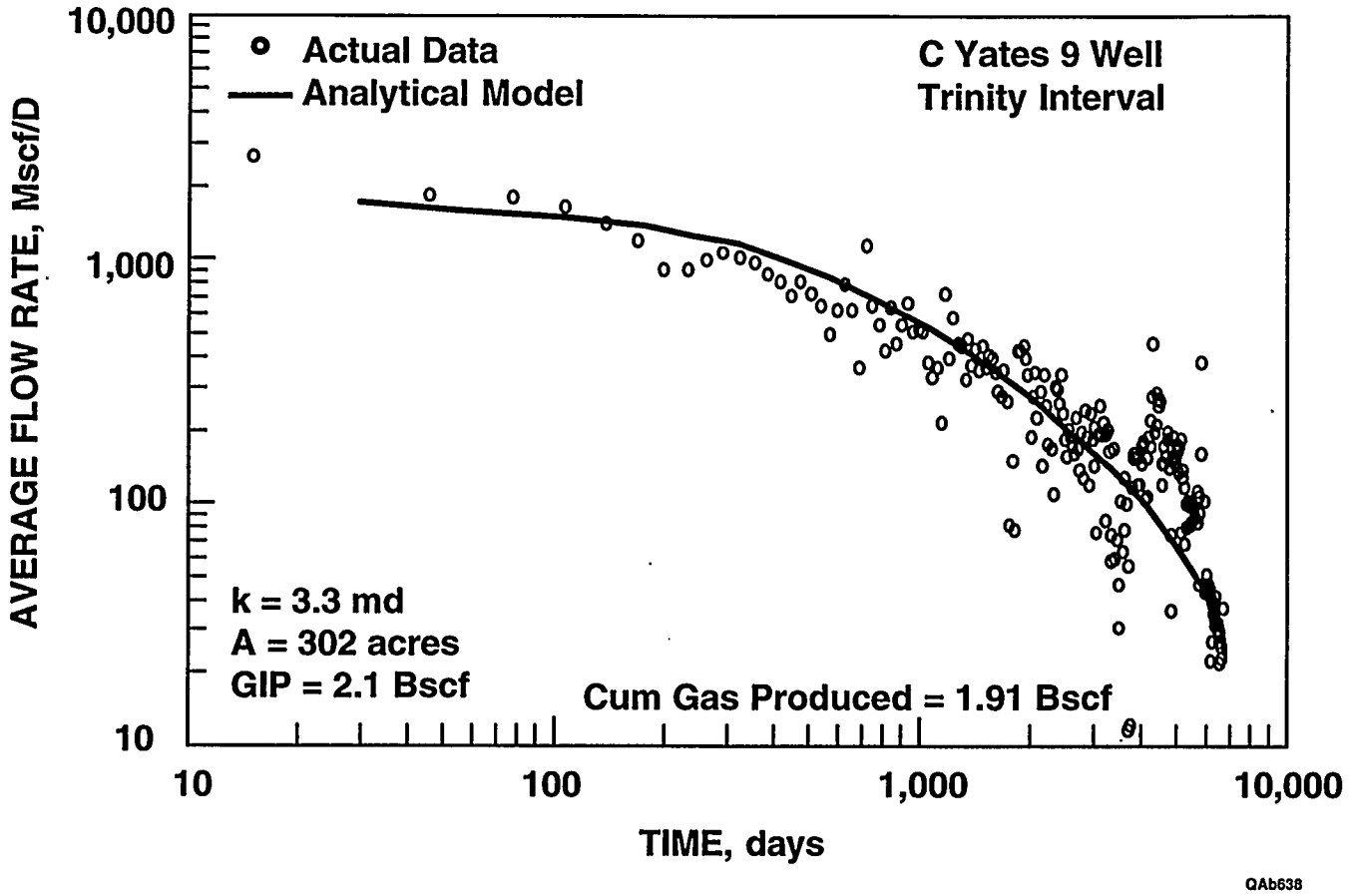

Figure B26. Log-log plot of production data from the C Yates 9 well showing significant depletion of the Trinity reservoir. A history-match using an analytical model yields estimates for permeability, drainage area, and gas in place.

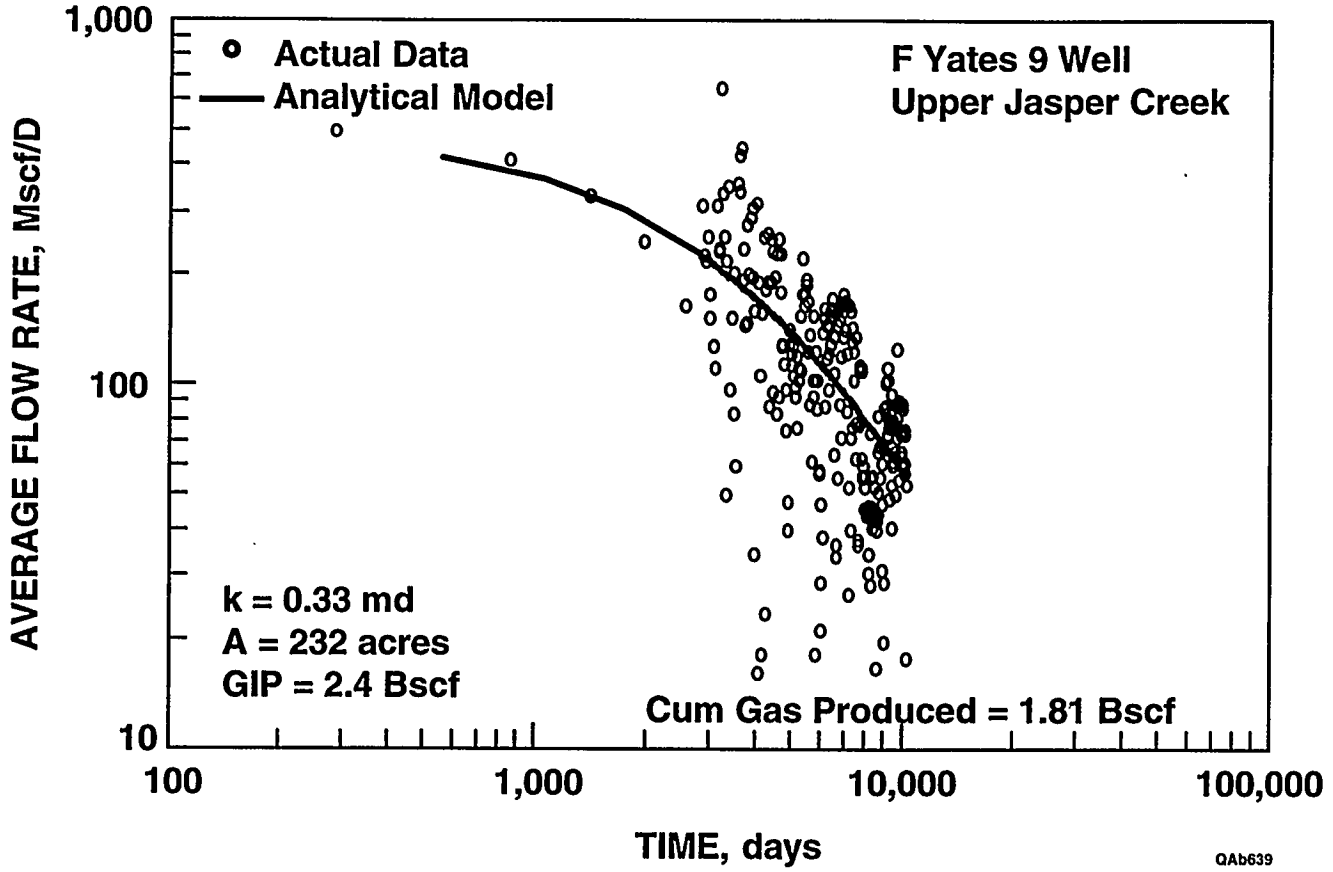

Figure B27. Log-log plot of production data from the F Yates 9 well showing significant depletion of the Upper Jasper Creek reservoir. A history-match using an analytical model yields estimates for permeability, drainage area, and gas in place.

B.57

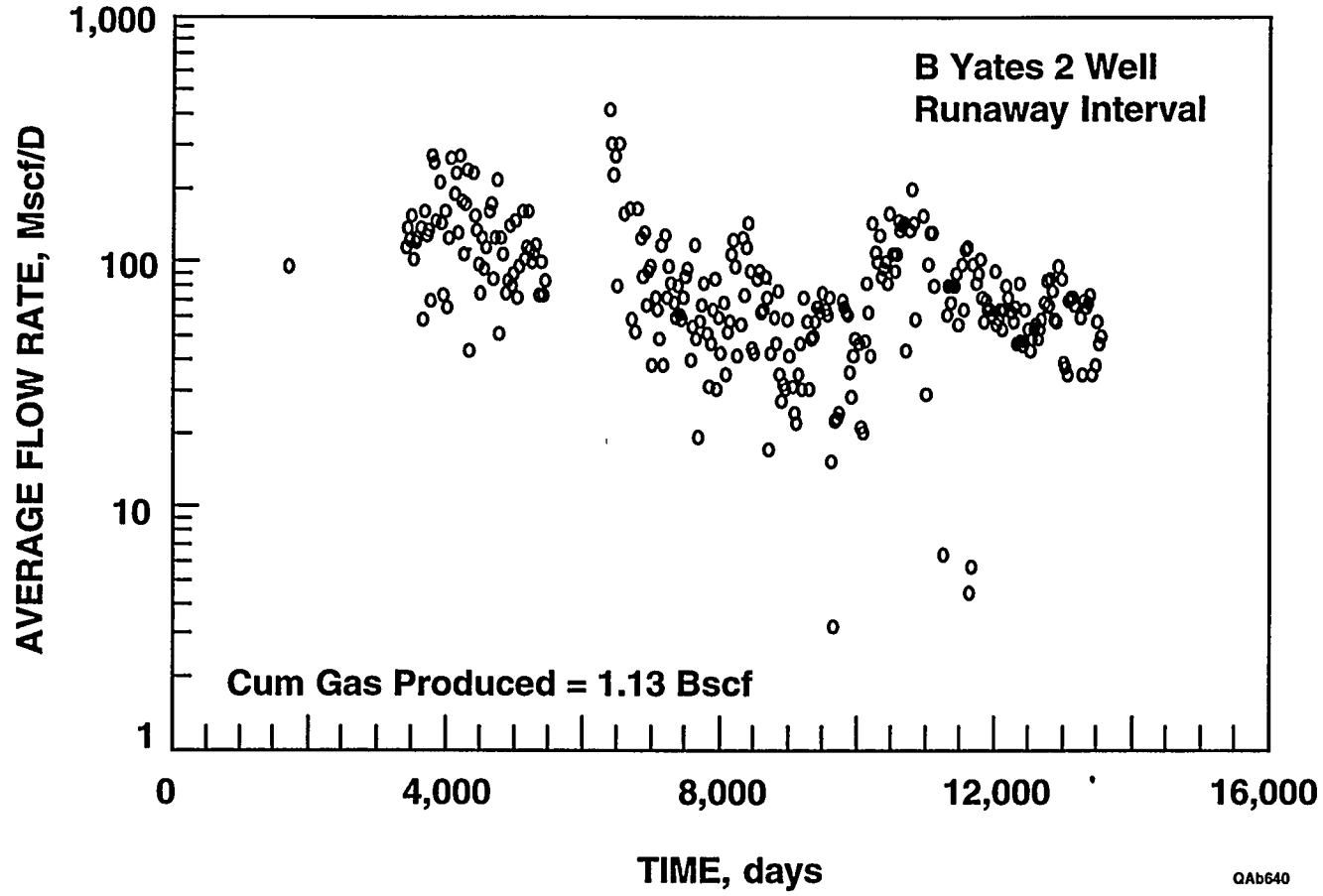

Figure B28. Production data from the Runaway interval in the B Yates 2 well. Note the relatively small decline in flow rate over time over about 40 yr, which is atypical of most Bend completions.

B.58

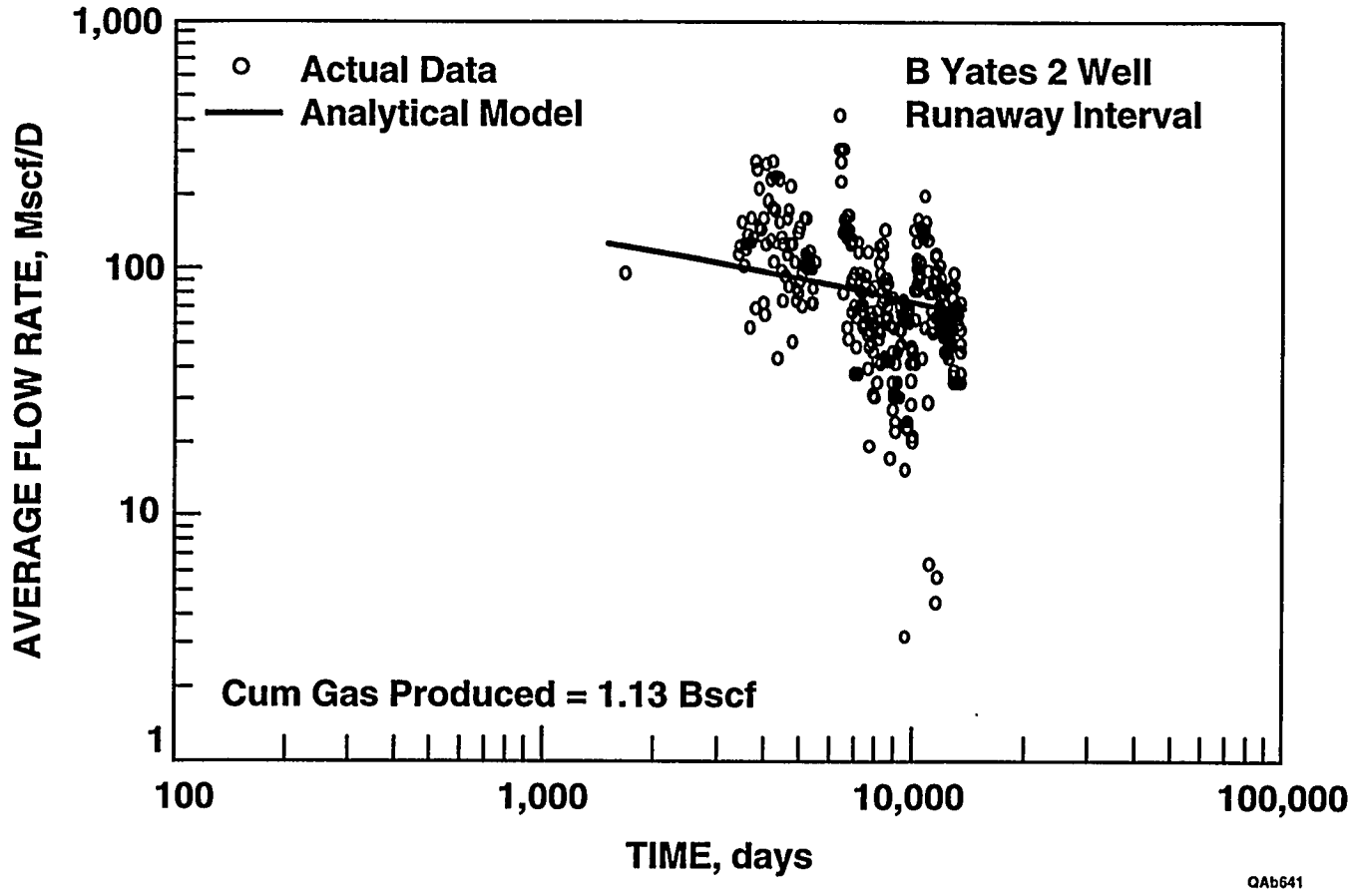

Figure B29. History-match of production data from the Runaway interval suggests that the B Yates 2 well may be in communication with a larger gas volume than it can drain effectively.

B.59

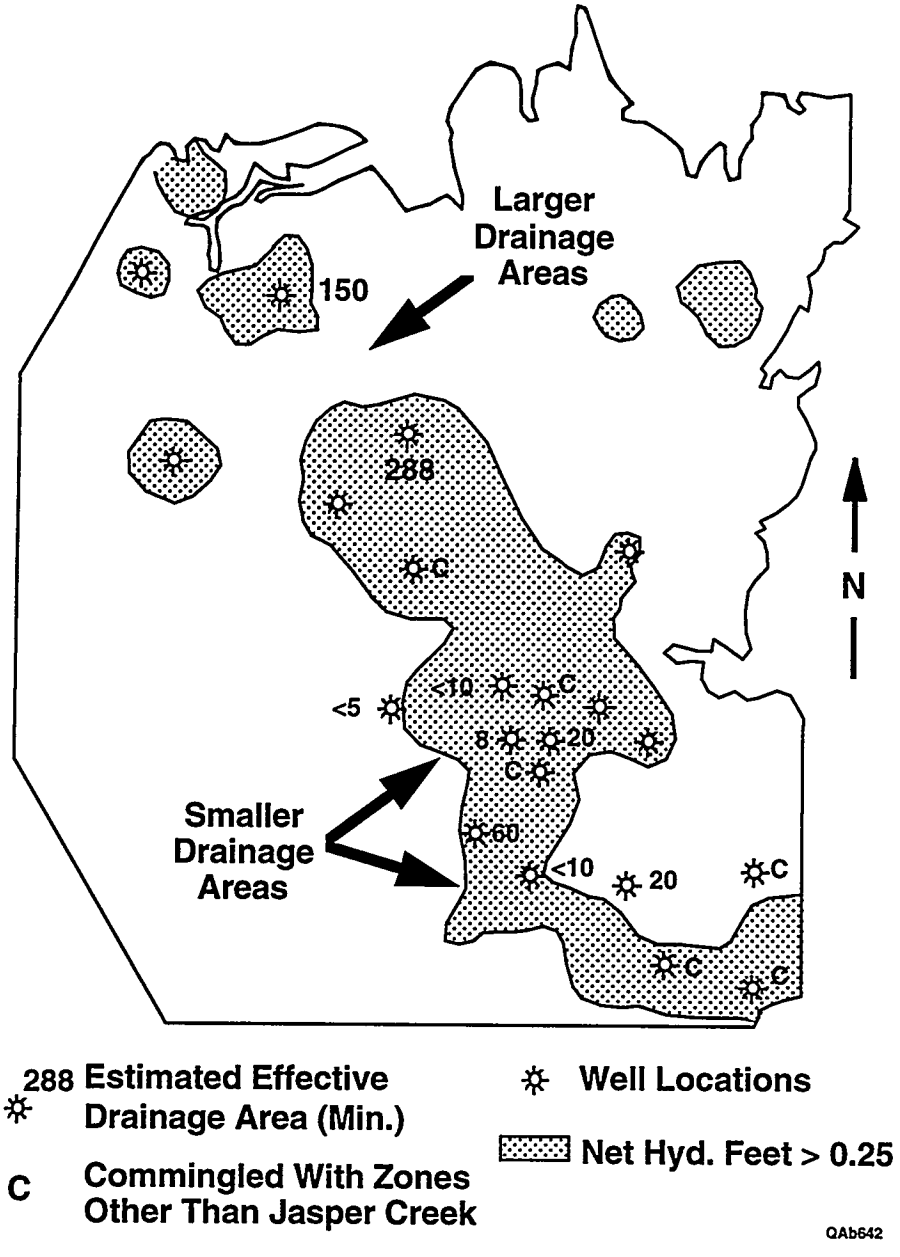

Figure B30. Map showing drainage areas estimated for Middle Jasper Creek completions from production data analysis.

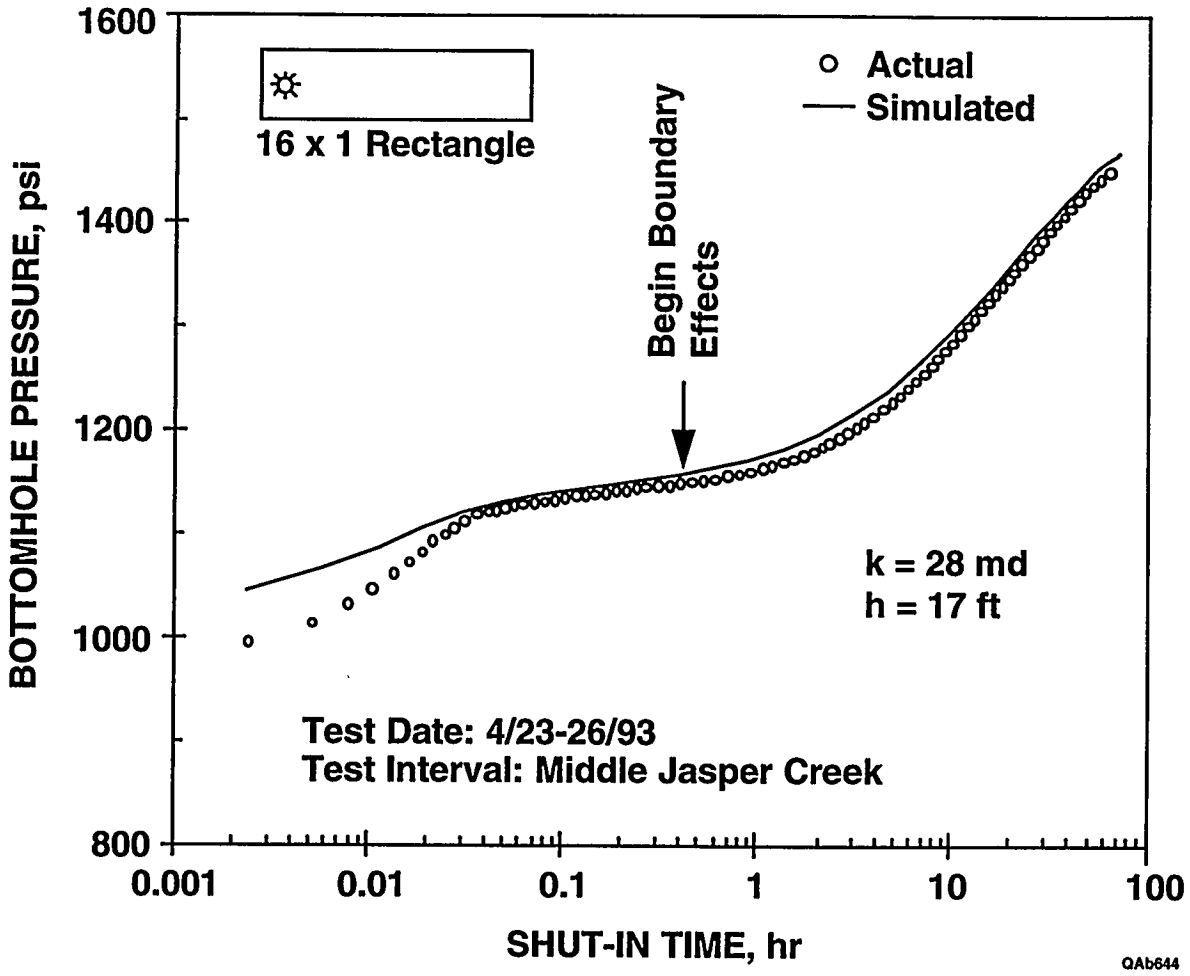

Figure B32. History-match of the pressure buildup test data from the April 1993 well test conducted on the I. G. Yates 33 well.

B.62

APPENDIX C

PETROPHYSICAL ANALYSIS OF THE BOONSVILLE PROJECT AREA

Petrophysical Data

Wells within and immediately surrounding the Boonsville 3-D seismic survey that had log data within the Bend Conglomerate were spotted on a base map. Two major petrophysical data bases were created from these log data using two different software packages—Scientific Software-Intercomp's WorkBench* and Occidental Petroleum's Stacked Curves (SCPC)*.

WorkBench is a reservoir management tool kit that includes a reservoir description module. The reservoir description module includes base map, cross section, advanced log analysis, summation calculations, and contouring. This system was used to edit the log data, depth-shift the various log suites to a common depth (usually on the basis of the resistivity suite), and perform environmental corrections before any log analyses were performed. Geological markers generated by SCPC were imported into WorkBench before summations were calculated for each of the layers. The summation results were contoured using several different software packages, including WorkBench.

Wireline Logs—A Historical Perspective of Available Data

Log analysis of Boonsville field involved interpreting several different types of log suites. Wells were logged from the discovery of the field in 1945 until the present time. During that period, the wireline logging industry developed and introduced a number of new logs and replaced older logging tools with newer tools. Figure C1 shows a rough

*The Bureau of Economic Geology (BEG), the Gas Research Institute (GRI), and the U.S. Department of Energy (DOE) do not endorse in any way the software, hardware, or any other commercial or noncommercial products mentioned in this report. Any references to these products should not be construed as such an endorsement.

time line of the available tool types along with a graph of drilling activity in the general area of study. Peaks of activity occurred when the field was first drilled at 320-acre spacing, then at 160-acre spacing, and most recently when 80-acre spacing was authorized.

In the 1940's and 1950's, only resistivity measurements were available. At first, these data consisted of electric sonde logs (ES logs), which made four measurements: Spontaneous Potential (SP), 16-inch Short Normal (SN), 64-inch Long Normal (LN), 18-ft, 8-inch Lateral Log (LAT). An additional log that was commonly run in Boonsville field was the microlog, which provided three measurements: Caliper, Micro Normal (2 inches), and Micro Inverse (1 inch × 1 inch). Later this microlog was sometimes replaced with newer devices such as Proximity logs, MicroLaterlog logs, and MicroSFL logs. These micrologging tools were used to find permeable zones in a qualitative way. Generally the curve cross-over that occurs when the resistivity is below 20 ohm-ms is a good indication of a permeable sand.

Although the Lateral Log measured resistivity values close to the true resistivity in sandstones that were at least five times as thick as the measure length (18 ft, 8 inches) of the tool, most sands in the Bend Conglomerate are not this thick. The asymmetrical nature of the Lateral Log measurement made it difficult to estimate true resistivity of the noninvaded sandstones. This log was later replaced by the Induction Log.

The first induction tools that were used in Boonsville field were the Induction Electric Logs (IES logs), which provided three measurements: Spontaneous Potential (SP), 16-inch Short Normal (SN), Deep Induction (ILD). Most of these logs were provided by Schlumberger Well Services, but several new wireline vendors soon appeared and offered their own versions of these logs. The differences in the tools of the various vendors are not enough to make any substantial difference to the water-saturation calculations; however, we did correct for differences using the automatic environmental corrections module of WorkBench.

In the late 1960's, the Short Normal was replaced by focused shallow resistivity tools, such as the Spherically Focused Log (SFL). The new resistivity tool was then known as the Induction SFL (I/SFL) tool and was often run with the newly developed borehole compensated sonic (BHS) tool and the gamma ray (GR) tool. The combined tool suite was referred to as the ISF/Sonic suite by Schlumberger. Other logging companies had different tool mnemonics, but the tools provided similar measurements.

In the 1970's, two new tools, the Compensated Neutron (CNL) and the Compensated Formation Density (FDC) devices, became commonly used. These tools were used to estimate porosities and lithologies of the formation, and they usually replaced sonic tools in Boonsville field. In fact, few sonic tools were run in the study area because at the time when these tools were popular, the area was not being drilled (see Figure C1).

In the 1980's, the density tool was enhanced to include a photoelectric effect measurement (PEF) that is very useful in determining lithology, particularly for detecting the presence of calcite. This density tool uses gamma rays at two different energies. The lower energy gamma rays interact with the formation by Compton scattering of the outer electron shells in component atoms, thus giving a measure of electron density which, in turn, allows the bulk density to be estimated. The higher energy gamma rays interact with the atoms by the photoelectric effect.

Other recently developed tools that have been used in Boonsville field include the microwave absorption tool (EPT) and formation scanning tools (FMS and FMI). The FMI, in particular, was used in three recent cooperative wells—the B Yates 17D, the B Yates 18D, and the I. G. Yates 33 wells. The microwave tool is used to measure water in the invaded zone, allowing invasion and porosity calculations to be performed. The FMS and FMI imaging tools use a series of microresistivity buttons on four calipers, and sophisticated processing of their resistivity data produces resistivity images covering

about 80 percent of the surface of the borehole. These images are valuable in determining the stratigraphic and structural environment of the formation.

Repeat Formation Tester

The Repeat Formation Tester (RFT) was run in many wells in the study area. This device is one of the most important wireline tools because it can measure pressure in formations having permeability down to about 0.1 md before running the risk of differential sticking. Pressure data are a good first indicator of whether a reservoir has been produced from another well or whether it resides in its own untapped compartment. Pressure data provided the first evidence of compartmented or incompletely drained gas in the Bend Conglomerate (see Appendix B).

The RFT tool estimates formation pressure and permeability by mechanically placing a probe against the formation and sealing it to the mud cake. A small prechamber is opened, creating a vacuum that the formation fluid will tend to fill if the fluid is capable of moving. The prechamber volume can be as large as 20 cm^3. Smaller prechambers are used in lower permeability zones. In the Bend sandstones, 2- to 5-cm^3 prechambers are commonly used. With this small prechamber, the tool is being influenced by the invaded zone, not by the virgin formation. The invaded zone is often damaged by invading fluids (mud filtrate), so the permeability data obtained using an RFT tool must be used with care. The permeability value obtained with the tool is usually pessimistic compared with the values determined by a full drill-stem test. The RFT pressure data can provide a good estimate of formation pressure, however, if sufficient time is allowed for pressure to build up to a value that is close enough to actual formation pressure to allow an accurate extrapolation.

Although the RFT tool is capable of obtaining fluid samples from the formation, this option is normally used only in zones of sufficiently high permeability that allow the samples to be obtained within a few minutes. Permeabilities in the Bend Conglomerate are not high enough to permit retrieving a fluid sample before running the risk of sticking the tool in the borehole.

Care must be taken to ensure that the probe of the RFT tool remain clean because the probe includes a fine filter that can easily become clogged. In the Bend Conglomerate, there are some potential "lost circulation" zones, particularly near the top of Marble Falls. When these lost circulation zones are penetrated, it is sometimes necessary to add fluid-loss materials to the mud to regain control of the mud column. This lost circulation material is usually some type of fibrous material, such as cottonseed hulls, which is designed to form a seal over higher permeability features (such as fractures and vugs), so that a mud cake can be formed at the borehole. Unfortunately, this material can also clog the filter and/or probe of the RFT tool.

If the probe becomes clogged by lost circulation material, the operator must normally pull the tool to the surface and clean the tool. Occasionally the probe can be cleaned by moving the tool to a high-permeability zone and allowing the formation fluid to move through the probe (as was done in the OXY Sealy C-3 well using the Upper Jasper Creek sand). In order to reduce the problem of lost circulation material clogging the RFT probe, we recommend that the mud be altered to a high viscosity and then circulated out from the bottom up for 2 h or more before pulling the drill string out of the hole for logging.

Core Data

Cores were obtained in four cooperative wells:

Well Name	Depths (ft)
I. G. Yates 33	5446-5472
Sealy C-2	4891-4910
Craft Tarrant Water Board 3	5370-5518
Tarrant A-4	4715-4750
Tarrant A-4	4800-4841
Tarrant A-4	5497-5566

The core data were divided into the 12 different facies shown in Table C1. Each facies is identified by a letter and is assigned a number that roughly describes the hardness of that facies. This hardness number is used in cross sections to graphically show the facies described from core and calculated from wireline logs.

Sample plugs were taken from representative zones and analyzed for porosity and permeability. Samples were taken from cores in both permeable and nonpermeable rock and analyzed for mineralogy by infrared (IR) spectroscopy. The results of this analysis are listed in Table C2 and show that the primary components of the samples are quartz, calcite, and clays. Note that although numbers are quoted for pyrite (all zeroes), the spectrometer was not capable of detecting pyrite. However, pyrite was seen visually in many parts of the cores. Thin sections were also prepared and petrographic analysis performed.

Table C1. The 12 primary facies identified from the core data for the Bend Conglomerate. The facies number is loosely based on the hardness of each facies. This number is used to display the facies on cross sections when the facies is derived from core or logs.

Facies name	Facies no.	Description	Interpretation
A	2	Fissile mudstone	Maximum flooding shale—outer shelf
B	3	Fossiliferous mudstone	Shelf, prodelta
C	8	Interbedded fossiliferous, calcareous sandstones and mudstones	Lower shoreface, distal delta front
D	15	Fossiliferous, calcareous sandstones (+conglomerate)	Upper shoreface
E	20	Conglomeratic sandstones	Active fluvial/deltaic channel fill
E2	18	Muddy, fine-grained sandstones	(High sinuosity?) fluvial channel fill
G	6	Burrowed, poorly fossiliferous interbedded sandstones and mudstones	Estuary or restricted bay fill
G2	9	Burrowed, poorly fossiliferous fine-grained sandstones	Estuarine channel fill
H	4	Carbonaceous, coaly mudstone	Marsh / swamp
I	13	Bioturbated calcareous fine sandstones	Transgressive shoreface
J	10	Bioturbated muddy skeletal wackestone	Interdeltaic shelf, lower shoreface
K	17	Skeletal packstone, wackestone	Shelf carbonate

Table C2. Results of infrared (IR) spectroscopy analysis on selected core samples. Note that although pyrite numbers were quoted, the spectrometer could not detect pyrite. The wells used were Sealy C-2 (SC2), I. G. Yates 33 (IGY33), and Craft TWB 3 (CTWB3). The minerals listed are Qtz (quartz), Plg (plagioclase), Ksp (K-feldspar), Cal (calcite), Dol (dolomite), Pyr (pyrite), Anh (anhydrite), Sid (siderite), Alb (albite), Arg (aragonite), Kao (kaolinite), Chl (chlorite), Ill + Smc (illite and smectite). The grain densities are calculated using average densities of the minerals detected.

Well	Depth	Grain density	Qtz	Plg	Ksp	Cal	Dol	Pyr	Anhy	Sid	Alb	Arg	Total clay	Kao	Chl	Ill+Smc
SC2	4,890.5	2.66	44	0	10	14	9	0	0	0	13	0	10	6	0	4
SC2	4,893.5	2.65	46	0	3	16	3	0	0	0	27	0	5	2	0	3
SC2	4,896.2	2.63	52	0	3	3	0	0	0	0	37	0	5	3	0	2
SC2	4,897.6	2.63	56	0	5	1	0	0	0	0	36	0	2	0	0	2
SC2	4,901.5	2.66	49	0	9	13	8	0	0	0	15	0	6	4	0	2
SC2	4,903.9	2.71	38	2	2	28	3	0	0	5	11	0	11	4	4	3
SC2	4,906.0	2.68	20	1	1	25	9	0	0	1	0	0	43	10	0	33
IGY33	5,457.8	2.66	83	0	0	0	0	0	0	0	2	0	15	0	11	4
IGY33	5,466.7	2.67	65	0	0	11	10	0	0	0	10	0	4	0	1	3
IGY33	5,469.4	2.64	86	0	3	0	0	0	0	0	7	0	4	0	0	4
IGY33	5,476.0	2.66	72	2	0	4	2	0	0	0	7	0	13	0	10	3
IGT33	5,478.0	2.77	54	0	5	4	3	0	0	13	2	0	19	3	7	9
CTWB3	5,371.3	2.69	28	0	0	47	14	0	0	0	0	0	11	3	0	8
CTWB3	5,421.1	2.65	95	0	0	2	0	0	0	0	0	0	3	0	3	1
CTWB3	5,428.1	2.65	60	0	0	0	0	0	0	0	2	0	38	18	2	18
CTWB3	5,440.2	2.66	83	0	0	8	0	0	0	0	1	0	8	2	4	2
CTWB3	5,444.8	2.67	80	0	0	9	1	0	0	0	0	0	10	0	8	2
CTWB3	5,477.7	2.69	49	0	0	37	8	0	0	0	0	0	6	0	4	2
CTWB3	5,483.9	2.69	60	0	0	15	8	0	0	0	0	0	17	0	14	3

Core Analysis

As mentioned earlier, core plug samples were analyzed in most of the sandy intervals. The results of the plug analysis are summarized in Figures C2 and C3 and show three distinct data groupings:

- The first grouping is in the region where porosity is less than 4 percent. These points are associated with the tighter facies that are well cemented, and they probably do not represent reservoir rock. The permeability values are probably the permeabilities related to induced microfractures formed during the coring and plugging processes.
- The second group of points runs generally from porosity = 6 percent, perm = 0.1 md to porosity = 16 percent, perm = 200 md. This group is dominated by a permeable sandstone facies.
- The third group of data is another linear set running from approximate porosity = 6 percent, perm = 0.1 md to porosity = 14 percent, perm = 0.6 md. This group is associated with low-permeability sandstones that may have some measure of cementation or other pore-blocking material.

The second and third groups of data indicate that the productive sands in the Bend Conglomerate are associated with two (or more) different facies. A key objective of the petrophysical analysis was to find a way to calculate the different sandstone facies in order to determine the importance of facies changes in reservoir compartmentalization.

Overview of Log-Analysis Techniques

Data Preparation

Once all the wireline data were located and digitized, the data were brought into the WorkBench environment. The locations of all the wells were entered into the base map

system of WorkBench, and appropriate API numbers were attached to each. The log data could then be entered for each well.

The log data were plotted to compare with the original paper logs and checked for digitizing quality. Any editing of the data was then done interactively on the graphic screen or by keyboard entering of data revisions. All the required header data from the logs were also entered into WorkBench. This included information on tool types and wireline vendor. This information was used later by the system for automatic environmental corrections and other operations.

SP base line shift

The Spontaneous Potential (SP) curves were compared for amplitudes, and the variations for sand and shale amplitudes were examined. All wells that penetrated the Bend Conglomerate had at least one sand that was clean and seemed to provide the amplitude of a clean sand for the SP. These wells often had the best sand development for the SP in the Vineyard zone at the bottom of the Bend sequence. Some wells penetrated only the Caddo zone, and, in these cases, the SP examination included the Strawn sequence above the Bend. The SP curves were straightened (i.e., the steady drift to the right was removed) through the Bend sequence for all the wells. The SP curves were then all rescaled to fall into the range of –100 to 0 millivolts. The SP curves needed to be set into the same scales so that meaningful cross sections could be produced in either Stacked Curves or WorkBench. In addition, the facies analysis from logs required all the curves to be normalized (see section after next).

Depth Shift

For wells than had multiple runs, the various runs were depth-shifted to match the resistivity suite to the nearest foot. This was done using sophisticated automatic depth-

shift algorithms in WorkBench. The results of this process were then displayed on the screen for visual verification. In the event that editing of the depth shifts was required, it was done interactively.

Normalization

Many neutron and density curves were found to disagree from one well to another. Crossplots of neutron and density curves were made for each well and then compared with each other. Patterns of lithological origin were easily recognized and showed clusters around tight limestones, clean gas-filled sandstones, and marine shales. Other clusters were recognizable, but either were not present in all wells, or doubt existed as to whether they were a consistent lithological facies across the field. All clusters that could be associated with a known lithological origin were then used for calibration.

Many of the wells gave essentially the same patterns for the calibration clusters, so these values were assumed to be correct and were chosen to be the standard crossplots. The well logs were checked for these wells, and the calibration tails (where available) all showed that these logs had been properly calibrated. The crossplots that deviated from the standard crossplots were then shifted linearly along the density axis and/or the neutron axis to fit the standard. These shifts were then applied to the raw data in the data base for the same well. Some shifts were as high as 10 porosity units. Generally Halliburton and Western Atlas logs required more of this recalibration than did Schlumberger logs.

No attempt was made to normalize the gamma-ray logs (except one well that was obviously grossly miscalibrated in the field). Because the gamma-ray shale and clean sand values were to be picked individually for each well at analysis time, the normalization of the gamma-ray curve was deemed unnecessary.

Environmental Corrections

WorkBench contains all the environmental correction charts for all major wireline vendors. This module corrects neutron, density, and gamma ray data for borehole effects such as temperature, pressure, mud, and washout.

The resistivity data were corrected through the appropriate charts and then used in tornado chart calculations to find a true resistivity of the virgin zone (Rt) and a resistivity of the flushed zone (Rxo), in instances where three or more resistivity curves existed. If only one or two curves existed, the deepest curve was assumed to equal Rt (this is the case on most of the old IES logs).

Dual-Water Method

Examination of the core data indicated that the Bend Conglomerate is composed mostly of fluvial sands and shales, with considerable carbonate material in the form of cements. In addition, marine shales and pure limestones are present. In order to determine the most accurate water saturations, the dual-water method was adopted. The dual-water method accounts for the electrical conductivity of the shales by assuming that the shales are porous and their pores are filled with salty water that may have a salinity different from that of the connate water. A diagrammatic representation of the dual-water model is shown in Figure C4.

Shale porosity is filled with water known as bound water. The resistivity of this water is Rwb. The water in effective porosity (the producible porosity associated with the sands) is filled with free water and any hydrocarbons that may be present. The free water is the same as connate water and has a resistivity of Rwf.

For a rock that has no hydrocarbons, the resistivity of the rock is Ro. Using the dual-water method, this value can be calculated from the equation

$$Ro = a * (Rwf * Rwb) / ((Rwb + Vsh * (Rwf - Rwb)) * PHIT ** m), \qquad C\text{-}1$$

where a = the Archie constant, m = the Archie exponent (cementation exponent), Vsh = the proportion of the matrix that is shale, and PHIT = the total porosity. For this study, Archie parameters were given the values a = 1.0 and m = 2.0.

Total porosity (PHIT) was found to be approximately 15 percent in both the sands and the shales. A lower value of PHIT was found in the carbonates. The observation that the value of the total porosity is constant for the sands and shales has been found to be true in many formations. This observation makes it possible to interpret old wells that have only resistivity logs with reasonable accuracy. This procedure is described in the next section.

IES/ES analysis

Introduction

In fields such as Boonsville that were discovered before the invention of neutron, density, and sonic tools, wells were logged only with resistivity tools. Of the 221 wells used in this study, 55 percent were from older wells that only had resistivity information. Only 45 percent of the well logs could be interpreted for porosity, water saturation, and lithology using standard log analysis techniques. This restriction on the number of interpretable wells represents a limitation in complex clastic reservoirs; therefore, a method had to be developed to interpret the old wells that only had IES logs.

A computer program was developed to interpret induction (IES) logs having deep induction, short normal, and spontaneous potential (SP) curves. The method was developed to interpret zones that consist of three major lithologies: (1) shale, (2) clean, productive sandstone, and (3) tight, carbonate cemented sandstones and siltstones.

Where possible, the logs must be used to determine the presence of productive sands (along with their characteristics such as porosity, water saturation, etc.) and to understand their structural and stratigraphic settings. Any log analysis that can determine lithologies

and porosities is therefore very valuable. When operators learn to interpret wells containing only resistivity logs, the number of interpreted wells available for geological modeling of the Bend formation in Boonsville field can be more than doubled. The same is true for many other Midcontinent clastic reservoir systems.

Description of the Petrophysical Analysis Technology

A program was developed using a well that had a complete suite of modern well logs. First, the well was interpreted using a standard interpretation program that took advantage of all the curves, including density (RHOB), lithodensity (PEF), and neutron (PHIN) curves. The same well was then interpreted using the new IES technique and recalibrated until the results matched the original analysis as closely as possible. The technique was subsequently used on other wells that had full modern logs. Without any further calibration, the results in these check wells were excellent, indicating that the technique could now be used with confidence in wells having only IES log suites. An example of one of the check wells is illustrated in Figures C5 through C7.

The program uses only two curves: the spontaneous potential (SP) and the deep induction (RILD). From these curves, we calculate the relative proportions of three lithologies, the porosity, and the water saturation. The program uses a dual-water model and assumes that the total porosity (PHIT) is constant through the zone(s) of interest. The total porosity (PHIT) is made up of effective porosity (the porosity associated with productive sands and containing connate water and possibly hydrocarbons) and shale porosity (nonproductive pore space in the shales that contains the bound water). The three lithologies that the program calculates are (1) clean sandstone with porosity, (2) clean calcite cemented (tight) sandstones and (tight) limestones, and (3) shale.

Clean sandstone has porosity and permeability and, therefore, is readily detected by the SP curve. The equations to determine the amount of clean sand and porosity are:

$$VSHS = (SP - SPCL)/(SPSH - SPCL) \qquad C\text{-}2$$

$$PHIE = PHIT * (1 - VSHS) \quad \text{C-3}$$

$$SAND = 1 - PHIE - VSHS \quad \text{C-4}$$

where SPCL = the clean sandstone value for the SP, SPSH = the shale value for the SP, PHIE = the effective porosity, which is the porosity that has the potential to contain movable fluids, PHIT = the total porosity, which must be estimated from nearby wells in the same formation and is generally taken as the maximum value of porosity in the nearby well, SAND = the amount of clean sandstone, and VSHS = the volume of shale in a sand.

Note that estimating the total porosity is a critical step. Total porosity can be determined by performing log analysis on any nearby wells that have neutron and density curves. The maximum PHIE calculated for these wells may be used for the PHIT value in the above equation. Analysts must be careful about using porosities measured by the neutron/density logs in washed-out shales; these are probably too high and will give a false value for PHIT. In the Bend formations, a value of 15 percent was often used during the SGR study. An alternative approach is to use any available core data and to take the maximum value of porosity found in the core analysis for PHIT.

The SPCL value is usually the minimum value of SP found in the zone. The well being studied must have at least one clean sand to obtain a valid interpretation. If the best sand is known to be partially contaminated by carbonate cement, then a lower value of SP must be estimated for the SPCL value.

The second formation type (tight limestones and tight carbonate cemented sandstones) is more difficult to find. Generally these rocks will have no SP response because they have no porosity, but they should have a resistivity higher than the value seen in the shales. The proportion of this facies is determined by:

$$VSHR = 1 - ((RILD - (RSH + 1)) / 12 \quad \text{C-5}$$

$$VSH = MIN(VSHS, VSHR) \quad \text{C-6}$$

$$CARB = 1 - SAND - VSH - PHIE \quad \text{C-7}$$

where RSH = the value of the deep resistivity in the shales, VSH = the volume of the shale, and CARB = the volume of the carbonate cemented sandstones.

Note that the numerical divisor in the VSHR equation (the value 12) works well in Boonsville field. In other fields in North and South America, this term can vary from 10 to 20, but is usually close to 12.

Water saturation is then calculated using the dual-water method. This method calculates the theoretical resistivity of the rock as if the rock were 100-percent wet (Ro) as follows:

$$Ro = 1 * (RWF*RWB)/((RWB+VSH*(RWF-RWB))*PHIT^2) \quad \text{C-8}$$

where RWF = connate water resistivity, and RWB = resistivity of the bound water (shale water). The program assumes a value of 1.0 for the Archie parameter "a" and a value of 2.0 for the Archie cementation exponent "m."

RWF and RWB are determined by looking at a calculated curve of Rwa. This curve is generated as part of the initial run in the program and is given by the relationship

$$Rwa = RILD * PHIT^2, \quad \text{C-9}$$

assuming that a=1 and m=2 for the Archie parameters. RWF is then the Rwa value in a clean wet sand and RWB is the average Rwa value in the pure shales.

Water saturation can now be calculated from the ratio of Ro to RILD.

$$SWR = (R0 / RILD)^(0.5) . \quad \text{C-10}$$

Two versions of this IES technique have been programmed—one version for the Macintosh computer and one for Windows 3.1 on MS-DOS computers. These programs are stand-alone versions that will read LAS format files that contain SP and deep resistivity curves and interpret these curves using the technique just outlined. The computed results are displayed on the screen and are also written into an LAS format file for use in other applications. Both source code and executable versions of the IES algorithm may be obtained from GRI or by contacting Robert Elphick with Scientific Software-Intercomp in Denver, Colorado.

ES Logs

ES logs consist of three resistivity measurements: the lateral log (LAT), the short normal (SN), and the long normal (LN). The lateral curve is eccentric and can be used to estimate true resistivity of a sand only if the thickness of the sand is at least five times the length of the tool and is homogenous (in terms of its porosity and water saturation). Because the lateral tools were 18 ft, 8 inches long, this requirement means that sands would have to be greater than 100 ft thick. Sands in the Bend Conglomerate do not get anywhere near this thick and are not homogeneous.

Two different techniques were used to calculate true resistivity from lateral logs. Both techniques involved the use of commercially available computer programs. The first is the ES-LOG program developed as part of a separate GRI research effort and marketed by Walt Whitman Software, Inc. This system performs forward modeling and inversion. The forward modeling generates synthetic logs from a specified Earth model, and the inversion algorithm interprets the logs and builds an Earth model. The program can run on an MS-DOS computer but is very CPU intensive and runs better on Unix workstations (such as DEC and IBM RS-6000 series computers). For further information on this software contact

Kent Gestring
Walt Whitman Software, Inc.
12600 West Colfax Ave., Suite A270
Lakewood
Colorado 80215
Phone: (303) 237-2523
Fax: (303) 237-3589

The second technique was the Old Electric Log Advisor (OEA) marketed by The Logic Group. This system uses a knowledge engineering approach to help the user

estimate true resistivity in each sand. The knowledge data base was provided by Dr. George Asquith of Texas Tech University, a petrophysicist with many years of experience using ES logs. Further information on this product can be obtained from

Diane Zbranak

The Logic Group

P.O. Box 50499

Austin

Texas 78763

Phone: (512) 451-5707

Fax: (512) 451-2300

The OEA technique lacks an inversion capability but runs fast on an MS-DOS computer. Generally all the sands in the Bend Conglomerate for one well could be computed in 1 or 2 h with OEA, whereas the ES-LOG program would run for 20 to 30 h on an RS-6000 to interpret 200 ft of data.

Because the normal logs are symmetrical and easier to understand, we looked at the long normal to estimate true resistivities. As a first approximation, the long normal reads true resistivity where the sands are reasonably homogeneous and at least 6 ft thick.

Modern Log Interpretation

Introduction

Nearly half the wells in the study area had neutron and density tools. The combination of neutron and density tools allows analysts to obtain good estimates of the total porosity. In addition, these curves are useful for estimating the lithology of the formation. The method used was also capable of using the photoelectric effect (PEF) curve when it was available.

The analysis of the wells having at least neutron and density curves was performed first. These wells were then used to calibrate the IES and ES logs as described in the previous section. Interpretation began with the wells that contained core data. The porosity/permeability data, along with the IR lithology data, were used to calibrate the log-analysis technique and to refine the program and parameters used for the remaining wells.

Log Analysis

The log analysis begins by calculating the volume of shale from the SP and/or the gamma ray using the normal routines.

$$VSHG = (GR - GRCL) / (GRSH - GRCL) \qquad \text{C-11}$$

$$VSHS = (SP - SPCL) / (SPSH - SPCL) \qquad \text{C-12}$$

where VSHG = shale volume calculated from the gamma ray, GR = gamma-ray value, GRCL = gamma-ray clean value chosen in the cleanest sandstone, GRSH = gamma-ray value chosen in a marine shale, VSHS = shale volume calculated from the SP, SPCL = SP value chosen in a clean sandstone, and SPSH = SP value in the shales.

These values are averaged together and an S curve modifier applied. Two other options available in the program allow the use of spectral gamma-ray data, when available, and the neutron/density curves as shale volume estimators. Neither of these options were used for this study because no spectral gamma-ray data were available and the neutron/density data are confused by the presence of carbonates and bad hole.

The presence of bad hole is determined by looking at the caliper, rugosity, and density curves. The rugosity curve is produced by the environmental correction submodule and determines the rate of change of the caliper. The sidewall tool (density) is more prone to be incorrect when the hole size is changing than when the hole size is large but constant. The density is also used to determine bad-hole conditions because the curve

tends to read very high porosities (low bulk densities) when the tool pad cannot make good contact with the side of the hole.

Once bad-hole conditions have been detected, the density is modified on the assumption that the shale volume calculation and the neutron reading are correct (not true at rare, extreme, bad-hole depths). In shaly sands, the position of the neutron and density points on a crossplot is determined by the amount of shale at a given depth. When bad-hole conditions are encountered, the density moves down in the plot along a line of constant neutron porosity until it reaches the appropriate shale volume line (see Figure C8).

Total porosity is then calculated from the neutron–density. A gas-correction algorithm is then applied to account for any gas that is present.

The value of the ideal resistivity in the water-filled rock (Ro) is then calculated using the dual-water model (see section on Dual-Water Model earlier). This value is then compared with the value for Rt, and the water saturation is calculated from the ratio. The effective porosity (porosity of the sand that is capable of giving up fluids) is then calculated as follows:

$$PHIE = PHIT * (1 - VSH) \qquad \text{C-13}$$

where PHIE = effective porosity (in fractional units), PHIT = total porosity (in fractional units), and VSH = calculated shale volume (in fractional units).
Some aesthetics are applied to the water saturation and porosity curves to reduce ridiculous answers in unstable situations.

The lithology is calculated using three algorithms. One algorithm is used when only neutron and density data are available; a second is used when a PEF curve is available. The third algorithm uses the resistivity data to determine the presence of calcite cemented sands and silts when the other techniques fail to find them; this is the same technique used in the IES method described above.

Apparent grain density is calculated from the original bulk density measurement and the total porosity.

$$RHOG = (RHOB - RHOF * PHIT) / (1 - PHIT) \quad \text{C-14}$$

where RHOG = apparent grain density, RHOB = bulk density from the log in g/cc, RHOF = the density of the fluid in g/cc (1.0 g/cc), and PHIT = total porosity in fractional units.

This value is then corrected for shale to give the value of the nonshale matrix. Using logs, we can determine only two or three minerals when only two curves are being used to differentiate them (in this case the neutron and density). Only three minerals are therefore determined: sand, calcite, and dolomite. In this case, the dolomite represents all the heavy minerals present in the Bend. The minerals are determined for only two possibilities—either sand/calcite (when the RHOG value is less than 2.71 g/cc) or calcite/dolomite (when the RHOG value is above 2.71 g/cc).

When a PEF curve exists, the apparent U value is calculated from

$$U = PEF * (RHOB + 0.1883) / 1.0704 \quad \text{C-15}$$

$$UMA = (U - UF * PHIT) / (1 - PHIT) \quad \text{C-16}$$

where RHOB = bulk density from the log in g/cc, PHIT = total porosity in fractional units, and UF = fluid value of U. The proportions of four minerals present are then determined from the UMA/RHOG crossplot (see Figure C9).

Summations

Once the log analysis was completed over the Bend Conglomerate in each of the wells, markers representing the surface boundaries for each of the critical zones were entered into the log-analysis program. Layers were defined on the basis of these markers. Summations were then run for both net reservoir (using a shale volume cutoff and a porosity cutoff) and net pay (using shale volume, porosity, and water saturation cutoffs) for each layer.

Cutoffs

The shale cutoff parameter was chosen to remove any shaly sections that may have too high a porosity calculation due to bad-hole conditions. Bad-hole conditions usually occur in the shalier zones and cause the density logs to read a porosity that is too high. Although the log-analysis program attempted to correct the density reading in these circumstances, the correction was not always successful. A value of 50 percent was chosen for the shale cutoff. For the most part, the porosity cutoff was much more severe and was the parameter that determined whether a data point was selected. Generally the shale cutoff parameter had no effect except to eliminate the occasional bad-hole data.

The porosity cutoff was chosen by examining the porosity versus permeability crossplots made from the core data (see Figures C2, C3, and C20). The permeability cutoff was difficult to determine, but the producible E and E2 sand facies seemed to occur with permeabilities down to about 0.05 md. From the crossplots, this value corresponds to a porosity of 4 percent for both the E and the E2 facies. A value of 4 percent was therefore chosen for the porosity cutoff. A water saturation cutoff of 60 percent was also used in the net pay summation calculations.

The results of the summation calculations were then used to map the sand characteristics for each of the layers. The net reservoir hydrocarbon pore-volume maps indicate varying hydrocarbon distribution within each layer. These net pay and net reservoir summations were also used extensively in the engineering analysis (see Appendix B).

Facies Determination

Introduction

When facies vary rapidly across a field, finding correlations can be difficult. The Bend Conglomerate is complex, and finding correct correlations is essential to identifying the compartments within the section. Correlations are traditionally done by hanging all or some of the wireline curves in a cross section and identifying certain curve patterns as belonging to given facies. This is easier when the logs are all of similar types and are all presented on similar scales. Nonetheless, identifying various facies from pattern recognition alone is often difficult.

Pattern recognition software designed to identify facies has existed for a number of years. Most of these packages involve sophisticated stochastic techniques and often provide impressive results when applied by skilled users. A principal component analysis technique was used by the analysis team, with the results being good when applied to well logs of similar curve suites but inconsistent when applied to nearby wells that had radically different log suites.

Therefore, a deterministic method for recognizing facies from logs was developed for use in the Bend Conglomerate. Several different approaches were attempted until the final system was chosen. Although the original technique was developed on a Macintosh, it was transferred to the Stacked Curves program to take advantage of its geocolumn display capabilities. Five models were constructed for each of the possible curve suites that we wished to use. Table C3 shows which curves were set up as input curves for each of these five models.

Table C3.

MODEL	Res	GR	PEF	NPHI	RHOB
FaciesR	•				
FaciesG	•	•			
FaciesU	•	•	•		
FaciesN	•	•		•	•
FaciesP	•	•	•	•	•

The Res column refers to the suite of resistivity curves: SP, deep resistivity, and shallow resistivity curves. These curves were used in all the models.

Methodology

The facies technique is based on determining the ideal curve responses for each curve in each facies. The ideal responses were obtained from the cored intervals of the four cored wells. The logs for these cored intervals were shifted to the core (by matching the porosity from core to the porosity calculated from the logs). Histograms were then built for each curve in each facies—a total of 84 histograms because only seven curves were used. Many of the histograms provided a well-defined peak, but others were less well defined, and so some judgment had to be used to find the best value. Two examples of well-defined peaks are shown in Figures C10 and C11. An example of a less well defined peak is shown in Figure C12. The poorer quality peaks are associated with the nearness to a bed boundary (most of the logs used have about a 2-ft vertical resolution and therefore do not respond immediately to bed boundaries) or to hole washout as determined by the caliper and/or the rugosity curves. Table C4 shows the values for the curves in each facies that were chosen from the histograms. These values were used in the programs developed to find the facies from the logs.

Table C4. Ideal values for each curve in each facies, as chosen from histograms of these data sets.

Facies name	Facies no.	NPHI	DPHI	RHOB	PEF	GR	SP	Res deep	Res shal.
A	2	0.36	0.16	2.44	3.9	125	–15	3	7
B	3	0.30	0.08	2.57	3.2	105	–10	7	9
C	8	0.18	0.04	2.64	3.5	90	–10	15	9
D	15	0.05	0.03	2.66	3.5	60	–15	25	25
E	20	0.08	0.15	2.45	2.2	45	–80	60	200
E2	18	0.13	0.12	2.51	2.4	58	–40	20	90
G	6	0.20	0.10	2.54	4.0	115	–20	4	5
G2	9	0.20	0.08	2.58	3.5	102	–18	10	15
H	4	0.28	0.12	2.51	3.5	125	–15	7	10
I	13	0.10	0.05	2.63	3.2	88	–20	9	10
J	10	0.11	0.03	2.66	3.5	90	–15	9	10
K	17	0.02	0.02	2.68	5.0	60	–25	55	300

The programs are set up to determine the difference between the ideal value of a curve for each of the 12 possible facies (see Tables C1 and C3) and its actual value. The differences for each curve are added up and then divided by the number of curves used by the program. This difference then represents the error function for each facies.

$$errorf = [\, Nc * (Logc - Ic) \,] \qquad \text{C-17}$$

where errorf = total deviation from the ideal facies f, Nc = normalization for curve c, Logc = the log value of curve c, and Ic = the ideal value of curve c in facies f. The program then finds which of the facies has the smallest error function (errorf) and selects that facies for the depth being calculated. The procedure is continued for each depth.

All versions of the facies program output an error curve that is based on the error function described above—the errorf value divided by the number of input curves used by the program. This curve allows the user to see how well the program is matching the data; large values in the error curve indicate that the program is having some difficulty in choosing an appropriate facies.

A data set was made up of all the core data stacked end to end and the depth-corrected log data for the same interval. Each of the electrofacies programs was run

against this data set, and the calculated electrofacies were compared with the facies from the core descriptions. The results of these calculations are summarized here:

Table C5.

MODEL	Total Error	Average Error	Hits	% Hits
FaciesR	955	1.41	301	44
FaciesG	1057	1.56	349	51
FaciesU	1121	1.65	340	50
FaciesN	1745	2.57	288	42
FaciesP	1702	2.51	289	43

The average error is the total error for the whole interval divided by the footage of the interval. The hits are the number of times that the core facies agreed with the electrofacies. The number of hits is mostly affected by the bed boundary effects described earlier. The geocolumn displays show the comparisons of the core described facies with the electrofacies. Some of the facies are found remarkably well by the electrofacies. Others are harder to discriminate because the differences between some of the facies are easy to see when looking at core but are not resolved by logs. For example, the logs cannot tell the difference between a calcite cemented siltstone and a fossiliferous siltstone because the lithological makeup of these two rock types is the same. If we had a log that was sensitive to fossils, this difference could be resolved.

Comparisons of each of the five facies model results with each of the core facies are shown in Figures C13 through C17. These figures are geocolumn displays in which all the core data have been stacked on top of one another (shown on the left of the depth track). The corresponding log data, after being depth-shifted to match the core data and then run through one of the facies calculation models, are shown on the right side of the depth track. The depths displayed in the depth track are in arbitrary values that show the

relative depths and not true depths because these data come from four wells and a number of different sequences.

When applied to the cored data, the error curves indicate that the versions of the program that use the neutron and density curves find higher errors (presumably because of washout). In addition, the versions that include the neutron and density curves find fewer depths of agreement (hits) with the core data than do the other versions.

Before the models were run against the wireline data base, an additional few lines of code were added to the models to force them to predict the E facies when the SP was less than –80 mV and to predict the E2 facies when the SP was less than –40 mV. These facies were found in most cases without this artificial shove, but, in a few instances of poorly calibrated old resistivity logs, the change was required.

Stacked Curves was used to run all the models for each well. Those wells that did not have curves sufficient to run a particular model were automatically bypassed by the Stacked Curves system. Because all the wells had the minimum curves required to run the FaciesR model, this model was run on every well. Cross sections were then made through the study area. The cross sections were made so that the results of only one of the facies models were displayed. The hierarchy of models was set so that the preferred display was in the following order:

1. FaciesU
2. FaciesG
3. FaciesR

Note that the first model (FaciesU) required the greatest number of curves and that the last model (FaciesR) required the minimum set of resistivity curves.

The facies model used on the displays is indicated by the color of the bounding curve on the geocolumn for each well in the cross sections. FaciesU is indicated by a black bounding curve, FaciesG by a blue bounding curve, and FaciesR by a red bounding curve. The bounding curve is set by the values of the facies as shown in column 2 of

Table C3. These facies numbers are loosely related to the hardness of each of the facies, so that the geocolumn display resembles an outcrop display. Note also that the color of each facies is also determined by this same number.

Figure C18 shows a typical cross section through the Caddo sequence using the geocolumn display. Note that the marine limestone facies (K) is predominant in the B Yates 12, B Yates 6, and Ashe A5 wells; in the other wells, this facies has been replaced by sandstone facies (E and E2). Figure C19 shows the interpretation of this cross section, indicating that the marine sequence has been eroded by erosional surface ES 95 and replaced by fluvial deposits, with sandstone associated with the greater accommodation space. The marine limestone (K facies) in the B Yates 12 well has a square boundary into the shaly facies above and below it. The sandstones (E facies) in the C Yates 1 and Ashe A1 wells terminate upward through a series of facies into the shaly facies, indicating an upward-fining sequence similar to that represented in the ideal genetic sequence described in the geologic interpretation presented in Appendix A. It is worth noting that even though the actual facies in these upward-fining sequences may be in error at any given depth due to the vertical resolution of the wireline tools, the pattern of the sequence is still maintained.

Figure C20 shows a cross plot of porosity versus the permeability of all the core plugs taken from the four cored wells. The colors represent the 12 facies described from core. Note that the E facies belongs to the higher permeability sands in the trend from porosity = 6 percent, permeability = 0.1 md to porosity = 15 percent, permeability = 60 md. The E2 facies is associated with the lower trend, indicating sandstones and/or siltstones of a lower permeability. In the cross section shown in Figure C21, the Sealy C-2 well shows a sandstone with a predominant E facies developed above the ES95 erosional surface (the Upper Caddo zone). The Sealy B-3 well has a sandstone above the ES95 surface that is entirely E2 facies according to the facies from wireline logs computation. Figure C22 shows the production histories for these two wells in the Upper

Caddo zone; the production was isolated (i.e., not commingled) in both of these wells. Production data analysis calculates a lower average permeability (0.5 md) in the Sealy B-3 well and a higher value (2.2 md) in the Sealy C-2 well (see Appendix B). The facies determination from logs appears able to distinguish between the higher and lower permeability sandstones that were detected from the core data (see Figure C20).

Advantages of the Facies Technique

The facies technique developed for this study has several advantages when using log data to interpret the geology of the Bend Conglomerate:

- This deterministic technique is much easier to use than the complex stochastic methods, including principal component analyses that require specialized computer programs and extensive knowledge and experience to run.
- The procedure can be used over a broad range of tools suites, including wells that have only old resistivity logs.
- The calculation generates good pattern recognition (for example, the upward-fining sequence described earlier), even where the vertical resolution of the logging tool is less than the thickness of some of the beds in the sequence.
- The algorithm appears to be able to distinguish between sandstones of different permeability characteristics.
- The results are valuable in sequence stratigraphy interpretation.
- The technique is readily adapted to other fields with similar facies recognition problems.

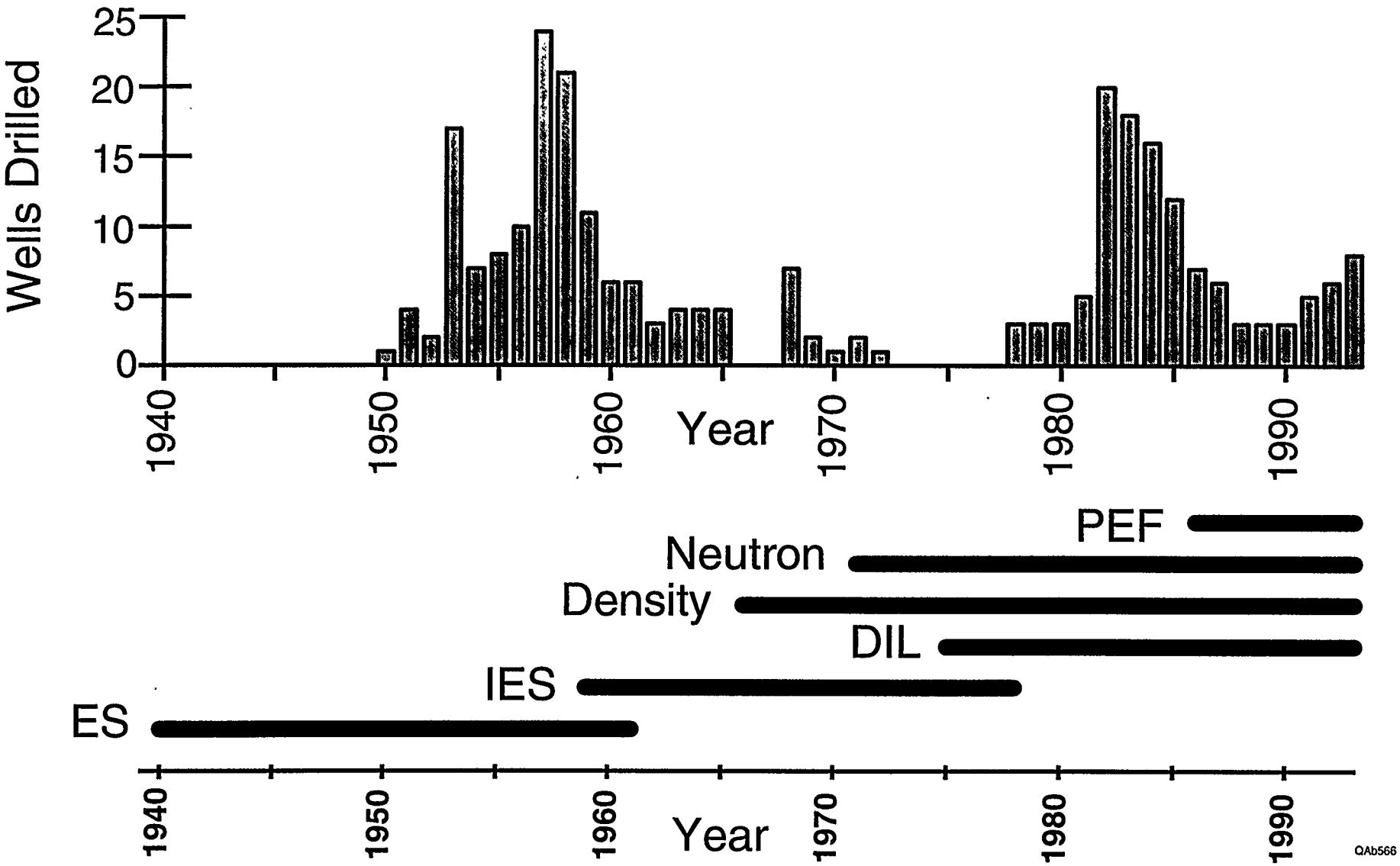

Figure C1. Time line showing available tool types and a graph of the drilling activity in the general area of the study.

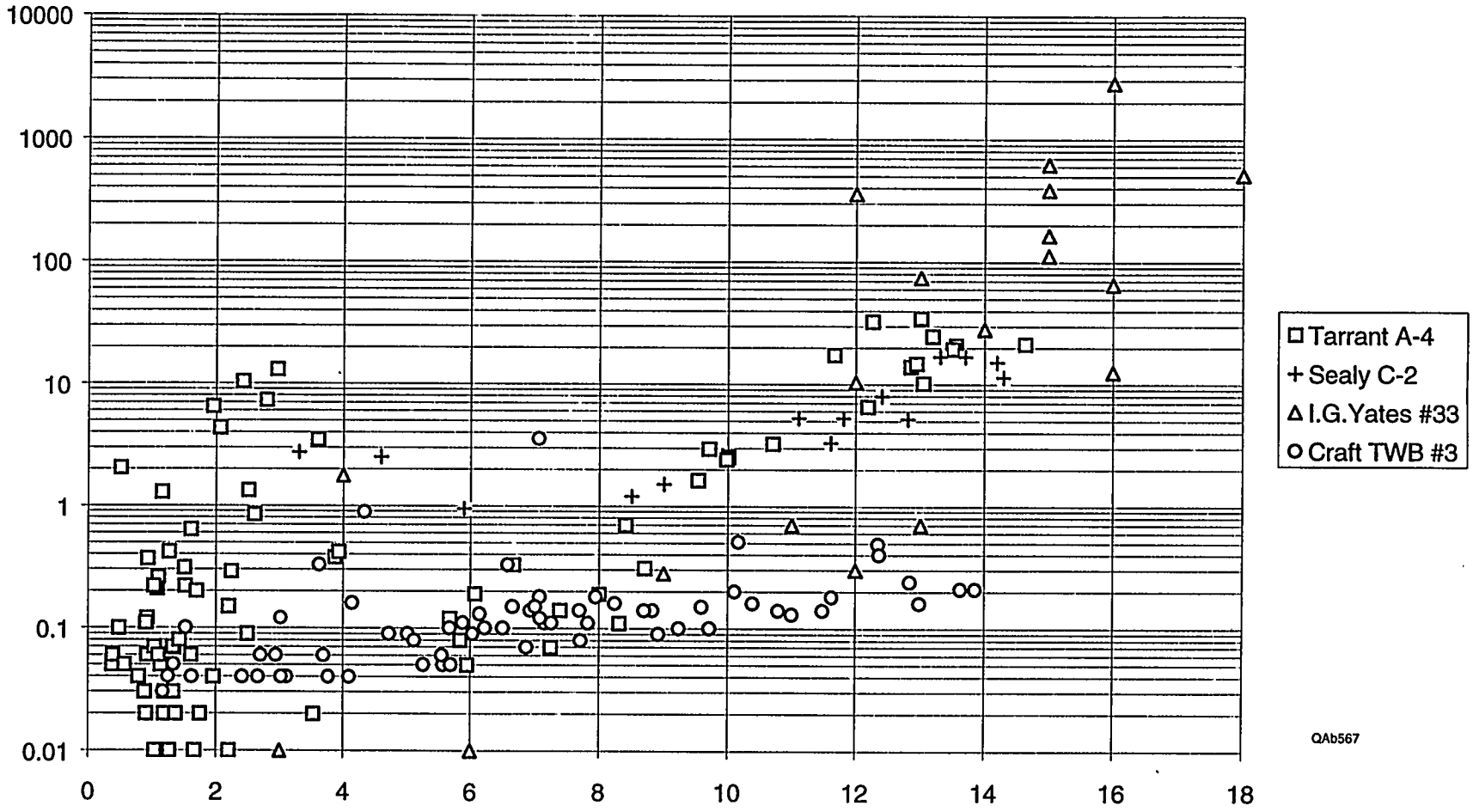

Figure C2. Porosity vs. permeability cross plot of all sample plugs from the four cored wells. The symbols indicate the well from which each plug was taken.

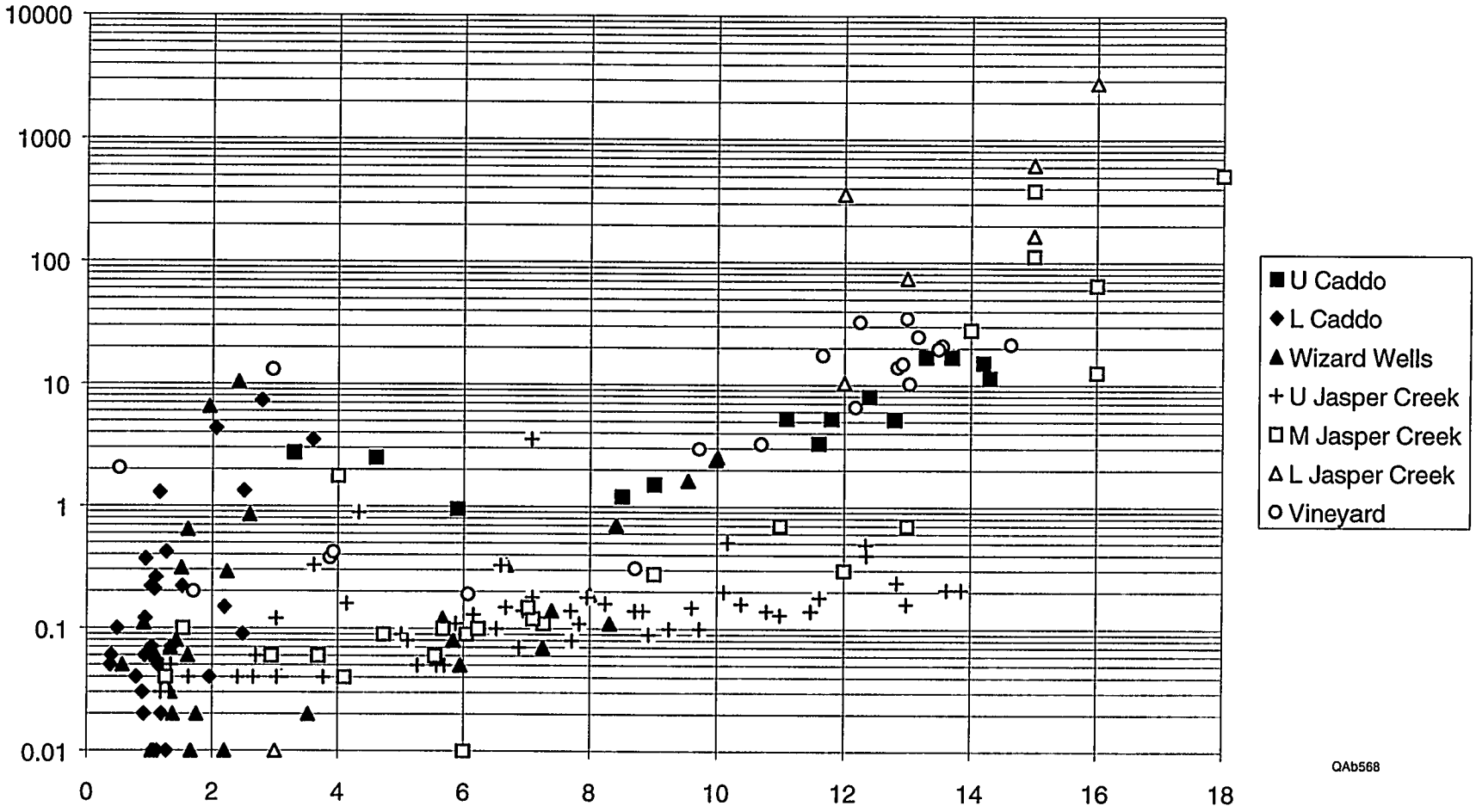

Figure C3. Porosity vs. permeability cross plot of all sample plugs from the four cored wells' zones. The symbols indicate the zones from which the plugs were taken.

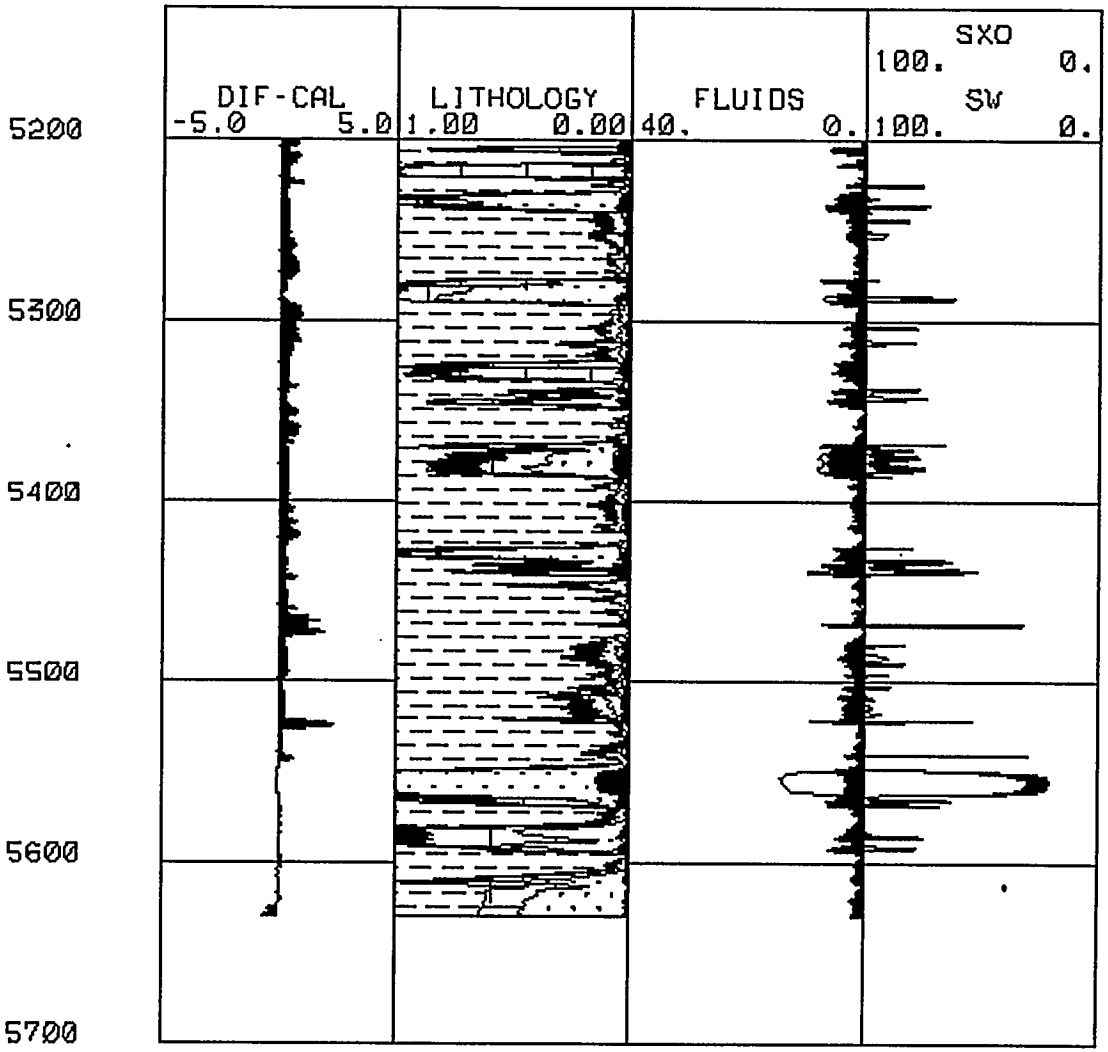

Figure C6. Log interpretation of the Tarrant A-4 well using all available curves in a standard log analysis. The lithology track indicates the proportions of shale, sandstone, calcite, and dolomite. The fluid track shows effective porosity with the hydrocarbons and the water. Water saturations are shown in the fourth track. Note the porous sand at about 5,580 ft, the many tight carbonate cemented sands, and the limestone at about 5,220 ft.

C.36

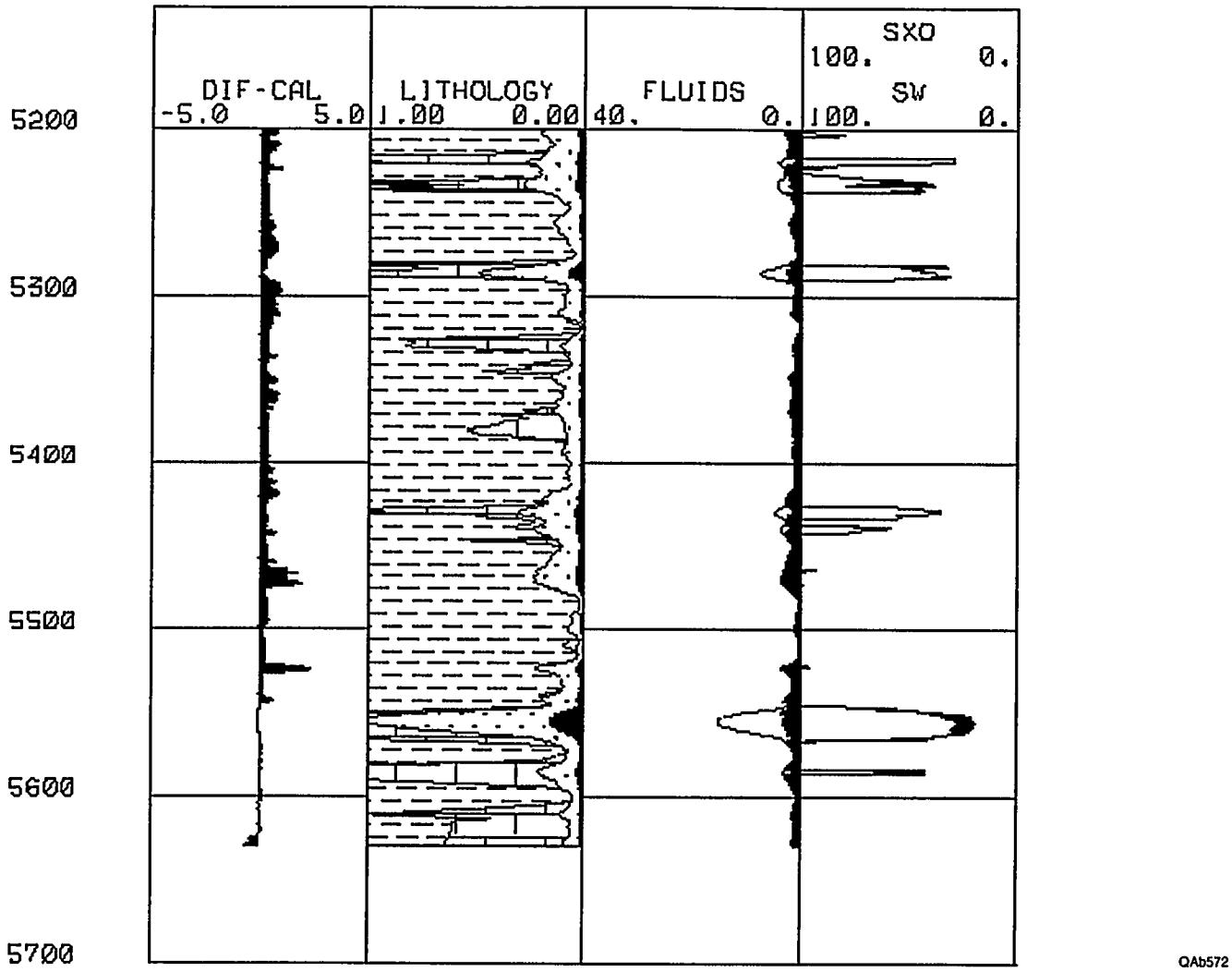

Figure C7. Log interpretation of the Tarrant A-4 well using only the SP and deep resistivity curves in the IES log analysis. Note the porous sand at about 5,580 ft and compare it with the interpretation in Figure C6. Also note that most of the carbonate cemented sandstones shown in Figure C6 are also being found by the IES log-analysis technique.

C.37

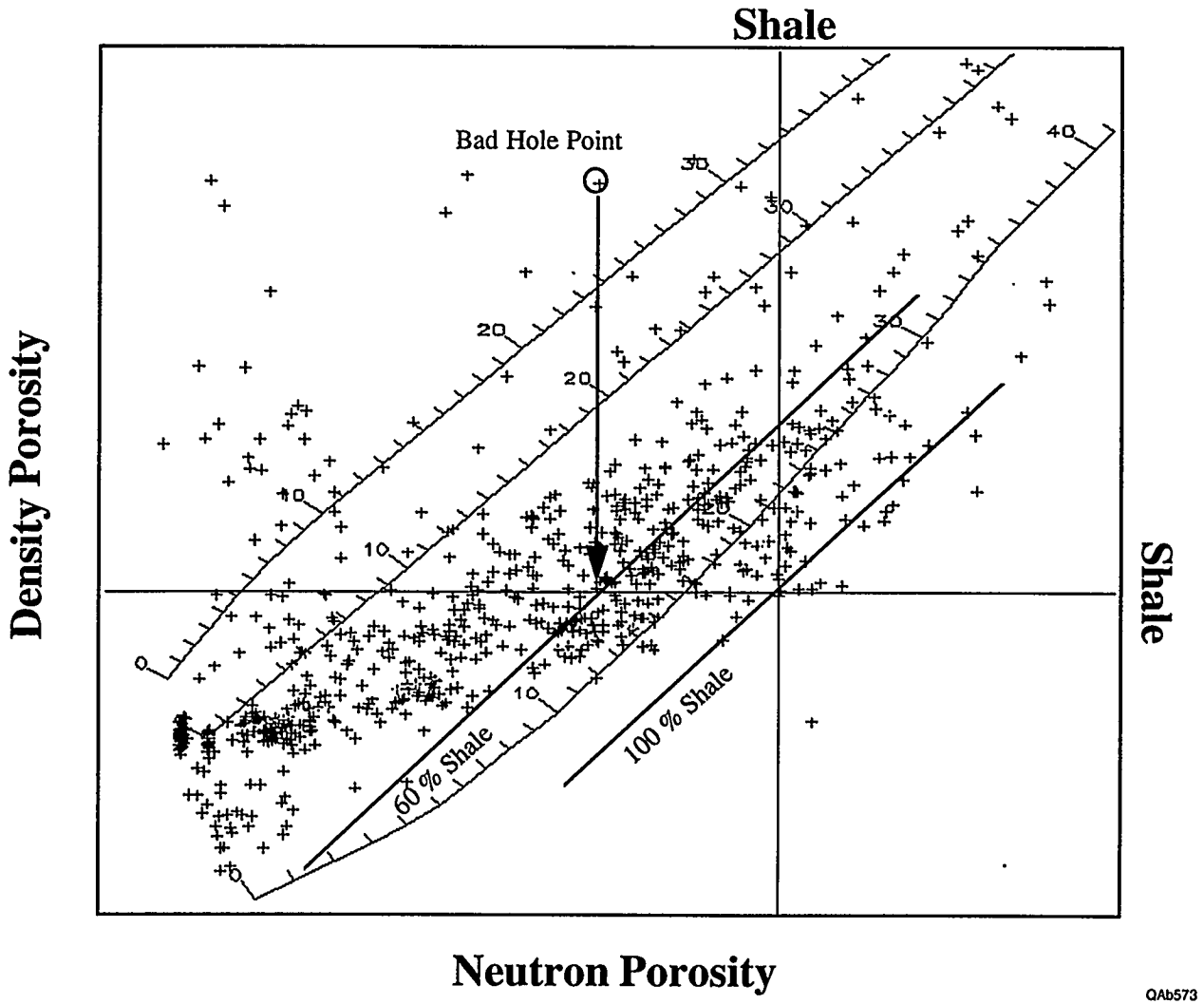

Figure C8. In bad hole, a density point is relocated along the line of the neutron porosity value until it intercepts the appropriate shale volume value. In this example, the shale volume has been calculated from the gamma-ray log to be about 60 percent.

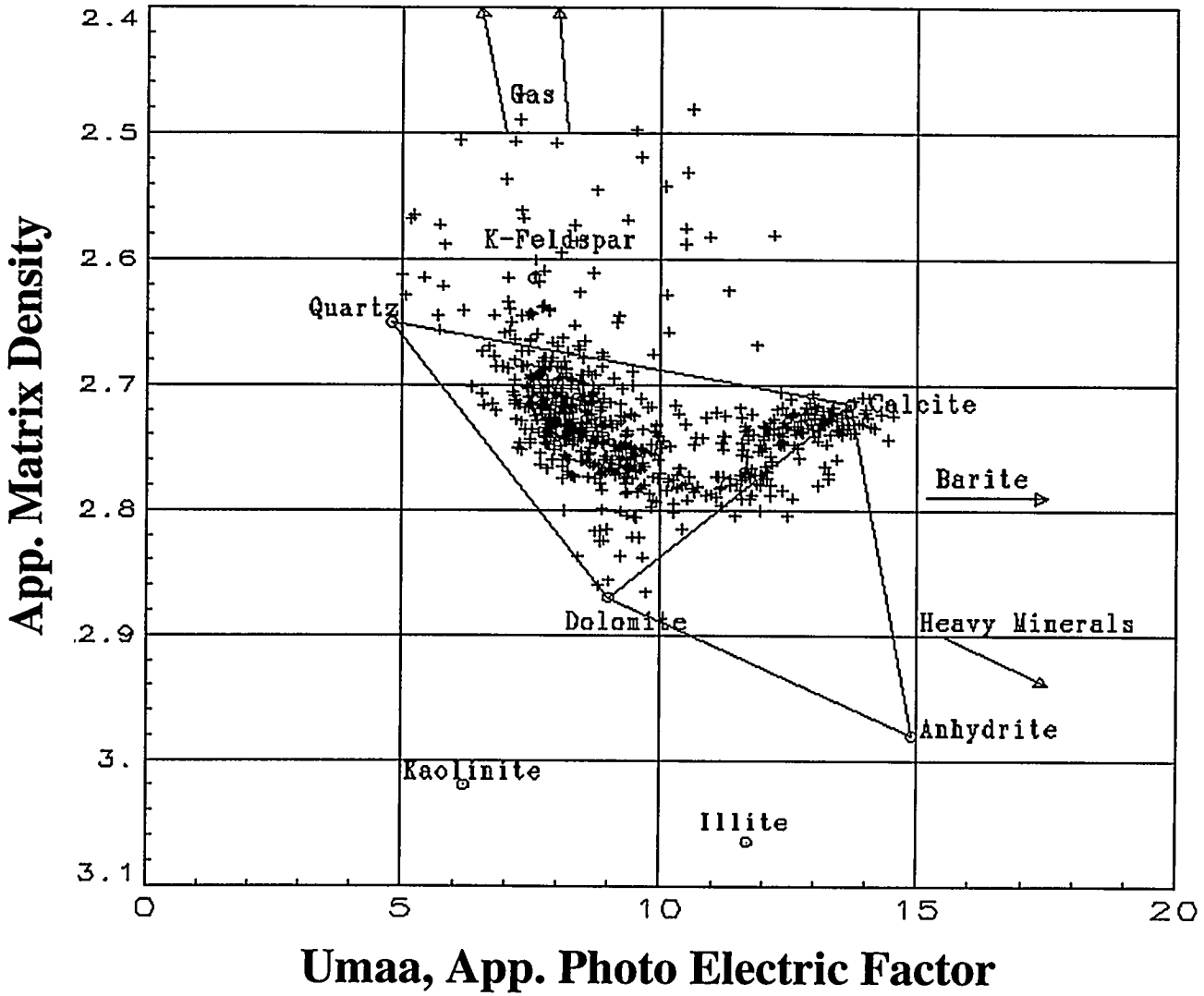

Figure C9. Cross plot of UMA/RHOG used to determine the proportions of up to four minerals in the rock.

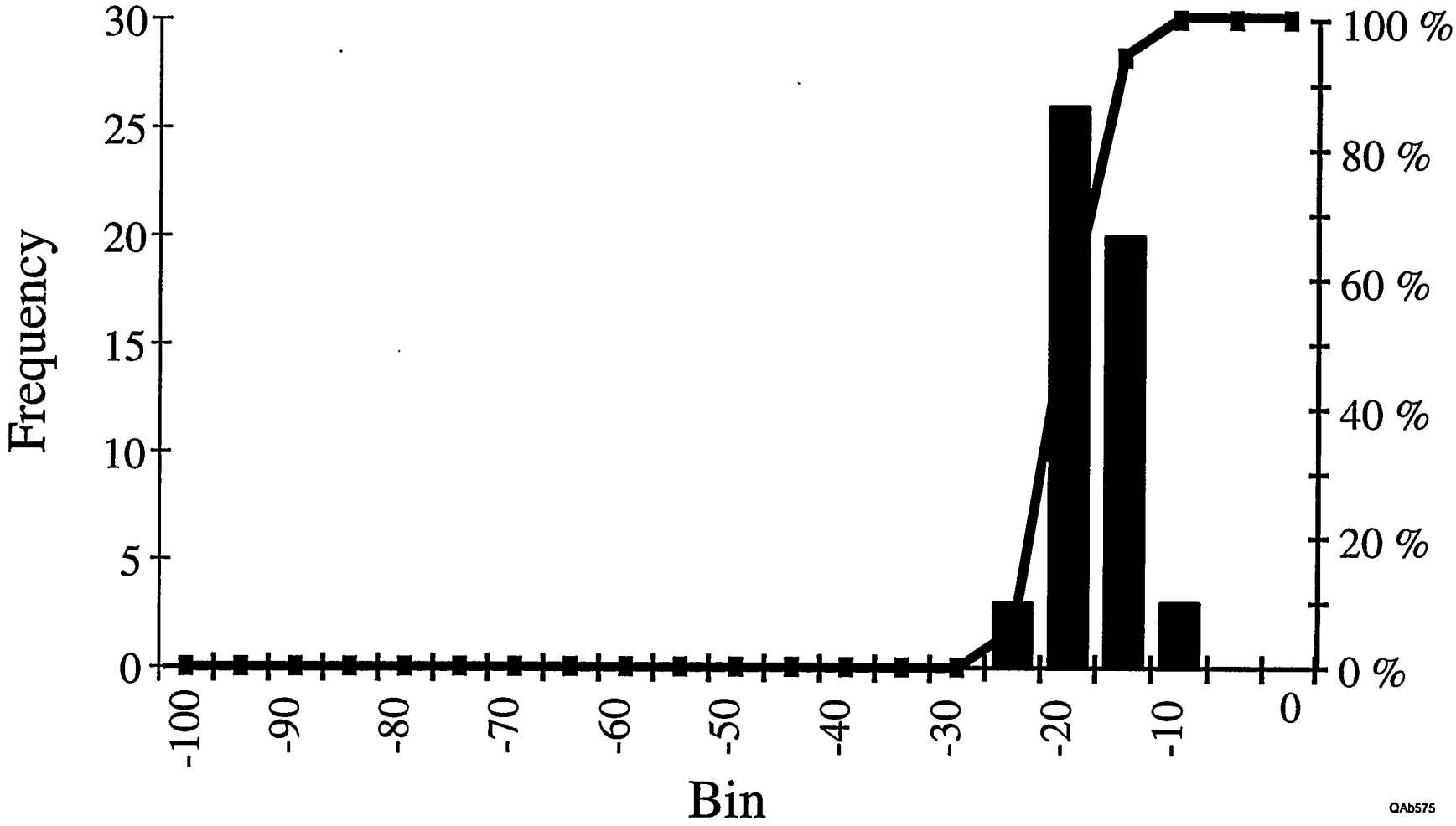

Figure C10. Histogram of the SP curve in the "A" facies.

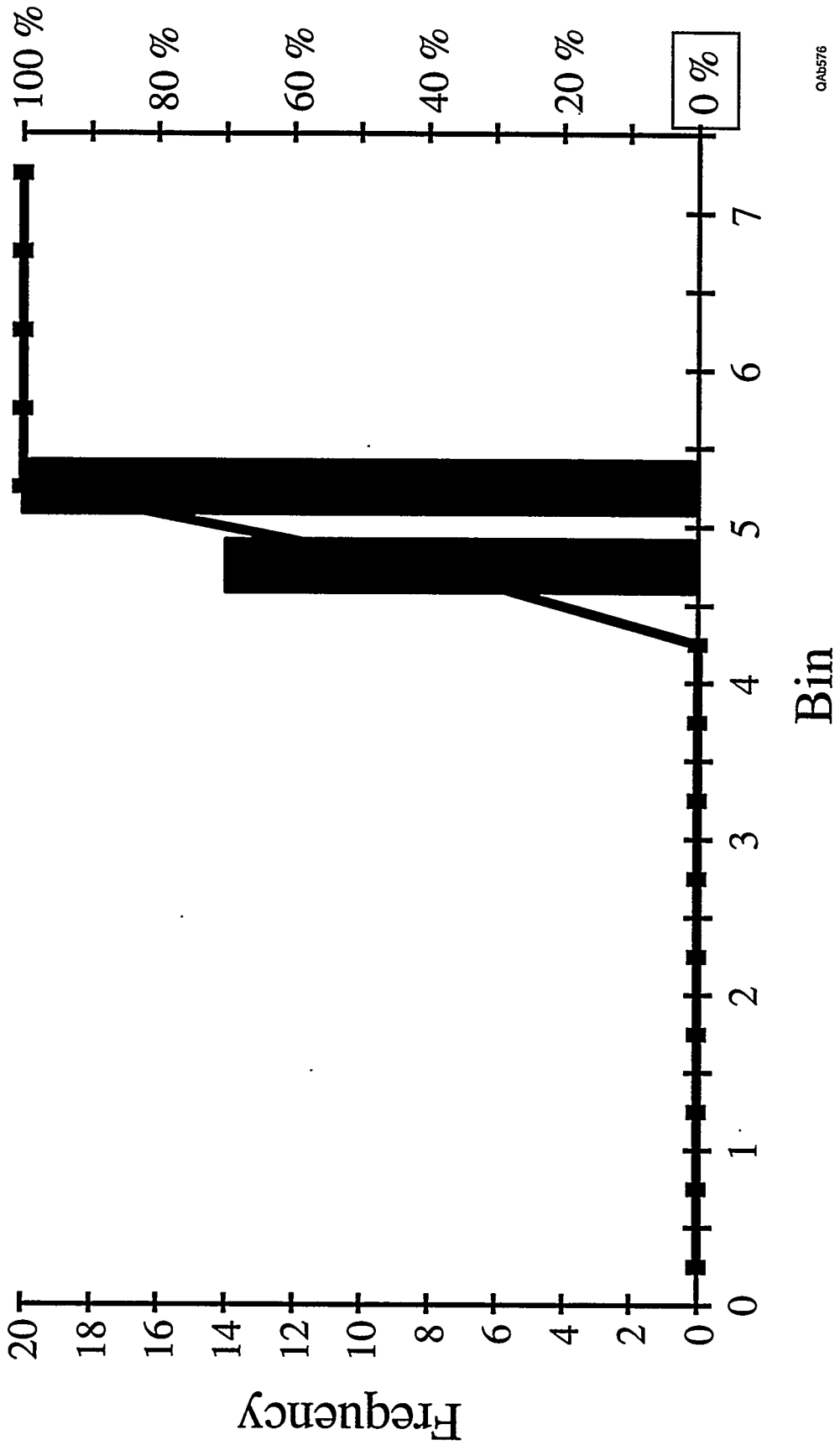

Figure C11. Histogram of the PEF curve in the "K" facies.

C.41

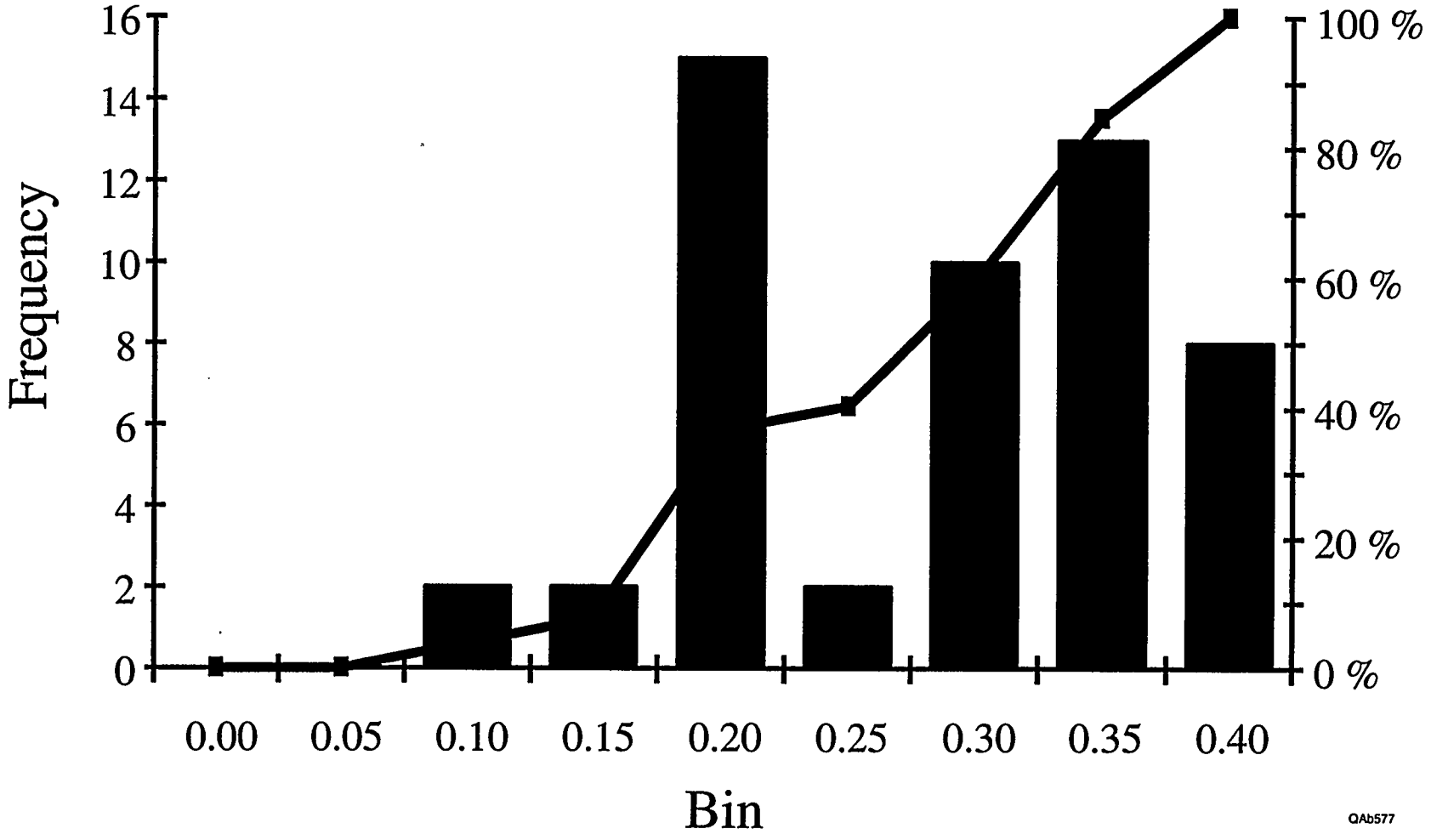

Figure C12. Histogram of the neutron curve in the "A" facies.

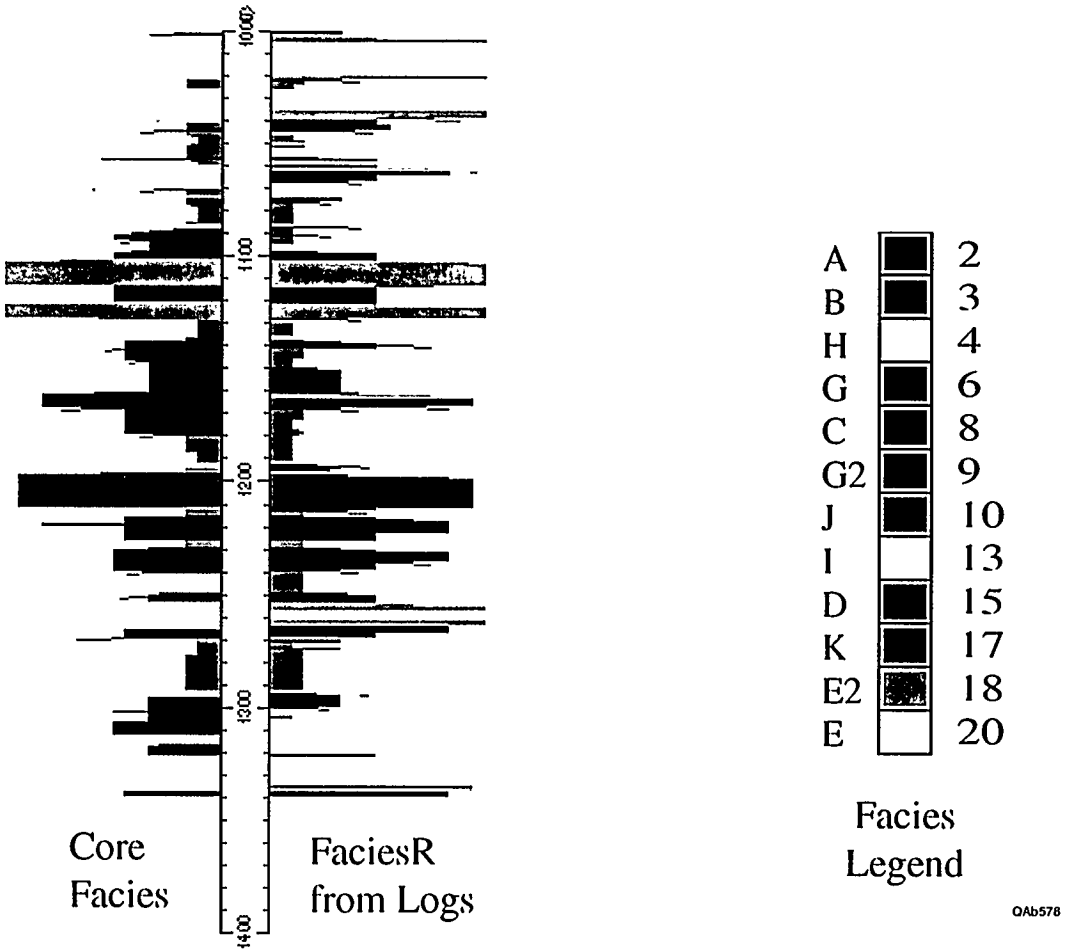

Figure C13. Geocolumn display of all core data stacked on top of one another to the left of the depth track and the corresponding log-derived facies using the FaciesR model to the right of the depth track.

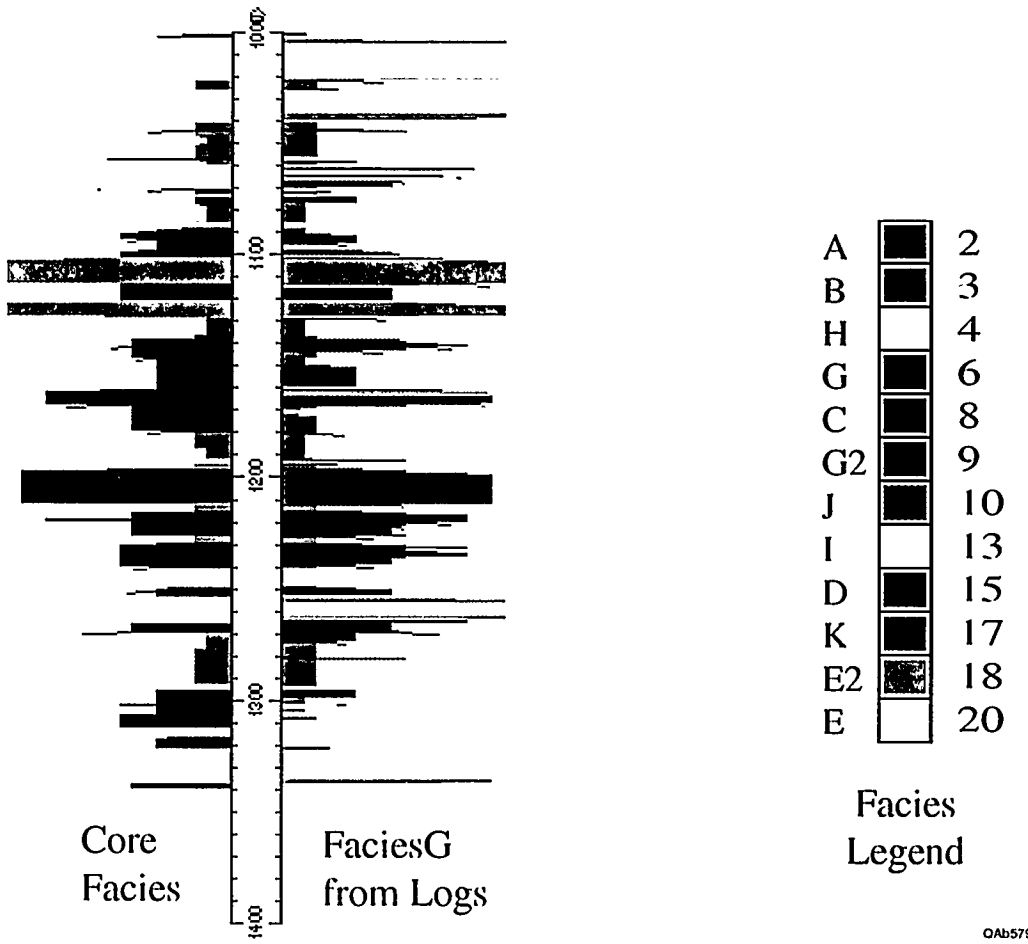

Figure C14. Geocolumn display of all core data stacked on top of one another to the left of the depth track and the corresponding log-derived facies using the FaciesG model to the right of the depth track.

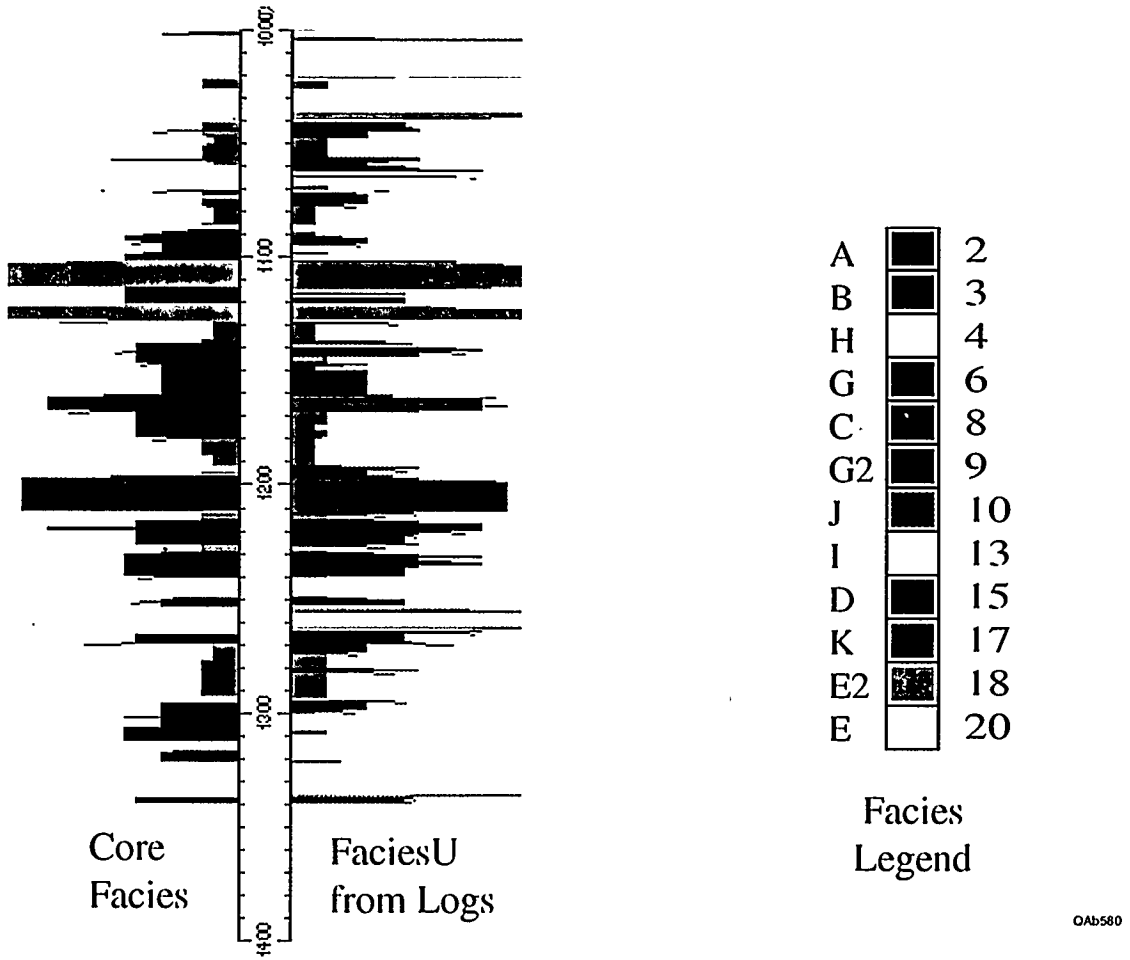

Figure C15. Geocolumn display of all core data stacked on top on one another to the left of the depth track and the corresponding log-derived facies using the FaciesU model to the right of the depth track.

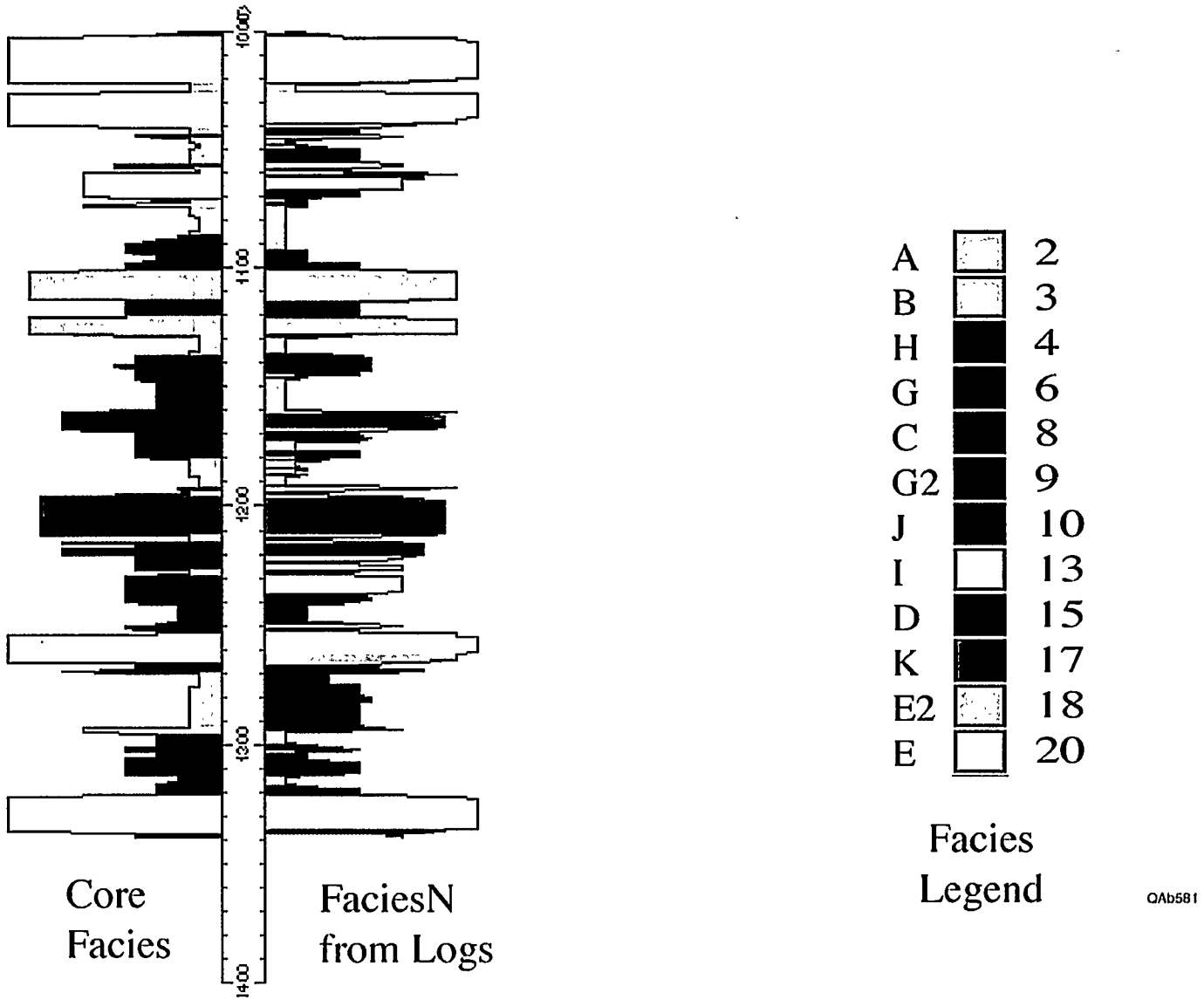

Figure C16. Geocolumn display of all core data stacked on top of one another to the left of the depth track and the corresponding log-derived facies using the FaciesN model to the right of the depth track.

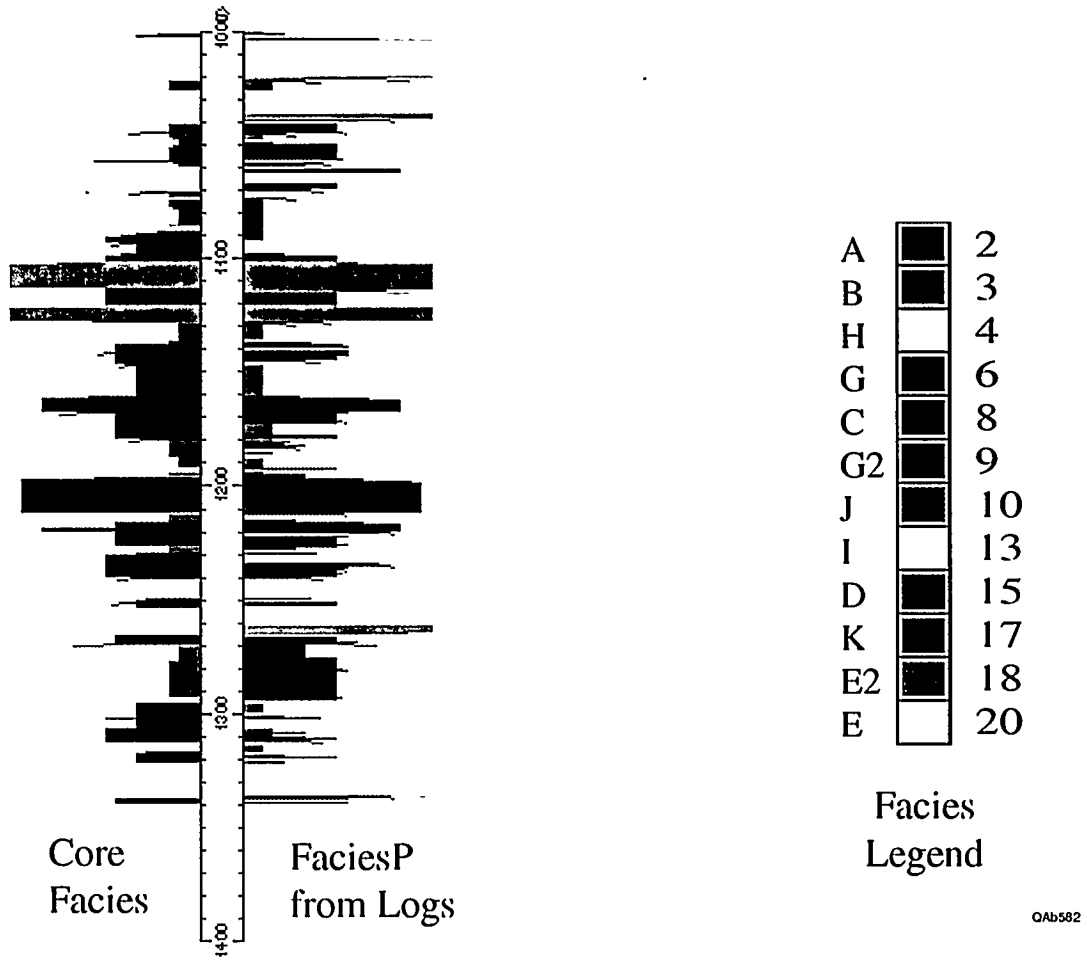

Figure C17. Geocolumn display of all core data stacked on top of one another to the left of the depth track and the corresponding log-derived facies using the FaciesP model to the right of the depth track.

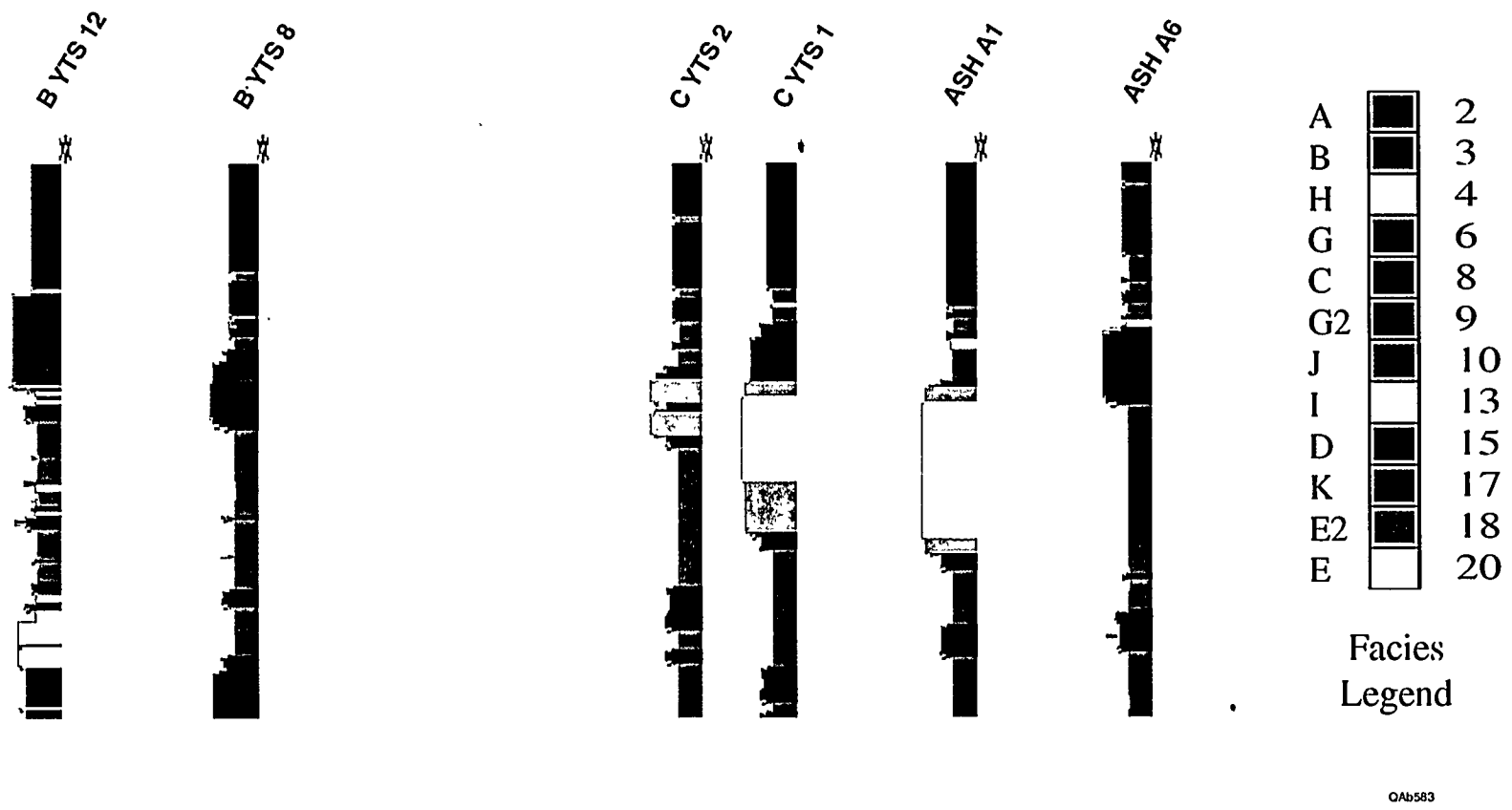

Figure C18. A geocolumn display cross section. This section is through the Caddo sequence.

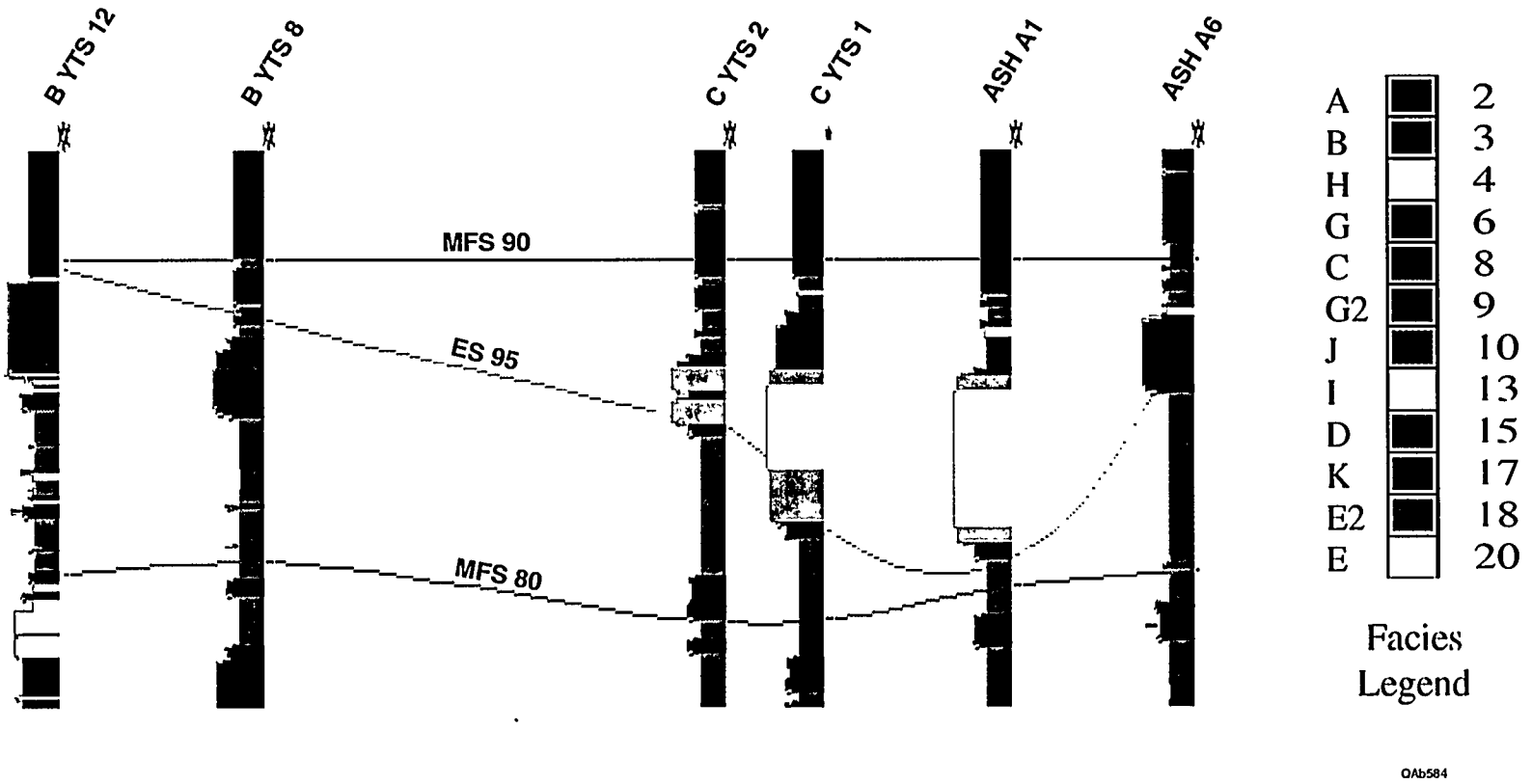

Figure C19. Interpreted version of the cross section shown in Figure C18.

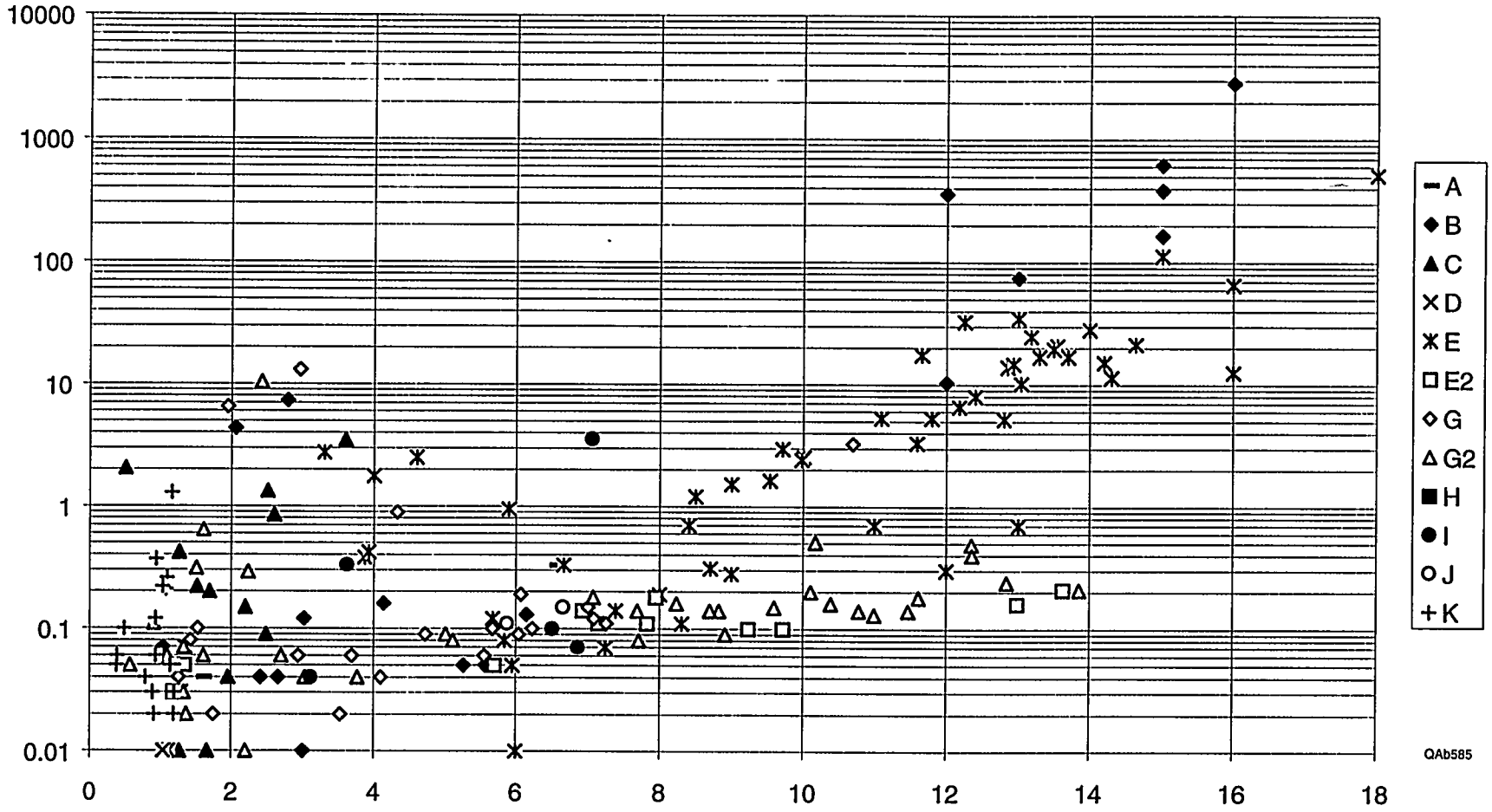

Figure C20. Cross plot of porosity vs. permeability for all core plugs from the four cored wells. The symbols represent the 12 facies described using the core data.

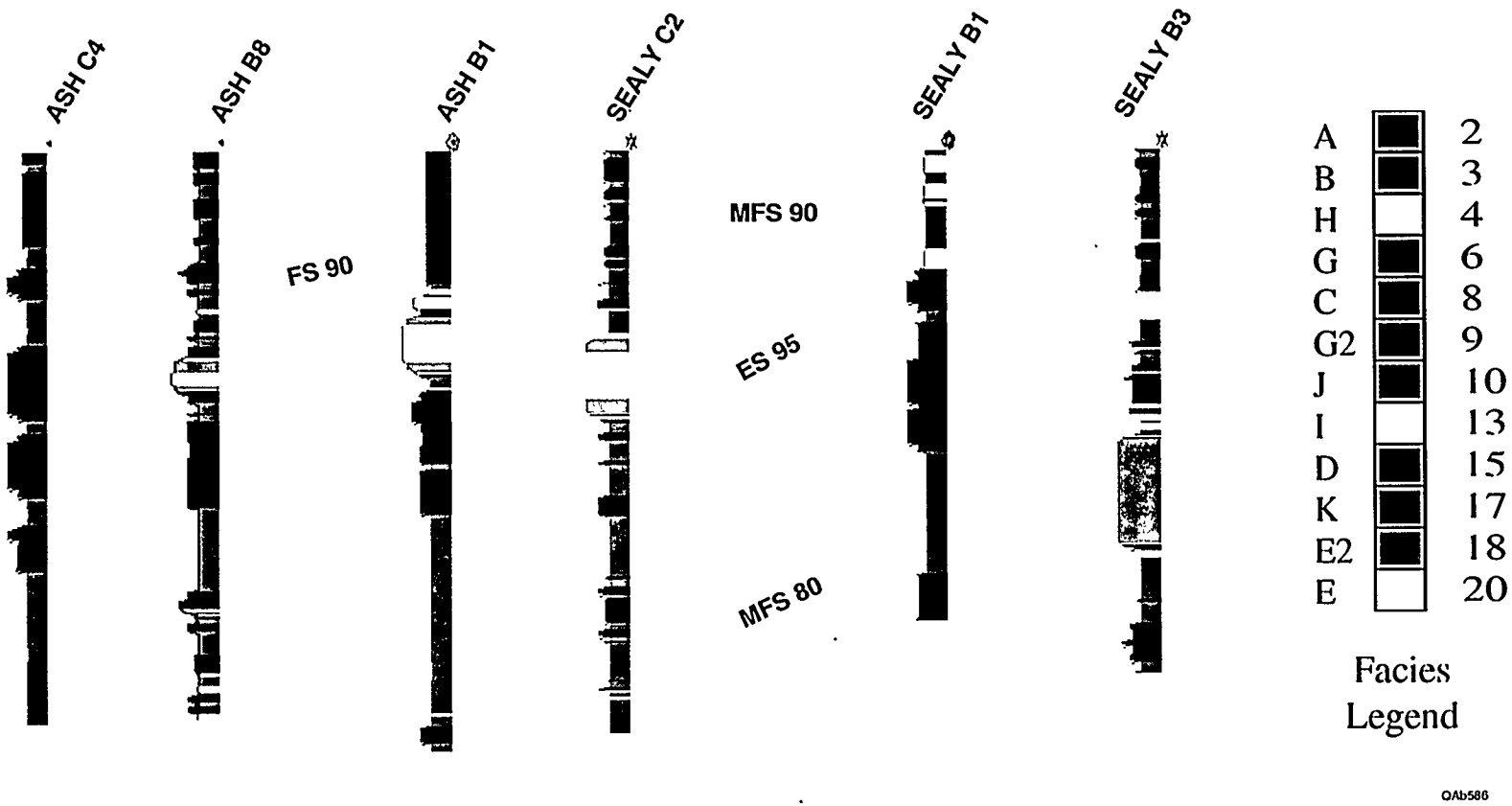

Figure C21. Cross section through the Upper Caddo in the northeast part of the study area.

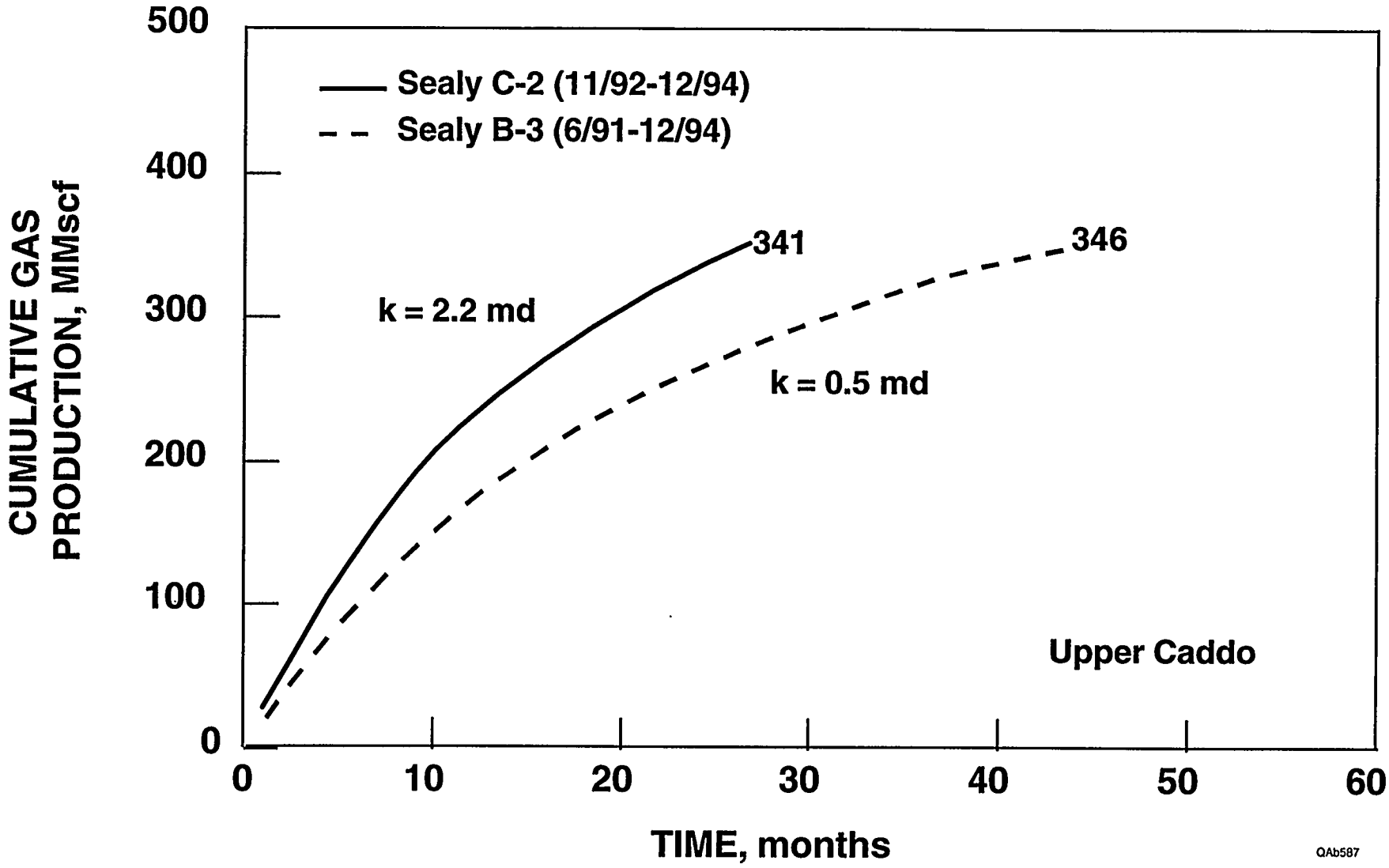

Figure C22. Production histories of the Sealy C-2 and Sealy B-3 wells; both wells are completed in the Upper Caddo.

APPENDIX D

BOONSVILLE 3-D SEISMIC PROGRAM—WAVETESTING, DESIGN, ACQUISITION, AND PROCESSING

Introduction

The 3-D seismic grid at Boonsville field covered approximately 26 mi^2, starting at the west shore of Lake Bridgeport and extending westward across Wise County and into Jack County. The positions of the source and receiver lines within the 26-mi^2 area are shown in Figure D1. Approximately half of the survey was positioned in Wise County and half in Jack County.

An extensive research effort was conducted to determine the optimal 3-D seismic field procedures that should be used to image the thin-bed reservoirs deposited in the low-accommodation conditions that existed during Atoka time on this shelf margin of the Fort Worth basin. This seismic field program involved the following research efforts:

1. Establishing vertical wavetesting as a technique for comparing seismic sources and for selecting the optimal source parameters for imaging midcontinent thin-bed reservoirs.
2. Demonstrating the value of horizontal wavetesting as a technique for determining the optimal receiver geometry to use in a 3-D seismic survey so that the recorded data have a maximum bandwidth.
3. Verifying the interpretational value of a novel, staggered-source-line, staggered-receiver-line recording geometry, which allows 3-D data to be sorted into (a) large bins with high stacking fold or (b) small bins with low stacking fold.
4. Documenting the traveltime differences, if any, exhibited by an explosive source and a swept-frequency source in midcontinent rocks.

5. Demonstrating the economic and technical advantages of using small explosive charges in shallow holes, rather than the usual convention of large charges in deep holes, as a 3-D seismic energy source in midcontinent prospects.

This section documents the research techniques used in these investigations and the technical conclusions that resulted. These research findings should apply in midcontinent basins other than the Fort Worth basin.

Wavetesting

Both vertical and conventional horizontal wavetesting were done at Boonsville field to determine the type of source that should be used and the type of receiver array geometry that should be deployed to optimize 3-D seismic data quality and to maximize seismic signal bandwidth. The first phase of the 3-D seismic program was to conduct a vertical wavetest and to record a vertical seismic profile (VSP) in the Billie Yates 11 well inside the planned 3-D seismic grid (see Figure D1 for well location).

On-site inspection of the 3-D seismic area showed that about one-third of the 26-mi^2 grid was heavily timbered, particularly in the northern and eastern portions abutted to Lake Bridgeport. Vibroseis sources could not be used in these forested areas because permitting restrictions in some properties prohibited clearing vibroseis driving lanes through the timber, and in other properties, landowners imposed excessive costs for disposing of all felled trees. As a consequence, the most logical sources to use in these timbered areas were explosives in shot holes, although these shot holes had be prepared by drills that were small enough to wend their way through the timber without having to cut any trees.

Thus, the planning for the 3-D seismic wavetesting began with the requirement that explosive sources had to be used in a large part of the survey area. Because vibroseis sources could be used in the lightly timbered southwestern half of the area and would be a more economical source than drilled shot holes, the objectives of the vertical wavetest were to

compare the effective bandwidths of vibroseis and explosives and to determine whether these two sources could (and should) be intermingled in the subsequent 3-D data acquisition effort.

Vertical Wavetesting

In Texas, different legal requirements must be met for shot hole construction, depending on whether the hole depth is less than 20 ft or more than 20 ft (Fig. D2). When a shot hole is 20 ft or more deep, a plug of bentonite at least 13 ft thick must be placed in the hole, and then a special plastic cap must be secured at the top of the hole (Fig. D2b). This shot hole construction design is a legal requirement that has been imposed in an effort to prevent surface contaminants from gaining access to subsurface aquifers. These construction requirements add a cost of about $40 to each shot hole and significantly impact the economics of 3-D seismic data acquisition.

None of these requirements is imposed when the shot hole depth is less than 20 ft (Fig. D2a). Thus, one objective of the Boonsville wavetesting was to verify whether explosives detonated in shallow holes could be an effective 3-D seismic source. Shallow holes were desired, not only for reasons of economy, but because shallow holes would be much easier to prepare by the small drill rigs that would have to be used in the timbered portions of the survey area.

The explosive charge selected for testing was the C-10 design, comprised of 10 ounces of high-velocity pentolite molded into a directional charge that focuses the energy downward (Fig. D3). These charges were planted in holes 10 ft deep with the assumption that this hole depth was adequate for good energy coupling, and yet minimal rifling (i.e., hole blowouts) would occur. This directional charge is also available as C-20 and C-30 options (20 and 30 ounces of pentolite, respectively), but these larger explosives were thought to be too powerful for a 10-ft hole depth and were not tested. C-20 and C-30 charges should be considered for programs in which shot holes are deeper than 10 ft or in which charges can be cemented in place.

During wavetesting, the C-10 charges were shot in a five-hole pattern so that 50 ounces of high-velocity pentolite were detonated as a uniformly distributed source spanning 40 ft centered about the source flag (Fig. D4). This design is a reasonable approximation of a seismic point

source. All five holes were wired in series so that if an electrical break occurred in any one of the five detonating caps, none of the charges would fire. This technique ensured that all shots recorded during wavetesting and during the subsequent 3-D recording would be consistent, in that they each involved simultaneous detonation of five 10-oz charges distributed as shown in Figure D4. No shot holes blew out during the vertical wavetesting at the Billie Yates 11 well, so it was decided that 10-ft shot holes would indeed be appropriate for the subsequent 26-mi^2 3-D grid. Later, during the 3-D seismic data acquisition, sometimes one shot hole (and in a few rare occasions, two) blew out in the five-hole arrays, but the overall negative effect of this reduced energy output for a few shotpoints randomly dispersed throughout the 3-D survey area was minimal.

The vertical wavetesting geometry used at Boonsville field is illustrated in Figure D5. Twelve five-hole arrays, each array designed as diagrammed in Figure D4, were prepared at an offset distance of 420 ft (Fig. D5b), and the wavefields generated by these shots were recorded at vertical intervals of 500 ft as the receiver was lowered down the Billie Yates 11 well (Fig. D6). These vertical wavetest data were numerically analyzed on site to determine the energy level and the spectral bandwidth of the pentolite-generated wavelet as it propagated down to, and through, the targeted Atokan-age Bend reservoirs occurring between depths of 4,500 and 6,000 ft (approximately) in the Billie Yates 11 well.

The spectra of the down-going pentolite wavelets were calculated within minutes of recording each wavelet so that on-site decisions could be made about how to set vibrator parameters to create a vibroseis wavelet that would equal or surpass the energy content and the bandwidth of the pentolite wavelet. These on-site spectral calculations are plotted in Figure D7 and show that these small, shallow, directional charges produce a remarkably broadband signal spectrum exceeding 200 Hz.

Western Geophysical, having been alerted that the Bureau wanted to achieve the widest possible bandwidth in this vertical wavetest, had its chief vibrator engineer, together with Pelton's Vice President of Research, on site to test Pelton's newest vibrator electronics control

system. On the basis of the pentolite bandwidth evidence (Fig. D7), these engineers were instructed to begin tests to confirm that the vibrator to be used for the vibroseis portion of the vertical wavetesting could demonstrate acceptable ground-force-phase-locking between 10 and 200 Hz. After extensive effort, it was decided that ground-force-phase-locking could not be achieved above 160 Hz, so the vibroseis vertical wavetesting, conducted on the upward trip of the downhole receiver, was done using a 6–160-Hz nonlinear sweep. The resulting wavetest data comprised a zero-offset VSP (Fig. D8) and also allowed the spectra of the down-going vibroseis wavelets to be calculated at the same receiver depths that pentolite wavelets had been analyzed (Fig. D9).

These vertical wavetest data demonstrated that both pentolite and vibroseis sources would produce exceptional wideband data in the Boonsville survey area. Most important, the vertical wavetests confirmed that the small C-10 directional charges would be an excellent source option when they were detonated in shallow (10-ft) shot holes. On the basis of this vertical wavetest, it was decided that the shot hole array design shown in Figure D4 would be used for the entire 26-mi^2 survey, and that pentolite and vibroseis sources would not be intermingled in the data recording.

Horizontal Wavetesting

The vertical wavetesting program conducted in the Billie Yates 11 well defined the source (C-10 directional charges) that should be used in the Boonsville 3-D seismic program. The next phase of the seismic program was to conduct horizontal wavetesting to determine the receiver array design that should be used. This receiver testing was done approximately 1 mile north of the Billie Yates 11 well (Fig. D1).

The vertical wavetesting had already documented that the C-10 directional charges selected for the Boonsville energy source, when deployed in shallow 10-ft holes, could illuminate the targeted thin-bed, Atokan-age reservoirs with a wavelet having a frequency content as high as

200 Hz (Fig. D7). The objective of the horizontal wavetesting was to determine what receiver array geometry would best preserve these high frequencies in the reflected wavefield.

The basic concepts of receiver array design are summarized in Figures D10 and D11. Receiver design theory requires that the time-moveout across a receiver array not exceed one-half of the time period associated with the highest frequency component that is to be recorded. If we assume that the maximum recorded frequency is 200 Hz, this requirement means that the array moveout cannot exceed (1/2)(1/200 Hz) = 2.5 ms. According to the array moveout equation in Figure D10, the array length L that satisfies this design criterion is

$$L = (0.0025\, t_o\, V^2)/X, \tag{1}$$

where t_o is the one-way travel time to the reflector that is to be imaged, V is the average velocity to that reflector depth, and X is the offset distance between the subsurface reflection point and the center of the receiver array. Using the values

$t_o = 0.45$ s for the Atoka reservoirs,

V = 12,000 ft/s for the average velocity to these reservoirs, and

X = 5,000 ft for the maximum offset

results in L having a value of 32 ft.

Now that theory has specified the desired length L of the surface receiver array that will not attenuate 200 Hz data in the reflected wavefield, the next requirement is to decide how far apart adjacent receiver arrays should be so that this 200-Hz-frequency component is not attenuated by the trace-to-trace normal moveout (NMO) corrections that are done to the recorded data. The NMO requirement that has to be imposed on the receiver spacing is shown in Figure D11. This requirement states that the time moveout DT between adjacent receiver stations N and (N-1), which are a distance DX apart, should not exceed the time moveout dt across the array of length L, or

$$(DT/DX) \leq (dt/L). \tag{2}$$

The objective is to determine what the receiver spacing DX should be. Reordering equation 2 and ignoring the inequality sign gives

$$DX \sim (DT/dt)L. \tag{3}$$

The maximum allowable array moveout dt has already been defined as $(0.5/f_m)$, where $(1/f_m)$ is the time period of the maximum frequency component in the reflected wavefield. Array designers use a similar logic to define the maximum trace-to-trace moveout DT and set DT equal to $(0.5/f_d)$, where $(1/f_d)$ is the time period of the dominant frequency component in the reflection data. This logic is followed because as long as the dominant wavefield frequency is preserved in the trace-to-trace reflection moveouts, the normal moveout corrections for the reflection event can be accurately calculated. Equation 3 can thus be rewritten as

$$DX \sim (f_m/f_d)\, L. \tag{4}$$

If $f_m = 200$ Hz and we assume $f_d \sim 40$ Hz, then

$$DX \sim 5\, L, \tag{5}$$

or DX ~ 160 ft. On the basis of this theory and the attendant assumptions, receiver groups should not be separated much more than 200 ft, and preferably less than 200 ft.

Using this array design theory, the horizontal wavetest program was laid out as illustrated in Figure D12. Three source stations, spaced at intervals of 2,640 ft, were prepared in an east-west direction. Three five-hole arrays were drilled and loaded at each of these source stations, following the design shown in Figure D4. To measure reflection wavefields in both the inline and crossline directions relative to each shot, receiver lines were laid out in both east-west and north-south directions. Each line had 24 receiver stations with a spacing of 220 ft between adjacent receiver flags, which is a spacing roughly equivalent to that determined by the logic leading to equation 5. This geometry allowed reflection wavefields to be recorded for source-to-receiver offsets ranging from 220 ft to 10,560 ft, an offset range greater than what would be

required to image the targeted Atokan-age reservoirs occurring at depths between 4,500 and 6,000 ft.

Three receiver array designs were deployed at each receiver flag (Fig. D12b). In design 1, 12 inline geophones were spaced 10 ft apart to form a linear array 110 ft long; in design 2, 12 geophones were spaced 3 ft apart to form a linear array 33 ft long; and in design 3, 12 geophones were clustered inside a circle having a diameter of approximately 3 ft. In concept, the two smaller arrays should preserve the high-frequency components of the reflected wavefield (see comments related to equation 1) but should not cancel low-frequency ground roll, whereas the larger 110-ft array should attenuate some of the ground roll but perhaps also attenuate some of the high frequencies in the reflected signal. The purpose of the horizontal wavetesting was to determine which array design recorded a wavefield that had the desired wide reflection bandwidth but still reduced the ground roll noise to an acceptable level.

Some of the wavetest data recorded with these receiver design options are shown in Figures D13 and D14. In each array geometry, the data are dominated by ground roll noise, and no reflection events are obvious in any of the receiver responses. To determine whether reflections were present underneath the high-amplitude noise, the data were transformed into the frequency-wavenumber (f-k) domain. The value of these transforms (Figs. D15 and D16) is that they reveal energy alignments over a much wider range of amplitudes (typically 60 dB or more) than can be determined by a visual inspection of wiggle trace data (typically a range of only 20 dB or less).

Even in this high-resolution f-k domain, there was little evidence of reflection events, and the obvious implications were that the minihole shots created a strong ground roll and that there was probably a considerable amount of near-surface scattered noise also. On the basis of these horizontal wavetests, a 3-D receiver array length of 110 ft was selected over the shorter length of ~30 ft, which was anticipated would be supported by the test results. This longer array length was chosen because, due to the obvious generation of strong ground roll at this test site, it seemed wiser to have a reasonably long array that would partially attenuate ground roll than to

have a short array that would ensure that frequencies greater than 150 Hz were not severely attenuated.

Design

Staggered-Line Geometry

A unique 3-D source-receiver geometry, referred to as a staggered-line grid, was implemented at Boonsville field. The geometrical pattern that was used is illustrated in Figure D17. In this geometry, adjacent source lines were shifted by one-half of the source interval, and, likewise, adjacent receiver lines were shifted by one-half of the receiver interval. This recording technique allowed the data to be sorted into large, higher fold bins [measuring (0.5 × source interval) × (0.5 × receiver interval)] or into small, lower fold bins [measuring (0.25 × source interval) × (0.25 × receiver interval)]. At Boonsville, the receiver and source intervals were both 220 ft, so the sizes of the two stacking-bin options provided by this staggered-line geometry were 110 × 110 ft and 55 × 55 ft, as shown in Figure D17.

This recording geometry allowed higher fold, large-bin data to be used as the primary data set for determining accurate residual statics and precise stacking velocities and for a first-pass interpretation, and lower fold, small-bin data to be used when greater lateral resolution was needed in the interpretation process. The advantage of this staggered-line technique is that the increased lateral resolution it provides is accomplished by directly sorting the data into small bins during the stacking process and not by doing some type of poststack trace interpolation that converts a large trace spacing to a smaller trace spacing.

Line Spacing and Stacking Fold

As shown in Figure D17, the basic field design plan was to space receiver lines 880 ft apart and to separate source lines a distance of 1,320 ft. This source-receiver line geometry was surveyed over the 26-mi^2 3-D seismic area, except that in some locations, the line spacings were

varied to avoid production facilities and to minimize cultural problems. The stacking folds that resulted from this geometry when the data were sorted into 110- × 110-ft bins and then into 55- × 55-ft bins are shown in Figures D18 and D19, respectively. The increased stacking fold shown along the east and south margins of the grid resulted because extra source stations were drilled in these areas to cause the stacking fold to build to a high level rapidly. The two stacking-fold distributions in Figures D18 and D19 differed by a factor of 4, as expected, because the respective stacking bin areas differed by a factor of 4.

Acquisition

Recording System

Northern Geophysical used an I/O System Two to record the Boonsville 3-D data. This modern seismic recording system was important in the project because it generated 24-bit data words to increase dynamic resolution and to allow lower amplitude reflection signals to be extracted from noisy field records than could have been if the data had been recorded with a system that generated 16- or 18-bit data words. Horizontal wavetesting had already shown that noisy field records and weak reflection amplitudes would be common inside the Boonsville grid (Figs. D13–D16).

Recording Aperture

The Atokan-age reservoirs at Boonsville field occur at depths from 4,500 to 6,000 ft, so the 3-D receiver aperture was designed as eight adjacent receiver lines, each 2.5 mi long, as shown in Figure D20. This aperture created a maximum source-receiver offset of 6,600 ft in the north-south direction and 3,520 ft in the east-west direction (Fig. D20). Ideally, the east-west offset should also have been ~6,000 ft (the depth of the deepest reservoir to image), but an aperture of this size was not possible because the data were recorded at a sample rate of 1 ms. The eight-line aperture in Figure D20 contains 468 receiver stations (61 stations/line × 8 lines), and the I/O

System Two could not record significantly more data channels without resorting to a data sample rate of 2 ms. A sample rate of 1 ms was preferred over 2 ms so that the high-frequency components of the wavefield (>150 Hz) would not be attenuated by the alias filter in the recording system. Subsequent data analysis showed that this aliasing concern was not justified, and a sample rate of 2 ms and a wider east-west recording aperture could have been used.

Data Recording in Nonoverlapping Apertures

Typically, 3-D seismic data are recorded using continuously overlapping receiver apertures. In this standard industry technique, energy sources are activated at successive source stations that are juxtaposed immediately next to each other to form a continuous, unbroken movement of the seismic source across the survey area. Each source wavefield is recorded by an appropriate receiver aperture that also moves uniformly and continuously in space to stay centered about the moving source point; i.e., the receiver apertures continuously overlap from source point to source point.

The I/O System Two seismic recording system used in the Boonsville study allowed a much greater flexibility for defining which source points and what receiver apertures could be recorded. Specifically, the system removed the requirement of a continuous overlapping receiver aperture and allowed data to be recorded in widely separated, nonoverlapping receiver apertures whenever that procedure expedited the data collection activity.

All of the shot hole arrays inside the 26-mi^2 Boonsville survey were drilled and loaded before any receivers were deployed. Once an appropriate number of receiver lines (12 to 15) were laid out across the entire north-south extent of the grid (typically 5 mi of cable per line, Fig. D1), the flexible I/O software allowed the receiver aperture diagrammed in Figure D20 to be activated about any source point falling inside a north-south-oriented strip roughly 1 mi wide (east-west) passing through the center of this grid of 12 to 15 north-south receiver lines.

This ability to *turn on* a receiver aperture anywhere within this large recording strip introduced considerable efficiency into the field recording process. Specifically, with this

capability the speed of data recording was controlled more by how many shooters were in the field than by any other factor. To illustrate the concept, a hypothetical recording scenario using this flexible positioning of a receiver aperture is depicted in Figure D21. In this example, 22 receiver lines are assumed to be laid out, and three shooters are positioned across the receiver grid at locations S_1, S_2, and S_3. The recording truck can be positioned anywhere in this 22-line grid and still be electrically connected to the entire grid. At Boonsville, each source line segment S_1, S_2, and S_3 spanned four shotpoints because the receiver line spacing was 880 ft and the shotpoint interval was 220 ft (Fig. D17). Receiver aperture $A_1B_1C_1D_1$ is turned on first, and shooter S_1 connects a shooting box to one of the four minihole arrays spanned by distance S_1. Once the data from this shot are recorded, receiver aperture $A_2B_2C_2D_2$ is activated, and shooter number 2 electrically connects a minihole array inside source segment S_2 to the recording truck. As soon as this shot is recorded, receiver aperture $A_3B_3C_3D_3$ is turned on, and shooter number 3 electrically connects a shotpoint inside segment S_3 to the recording truck. The shooting sequence then returns to shooter 1, who has moved to a new shotpoint inside segment S_1.

This technique of recording arbitrarily positioned receiver apertures allows shooters to be widely separated over a 3-D grid for optimal field flexibility, and modern recording systems, like the I/O Systems Two or its equivalent, allow the appropriate receiver aperture to be quickly centered (in an electrical sense) about the X-Y coordinates of the selected shotpoint. This technique cannot be used easily with most older recording systems, so when it is desired to implement this procedure of recording nonoverlapping receiver apertures, a modern recording system with the proper acquisition software should be contracted.

Although this technique of using nonoverlapping receiver apertures is attractive for dynamite shooting when a large area of shot holes has been drilled and preloaded, it does not have as much appeal for vibroseis recording unless a large number of vibrators are mobilized so that two or more vibrator source arrays can be created and positioned at different locations inside the 3-D grid.

Data Quality

An example of the Boonsville data recorded using the source-receiver concepts and the recording geometry described in the preceding sections is shown in Figure D22. Data from only five of the eight receiver lines involved in this particular recording aperture (see Fig. D20) are shown. Each displayed line contains 61 traces representing the responses recorded at the 61 receiver stations distributed over the north-south extent of the receiver line.

These records are typical of most data recorded across the Boonsville grid in that they contain a considerable amount of ground roll noise, and only a few reflection events can be seen. The strong ground roll noise was not unexpected, on the basis of the horizontal wavetesting results (Figs. D13–D16). Vertical seismic profiling had already confirmed that numerous reflection events would be created (Fig. D8), so the extraction of these relatively weak, wideband reflection signals from field records of this quality presented a challenging data-processing problem. The data-processing techniques used to create 3-D seismic images from these Boonsville records are discussed in the following sections.

Processing

The Boonsville 3-D data were processed by Trend Technology, Inc., Midland, Texas. Trend imposed stringent processing requirements to preserve the high frequencies that were known, from vertical wavetesting, to exist in the reflection signals generated by the C-10 directional charges used as the energy source at Boonsville field. Because many field records had a high level of noise contamination (Fig. D22), the processing procedures that Trend used produced remarkably good 3-D images of the targeted Atokan thin-bed stratigraphy. The data-processing technology used to image the thin-bed reservoirs distributed throughout Boonsville field are summarized in Table D1, and the more critical components of this processing procedure are described in the following sections.

Table D1. Boonsville 3-D processing sequence.

(1)	Surface and Subsurface Maps
(2)	Geometry Definition and Application
(3)	Prefilter 17-250 Hz
(4)	Surface-Consistent Deconvolution
(5)	Refraction Statics: Datum = 900 ft, Velocity = 8000 ft/s
(6)	Velocity Analysis
(7)	Refraction Statics: Datum = 900 ft, Velocity = 8000 ft/s
(8)	CDP Stack
(9)	Automatic Residual Statics: Iterate 6 Times
(10)	Velocity Analysis
(11)	Normal Moveout
(12)	Spectral Balance
(13)	CDP Residual Statics
(14)	CDP Stack (55- and 110-ft bins)
(15)	Interpolate Missing CDP's at edges of data volume (55-ft bins only)
(16)	3-D Migration

Deconvolution Tests

Vertical wavetesting demonstrated that the small C-10 directional charges used as the seismic source at Boonsville field produced a seismic wavelet having frequencies of up to 200 Hz (Fig. D7). However, horizontal wavetesting showed that reflection signals having this wide bandwidth would be masked by strong, low-frequency ground roll and surface-related noise (Figs. D13–D16). Consequently, one of the early processing tests was to determine what usable signal bandwidth actually existed in the 3-D field records because the dynamic range of the data was significantly enhanced by the availability of the 24-bit data words created by the I/O System Two data acquisition hardware.

Some of these bandwidth investigation results are shown in Figures D23 and D24. In each example, the raw field record and its associated frequency analysis are displayed on the left. The right-hand display shows the same field record after the noise has been attenuated by a low-cut

filter, and the higher frequency components have been emphasized by an appropriate deconvolution operator. These tests demonstrated that wideband reflections did indeed exist throughout the Atokan interval (approximately 0.8 to 1.0 s) and that the reflection signals contained robust energy spanning a frequency range from about 10 Hz up to approximately 150 Hz. Although the initial goal of preserving frequencies up to 200 Hz in the raw field records appears not to have been realized, the spectra resulting from these tests still had impressive bandwidths that spanned almost four octaves.

Static Corrections

Because the Boonsville data contained reflection signals with frequencies as high as 150 Hz, precise static corrections were essential to preserve the high-frequency components of these signals in the final 3-D images. In addition to correcting the shot and receiver elevations to a uniform depth datum, both refraction statics and residual statics were calculated and applied as iterative processes until the time shifts that had to be applied to the traces that were summed in each stacking bin converged to an acceptably small value.

The refraction statics calculated for the Boonsville survey are shown in Figure D25. Two iterations of refraction statics were done (Table D1), with each iteration improving the accuracy of the velocity analysis and the resulting stacked image. The large corrections shown at the edges of the maps in Figure D25 should be ignored because these values are extrapolations of the real static corrections beyond the boundaries of the actual seismic grid. However, valid static corrections as large as 30 ms were required at some source and/or receiver coordinates, which are significant time shifts for frequencies exceeding 100 Hz. For example, the 100- and 150-Hz components of the reflected wavefield have time periods of 10 and 6.7 ms, respectively. Thus, a static correction of 20 ms is equivalent to a time misalignment of two full wavelengths of the 100-Hz component of the reflection signal and three full wavelengths of the 150-Hz component, which is the upper bound of usable signal frequency at Boonsville.

Normally, refraction statics are calculated only once. A second refraction statics analysis was done with the Boonsville data to confirm that the time picks used in the first analysis were correct. A two-pass refraction statics effort is a good procedure to use when the processing objective is to ensure that high-frequency stacked data are to be created.

The residual static calculation procedure in Table D1 was a six-stage iteration process, and the static corrections determined in the first and fourth iterations are displayed in Figure D26. (The fifth and sixth iterations were localized to small areas where there appeared to be cycle skips in the static calculations.) The first residual static calculation showed that, although the preceding refraction static corrections (Fig. D25) had significantly improved the trace alignments needed for optimum stacking, major static errors of 6 to 8 ms (approximately one wavelength of the higher frequency components) still existed in much of the 3-D grid. As shown in Figure D26, the residual static corrections converged with each iteration, finally reaching the desired objective where no static correction exceeded one time sample (± 1 ms) anywhere inside the 3-D grid. (During the 3-D data interpretation, two locations were found where the migrated data appeared to have a static-induced cycle skip.)

Velocity Analysis

Often velocity analyses are performed at intervals of approximately .5 mi across a 3-D seismic grid, and the optimal stacking velocities at these analysis sites are then used to construct an areal velocity map that can be used to stack data at every common depth point (CDP) in the grid. A much more detailed velocity analysis was done at Boonsville field so that the high-frequency portion of the reflection wavefield would be properly time shifted by the velocity moveout corrections before traces were summed at any of the CDP locations.

Specifically, velocity analyses were done along east-west lines separated by only 440 ft; i.e., along every fourth row of the 110- × 110-ft stacking bins inside the 3-D grid. Within each of these east-west lines, a velocity analysis was done at every CDP, not at CDP's spaced .25 or .5 mi apart, using 50 different velocity functions. As a consequence, approximately 850,000

velocity panels were created across the Boonsville survey area, which is about two orders of magnitude more velocity information than is usually used to determine stacking velocities.

The reason for doing such detailed velocity analyses can be demonstrated by considering a simple mathematical approximation of the normal moveout experienced by a reflection event from the Atoka interval at Boonsville field. Mathematically, the normal moveout of a reflection event (i.e., the difference between the reflection arrival times at a zero-offset receiver and at a far-offset receiver) can be approximated by the equation,

$$\Delta t = \frac{X^2}{2V^2 t_o}, \tag{6}$$

where Δt is the normal moveout in seconds, X is the offset distance to the receiver in feet, V is the average velocity in ft/s down to the reflector depth, and t_o is the reflection arrival time in seconds at the zero-offset receiver position (i.e., at X=0). If we assign the values,

X = 6,000 ft (approximately the largest receiver offset) and

t_o = 0.8 s (approximately the top of the Bend interval),

and allow the average velocity V to have first a value of 12,000 ft/s and then a value of 12,200 ft/s, then the moveout corrections applied to a trace at an offset of 6,000 ft for each of these velocity possibilities are 156 and 151 ms, respectively. The time difference of 5 ms between these two time adjustments is approximately the same as the 6.7-ms time period of the 150-Hz component of the reflection signal. Thus, the objective that frequencies as high as 150 Hz be preserved during the Boonsville data processing required that the stacking velocities be determined over the complete 3-D grid to an accuracy of approximately ± 50 ft/s, which is a demanding requirement.

This type of detailed velocity study was done twice during the data processing (Table D1). Examples of the final stacking velocities determined at Boonsville are given in Figures D27 through D29. Figure 27 shows the north-south velocity behavior along inlines 100 and 200, whereas Figure D28 shows how the stacking velocity varies in an east-west direction along

crossline 200. Figure D29 is a time slice through the 3-D velocity volume at 1,100 ms, showing how the velocity varies in an areal sense just below the lowest Atokan-age reservoir.

Spectral Balancing

Of all the numerical procedures used during the processing of the Boonsville 3-D data, spectral balancing probably had the greatest positive impact on data quality. Because spectral balancing is a lengthy numerical calculation, as will be explained, the Boonsville data were stacked first without using spectral balancing to determine whether acceptable reservoir images could be produced by conventional processing. In this preliminary stacking effort, the application of standard deconvolution algorithms comprised the principal procedures used to preserve the widest possible data bandwidth. The resulting stacked data were judged not to have the bandwidth nor the signal-to-noise character that were needed for imaging the thin-bed Atokan-age reservoirs in Boonsville field. Consequently, the processing was redone by first spectrally balancing all field records, then calculating new statics and stacking velocities, and restacking the data. Comparisons of stacked lines created with and without spectral balancing during these two tests are shown in Figures D30 and D31. The spectrally balanced data have a wider bandwidth, superior resolution, and better signal-to-noise character, demonstrating the importance of the spectral balancing procedure for imaging thin-bed midcontinent reservoirs.

Spectral balancing is a demanding computational procedure. The lengthy computation time results because the process is not a poststack procedure, but a prestack calculation that is applied to every trace of every field record on a trace-by-trace basis. In the case of the Boonsville 3-D data, the spectral balancing computation required 6 days (144 hours) of continuous runtime on a Sun SPARC 10, which is a significant demand on computer resources. The objectives of spectral balancing are to cause all traces of all field records to have equivalent frequency spectra and for these spectra to exhibit a flat response over the widest possible bandwidth. A hypothetical example of the concept is shown in Figure D32 where the frequency content of a wideband spectrum (top) is altered so that the energy content is uniformly distributed across the complete

frequency range of the data (bottom); i.e., the bottom spectrum is balanced across the complete signal bandwidth.

Spectral balancing is done in successive, narrow passbands such as those indicated by the twelve frequency intervals in Figure D32. In practice, the computation is not done in the frequency domain as one might assume from this figure but is implemented in the time domain following the procedural path(s) diagrammed in Figure D33.

Analysis of the Boonsville seismic field records showed that the signal bandwidth diminished significantly above 150 Hz, so spectral balancing was not attempted for frequencies that greatly exceeded this signal cutoff. The specific filters used to spectrally balance the Boonsville data are shown in Figure D34. Each filter had a passband width of 10 Hz and rolloff widths of 5 Hz at the low end and 20 Hz at the high end. The first full-pass frequency was set at 15 Hz, and the low-end rolloff for this filter (filter 1 in Fig. D34) eliminated most of the low-frequency ground roll noise as well as much of the cultural noise created by gas compressors and other surface-based mechanical equipment operating throughout the 3-D grid. The full-pass portion of each filter overlapped the full-pass portion of the preceding filter by 25 percent (i.e., by 2.5 Hz). The full-pass portion of the eighteenth, and last, bandpass filter in the sequence ended at 152.5 Hz, where the signal frequency effectively ended in the field records. This filter suite resulted in computation loop A (Fig. D33) being exercised 18 times for each data trace of every Boonsville field record. Because the Boonsville data were sampled at 1 ms and the record length was 2 s, computation loop B (Fig. D33) generated 2,000 trace amplitude scaling factors, one for each data sample of the trace being processed, during each execution of loop A. The result of this extensive trace-by-trace spectral balancing was the improvement in the stacked 3-D image documented in Figures D30 and D31.

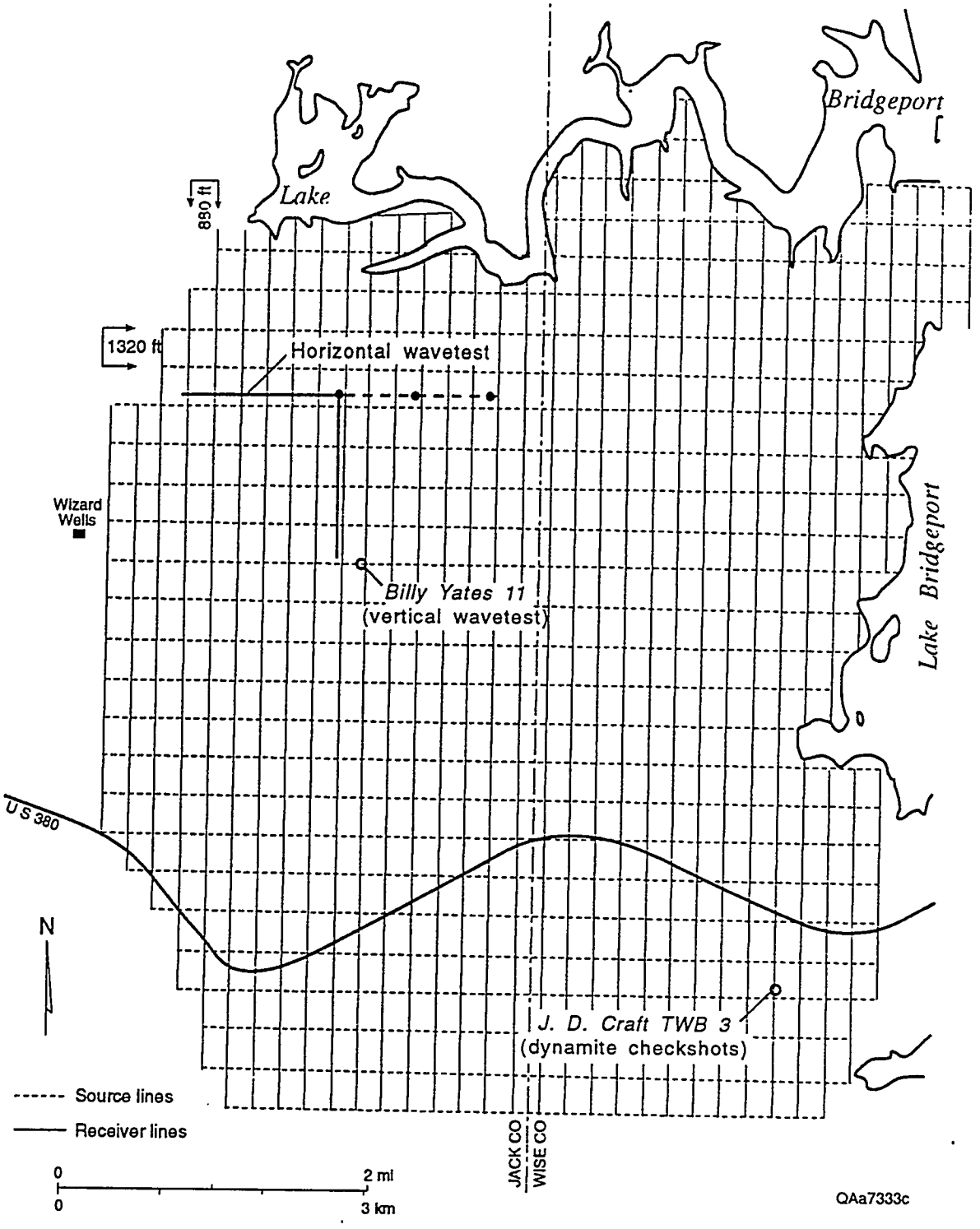

Figure D1. The source-receiver grid used to record the Boonsville 3-D seismic data. The locations of key velocity control wells and wavetest sites are indicated. The north-south receiver lines are spaced at intervals of 880 ft, and the east-west source lines are separated a distance of 1,320 ft. The horizontal wavetest site is further explained in Figure D12.

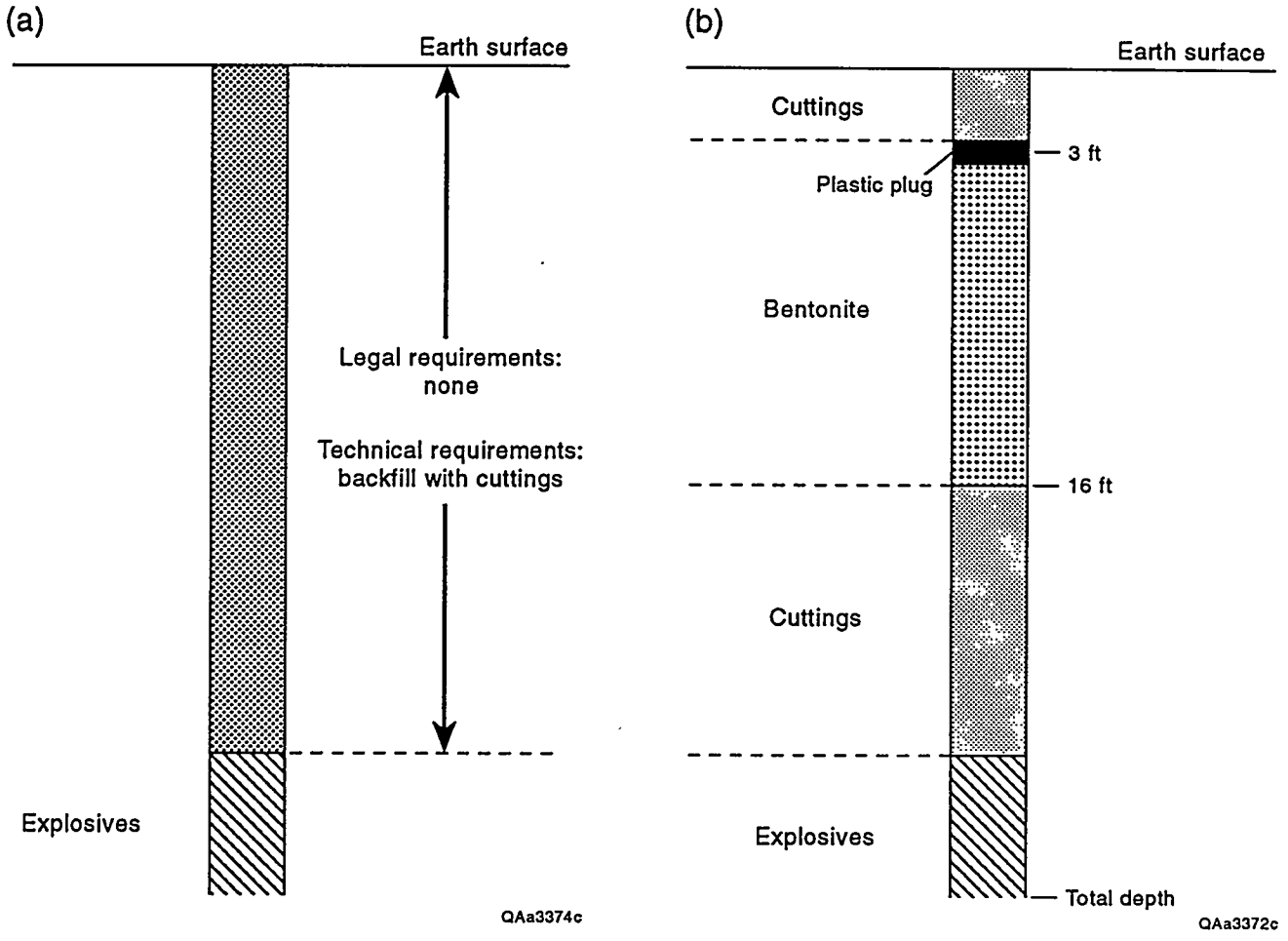

Figure D2. The construction requirements for shot holes in Texas when the hole depth is (a) less than 20 ft and (b) 20 ft or more.

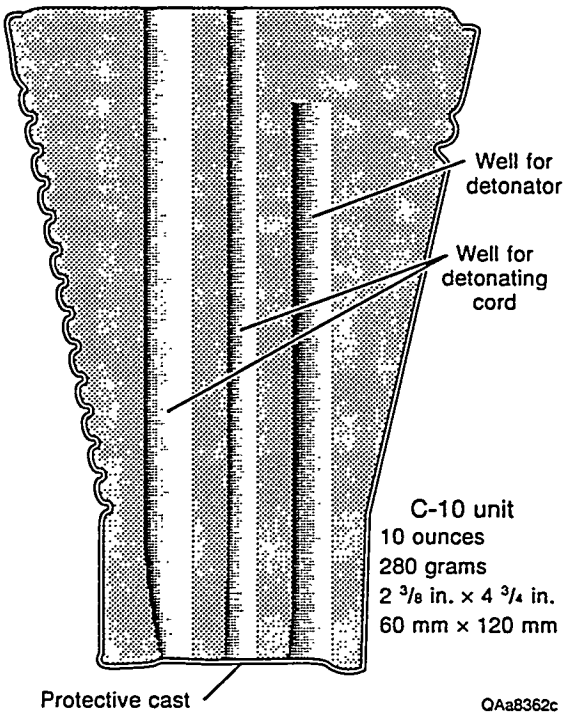

Figure D3. The C-10 directional charge used as the seismic energy source in the Boonsville 3-D survey. The C-10 package contains 10 ounces of high-velocity pentolite, and when the package is buried with the large end downward, the molded shape of the charge creates a large downward force.

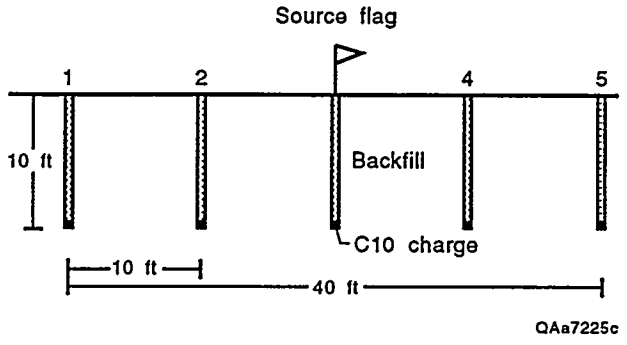

Figure D4. The five-hole source array geometry used at each source station within the Boonsville grid. Five shot holes were drilled inline, centered on the source flag, and spaced 10 ft apart. Each hole was 10 ft deep and loaded with a C-10 directional charge. All five holes were detonated simultaneously.

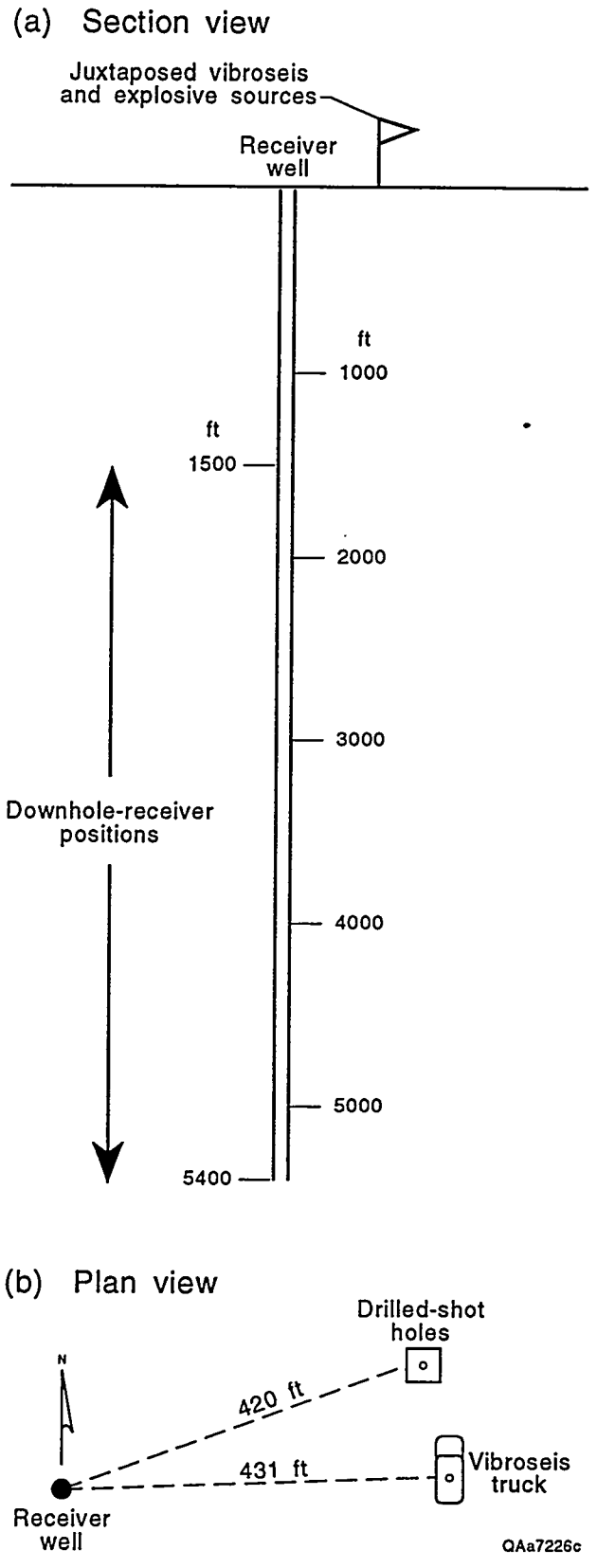

Figure D5. The geometry used to record vertical wavetest data in the Billy Yates 11 well. Well location shown in Figure D1. The objective of the test was to determine the relative bandwidths and vertical traveltimes of vibroseis and pentolite wavelets.

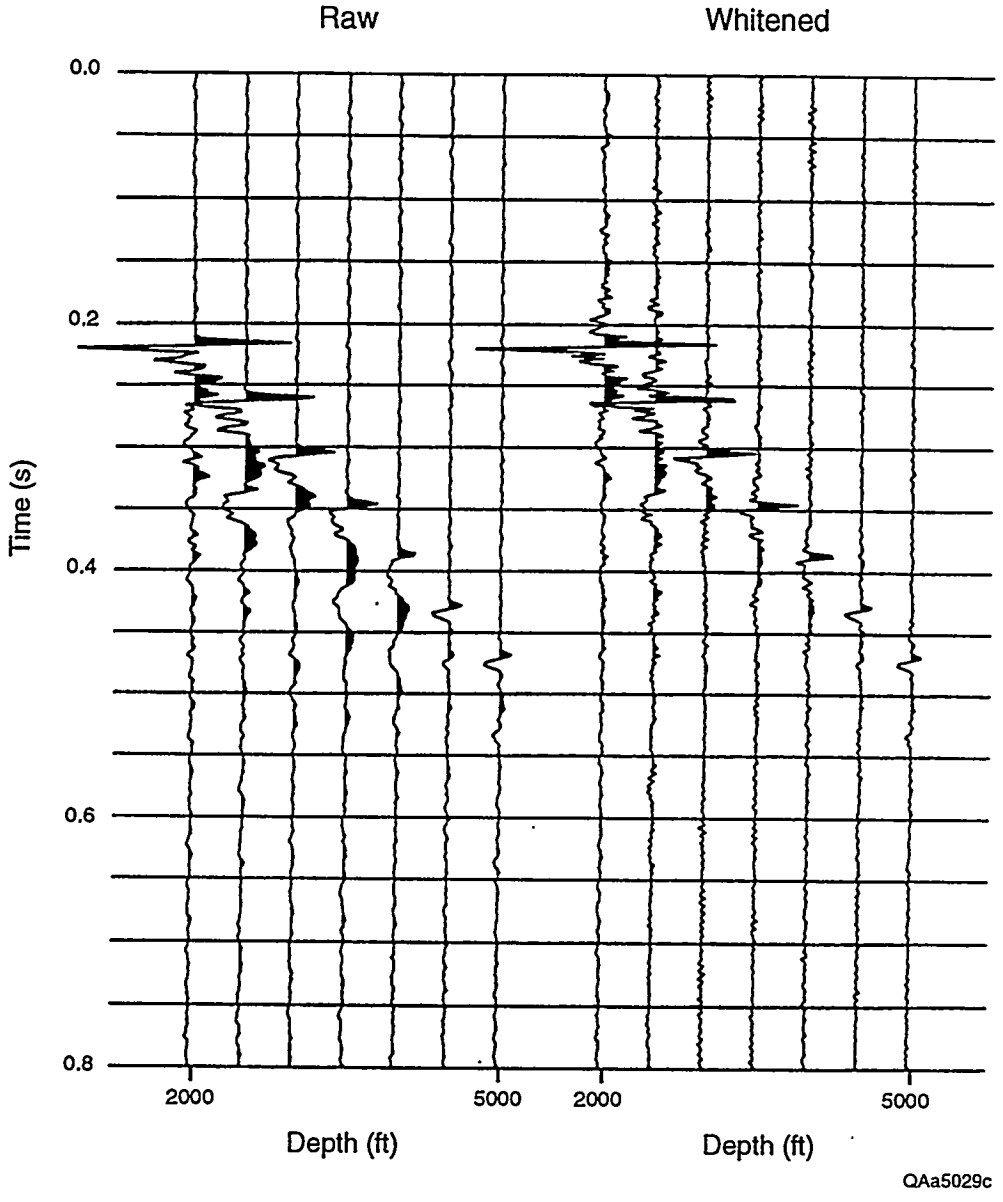

Figure D6. Some of the vertical wavetest data generated by C-10 directional charges detonated in five-hole patterns constructed as shown in Figure D4 and recorded in the Billy Yates 11 well. The source-receiver geometry used to record these data is diagrammed in Figure D5.

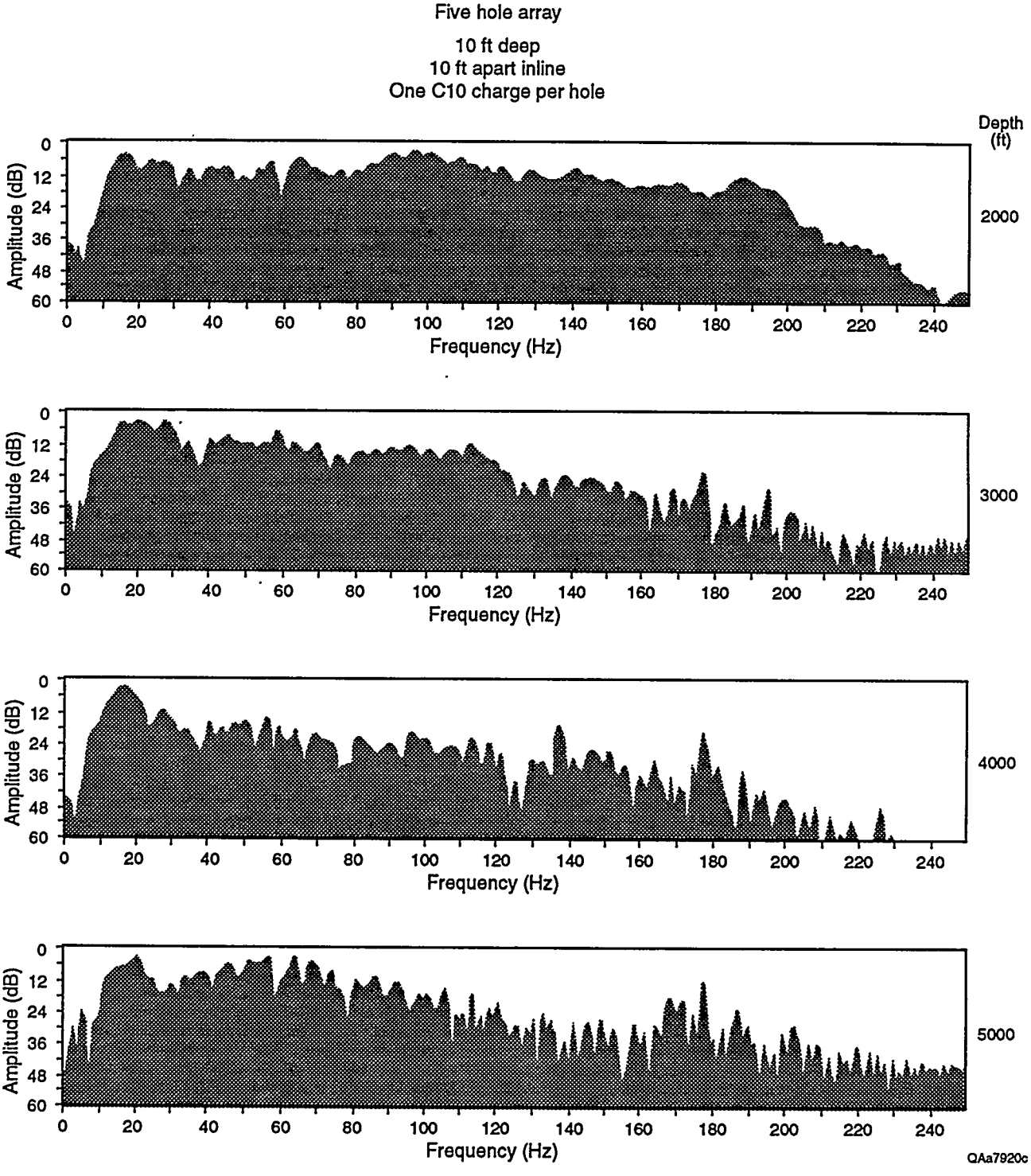

Figure D7. Amplitude spectra of the pentolite-generated vertical wavetest data shown in Figure D6. These spectra document that the pentolite wavelets are extremely broadband and contain frequency components exceeding 200 Hz. The recording system used in this test required that the wavelets be recorded at a sample rate of 2 ms, so the spectral roll-off above 180 Hz is produced by the 2-ms alias filter in the recording system and is not a true reduction of the wavelet energy. The numbers labeled on the right margin indicate the depths where the spectral analyses were done. The Atoka-age reservoirs begin at a depth of about 4,500 ft.

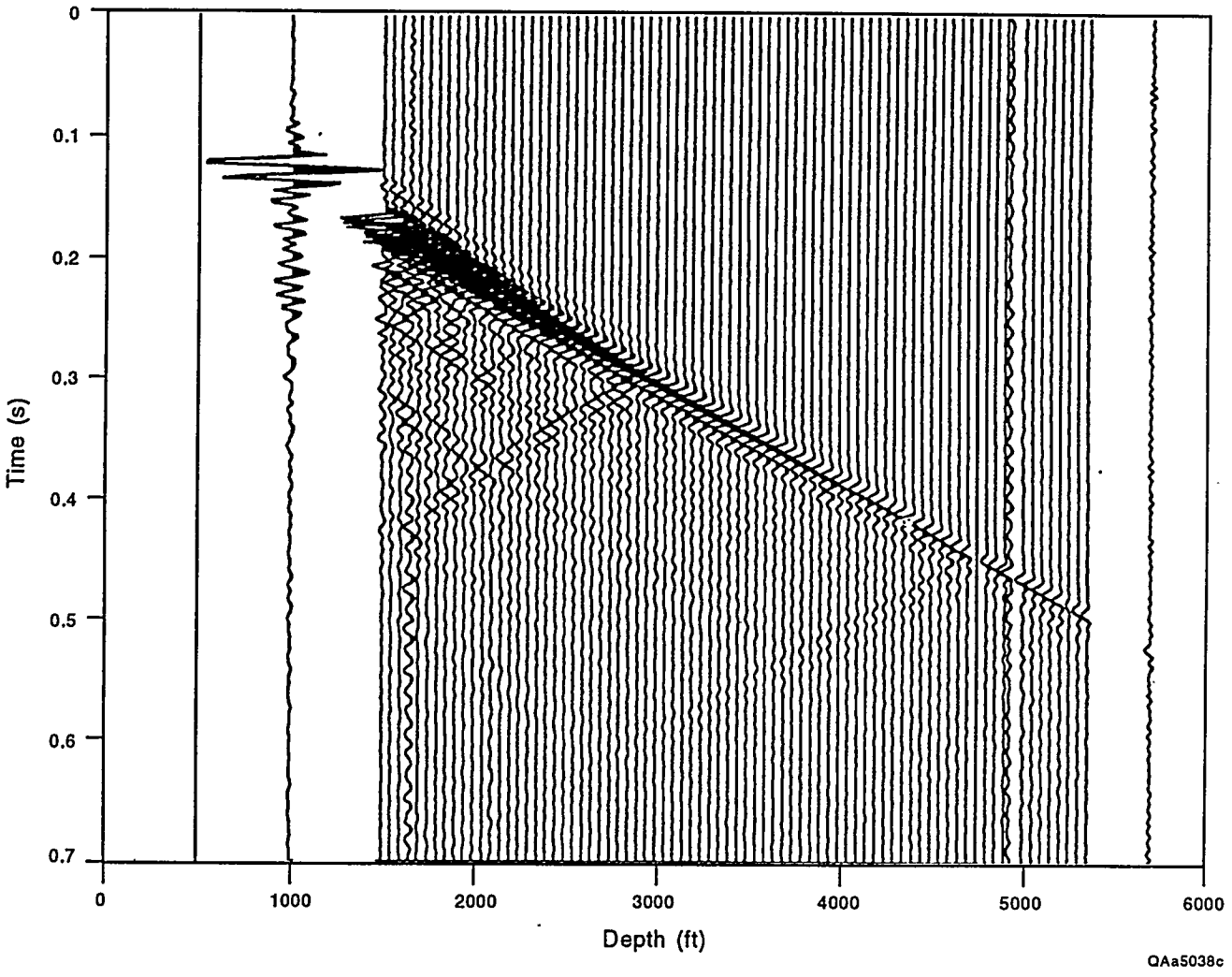

Figure D8. Vibroseis vertical seismic profile recorded in the Billy Yates 11 well. Well location shown in Figure D1. The source-receiver geometry used when recording these data is diagrammed in Figure D5.

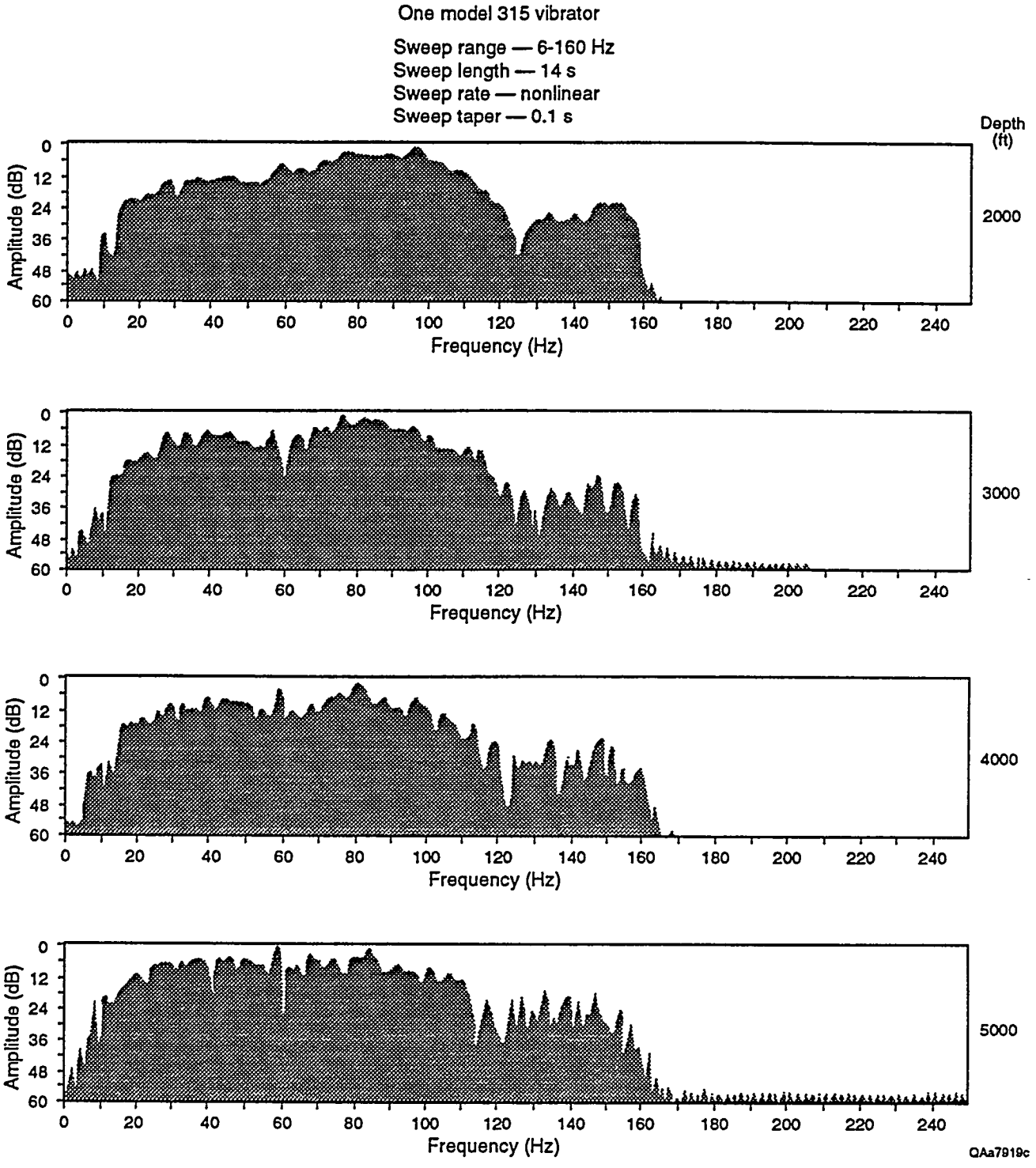

Figure D9. Amplitude spectra of vibroseis vertical wavetest data recorded at the same receiver depths as the pentolite data in Figure D6. After extensive testing, the source vibrator could not demonstrate acceptable ground-force-phase-locking above 160 Hz, so the VSP data were generated using a nonlinear 3-dB/octave sweep, 14 s long that began at 6 Hz and ended at 160 Hz. A nonlinear sweep was used to maximize the energy content at the higher frequencies.

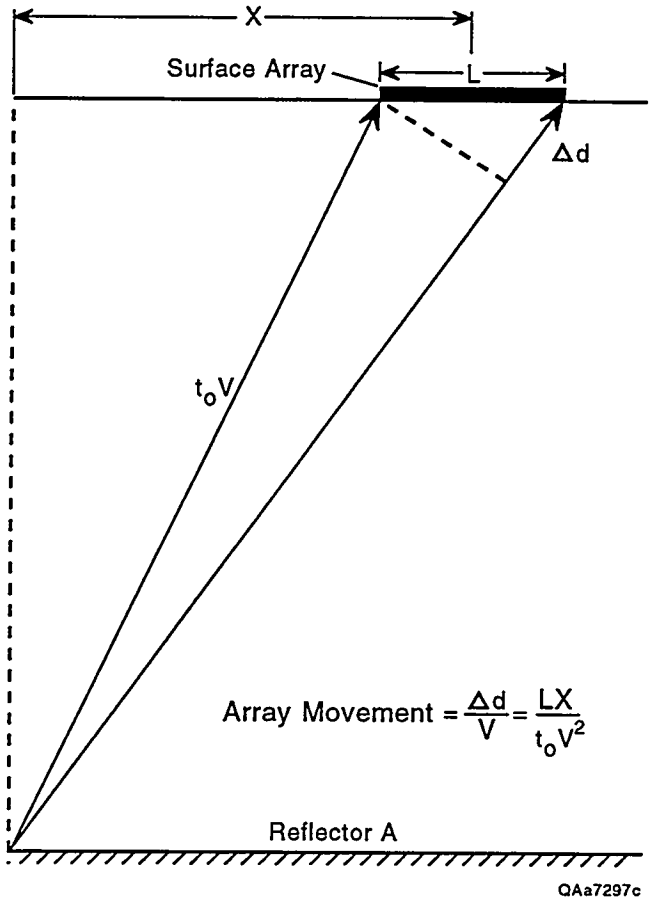

Figure D10. Geometrical theory used to design the dimensions of the surface-positioned seismic receiver arrays at Boonsville field. The magnitude of the array moveout (i.e., the time shift across the array) for an array of length L is the time required for an upgoing reflection to traverse the extra path length Δd between the raypaths to the receivers at opposite ends of the array. The time smearing of the reflection arrival time resulting from this moveout defines the maximum frequency that can be correctly preserved in the recorded data. If high frequencies are to be preserved, the array length L must be short so that this time shift and wavelet smearing are small.

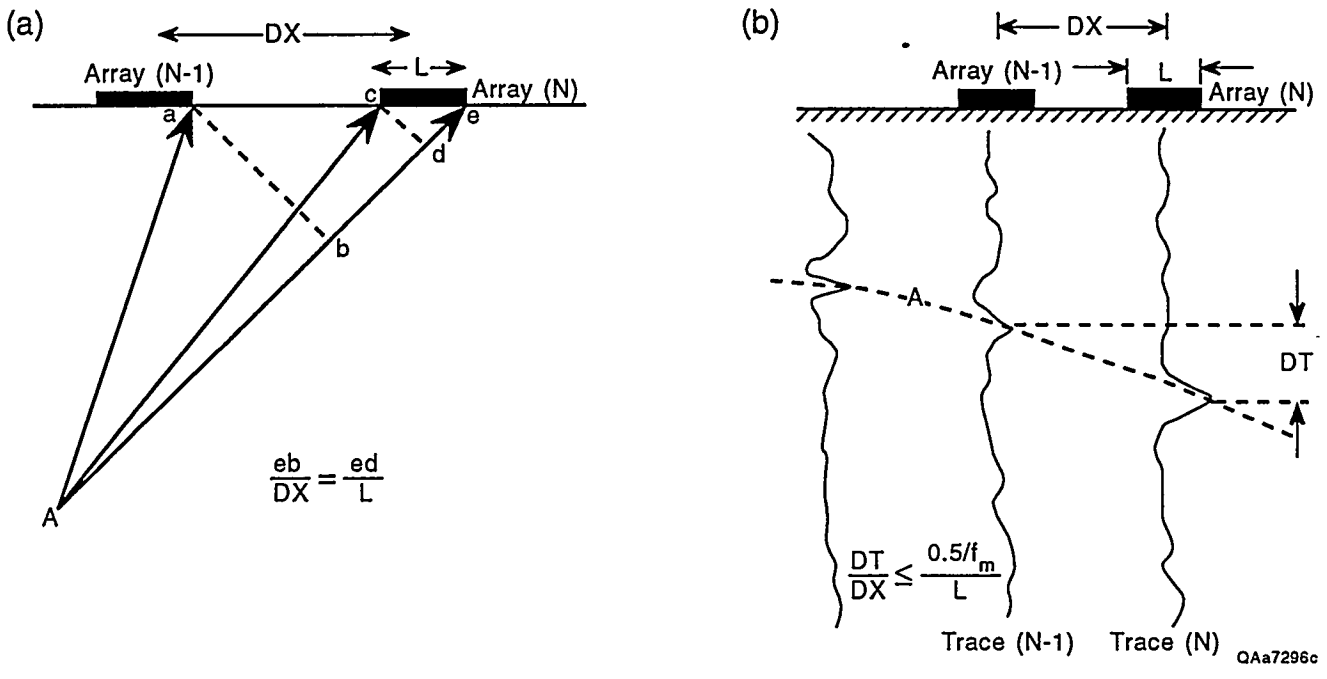

Figure D11. The theory in Figure D10 defines the criteria used to select the proper length L of a single receiver array. The theory shown here expands that design concept to define how far apart adjacent receiver arrays should be. Panel (a) shows the geometrical relationships between the reflected raypaths that arrive at two receiver arrays separated a distance DX. Panel (b) illustrates how this receiver interval DX can be calculated by defining the maximum time moveout DT that should exist for a reflection signal A recorded by these two arrays. The moveout DT should not exceed one-half of the time period associated with the dominant frequency f_d in the reflection signal; i.e., DT should be $\leq 0.5/f_d$. The equation in (b) follows from the equation in (a) by defining the traveltime over distance *eb* to be DT, the traveltime over distance *ed* to be dt, and then setting dt equal to one-half of the time period of the highest frequency component, or 0.5/fm.

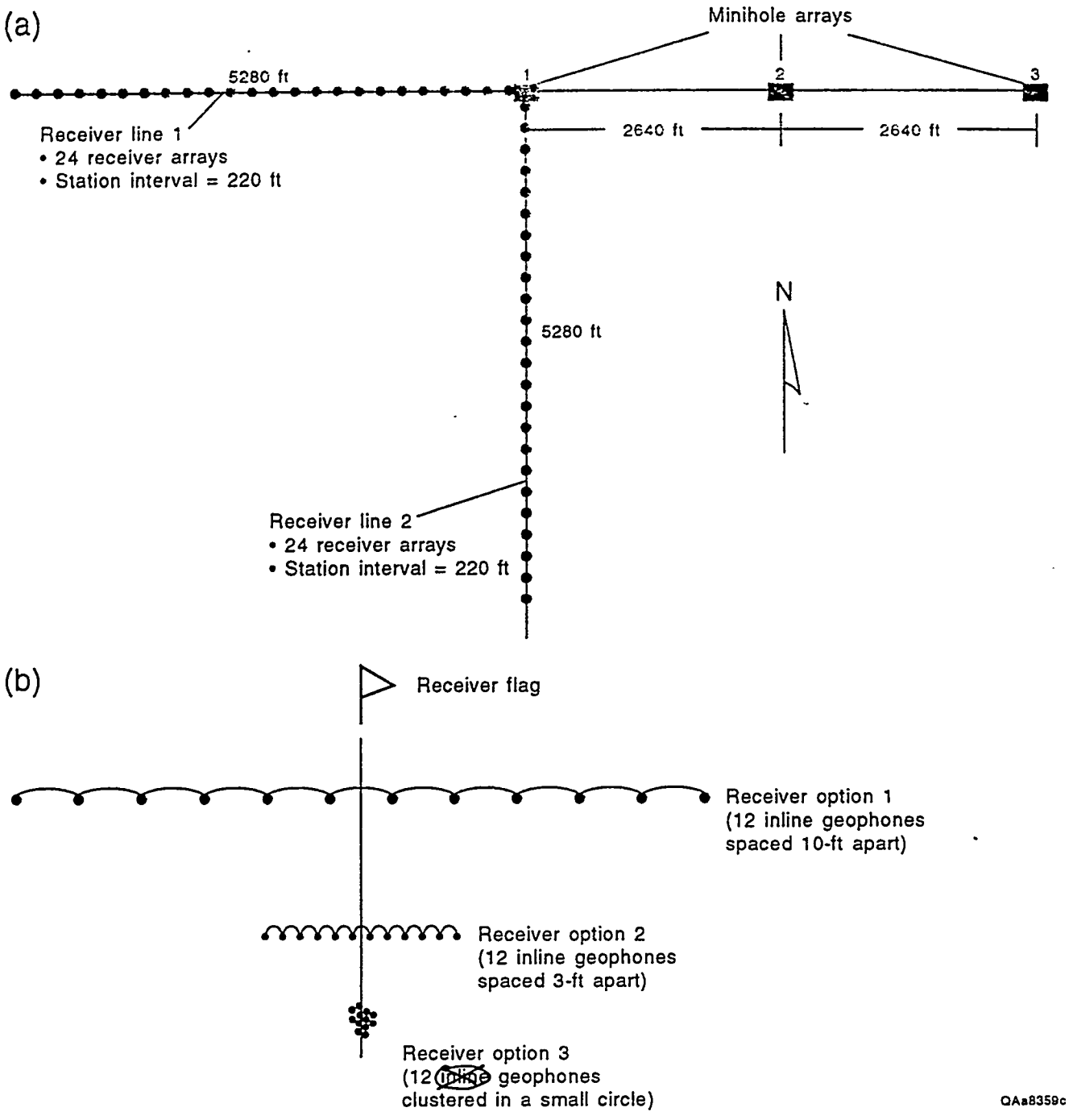

Figure D12. Horizontal wavetesting concepts implemented at Boonsville field. The test site is indicated in Figure D1. In (a), five-hole arrays were constructed at each of the three east-west source stations (solid rectangles) following the design concept shown in Figure D4. Receiver flags were surveyed at the locations indicated by the solid circles to create two receiver lines, one oriented east-west and one oriented north-south. The three receiver array options shown in (b) were constructed at each of these receiver flags.

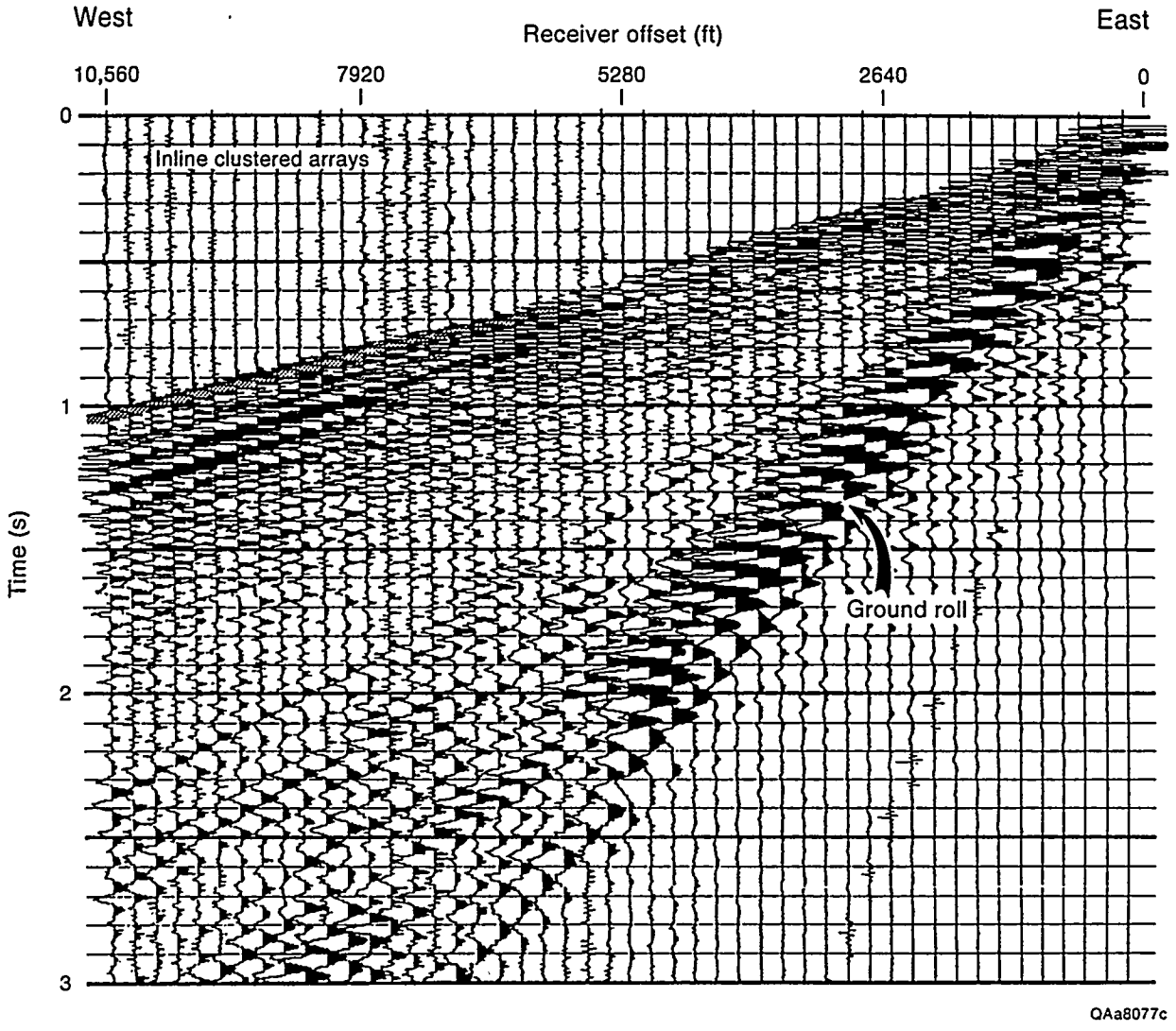

Figure D13. An example of the horizontal wavetest data recorded using the point receiver option (12 geophones clustered inside a circle having a diameter of approximately 5 ft). The receivers were deployed along receiver line 1, the east-west arm of the wavetest array (Fig. D12). This display combines the responses of two different explosive shots. The traces between offset distances of 0 and 5,280 ft are the response of the 24 east-west clustered receiver stations to a shot from minihole array 1 (Fig. D12), and the traces between receiver offsets of 5,280 and 10,560 ft are the response of these same 24 receiver stations to a shot from minihole array 3.

D 32

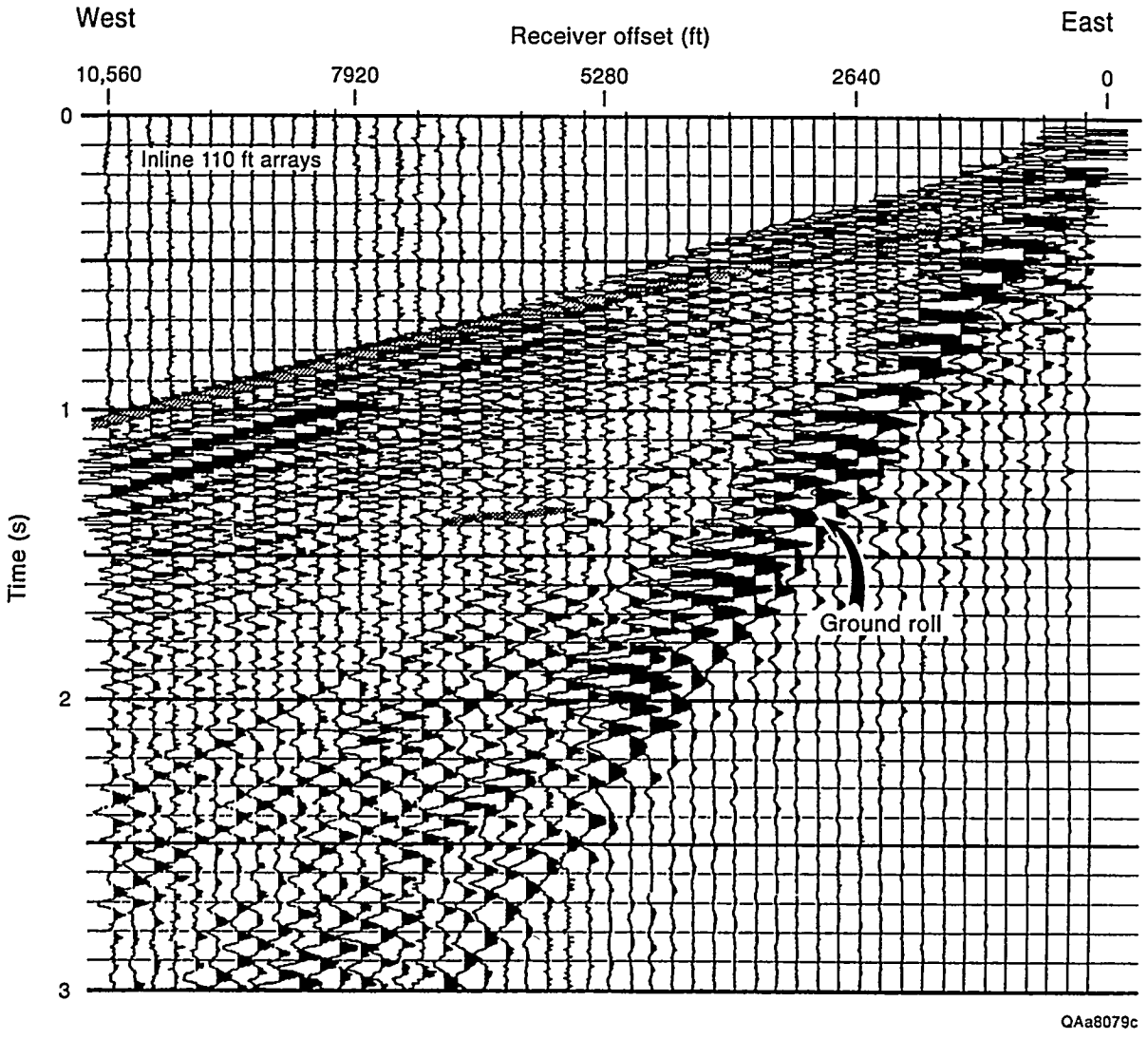

Figure D14. Horizontal wavetest data recorded using a moderately long receiver array (12 geophones spaced 10 ft apart to form a 110-ft array). The receivers were deployed along receiver line 1, the east-west arm of the wavetest array (Fig. D12). This display combines the responses of two different explosive shots. The traces between offset distances of 0 and 5,280 ft are the response of the 24 east-west, long (110-ft) receiver stations to a shot from minihole array 1 (Fig. D12), and the traces between receiver offsets of 5,280 and 10,560 ft are the response of these same 24 receiver stations to a shot from minihole array 3.

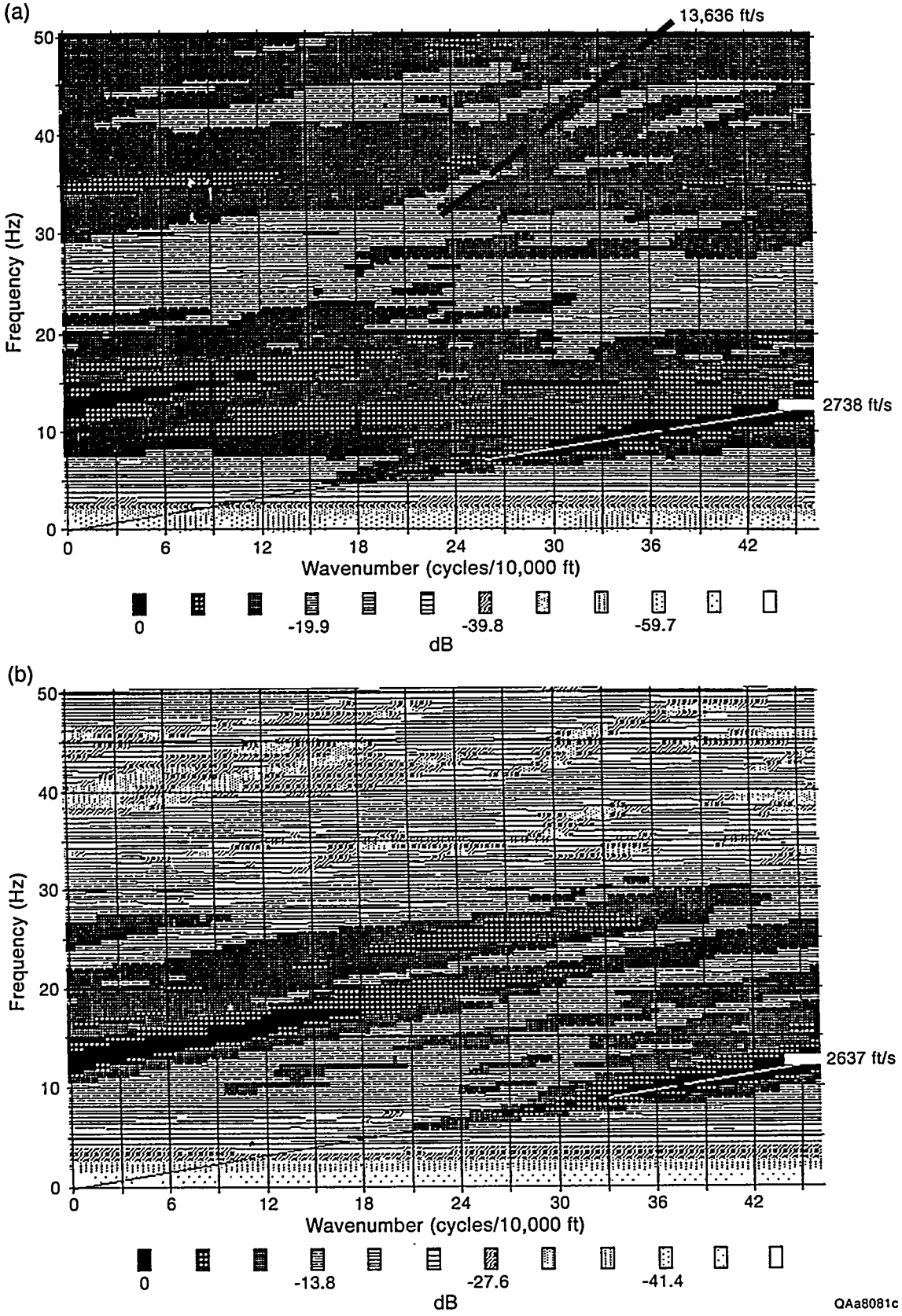

Figure D15. The horizontal wavetest data recorded on east-west receiver line 1 after transforming to the f-k domain. (a) The f-k spectrum of the 110-ft long receiver arrays. The f-k energy alignment exhibiting a velocity of 2,738 ft/s is the ground roll event labeled in Figures D13 and D14. Only hints of reflection signal exist, such as the modest energy alignment with a velocity of 13,636 ft/s. (b) The f-k spectrum of the clustered receiver array responses. Ground roll energy (velocity 2,637 ft/s) dominates the data, and it is difficult to find any evidence of reflected signal.

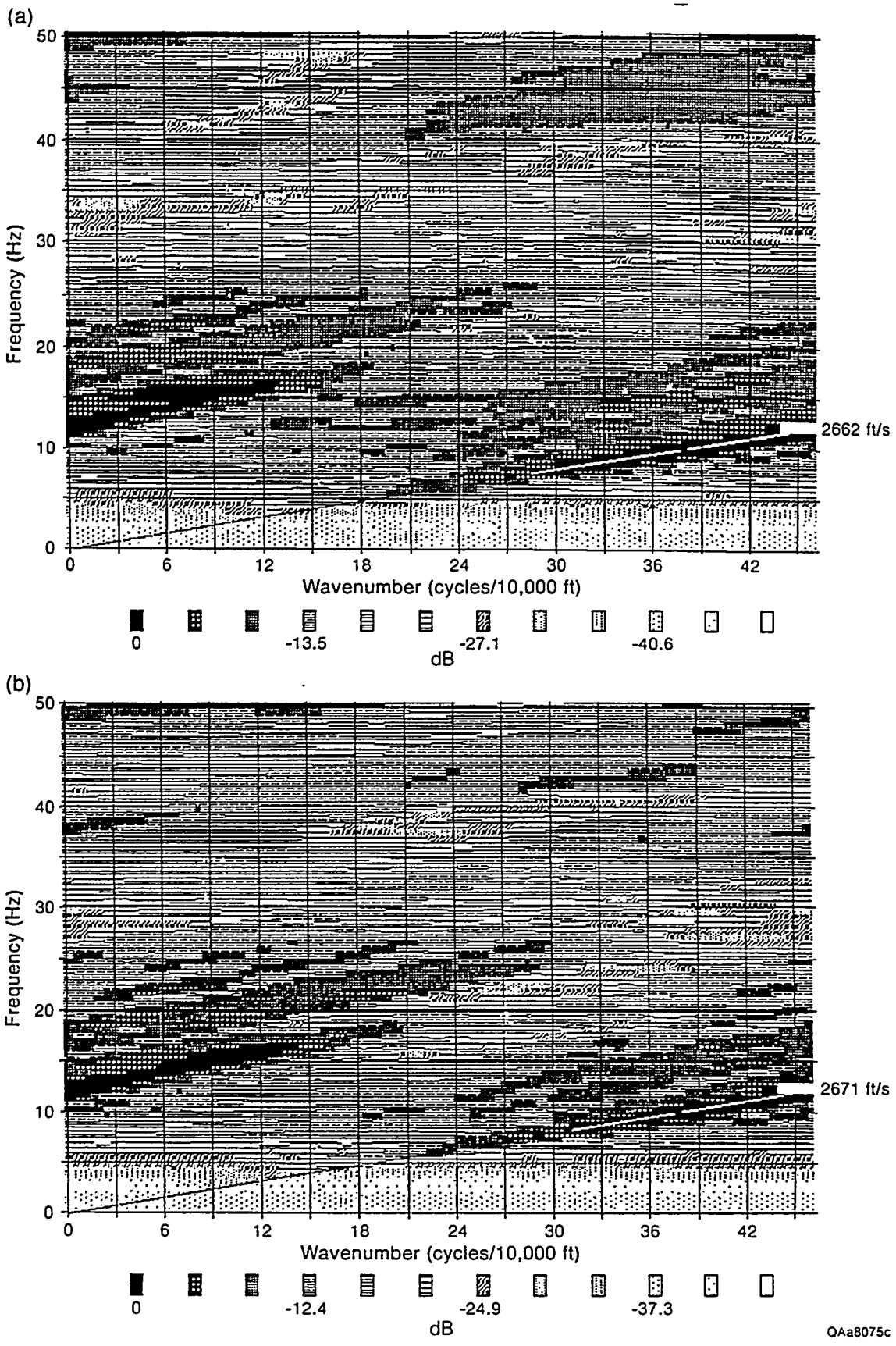

Figure D16. The horizontal wavetest data recorded on north-south receiver line 2 (Fig. D12) after transforming to the f-k domain. (a) The f-k spectrum of the 110-ft long receiver arrays. (b) The f-k spectrum of the clustered receiver arrays. Both spectra are dominated by ground roll and there is little evidence of reflected signal. Ground roll was expected to be strong on this test line because the receiver arrays were broadside to the shot.

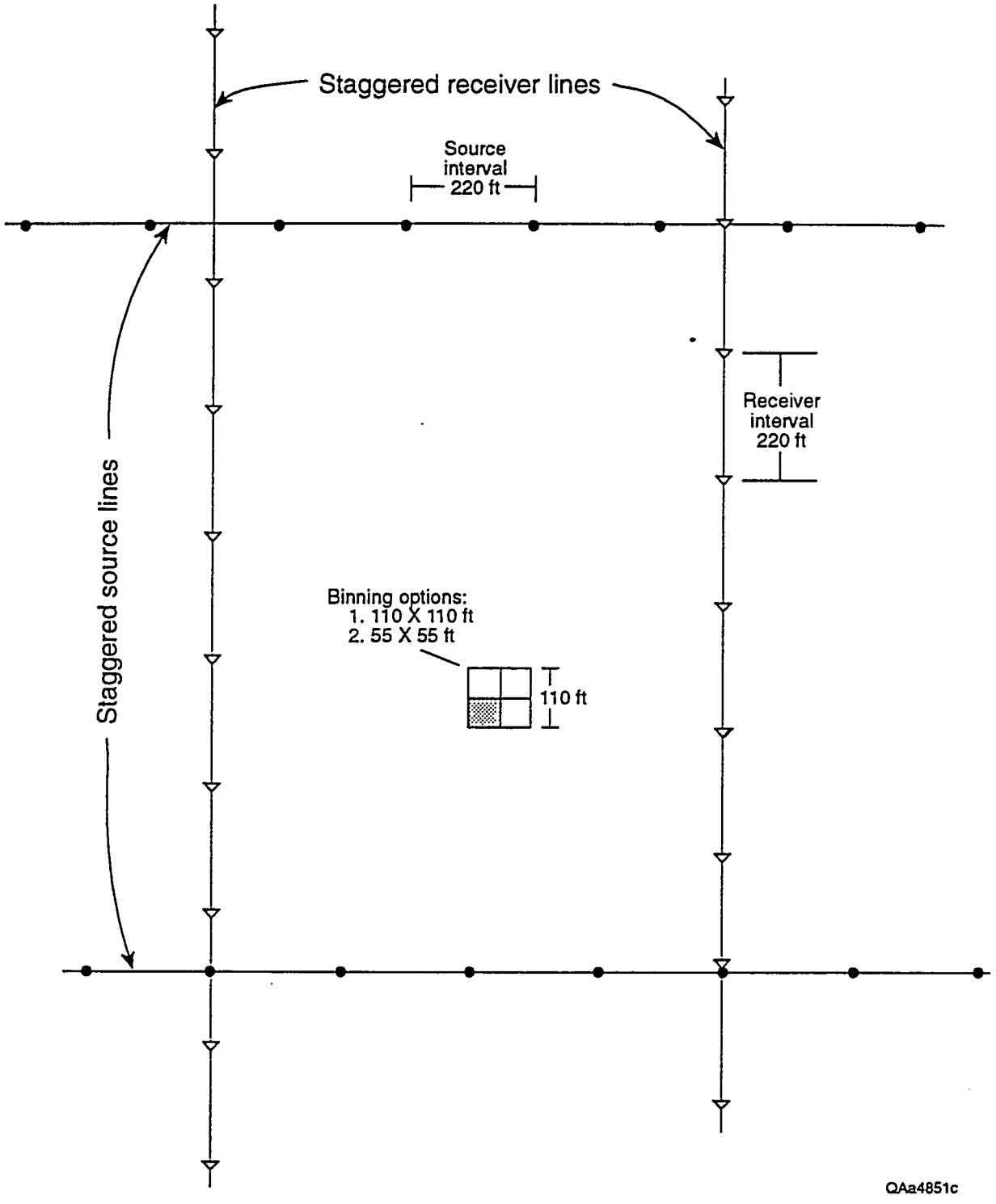

Figure D17. The staggered-line geometry used at Boonsville field. Source flags and receiver flags were stationed 220 ft apart so that the size of the conventionally defined stacking bin was 110 × 110 ft. In the staggered-line technique, adjacent receiver lines were shifted north or south by one-half of the receiver interval (a shift of 110 ft), and adjacent source lines were shifted east-west by one-half of the source interval (a shift of 110 ft). This geometry allows the data to be sorted into stacking bins measuring 110 × 110 ft or into smaller bins measuring 55 × 55 ft.

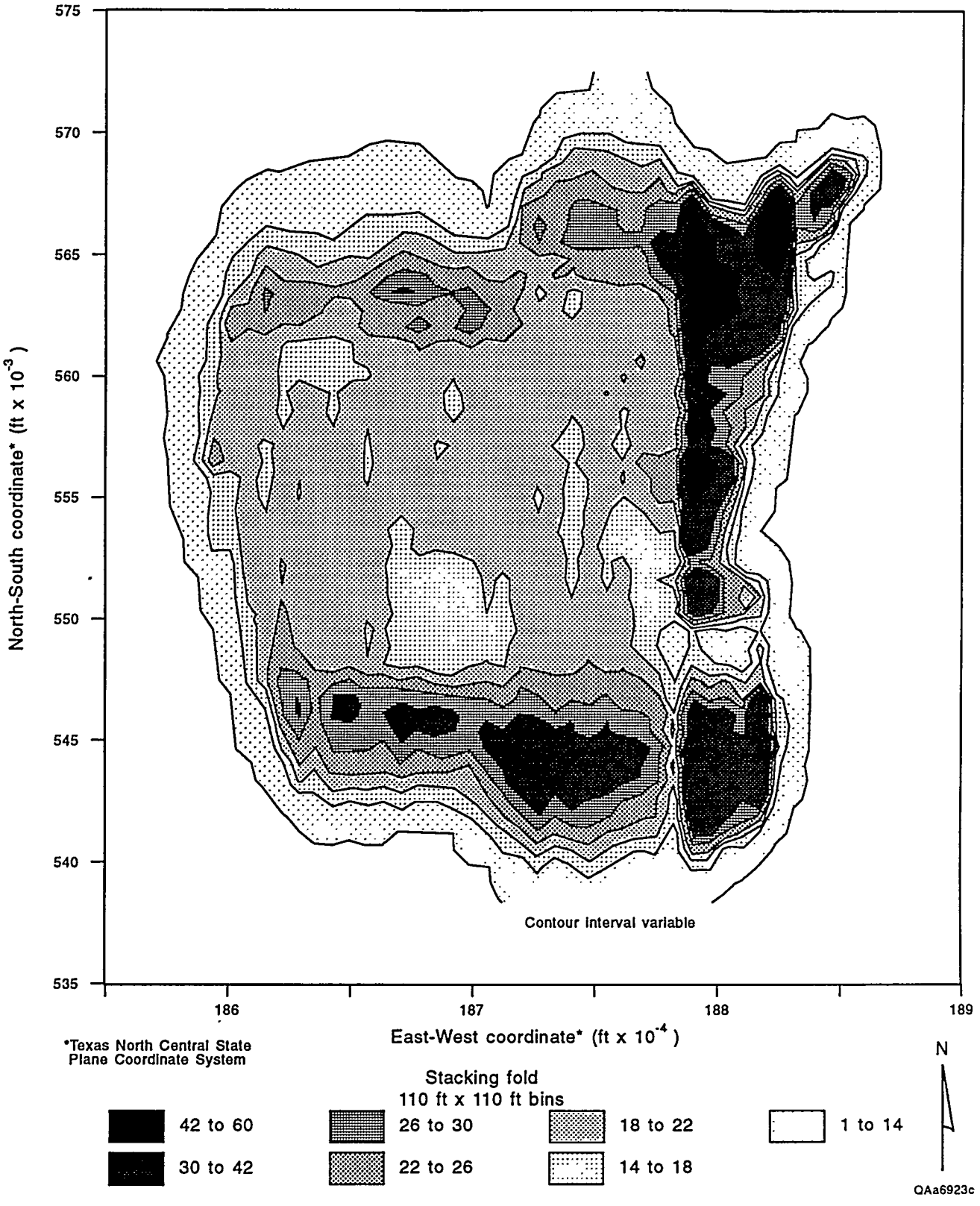

Figure D18. Stacking fold for the 110- × 110-ft bins as determined by trace sorting during data processing.

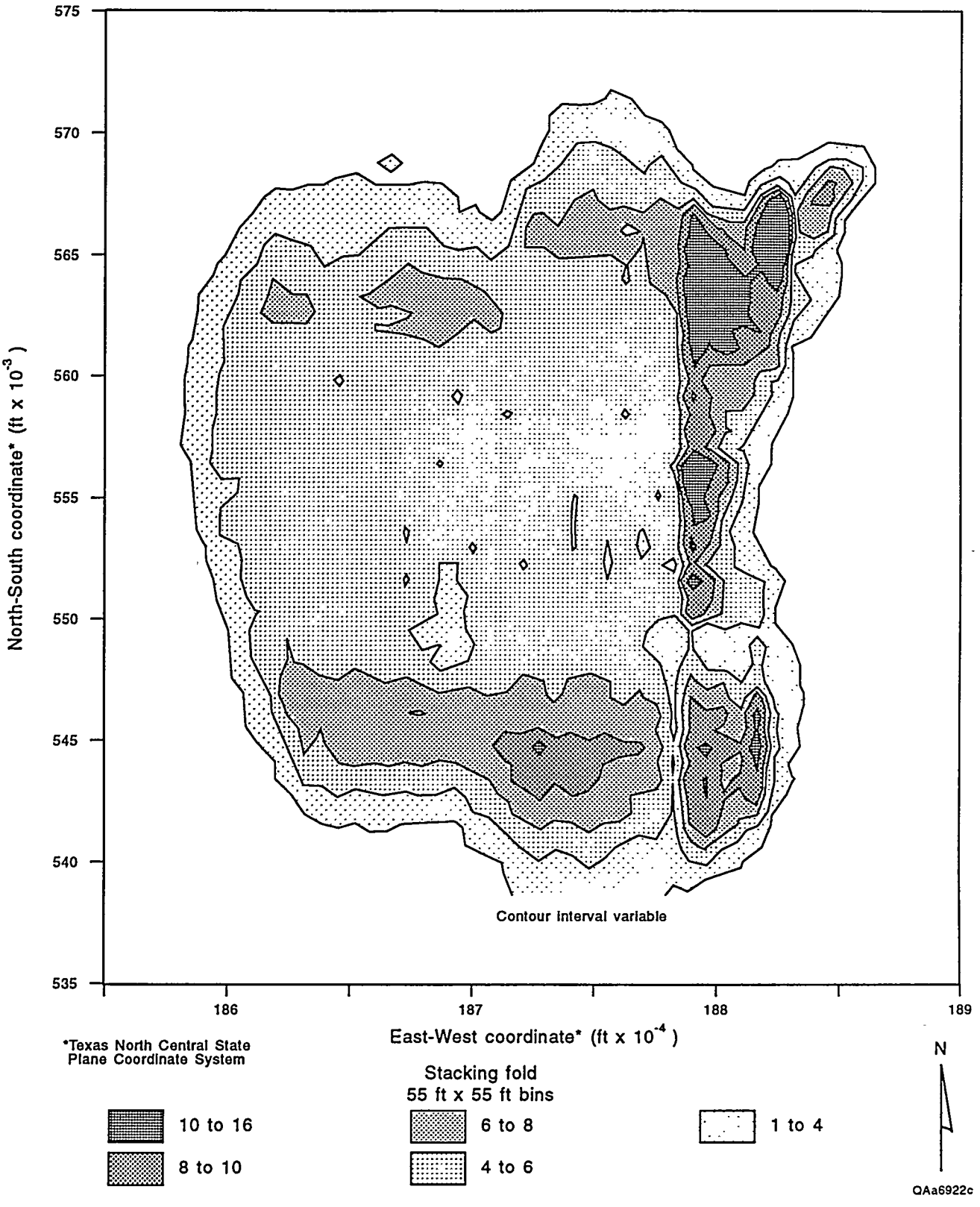

Figure D19. Stacking fold for the 55- × 55-ft bins as determined by trace sorting during data processing.

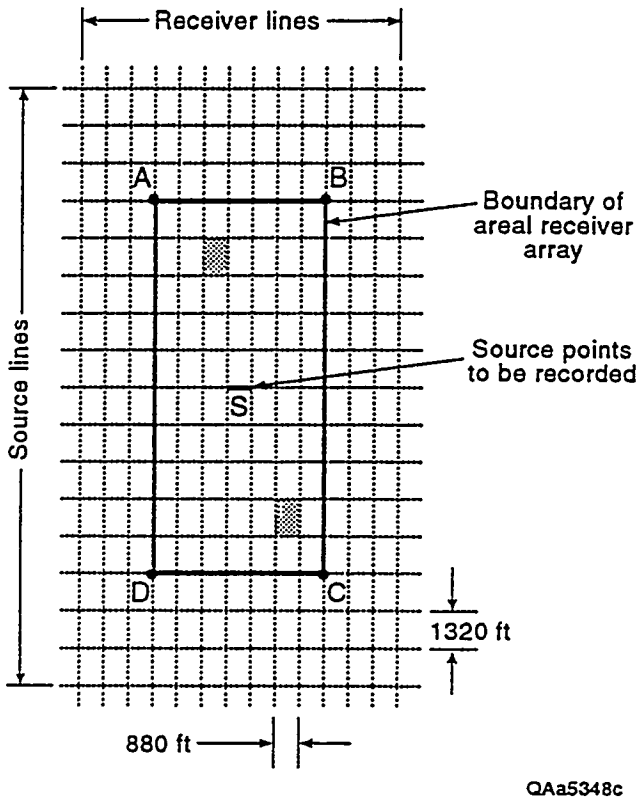

Figure D20. The receiver aperture ABCD used at Boonsville field. The aperture involved eight north-south receiver lines, each 2.5 mi long and spanning 10 source line intervals. The east-west width of the aperture was 1 1/6 mi (i.e., seven receiver line intervals of 880 ft). The shotpoint was always at S, the center of the aperture. The local source-receiver geometry within each cell of this aperture (such as either of the two shaded cells) is defined in Figure D17.

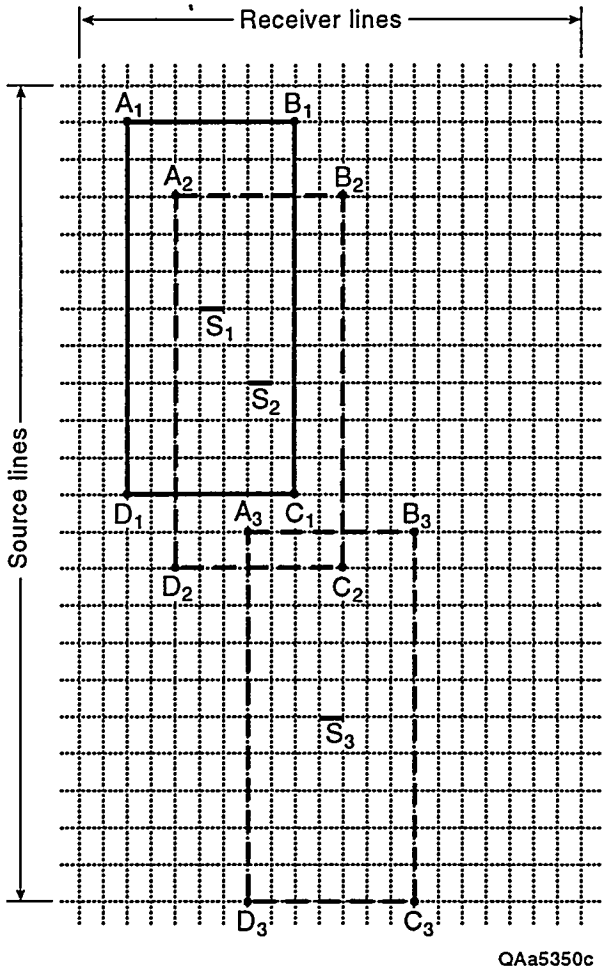

Figure D21. To increase the number of shots recorded per day, the Boonsville data were recorded using multiple shooters positioned at preplanned locations S_1, S_2, and S_3. A state-of-the-art recording system (I/O System Two) was used, which allowed receiver apertures $A_1B_1C_1D_1$, $A_2B_2C_2D_2$, and $A_3B_3C_3D_3$ to be quickly activated about S_1, S_2, and S_3 as soon as the shooters at these locations were ready to power their shooting boxes. This shooting technique differs from the usual industry practice of moving successive receiver apertures no farther than one receiver line spacing or one receiver interval.

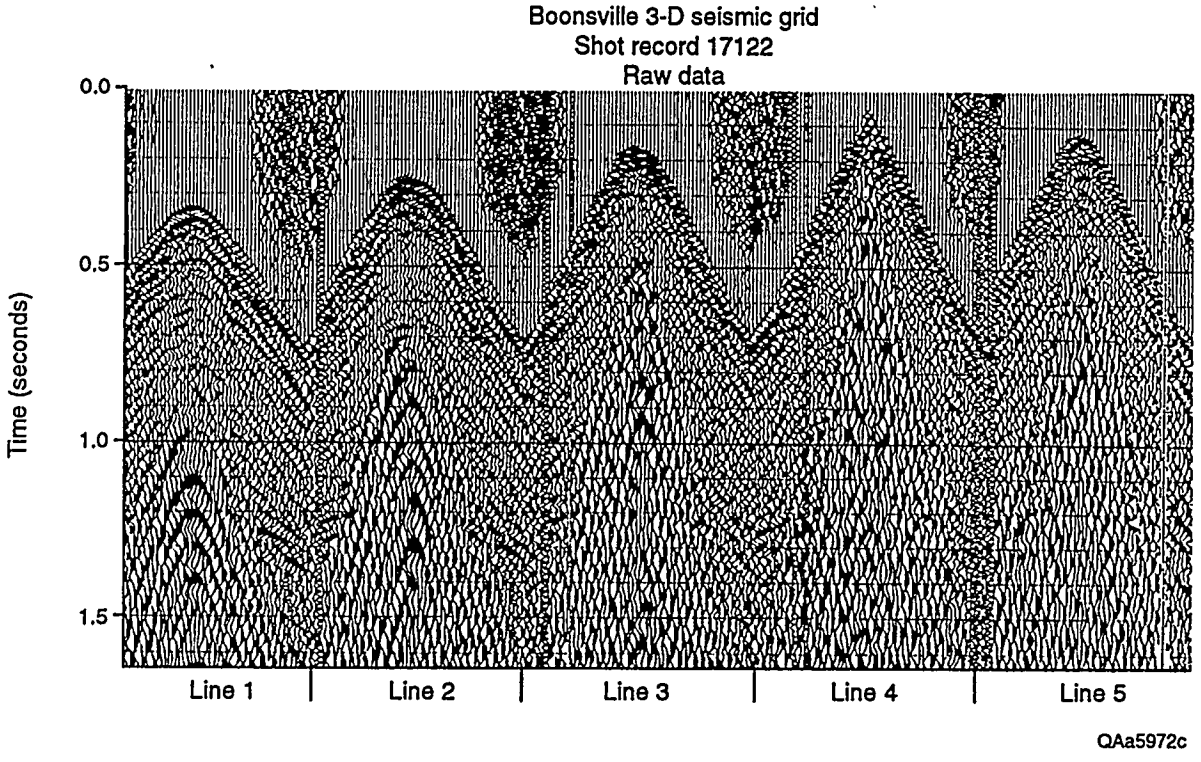

Figure D22. Typical field data recorded across the Boonsville 3-D grid. Each "line" represents the response of a single north-south receiver line inside the recording aperture (Fig. D20). Only five of the eight receiver lines involved in the receiver aperture are shown. Each line has 61 receiver stations within its 2.5-mi length; hence, there are 61 data traces in each line display. The data exhibit strong ground roll noise that camouflages most of the reflection events.

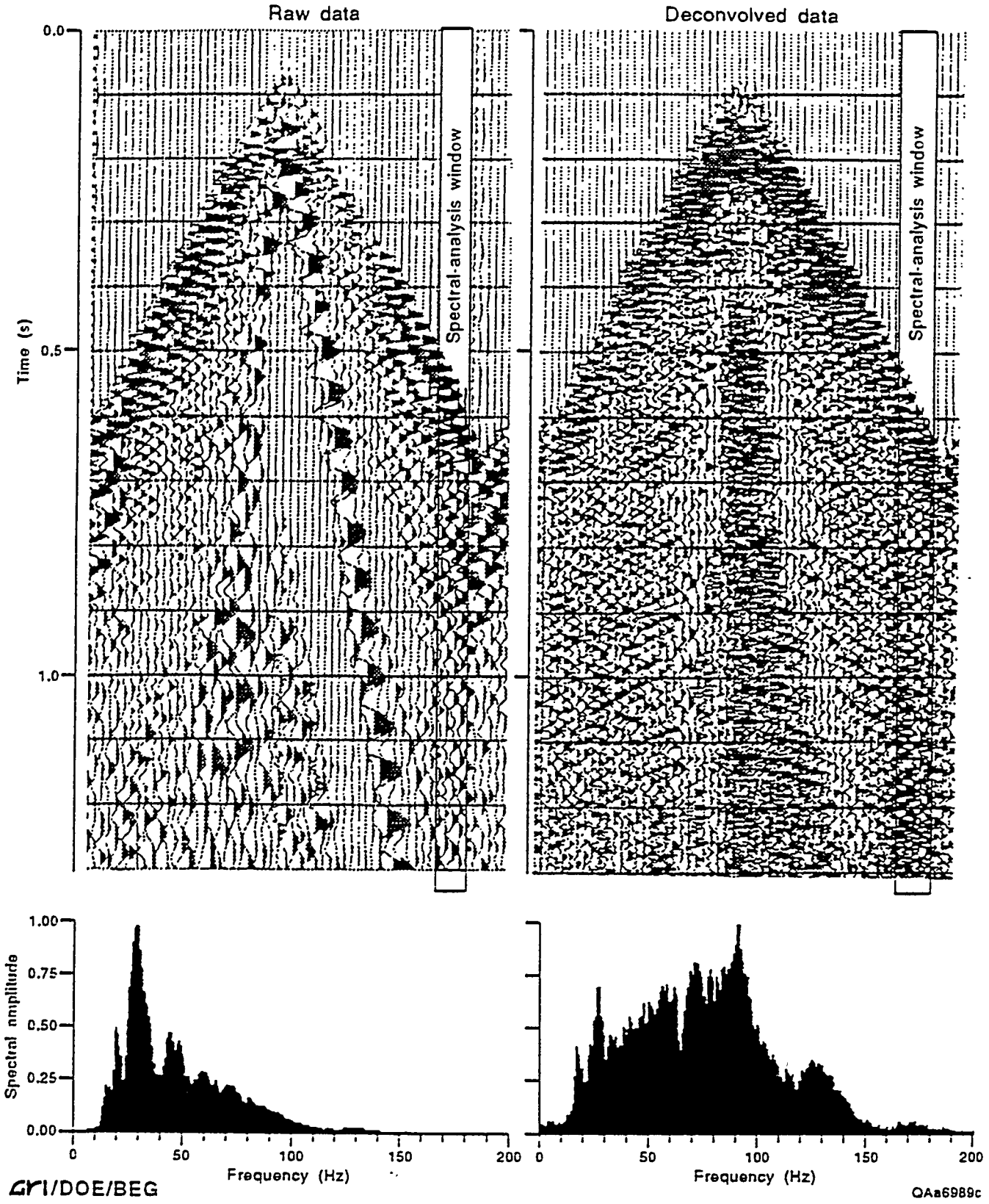

Figure D23. Deconvolution test of the far-offset traces of a Boonsville field record to determine the usable bandwidth of the reflection signals. A low-cut filter removed most of the low-frequency ground roll and other surface-related noises that are evident in the raw field record (Fig. D22) before the deconvolution operator was applied to the data. After deconvolution, the reflection signal spectrum for the far-offset traces extends from 10 to 150 Hz, which is a spectral width of almost four octaves.

D.43
D.44

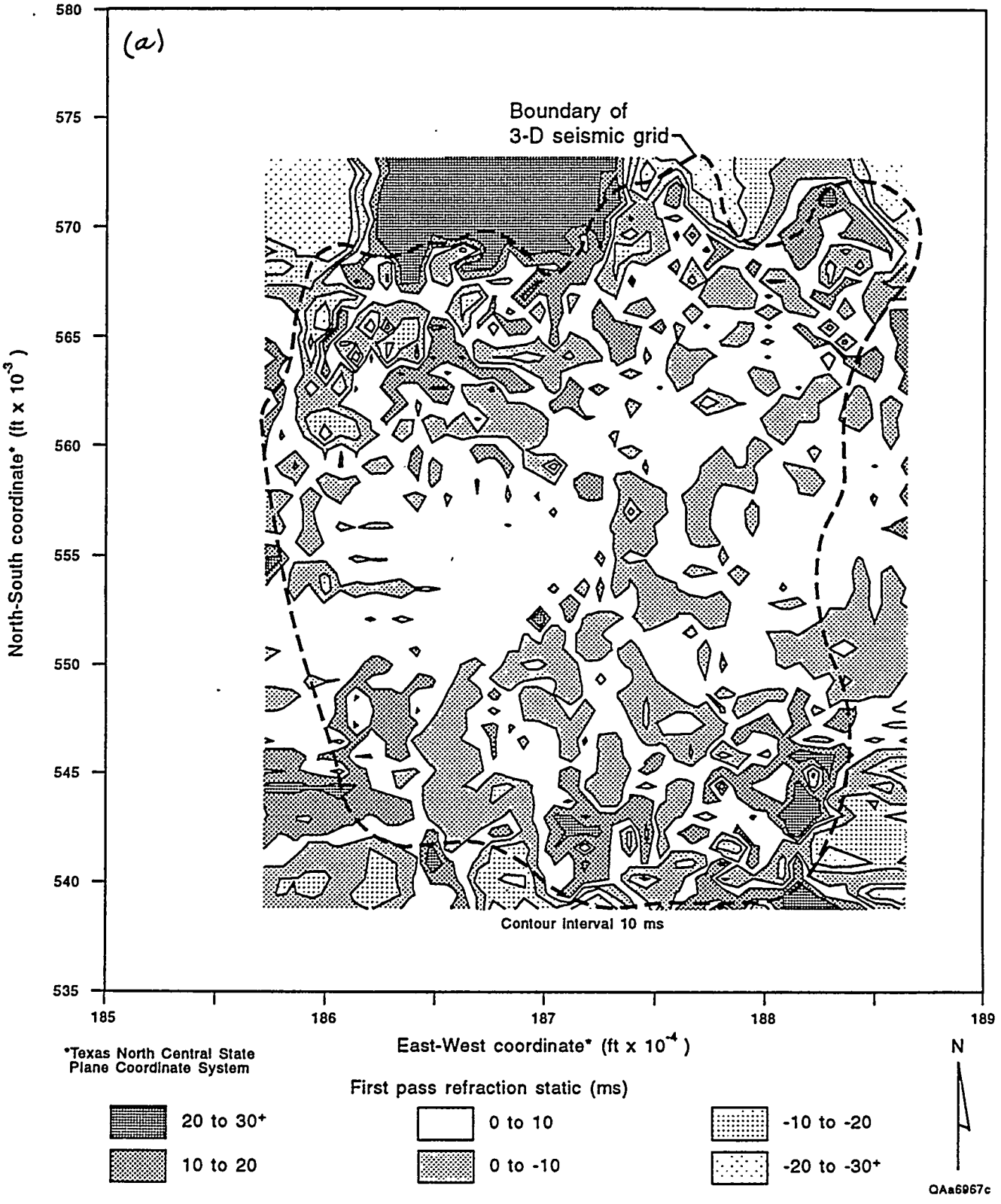

Figure D25. Refraction statics, (a) first pass and (b) second pass, applied to the Boonsville 3-D data. The boundary of the 3-D grid is superimposed on the statics map to separate valid static values inside the grid from invalid values around the edges of the map, which exist only because the mapping software extrapolates data all the way to the edges of the map coordinates.

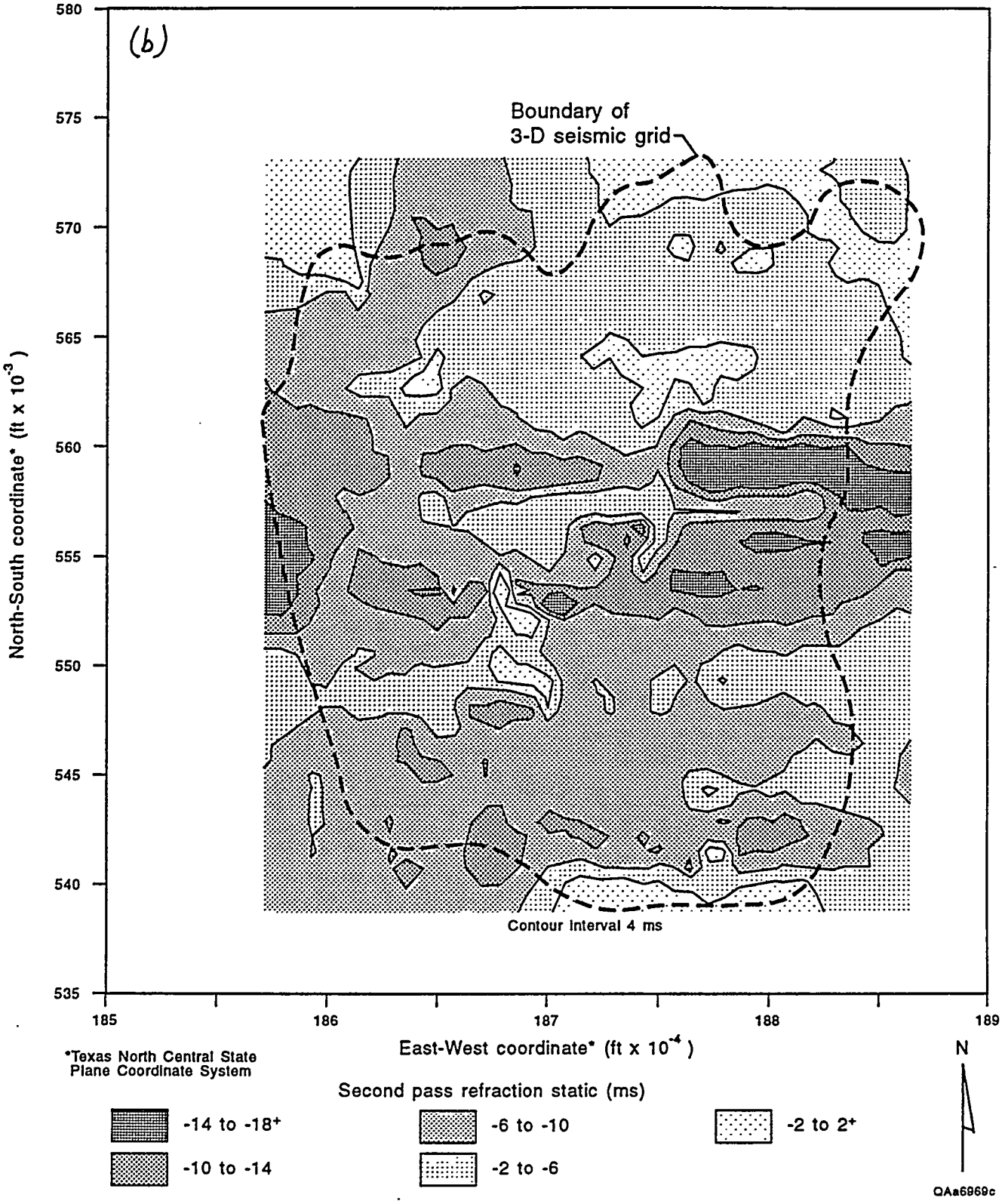
(b)
Boundary of
3-D seismic grid
580
575
570
565
560
555
550
545
540
535
North-South coordinate* (ft x 10^-3)
185
186
187
188
189
East-West coordinate* (ft x 10^-4)
Contour Interval 4 ms
*Texas North Central State
Plane Coordinate System
Second pass refraction static (ms)
-14 to -18+
-10 to -14
-6 to -10
-2 to -6
-2 to 2+
N
QAa6969c

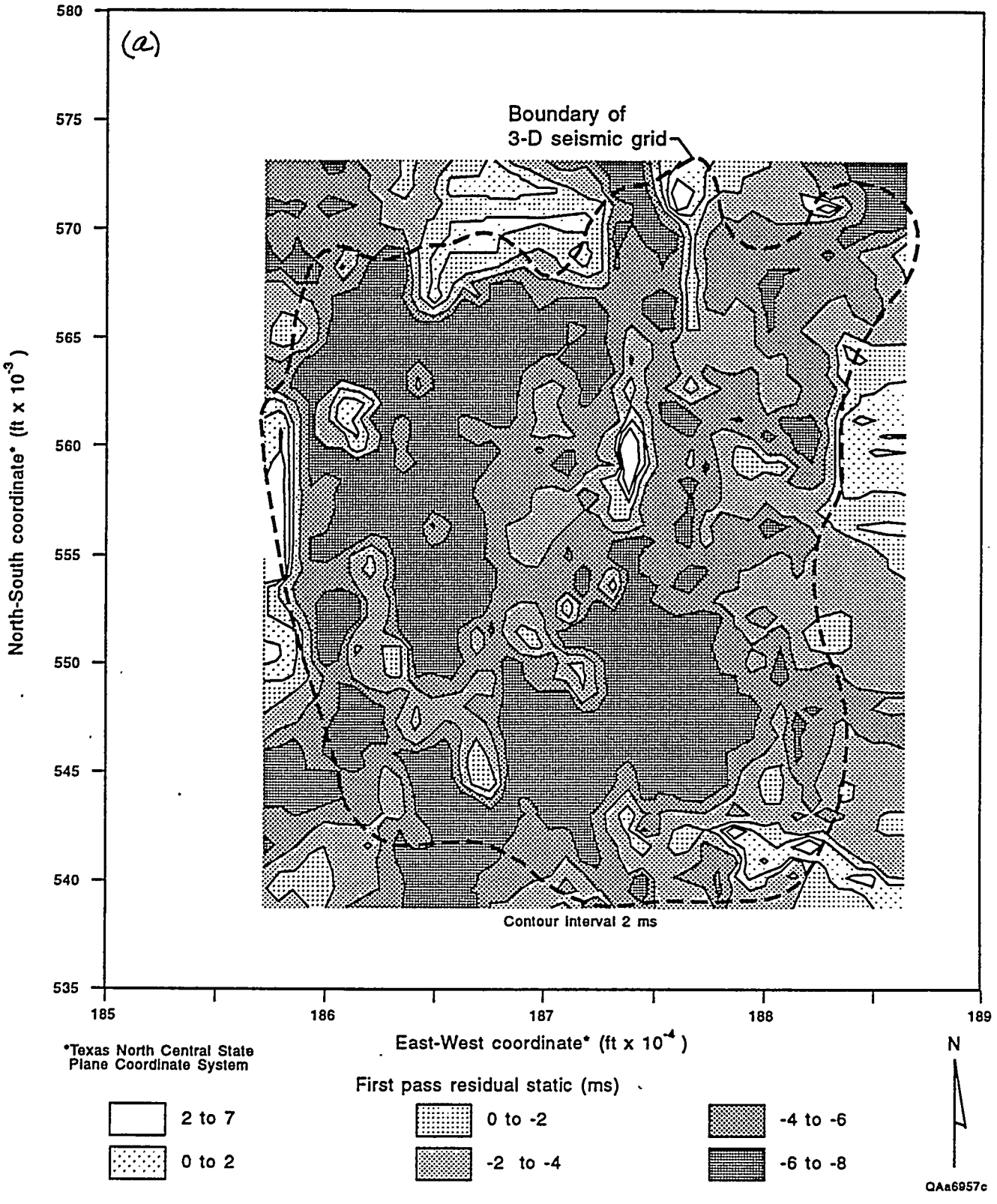

Figure D26. Residual statics, (a) first pass and (b) second pass, applied to the Boonsville 3-D data. The boundary of the 3-D grid is shown to isolate the valid static calculations inside the 3-D area from the invalid values outside the boundary that are simply the result of the mapping software extrapolating values to fill all of the mapping space.

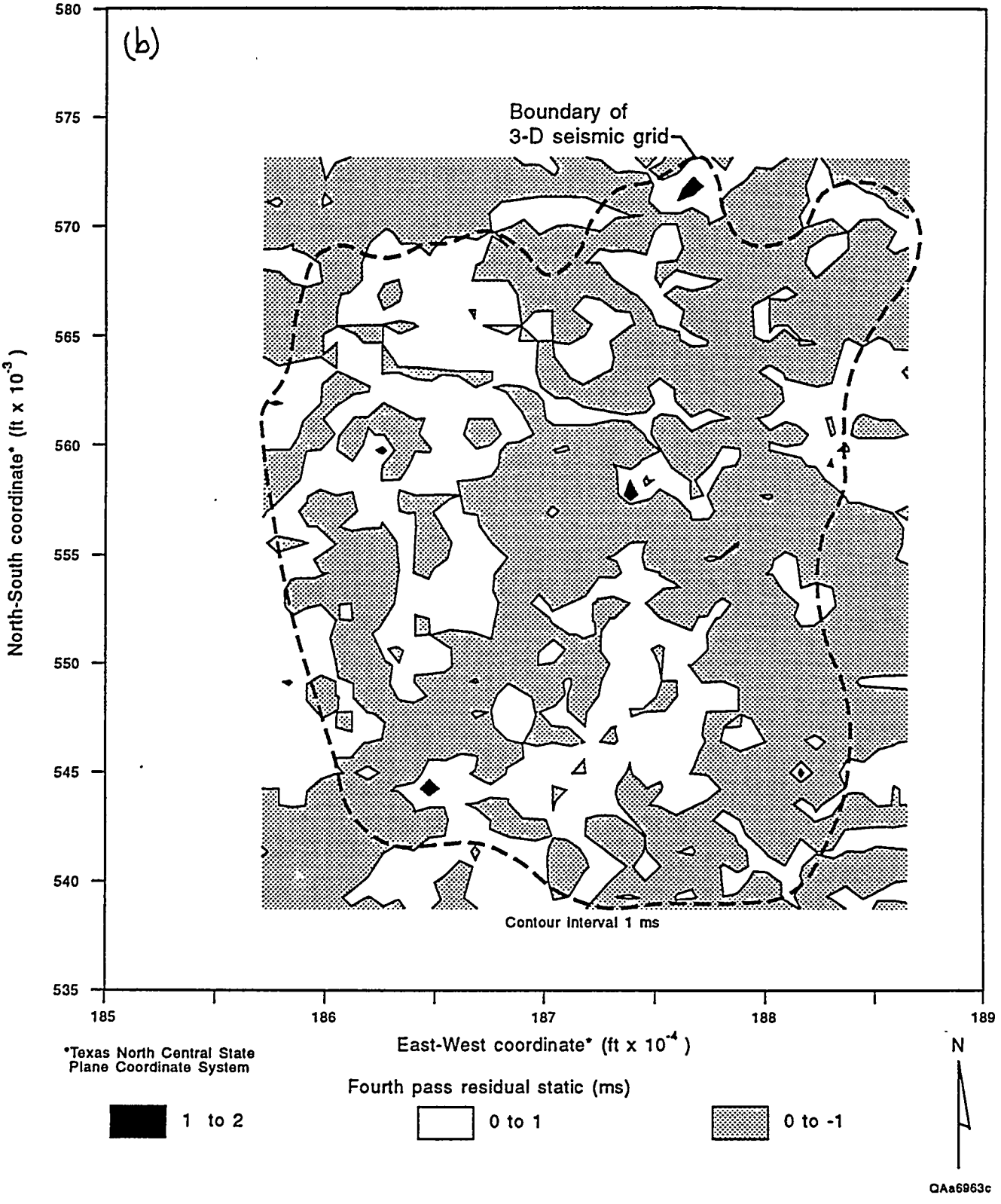
(b)
Boundary of
3-D seismic grid
Contour Interval 1 ms
North-South coordinate* (ft x 10^{-3})
East-West coordinate* (ft x 10^{-4})
580
575
570
565
560
555
550
545
540
535
185
186
187
188
189
*Texas North Central State
Plane Coordinate System
Fourth pass residual static (ms)
1 to 2
0 to 1
0 to -1
N
QAa6963c

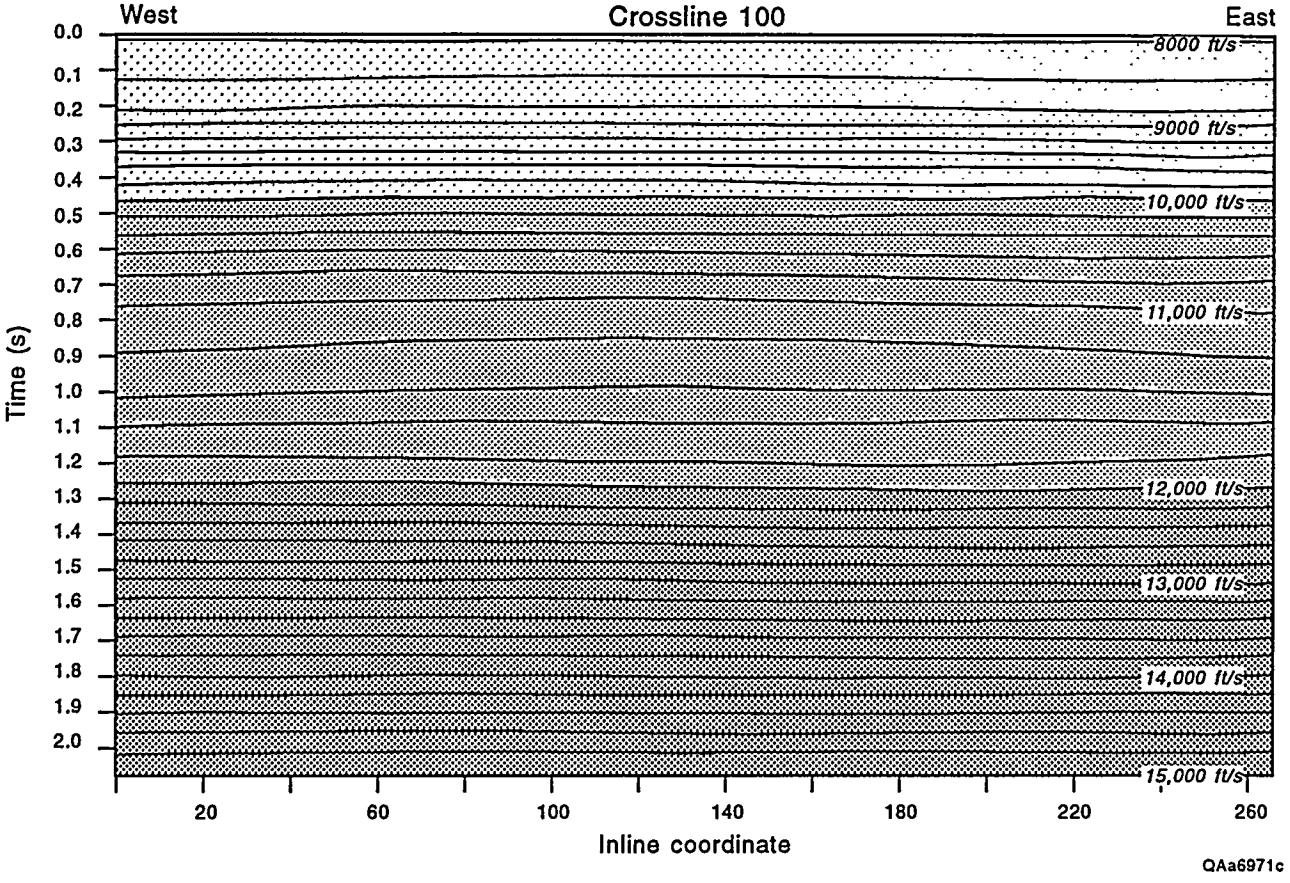

Figure D28. West-east profile of the final stacking velocities along crossline 100. See Figure D29 to locate this crossline coordinate. The velocity behavior is relatively smooth along this profile.

D.48

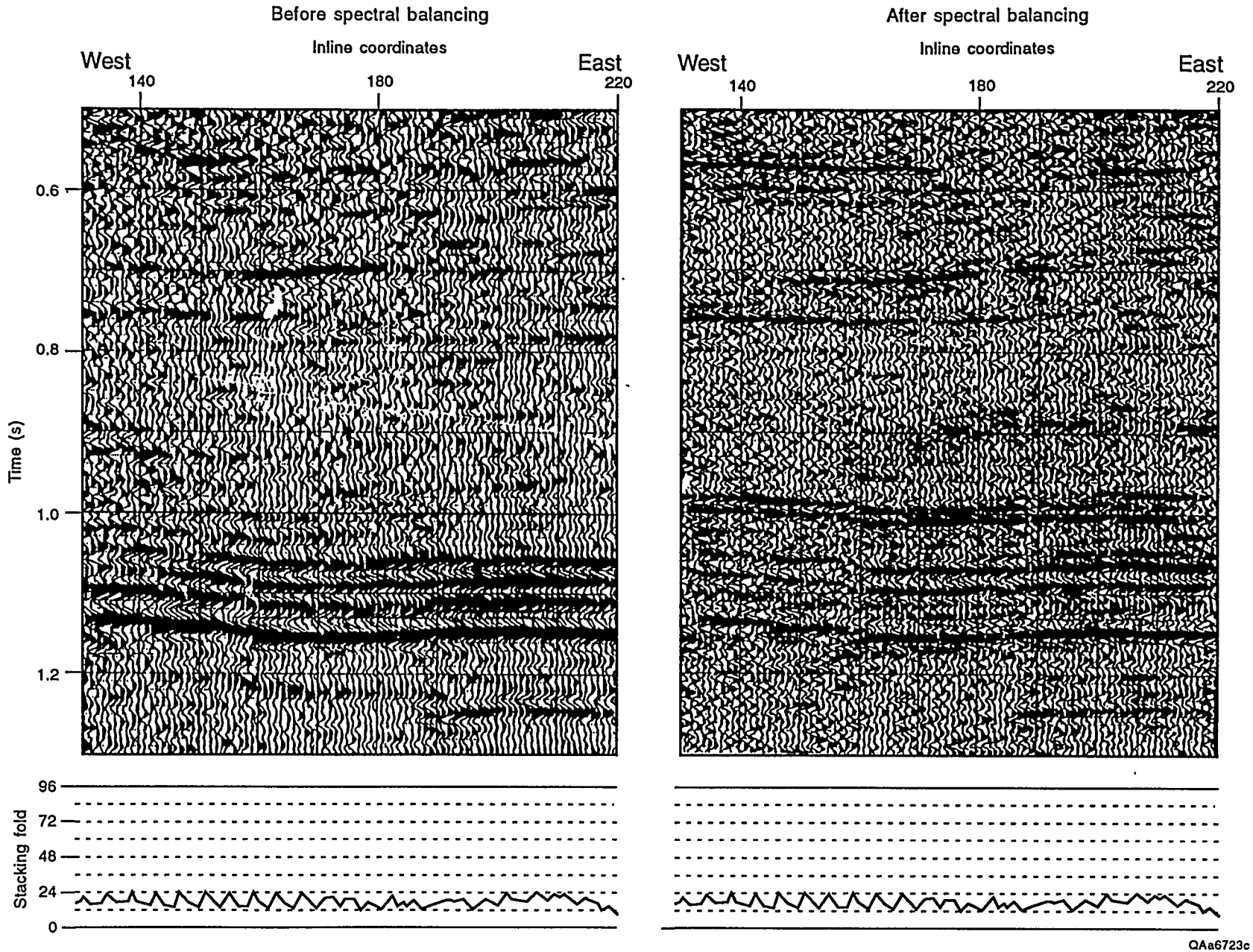

Figure D30. A comparison between Boonsville data stacked without spectral balancing (left) and with spectral balancing (right). The spectrally balanced data have better resolution and exhibit dramatic improvements in signal-to-noise in some time intervals. See, for example, the strong reflection signal near 1.0 s in the spectrally balanced data. This reflection event is critical for interpreting the Atoka interval, which extends from 0.8 to 1.1 s (approximately), but this reflection signal is overwhelmed by noise in the image on the left.

D.59

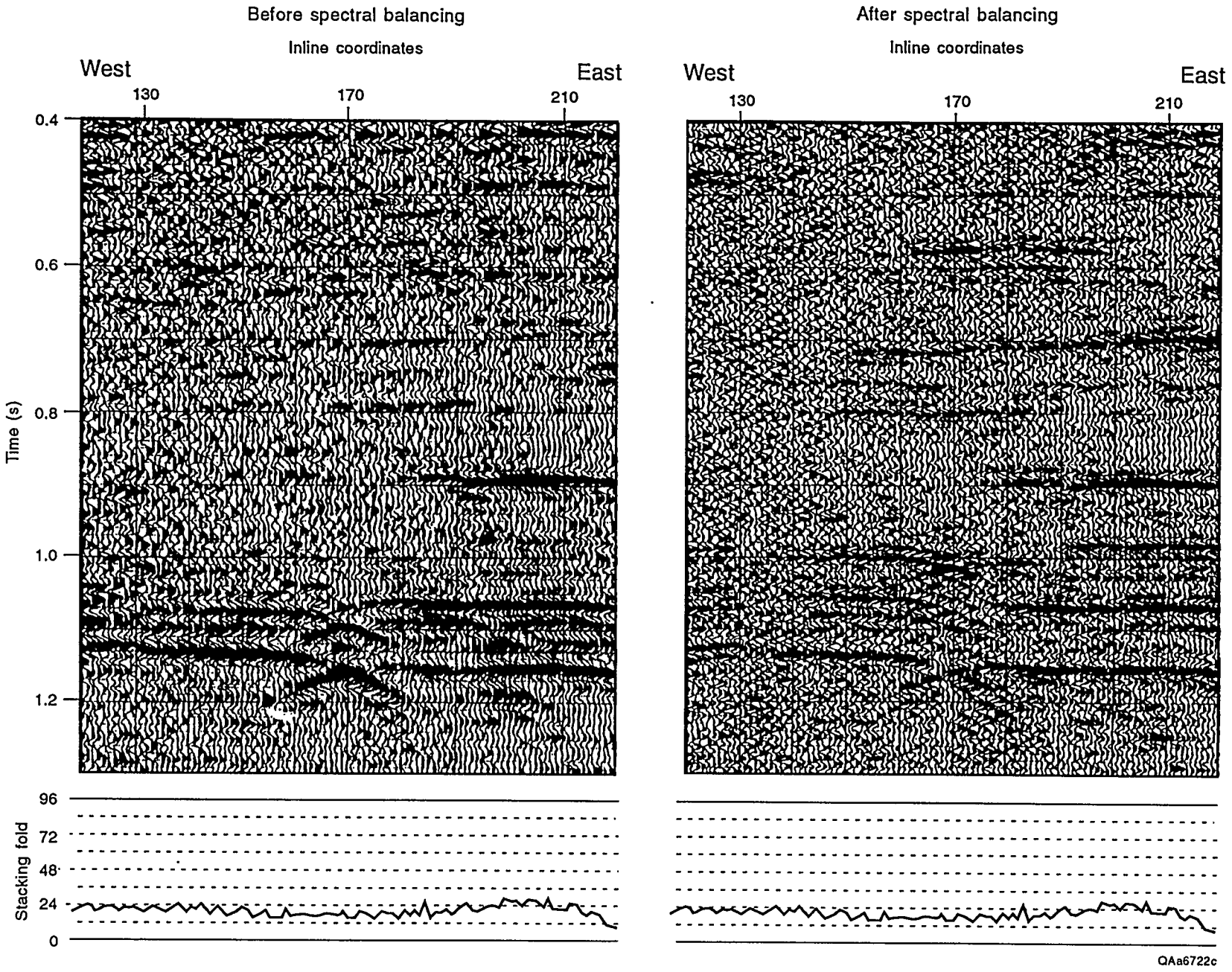

Figure D31. A second comparison between Boonsville data stacked without spectral balancing (left) and with spectral balancing (right). Again, the spectrally balanced data have a superior resolution and reveal reflection events in the Atoka interval (~0.8 to 1.1 s), which cannot be easily interpreted in the image on the left.

D.51

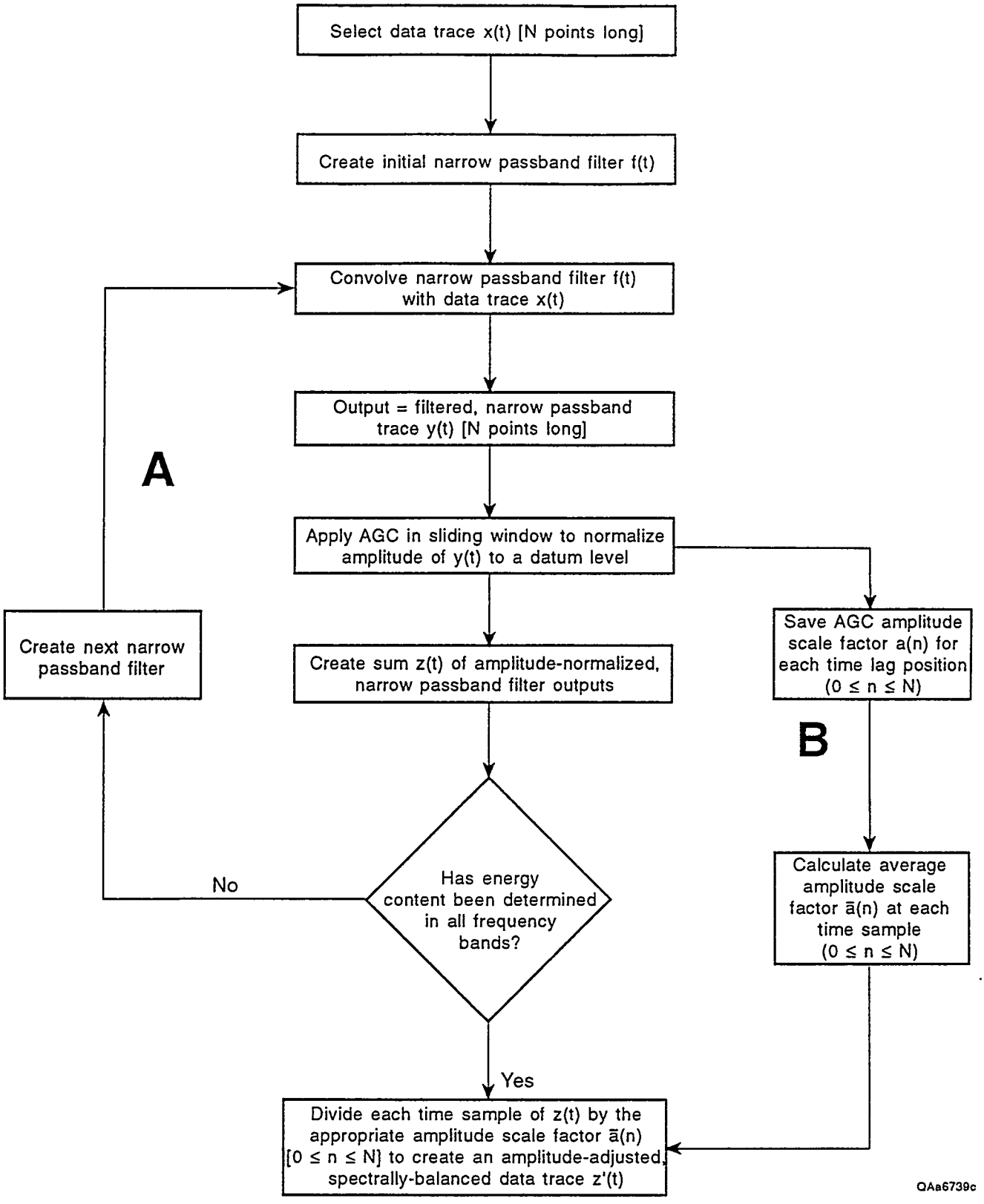

Figure D33. Flow chart showing the numerical steps involved in spectral balancing. Computation loop A creates the overlapping narrow passband filters and applies them in the time domain. Computation loop B creates the scale factors used to adjust each data sample of the output trace, a different scale factor being used for each data sample.

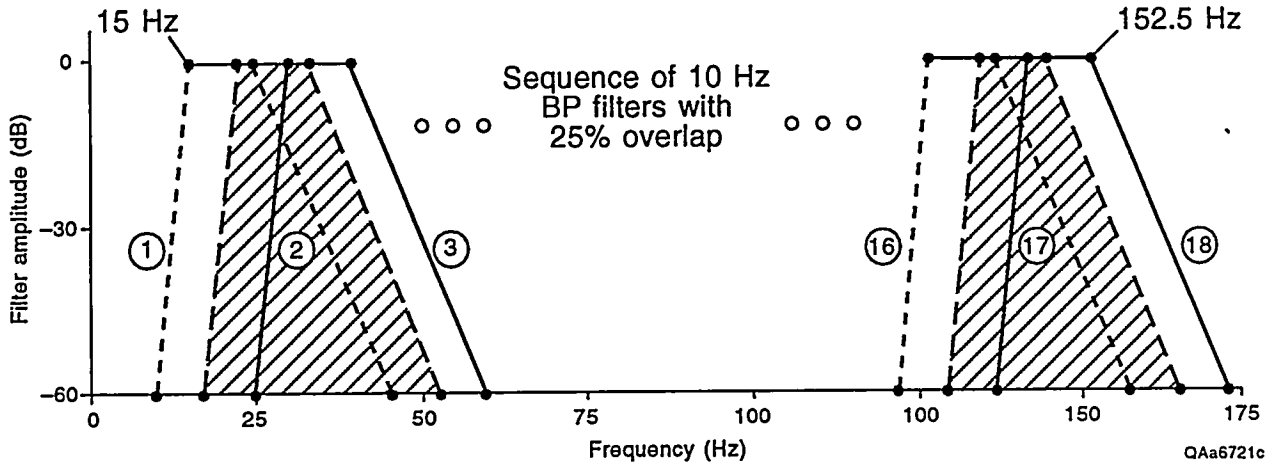

Figure D34. The specific bandpass (BP) filters created in computation loop A (Fig. D33) for the Boonsville data. A total of 18 filters were used to span the signal bandwidth extending from 15 to 152.5 Hz. Each filter had a full-pass interval that was 10 Hz wide, and the width of the rolloffs at the lower and upper ends of each filter was 5 and 20 Hz, respectively. The full-pass interval of each filter overlapped the full-pass interval of the preceding filter by 25 percent (i.e., by 2.5 Hz).

APPENDIX E
SEISMIC ATTRIBUTES

The numerical attributes that are traditionally extracted from seismic data are instantaneous amplitude, instantaneous phase, and instantaneous frequency. Taner and Sheriff (1977) and Taner et al. (1979) introduced seismic interpreters to these attributes, and since that introduction almost 20 years ago, numerous algorithms have been implemented to calculate these seismic properties (for example, Hardage, 1987, p. 199–206). All of these attributes are based on using the Hilbert transform to convert a real seismic trace into a complex seismic trace having an imaginary and a real component, the real component being an exact replication of the original seismic trace. The mathematical details of these computational algorithms will not be described; the calculation procedure will instead be described graphically.

Fundamental Principles

The concept of a complex seismic trace is illustrated in Figure E1. In this illustration, x(t) represents the real seismic trace, which in this study would be a single trace from the Boonsville 3-D migrated data volume, and y(t) is the Hilbert transform of x(t). Present algorithms calculate y(t) quite rapidly. These two data vectors are displayed in a complex (mathematically) 3-dimensional (x,y,t) space, where t is seismic traveltime, x is the real data plane, and y is the imaginary plane. The actual seismic trace x(t) is confined to the real x-plane, and y(t), the Hilbert transform of x(t), is confined to the imaginary y-plane. When x(t) and y(t) are added vectorally, the result is a complex (mathematically) seismic trace z(t), which has the shape of a helical spiral extending along, and centered about, the time axis, t. The projection of this complex function z(t) onto the real plane is the real seismic trace x(t), and the projection of z(t) onto the imaginary plane is y(t), the calculated Hilbert transform of x(t).

The reason for converting the real seismic trace x(t) into a seemingly more mysterious complex seismic trace z(t) is illustrated in Figure E2, where the concepts of instantaneous seismic amplitude, phase, and frequency are introduced. At any point on the time axis, a vector a(t) can be calculated that extends away from the t axis in a perpendicular plane to intersect the helically shaped complex seismic trace z(t). The length of this vector is the amplitude of the complex trace at that particular instant of time, hence the term *instantaneous amplitude*. Mathematically, this amplitude value a(t) can be calculated as

$$a(t) = \sqrt{x^2(t) + y^2(t)}\ , \tag{1}$$

because both x(t) and y(t) are known quantities, x(t) being the actual seismic trace and y(t) being the calculated Hilbert transform of x(t).

The orientation angle $\phi(t)$ of this vector a(t), which is usually measured relative to the positive axis of the real x-plane, is defined as the phase of z(t) at that instant in time, hence the term *instantaneous phase*. Numerically, the phase angle is calculated as

$$\phi(t) = \tan^{-1} \frac{y(t)}{x(t)}\ . \tag{2}$$

As seismic time progresses, the vector a(t) not only moves along the t axis, but it also continually rotates about the time axis to maintain contact with the spiraling complex trace z(t). Each full rotation of the vector about the time axis increases the phase value by 360°.

In any oscillating system, and specifically for a seismic trace, frequency can be defined as the time rate of change of the phase angle. This fundamental definition is used to describe the frequency behavior of the complex seismic trace, so that the *instantaneous frequency* $\omega(t)$ at any seismic time sample is given by

$$\omega(t) = \frac{d}{dt}\,\phi(t)\ . \tag{3}$$

Graphical Example of Instantaneous Amplitude

Equations 1, 2, and 3 will now be applied to a single seismic trace to illustrate some of the characteristics of the instantaneous amplitude, phase, and frequency functions that are used in seismic interpretation. An example of an instantaneous amplitude calculation is illustrated in Figure E3. The data trace in the bottom panel is the actual seismic trace; the real and imaginary components of the associated complex seismic trace **z**(t) are identified in the top panel. As in all Hilbert transform processes, the real part of this complex trace is identical to the actual seismic trace in the bottom panel. The instantaneous amplitude function a(t) that results when equation 1 is applied to the complex trace components **x**(t) and **y**(t) is shown in the top panel. Because this a(t) function is a smooth curve passing through the apices of all the peaks and troughs of the real seismic trace, it is sometimes referred to as an *envelope function*.

Importantly, the extrema of the instantaneous amplitude function do not occur at the same seismic times as do the extrema of the real seismic trace **x**(t). Thus, when doing an amplitude interpretation of seismic data within a specific time window, two different answers can be obtained, depending on whether the interpreter analyzes the amplitudes of the actual data or the magnitudes of the instantaneous amplitude functions.

Graphical Example of Instantaneous Phase

A calculation of the instantaneous phase associated with a typical seismic trace is illustrated in Figure E4. The bottom panel in the figure is the actual seismic trace, and the real and imaginary components of the associated complex trace are shown in the center panel. Applying equation 2 to the real and imaginary components of the complex seismic trace (center panel) produces the instantaneous phase function at the top of the figure. Although phase is a positive function that monotonically increases in magnitude with seismic time, it is customarily plotted as a repetitive, wraparound function with plot limits of 0 to 360° (or –180° to +180°), as is done in this display. Each wraparound of

360° corresponds to a full rotation of the a(t) vector about the time axis as that vector stays in contact with the spiraling complex seismic trace z(t) (refer to Fig. E2).

Instantaneous phase can be calculated with the same ease and the same accuracy in the low amplitude zones of a seismic trace as it can in the high amplitude regions. Thus, a chronostratigraphic surface in a low-amplitude region of a 3-D seismic data volume can usually be constructed quicker and more accurately by interpreting the surface in a 3-D volume of instantaneous phase than by trying to track a constant phase value across the low-amplitude seismic wiggle traces.

Graphical Example of Instantaneous Frequency

The instantaneous frequencies calculated for this same seismic trace are shown in the top panel of Figure E5. The bottom two panels in this display are identical to those described in Figure E4. Although negative frequencies cannot exist physically, this instantaneous frequency function exhibits negative values at time positions t_1 and t_2. Comparing the time coordinates of these anomalous frequency values with the time coordinates of the instantaneous phase function in Figure E4 shows that the phase does not exhibit its usual, monotonically increasing behavior in these time intervals, causing the time rate of change of phase (or the slope of the phase function), which is the instantaneous frequency, to be negative at time samples t_1 and t_2.

It will be shown later that these anomalous negative frequency values are often the most important information provided by any of the seismic attributes. It is thus essential that the software that calculates instantaneous frequencies not camouflage these physically unrealizable negative frequency values, which is what some algorithms have done, and some still do. Commonly negative frequencies are camouflaged to unsuspecting interpreters when the software simply changes the algebraic sign of any negative value to a positive sign. At times t_1 and t_2 in Figure E5, such software would create frequency values that follow the dashed curves shown in the enlarged view (always

positive numbers), rather than the correct solid-line curve (negative numbers). The Boonsville 3-D seismic interpretation was done with Landmark software, which preserves anomalous negative instantaneous frequencies, as a robust interpretation system should.

It should also be emphasized that a digitally sampled time function such as a seismic trace cannot contain positive frequencies that exceed the Nyquist frequency limit f_n, which is given by

$$f_n = \frac{1}{2\Delta t}, \tag{4}$$

where Δt is the time sampling interval of the seismic data. Because the seismic trace example used in Figure E5 was sampled at 4 ms, from the above equation, the highest positive frequency that can exist in this data trace is 125 Hz. Yet at time position t_3, the instantaneous frequency exceeds the allowed Nyquist bound (125 Hz). According to Figure E4, the instantaneous phase exhibits an extremely steep slope in the vicinity of this time value, causing the instantaneous frequency to achieve anomalous positive values that exceed the Nyquist limit.

It will be shown that these anomalous positive frequencies, like the anomalous negative frequencies previously discussed, are invaluable in seismic interpretation. Thus, it is essential that the interpretation software not camouflage these anomalous positive values either, which some algorithms have done by simply clipping the anomalous high positive magnitudes to a value equal to or slightly less than the Nyquist limit f_n. The Landmark software used to interpret the Boonsville data preserved the anomalous positive frequencies created by the Hilbert transform, which was a great benefit when interpreting subtle stratigraphic boundaries in the Bend Conglomerate interval, as will be emphasized in the remainder of this appendix and also in the main text of this report.

Using Anomalous Frequency Values to Define Stratigraphic and Structural Discontinuities

A fundamental objective of the Boonsville research was to determine what seismic attributes, if any, could reveal potential compartment boundaries in the Bend Conglomerate interval. Historically some seismic stratigraphers who have used Hilbert transform attributes as interpretational aids have found that the anomalous frequency values just described (i.e., any positive values that exceed the Nyquist limit or any negative values) are extremely valuable because these anomalous values pinpoint where stratigraphic and/or structural discontinuities occur, even when these discontinuities are subtle, semi-invisible features in the seismic wiggle trace data. Unfortunately, these stratigraphic interpretations have been largely confined to proprietary reports, and essentially none have entered the public domain. The remainder of this appendix will provide a public documentation of the interpretive value of these anomalous instantaneous frequencies.

Anomalous Frequency Behavior at Stratigraphic Pinch-Outs

The Boonsville 3-D seismic data volume was converted to a 3-D volume of instantaneous frequencies so that time slices could be made to show the areal mathematical behavior of instantaneous frequencies associated with interesting geologic features. One of these time slices is shown in Figure E6. The color bar used in this display shades all negative frequency values as a dark black, and an inspection of the time slice shows numerous small black areas of negative frequencies distributed over this constant-time surface. Random patterns of theses black areas have no geological significance, but patterns that align in narrow continuous trends, whether linear or sinuous, are highly significant. Three examples where anomalous frequencies develop such trends will be examined.

The first pattern is the east-west-meandering trend occurring along crossline coordinate 80 (approximately) between inline coordinates 40 to 80. Inline profile 52 crosses this anomaly and is shown as Figure E7. Note the stratigraphic pinch-out occurring at a two-way time of 900 ms (the position of the time slice in Figure E6 at crossline coordinate 80 (the position of the anomalous frequency trend). Similar anomalous frequencies occur at pinch-outs that are considerably more subtle than the one shown here. Examples of instantaneous frequency imaging subtle pinch-outs will be emphasized in the main body of the text because such pinch-outs are important indicators of compartment boundaries.

Anomalous Frequency Behavior at Reef Buildups

Referring again to the time slice in Figure E6, there is an interesting circular pattern of anomalous frequencies near the intersection of crossline coordinate 160 and inline coordinate 110. Inline 111, which crosses this anomaly, is shown as Figure E8. At a two-way time of 900 ms (the position of the time slice), there is a mounded feature at crossline coordinate 160. Although no well penetrates this feature, nearby log control from the B Yates 18D well shows that limestone units exist at this stratigraphic level, suggesting that the feature is a small reef. The boundary of this mounded buildup, be it reef or whatever, is precisely imaged by anomalous frequency values.

Anomalous Frequency Behavior at Collapsed Zones

A second circular pattern of anomalous frequencies exists near crossline coordinate 180 and inline coordinate 45 in Figure E6. Crossline profile 186 is chosen to illustrate this feature and is shown in Figure E9. In this instance, the circular feature is one of the numerous collapsed zones that exist throughout the Boonsville study area. Again, anomalous frequency values align along the circumference of this stratigraphic disruption of the Bend Conglomerate section.

Anomalous Frequency Behavior at Faults

A deeper time slice through the 3-D volume of instantaneous frequencies at 980 ms is shown in Figure E10. In this image, there is a linear east-west trend of anomalous frequencies along crossline 170 (approximately) between inline coordinates 130 and 180. Inline profile 147 (Figure E11) crosses this frequency anomaly and shows that at 980 ms, there is a fault break at crossline coordinate 170. Investigation of the Boonsville 3-D data shows that anomalous frequencies consistently pinpoint faults that are much more subtle than the one shown in this example.

Interpretational Applications

The principle shown by these examples is that most anomalous instantaneous frequency values indicate some type of distortion in the seismic reflection waveform. Because waveform distortions are often associated with pinch-outs, faults, and lateral facies changes, these anomalous frequencies tend to be direct indicators of lateral structural or stratigraphic discontinuities. These frequency attributes are thus valuable indicators of reservoir compartment boundaries, and examples of instantaneous frequency being used to analyze reservoir compartment size and shape are distributed throughout this report.

References

Hardage, B. A., 1987, Seismic stratigraphy: Geophysical Press, London, 432 p. (Now available from Elsevier Science Ltd., Oxford, England.)

Taner, M. T., Koehler, F., and Sheriff, R. E., 1979, Complex seismic trace analysis: Geophysics, 44, p. 1041–1063.

Taner, M. T., and Sheriff, R. E., 1977, Application of amplitude, frequency, and other attributes to stratigraphic and hydrocarbon determination: American Association of Petroleum Geologists Memoir 26, p. 301–327.

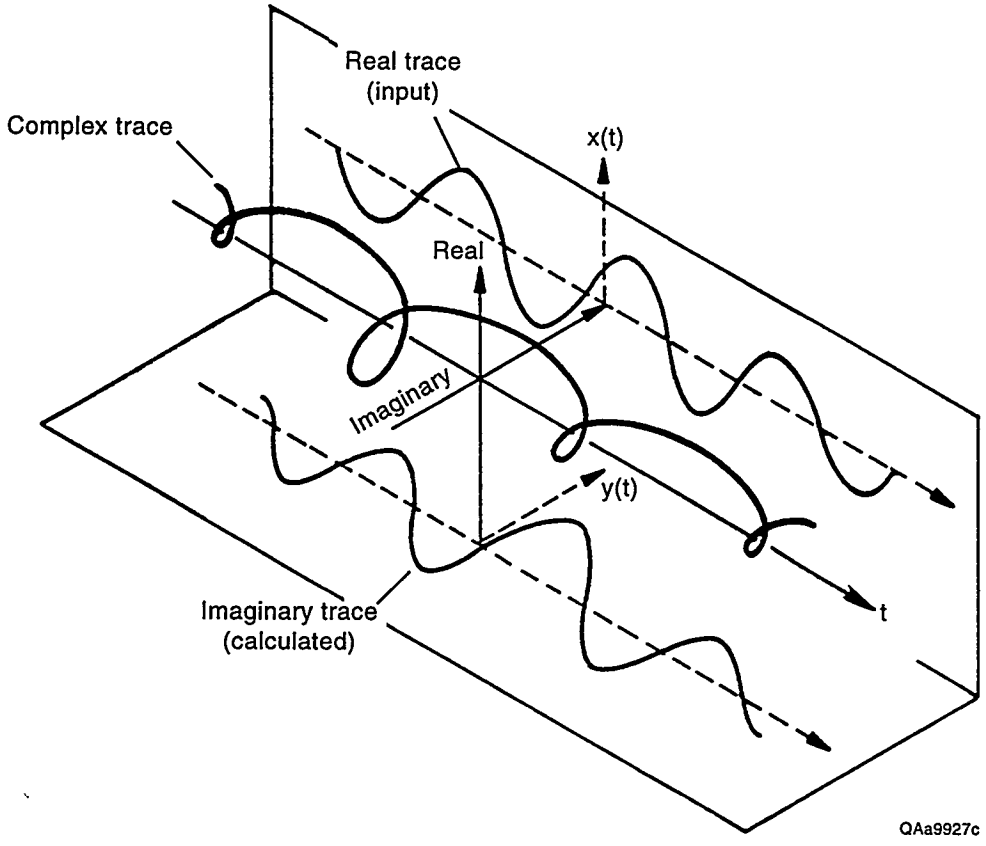

Figure E1. Graphical illustration of a complex seismic trace. The real part of the complex trace is an actual seismic trace, which in this study would be a single trace from the final migrated 3-D seismic data volume. The imaginary part is a mathematical function calculated from the real trace by a Hilbert transform process. When the real and imaginary traces are added in a vector sense, the result is a helical spiral centered about the seismic time axis. This helical trace is the complex seismic trace.

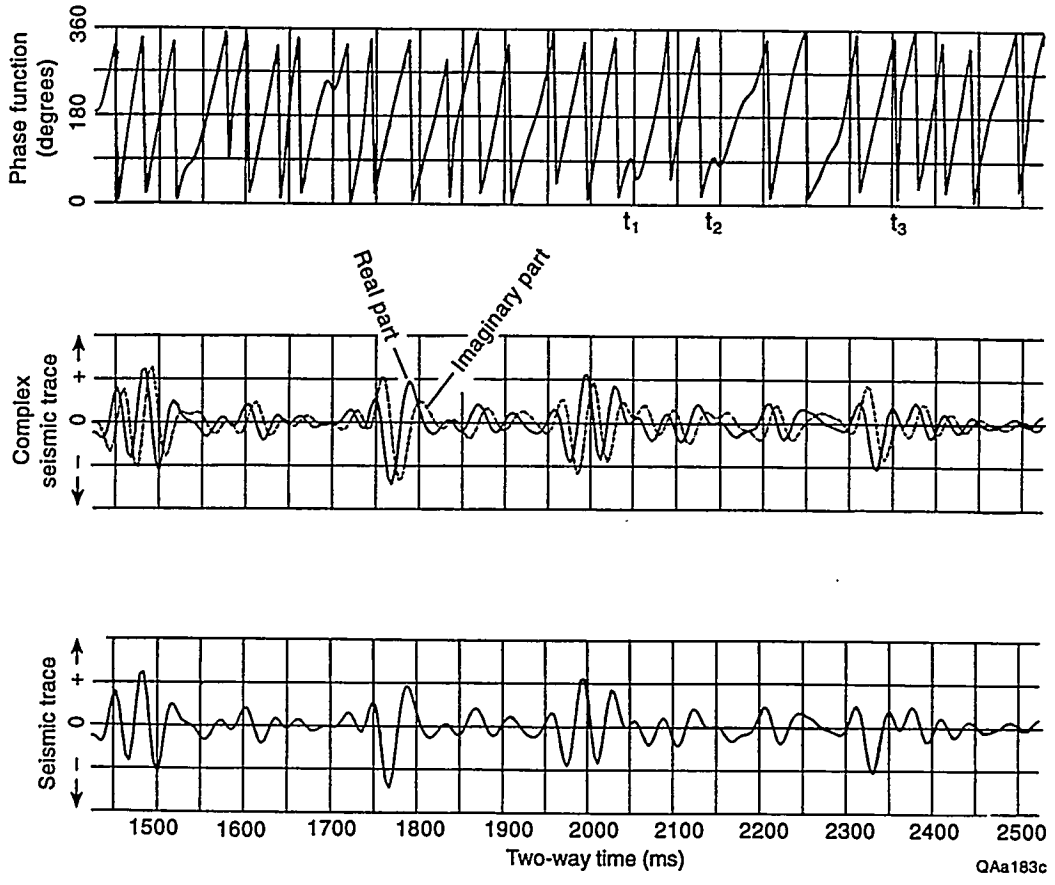

Figure E4. The instantaneous phase seismic attribute function. The real seismic trace is shown in the bottom panel, the real and imaginary components of the associated complex seismic trace are shown in the center panel, and the calculated instantaneous phase is shown in the top panel. The phase behavior at times t_1, t_2, and t_3 is discussed in the text of this appendix.

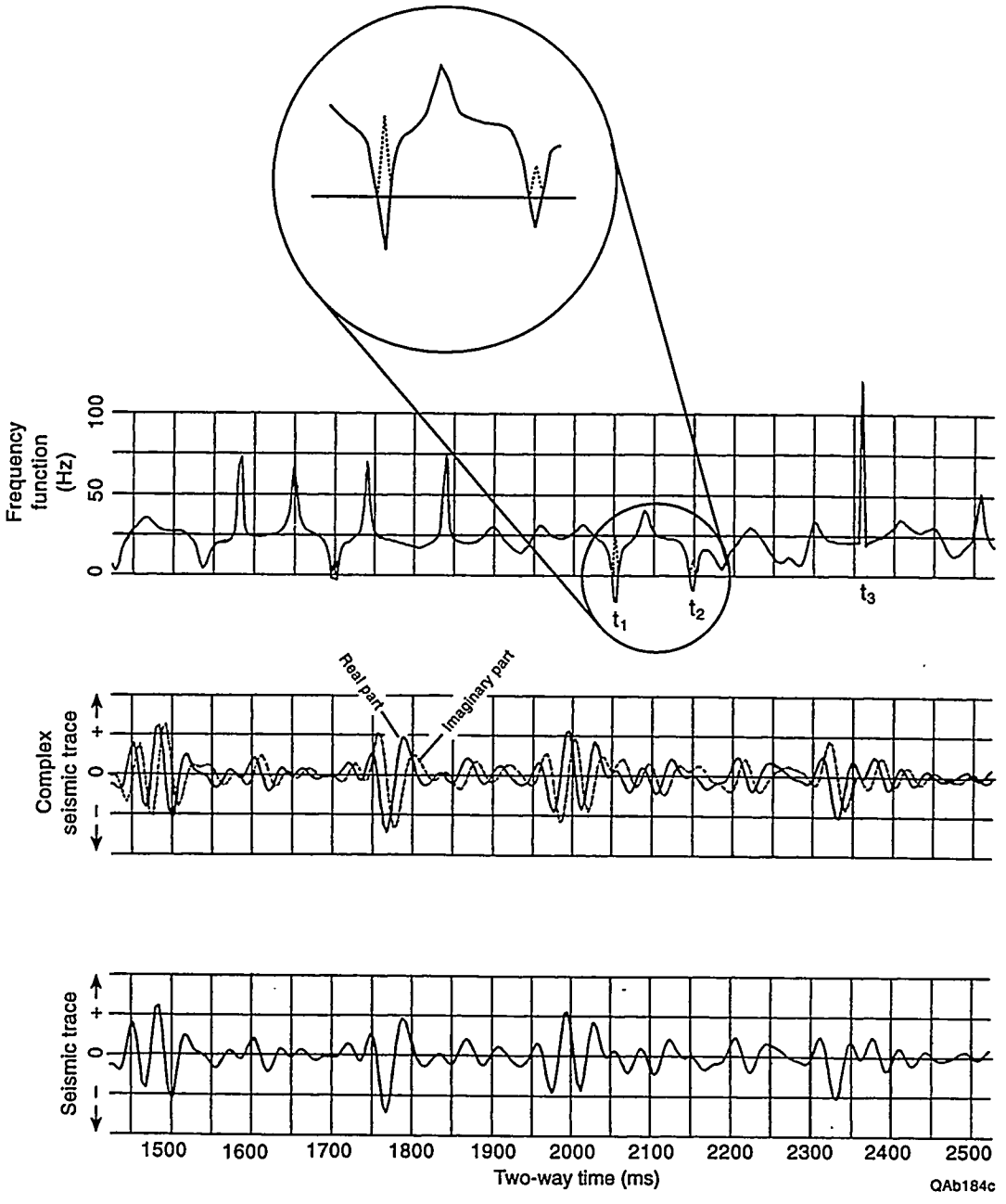

Figure E5. The instantaneous frequency seismic attribute function calculated for the same seismic trace discussed in Figure E4. The bottom two panels are identical to the two bottom data panels in Figure E4. The calculated instantaneous frequency function is shown in the top panel. The frequency behavior at times t_1, t_2, and t_3 is discussed in the text of this appendix.

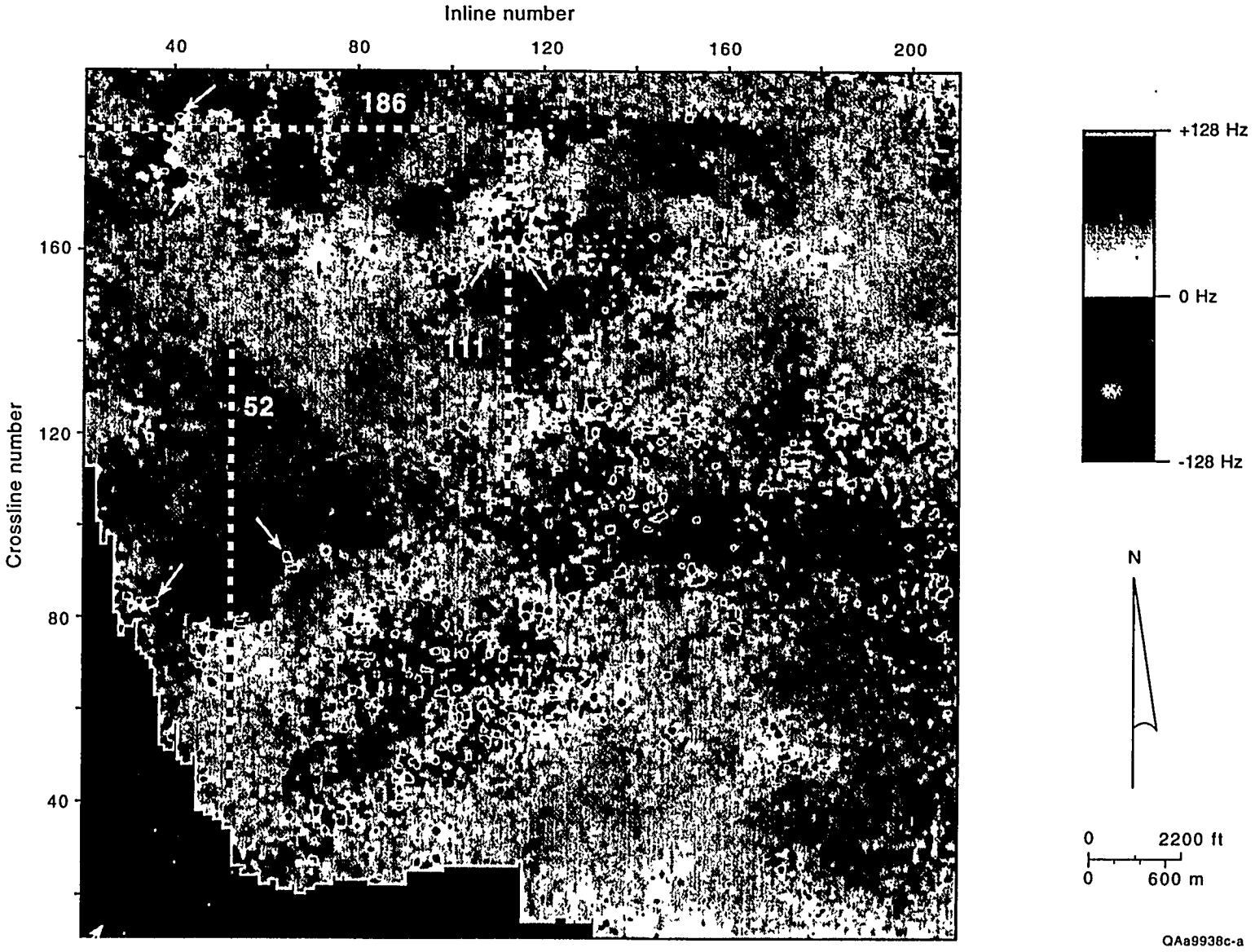

Figure E6. A time slice cutting through the Boonsville 3-D instantaneous frequency volume at a two-way time of 900 ms. The color bar is chosen so that anomalous frequency values (any negative value or any extreme positive value) are emphasized. The arrows point to locations on this image where such anomalous instantaneous frequency occurs. Seismic profiles 52, 111, and 186 will be used to illustrate how these anomalous instantaneous frequency values define structural and stratigraphic discontinuities.

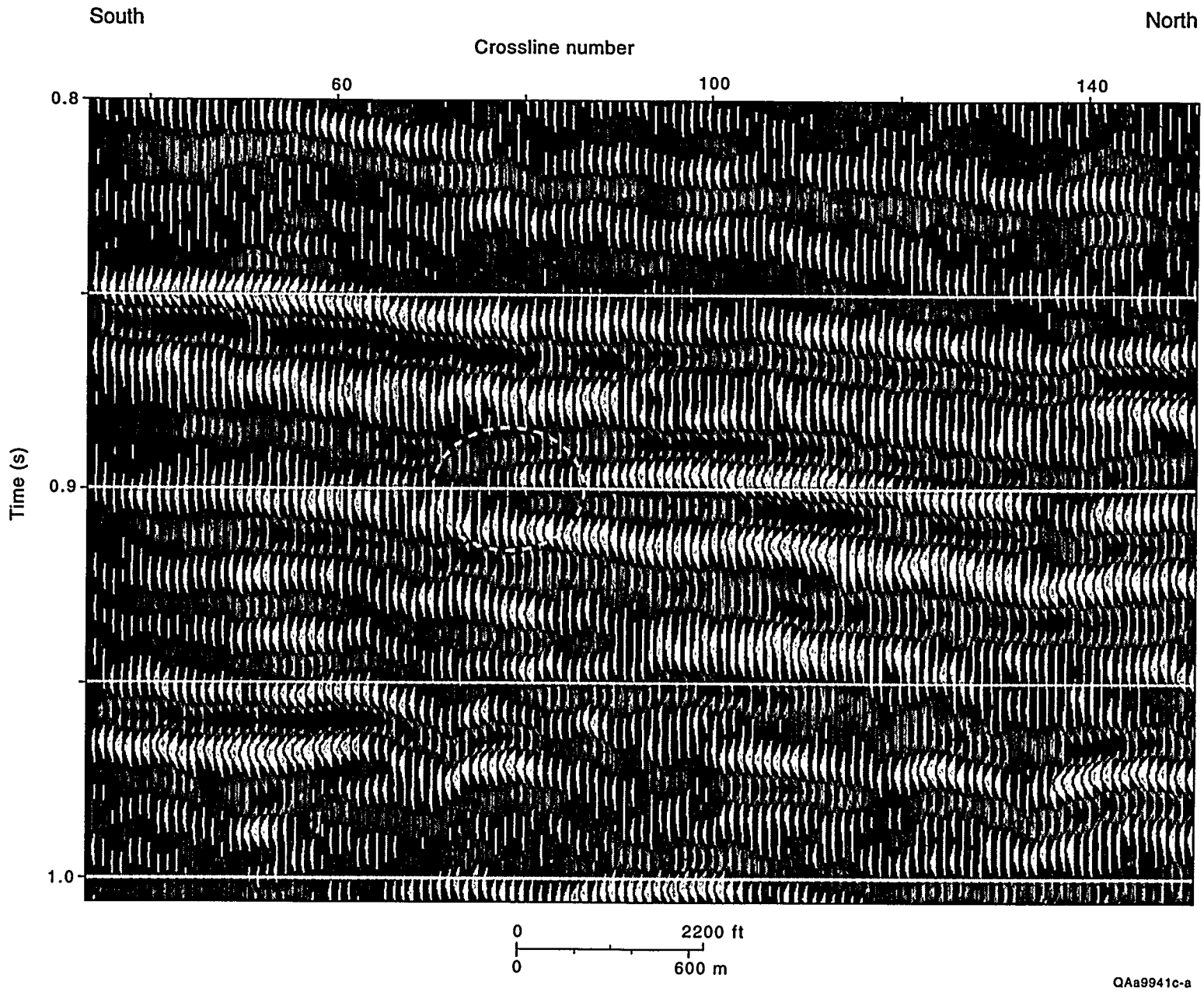

Figure E7. Inline profile 52 showing that the anomalous instantaneous frequency values in the vicinity of crossline coordinate 80, which form part of the east-west trend shown in the 900-ms time slice in Figure E6, are associated with a stratigraphic pinch-out. These anomalous frequencies occur at 900 ms near the center of the circled area.

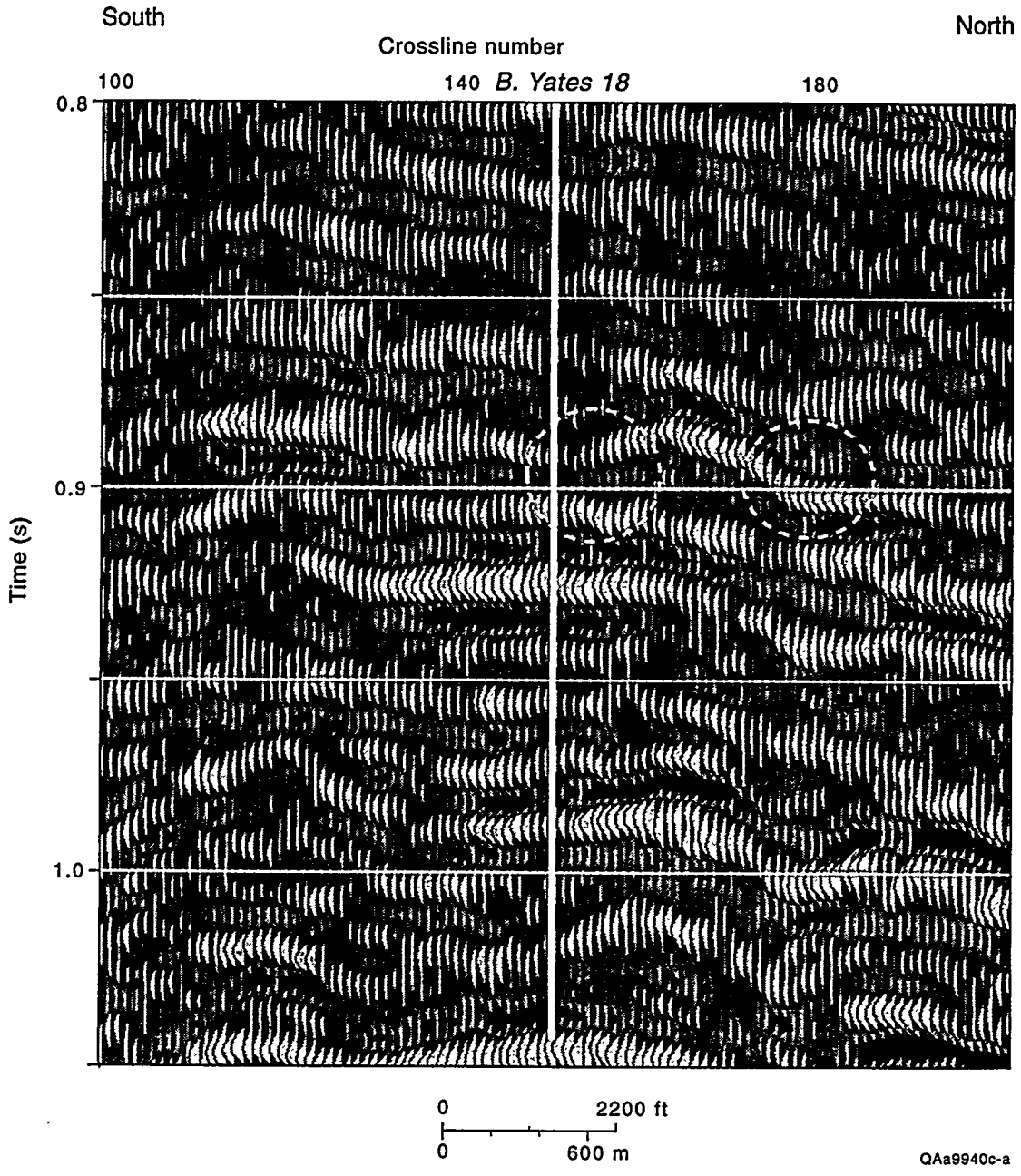

Figure E8. Inline profile 111 showing that the anomalous instantaneous frequency values in the vicinity of crossline coordinate 165, which form a ring in the 900-ms time slice in Figure E6, are associated with a stratigraphic mound (reef?). These anomalous frequencies occur at 900 ms near the centers of the two circled areas.

E.16

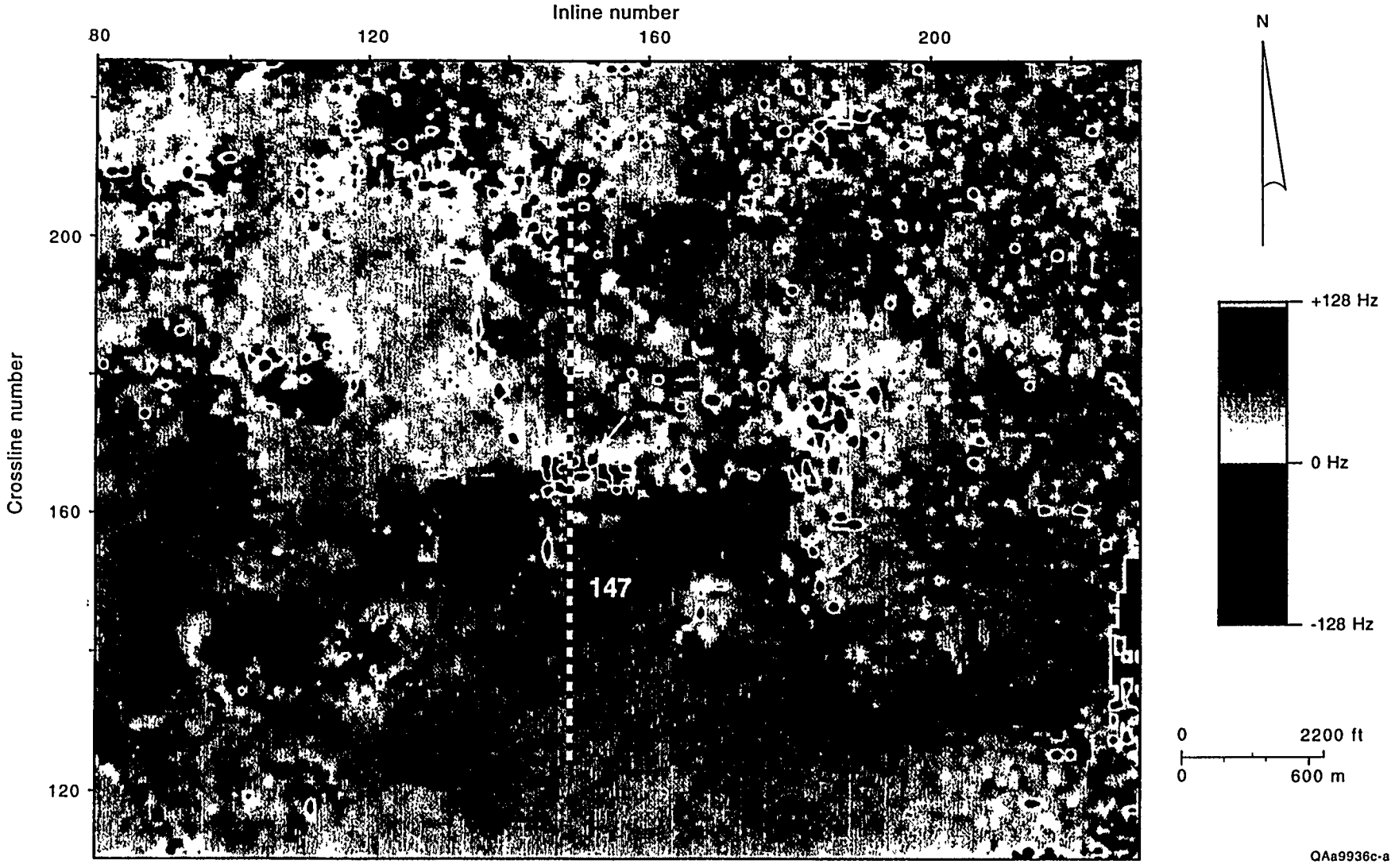

Figure E10. A time slice cutting through the Boonsville 3-D instantaneous frequency volume at a two-way time of 980 ms. The color bar is chosen so that anomalous frequency values (any negative value or any extreme positive value) are emphasized. The arrows point to locations where such anomalous instantaneous frequencies occur. Seismic profile 147 will be used to illustrate how the east-west linear trend of anomalous frequencies near crossline coordinate 170 maps a fault.

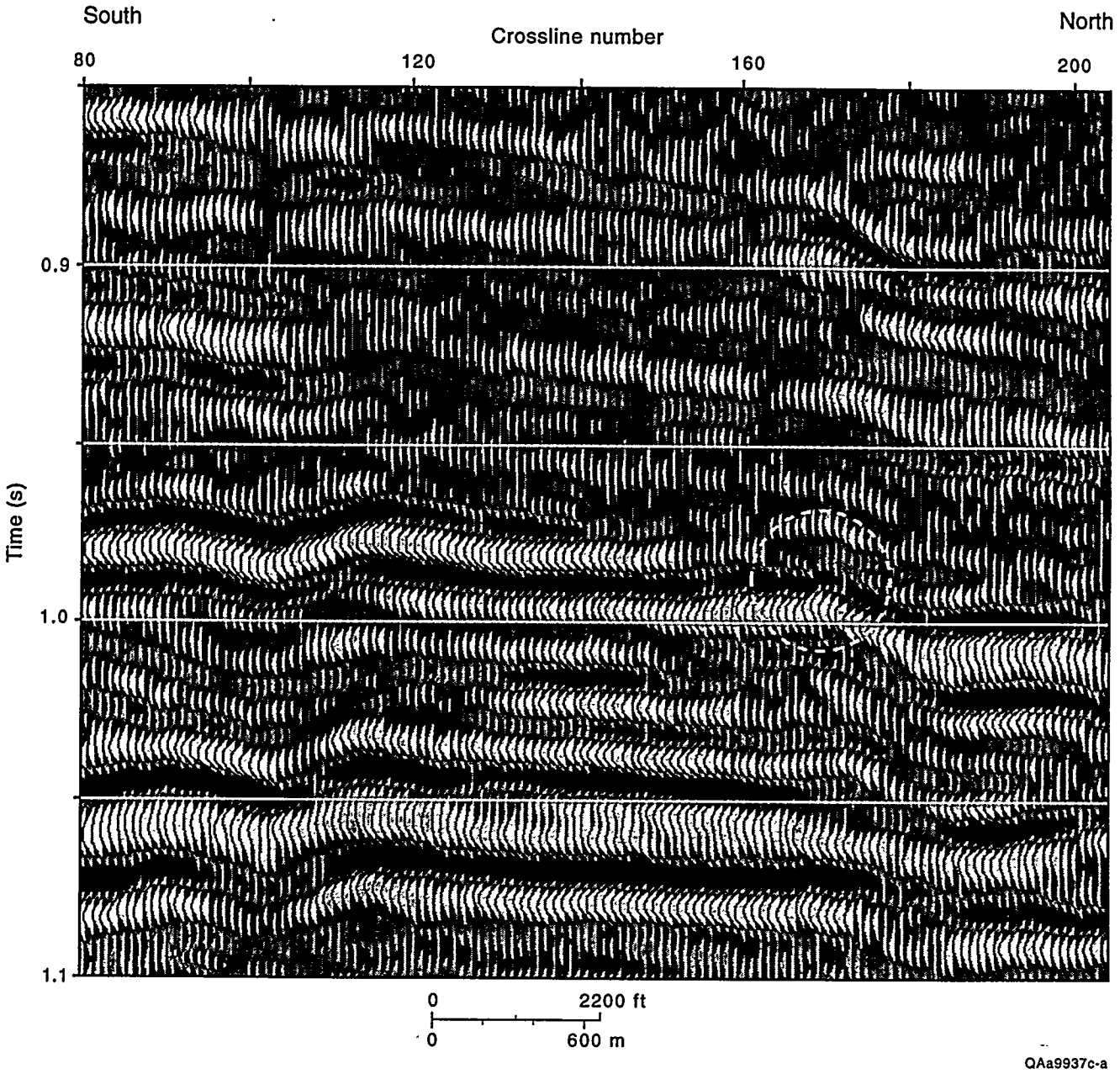

Figure E11. Inline profile 147 showing that the anomalous instantaneous frequency values in the vicinity of crossline coordinate 170, which form an east-west linear trend in the 980-ms time slice in Figure E10, are associated with a fault. These anomalous frequencies occur at 980 ms near the center of the circled area.

APPENDIX F

INTERPRETING THIN-BED STRATIGRAPHY IN 3-D SEISMIC DATA VOLUMES

Probably the most challenging problem in constructing seismic images of thin-bed reservoirs is to define precisely where the stratal surface representing a specific targeted thin bed is located in the seismic reflection response. This appendix describes a methodology that can be used to position thin-bed stratigraphy accurately in 3-D seismic data volumes. This methodology was particularly important in the Boonsville project because many of the depositional sequences that had to be seismically imaged were thin beds, which could not be seismically *resolved*; that is, there were no distinct peaks and troughs at the top and bottom boundaries of the bed. Even though the time thickness of these thin beds could not be resolved, the beds could usually be *detected* because they were positioned within a specific reflection peak or trough whose time coordinate could be defined by an appropriate depth-to-time calibration function. The challenge faced by a seismic interpreter is to select the correct peak or trough that contains the targeted thin bed.

Correcting for Velocity Anisotropy and for Time Shifts Produced by Data Processing, Source Wavelets, and Variation in Depth Datum

The critical measurement needed for calibrating seismic traveltime with stratigraphic depth is a zero-offset, or a moderate-offset, vertical seismic profile (VSP) because VSP data provide the following information, which is most important when positioning thin-bed images in a 3-D seismic data volume:

(1) a precise relationship between vertical traveltime and stratigraphic depth and

(2) an image, based on vertical seismic velocities and vertical seismic traveltimes, of the stratigraphic thin beds penetrated by the VSP well.

These interpretational benefits of VSP-derived data are emphasized in Figure F1.

The key phrases used here to describe the information provided by a zero-offset VSP (and a moderate-offset VSP also) are *vertical seismic velocities* and *vertical seismic traveltimes*. The word *vertical* is stressed because vertical ray paths and a vertical source-receiver geometry are involved in VSP data recording (Fig. F1a). In contrast, it is *horizontal* velocity that controls the time positions of reflection events that are generated by surface sources and then recorded by offset surface-based receivers, which is the geometry used in a 3-D seismic grid (Fig. F1a and F1b). This observation results because velocity V in the normal moveout equation that time-shifts reflections before stacking is the velocity in the horizontal direction. In general, seismic velocities measured in the Earth are anisotropic, with velocity V_x in the horizontal direction usually being faster than velocity V_z in the vertical direction. This anisotropic behavior is the reason the wavefront in Figure F1a is drawn as an ellipse in which the wavefront has traveled farther in the horizontal direction than in the vertical direction. This velocity anisotropy ($V_z<V_x$) exists because the Earth is more layered, and therefore more heterogeneous, in the vertical direction than it is in the horizontal direction.

Recording zero-offset and moderate-offset VSP data at depth increments of 50 ft or so through a stratigraphic interval provides a detailed and precise relationship between *vertical* traveltime and stratigraphic depth. This depth-versus-time calibration allows any geologic or engineering measurement that is known as a function of depth to be accurately positioned as a function of time in zero-offset and moderate-offset VSP images. The next (and last) critical step of seismic thin-bed interpretation is to determine how these VSP images (which are images in which reflections are positioned in terms of vertical traveltime and where vertical traveltime can be directly associated with depth) should be shifted in time to correlate with a 3-D image (which is an image in which reflection events are positioned in terms of horizontal traveltime, not vertical traveltime, and where there is no defined relationship between horizontal traveltime and depth).

This last step of the thin-bed calibration procedure is done by time-shifting the VSP image relative to the 3-D image at the VSP control well until the VSP reflection events and the 3-D reflection events align in an optimal manner. Often a VSP reflection event occurs at a time that is slightly greater than where it occurs in 3-D data because the vertical velocity V_z is usually less than the horizontal velocity V_x. The amount of time shift required for optimal alignment of the VSP and 3-D images may not be the same for shallow reflection events as for deep reflection events if the magnitude of the velocity anisotropy changes with depth.

In addition to accounting for the traveltime differences caused by velocity anisotropy, this time shifting of VSP and 3-D images to determine optimal image alignment also removes any timing differences that exist in the two images due to (1) different wavelets being involved in the VSP and 3-D data, (2) different data-processing procedures being used to create the two images, and (3) a different depth datum being used to define when $t = 0$ in each image. These observations are emphasized in Figure F1d. This time shifting and alignment of VSP and 3-D images to adjust for any phase differences that exist between the 3-D and VSP data due to different wavelets being involved in the respective data recordings and different data-processing procedures being used to make the images is the major reason VSP data, rather than velocity checkshots, are preferred for depth-to-time calibration. Velocity checkshots do not provide an independent image of the subsurface that can be correlated with the 3-D image to confirm whether wavelet phase differences, and therefore timing differences, exist between the 3-D data and the data used to define the depth-to-time calibration function. Both checkshot and VSP data were used for depth-to-time calibration in the Boonsville study.

Equivalent Source Requirement

It is not unusual to observe slightly different traveltimes between seismic wavefields generated by impulsive sources and wavefields produced by vibratory sources.

Sometimes small traveltime differences are noted even between wavefields generated by different impulsive sources—for example, when air-gun wavefields are compared with explosive wavefields or with weight-drop wavefields. These traveltime differences can sometimes be removed by numerical equalization procedures during data processing, but when confronted with the problem of interpreting thin sequences in a 3-D seismic data volume, one should use the same energy source for recording the depth-to-time calibrating data (velocity checkshot and VSP data) as the source that is used to produce the 3-D seismic wavefields. If a vibroseis source is used for the 3-D survey, a vibroseis source should be used to acquire the checkshot and/or VSP data. If explosives were used to generate the 3-D data, explosives should be used as the checkshot source and as the VSP source.

To calibrate the Boonsville sequence stratigraphy of the Boonsville 3-D seismic data, velocity checkshots were recorded in four wells across the study area. Because small directional charges deployed in 10-ft shot holes were used to generate the 3-D data, these same directional charges were detonated in 10-ft holes to produce the checkshot data. The checkshots were typically recorded at vertical intervals of 500 ft.

It is quite expensive to prepare the large number (approximately 300) of loaded shot holes needed for an explosive-source vertical seismic profile because VSP data are typically recorded at vertical intervals of 50 ft over a vertical aperture of approximately 3,000 ft. For reasons of economy, therefore, when VSP data were recorded in three of these four Boonsville velocity control wells, the energy source that was used was vibroseis rather than loaded shot holes. Numerical wavelet equalization techniques were then used to adjust the vibroseis VSP images to a vertical traveltime coordinate frame equivalent to that which would have resulted if loaded shot holes had been used. An explosive-source VSP image was thus created in each well from a less costly vibroseis VSP image.

Measuring Vertical Traveltime-versus-Depth inside the Boonsville 3-D Grid

The relationship between stratigraphic depth and vertical seismic traveltime was determined at four locations inside the 26-mi^2 Boonsville 3-D grid: the B. Yates 11, B. Yates 17D, B. Yates 18D, and J. D. Craft TWB 3 wells (Fig. F2). Two measurements were made in the B. Yates 11, 17D, and 18D wells—(1) VSP data were recorded using a surface vibrator as the energy source and (2) a checkshot survey was done in which C-10 directional charges deployed in 10-ft holes were used as the energy source. These directional charges are described in Appendix D.

The depth-versus-time curves observed in the B Yates 11 and 18D wells are shown in Figure F3. A comparison of these curves is essential for two reasons:

1. It is important to know whether vibroseis and pentolite wavelets exhibit significantly different traveltimes. If there are major differences in the traveltimes of the wavelets emitted by these two sources, then special steps must be taken if the Boonsville VSP data (which are generated by vibroseis sources) are used to calibrate the 3-D seismic data (which are generated by pentolite sources).
2. It is important to know whether anisotropy causes significant traveltime differences to exist between vertical travel paths (the pentolite checkshot curves) and slant travel paths (the offset VSP curves). If the traveltime differences are minor, then the pentolite checkshot data can be used as depth-to-time calibration data for the 3-D seismic data without our having to apply dynamic adjustments to the checkshot times.

Visual inspection of Figure F3 shows that the two traveltime curves measured for vertically traveling pentolite checkshot wavelets and the two traveltime curves measured for vibroseis VSP wavelets (one based on vertical travel paths and one based on slant paths) follow a similar, but not identical, trend. To determine the potential impact of the

traveltime variations manifested by these pentolite and vibroseis wavelets, and by their vertical and slant travel-path geometries, we show the same data in a different format in Figure F4. Here we plot the difference between the depth predicted by each traveltime curve and the depth predicted by the average of all four traveltime curves. This plot allows these important conclusions to be made:

1. Pentolite and vibroseis wavelets do not exhibit significant traveltime differences in our study area. This conclusion is supported by the pentolite and vibroseis traveltime curves measured in the B Yates 11 well, which compare traveltimes along the same vertical travel paths. The depths predicted by these two traveltime curves differ by no more than 50 ft within the Bend Conglomerate, which is not a significant difference because slight errors in picking first-arrival times in these high-velocity rocks can create depth differences of 20 to 30 ft.
2. Velocity anisotropy may indeed be a problem that has to be dealt with when calibrating stratigraphic depth to the Boonsville 3-D seismic data. This concern is supported by the depth difference of approximately 100 ft, which the two traveltime curves that were recorded in the B Yates 18D well (one a measurement using vertical travel paths and one a measurement using slant travel paths) define for the Bend Conglomerate interval. A depth difference of this magnitude concerns us because (1) it cannot be attributed to imprecise picking of first arrivals and (2) some of the Bend Conglomerate sequences are thinner than 100 ft.

On the basis of this concern, we decided to investigate the problem of velocity anisotropy across the project area. A part of this investigation was to determine whether the variation of vertical traveltimes, measured at different sites across the 3-D seismic grid, was approximately the same magnitude as the variation seen between vertical and slant travel paths at the B Yates 18D well (Fig. F4). Vertical traveltimes for pentolite

wavelets were measured at four wells, the B Yates 11, 17D, 18D, and Craft TWB No. 3 (see Fig. F1). These traveltime curves are displayed in Figure F5, and the variances in the depth predictions provided by these traveltime curves are shown in Figure F6.

We analyzed velocity anisotropy by concentrating on the data display in Figure F6. Because the Craft TWB No. 3 curve had an erratic behavior compared with those of the other traveltime curves, we reviewed the Craft TWB No. 3 data but could not find any significant errors in our first break picks. These Craft TWB No. 3 data may simply have inherent time-zero errors introduced by the recording systems and/or the shooting box; we put less weight on these data, than on the other traveltime data, when doing depth-to-time conversions.

The traveltime data recorded in the B Yates 11, 17D, and 18D wells are quite reliable, and the curves in Figure F6 show that vertical traveltimes vary in a way that causes depth differences of 100 ft to occur over distances of less than 1 mi (the distance between the B Yates 11 and 18D wells). These depth differences are the same order of magnitude as the depth differences observed for vertical and slant path traveltimes at the B Yates 18D well, so we concluded that we could ignore velocity anisotropy as a potential source of depth-to-time error because we had vertical traveltime control wells distributed across the 3-D seismic grid. In other words, we established enough vertical traveltime control wells across the project area so that regardless of where we did a depth-to-time conversion inside the 3-D seismic grid, one of these velocity control wells was close enough to that site to allow a local depth-to-time calibration function to be used. This interpretational approach ensures that a correct vertical velocity function is used for the calibration, even if the rocks do exhibit anisotropic velocity behavior. Our experience leads us to make the following recommendation:

> *For precise depth-to-time conversion across a sizable 3-D seismic grid, vertical traveltime calibration functions should be established at intervals of approximately 2 mi across the grid.*

Comparison of VSP and 3-D Seismic Images

Regardless of how much care is used in 3-D seismic data recording and processing, interpreters often have lingering doubts about the accuracy of the 3-D images once they begin to use the data for thin-bed interpretation. It is, therefore, important to obtain one or more independent seismic images of the thin-bed stratigraphy and compare these images with the 3-D seismic images. At Boonsville, we acquired these independent images by recording offset VSP's at two wells, the B Yates 17D and 18D.

A comparison between the VSP and 3-D images at the B Yates 18D well is given in Figure F7. These two images are quite similar and indicate that the 3-D seismic data are reliable for thin-bed interpretation. Most of the differences between VSP and 3-D seismic images, and specifically between these shown here for the 18D well, are due to three factors:

1. Different source wavelets are involved in the two images—a vibroseis wavelet in the VSP data and a pentolite wavelet in the 3-D data.
2. Different wavelet processing procedures are used in the two image constructions.
3. A VSP image is a 2-D stack of VSP traces, but a 3-D image is a 3-D migration of 3-D traces. By definition, 2-D stacking and 3-D migration produce different images.

Considering these factors, it is remarkable that the VSP and 3-D images are as similar as they are. The wavelet differences resulting from factors 1 and 2 can be minimized by applying a numerical equalization operator to the VSP image that causes its basic wavelet to have the same phase and amplitude spectra as does the basic wavelet in the 3-D data. Figure F8 shows the image comparison after such an equalization procedure and demonstrates that the images are even more alike once they contain basic wavelets

that are numerically equivalent. Note particularly the improved image match that occurs between 0.8 and 1.0 s.

At the B Yates 17D well, we recorded two offset VSP's to further confirm whether the 3-D seismic images accurately portrayed the Bend Conglomerate stratigraphy. The comparison between the contractor-delivered VSP images and the 3-D seismic images at the B Yates 17D well are shown in Figures F9 and F11; the comparison between our numerically equalized VSP images and the 3-D image are shown in Figures F10 and F12. Like the situation at the B Yates 18D well (Fig. F8), these image comparisons confirm that the Boonsville 3-D seismic data are quite accurate and can be used for interpreting thin Bend Conglomerate sequences with high confidence. We recommend that all 3-D seismic interpreters follow our procedure if possible:

> *To confirm that a 3-D seismic image is sufficiently accurate for thin-bed interpretation, one or more VSP images should be recorded inside the 3-D grid and compared with the 3-D image.*

SEISMIC INTERPRETATION PROCEDURE USED TO IMAGE BEND CONGLOMERATE THIN BEDS

An important assumption was invoked when interpreting the thin-bed images in the Boonsville 3-D seismic data volume, namely,

> *A seismic reflection event (i.e., a reflection peak or trough) follows a chronostratigraphic surface, which is a depositional surface that existed at a fixed geologic time. Because different lithological facies occur across a depositional surface, a seismic reflection may image different lithological contrasts at different reflection points along the stratal surface that it defines.*

This assumption is not accepted by all seismic interpreters, but it is a basic premise of seismic stratigraphy and was used in the Boonsville interpretation.

To create a 3-D seismic image of a thin bed, it is essential that a chronostratigraphic surface be constructed that is seismically conformable to the thin bed in the local area where the thin-bed interpretation is being done. Once such a surface is created, all of the traces in the 3-D volume can then be time shifted so that this chronostratigraphic interface is flat everywhere in the data volume. There are two reasons for doing such a time shift:

(1) At the time of deposition, most depositional surfaces are reasonably flat in a local sense. Thus, this time shifting restores the ancient topographic surface that existed locally at the time the targeted thin-bed sedimentation occurred, and this time-shifted image often allows seismic interpreters to more easily see the stratigraphic relationships that immediately preceded and followed the local thin-bed deposition.

(2) It is easier to write software that rapidly extracts and exhibits a seismic imaging surface when all the data points on that surface are forced to occur at the same seismic traveltime rather than allowing the data points to remain on a time-varying seismic surface.

Any constant-time slice made within a reasonably narrow time window immediately above or below a flattened chronostratigraphic surface is assumed to be a single depositional surface that is conformable to the flattened reference surface. That is, each such time slice is assumed to also be a chronostratigraphic surface. When one of these horizon slices is made at the seismic traveltime where VSP (or checkshot) control defines a particular thin bed is positioned, that horizon slice is assumed to be an image that is dominated by the sedimentation pattern and the stratigraphy of the targeted thin bed, but which also contains some less-dominating, but observable, phasing effects created by stratigraphy extending a few tens of feet above and below the target thin bed.

Present interpretation software defines one of the three following features of a reflection wavelet as the phase point that can be represented as an interpreted seismic surface: (1) the extremum of the wavelet peak, (2) the extremum of the wavelet trough, or (3) the zero-crossing between the peak and trough. In the Boonsville 3-D interpretation, either peaks or troughs, not zero-crossings, were used to construct chronostratigraphic surfaces.

Any reflection event that is chosen to be a reference chronostratigraphic surface and that will then be used to flatten a 3-D data volume for time slicing purposes should exhibit the following properties:

1. The event should have a signal-to-noise character that is of sufficient quality to allow a reliable interpretation.
2. The event should be continuous and extend across all, or a large portion of, the area spanned by the 3-D data volume.
3. The event should be reasonably close to the time position of the thin bed that is to be imaged so that the assumption of conformability between the chronostratigraphic surface and the thin bed is more likely to be correct.

Sometimes all three of these conditions cannot be satisfied and compromises have to be made. Common compromises are to allow a deviation in condition 3 by selecting a

good-quality, areally pervasive reflection event that is slightly unconformable to the targeted thin bed, or to alter requirement 2 by choosing a flattening event that does not extend over a large area but is conformable to the targeted thin bed in a critical portion of the study area. The implementation of the preceding assumptions and procedures during the Boonsville data interpretation is described in the following sections.

Defining Areally Pervasive Chronostratigraphic Surfaces

Inspection of the Boonsville 3-D data volume led to the conclusion that many of the thin-bed reservoirs in the Atokan interval could be assumed to be conformable, at least in a local sense, to one of four seismic chronostratigraphic surfaces that extended across the complete 3-D survey area, and which divided the Bend Conglomerate interval into three intervals of almost equal thickness. These four sequence boundaries are defined in Figure F13 as:

1—Caddo (MFS90),
2—Davis (MFS70),
3—Runaway (MFS53), and
4—Vineyard (MFS20 for the top and MFS10 for the base),

where MFS is an abbreviation for *maximum flooding surface*.

The areally consistent reflection event defining each of these chronostratigraphic surfaces was selected in the following way:

1. Several wells (typically 25 to 30) were chosen that were distributed in an approximately uniform manner over the complete 26-mi^2 3-D grid and in which the stratigraphic depths of the Vineyard, Runaway, Davis, and Caddo boundaries were known.
2. A series of meandering seismic lines, each line connecting 4 to 6 of these calibration wells, were extracted from the 3-D data volume. An example showing the paths taken by two of these well-tie lines is shown in Figure F14.

3. The vertical traveltime required for a pentolite-generated wavelet to travel to the depth of each of the four sequence boundaries in each of the calibration wells was determined using the average of the B Yates 11, 17D, and 18D pentolite traveltime functions specified in Figure F5.
4. At each well coordinate on each of these tie lines, tic marks were superimposed on the 3-D reflection data at the vertical traveltimes determined in step 3 to show where each of the four chosen chronostratigraphic surfaces should be positioned in the 3-D image at that particular well site.
5. A judgment was then made as to which seismic reflection event (i.e., which reflection peak or which reflection trough) was reasonably conformable to all of the tic marks made for each of the four sequence boundaries and which also met the other criteria required for a chronostratigraphic surface (i.e., good signal-to-noise and lateral continuity over an acceptable portion of the 3-D area). Two examples of the tic-mark positions and the seismic chronostratigraphic surfaces that were judged to best fit each set of tic marks are illustrated as Figures F15 and F16. These well-tie lines are the arbitrary profiles labeled Line 2 and Line 5 in Figure F14.

In the two examples illustrated in Figures F15 and F16, the time picks for the top and base of the Vineyard were positioned on a reasonably consistent reflection phase, and there was little doubt where to position the chronostratigraphic reference surface (surface No. 4) that would be used to flatten and extract images of thin-bed units deposited in the lower Atoka interval. Similarly the time picks for the top of the Runaway sequence fell on a consistent reflection waveform feature, and the final interpreted Runaway horizon surface No. 3 (Figs. F15 and F16) was chosen to be a good-quality reflection trough below and conformable with these calibration tic marks.

The time picks for the top of the Davis sequence occurred on a consistent reflection trough in Figure F16, but these picks are slightly above this same trough in Figure F15.

Some judgment had to be used to decide which reflection event near these Davis picks was the best choice for a Davis-age chronostratigraphic surface. After inspecting well-tie lines over the complete 26-mi^2 area, the best-quality, areally pervasive reflection that could serve as a Davis-age chronostratigraphic surface was judged to be the event labeled 2 in Figures F15 and F16.

In the northern part of the 3-D grid, the well picks for the Caddo fell on a consistently robust reflection event (Fig. F16), but in the northern part of the grid, the Caddo picks fell slightly below this same reflective event (Fig. F15). Surface No. 1 shown in Figures F15 and F16 was judged to be the best choice for a continuous seismic event that was conformable to all of the Caddo picks.

Building Areally Continuous Chronostratigraphic Surfaces

Once the four chronostratigraphic surfaces shown in Figures F15 and F16 were defined on a number of arbitrary well-tie lines across the Boonsville 3-D grid, the surfaces were then manually transferred onto a regularly spaced grid of inlines and crosslines that intersected these meandering, randomly spaced well-tie lines. This regularly spaced line grid is referred to as a *seeding grid* because it served as the seed information to drive the automatic event-picker software that converted the interpreted horizons on each individual line of the grid into an areally continuous surface. The seeding grid used for the Caddo chronostratigraphic surface is shown in Figure F17. The line spacing was smaller along the northern edge of the survey and in a narrow east-west strip just south of crossline 200 because the data quality deteriorated in these areas, making it more difficult for the automatic interpolation software to construct a continuous chronostratigraphic surface in these regions. The seeding grids for the other three Atokan-age seismic chronostratigraphic surfaces were similar to this Caddo grid. This interpretational procedure was used to generate all seismic structure and attribute maps shown in this report.

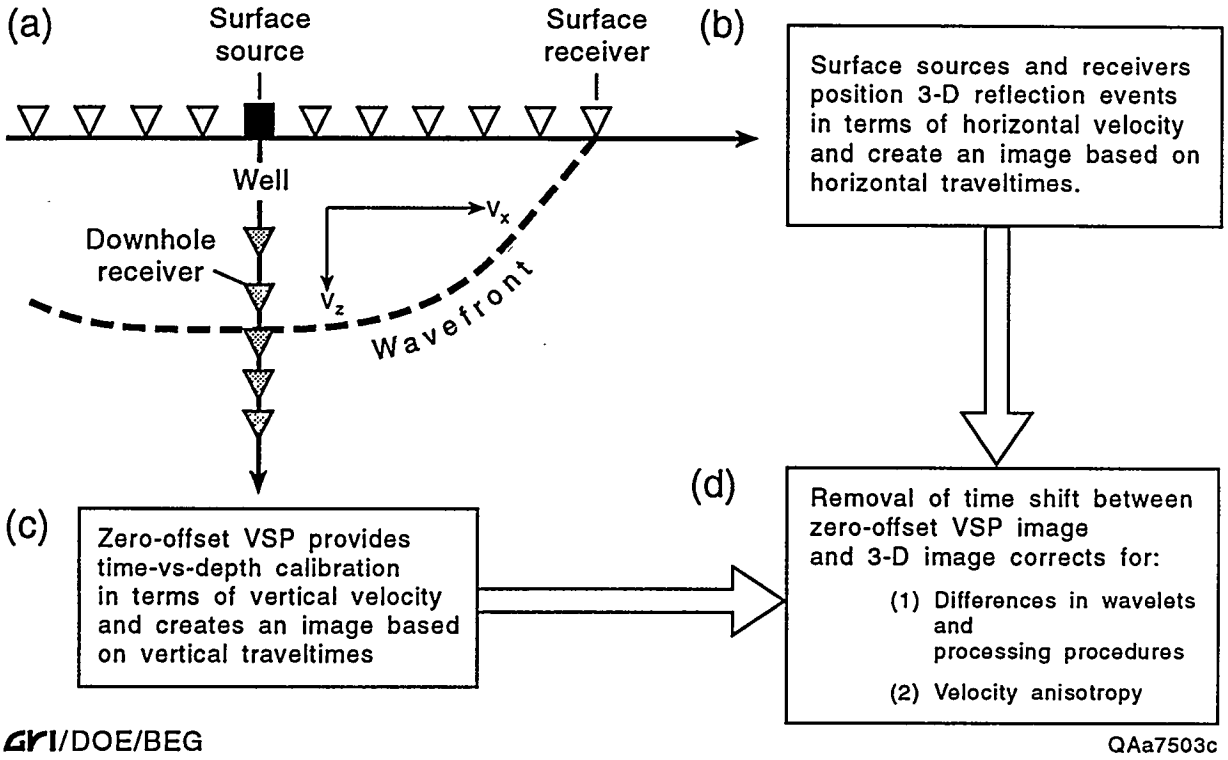

Figure F1. The concept of positioning thin beds in 3-D seismic images. (a) Source-receiver geometry involved in zero-offset VSP acquisition and 3-D data acquisition. The dashed wavefront is elliptical, not spherical, because of velocity anisotropy caused by the horizontal seismic velocity Vx in the Earth being faster than the vertical seismic velocity Vz. (b) Statement emphasizing that the time positions of surface-recorded 3-D reflection events are controlled by horizontal seismic velocity Vx. (c) Statement that the time positions of reflection events in a zero-offset VSP are controlled by vertical seismic velocity Vz. The VSP data provide a rigorous linkage between the stratigraphic depth of a thin bed and the vertical traveltime to that depth. (d) The final step in calibrating the correct time position of a thin bed in a 3-D image is to determine the time shift between the VSP image (where the time positions of thin beds are known) and the 3-D image.

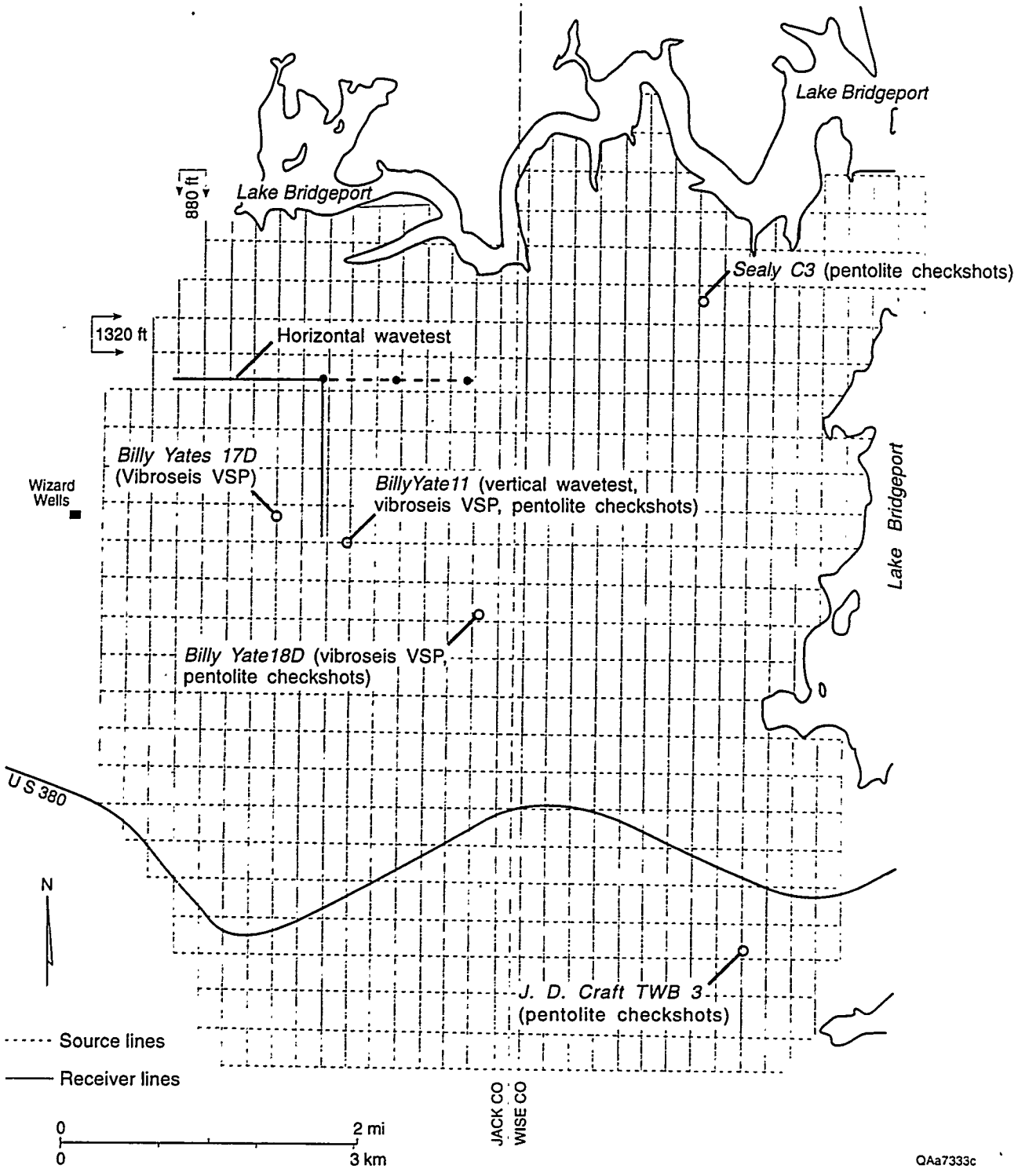

Figure F2. Location of wells where velocity checkshots and VSP data were recorded.

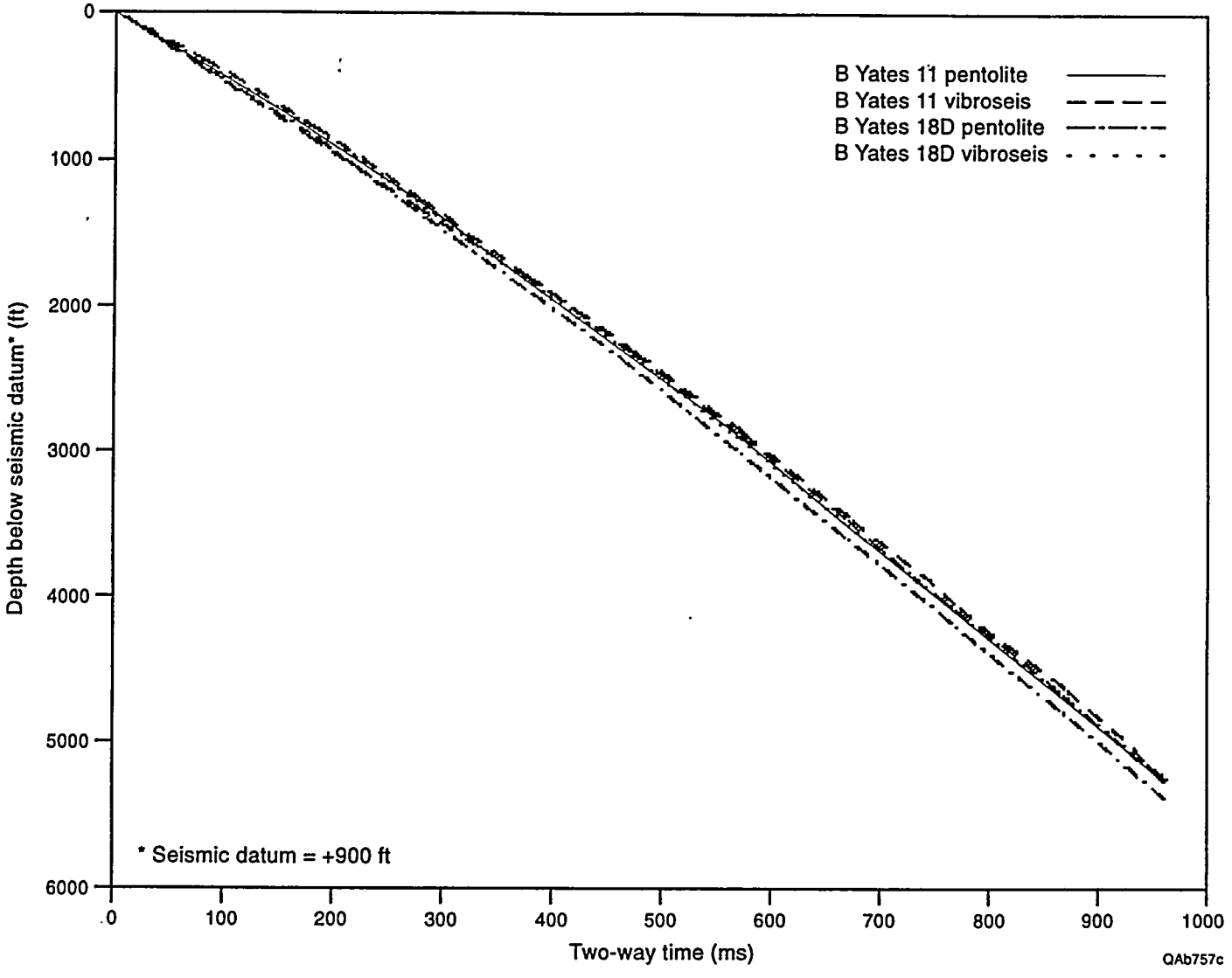

Figure F3. Time-vs-depth functions measured for vibroseis and pentolite (C-10 directional charges) wavelets inside the Boonsville 3-D seismic grid. Well locations are shown in Figure F2.

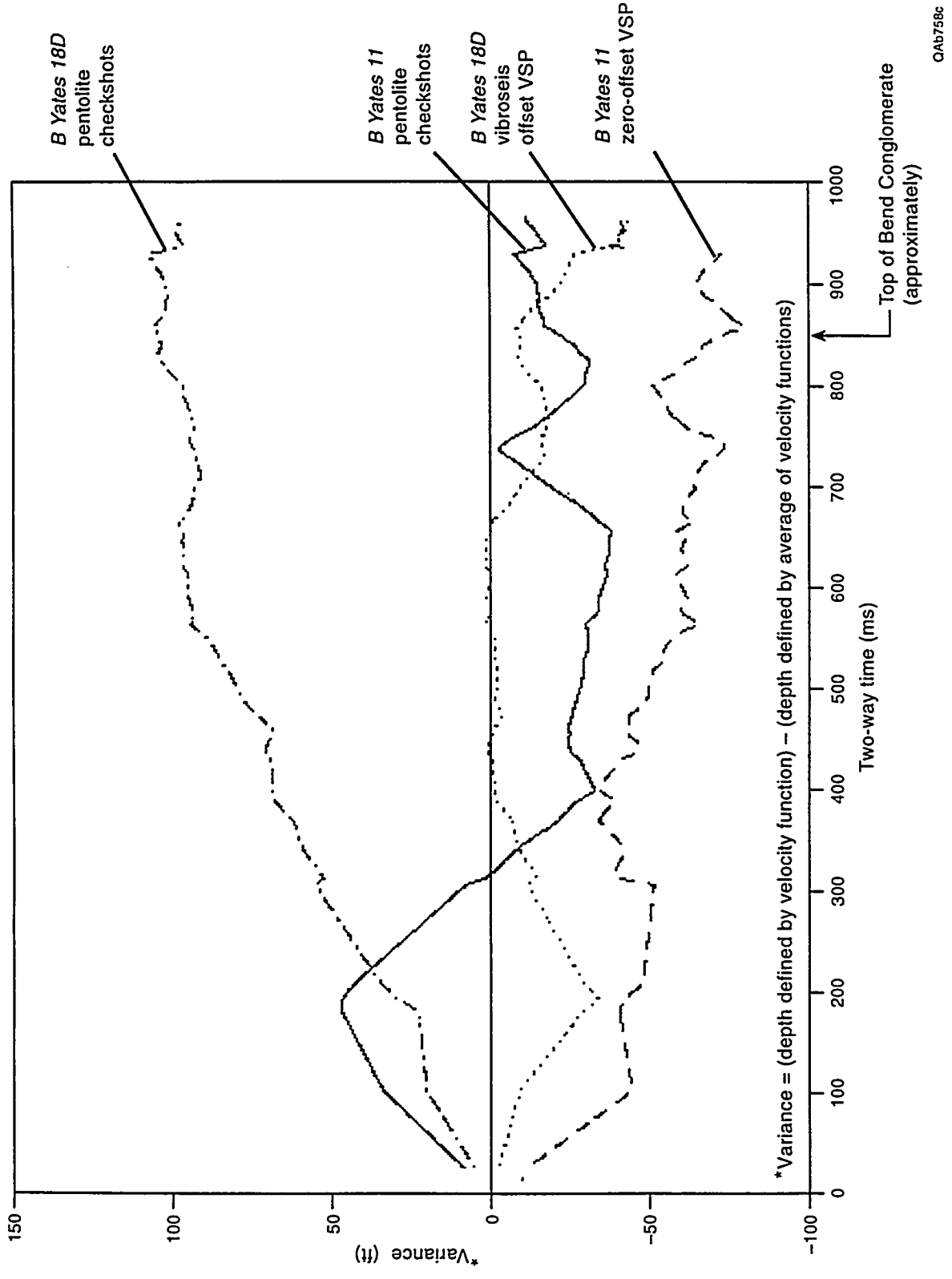

Figure F4. Variance in depth predictions associated with the traveltime functions shown in Figure F3.

F.18

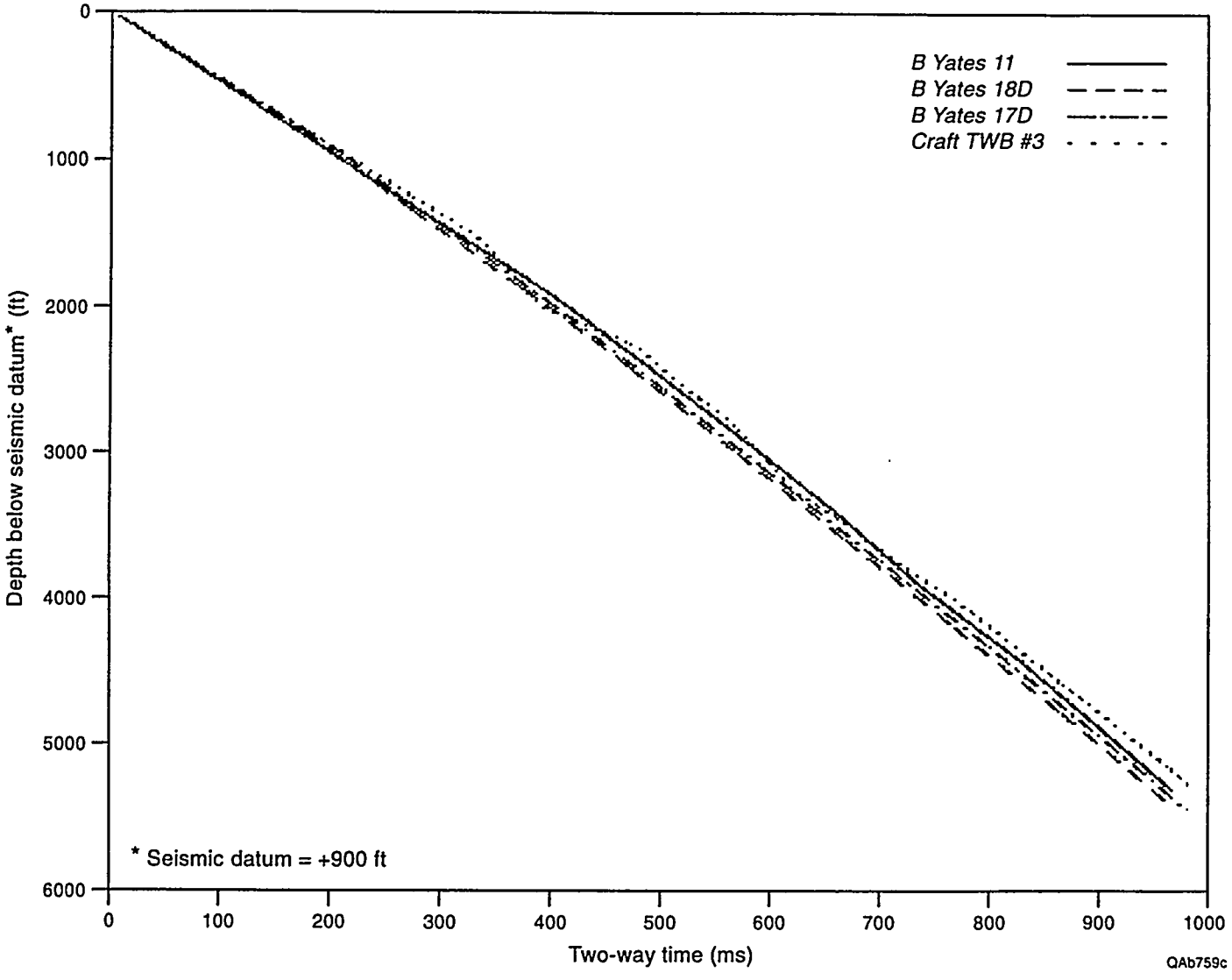

Figure F5. Time-vs-depth functions derived from pentolite-wavelet checkshot data recorded in different wells within the Boonsville 3-D seismic grid. Well locations shown in Figure F2.

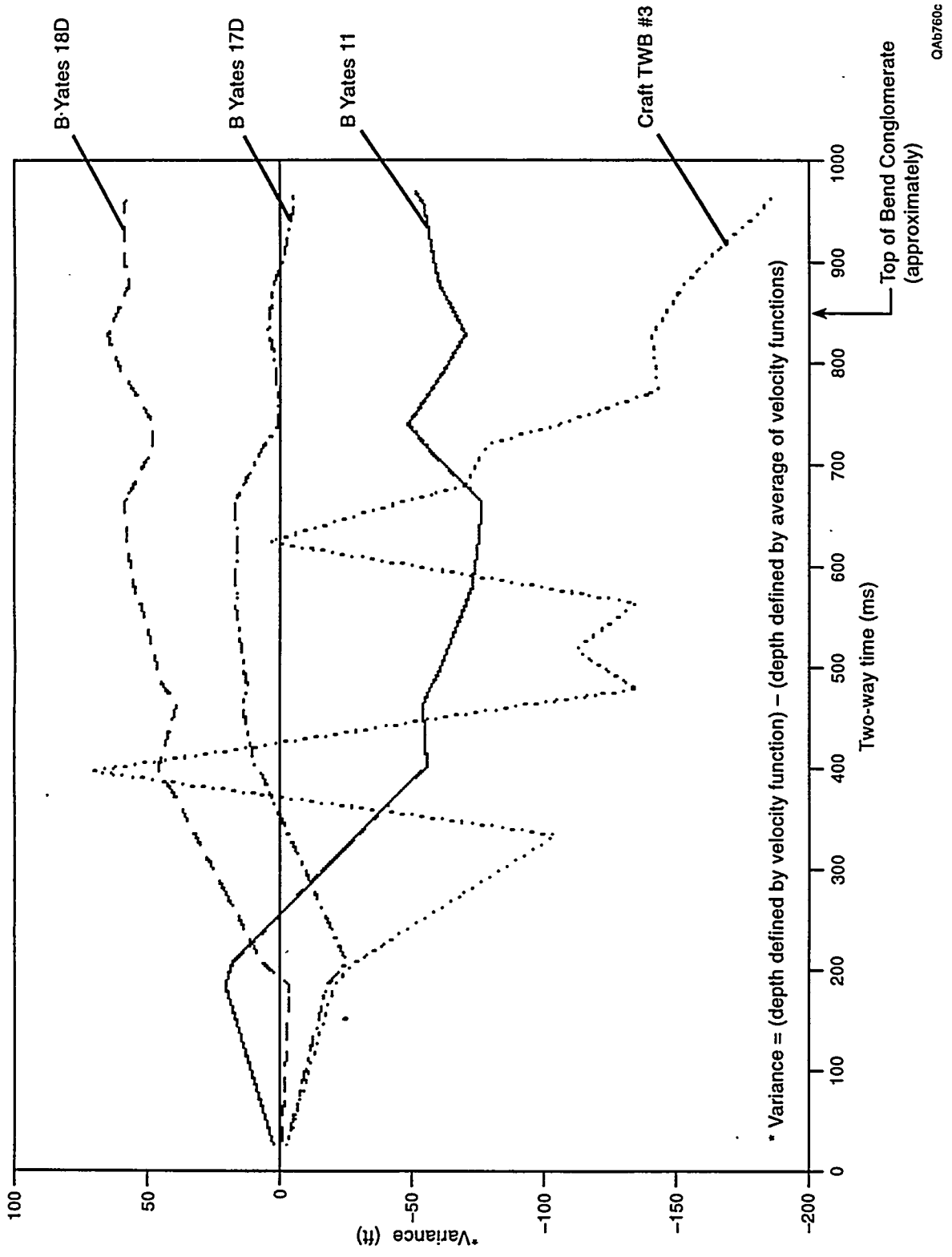

Figure F6. Variation in depth predictions associated with the traveltime functions shown in Figure F5.

F.20

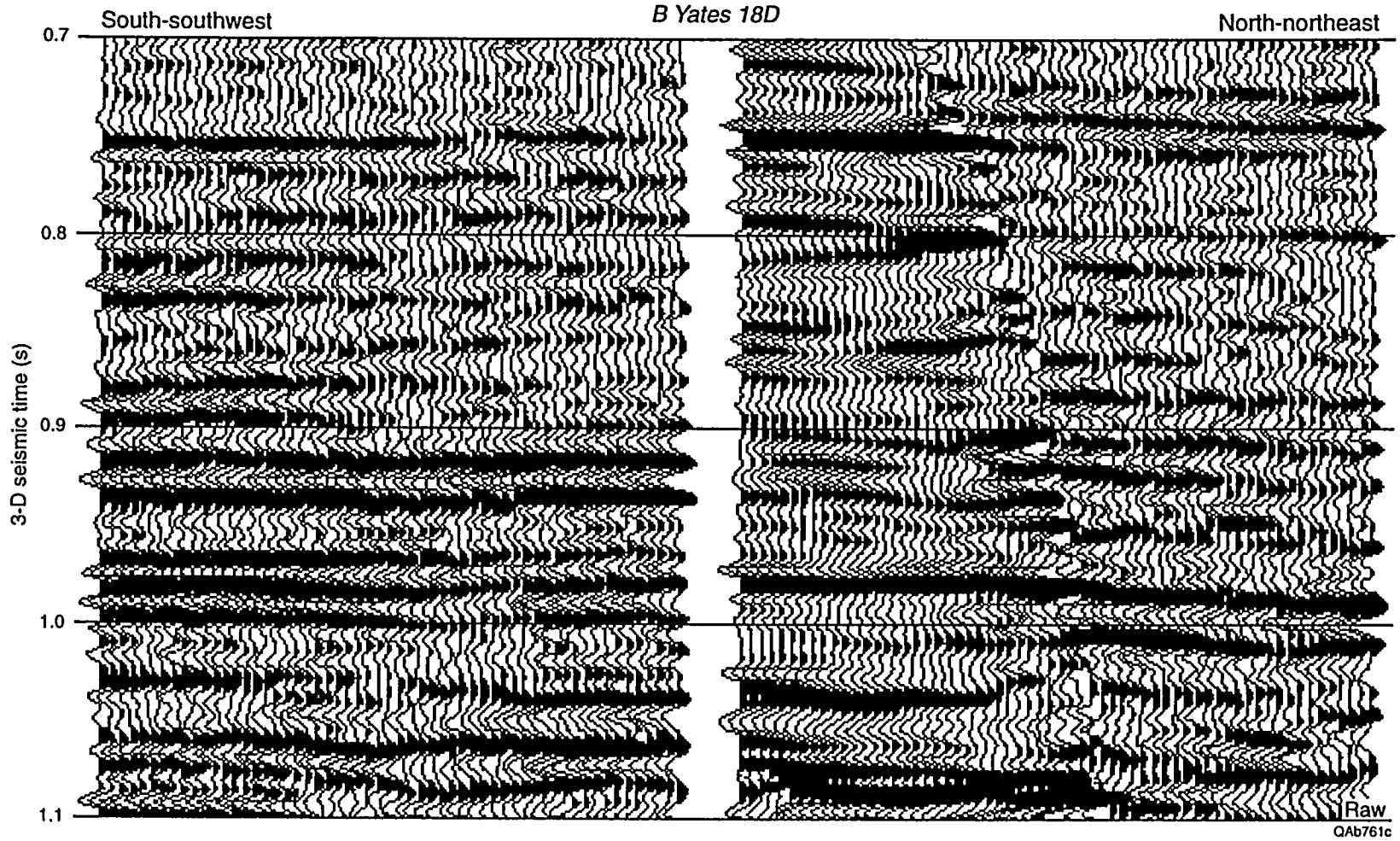

Figure F7. Comparison between contractor-delivered VSP images and 3-D seismic images at the B Yates 18D well.

F.21

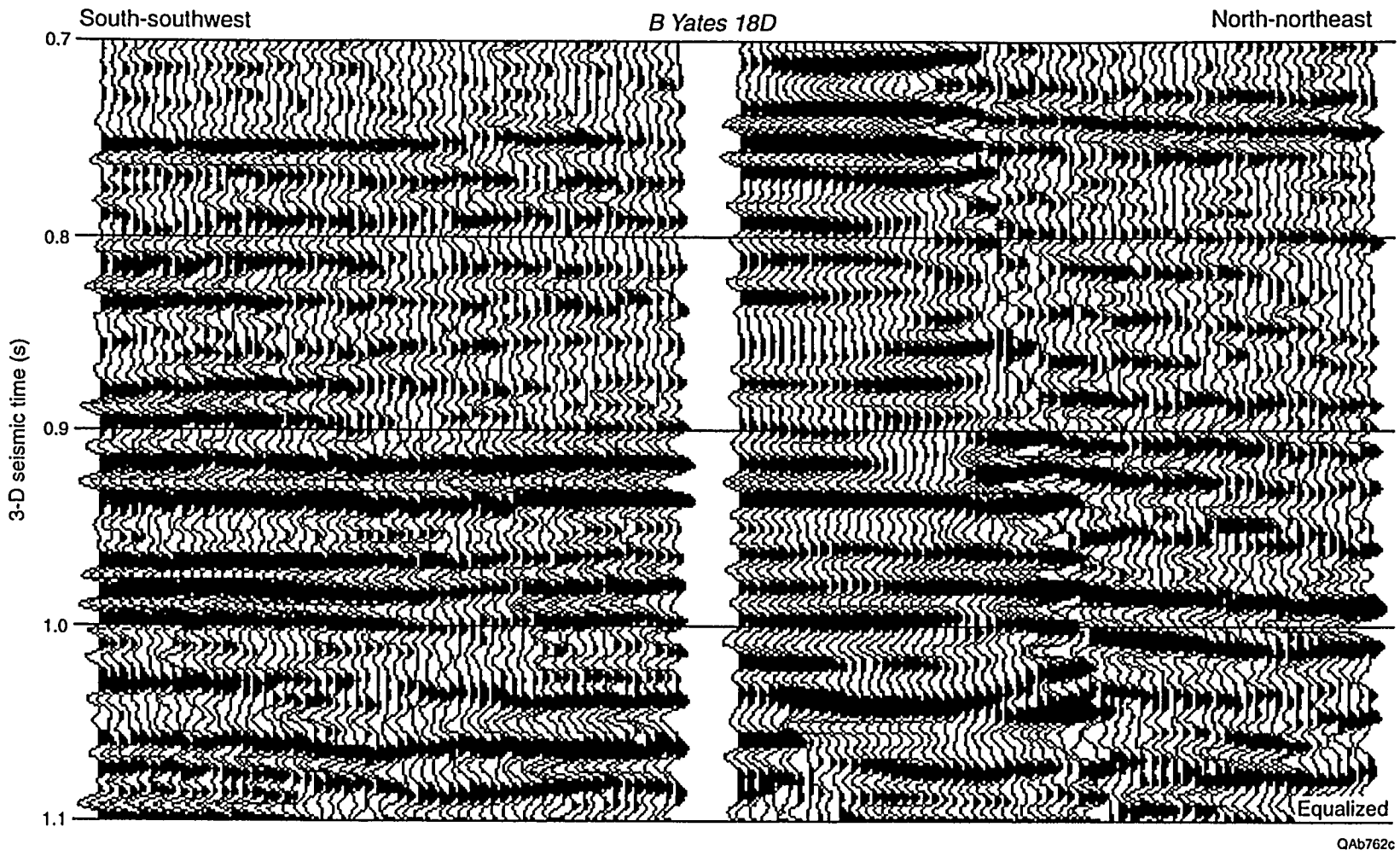

Figure F8. Comparison between wavelet-equalized VSP and 3-D images at the B Yates 18D well.

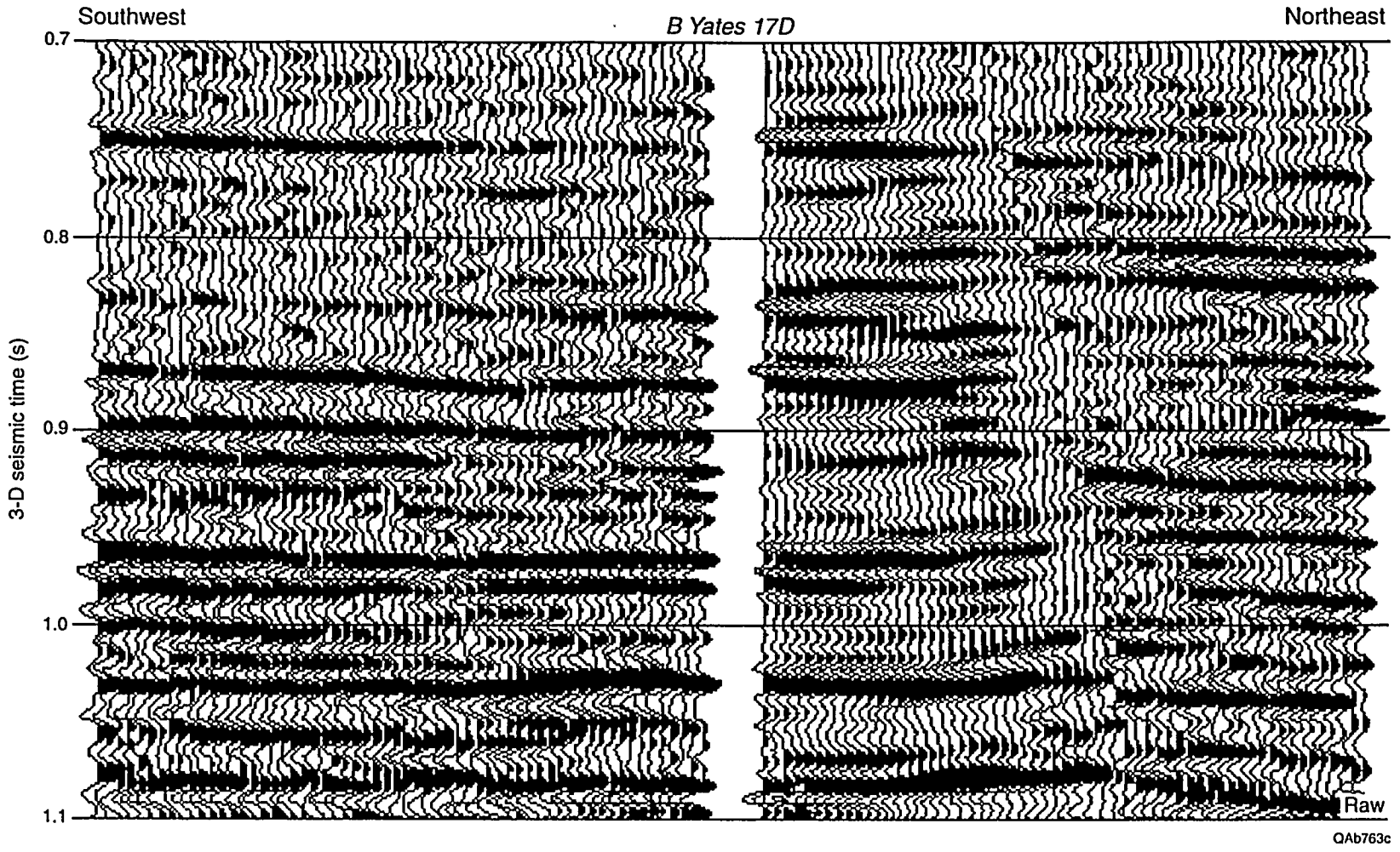

Figure F9. Comparison between contractor-delivered VSP image (northeast source offset location) and 3-D seismic image at the B Yates 17D well. VSP images are usually not accurate near the outer curved edge of the image, and interpretation should concentrate on comparing 3-D and VSP reflection waveshapes close to the VSP well.

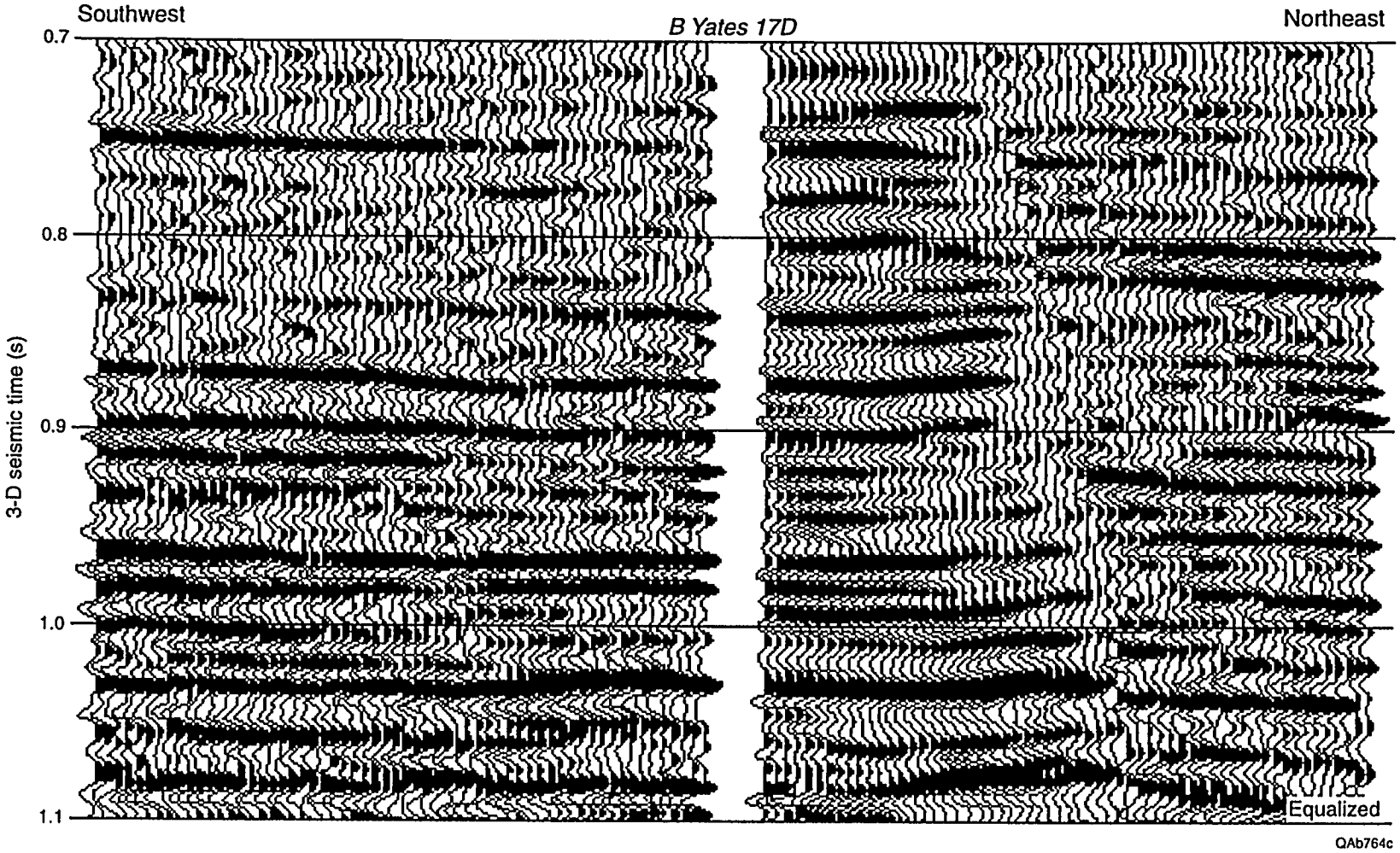

Figure F10. Comparison between wavelet-equalized VSP image (northeast source offset location) and 3-D seismic image at the B Yates 17D well. VSP images are usually not accurate near the outer curved edge of the image, and interpretation should concentrate on comparing 3-D and VSP reflection waveshapes close to the VSP well.

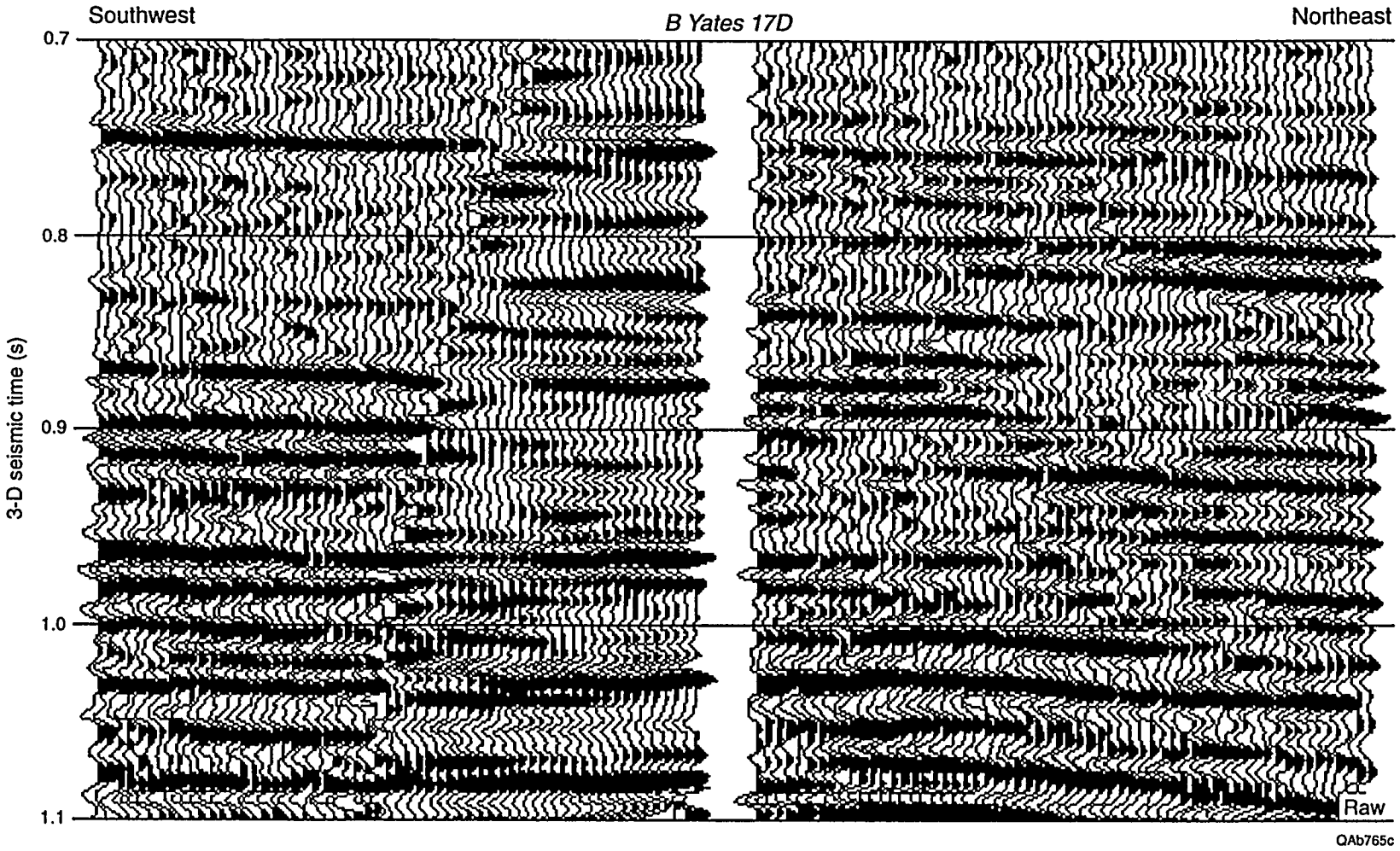

Figure F11. Comparison between contractor-delivered VSP image (southwest source offset location) and 3-D seismic image at the B Yates 17D well. VSP images are usually not accurate near the outer curved edge of the image, and interpretation should concentrate on comparing 3-D and VSP reflection waveshapes close to the VSP well.

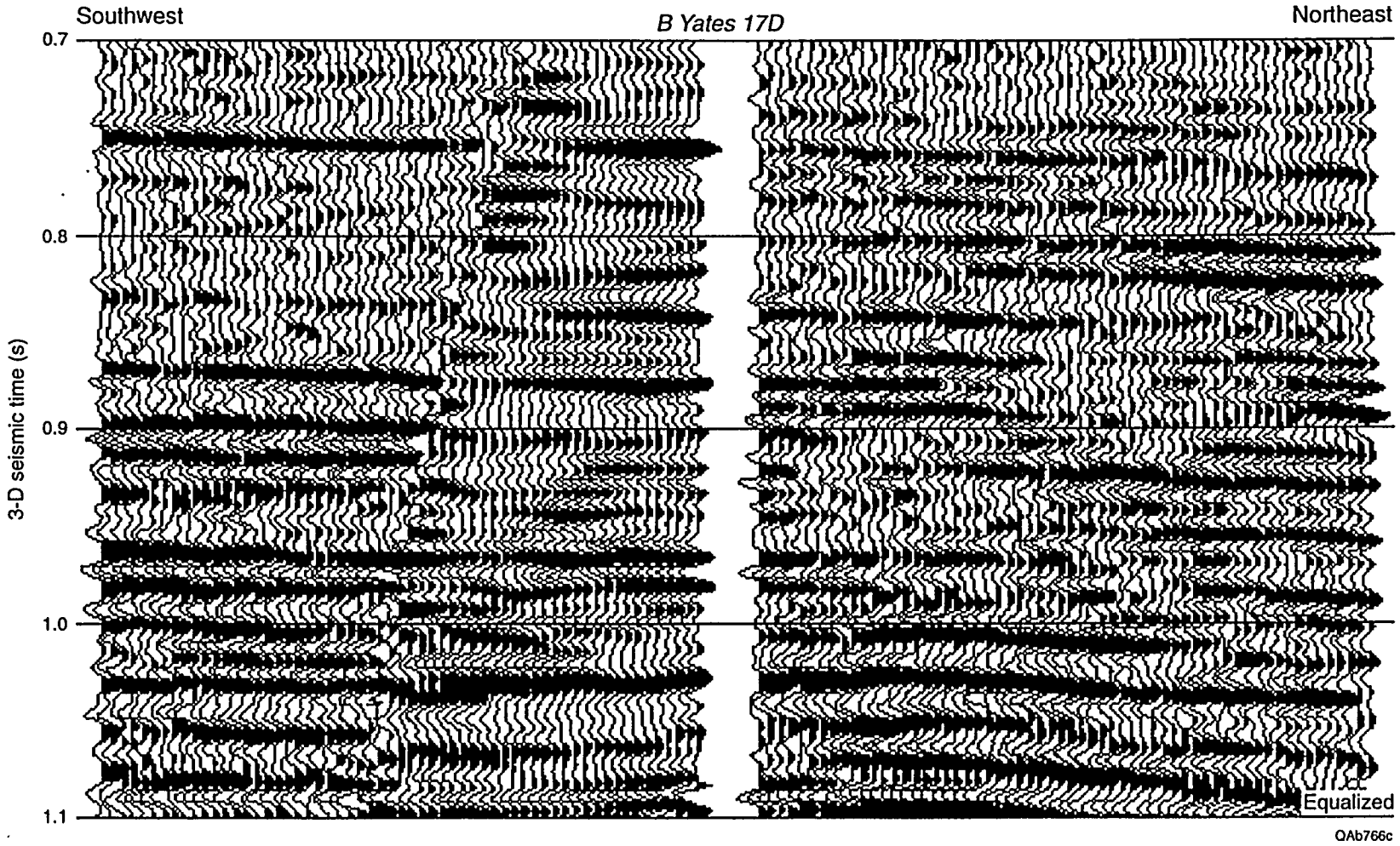

Figure F12. Comparison between wavelet-equalized VSP image (southwest source offset location) and 3-D seismic image at the B Yates 17D well. VSP images are usually not accurate near the outer curved edge of the image, and interpretation should concentrate on comparing 3-D and VSP reflection waveshapes close to the VSP well.

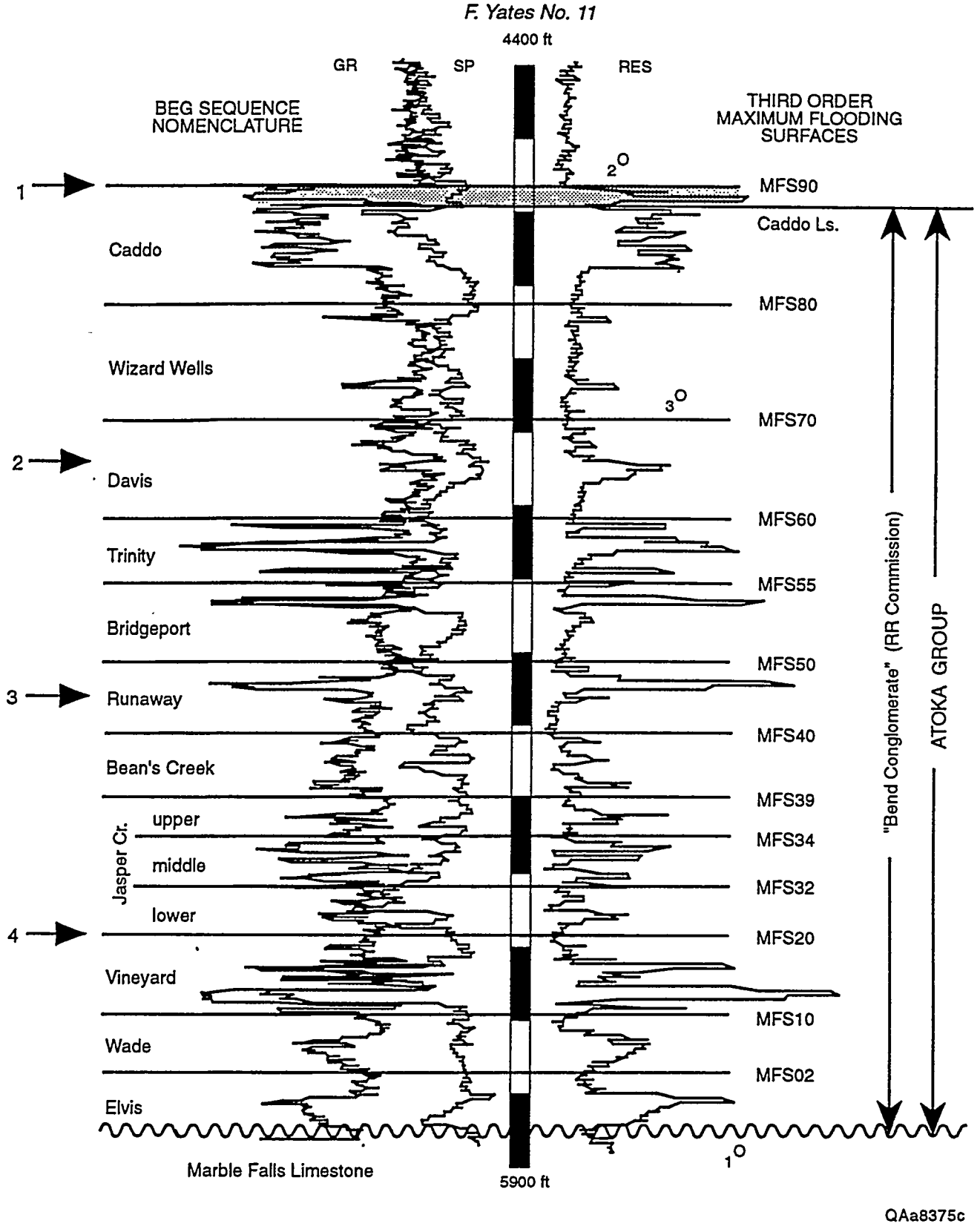

Figure F13. Stratigraphic nomenclature used to define depositional units and sequence boundaries in Boonsville field. The numbers 1, 2, 3, 4 in the left margin define the stratigraphic positions of four seismic chronostratigraphic surfaces that were interpreted across the complete 26-mi^2 3-D survey.

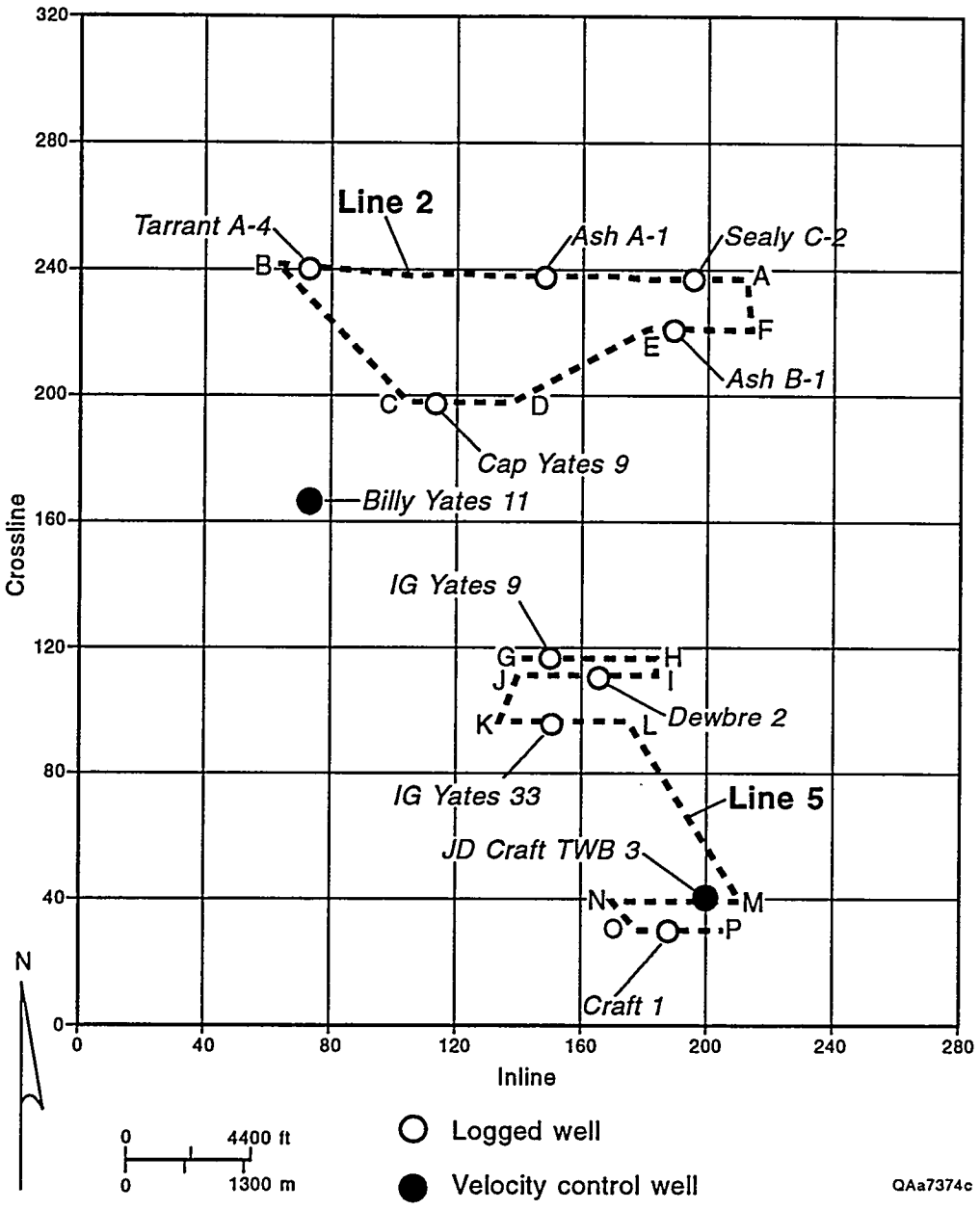

Figure F14. A map showing some of the wells used to identify the time positions of chronostratigraphic surfaces inside the Boonsville 3-D grid. Meandering lines, such as Line 2 and Line 5, were extracted from the 3-D data volume to define the two-way traveltime positions of key sequence boundaries among small subsets of the wells, with each line establishing a seismic stratigraphic tie among 4 to 6 wells. Wells were chosen so that these tie lines could be created over the entire 26-mi^2 area spanned by the 3-D survey.

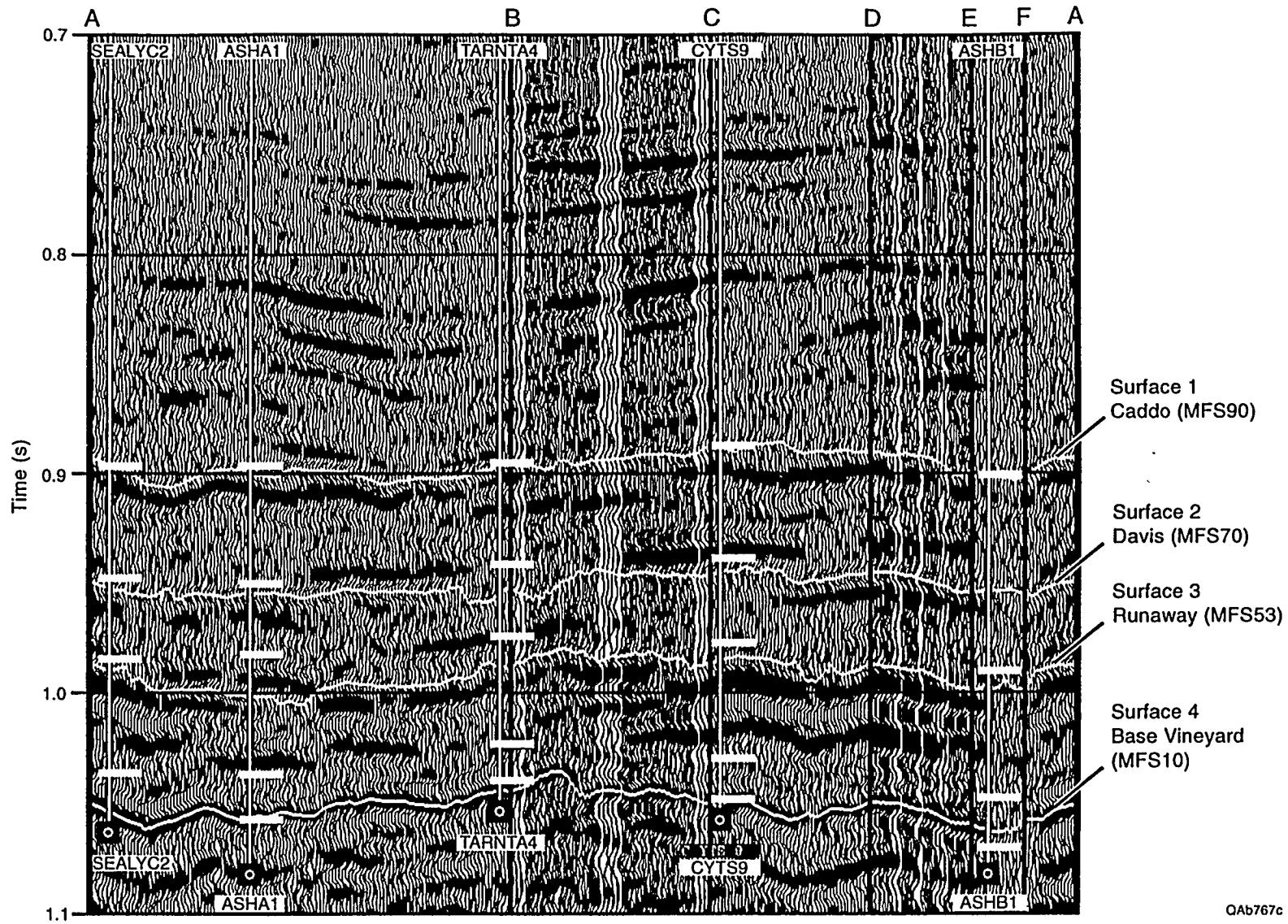

Figure F15. Arbitrary seismic line following the path labeled Line 2 in Figure F7. The positions of the labels ABCDEF correspond to the coordinates labeled ABCDEF on the map (Fig. F14). At each well location, heavy white tic marks are drawn so that they pass through the pentolite-based vertical traveltime corresponding to the depth of the Caddo, Davis, Runaway, and Vineyard sequence boundaries penetrated by the well. The time-versus-depth calibration curves in Figure F5 were used to define these time coordinates. The horizons labeled 1, 2, 3, 4 are the seismic events that were selected as the best choices for the chronostratigraphic surfaces that are closest to, and conformable with, the traveltime tic marks for the top of the Caddo, Davis, and Runaway, and the base of Vineyard sequences, respectively.

F.29

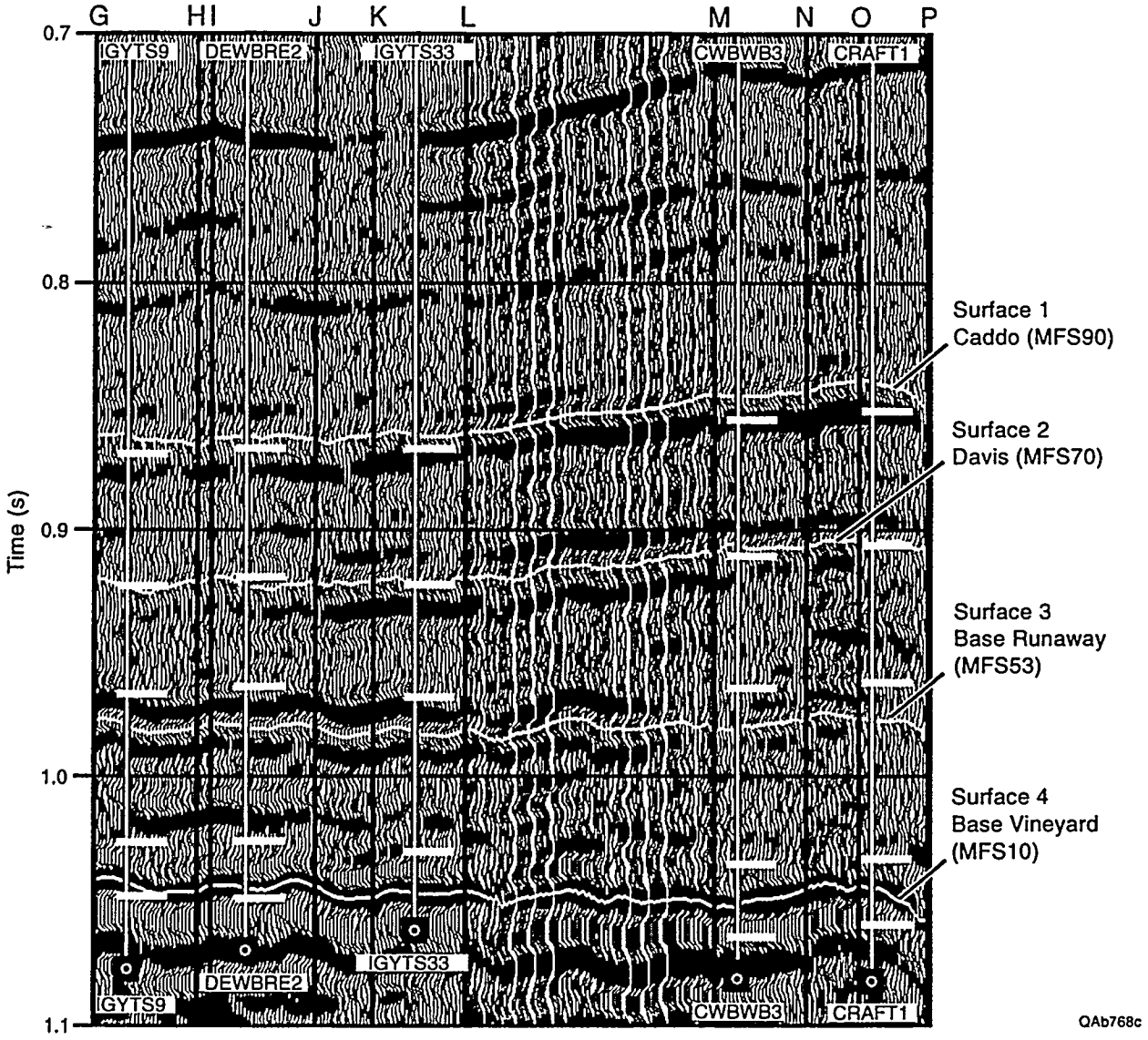

Figure F16. Arbitrary seismic line following the path labeled Line 5 in Figure F14. The positions of the labels GHIJKLMNOP correspond to the coordinates labeled GHIJKLMNOP in the map (Fig. F14). At each well location, heavy white tic marks are drawn so that they pass through the pentolite-based vertical traveltime corresponding to the depth of the Caddo, Davis, Runaway, and Vineyard sequence boundaries penetrated by that well. The time versus-depth calibration curves shown in Figure F5 were used to define these time coordinates. The horizons labeled 1, 2, 3, 4 are the seismic events that were selected as the best choices for the chronostratigraphic surfaces that are closest to, and conformable with, the traveltime tic marks for the top of the Caddo, Davis, and Runaway, and the base of the Vineyard sequences, respectively.

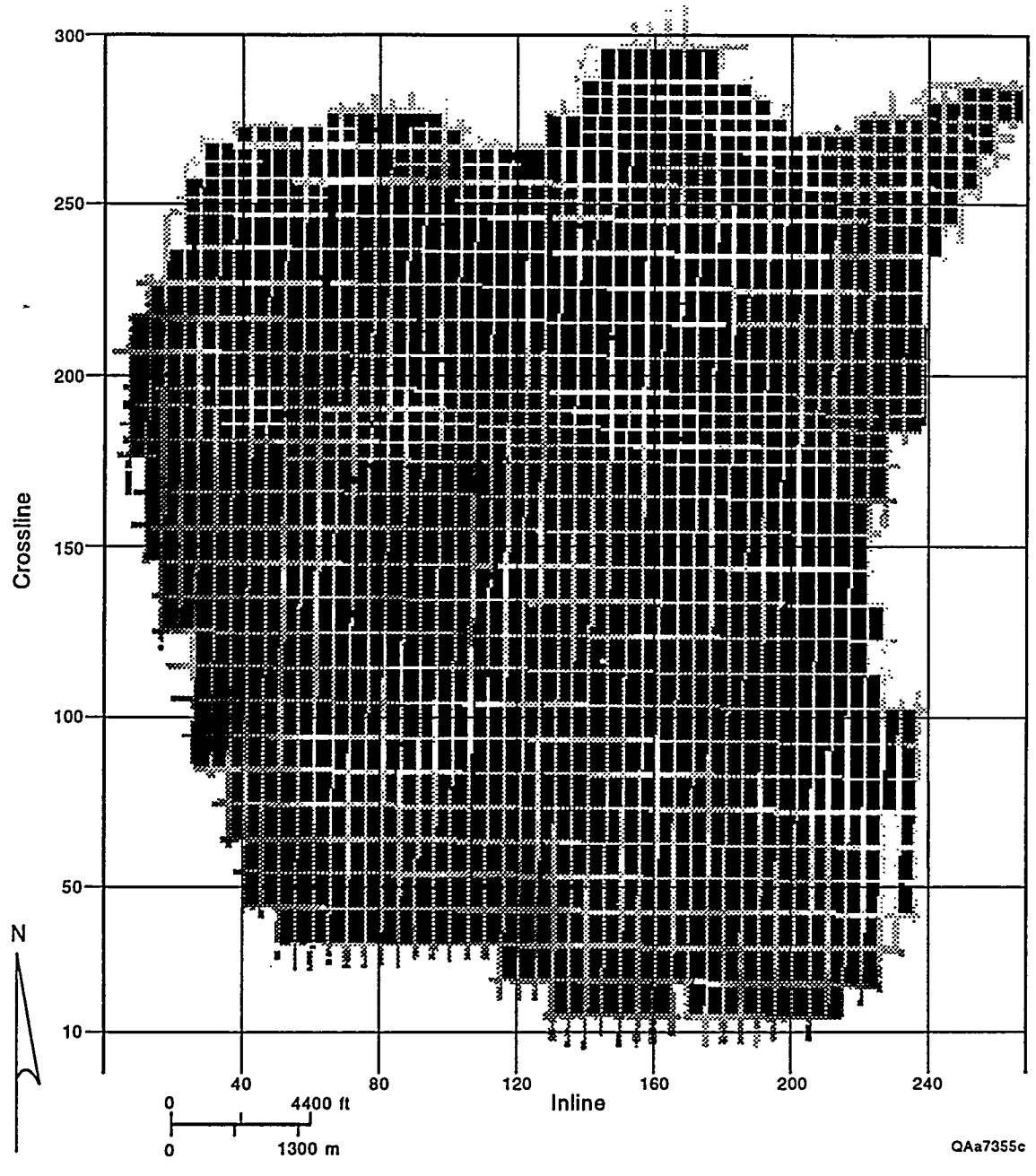

Figure F17. The seeding grid for the Caddo chronostratigraphic surface. The Caddo chronostratigraphic horizon was first defined on a series of arbitrary well-tie lines, such as those shown in Figures F15 and F16, and this horizon was then transferred to each of the lines in this seeding grid. In areas of difficult interpretation, such as the northern edge of the survey and the region south of crossline 200, the line spacing of the seeding grid was reduced. Once the horizon interpretation was satisfactorily tied across the grid, the Landmark software used by Bureau interpreters then created a continuous, smooth chronostratigraphic surface that connected the manually interpreted horizons defined across this seeding grid.

1

Here are the color graphs that were in the document

DOE/MC/25031-5097

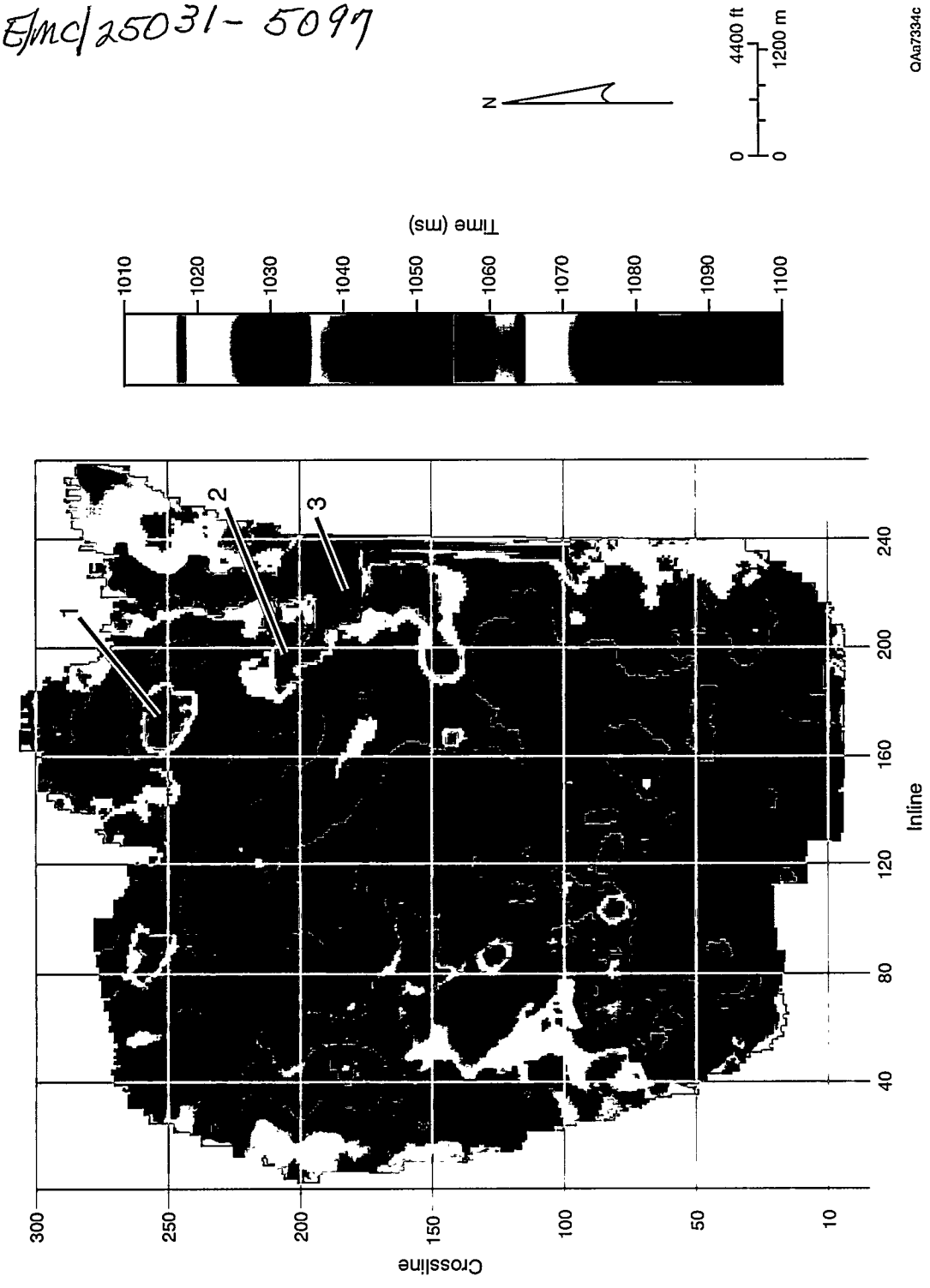

Figure 2.1. Seismic time structure map showing the topography of the Vineyard chronostratigraphic surface (base of the Bend Conglomerate). The numbered features identify karst collapse areas.

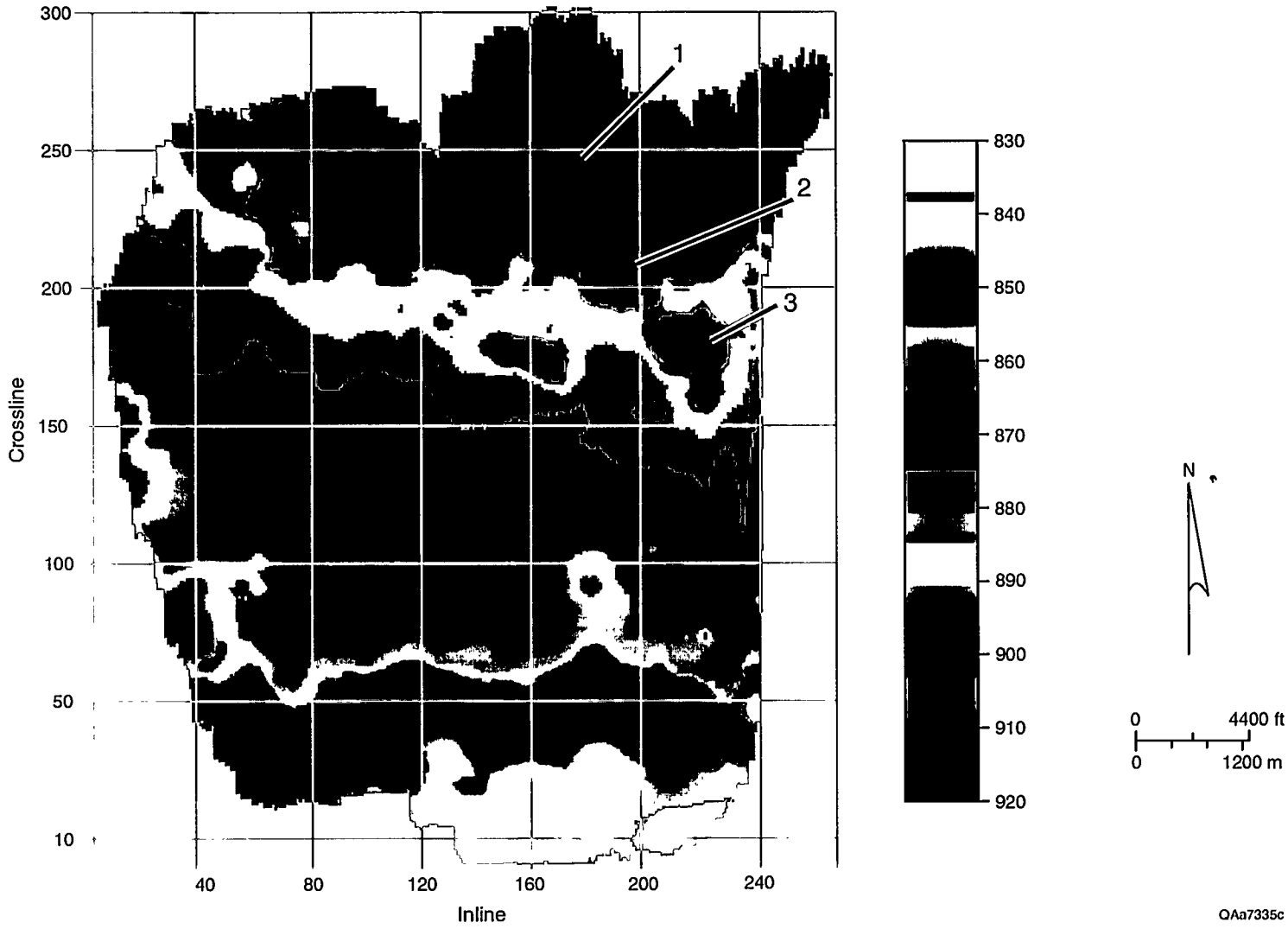

Figure 2.2. Seismic time structure map showing the topography of the Caddo chronostratigraphic surface (top of the Bend Conglomerate). The numbered features identify karst collapse areas. Note that these karst depressions are positioned directly above the depressions in the Vineyard surface (previous figure).

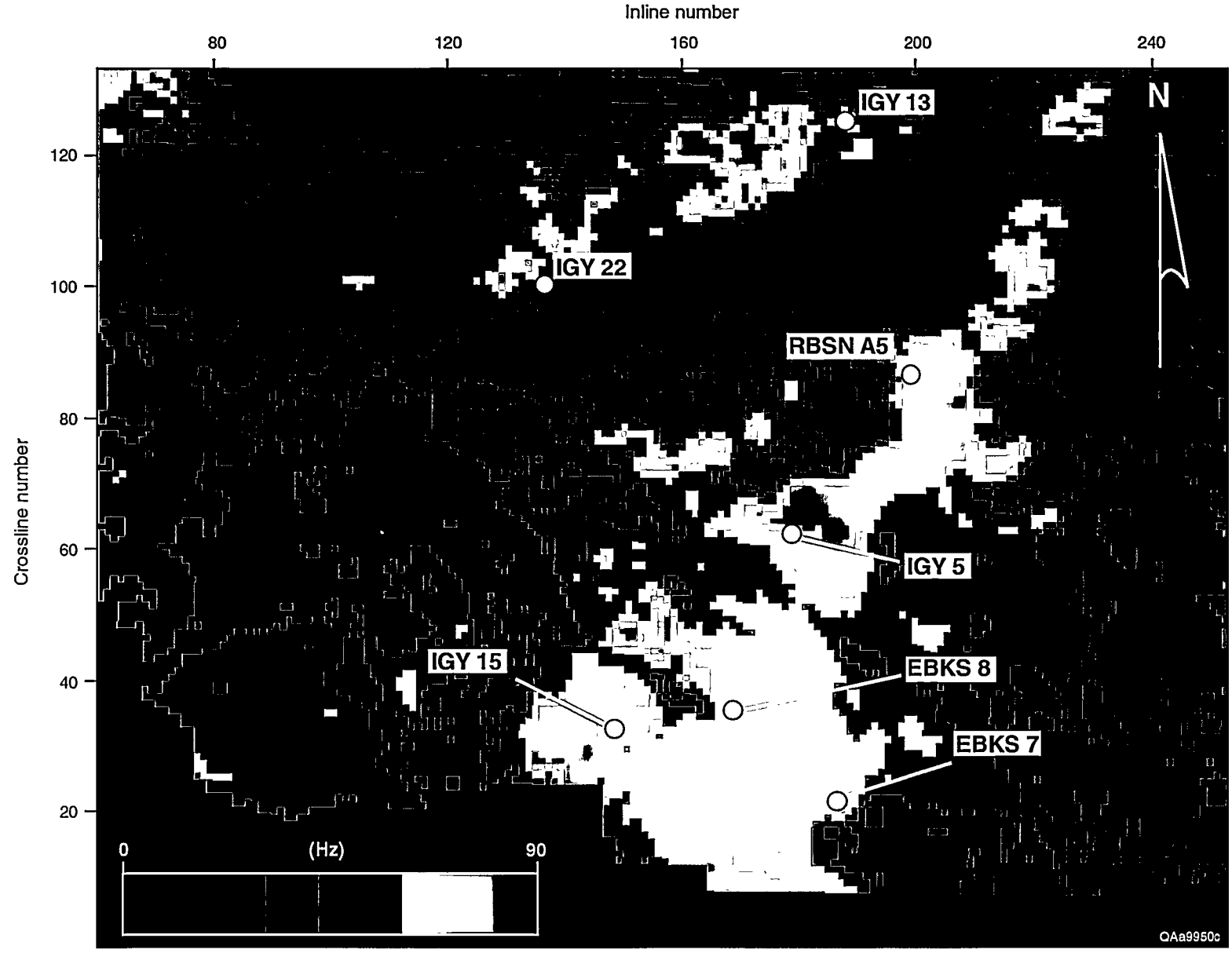

Figure 3.2. Average instantaneous seismic frequency calculated within the Lower Caddo sequence. This map should be compared with the preceding Lower Caddo net reservoir map. The parameter that is mapped is the average instantaneous frequency in a 10-ms window that is conformable to the seismically derived Caddo chronostratigraphic boundary and starting 10 ms below that boundary. The correspondence between this seismic attribute map and the log-based net reservoir map is striking, and shows that, in some circumstances, 3-D seismic data provide a valuable predictive tool for locating stratigraphically trapped reservoirs. The theory of instantaneous frequency is discussed in Appendix E.

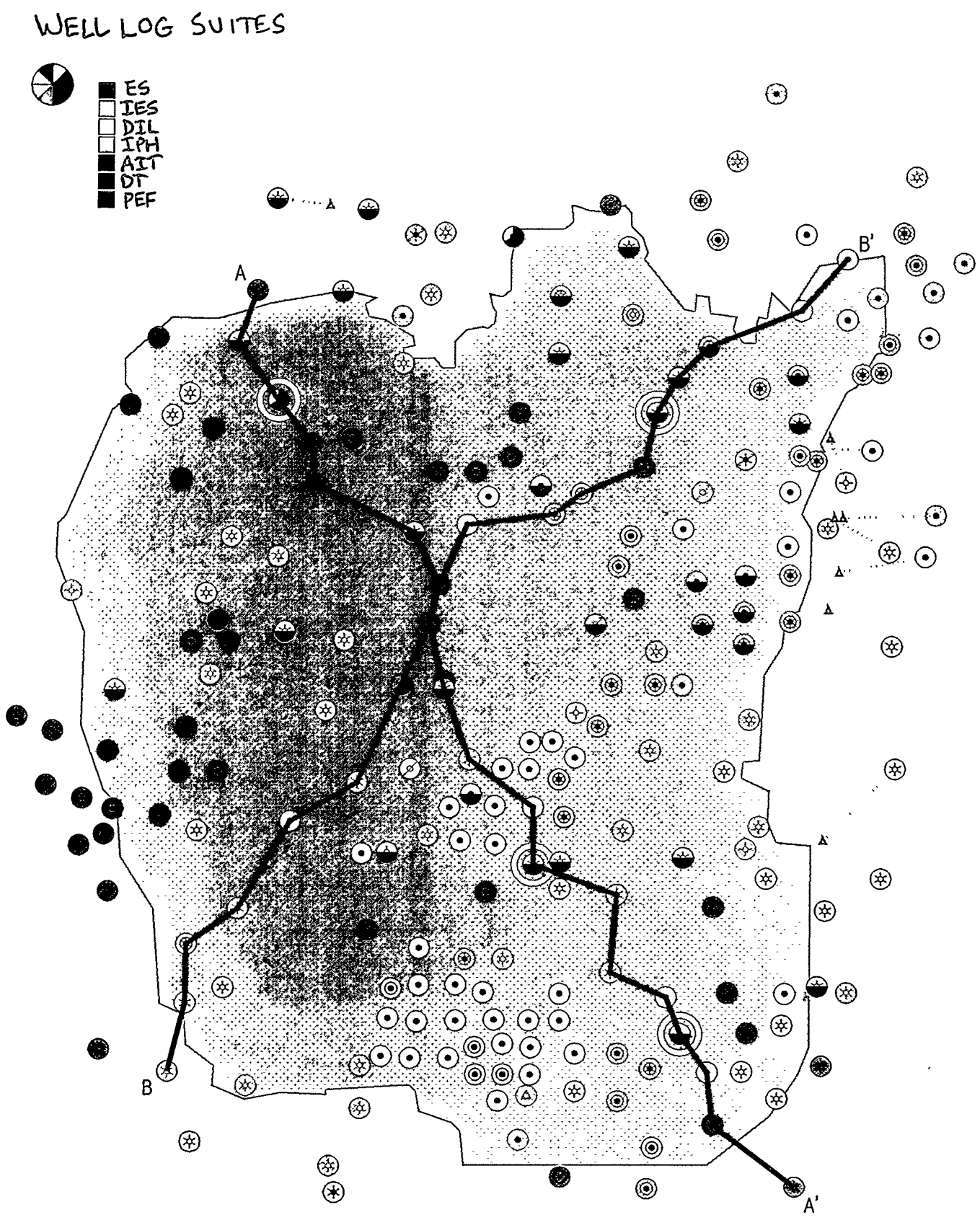

Figure A8. Distribution of well-log suites and cores (yellow open circles) used in the geologic evaluation of the Boonsville Project Area. Dark cyan colored-filled area represents outline of the 3-D seismic survey

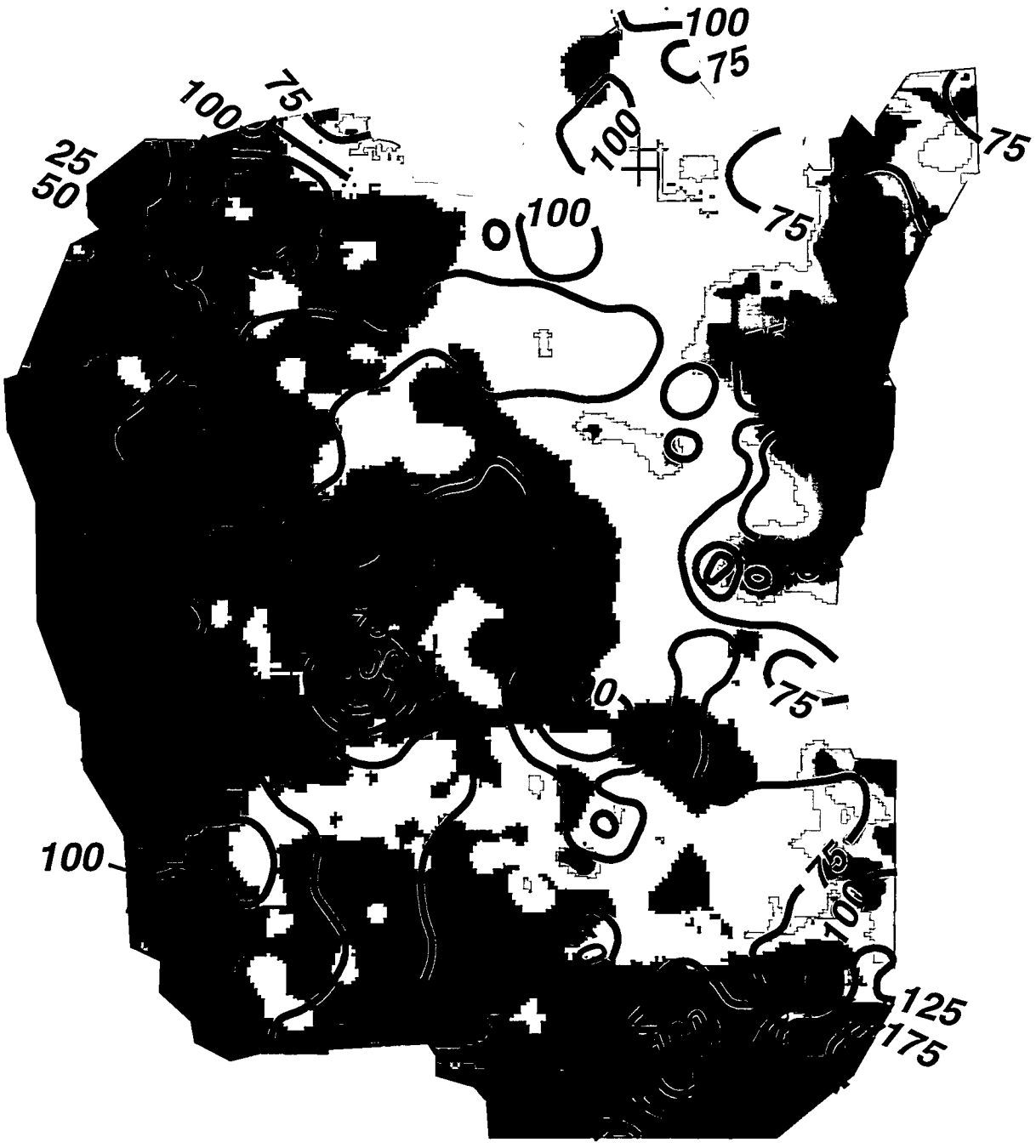

Figure A20. Map of Boonsville project area showing the relationship between total Atoka (MFS90-MFS10) net reservoir thickness and deep subsurface structure, as indicated by the top of the Marble Falls Limestone interpreted from 3D seismic data. Dark colors represent higher elevations and grade to lower elevations colored in lighter shades.

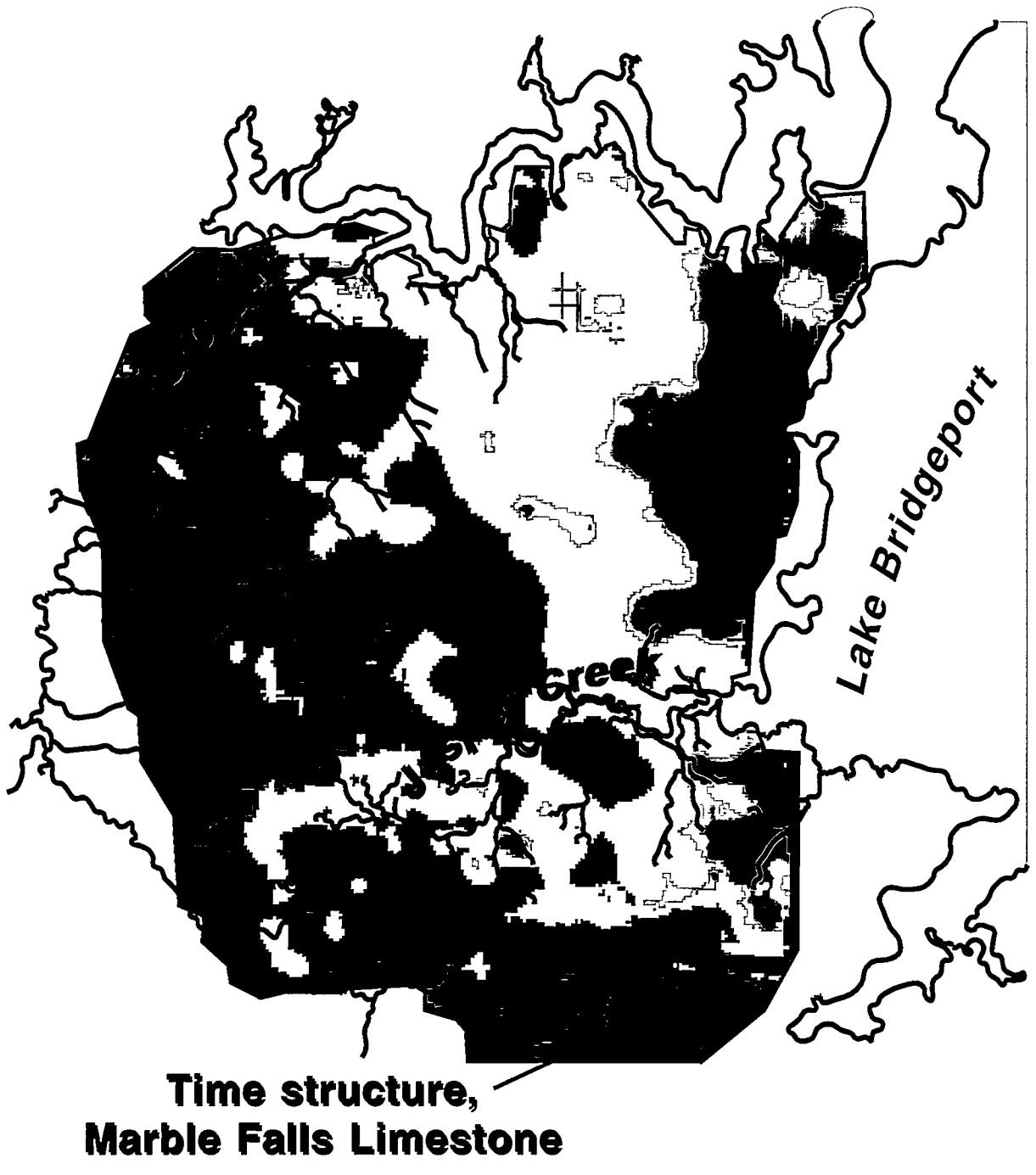

Figure A21. Map of Boonsville project area showing the relationship between modern stream drainage and deep subsurface structure, as indicated by the top of the Marble Falls Limestone interpreted from 3D seismic data. Dark colors represent higher elevations and grade to lower elevations colored in lighter shades.

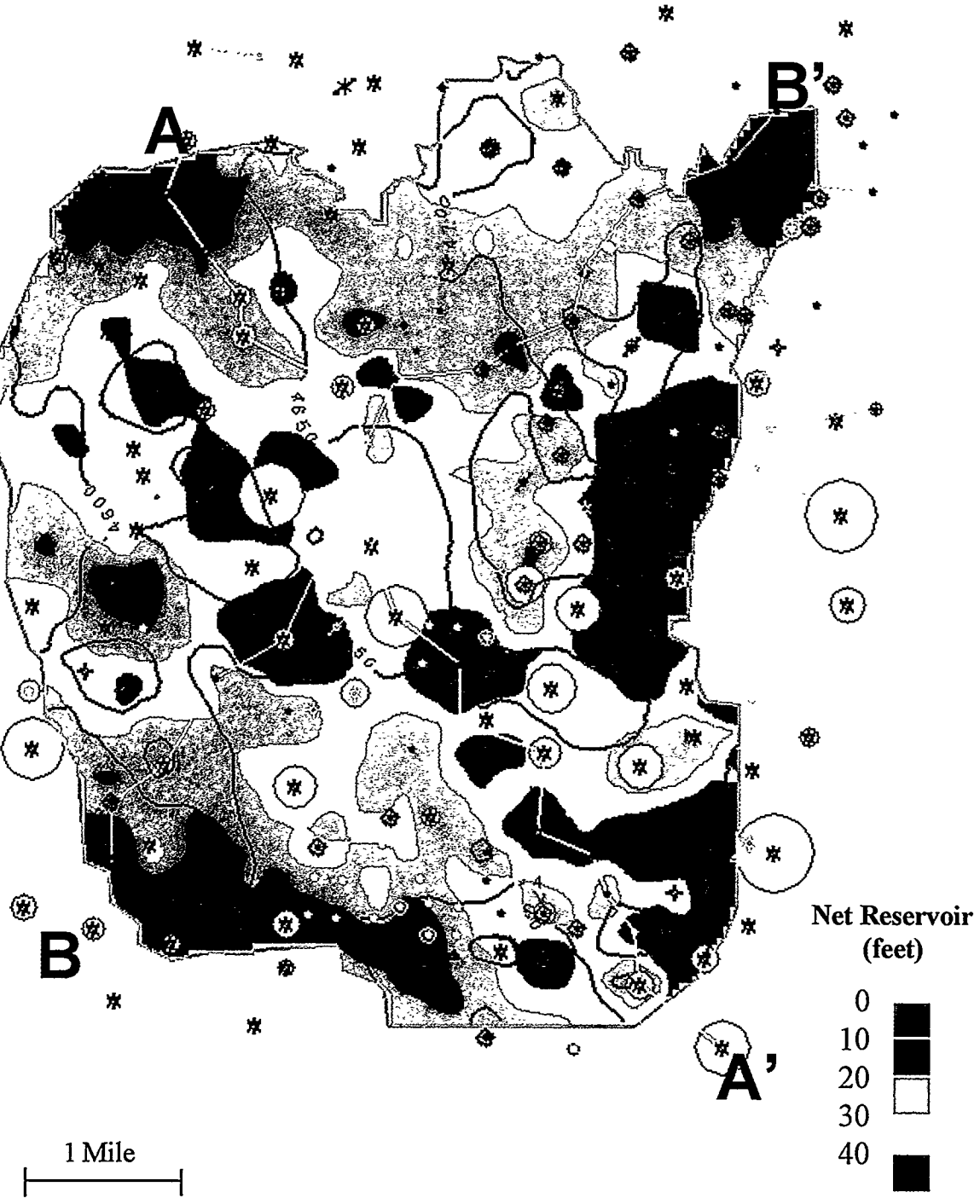

Figure A22. Thick sandstone and subtle structural controls on gas production in the Vineyard sequence. Note the southeast-northwest trending line of large cumulative gas production coincides with the thick net reservoir "sweetspot" draped over "Noles' Nose". Color fill = Vineyard net reservoir isopach; bubbles = cumulative gas production. Net reservoir cutoffs: SP < -30 mv, res > 10 ohmm.

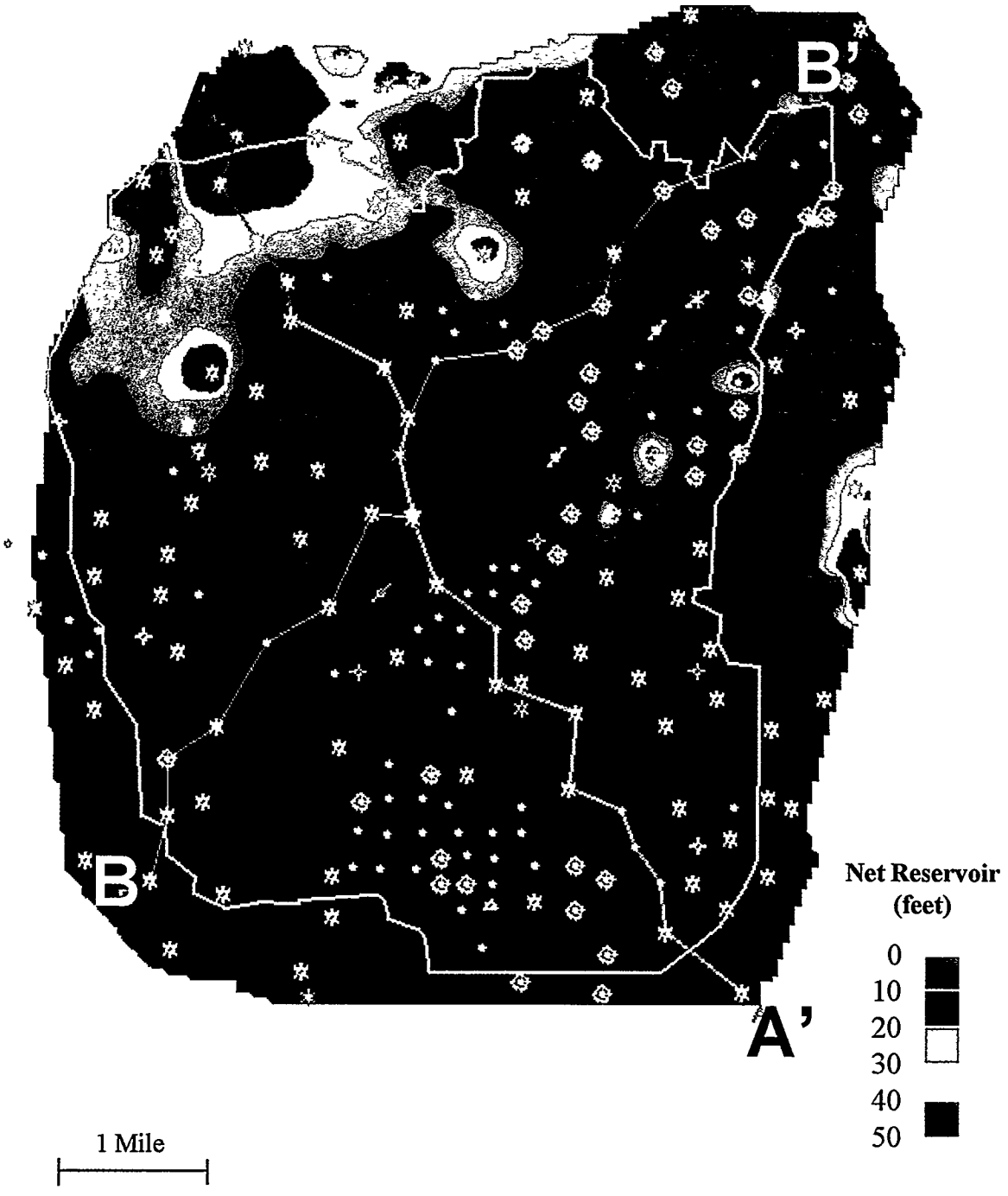

Figure A24. Wizard Wells genetic sequence net reservoir isopach (MFS80-MFS70). Net reservoir cutoffs: SP < -30 mv, Res > 10 ohmm.

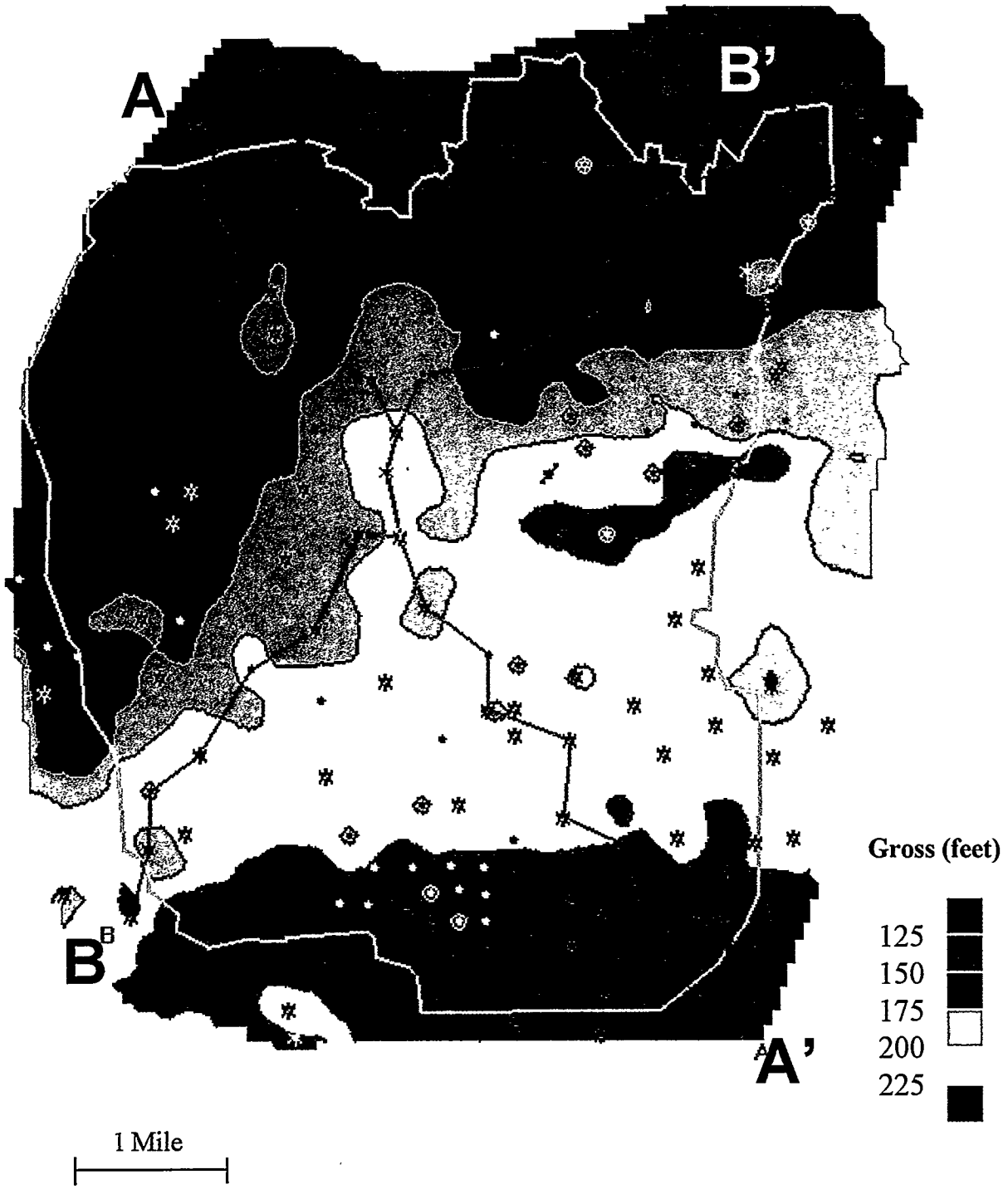

Figure A26. Jasper Creek "Exxon" sequence total gross interval isopach (ES40-ES30).

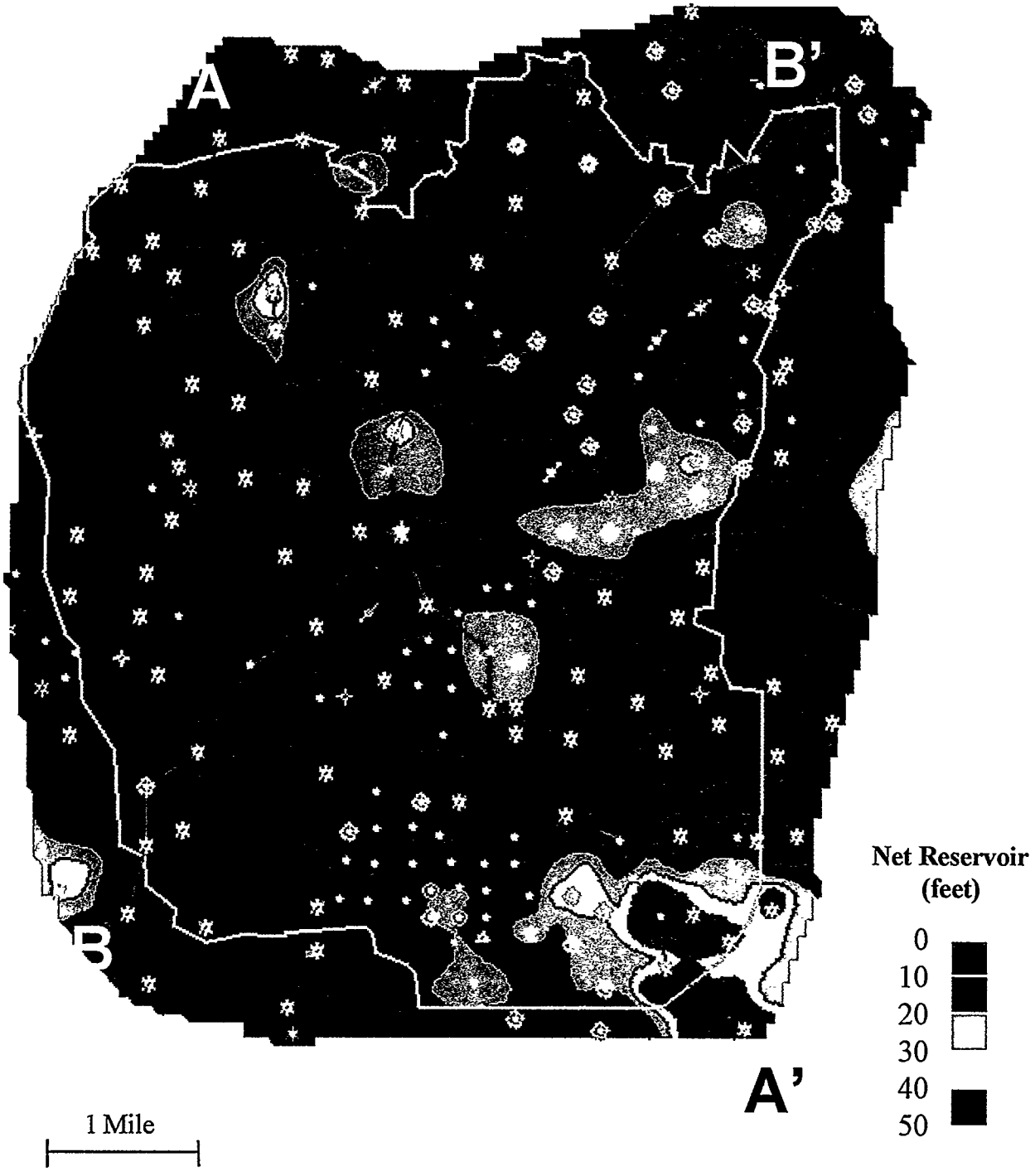

Figure A27. Jasper Creek "Exxon" sequence total net reservoir isopach (ES40-ES30). Net reservoir cutoffs: SP < -30 mv, Res > 10 ohmm.

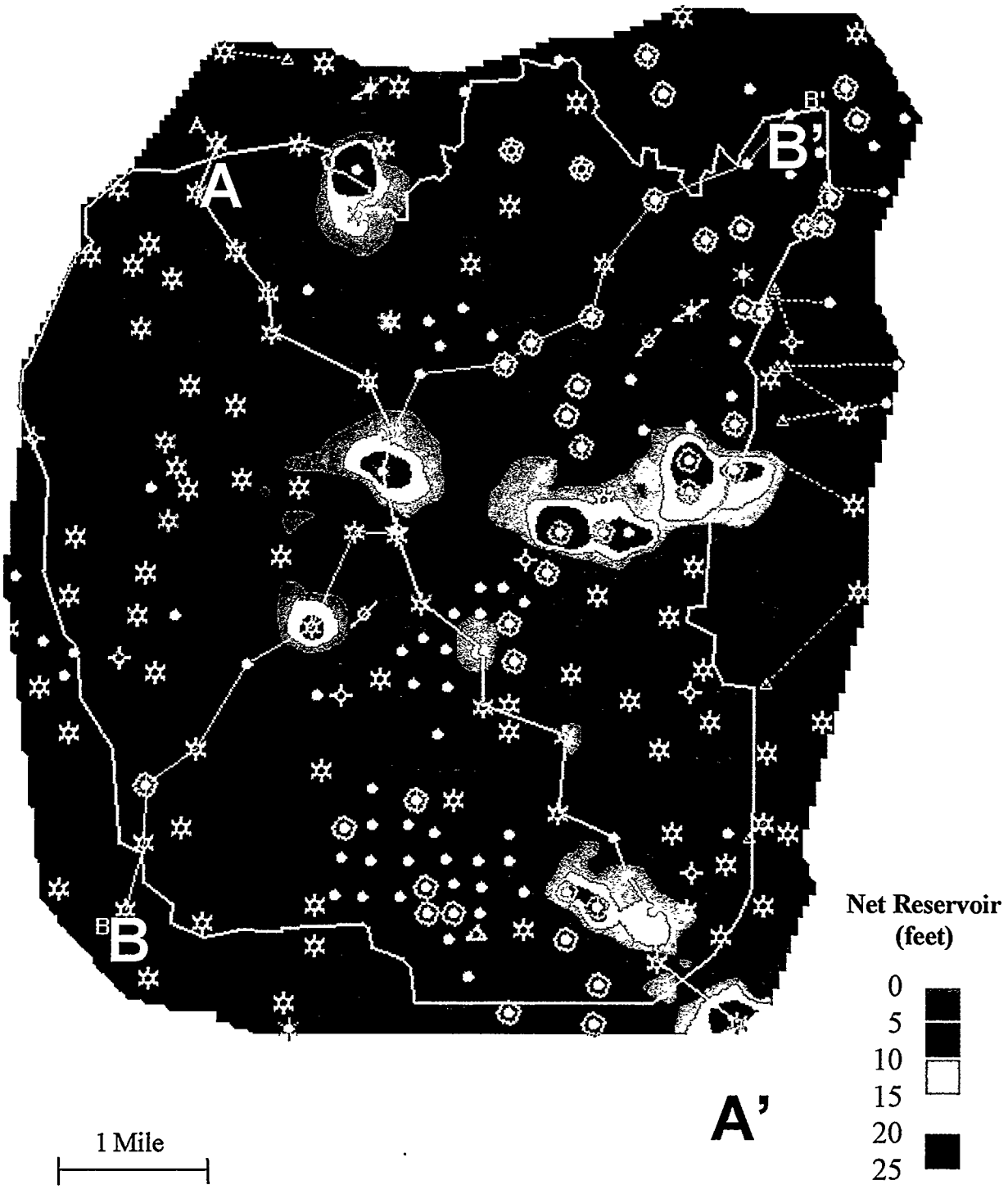

Figure A29. Lower Jasper Creek "Exxon" sequence total net reservoir isopach (ES34-ES30). Net reservoir cutoffs: SP < -30 mv, Res > 10 ohmm.

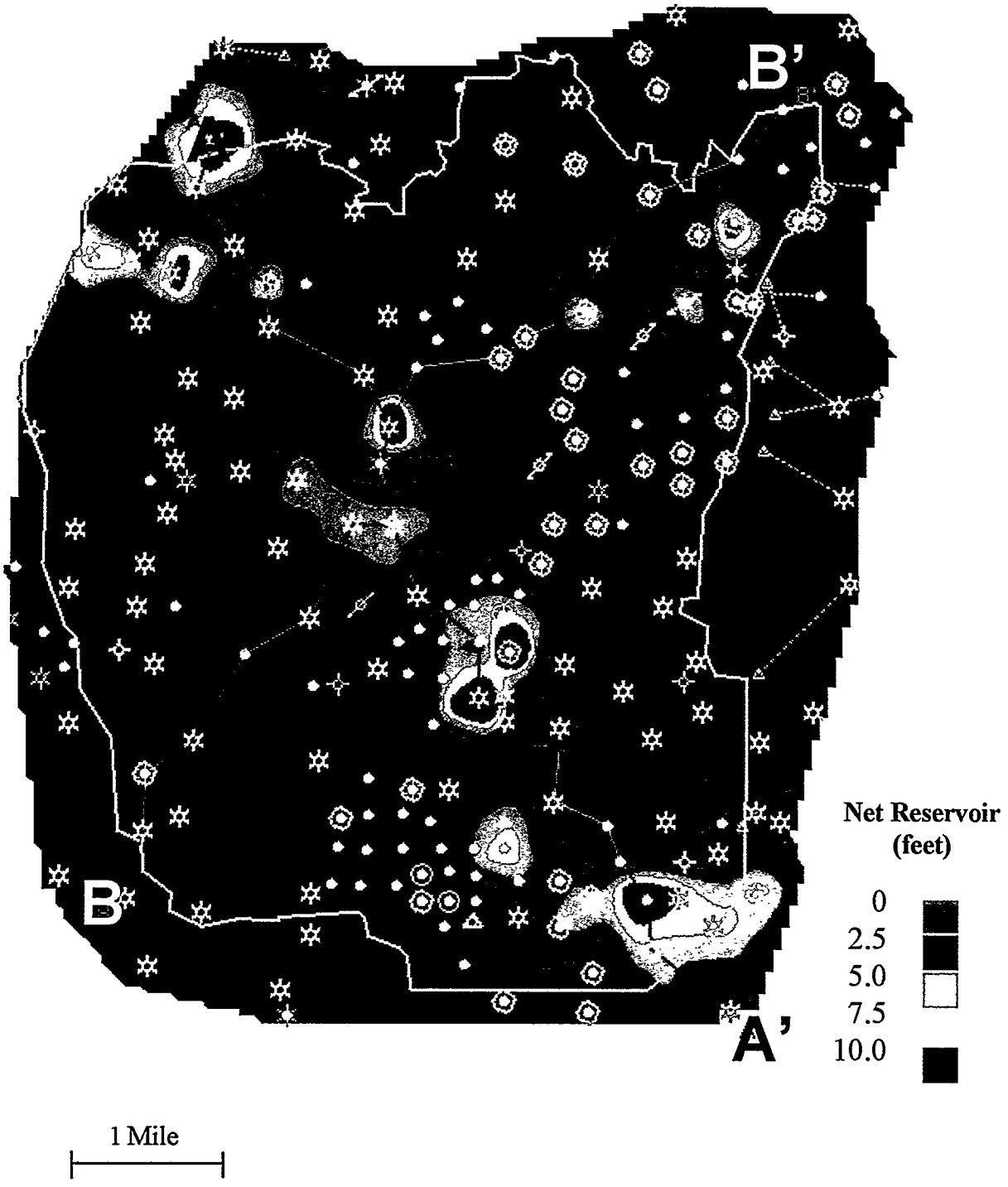

Figure A30. Middle Jasper Creek lowstand valley fill net reservoir isopach (FS34-ES34). Net reservoir cutoffs: SP < -30 mv, Res > 10 ohmm.

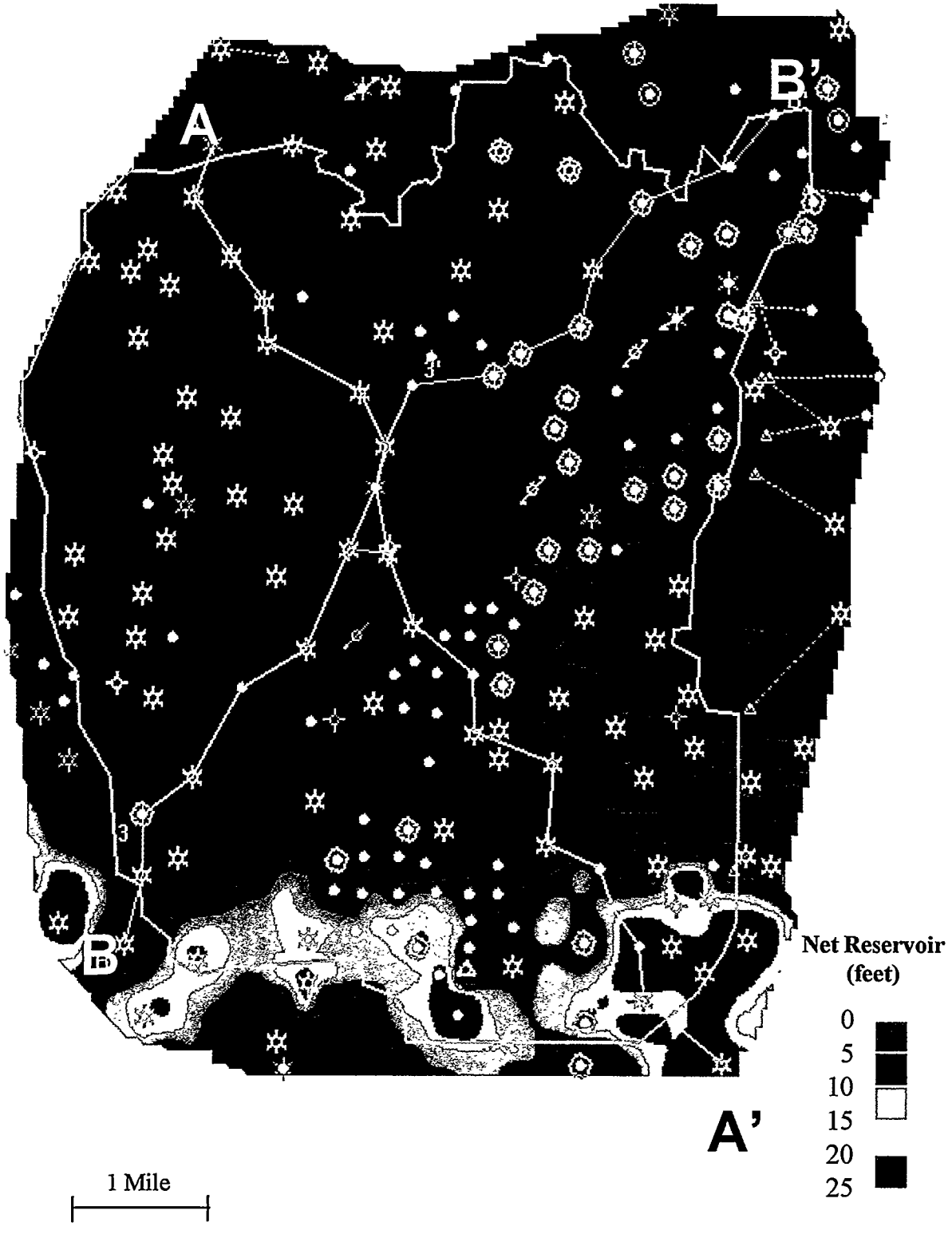

Figure A31. Upper Jasper Creek "Exxon" sequence net reservoir isopach (ES38-ES36). Net reservoir cutoffs: SP < -30 mv, Res > 10 ohmm.

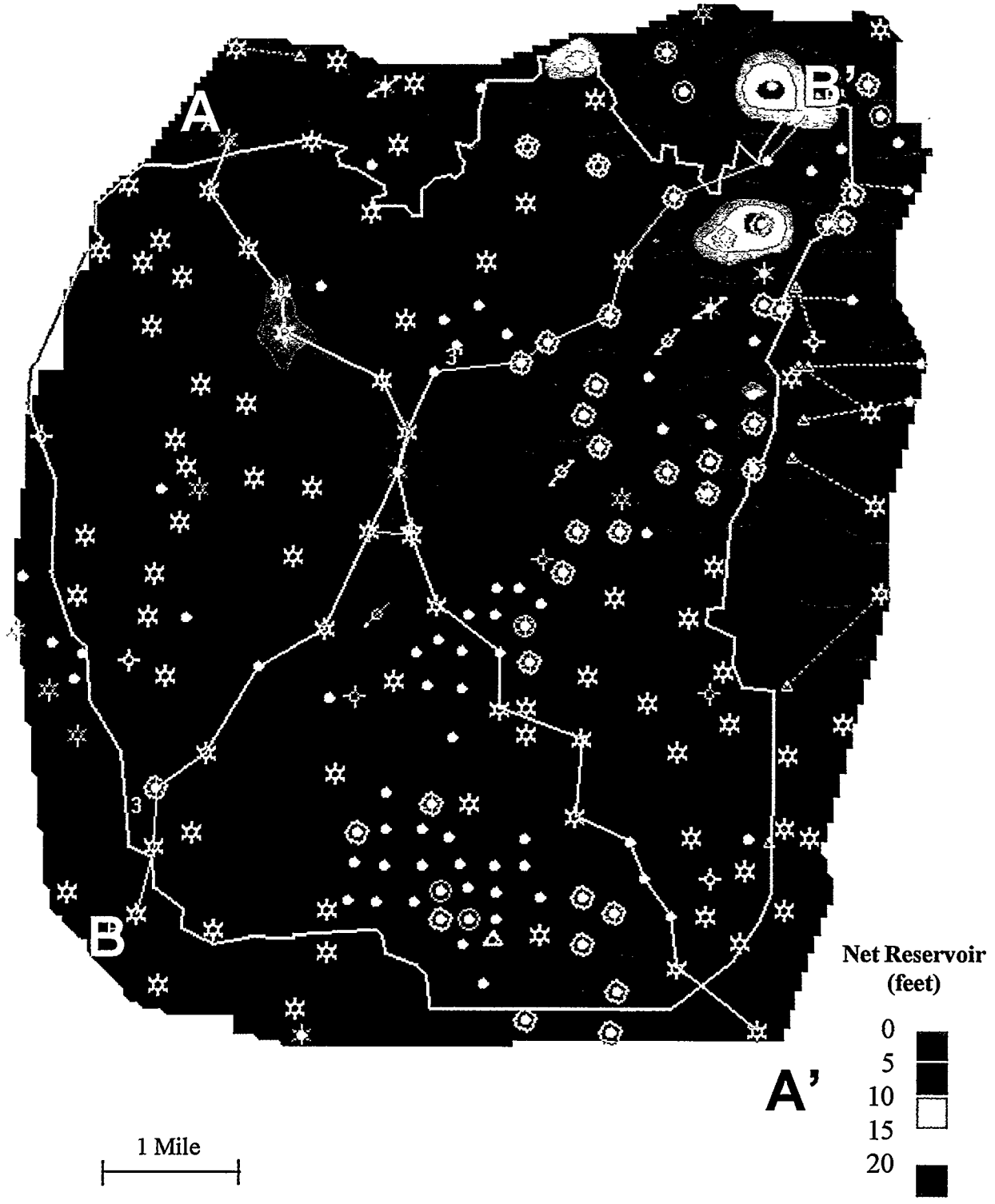

Figure A32. Fourth Jasper Creek "Exxon" sequence net reservoir isopach (ES40-ES38). Net reservoir cutoffs: SP < -30 mv, Res > 10 ohmm.

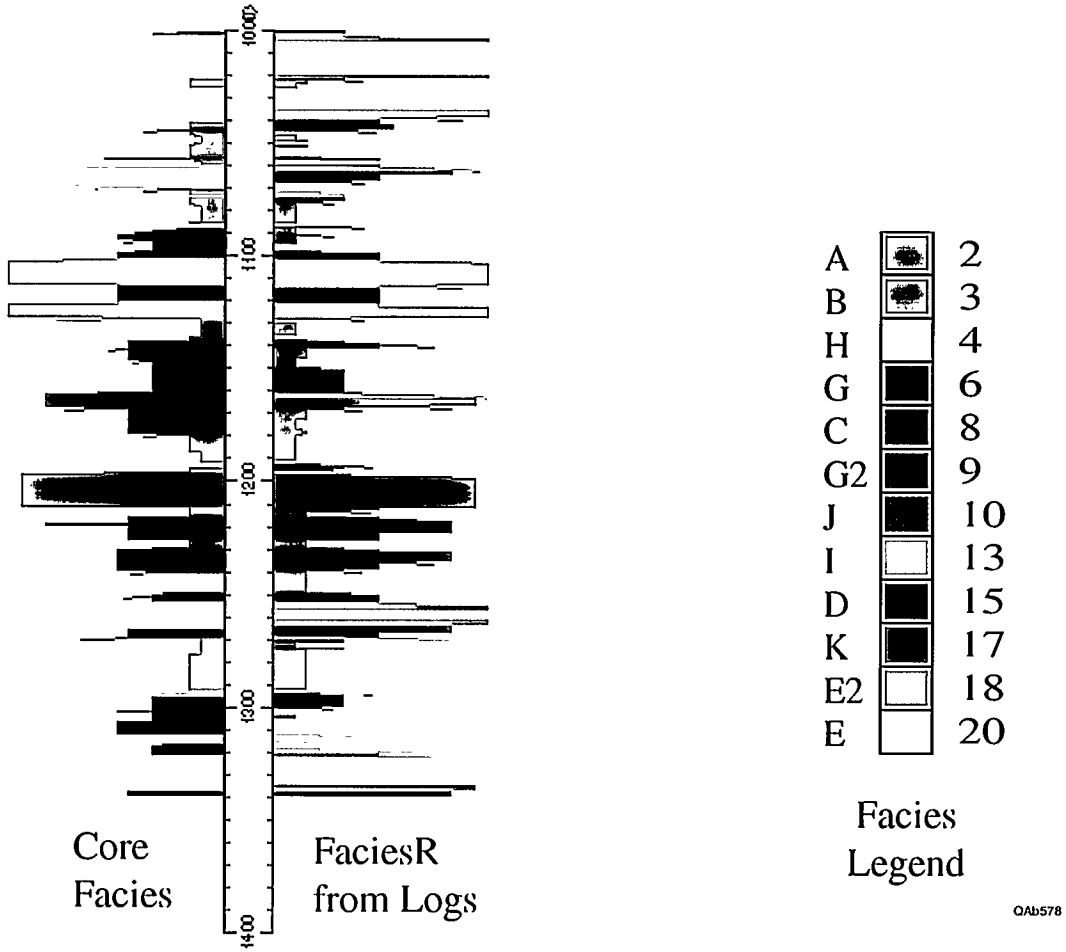

Figure C13. Geocolumn display of all core data stacked on top of one another to the left of the depth track and the corresponding log-derived facies using the FaciesR model to the right of the depth track.

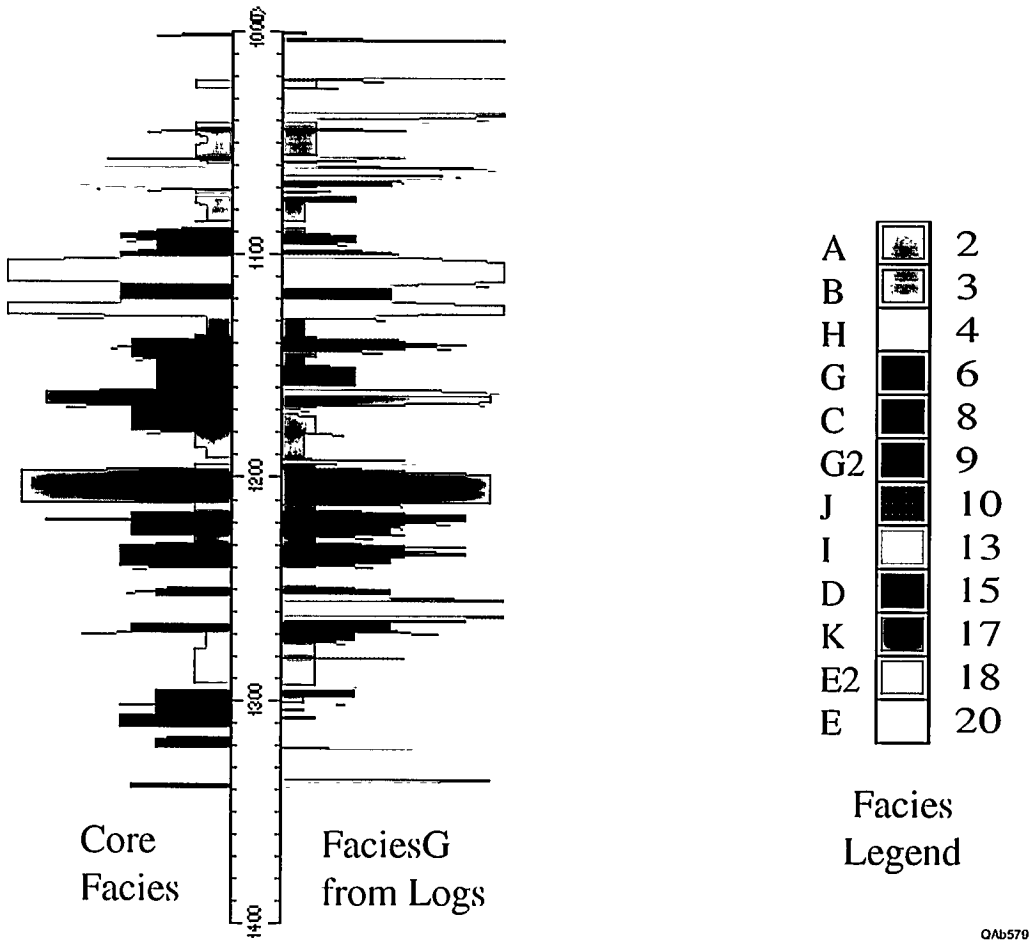

Figure C14. Geocolumn display of all core data stacked on top of one another to the left of the depth track and the corresponding log-derived facies using the FaciesG model to the right of the depth track.

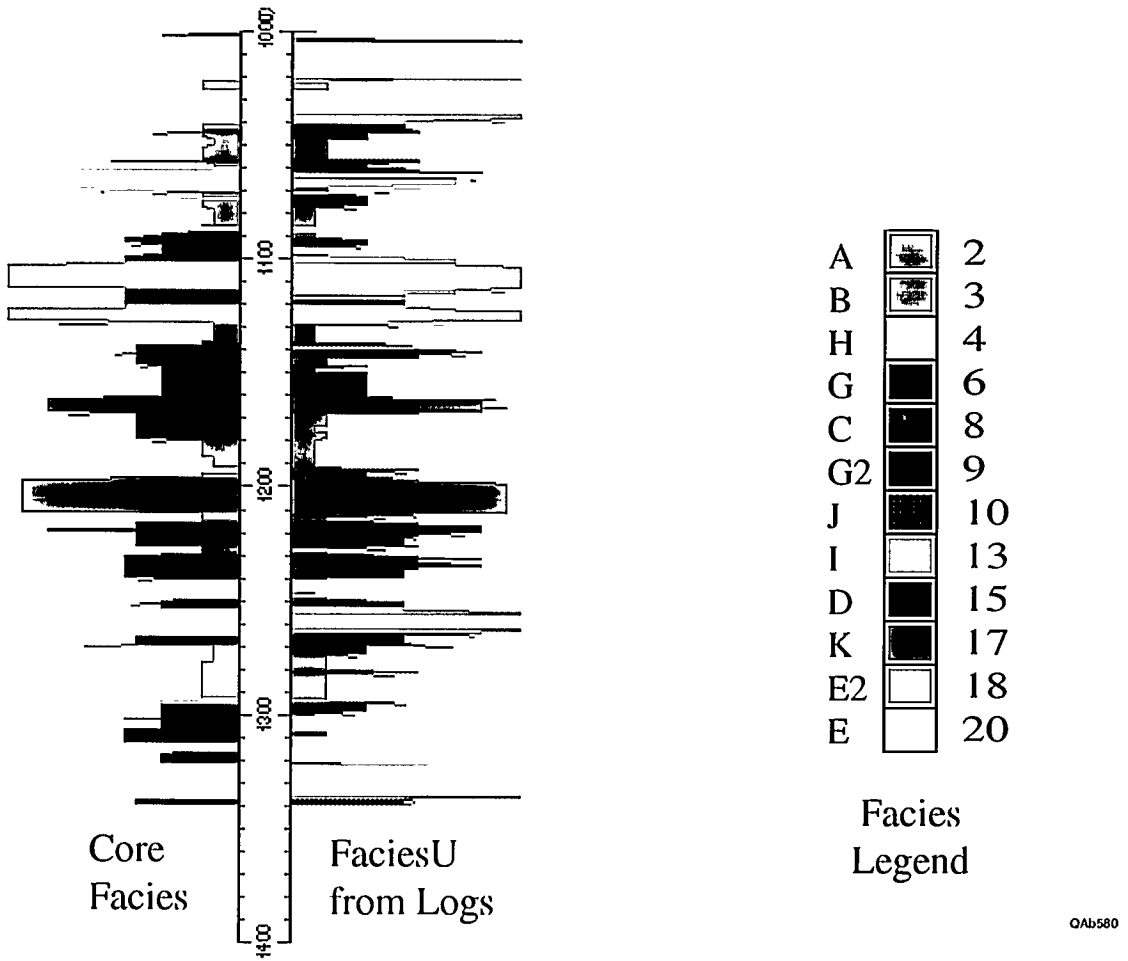

Figure C15. Geocolumn display of all core data stacked on top on one another to the left of the depth track and the corresponding log-derived facies using the FaciesU model to the right of the depth track.

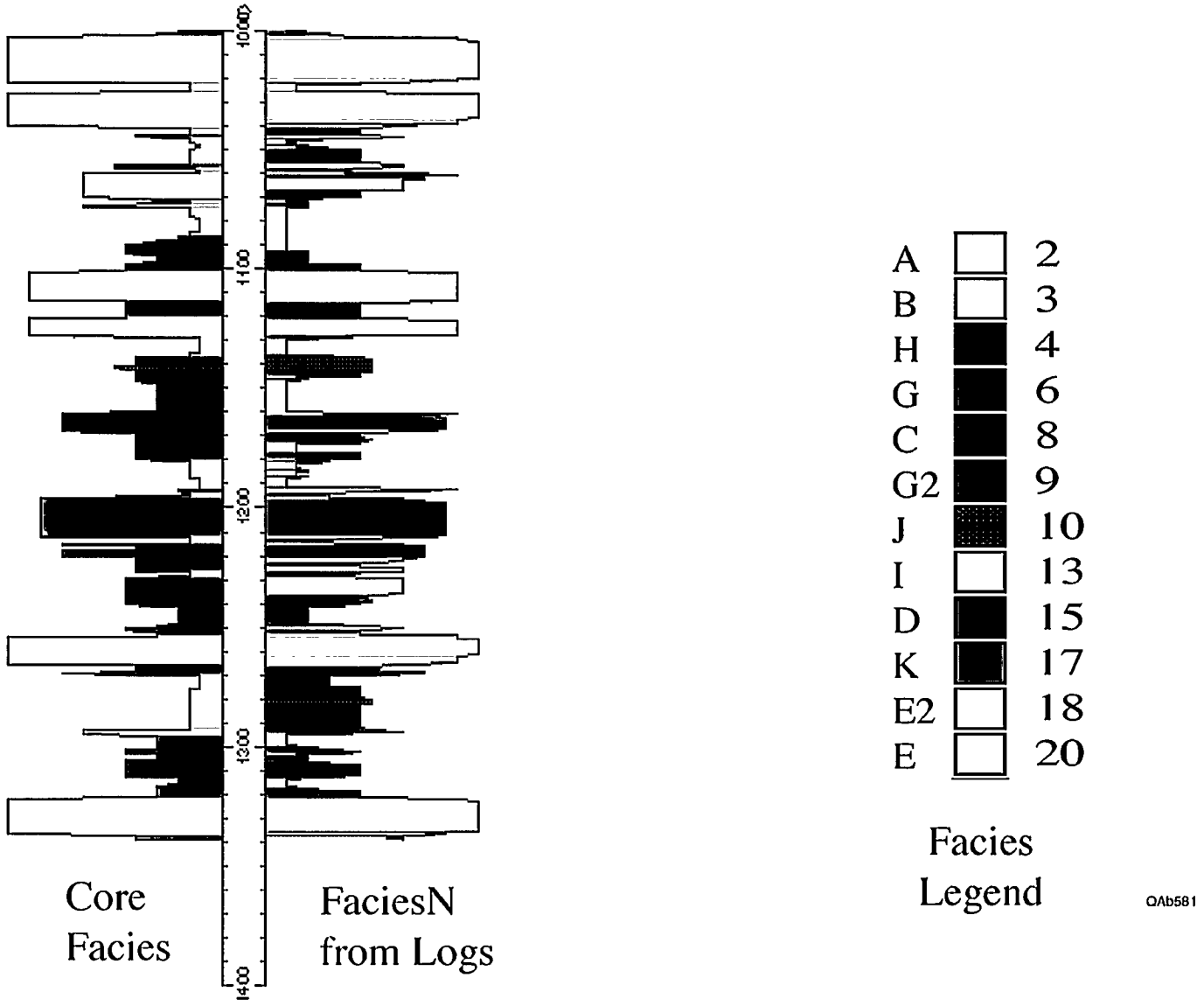

Figure C16. Geocolumn display of all core data stacked on top of one another to the left of the depth track and the corresponding log-derived facies using the FaciesN model to the right of the depth track.

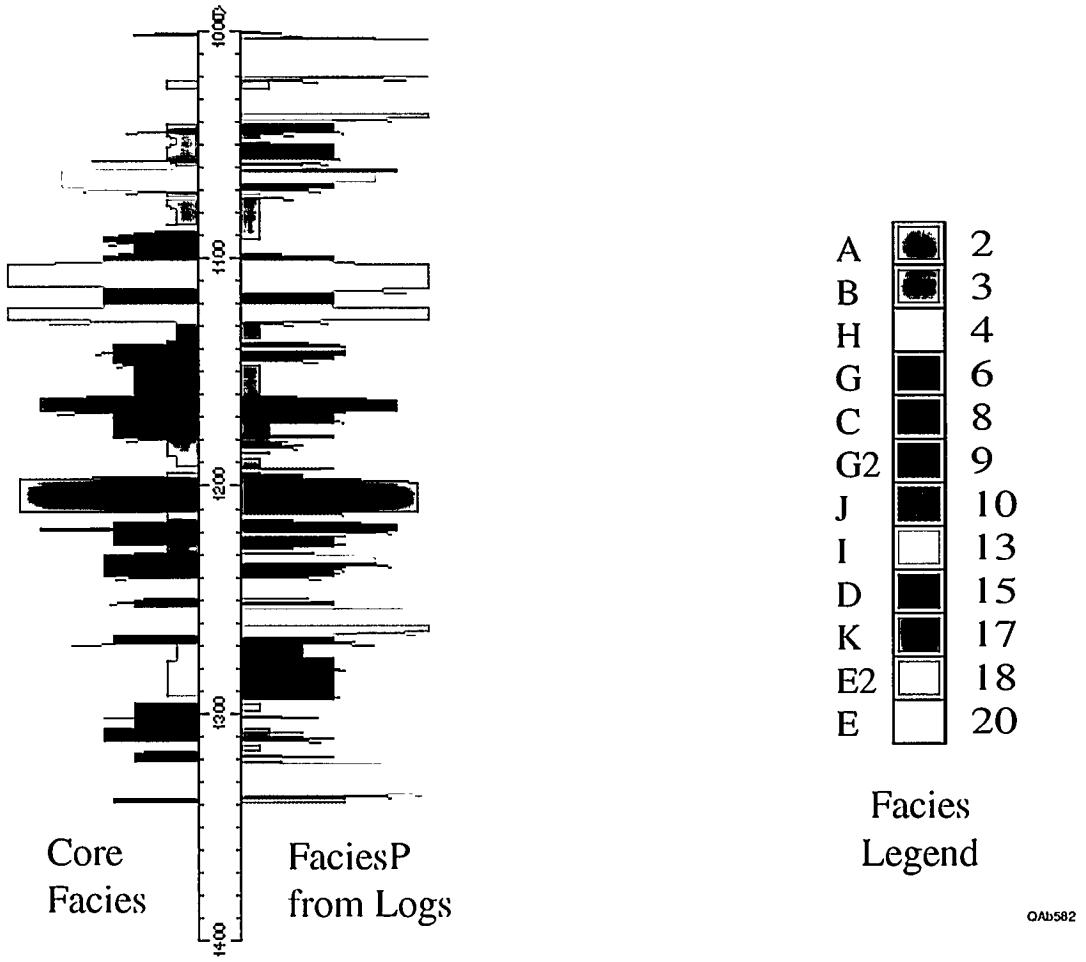

Figure C17. Geocolumn display of all core data stacked on top of one another to the left of the depth track and the corresponding log-derived facies using the FaciesP model to the right of the depth track.

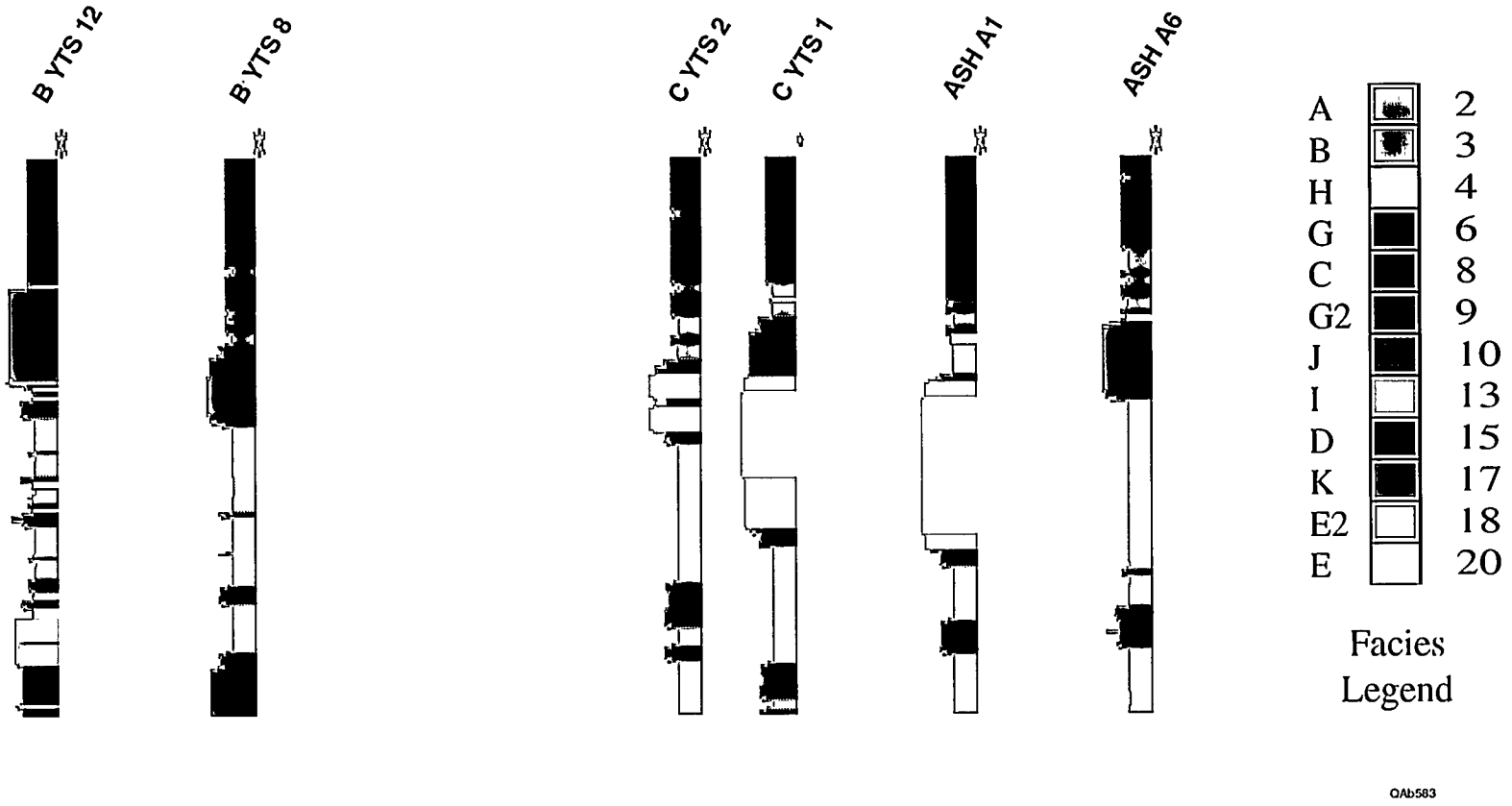

Figure C18. A geocolumn display cross section. This section is through the Caddo sequence.

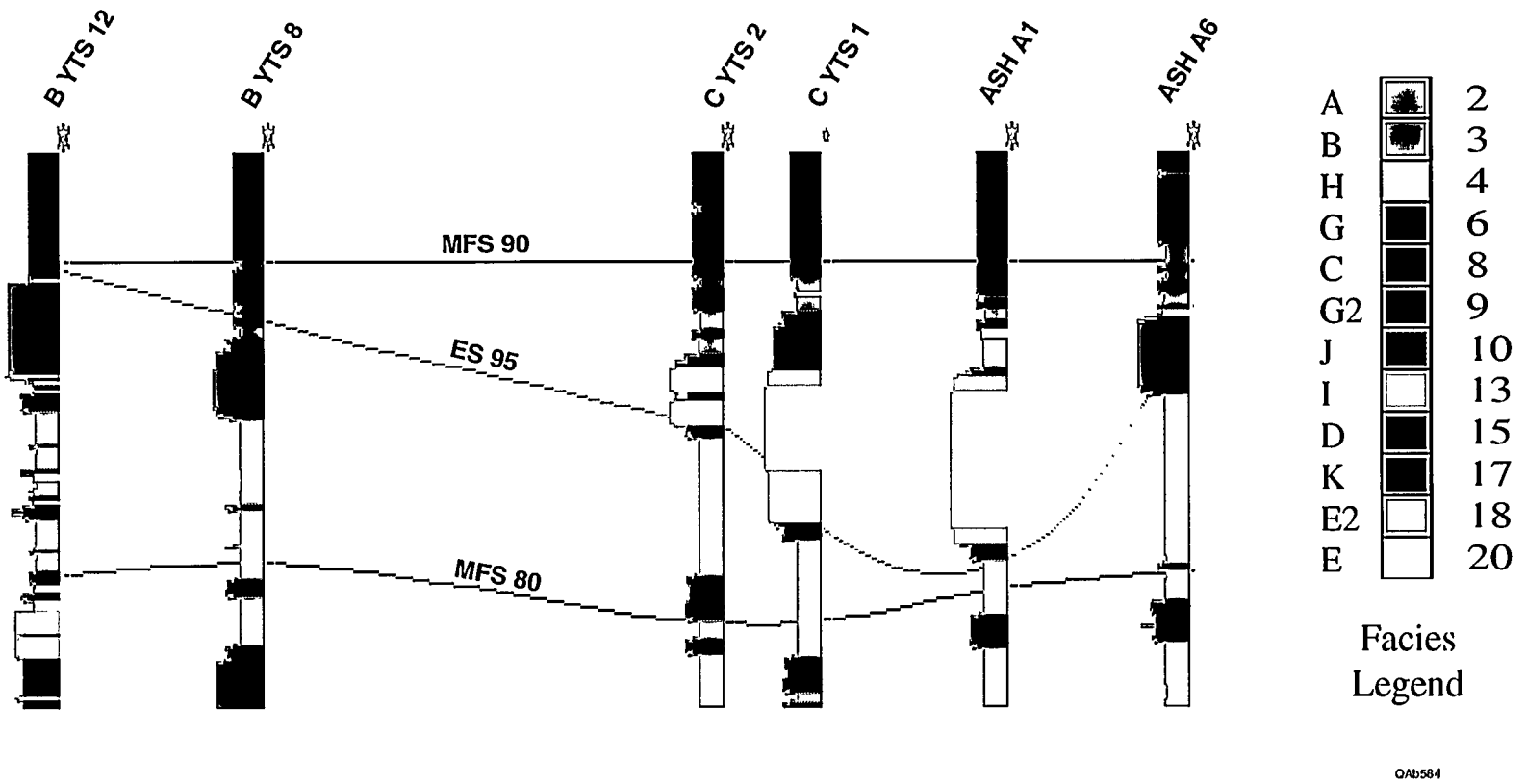

Figure C19. Interpreted version of the cross section shown in Figure C18.

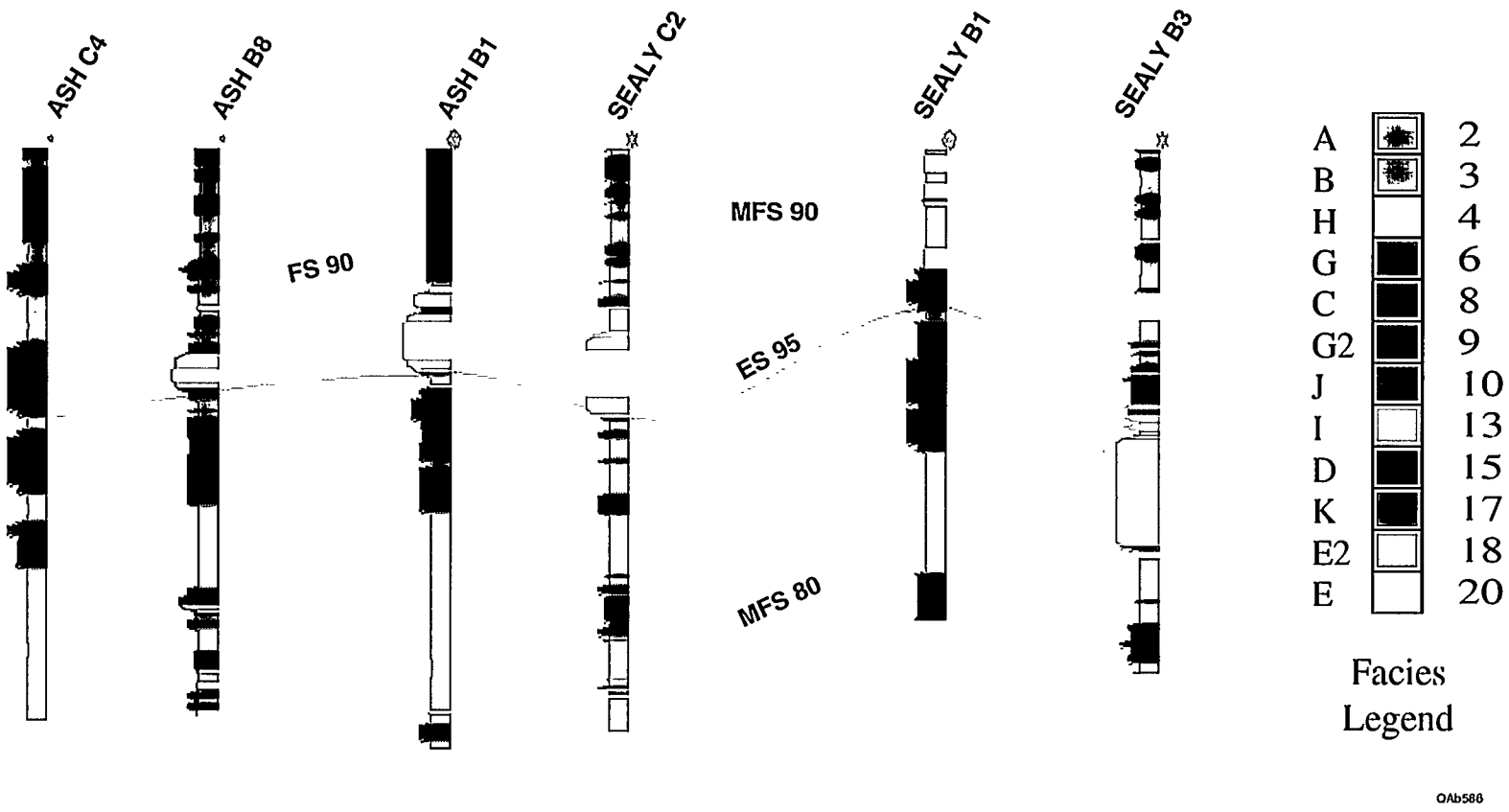

Figure C21. Cross section through the Upper Caddo in the northeast part of the study area.